THE FOURTH IAEA SYMPOSIUM ON

NEUTRON INELASTIC SCATTERING

VOL. I

PROCEEDINGS OF A
SYMPOSIUM, COPENHAGEN,
20-25 MAY 1968

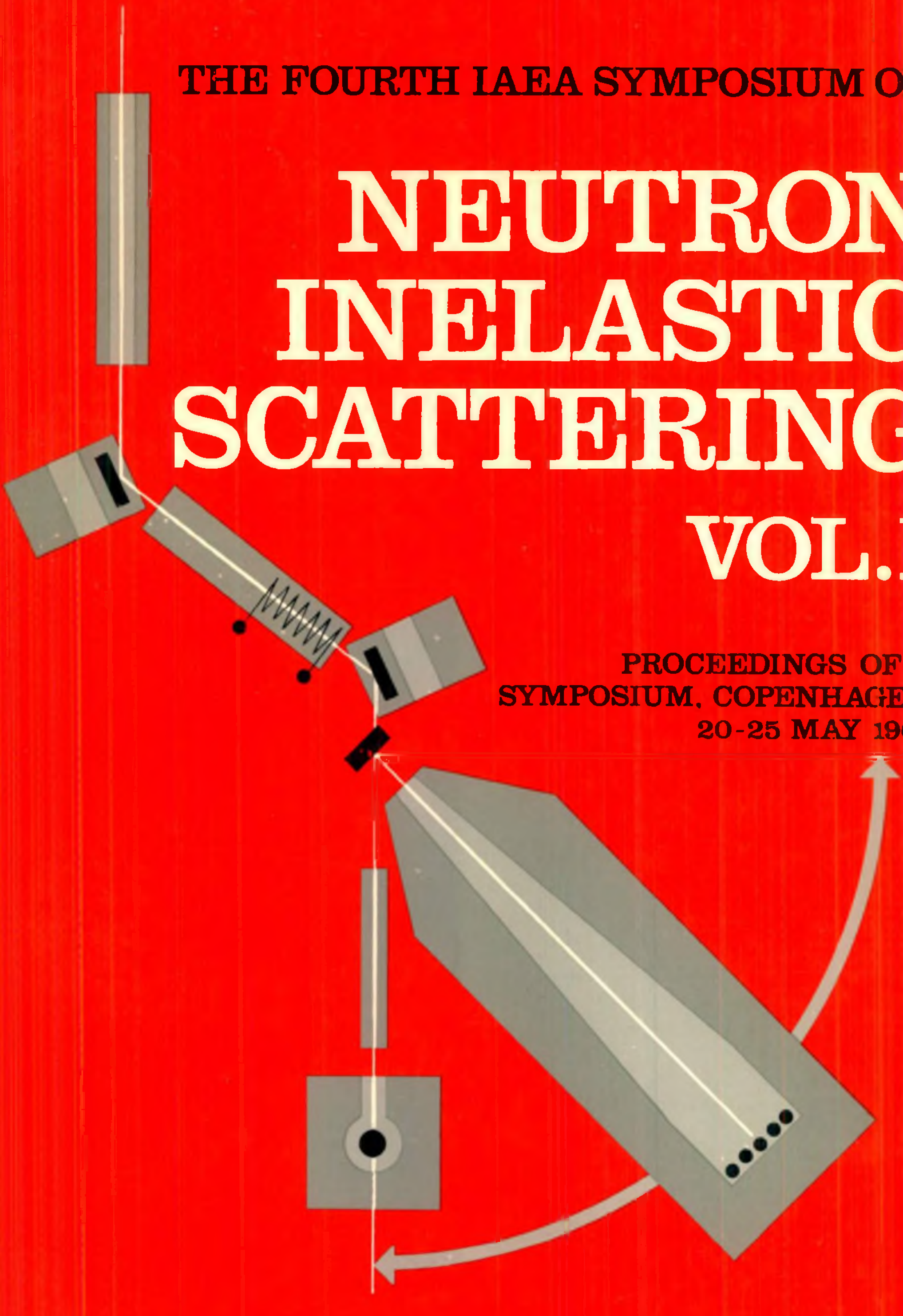

INTERNATIONAL ATOMIC ENERGY AGENCY, VIENNA, 1968

NEUTRON INELASTIC SCATTERING, VOLUME I

ERRATA AND CORRIGENDA

Separator page 1

For DYNAMICS OF LIQUIDS read DYNAMICS OF SOLIDS

Page 47 paper title

For Cua_{1-x} read Cu_{1-x}

Page 119

Add footnotes
*This work has been partly supported by the Office of Naval Research.
**National Science Foundation Predoctoral Fellow.
†On leave from CEN-Saclay, France, where part of the present work was also performed.

Page 289

Add footnote *Faculté des sciences de Montpellier, France.

Page 352, Table I

For	H_θ	0.0428	0.0428	read	F_θ	0.0428	0.02320
	H_ϕ	0.0151	0.0151		F_ϕ	0.0151	0.00824
	$H_{\phi'}$	0.0109	0.0109		$F_{\phi'}$	0.0109	0.00595

Separator page 395

For DYNAMICS OF SOLIDS read DYNAMICS OF LIQUIDS
(Session B)

Page 581

Add footnote *Guest scientist from Jozef Stefan Nuclear Institute, Ljubljana, Yugoslavia, since returned.

Page 639

The name of the Scientific Secretary should read: J. DOLNIČAR

NEUTRON INELASTIC SCATTERING
VOL.I

The following States are Members of the International Atomic Energy Agency:

AFGHANISTAN
ALBANIA
ALGERIA
ARGENTINA
AUSTRALIA
AUSTRIA
BELGIUM
BOLIVIA
BRAZIL
BULGARIA
BURMA
BYELORUSSIAN SOVIET SOCIALIST REPUBLIC
CAMBODIA
CAMEROON
CANADA
CEYLON
CHILE
CHINA
COLOMBIA
CONGO, DEMOCRATIC REPUBLIC OF
COSTA RICA
CUBA
CYPRUS
CZECHOSLOVAK SOCIALIST REPUBLIC
DENMARK
DOMINICAN REPUBLIC
ECUADOR
EL SALVADOR
ETHIOPIA
FINLAND
FRANCE
GABON
GERMANY, FEDERAL REPUBLIC OF
GHANA
GREECE
GUATEMALA
HAITI
HOLY SEE
HUNGARY
ICELAND
INDIA
INDONESIA
IRAN
IRAQ
ISRAEL
ITALY
IVORY COAST
JAMAICA
JAPAN
JORDAN
KENYA
KOREA, REPUBLIC OF
KUWAIT
LEBANON
LIBERIA
LIBYA
LUXEMBOURG
MADAGASCAR
MALI
MEXICO
MONACO
MOROCCO
NETHERLANDS
NEW ZEALAND
NICARAGUA
NIGERIA
NORWAY
PAKISTAN
PANAMA
PARAGUAY
PERU
PHILIPPINES
POLAND
PORTUGAL
ROMANIA
SAUDI ARABIA
SENEGAL
SIERRA LEONE
SINGAPORE
SOUTH AFRICA
SPAIN
SUDAN
SWEDEN
SWITZERLAND
SYRIAN ARAB REPUBLIC
THAILAND
TUNISIA
TURKEY
UGANDA
UKRAINIAN SOVIET SOCIALIST REPUBLIC
UNION OF SOVIET SOCIALIST REPUBLICS
UNITED ARAB REPUBLIC
UNITED KINGDOM OF GREAT BRITAIN AND NORTHERN IRELAND
UNITED STATES OF AMERICA
URUGUAY
VENEZUELA
VIET-NAM
YUGOSLAVIA

The Agency's Statute was approved on 23 October 1956 by the Conference on the Statute of the IAEA held at United Nations Headquarters, New York; it entered into force on 29 July 1957. The Headquarters of the Agency are situated in Vienna. Its principal objective is "to accelerate and enlarge the contribution of atomic energy to peace, health and prosperity throughout the world".

Printed by the IAEA in Austria
September 1968

PROCEEDINGS SERIES

NEUTRON INELASTIC SCATTERING

PROCEEDINGS OF A SYMPOSIUM ON
NEUTRON INELASTIC SCATTERING
HELD BY THE
INTERNATIONAL ATOMIC ENERGY AGENCY
IN COPENHAGEN, 20-25 MAY, 1968

In two volumes

VOL. I

INTERNATIONAL ATOMIC ENERGY AGENCY
VIENNA, 1968

NEUTRON INELASTIC SCATTERING
(Proceedings Series)

ABSTRACT. Proceedings of a Symposium convened by the IAEA and held in Copenhagen, 20-25 May 1968. The meeting was attended by 167 participants from 29 Member States and 4 international organizations. These are the fourth IAEA Symposium Proceedings to have neutron inelastic scattering as their main theme, the previous ones being Inelastic Scattering of Neutrons in Solids and Liquids (Vienna), IAEA (1961), Inelastic Scattering of Neutrons in Solids and Liquids (Chalk River), IAEA (1963), and Inelastic Scattering of Neutrons (Bombay), IAEA (1965).

Contents: Dynamics of solids, including: lattice vibrations and local modes (6 papers), lattice dynamics in metals (7 papers), lattice dynamics of metals and alloys (13 papers), lattice dynamics of non-metals (11 papers) and review paper; Dynamics of liquids, including: coherent neutron scattering on liquids (5 papers), neutron scattering on hydrogenous liquids (14 papers) and 2 review papers; Magnetic systems (13 papers and review paper); Molecular dynamics (9 papers); Experimental methods (17 papers); and Summary.

Each paper is in its original language (93 English, 2 French, 4 Russian) and is preceded by an abstract in English with one in the original language where this is not English. Discussions are in English.

(Vol. I: 642 pp., 16×24 cm, paper-bound, 306 figures)
(1968) Price: US $15.00; £ 6.5.0

NEUTRON INELASTIC SCATTERING
IAEA, VIENNA, 1968
STI/PUB/187

FOREWORD

Three and a half years have passed since the IAEA held its third Symposium on Neutron Inelastic Scattering in Bombay, India. During this period, studies of the dynamics of liquids, solids and magnetic systems by inelastic scattering of neutrons have resulted in the maturing of the theoretical aspects, and in more sophisticated interpretation of experimental data. From the many laboratories where neutron scattering research was recently introduced, the first results have now been obtained. This situation was reflected in the very large number of abstracts submitted to the selection committee that prepared the program for the Fourth Symposium held in Copenhagen from 20 to 25 May 1968. In the event, 99 papers from 21 countries and two international organizations were selected for presentation. Because of this large number of contributions, 53 papers were summarized by seven rapporteurs. These papers were discussed in groups and the discussion is included in these Proceedings after the full texts of the contributions; the rapporteurs' texts, however, have not been included.

Although the meeting concentrated on experimental results and their interpretation, it was realized that experimental methods and techniques have been greatly improved during the last few years. Consequently, a Special Session was organized, devoted entirely to this topic. Several of the new experimental techniques are arousing interest.

Three prominent experts were invited to present review papers covering the advances of recent years. In addition, two invited papers on competitive, non-neutron techniques for dynamics studies were included in the program, thereby establishing a connection between neutron inelastic scattering and nuclear magnetic resonance, optical and other techniques for investigating the dynamics of solids and liquids.

The Symposium was held at the kind invitation of the Danish Government. Gratitude is also expressed to the authors of the papers, the rapporteurs, the chairmen of sessions and the discussion participants for their contributions to the success of the Symposium.

EDITORIAL NOTE

The papers and discussions incorporated in the proceedings published by the International Atomic Energy Agency are edited by the Agency's editorial staff to the extent considered necessary for the reader's assistance. The views expressed and the general style adopted remain, however, the responsibility of the named authors or participants.

For the sake of speed of publication the present Proceedings have been printed by composition typing and photo-offset lithography. Within the limitations imposed by this method, every effort has been made to maintain a high editorial standard; in particular, the units and symbols employed are to the fullest practicable extent those standardized or recommended by the competent international scientific bodies.

The affiliations of authors are those given at the time of nomination.

The use in these Proceedings of particular designations of countries or territories does not imply any judgement by the Agency as to the legal status of such countries or territories, of their authorities and institutions or of the delimitation of their boundaries.

The mention of specific companies or of their products or brand-names does not imply any endorsement or recommendation on the part of the International Atomic Energy Agency.

CONTENTS OF VOL. I

DYNAMICS OF SOLIDS (Session A)

Lattice vibrations and local modes

Lattice dynamics in metals

Lattice dynamics of metals and alloys

Lattice dynamics of non-metals

DYNAMICS OF LIQUIDS (Session B)

Coherent neutron scattering on liquids

Neutron scattering on hydrogenous liquids

DYNAMICS OF LIQUIDS

(Session A)

Chairmen: W.HÄLG
J.ALS-NIELSEN
Yu.M.KAGAN

Rapporteurs for this Session were:

B.MOZER for SM—104/18, 42, 85 and 78
W.COCHRAN for SM—104/1, 4, 29, 47, 86 and 132
R.M.NICKLOW for SM—104/24, 40, 124, 66, 54, 120, 128 and 137
R.STEDMAN for SM—104/46, 33, 41, 75, 93 and 109

All other papers were presented in the usual way.

РОЛЬ ЭЛЕКТРОНОВ В ФОРМИРОВАНИИ ФОНОННОГО СПЕКТРА МЕТАЛЛОВ

Ю.КАГАН, Е.Г.БРОВМАН
ИНСТИТУТ АТОМНОЙ ЭНЕРГИИ
им.И.В.КУРЧАТОВА, МОСКВА,
СССР

Abstract — Аннотация

THE ROLE OF ELECTRONS IN PHONON SPECTRUM FORMATION IN METALS.* The explanation of phonon spectra in simple metals is based on long-range interaction between ions. A better description can be obtained if the electrons are included in the treatment. A theory based on the electron-ion system enables a better understanding of the indirect interaction between ions for a majority of non-transient metals. The physical and mathematical foundations are constituted, and the theoretical elaboration of this model is presented.

The role of electrons in formations of the phonon spectra in metals is illustrated on examples of simple metals and metals with hexagonal structure. It is shown that the phonon spectra of complex metals could be satisfactorily explained by treating the short-range non-pair and the long-range pair interactions separately.

РОЛЬ ЭЛЕКТРОНОВ В ФОРМИРОВАНИИ ФОНОННОГО СПЕКТРА МЕТАЛЛОВ. Фононный спектр простых металлов основывается на дальнодействующем взаимодействии между ионами. Более полно фононный спектр металлов можно объяснить, если учесть наличие электронов. Теория, основанная на электрон-ионной системе металла, дает возможность лучше понять косвенное взаимодействие между ионами для большинства непереходных металлов. В данной работе приводятся физические и математические основы, а также дается теоретическая разработка такой модели.

Роль электронов в формировании фононного спектра металлов иллюстрируется на примерах простых металлов и металлов с гексагональной структурой. Показано, что фононный спектр сложных металлов можно достаточно хорошо описать, выделяя в явной форме непарное короткодействующее и парное дальнодействующее взаимодействия.

ВВЕДЕНИЕ

В последние годы стало отчетливо ясно, что для фононного спектра металлов характерно существование дальнодействующего взаимодействия между ионами. Этот факт был обнаружен уже в известной работе Брокхауза и др. [I] , в которой изучался фононный спектр свинца. Однако, пожалуй, наиболее ярко роль дальнодействующего взаимодействия проявилась тогда, когда начались исследования фононного спектра более сложных металлов, таких, например, как олово [2]—[4] или цинк [5] , [6] , т.е. некубических металлов с двумя атомами в элементарной ячейке. Это обстоятельство не случайно. Дело в том, что сравнительная простота дисперсионных кривых в случае простых металлов почти всегда допускает альтернативное описание на языке короткодействующего

---

[*] An English translation of this paper is available on request from the Editorial and Publications Section, IAEA.

взаимодействия с ближайшими координационными сферами. При этом схватываются основные черты спектра и уж, во всяком случае, хорошо описываются интегральные по спектру физические величины. Для сложных металлов картина оказывается иной. Так,в случае олова попытки учесть только взаимодействие с ближайшими координационными сферами привели к неправильному виду спектра, на основе которого не удавалось объяснить даже интегральные по спектру величины.

Для более или менее разумного описания дисперсионных кривых и всего спектра в целом потребовалось учесть, по крайней мере, 6 координационных сфер и 14 независимых констант [7] , а чуть более хорошее согласие между вычисленными и измеренными дисперсионными кривыми достигалось уже за счет учета 12 координационных сфер и 26 силовых констант [8].

Объяснение дальнодействующего взаимодействия,как и вообще всей тонкой структуры дисперсионных кривых, лежит в особой роли электронов проводимости в формировании фононного спектра металлов, точнее говоря, в характере косвенного взаимодействия между ионами через электроны. Однако развитые в последние годы общие представления об электрон-ионной системе металла позволяют последовательно решить вопрос о косвенном взаимодействии между ионами для большинства непереходных металлов. Тем самым возникает заманчивая возможность определения фононного спектра широкого класса металлов, исходя из первых принципов или же привлекая очень небольшое число экспериментальных констант.

Сформулируем кратко те современные представления о металле, которые существенны для дальнейшего анализа.

1. В металле все валентные электроны коллективизируются, образуя квазисвободную электронную подсистему. Экспериментально это легко проверяется по объему, который занимают электроны в импульсном пространстве.

2. Оставшиеся ионы обладают сравнительно малым размером, занимая примерно 10% от объема, приходящегося на 1 атом кристалла. При этом ионы не перекрываются, сохраняют практически свойства изолированного иона и взаимодействие между ними носит главным образом, кулоновский характер с возможной малой примесью Ван-дер-Ваальсовских сил. В силу этого, по крайней мере на современном уровне, мы должны считать прямое короткодействующее взаимодействие между ионами, например Борн-Майеревского типа, отсутствующим. На примере натрия это было четко продемонстрировано Воско [9] .

3. В основной части объема отдельный электрон взаимодействует с ионом чисто кулоновским образом. В пределах же иона истинная ψ -функция электрона испытывает сильные осцилляции, поскольку она должна быть ортогональна к собственным функциям ионного остова. Это приводит к резкому уменьшению эффективного взаимодействия электрона с ионом и, следовательно, амплитуды

рассеяния электрона на ионе при больших передачах импульса. Такое уменьшение взаимодействия эквивалентно появлению в пределах иона некоторого эффективного отталкивающего потенциала, который в значительной степени компенсирует самосогласованный потенциал ионного остова. В результате появляется возможность замены истинного потенциала на некоторый эффективный псевдопотенциал, в общем случае нелокальный, дающий близкое к истинному значение амплитуды рассеяния и близкое к плоской волне поведение Ψ - функции электрона уже во всем пространстве. Концепция псевдопотенциала (см., например, [10]- [12]) оказалась очень эффективной для рассмотрения самых различных свойств металлов.

4. Эффективное уменьшение взаимодействия в пределах иона приводит к появлению малого параметра в теории металла. Этим параметром является отношение фурье-компоненты псевдопотенциала в ближайших узлах обратной решетки $V_{\vec{K}}$ к энергии Ферми E_F (для простоты рассуждения мы предполагаем псевдопотенциал локальным). Именно наличие этого малого параметра определило большой успех модели квазисвободных электронов при описании электронных свойств металлов (см., например, [12]).

Пусть для металла справедливо адиабатическое приближение. (Обсуждение этого вопроса проведено в следующем разделе). Тогда на основе сказанного можно заключить, что, если известен эффективный потенциал, описывающий взаимодействие электрона с изолированным ионом, то энергия всей системы при фиксированном положении ионов, а следовательно, и соответствующая динамическая матрица колебаний,в принципе, являются функционалом от этого взаимодействия и не должна содержать никаких других параметров или величин, кроме тривиальных.

Решая задачу во втором порядке теории возмущения по псевдопотенциалу, приходим к парному взаимодействию между ионами центрального типа. Именно в этом приближении и были получены все конкретные результаты в работах Тойи [13] ,[14], Шама [15]и Воско [16] , где рассматривался фононный спектр простых металлов, главным образом, натрия. Вычисления различались только разным выбором эффективного электрон-ионного взаимодействия и разным характером учета электронного экранирования. (При этом в первых двух работах учитывалось короткодействующее взаимодействие между ионами типа Борна-Майера, а в третьей работе совершенно разумно оно было опущено). Анализ характера возникающего центрального взаимодействия между ионами и роль его в образовании фононного спектра металлов типа натрия подробно рассматривалось в докладе Кокрана [17] на предыдущем симпозиуме (см. также [18]),и мы специально на этом останавливаться не будем.

В работах авторов [19, 20] было показано, что для анализа фононного спектра очень важно учесть следующие члены разложения электронной энергии по степеням псевдопотенциала. Оказывается,эти члены приводят к появлению непарного взаимодействия между ионами. Следовательно, само косвенное взаимодействие через электроны предопределяет возникновение в молекуле сил ковалентного типа. Хотя следующий член разложения электронной энергии содержит параметр малости $V_{\vec{K}}/\varepsilon_F$, но в колебательной задаче это короткодействующее взаимодействие может играть весьма существенную роль. В частности, это связано с тем, что вклад в фононный спектр от прямого кулоновского взаимодействия между ионами и от парного косвенного взаимодействия могут заметно компенсировать друг друга. По-видимому, в некоторых случаях только учет этого взаимодействия приводит к динамической стабильности решетки.

С точки зрения справедливости приведенных выше соображений о характере взаимодействия в электрон-ионной системе металла простые металлы не имеют преимущества перед сложными. Это наглядно видно на примере табл. I, где приведено отношение объема иона к объему, приходящемуся на I атом в кристалле для ряда металлов. (Значения заимствованы из работы [34]).

Таблица I

Li	Na	K	Rb	Be	Mg	Ca
0,092	0,I04	0,I38	0,I6	0,02	0,086	0,II4

Zn	Al	Ga	In	Sn	Pb
0,I58	0,048	0,052	0,I26	0,064	0,082

Действительно, это отношение в таких сложных металлах, как Sn , Be , Mg , меньше чем в случае Na или K .

В этой связи ,естественно, встает вопрос о возможности описания фононного спектра сложных металлов, используя только представление об электрон-ионном взаимодействии. Однако до сих пор основной успех в описании фононного спектра металлов был связан, главным образом, с металлами типа натрия. Как мы увидим ниже, это обстоятельство не случайно - оно связано с малой ролью процессов переброса и, следовательно, с малой ролью непарного взаимодействия. В общем случае картина резко иная, особенно в сложных металлах.

Считая, что "век натрия" кончается, мы уделяем основное внимание анализу роли парного и непарного взаимодействия, природе появляющихся ковалентных по типу сил между ионами, роли процессов переброса и покажем, что в настоящее время имеется реальная возможность дать разумное описание фононного спектра сложных металлов на сравнительно простом языке.

2. АДИАБАТИЧЕСКОЕ ПРИБЛИЖЕНИЕ В МЕТАЛЛЕ

Для нахождения фононного спектра металлов существенен вопрос о справедливости адиабатического приближения. Если мы ищем фононный спектр в электрон-ионной системе металла, опираясь на адиабатическое приближение, то вопрос фактически сводится к тому, должны ли мы затем проводить перенормировку такого адиабатического спектра за счет уже электрон-фононного взаимодействия. Это вопрос был подробно изучен в [20], и мы наметим здесь только путь рассмотрения и приведем результаты.

Проводя обычную для адиабатического приближения Борна-Оппенгеймера процедуру (см., например, [21]) и выделяя сначала электронную энергию $E_n(\vec{R})$ при фиксированном положении ионов, легко придти к следующей системе уравнений, описывающих колебания ионов:

$$\left[H_i(\vec{R})+E_n(\vec{R})\right]\Phi_n(\vec{R})+\sum_m C_{nm}\,\Phi_m(\vec{R})=E\,\Phi_n(\vec{R}) \qquad (2.1)$$

где:
$$C_{nm}=A_{nm}+B_{nm}$$
$$A_{nm}=-\frac{1}{M}\sum_p\int d\vec{r}\,\psi_n^*(\vec{r},\vec{R})\nabla_{\vec{R}_p}\psi_m(\vec{r},\vec{R})\nabla_{\vec{R}_p}$$
$$B_{nm}=-\frac{1}{2M}\sum_p\int d\vec{r}\,\psi_n^*(\vec{r},\vec{R})\Delta_{\vec{R}_p}\psi_m(\vec{r},\vec{R}) \qquad (2.2)$$

Здесь $H_i(\vec{R})$ - гамильтониан ионной системы, а $\psi_n(\vec{r},\vec{R})$ - волновая функция электронной системы при фиксированном положении иона. Форма (2.1), (2.2) - совершенно стандартная.

Если пренебречь недиагональными членами C_{nm} , то (2.1) представляет собой "адиабатическое" уравнение, решение которого дает нам "адиабатический" колебательный спектр. Недиагональные члены описывают взаимодействие этих фононов с электронами.

Вводя вторичное квантование и рассматривая теорию возмущения по недиагональным членам, можно найти вклад в общую энергию системы за счет электрон-фононного взаимодействия ΔE . Тогда для определения перенормировки "адиабатических"фононнов с волновым вектором $\vec{q}$ и номером ветви λ оказывается достаточным проварьировать эту энергию по числам заполнения фононов $N_{\vec{q}\lambda}$, т.е.:

$$\Delta\omega_{\vec{q}\lambda}=\frac{\delta\Delta E}{\delta N_{\vec{q}\lambda}} \qquad (2.3)$$

и аналогично для перенормировки электронов:

$$\Delta E_{\vec{k}}=\frac{\delta\Delta E}{\delta n_{\vec{k}}} \qquad (2.4)$$

В соответствии с результатом, найденным в [20]:

$$\Delta\omega_{\vec{q}\lambda}=\sum_{\vec{k}}|M_{\vec{k}\vec{q}\lambda}|^2\frac{n_{\vec{k}}-n_{\vec{k}+\vec{q}}}{E_{\vec{k}}-E_{\vec{k}+\vec{q}}-\omega_{\vec{q}\lambda}}-\sum_{\vec{k}}|M_{\vec{k}\vec{q}\lambda}|^2\frac{n_{\vec{k}}-n_{\vec{k}+\vec{q}}}{E_{\vec{k}}-E_{\vec{k}+\vec{q}}} \qquad (2.5)$$

где $M_{\vec{k}\vec{q}\lambda}$ - блоховский матричный элемент.

Легко понять смысл полученного выражения. Второй член в нем описывает адиабатический вклад электронов в фононную частоту и сам по себе он порядка самой частоты $\omega_{\vec{q}\lambda}$. Однако собственно неадиабатическая перенормировка оказывается весьма слабой. Для основной части фазового пространства (2.5) дает:

$$\Delta\omega_{\vec{q}\lambda} \sim \omega_{\vec{q}\lambda}\left(\frac{\omega_0}{E_F}\right)^2 \tag{2.6}$$

где ω_0 - характерная частота фононного спектра.

В узкой области импульсов, где $\frac{|q-2K_F|}{K_F} \sim \frac{\omega_0}{E_F}$, малость перенормировки сказывается слабее:

$$\Delta\omega_{\vec{q}\lambda} \sim \omega_{\vec{q}\lambda}\frac{\omega_0}{E_F}$$

Если определить (2.4), то оказывается, что перенормировка электронов за счет электрон-фононного взаимодействия, точнее скорости электронов, оказывается очень существенной для состояний, лежащих вблизи E_F в интервале энергии порядка ω_0, в полном соответствии с результатом Мигдала [22].

Приведенные результаты позволяют четко представить физическую картину. Для электронов в узкой "корочке" вблизи поверхности Ферми адиабатическое приближение несправедливо, поскольку имеет место сильное перемешивание электронных состояний. С другой стороны, электроны, лежащие в основной части фазового объема под поверхностью Ферми, движутся адиабатически за ионами и для них перемешивание состояний отсутствует.

В образовании фононов участвуют все электроны. Поэтому, естественно, возникает параметр малости, характеризующий отношение фазового объема неадиабатически возмущенных электронов к общему фазовому объему электронов, т.е. $\frac{\omega_0}{E_F}$. Результат (2.5) является фактически отражением этого обстоятельства.

Таким образом, найдя фононный спектр в адиабатическом приближении, мы не должны совсем его перенормировать за счет электрон-фононного взаимодействия.

3. ЭЛЕКТРОННАЯ ЭНЕРГИЯ

Итак, для определения фононного спектра нам необходимо найти энергию электронной системы в поле фиксированных ионов, т.е. $E(\vec{R}_1,\ldots,\vec{R}_n)$. Пусть мы знаем эффективный псевдопотенциал $V(\vec{r}-\vec{R}_m)$, описывающий взаимодействие электрона с отдельным ионом. Тогда соответствующий гамильтониан электронной системы в представлении вторичного квантования запишется в виде (везде полный объем системы положен единице);

$$H=\sum_{\vec{K}} E_{\vec{K}} a^{+}_{\vec{K}} a_{\vec{K}} + \frac{1}{2}\sum_{\vec{K},\vec{K}',\vec{q}}{}' \frac{4\pi e^2}{q^2} a^{+}_{\vec{K}-\vec{q}} a^{+}_{\vec{K}'+\vec{q}} a_{\vec{K}'} a_{\vec{K}} + \sum_{\vec{K},\vec{q}}{}' U_{\vec{K}+\vec{q},\vec{K}} a^{+}_{\vec{K}+\vec{q}} a_{\vec{K}}; \qquad E_{\vec{K}} = \frac{K^2}{2m} \tag{3.I}$$

Здесь первые два члена соответствуют гамильтониану электронного газа при учете кулоновского взаимодействия, а последний член описывает электрон-ионное взаимодействие. При этом:

$$U_{\vec{K}+\vec{q},\vec{K}}=\frac{1}{N}\sum_{n} e^{i\vec{q}\vec{R}_n}\,V_{\vec{K}+\vec{q},\vec{K}} \tag{3.2}$$

$$V_{\vec{K}+\vec{q},\vec{K}}=\langle\vec{K}+\vec{q}|V|\vec{K}\rangle \tag{3.3}$$

где N - число элементарных ячеек.

Ограничимся рассмотрением моноатомного металла с произвольным числом атомов ν в элементарной ячейке . Обобщение на общий случай - тривиально. Учтем, что рассматриваемая система в целом электронейтральна.

Легко показать, что в представлении (3.I) это соответствует отсутствию члена с $\vec{q}=0$ во второй сумме и отсутствию кулоновской части при $\vec{q}=0$ в $U_{\vec{K},\vec{K}}$ в третьей сумме.

В случае локального псевдопотенциала матричный элемент электрон-ионного взаимодействия зависит только от разности импульсов

$$V_{\vec{K}+\vec{q},\vec{K}}\rightarrow V_{\vec{q}} \tag{3.3a}$$

Дальнейший анализ мы проведем на языке локального псевдопотенциала.(О роли нелокальности - см. в разд. 6).

Вычисление энергии основного состояния, соответствующего гамильтониану (3.I), будем производить в виде разложения по степеням псевдопотенциала

$$E=E^{(0)}+E^{(1)}+E^{(2)}+\ldots \tag{3.4}$$

Для этого можно воспользоваться обычным анализом, рассматривая в качестве возмущения H' оба последних члена в (3.1) и используя развитую диаграммную технику. При этом задача сводится к суммированию связанных диаграмм (см., например, [23, 24]), причем электрон-ионное взаимодействие играет роль внешнего поля.

Отбирая совокупность диаграмм, содержащих определенное число линий внешнего поля, т.е. определенное число множителей $U_{\vec{q}}$, мы можем, в принципе, определить разложение (3.4). Нулевой член этого ряда описывает энергию взаимодействия электронного газа и для дальнейшего анализа интереса не представляет. Члены линейные по псевдопотенциалу обращаются в нуль, что является следствием электронейтральности системы. (При учете нелокальности псевдопотенциала $E^{(1)}$может оказаться отличным от нуля, поскольку $V_{\vec{K},\vec{K}}\neq 0$. Однако, этот член не будет содержать координат, что сразу видно из (3.2), если принять во внимание возникающее условие $\vec{q}=0$).

Для квадратичных по V членов поправка к энергии в графической форме может быть представлена следующим образом:

$E^{(2)}=$ 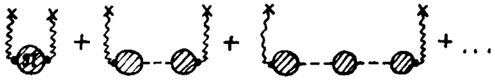 (3.5)

Здесь крестом с волнистой линией обозначено действие внешнего поля (электрон-ионное взаимодействие), пунктиром - линия межэлектронного взаимодействия, а через π обозначен неразрезаемый по линии этого взаимодействия блок (поляризационный оператор).

В результате суммирования (3.5) находим:

$$E^{(2)}=\sum_{\vec{q}_1}\Gamma^{(2)}(\vec{q}_1,-\vec{q}_1)\,|U_{\vec{q}_1}|^2 \tag{3.6}$$

$$\Gamma^{(2)}(\vec{q}_1,-\vec{q}_1)=-\frac{1}{2}\,\frac{\pi(\vec{q}_1)}{\varepsilon(\vec{q}_1)},\qquad \varepsilon(\vec{q}_1)=1+\frac{4\pi e^2}{q_1^2\,\Omega_0}\,\pi(\vec{q}_1) \tag{3.7}$$

Фигурирующее в (3.7) $\varepsilon(\vec{q})$ есть не что иное, как диэлектрическая проницаемость электронного газа.

Выражение для произвольного члена разложения (3.4) можно представить в следующем виде:

$$E^{(n)}=\sum_{\vec{q}_1,\dots,\vec{q}_n}\Gamma^{(n)}(\vec{q}_1,\dots,\vec{q}_n)\,U_{\vec{q}_1}\dots U_{\vec{q}_n}\,\Delta(\vec{q}_1+\dots+\vec{q}_n)$$
$$\Delta(\vec{q})=\begin{cases}1, & \vec{q}=0\\ 0, & \vec{q}\neq 0\end{cases} \tag{3.8}$$

(Закон сохранения импульса в этом выражении является следствием однородности пространства).

Здесь $\Gamma^{(n)}$ определяется совокупностью всех связанных диаграмм, имеющих n "хвостов" внешнего поля. Хотя выражение для $\Gamma^{(n)}$ с $n>2$ не может быть получено в столь простой форме как (3.7), однако можно провести важное частичное суммирование, введя "жирную" вершину внешнего поля с помощью следующего выражения

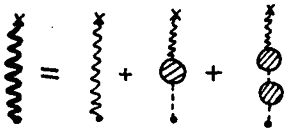

Таким образом в явной форме выделяется экранировка внешнего поля. При этом выражение (3.8) перепишется в виде:

$$E^{(n)}=\sum_{\vec{q}_1,\dots,\vec{q}_n}\Lambda^{(n)}(\vec{q}_1,\dots,\vec{q}_n)\,\frac{U_{\vec{q}_1}}{\varepsilon(\vec{q}_1)}\,\frac{U_{\vec{q}_2}}{\varepsilon(\vec{q}_2)}\cdots\frac{U_{\vec{q}_n}}{\varepsilon(\vec{q}_n)}\,\Delta(\vec{q}_1+\dots+\vec{q}_n)\qquad n>2 \tag{3.9}$$

$\Lambda^{(n)}$ теперь определяется совокупностью диаграмм с n входами, не имеющих частей, которые могли бы быть отнесены к одной из "жирных" вершин внешнего поля.

Отметим, что случай $n=2$ (3.6) оказывается выделенным, так как в этом случае нельзя отделить экранировку одной вершины от другой и "жирной" может быть только одна вершина.

Для $n=3$ приведем диаграмму, которая, нам представляется , дает основной вклад

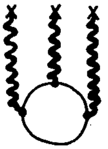

(3.10)

(Сплошной линией здесь обозначены электронные гриновские функции G_0 -см., например, [24]).

После того как ясна общая структура выражения для энергии при произвольном расположении ионов, можно рассмотреть задачу о малых колебаниях и разложить E по степеням смещения ионов $\vec{u}_m$. При этом от смещения зависит только структурный множитель в определении $U_{\vec{q}}$ (3.2).

Нулевой член разложения представляет собой энергию электронного газа в поле периодически расположенных ионов. Линейный член разложения, если воспользоваться тем, что $U^*_{\vec{q}} = U_{-\vec{q}}$, можно представить в виде:

$$E_1^{(n)} = -n \sum_{\substack{\vec{K}_1 \neq 0, \\ \vdots \\ \vec{K}_n \neq 0.}} \sum_{m} (\vec{u}_m \vec{K}_n) \Gamma^{(n)}(\vec{K}_1, \dots, \vec{K}_n) \times \operatorname{Im}\left[U_{\vec{K}_1} \dots U_{\vec{K}_{n-1}} V_{\vec{K}_n} e^{i\vec{K}\vec{R}^0_m} \right] \Delta(\vec{K}_1 + \dots + \vec{K}_n) \qquad (3.11)$$

где $\vec{K}_i$ - вектор обратной решетки (умноженный на 2π). Естественно, что в случае решеток с одним атомом в элементарной ячейке E_1 тождественно обращается в 0. В случае же решеток с большим числом атомов в элементарной ячейке этого уже нельзя утверждать и сила, действующая на отдельный ион со стороны электронной системы $\frac{\partial E_1}{\partial \vec{u}_m}$, вообще говоря, отлична от нуля. Она должна компенсироваться суммарной силой, действующей на данный ион непосредственно со стороны других ионов. Только при достаточной симметрии расположения ионов каждая из этих сил по отдельности обращается в нуль.

Квадратичный член разложения по смещениям E_2 определяет, очевидно, вклад в колебательную матрицу косвенного взаимодействия между ионами через электроны и является для нашего анализа основным.

4. КОСВЕННОЕ ВЗАИМОДЕЙСТВИЕ МЕЖДУ ИОНАМИ В МЕТАЛЛЕ "КОВАЛЕНТНОСТЬ"

Представим E_2 в традиционной форме:

$$E_2 = \frac{1}{2} \sum_{m,m'} A^{\alpha\beta}_{mm'} u^\alpha_m u^\beta_{m'} \qquad (4.1)$$

(В общем случае $m \equiv \{\vec{m}, s\}$, где $\vec{m}$ -номер элементарной ячейки, а s -номер атома в элементарной ячейке).

Тогда, в соответствии с (3.8) и (3.2), для вклада n -го члена в колебательную матрицу имеем:

$$\left(A^{(n)}\right)^{\alpha\beta}_{mm'} = -n(n-1)\sum_{\vec q,\vec q_1}\;\sum'_{\vec K_1,\dots,\vec K_{n-2}} \Gamma^{(n)}(\vec K_1,\dots,\vec K_{n-2},\vec q,\vec q_1)\,U_{\vec K_1}\dots U_{\vec K_{n-2}}$$
$$\times q^\alpha q_1^\beta V_{\vec q} V_{\vec q_1} e^{i\vec q(\vec R^0_m-\vec R^0_{m'})+i\vec q\vec\rho_s+i\vec q_1\vec\rho_{s'}}\Delta(\vec K_1+\dots+\vec K_{n-2}+\vec q+\vec q_1),\; m\neq m' \qquad (4.2)$$

$$\left(A^{(n)}\right)^{\alpha\beta}_{mm} = -\sum_{m'\neq m}\left(A^{(n)}\right)^{\alpha\beta}_{mm'} \qquad (4.3)$$

Выражение (4.2) позволяет четко проанализировать характер влияния электронов на косвенное взаимодействие между ионами, а точнее непосредственно на колебательную матрицу. Первый член в разложении $\hat{A}$ по степеням псевдопотенциала, соответствующий $n=2$, равен просто:

$$\left(A^{(2)}\right)^{\alpha\beta}_{mm'} = -\sum_{\vec q} q^\alpha q^\beta |V_{\vec q}|^2 \frac{\pi(\vec q)}{\varepsilon(\vec q)} e^{i\vec q(\vec R^0_m-\vec R^0_{m'})} \qquad (4.4)$$

В такой форме обычно и представляется электронная часть колебательной матрицы. Соответствующая ей энергия $E^{(2)}$ (3.6) описывает центральное взаимодействие между парами ионов, а сама матрица (4.4) обладает аксиальной симметрией [17] .

Однако помимо (4.4) матрица $\hat{A}$ содержит члены вида (4.2) с $n > 2$. В энергии этим членам соответствует косвенное взаимодействие между n ионами одновременно (n - кратное рассеяние электронов на ионах системы). В колебательной задаче наличие этих членов приводит к появлению непарного взаимодействия между ионами нецентрального типа. Это непосредственно видно из (4.2), поскольку при $n > 2$ члены суммы содержат помимо вектора $\vec R^0_m - \vec R^0_{m'}$ векторы обратной решетки. В результате колебательная матрица $\hat{A}$ теряет аксиальную симметрию,и возникает взаимодействие общего типа, имеющее симметрию кристалла. Таким образом, несмотря на отсутствие перекрытия между ионами, появляется взаимодействие ковалентного типа.

Из вида выражения (4.2) следует, что каждый следующий член разложения содержит по отношению к предыдущему лишний малый множитель вида $U_{\vec K}/E_F$, где $U_{\vec K} = V_{\vec K}\sum_s e^{i\vec K\vec\rho_s}$. В силу этого члены, соответствующие непарному взаимодействию,малы по сравнению с членом (4.4). Однако есть одно обстоятельство, которое может делать учет этих членов существенным. Дело в том, что полная колебательная матрица,помимо $\hat{A}$, будет содержать матрицу $\hat{B}$, соответствующую прямому кулоновскому взаимодействию. Во многих случаях происходит существенная компенсация прямого и косвенного взаимодействия: и, естественно, что мы должны сравнивать вклад членов непарного взаимодействия с вкладом от суммы $\hat{A}^{(2)} + \hat{B}$. В этой связи, очевидно, становится важным учет третьего члена разложения.

Вычисляя диаграмму (3.10) в явном виде и разлагая результаты по степеням смещения, можно непосредственно найти следующее выражение:

$$\left(A^{(3)}\right)^{\alpha\beta}_{mm'}=\frac{1}{N}\sum_{\vec{K}\neq 0,\vec{q}} q^{\alpha}(\vec{q}+\vec{K})^{\beta}\,\frac{V_{\vec{q}}}{\varepsilon(\vec{q})}\,\frac{V_{\vec{q}+\vec{K}}}{\varepsilon(\vec{q}+\vec{K})}\,\frac{U_{\vec{K}}}{\varepsilon(\vec{K})} \tag{4.5}$$

$$\times e^{i\vec{q}(\vec{R}^{o}_{m}-\vec{R}^{o}_{m'})}e^{-i\vec{K}\vec{\rho}_{s'}}\;P_{\vec{q},\vec{q}+\vec{K}}$$

$$P_{\vec{q},\vec{q}+\vec{K}}=\frac{1}{N}\sum_{\vec{\varkappa}} n_{\vec{\varkappa}}\left\{\frac{1}{(E_{\vec{\varkappa}}-E_{\vec{\varkappa}+\vec{q}})(E_{\vec{\varkappa}}-E_{\vec{\varkappa}-\vec{K}})}+\frac{}{(E_{\vec{\varkappa}}-E_{\vec{\varkappa}+\vec{q}+\vec{K}})(E_{\vec{\varkappa}}-E_{\vec{\varkappa}+\vec{K}})}+\frac{1}{(E_{\vec{\varkappa}}-E_{\vec{x}+\vec{q}})(E_{\vec{\varkappa}}-E_{\vec{\varkappa}+\vec{q}+\vec{K}})}\right\} \tag{4.6}$$

(4.4) и (4.5) в существенной степени решают задачу учета влияния электронов на колебательную матрицу.

Как известно, наличие резкой границы фермиевского спектра приводит к неаналитичности поляризационного оператора $\mathcal{П}(\vec{q})$ при $q=2K_F$, что влечет за собой появление особенности Кона [25] в фононном спектре металла, а с другой стороны, к наличию неэкспоненциальных осциллирующих членов в асимптотическом поведении парного взаимодействия вида:

$$\left(A^{(2)}\right)^{\alpha\beta}_{mm'}\sim\left.\frac{\cos q\,|\vec{R}^{o}_{m}-\vec{R}^{o}_{m'}|}{|\vec{R}^{o}_{m}-\vec{R}^{o}_{m'}|^{3}}\right|_{q=2K_F} \tag{4.7}$$

Из вида (4.5) можно непосредственно заключить, что асимптотическое поведение непарных членов матрицы $\hat{A}$, если принять аналитичность функции $V_{\vec{q}}$, характеризуется появлением набора осциллирующих "хвостов" вида (4.7), но с отличающимися периодами. Эти периоды характеризуются значениями $\vec{q}$, получающимися из соотношения:

$$|\vec{q}+\vec{K}|=2K_F$$

Это должно приводить во многих случаях, особенно в поливалентных металлах, к заметной взаимной компенсации этих "хвостов". С другой стороны как показывает анализ парных сил (см., например, [26]), взаимодействие с ближайшими координационными сферами, хотя и носит осциллирующий характер, но определяется целиком характером поведения подынтегральной функции в (4.4). В связи с этим, с ростом $|\vec{R}^{o}_{m}-\vec{R}^{o}_{m'}|$ в (4.5) существенной становится область ограниченных q. При этом возникает тенденция к появлению вместо $V_{\vec{K}}/E_F$, квадрата этого малого параметра.

Все сказанное позволяет полагать, что непарная часть взаимодействия будет проявляться в колебательной задаче в первую очередь как относительно короткодействующее взаимодействие. В этом смысле непарное взаимодействие приобретает традиционные черты ковалентности.

Таким образом, в металле даже при полном отсутствии перекрытия ионных остовов будет существовать взаимодействие между ионами ковалентного типа. Оно будет тем сильнее выражено, чем большую роль играют процессы переброса в динамической матрице, отвечающей парному взаимодействию между ионами через электроны, т.е. чем больше значения $V_{\vec{K}}$. В металлах типа Na, где процессы переброса проявляются слабо, вполне адэкватное описание можно получить в рамках учета только парного взаимодействия (4.2). И, действительно, во всех работах (см. [13], [15] , [16]), а также недавнюю работу [27]) наблюдается сравнительно хорошее согласие между теорией и экспериментом. Однако в металлах, где процессы переброса играют заметную роль, описание, использующее только парное взаимодействие (4.4), становится сугубо недостаточным. С какими трудностями при этом сталкиваются, можно наглядно проследить на примере исследования фононного спектра свинца, проведенного в работе Воско и др. [16] , или же на примере более сложных металлов, как олово [19], [20] , или группы гексагональных металлов [28] .

Заметим в заключение этого раздела, что при рассмотрении ангармонического взаимодействия учет $E^{(3)}$ наряду с $E^{(2)}$ очень существенен, поскольку в 3-м порядке по смещению $E^{(3)}$ уже не содержит обязательно малого множителя $V_{\vec{K}}/E_F$.

5. ДИНАМИЧЕСКАЯ МАТРИЦА. ЗВУК. ПРЕДЕЛЬНЫЕ ОПТИЧЕСКИЕ ЧАСТОТЫ

Зная колебательную матрицу (4.4), (4.5), не представляет труда найти динамическую матрицу $\hat{\mathcal{D}}$ ($\vec{q}$), диагонализация которой определяет фононный спектр. Объединим прямое кулоновское взаимодействие между ионами и парное косвенное взаимодействие (4.4) в отдельную матрицу $\mathcal{D}_1(\vec{q})$. Тогда:

$$\hat{\mathcal{D}}(\vec{q})=\hat{\mathcal{D}}_1(\vec{q})+\hat{\mathcal{D}}_2(\vec{q}) \tag{5.1}$$

где:

$$\mathcal{D}^{\alpha\beta}_{1ss'}(\vec{q})=\frac{\omega_0^2}{\nu}\Big\{\sum_{\vec{K}}\Big[\frac{(\vec{q}+\vec{K})^{\alpha}(\vec{q}+\vec{K})^{\beta}}{|\vec{q}+\vec{K}|^2}\big(1-\psi(\vec{q}+\vec{K})\big)e^{i\vec{K}(\vec{\rho}_s-\vec{\rho}_{s'})}\Big] \tag{5.2}$$

$$-\delta_{ss'}\sum_{\vec{K}\neq 0}\sum_{s''}\big[\vec{q}=0,\, s'\to s''\big]\Big\}$$

$$\psi(\vec{q})=\frac{|V_{\vec{q}}|^2\,\Pi(\vec{q})\,q^2}{\varepsilon(\vec{q})}\;\frac{\Omega_0}{4\pi Z^2e^2},\quad \omega_0^2=\frac{4\pi Z^2e^2}{M\Omega_0}\nu \tag{5.3}$$

(ν -число атомов в элементарной ячейке Ω_0).

Первый член в круглых скобках (5.2) возник от прямого взаимодействия ионов, а $\psi(\vec{q})$ – от косвенного.

Матрица $\hat{\mathcal{D}}_2(\vec{q})$ учитывает непарное взаимодействие. При ограничении третьим членом разложения (4.5), она имеет вид:

$$\mathcal{D}_{2\,ss'}^{\alpha\beta}(\vec{q})=\frac{1}{M}\Big\{\sum_{\vec{K}_1\neq\vec{K}}\Big[(\vec{q}+\vec{K})^{\alpha}(\vec{q}+\vec{K}_1)^{\beta}\frac{V_{\vec{q}+\vec{K}}}{\varepsilon(\vec{q}+\vec{K})} \tag{5.4}$$

$$\times\frac{V_{\vec{q}+\vec{K}_1}}{\varepsilon(\vec{q}+\vec{K}_1)}\,\frac{U_{\vec{K}-\vec{K}_1}}{\varepsilon(\vec{K}-\vec{K}_1)}\,P_{\vec{q}+\vec{K},\,\vec{q}+\vec{K}_1}\,e^{i\vec{K}\vec{\rho}_s-i\vec{K}_1\vec{\rho}_{s'}}-\delta_{ss'}{\sum_{\vec{K}_1\neq\vec{K}}}'\sum_{s''}\big[\vec{q}=0,\,s'\to s''\big]\Big\}$$

(Штрих у суммы означает отсутствие членов с $\vec{K}, \vec{K}_1 = 0$).

Рассмотрим поведение динамической матрицы при малых $\vec{q}$. Для простоты ограничимся сначала случаем одного атома в элементарной ячейке.

На достаточно больших расстояниях электрон-ионное взаимодействие носит чисто кулоновский характер. В силу этого, принимая во внимание, что $V_{\vec{q}}$ есть четная функция $\vec{q}$, при $\vec{q} \to 0$ имеем:

$$V_{\vec{q}} = -\frac{4\pi z e^2}{q^2 \Omega_0} + b \qquad (5.5)$$

Если воспользоваться выражением для диэлектрической проницаемости (3.7), то легко установить, что $\Psi(\vec{q} \to 0) \to 1$ и $\hat{\mathcal{D}}_1(\vec{q})$ имеет следующий вид:

$$\mathcal{D}_1^{\alpha\beta}(\vec{q}) = \frac{q^\alpha q^\beta}{M}\left[\frac{z^2}{\Pi(\vec{q}=0)} + 2bz\right] + \frac{1}{M\Omega_0}\sum_{\vec{K}\neq 0}\Big[q^\alpha q^\beta \varphi(\vec{K}) + q^\alpha q^\gamma K^\beta \left(\frac{\partial \varphi(\vec{f})}{\partial f^\gamma}\right)_{\vec{f}=\vec{K}} + \frac{1}{2} K^\alpha K^\beta q^\gamma q^\delta \left(\frac{\partial^2 \varphi(\vec{f})}{\partial f^\gamma \partial f^\delta}\right)_{\vec{f}=\vec{K}}\Big] \qquad (5.6)$$

где
$$\varphi(\vec{f}) = \frac{4\pi z^2 e^2}{f^2}\left[1 - \Psi(\vec{f})\right]$$

Аналогично может быть непосредственно из (5.4) получено выражение и для $\mathcal{D}_2^{\alpha\beta}(\vec{q} \to 0)$, которое мы не приводим из-за громоздкости.

Если пренебречь вкладом процессов переброса, то мы приходим к хорошо известному результату Бардина-Пайнса [29] для продольного звука. Последний результат получается, если для $\Pi(\vec{q})$ в (5.6) воспользоваться значением, которое находится в рамках метода случайных фаз (см., например, [30]):

$$\Pi^0(\vec{q}) = -\frac{1}{N}\sum_{\vec{K}} \frac{n_{\vec{K}+\vec{q}} - n_{\vec{K}}}{E_{\vec{K}+\vec{q}} - E_{\vec{K}}} \qquad (5.7)$$

Если положить $b = 0$ и принять во внимание, что $\Pi^0(\vec{q}=0) = \frac{3}{2}\frac{Z}{E_F}$, то, используя (5.7), приходим для скорости продольного звука к результату Бома-Стайвера [31] .

Если процессами переброса пренебречь нельзя, то продольный звук может заметно измениться. При этом существенно, что, как непосредственно следует из (5.4), непарное взаимодействие будет приводить к поправкам того же порядка, что и при учете членов с $\vec{K} \neq 0$ в парном взаимодействии. (Заметим, что $\left(V_{\vec{q}}/\varepsilon(\vec{q})\right)_{\vec{q}\to 0} \to \frac{Z}{\Pi(\vec{q}=0)}$. Поскольку поперечный звук целиком обусловлен процессами переброса, то роль вклада (5.4) в электронную часть звука может стать еще более существенной. В простых металлах типа Na поперечный звук в значительной степени определяется просто ионной решеткой. При этом оказывается малой суммарная роль электронов. Однако в общем случае роль электронов велика и тогда надо одновременно учитывать вклад как от парного, так и непарного взаимодействий.

Так, в ионной решетке олова [20] и цинка (см. раздел 7) поперечный звук по некоторым направлениям вообще оказался неустойчивым. Отсюда сразу ясно, какую существенную роль должен играть именно электронный вклад и как раз целиком за счет членов с $\vec K \neq 0$.

Отметим одно существенное обстоятельство. Из (5.6) следует, что поведение $\hat{\mathcal{D}}_1(\vec q)$ при малых $\vec q$ (и аналогично $\hat{\mathcal{D}}_2(\vec q)$) зависит от первой и второй производной псевдопотенциала в точках $\vec q = \vec K$. В связи с ограниченной точностью, с которой обычно известно поведение $V_{\vec q}$ при больших $\vec q$, могут возникать заметные ошибки в определении скоростей звука или модулей упругости, особенно соответствующих поперечным ветвям, если члены с $\vec K \neq 0$ играют существенную роль. Поэтому, в частности, очень трудно в случае сложных металлов использовать модули упругости для решения обратных задач.

Наличие вклада непарного взаимодействия в звук и вообще в динамическую матрицу при малых $\vec q$ само по себе уже снимает проблему, связанную с несоблюдением условия Коши в металлах. Поэтому в настоящем докладе мы не будем вообще дискутировать эту проблему (соответствующее обсуждение в случае парного взаимодействия см. в [17]).

Отметим еще одно важное обстоятельство. Известно, что правильно построенная динамическая матрица должна удовлетворять условию отсутствия анизотропных напряжений - т.е. условию Борна-Хуанга (см. [21]). Существенно, однако, что это условие не выполняется автоматически для матрицы $\hat{\mathcal{D}}_1(\vec q)$ (5.2). Это связано с тем, что при парном взаимодействии вторые производные от взаимодействия обладают не центральной симметрией, а только аксиальной. Но в достаточно несимметричном кристалле это в общем случае приводит к нарушению условий Борна-Хуанга для $\hat{\mathcal{D}}_1(\vec q)$. Отсюда следует важное заключение, что условию Борна-Хуанга должна подчиняться только динамическая матрица в целом, т.е. $\hat{\mathcal{D}}(\vec q)$ (5.1).

Рассмотрим теперь решетку с двумя одинаковыми атомами в элементарной ячейке. Пусть симметрия кристалла достаточно высока, чтобы матрица $\mathcal{D}^{\alpha\beta}_{ss'}(\vec q = 0)$ являлась диагональной по декартовым индексам. Тогда возникает распад на три независимых оптических колебания с поляризацией вдоль избранных осей. Используя выражение (5.2), можно найти следующее представление для предельных частот:

$$\omega_\alpha^2(\vec q=0) = -\sum_{\vec K\neq 0}\left(\frac{K^\alpha}{K}\right)^2\left(1-\psi(\vec K)\right)\cos(\vec K\vec\rho) + \omega_{2\alpha}^2 \qquad \alpha = x,y,z \tag{5.8}$$

где второй член связан с учетом матрицы $\hat{\mathcal{D}}_2$, а $\vec\rho$ есть расстояние между атомами в элементарной ячейке.

Отметим, что предельные оптические частоты зависят только от значения псевдопотенциала в узлах обратной решетки, но не от его производных. Это, естественно, делает эти частоты очень удобными для использования в обратной задаче.

Из вида (5.8) следует, что в продольную и поперечные частоты вносит вклад разная совокупность узлов обратной решетки.

Если наиболее близкие узлы обратной решетки, где псевдопотенциал относительно велик, вносят вклад только в один тип колебания, то возникает резко отличное электронное экранирование для продольных и поперечных частот.

Это обстоятельство очень ярко проявляется в анизотропных металлах.

6. ПСЕВДОПОТЕНЦИАЛ. ПРЯМАЯ И ОБРАТНАЯ ЗАДАЧИ ПРИ ОПИСАНИИ ФОНОННОГО СПЕКТРА МЕТАЛЛОВ

В соответствии с полученными в предыдущих разделах результатами, фононный спектр металлов может быть найден, если известен псевдопотенциал, описывающий эффективное взаимодействие электрона с отдельным ионом $\hat{V}$ и статическая диэлектрическая проницаемость электронного газа $\varepsilon(\vec{q})$

Определение $\hat{V}$ с той или иной точностью может быть проведено в рамках двух различных направлений. Первое из них предполагает прямое вычисление псевдопотенциала из первых принципов, опирающееся на те или иные предположения (см. подробнее, например, [12]). Второе направление предполагает для нахождения псевдопотенциала использование хотя бы частичной экспериментальной информации. Надо сразу сказать, что результаты последних лет по анализу различных свойств металлов отдают предпочтение последнему направлению, ибо точность вычисления из первых принципов оказывается пока весьма ограниченной. В этом смысле весьма примечателен результат, найденный Воско и др. [16] . Оказалось, что даже в случае Na самосогласованняя процедура для нахождения потенциала голого иона ведет к потенциалу, существенно отличающемуся от эффективного одноэлектронного потенциала Прокофьева, который был специально подобран для описания спектроскопических данных. При этом фононный спектр Na хорошо описывается именно при использовании результатов, опирающихся на эмпирический потенциал Прокофьева.

Наиболее прямое определение псевдопотенциала могло бы быть получено при измерении амплитуды рассеяния $f(\vec{k},\vec{k}')$ электронов на отдельном ионе в интересующем нас в металле интервале энергий. В принципе, такие измерения могли бы дать сравнительно исчерпывающую информацию о псевдопотенциале. Другой метод может состоять в использовании частичной экспериментальной информации, которую, например, дают спектроскопические исследования ионов. Именно эта идея была использована в методе Хейне и Абаренкова [32, 33] (см. также работу Анималу, Хейне [34]). Суть этого метода состоит в следующем. Вне иона, начиная с некоторого радиуса R_M, электрон-ионный потенциал принимается равным $-\frac{ze^2}{r}$. Внутри этого радиуса потенциал заменяется ямой, причём для каждой порциальной волны с орбитальным моментом ℓ глубина ямы - A_ℓ различна. Значение A_ℓ находится из соответствующих спектроскопических данных. Таким образом, находится модельный псевдопотенциал, который, с одной стороны, автоматически учитывает эффективное сокращение потенциала внутри ионного остова, а с другой - дает сглаженное описание интересующих нас величин. По-видимому, модельный псевдопотенциал, получающийся в рамках метода Хейне-Абаренкова, дает сейчас сравнительно наиболее надежное описание взаимодействия отдельного электрона с ионом, хотя, конечно, в рамках определенной точности. (Параметры модельного псевдопотенциала известны сейчас для большинства непереходных элементов [34]).

Из других экспериментальных величин, которые могут быть использованы для уточнения псевдопотенциала, следует выделить измерение энергетической щели, которая возникает в электронном спектре на границе зоны Бриллюэна. Это тем более важно, что эта щель равна просто удвоенной фурье-компоненте псевдопотенциала в соответствующем узле обратной решетки, что позволяет верифицировать значения псевдопотенциала в некоторых точках при заметных импульсах, где определение фурье-компоненты наименее надежно.

Псевдопотенциал, который получается в рамках метода Хейне-Абаренкова или какого-либо другого метода носит нелокальный характер. Однако как показывает непосредственный анализ, появляющаяся в результате нелокальности зависимость матричного элемента (3.3) от $\vec{K}$ оказывается весьма слабой. Поэтому во многих случаях нелокальный псевдопотенциал может быть заменен эффективным (усредненным) локальным. Это приближение, по-видимому, во всяком случае можно использовать для вычисления $\hat{A}^{(3)}$ (4.5) и соответственно $\hat{\mathcal{D}}_2(\vec{q})$ (5.4). Что же касается $\hat{A}^{(2)}$ и $\hat{\mathcal{D}}_1(\vec{q})$ (5.2), то , в принципе, можно воспользоваться непосредственным вычислением $\Psi(\vec{q})$, которое с определенной точностью проводится для нелокального псевдопотенциала (см., например, [35]). При этом эффективный локальный псевдопотенциал может быть получен, например, из соотношения (5.3) по известному $\Psi(\vec{q})$.

Таким образом, опираясь каждый раз на сегодняшний уровень знания эффективного псевдопотенциала электрон-ионного взаимодействия, мы можем, используя (5.2) и (5.4), провести прямое определение фононного спектра металла. Такая задача решается в настоящее время. Следует также заметить, что среди величин, значение которых будет несколько меняться по мере углубления знаний находится и статическая диэлектрическая проницаемость $\varepsilon(\vec{q})$ (3.7).

Как известно, при определении поляризационного оператора в приближении (5.7), соответствующему приближению хаотических фаз, не содержится последовательный учёт обменного взаимодействия.

Приближенное решение этой проблемы было дано Хаббардом [36] . Он показал, что при учёте обмена поляризационный оператор будет иметь вид:

$$\mathcal{T}(\vec{q}) = \frac{\mathcal{T}^{o}(\vec{q})}{1 - f(\vec{q})\,\frac{4\pi e^2}{q^2}\,\mathcal{T}^{o}(\vec{q})} \qquad (6.1)$$

По-видимому, наиболее последовательное выражение для $f(\vec{q})$ может быть представлено в форме:

$$f(\vec{q}) = \frac{1}{2}\,\frac{q^2}{q^2 + \lambda K_F^2} \qquad (6.2)$$

где λ может быть определено из условия, чтобы (6.1) давало бы правильное значение сжимаемости для взаимодействующего электронного газа [37].

Многие авторы используют для $f(\vec{q})$ близкое выражение, предложенное Хаббардом:

$$f(\vec{q}) = \frac{1}{2}\,\frac{1}{q^2 + K_F^2 + K_{TF}^2} \qquad (6.3)$$

где K_{TF} - экранирующий фактор в приближении Томаса-Ферми.

Ограниченная точность в определении псевдопотенциала делает разумным анализ фононного спектра металлов в рамках обратной задачи. При этом можно мыслить три типа обратных задач.

1. Из сравнения вычисленных на основе (5.1), (5.2) и (5.4) и измеренных дисперсионных кривых ищется значение эффективного локального псевдопотенциала $V_{\vec{q}}$. При этом для простоты $V_{\vec{q}}$ может быть выбрано в некотором параметрическом виде и тогда определению подлежат соответствующие параметры. Здесь особенно существенно определение поведения $V_{\vec{q}}$ при $q \gtrsim 2K_F$. Наличие члена 3-го порядка по псевдопотенциалу в динамической матрице, по-видимому, резко сужает полосу возможных значений $V_{\vec{q}}$. Следует отметить, что анализ фононного спектра позволяет определить псевдопотенциал в той области по $\vec{q}$, которая совершенно не верифицируется по измерениям электронных свойств металла.

Если процессы переброса играют очень слабую роль и можно пренебречь как $\hat{\mathcal{D}}_2(\vec{q})$, так и членами с $\vec{K} \neq 0$ в (5.2), то появляется возможность прямого определения функции $\Psi(\vec{q})$, а следовательно, и эффективного $V_{\vec{q}}$ по результатам измерения закона дисперсии для симметричного направления. Эта мысль впервые была высказана Кокраном [18], [17].

2. Матрица $\hat{\mathcal{D}}_1(\vec{q})$ определяется на основе существующих представлений о $V_{\vec{q}}$ или прямо $\Psi(\vec{q})$ для соответствующего металла. Что же касается $\hat{\mathcal{D}}_2(\vec{q})$, то, учитывая относительно короткодействующий характер непарного взаимодействия, можно предположить, что это взаимодействие сконцентрировано главным образом на самых ближайших координационных сферах. Тогда $\hat{\mathcal{D}}_2(\vec{q})$ строится обычным для схемы Борна-

Кармана методом, а малое число независимых силовых констант определяется из сравнения с экспериментом.

3. При определении $\hat{\mathcal{D}}_1(\vec{q})$ выбирается модельный псевдопотенциал со свободными параметрами. $\hat{\mathcal{D}}_2(\vec{q})$ определяется так же как в предыдущем случае. После этого решается обратная задача, в результате чего находятся не только параметры, описывающие короткодействие, но и значения эффективного псевдопотенциала.

При анализе фононного спектра сложных металлов мы рассматривали второй и третий тип обратной задачи [19], [20], [28]. При этом в качестве модельного псевдопотенциала принимался простой потенциал вида:

$$V(r)=\begin{cases} V_0\,, & r_0>r \\ -\dfrac{ze^2}{r}\,, & r_0<r \end{cases} \qquad (6.4)$$

который представляется весьма естественным для всей концепции псевдопотенциала (параметры r_0 и V_0 являются свободными).

7. РОЛЬ ЭЛЕКТРОНОВ В ОБРАЗОВАНИИ ФОНОННОГО СПЕКТРА КОНКРЕТНЫХ МЕТАЛЛОВ

Проанализируем теперь в свете изложенного в предыдущих разделах фононный спектр конкретных непереходных металлов.

Фононный спектр простых металлов

На рис. I приведена функция $\Psi(\vec{q})$ (5.3) для четырех непереходных металлов кубической симметрии, для которых измерен фононный спектр: Na, K, Al, Pb, построенная на основе вычислений, проведенных Анималу [35], в рамках метода Хейне-Абаренкова. На горизонтальных осях отложено положение узлов обратной решетки и указано число эквивалентных узлов.

В случае Na и K ближайший узел обратной решетки лежит далеко правее точки q_0, где псевдопотенциал пересекает ось абсцисс, а следующий узел попадает уже в область, где функция $\Psi(\vec{q})$ практически равна нулю. В силу этого процессы переброса играют в металлах типа Na очень слабую роль. Естественно, что при этом непарное взаимодействие, содержащее параметр малости $V_{\vec{k}}/\varepsilon_F$, очень мало, и для определения фононного спектра достаточно воспользоваться только матрицей $\hat{\mathcal{D}}_1(\vec{q})$ (5.2). Поэтому вычисления, в которых вообще пренебрегалось короткодействующим взаимодействием, давали хорошее описание спектра. Это можно наглядно видеть на рис. 2 и 3, заимствованных из работы [27], где приведены дисперсионные кривые для Na и K, полученные при использовании функции $\Psi(\vec{q})$ рис. I, а также более ранние расчёты Воско и др. [16] (Na, зачернен-

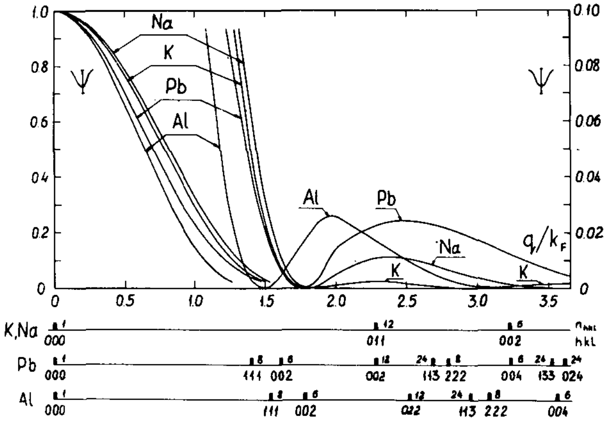

Рис. 1.

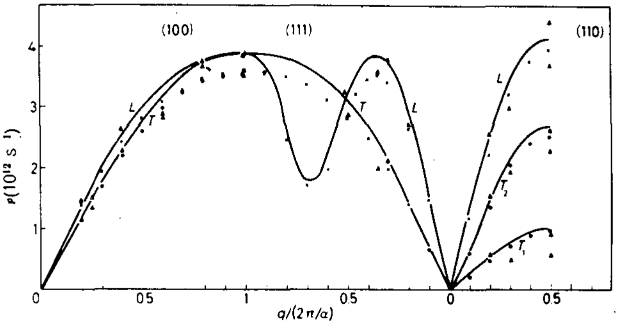

Рис. 2.

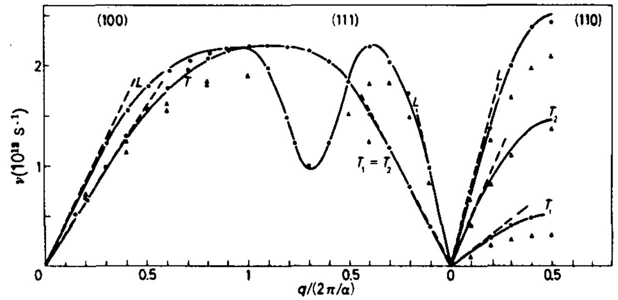

Рис. 3.

ные треугольники), Шама [15] (Na , простые треугольники) и Тойи [13] (K , простые треугольники). Одновременно точками нанесены экспериментальные результаты, полученные для Na в работе Вудса и др. [38] , а для K в работе Коулея [39] . (В работах [15] и [13] вводилось короткодействующее взаимодействие типа Борна-Майера).

Когда мы переходим к поливалентным гранецентрированным металлам Al и Pb , картина существенно меняется. Теперь появляются узлы обратной решетки, которые лежат при гораздо меньших значениях q/K_F (узлы [111] и [002]), кроме того, более интенсивны "хвосты" функции $\psi(\vec{q})$. Однако легко проследить, что поведение Al и Pb должно существенно отличаться друг от друга. Действительно, узлы [111] и [002] в Al попадают как раз в область q в непосредственной близости от q_0 и поэтому отношение $V_{\vec{K}}/E_F$ в этих точках мало. Наоборот в Pb оба эти узла лежат левее q_0, причем роль узла [111] весьма значительна. Кроме того, "хвост" функции $\psi(\vec{q})$ в случае Pb затянут гораздо сильнее, чем в Al. В соответствии с этим, можно утверждать, что в Al и Pb должно существовать взаимодействие ковалентного типа, но в Al оно будет представлено относительно слабо, а в Pb весьма сильно. В последнем случае это усугубляется тем, что в свинце имеет место сильнейшее взаимное сокращение вклада от ионной решетки и от электронов в парной части взаимодействия, на которое впервые было обращено внимание в работе [16]. Для того чтобы это проиллюстрировать, в таблице II приведены значения квадрата продольной частоты на границе зоны при $\vec{q}\uparrow\uparrow$ [001], отдельно для вклада от ионов ω_i^2/ω_0^2 и от электронов ω_e^2/ω_0^2. (Последняя величина считалась с функцией $\psi(\vec{q})$, приведенной на рис. 1).

Таблица II

	ω_i^2/ω_0^2	ω_e^2/ω_0^2
Na	0,3333	0,07
K	0,3333	-0,03
Al	0,678	-0,558
Pb	0,678	-0,636

Видно, что уже в случае Al имеет место сильная компенсация, но в случае Pb она становится "катастрофической". Поэтому, с одной стороны, в Pb должно быть заметное ковалентное взаимодействие, а с другой - сильная чувствительность окончательного спектра к виду эффективного потенциала электрон-ионного взаимодействия. Оба эти обстоятельства привели к тому, что единственная попытка теоретического объяснения спектра [16] на основе использования только парного взаимодействия оказалась не очень удачной. Соответствующие кривые, заимствованные из работы [16], приведены на рис. 4. Сплошными кривыми на этом рисунке нанесены результаты расчёта с подогнанным эффективным электрон-ионным взаимодействием, а пунктиром - результаты расчёта с использованием потенциала Бардина, но с подогнанным параметром. Экспериментальные точки взяты из работы [1].

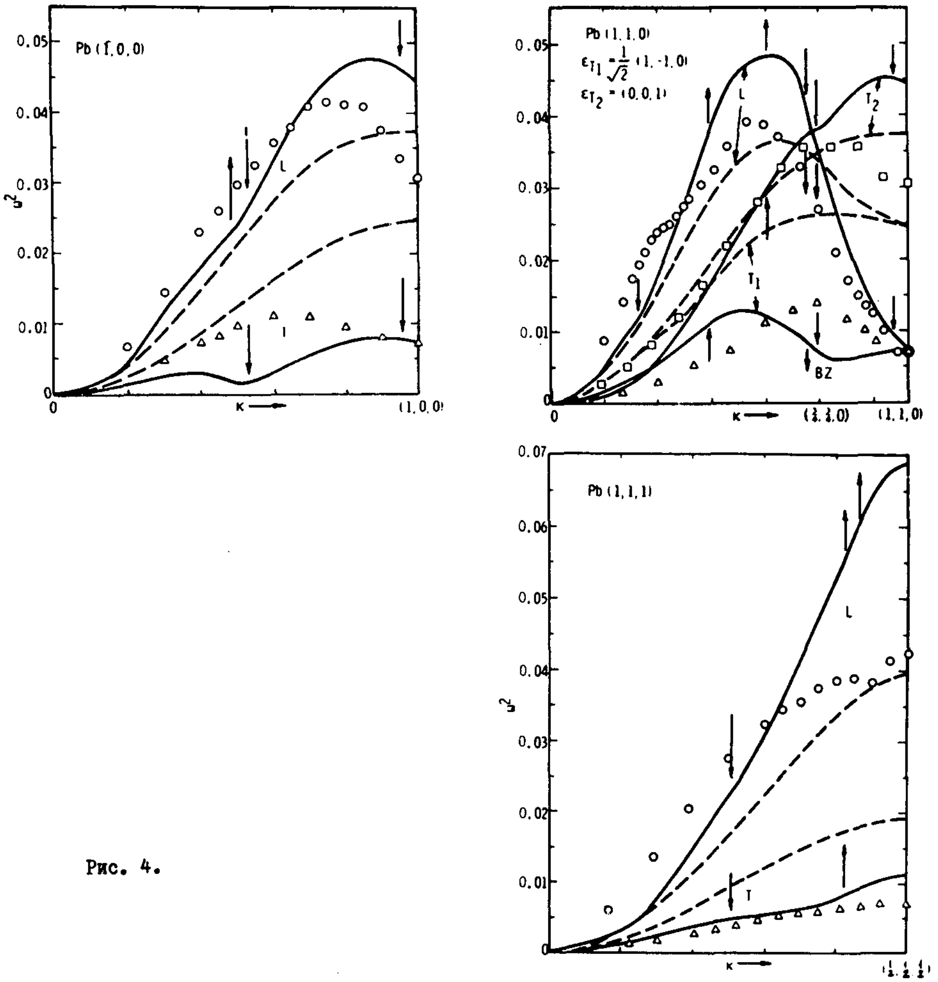

Рис. 4.

Что касается *Al* , то для него расчёты с учётом только парного взаимодействия между ионами через электроны [16] демонстрируют сравнительно хорошее согласие с экспериментом.

Фононный спектр белого олова

Анализ фононного спектра олова представляется весьма поучительным, поскольку речь идет о металле с двумя атомами в элементарной ячейке и сильно выраженной анизотропией решетки. Заметим, что олово было первым сложным металлом, для которого была проанализирована в явной форме роль электронов в образовании фононного спектра [19] , [20] .

Аномалии в таком металле начинаются уже на уровне ионной решетки. На рис. 5 построен колебательный спектр ионной решетки олова при наличии компенсирующего однородного электронного

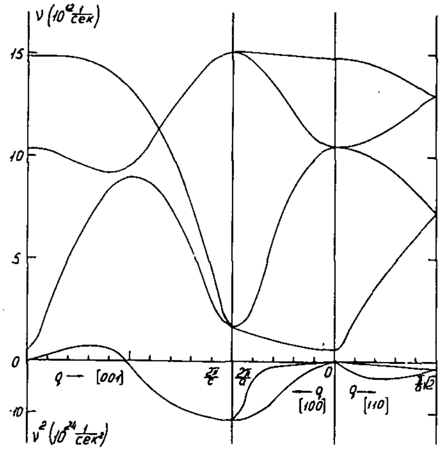

Рис. 5.

фона. Для нахождения спектра использовался метод, аналогичный хорошо известному методу Эвальда [21]. Первое, что бросается в глаза - это неустойчивость решетки - фононные частоты в целой области фазового пространства становятся мнимыми. Такое поведение является прямым следствием структуры олова. Частота продольных акустических колебаний (два иона колеблются в фазе) при $\vec{q} \to 0$, естественно, стремится к значению, соответствующему плазменной частоте.

При учёте косвенного взаимодействия через электроны использовался модельный двухпараметрический потенциал, а непарное взаимодействие учитывалось как взаимодействие с ближайшей координационной сферой. Это взаимодействие описывается тремя независимыми константами, так что суммарное число независимых параметров было пять. Эти параметры находились из сравнения с 5-ю экспериментальными величинами (три модуля упругости и две предельные оптические частоты).

На рис. 6 приведен найденный модельный псевдопотенциал. Для сравнения на том же рисунке отложен псевдопотенциал (пунктирная линия), вычисленный Анималу и Хейне [34, 12]. Согласие между обоими результатами весьма хорошее.

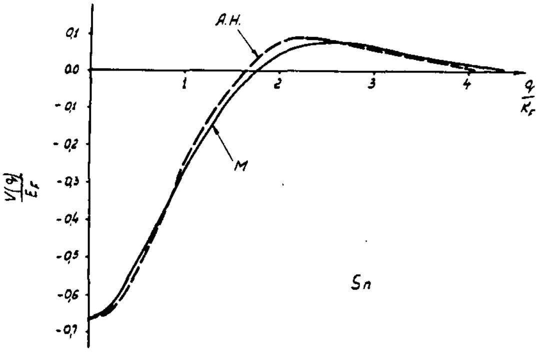

Рис. 6.

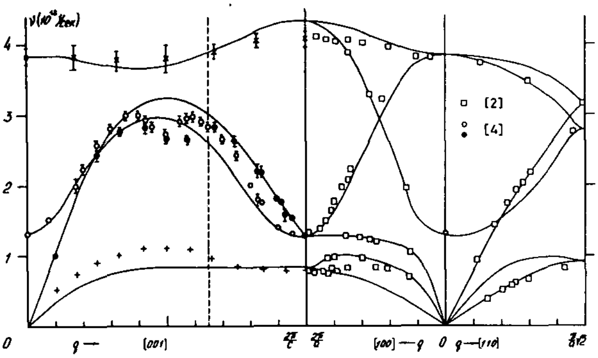

Рис. 7.

На рис. 7 показан окончательный вид фононного спектра, найденного на основе диагонализации суммарной матрицы (5.1), и нанесены экспериментальные точки, взятые из работ [2], [4]. (Рисунок заимствован из работы [20], поэтому на нем не нанесены точки, полученные в более поздних работах [8, 40]. Имеет место вполне хорошее согласие между теорией и экспериментом для всего спектра в целом, особенно если учесть нетривиальный характер поведения оптических и акустических ветвей спектра и малое количество свободных параметров.

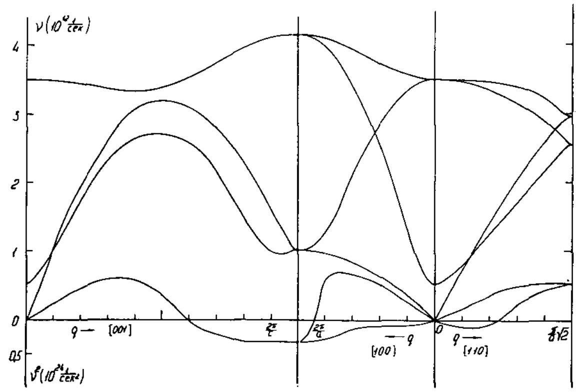

Рис. 8.

На рис. 8 приведен фононный спектр, получающийся при полном пренебрежении непарным короткодействующим взаимодействием, т.е. при $\hat{\mathcal{D}}_2 = 0$.

Прежде всего отметим большую количественную роль, которую играет взаимодействие через электроны. По сравнению с ионной решеткой весь спектр сжимается примерно в 3 раза. Получающиеся дисперсионные кривые демонстрируют многие черты окончательного спектра, особенно это касается оптических ветвей. Вместе с тем фононный спектр остается неустойчивым, а частоты в целых областях количественно сильно отличаются от своих истинных значений. Таким образом, мы сталкиваемся с ситуацией, когда в сильно анизотропном кристалле устойчивость обеспечивается только при

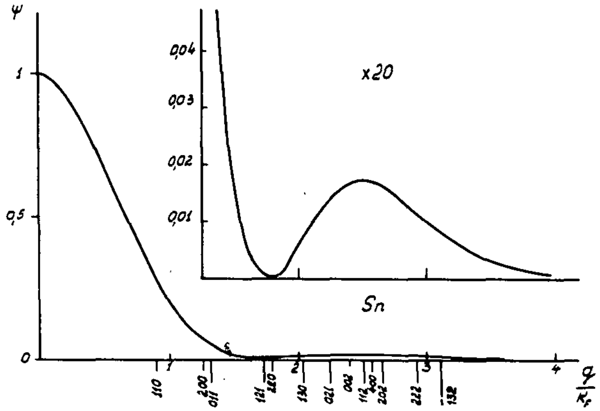

Рис. 9.

явном учёте короткодействующего взаимодействия ковалентного типа.

На рис. 9 приведена функция $\Psi(\vec{q})$ (5.3), соответствующая найденному псевдопотенциалу. Видно, что в случае олова целый ряд узлов обратной решетки лежит левее точки q_0, в которой псевдопотенциал обращается в нуль. Кроме того, большое число узлов расположено в области "хвоста", где Ψ еще имеет конечное значение. Все это предопределяет большую роль процессов переброса. Для того чтобы наглядно показать, сколь существенен вклад членов с $\vec{K} \neq 0$, мы на рис. 10 привели кривые, которые характеризуют вклад соответствующих членов в матрицу $\mathcal{D}_{1ss}^{zz}(\vec{q})$. Дело в том, что, рассматривая продольные колебания при $\vec{q}$ вдоль оси C, мы имеем просто:

$$\omega^2(\vec{q}) = \mathcal{D}_{11}^{zz}(\vec{q}) \pm \mathcal{D}_{12}^{zz}(\vec{q})$$

Основной вклад членов с $\vec{K} \neq 0$ в этом выражении связан с матрицей $\mathcal{D}_{11}^{zz}$, электронная часть которой имеет вид:

$$\mathcal{D}_{11}^{zz}(\vec{q}) = \omega_0^2 \frac{1}{2}\Big[\sum_{\vec{K}} \frac{(q^2-K^2)^2}{|\vec{q}-\vec{K}|^2}\psi(\vec{q}-\vec{K}) - \sum_{\vec{K}\neq 0}(1+\cos\vec{K}\vec{\rho}) \times \frac{K_z^2}{K^2}\psi(\vec{K})\Big] \equiv \omega_0^2 \sum_{\vec{K}} A_{\vec{K}}(\vec{q})$$

На рис. 10 как раз приведены величины $A_{\vec{K}}$. Видно, что члены с $\vec{K} \neq 0$ играют весьма значительную роль, определяя даже общий ход дисперсионных кривых.

Заметная роль процессов переброса должна приводить к существенной ковалентности, что, с одной стороны, и проявилось при анализе спектра, а с другой стороны, естественно для такого металла как олово.

Наконец, отметим, что из вида кривой $\Psi(\vec{q})$ и расположения узлов обратной решетки можно сразу понять природу

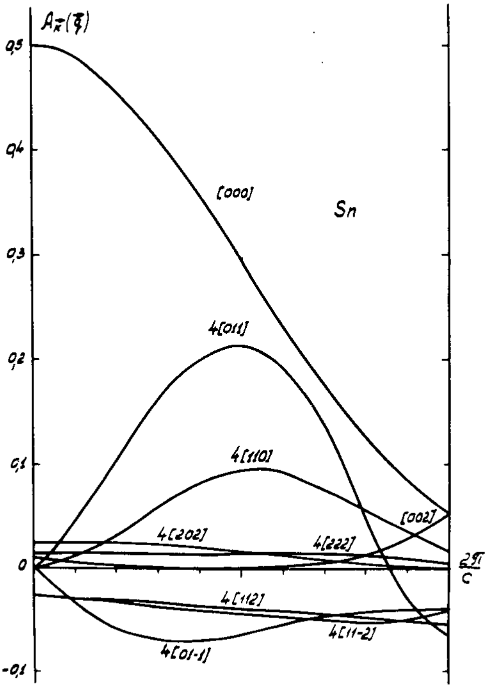

Рис. 10.

резко различного характера экранирования для предельной оптической частоты с поляризацией вдоль оси C и вдоль оси a. Действительно, из (5.7) следует, что в $\omega_a^2(0)$ будет вносить вклад самый мощный узел обратной решетки [110], тогда как для вклада в $\omega_c^2(0)$ ближайшим узлом будет только далеко лежащий узел [002]. В результате-сильнейший вклад электронов в частоту $\omega_a^2(0)$ и ничтожная экранировка в $\omega_c^2(0)$.

В заключение заметим, что, несмотря на хорошее согласие между теорией и экспериментом в целом, имеются особенности спектра, которые не были воспроизведены в расчёте. В первую очередь речь идет о тонкой структуре на продольных ветвях при $\vec{q}$ вдоль оси C [4]. Нам представляется, что эта структура целиком связана с реальным ходом псевдопотенциала при больших $\vec{q}$ и появляется в результате наложения вкладов от различных векторов $\vec{K}$. При некотором изменении параметров псевдопотенциала появлялась такая же тонкая структура, как и на экспериментальных кривых, но при сохранении двухпараметрического описания это влекло за собой искажение фононного спектра в целом. Требуется более гибкая форма модельного псевдопотенциала, и не вызывает сомнения, что при этом может быть достигнуто хорошее согласие между теорией и экспериментов в детальных чертах спектра. Заметим в этой связи, что решение обратной задачи для таких сложных металлов как олово, открывает большие возможности для верификации псевдопотенциала.

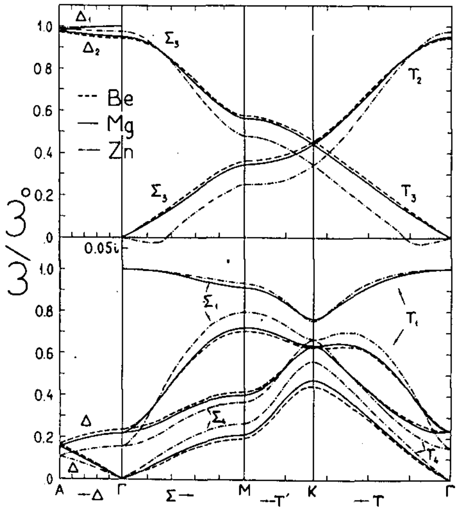

Рис. II.

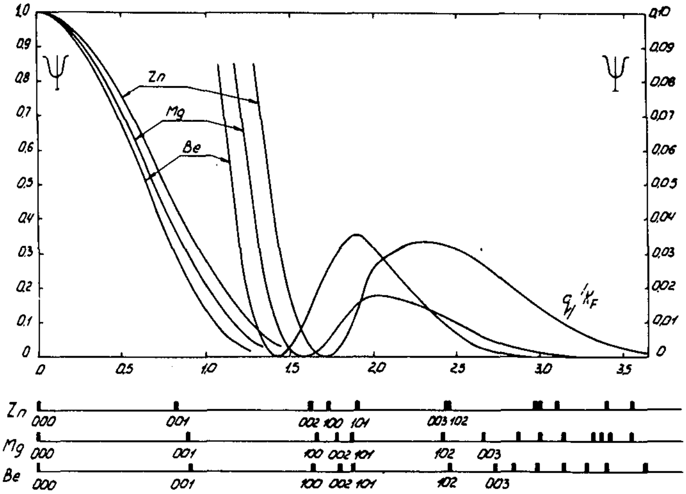

Рис. I2.

Фононный спектр гексагональных металлов

Фононный спектр сложных металлов, помимо олова, измерялся только для трех элементов гексагональной группы: Be, Mg и Zn. Поэтому рассмотрение этой группы металлов представляет большой интерес для анализа формирования спектра.

На рис. II приведены результаты расчёта спектра колебания ионной решетки при наличии компенсирующего отрицательного фона для этих металлов. Частоты отнесены к плазменной частоте ω_0 соответствующего металла. Видно, что в таком масштабе спектры весьма близки, особенно для Be и Mg. (Различие возникает за счёт изменения отношения c/a). Однако для Zn, как и для Sn, наблюдается неустойчивость ионной решетки и, соответственно, появление мнимых частей.

Хотя спектр ионной решетки и подобен для этих металлов, вид дисперсионных кривых, наблюдаемых на опыте, весьма различен. Это объясняется существенно разной ролью электронов проводимости.

На рис. 12 приведены кривые $\Psi(\vec{q})$ для трех гексагональных металлов, построенные на основе результатов работы [35]. На горизонтальных осях отложены положения узлов обратной решетки.

Из вида кривых и расположения узлов можно заключить, что для всех трех металлов процессы переброса будут играть существенную роль. При этом различие в поведении "хвоста" функции $\Psi(\vec{q})$ заставляет считать, что непарное взаимодействие в случае Be и Zn должно быть выражено сильнее, чем в случае магния. С другой стороны, ход кривых при $q < q_0$ показывает, что электронная экранировка максимальна в Zn и минимальна в Be. Чтобы проиллюстрировать масштаб этой экранировки, в таблице Ш приведен квадрат продольной оптической частоты при $q = 0$ отдельно для вклада от ионной решетки ω_i^2/ω_0^2 и для вклада от парного взаимодействия через электроны ω_e^2/ω_0^2. Из таблицы четко видна отмеченная выше тенденция

Таблица Ш

	ω_i^2/ω_0^2	ω_e^2/ω_0^2
Be	0,890	- 0,355
Mg	0,906	- 0,636
Zn	0,953	- 0,976

и, главное, чрезвычайно сильная электронная экранировка в случае Zn. Даже если окажется в результате уточнения псевдопотенциала, что переэкранировки нет, все равно картина почти полной компенсации останется. Отсюда ясно, что в Zn ковалентные эффекты должны играть очень существенную роль. (При использовании псевдопотенциала, полученного в рамках метода Хейне-Абаренкова, только они стабилизируют решетку - см. подробнее [28]). Следует отметить, что в каком-то смысле Zn ведет себя подобно Pb. Поэтому, в частности, весьма характерно, что в обоих случаях четко наблюдаются особенности Кона, выявление которых на фоне сильного сокращения, по-видимому, существенно облегчено (ср. соответствующее замечание в [16]).

Учёт роли электронов в образовании фононного спектра гексагональных металлов был проведен в рамках обратной задачи. При этом были рассмотрены два типа обратных задач. В первом - для описания парного взаимодействия использовались результаты Хейне-Абаренкова-Анималу, а учёт непарного взаимодействия проводился аналогично тому, как это делалось в олове. В другом - для описания дальнодействующего парного взаимодействия использовался модельный двухпараметрический потенциал вида (6.4). В обоих случаях для Mg и Be получались сравнительно близкие результаты. (В связи с отмеченной выше разной компенсацией в случае Zn последний тип обратной задачи для этого металла не рассматривался, ввиду необходимости использовать более гибкое представление для $V(\vec{r})$, нежели даваемое (6.4)). Результаты первой обратной задачи подробно изложены в [28] , и мы приведем здесь только результаты, основанные на использовании модельного псевдопотенциала.

В случае гексагональных металлов расстояния до ближайших двух координационных сфер мало отличаются друг от друга, поэтому мы считали необходимым учесть обе координационные сферы. Однако для простоты анализа взаимодействие принималось аксиально-симметричным, что при учёте условия Бона-Хуанга приводило к 3-м независимым константам. Таким образом, общее число параметров снова равнялось 5, которые находились из сравнения с 5 экспериментальными величинами (см. подробнее [28]).

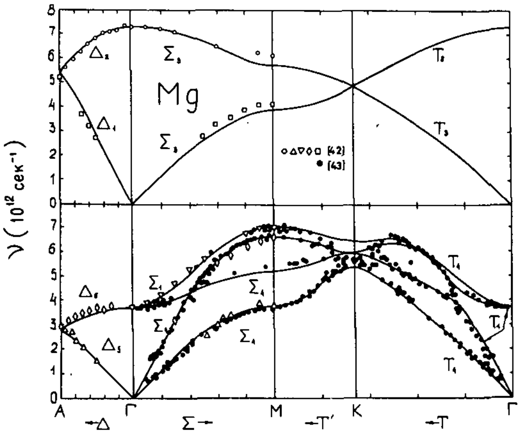

Рис. 13.

На рис. 13 приведен окончательный вид вычисленного фононного спектра Mg и нанесены экспериментальные точки, полученные в работах [42, 43]. Видно, что наблюдается хорошее согласие между теорией и экспериментом. На рис. 14 построен найденный модельный псевдопотенциал и для сравнения пунктиром приведен псевдопотенциал, вычисленный Анималу и Хейне [34], [12] .

На рис. 15 приведен вычисленный фононный спектр Be и нанесены экспериментальные точки, полученные в работе [41]. Снова наблюдается хорошее согласие между теорией и экспериментом.

На рис. 16 построен найденный нами в рамках обратной задачи псевдопотенциал. И пунктиром снова приведен псевдопотенциал, вычисленный Анималу и Хейне [34, 12].

Рис. I4.

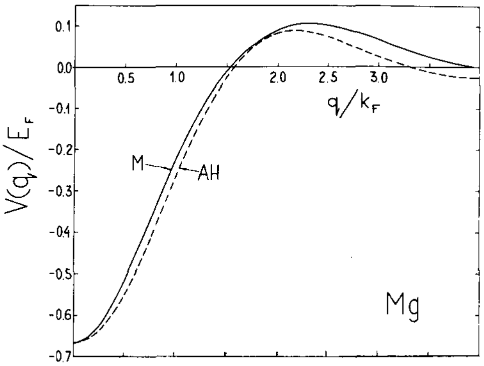

Рис. I5.

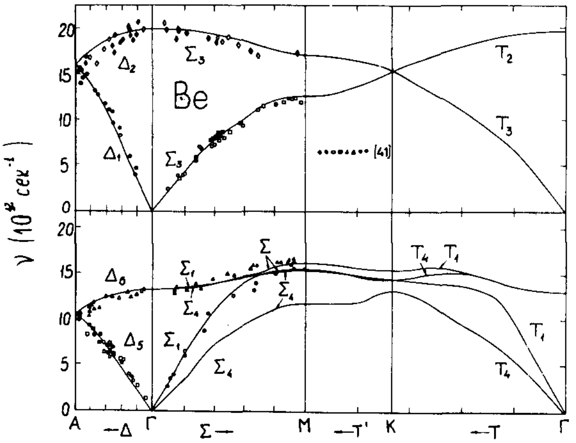

Мы не приводим здесь отдельно дисперсионных кривых, построенных без учёта короткодействующего взаимодействия. Отметим только, что учёт только парного взаимодействия схватывает основные черты спектра, однако количественное согласие достигается только при учёте короткодействующего взаимодействия. Роль этого взаимодействия, как и предсказывалось из общих соображений, оказалась в Be значительно большей чем в Mg, хотя и для Mg короткодействующее взаимодействие существенно. Следует думать, что в первую очередь по этой причине в работах [44, 45], где учитывалась роль электронов для описания динамики Be и Mg, но только в парном приближении, не удалось достичь хорошего согласия с экспериментом.

Мы ограничимся этими замечаниями о фононном спектре гексагональных металлов, отсылая за подробностями к работе [28].

Таким образом, как показывает приведенный анализ, схема рассмотрения, выделяющая в явной форме дальнодействующее парное взаимодействие и непарное короткодействующее взаимодействие оказывается весьма эффективной для описания фононного спектра сложных металлов. Заметим при этом, что неточность, которая

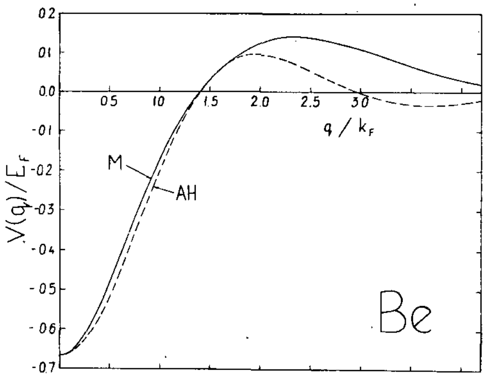

Рис. 16.

может быть связана со значением псевдопотенциала при $q \gtrsim 2K_F$ в парном взаимодействии будет в первую очередь сказываться, по-видимому, на взаимодействии с ближайшими координационными сферами. При этом нахождение $\mathcal{D}_2$ в рамках обратной задачи компенсирует эту неточность.

Авторы признательны А.Холасу за проведение ряда конкретных расчетов.

ЛИТЕРАТУРА

[1] BROCKHOUSE, B.N., ARASE, T., CAGLIOTI, G., RAO, K.R., WOODS, A.D.B., Phys. Rev. 128 (1962) 1099.
[2] PRICE, L.D., Inelastic Scattering of Neutrons (Proc. Symp. Bombay, 1964) 1, IAEA, Vienna (1965) 117.
[3] BORGONOVI, G., CAGLIOTI, C., ANTONINI, M., Inelastic Scattering of Neutrons (Proc. Symp. Bombay, 1964), 1, IAEA, Vienna (1965) 129.
[4] ROWE, I.M., BROCKHOUSE, B.N., SVENSSON, C., Phys. Rev. Lett. 14 (1965) 554.
[5] BOZGONOVI, G., CAGLIOTI, G., ANTAL, J.J., Phys. Rev. 132 (1963) 6.
[6] MALISZEWSKI, E., SOSNOWSKI, J., BLINOWSKI, K., KOZUBAWSKI, J., PADŁO, I., SLEDZIEWSKA, D., Inelastic Scattering of Neutrons (Proc. Symp. Chalk River, 1962) 2, IAEA, Vienna (1963) 87.
[7] БРОВМАН, Е.Г., КАГАН, Ю., ФТТ 8 (1966) 1402.
[8] PRICE, L.D., Proc. R. Soc. Ser. A300 (1967) 25.
[9] VOSKO, S.H., Phys. Lett. 13 (1964) 97.
[10] PHILLIPS, J.C., KLEINMAN, L., Phys. Rev. 116 (1959) 287, 880.
[11] AUSTIN, B.J., HEINE, V., SHAM, L.J., Phys. Rev. 127 (1962) 276.
[12] HARRISON, W., Pseudopotentials in the Theory of Metals, Benjamin, New York (1966).
[13] TOJA, T., J. Res. Inst. Cetalysis, Sapporo 6 (1958) 161, 183; 7 (1959) 60.
[14] TOJA, T., Inelastic Scattering of Neutrons (Proc. Symp. Bombay, 1964) 1, IAEA, Vienna (1965) 25.
[15] SHAM, L.J., Proc. R. Soc. Ser. A 283 (1965) 33.
[16] VOSCO, S.H., TAYLOR, R., KEECH, G.H., Can. J. Phys. 43 (1965) 1187.
[17] COCHRAN, W., Inelastic Scattering of Neutrons (Proc. Symp. Bombay, 1964) 1, IAEA, Vienna (1965) 3.
[18] COCHRAN, W., Proc. R. Soc. Ser. A 276 (1963) 308.
[19] БРОВМАН, Е.Г., КАГАН, Ю., Препринт ИАЭ-1186 (1966).
[20] БРОВМАН, Е.Г., КАГАН, Ю., ЖЭТФ 52 (1967) 557.
[21] БОРН, М., ХУАН КУНЬ., Динамическая теория кристаллических решеток, И.Л., Москва, 1958.

[22] МИГДАЛ, А.Б., ЖЭТФ 34 (1958) 1438.
[23] HUBBARD, J., Proc. R. Soc. Ser. A 240 (1967) 539.
[24] АБРИКОСОВ, А.А., ГОРЬКОВ, Л.П., ДЗЯЛОШИНСКИЙ, И.Е., Методы квантовой теории поля в статистической физике. Гостехиздат, Москва, 1962.
[25] KOHN, W., Phys. Rev. Lett. 2 (1959) 393.
[26] PICK, R., J. Physique 28 (1967) 539.
[27] ANIMALU, A.O.E., BONSIGNORI, F., BORTOLANI, V., Nuovo Cim. 44 (1966) 159.
[28] БРОВМАН, Е.Г., КАГАН, Ю., ХОЛАС, А., Доклад SM-104/145 на этой конференции.
[29] BARDEEN, J., PINES, D., Phys. Rev. 99 (1955) 1140.
[30] ПАЙНС, Д., Элементарные возбуждения в твердых телах, Мир, Москва, 1965.
[31] BOHM, D., STAVER, T., Phys. Rev. 84 (1950) 836.
[32] HEINE, V., ABARENKOV, I.V., Phil. Mag. 9 (1964) 451.
[33] ABARENKOV, I.V., HEINE, V., Phil. Mag. 12 (1915) 529.
[34] ANIMALU, A.O.E., HEINE, V., Phil. Mag. 12 (1965) 1249.
[35] ANIMALU, A.O.E., Proc. R. Soc. Ser. A 294 (1966) 376.
[36] HUBBARD, J., Proc. R. Soc. Ser. A 243 (1957) 336.
[37] GELDART, W., VOSKO, S.H., Can. J. Phys. 44 (1966) 2317.
[38] WOODS, A.D.B., BROCKHOUSE, B.N., MARCH, R.H., STEWART, A.T., BOWERS, R., Phys. Rev. 128 (1962) 1112.
[39] COWLEY, R.A., WOODS, A.D.B., DOLLING, G., Phys. Rev. 150 (1966) 487.
[40] ROWE, I.M., Phys. Rev. 163 (1967) 547.
[41] SCHMUNK, R.E., BRUGGER, R.M., RANDOLPH, P.D., STRONG, K.A., Phys. Rev. 128 (1962) 562.
[42] IYENGAR, P.K., VENKATARAMAN, C., VIJAYARAGHAVAN, P.R., ROY, A.P., Inelastic Scattering of Neutrons (Proc. Symp. Bombay, 1964) 1, IAEA, Vienna (1965) 153.
[43] SQUIRES, G.L., Proc. phys. Soc. 88 (1966) 919.
[44] KOPPEL, I.U., MARADUDIN, A.A., Phys. Lett. 24A (1967) 224.
[45] ROY, A.P., VENKATARAMAN, G., Phys. Rev. 156 (1967) 769.

DISCUSSION

B.N. BROCKHOUSE: In your presentation you described the strong anomaly in the longitudinal branch along the c-direction in β-tin as arising from the 'zero' in the pseudo-potential (a 'Harrison anomaly'?). Now, according to Rowe's results (Phys. Rev. 163 (1967) 547, Fig. 4), the anomaly decreases rapidly with distance from the c-axis. In view of the isotropy of the pseudo-potential, is this consistent with your interpretation?

Yu.M. KAGAN: As I indicated in my talk, the dip or anomaly in the longitudinal branch along the c-axis in β-tin may be explained in terms of interference by contributions from various reciprocal lattice sites. It is easy to reproduce this anomaly in our calculations by varying the pseudo-potential parameters. Since our simplest pseudo-potential was not sufficiently flexible, these variations resulted in a change in the remaining part of the dispersion curves. We very much doubt whether the use of a more flexible pseudo-potential will make it possible to reproduce the whole experimental dispersion curves.

As for the decrease of this anomaly with distance from the c-axis, I believe that this is connected with the change in the relative contribution from the reciprocal lattice sites, especially those lying in the basal plane (perpendicular to the c-axis).

S.K. SINHA: Do you consider that the local pseudo-potential which you described here would be valid for more complicated metals such as transition metals? It seems to me that the problem of getting a 'pseudo-potential' is one of the big difficulties as one departs from the simple metals. Similarly, do you believe that the treatment in terms of a simple scalar dielectric function $\psi(q)$ which you also mentioned would be applicable to such metals?

Yu. M. KAGAN: First, let me point out that everything in the paper relates to non-transition metals. Although the main results are quoted for a local pseudo-potential, non-locality can be taken into account in the normal way, at least for pair interaction. This will correspond simply to a more complex $\psi(q)$ function.

No artificial simplification of the dielectric function was carried out. By taking account of the subsequent terms of the pseudo-potential expansion one also describes the increased complexity of the dielectric function in a crystal as compared with the dielectric function of an electron gas. It is precisely herein that the advantage of this method of treatment lies.

With respect to transition elements, we have two problems: finding a pseudo-potential or scattering amplitude in an isolated ion, and overlapping of neighbouring ion shells in the crystal itself. These problems should preferably be considered separately, taking as subjects for investigation such substances as noble metals and specially selected rare-earth metals.

The problem of finding a pseudo-potential for a free ion in transition elements will be solved one way or another in the near future. As to the overlapping of inner shells, in a system where non-pair interaction is regarded as interaction with nearest neighbours, this overlapping can, it would appear, be taken into account directly.

LOCALIZED AND BAND PHONONS IN Ta_{88}-Nb_{12} STUDIED BY COHERENT INELASTIC NEUTRON SCATTERING

J. ALS-NIELSEN
RISØ, RESEARCH ESTABLISHMENT,
ROSKILDE, DENMARK

Abstract

LOCALIZED AND BAND PHONONS IN Ta_{88}-Nb_{12} STUDIED BY COHERENT INELASTIC NEUTRON SCATTERING. It is probable that substitution of Nb atoms in a Ta crystal does not alter the force constants significantly, so in a Ta-Nb alloy the Nb atoms can be regarded as nearly pure light-mass defects. These give rise to a localized mode of vibration with a frequency above the frequency band for pure Ta lattice vibrations. The lattice vibrations of an 88% Ta-12% Nb alloy have been studied by inelastic neutron scattering, using a triple-axis spectrometer in its constant-q mode of operation. In particular, the scattered intensity has been measured as a function of energy transfer, with q fixed along the (1, 0, 0) direction and perpendicular to the scattering vector. It has not been possible to resolve the band phonons from the localized phonon into two separate neutron energy groups. However, a tail at the high-energy side of the band phonon peak at $q = 1.5$ $Å^{-1}$ as well as an anomalous broadening of the peaks at $q = 1.7$ $Å^{-1}$ and $q = 1.9$ $Å^{-1}$ are interpreted as deriving from a localized mode of vibration. Its energy is 23.2 ± 0.2 meV, not far from the value of 22.55 meV calculated from the mass-defect theory using the frequency spectrum for Ta determined by Woods. The band phonons are shifted upwards in energy, although the dispersion curve becomes very flat or even decreases for $q > 1.5$ $Å^{-1}$. A comparison between the neutron groups from the alloy and a pure Ta crystal is being initiated.

1. INTRODUCTION

This paper deals with an inelastic neutron scattering study of the lattice vibrations of Ta alloyed with 12 at.% Nb to give substitutional defects in the crystal. The lattice constant is unaltered by the addition of Nb [1] and, as Ta and Nb are both column V transition metals, it is anticipated that the interatomic forces in the alloy are similar to those in the pure Ta crystal. The dispersion curves for Ta measured by Woods [2] and for Nb obtained by Nakagawa and Woods [3] do not scale very accurately as the square-root of the masses, but they do show many similarities in shape. Thus the Ta_{88}-Nb_{12} alloy is a fairly close approximation to a lattice with pure light-mass defects.

Qualitatively, the light impurities will introduce a mode of vibration with a frequency above the band-mode frequencies in the host lattice. The amplitude of this mode of vibration is maximum on the light impurity atom and decays with the distance from the impurity lattice site, it is therefore called a localized mode of vibration. As the cross-section for inelastic neutron scattering is essentially the Fourier transform in space and time of the dynamical pair-correlation function [4], it is in principle possible to measure the frequency and the spatial extension of the local mode of vibration.

The theory for lattice vibrations in a lattice with mass defects has been developed in recent years (see, e.g., the review article by Maradudin [5]), and it was the purpose of the present work to compare the theoretical predictions with experimental results.

2. THEORETICAL PREDICTIONS

In this section we recall the formulae given by Elliott [6] for localized phonons and give numerical results for the alloy Ta_{88}-Nb_{12}.

The localized mode frequency Ω is related to the frequency distribution $\nu(\omega)$ for the host lattice and to the relative mass difference $\epsilon = (M-M')/M$ between the host mass M and the impurity mass M' by

$$1 - \epsilon\Omega^2 \int \nu(\omega)\,(\Omega^2 - \omega^2)^{-1}\,d\omega = 0 \tag{1}$$

The band modes are modified slightly by the presence of impurities.

The frequency $\omega(\vec{q})$ at wavevector $\vec{q}$ is shifted by an amount $\Delta(\vec{q})$, where

$$\Delta(\vec{q}) = (c/2)\,\epsilon\omega(\vec{q})X_1\,[\omega(\vec{q})] \tag{2}$$

Here c denotes the concentration of impurities, and $X_1[\omega(\vec{q})]$ is the real part of a complex function, which is given in terms of $\nu(\omega)$ as

$$X_1[\omega(\vec{q})] + iX_2[\omega(\vec{q})] = \frac{[1 - \epsilon\omega^2\int\nu(\omega')\,(\omega^2 - \omega'^2)^{-1}\,d\omega'] + i(\pi/2)\,\epsilon\omega\,\nu(\omega)}{[1 - \epsilon\omega^2\int\nu(\omega')\,(\omega^2 - \omega'^2)^{-1}\,d\omega']^2 + [(\pi/2)\,\epsilon\omega\,\nu(\omega)]^2} \tag{3}$$

where the principal value of the integral is to be taken. Furthermore, the normal band modes will no longer have an infinite life-time. The life-time $\Gamma^{-1}(\vec{q})$ is related to $X_2[\omega(\vec{q})]$ in Eq. (3) by

$$\Gamma(q) = c\epsilon\omega(\vec{q})X_2[\omega(\vec{q})] \tag{4}$$

These effects may be observed experimentally by inelastic neutron scattering from a single crystal. The differential scattering cross-section for creation of a localized phonon of wavevector $\vec{q}$ is expressed by the scattering function $S(\vec{\kappa}, \omega)$:

$$S(\vec{\kappa}, \omega) \propto \frac{c}{\Omega}\left\{\frac{1}{\Omega^2 B(\Omega)}\left[\left(\frac{a' - a}{\epsilon} + \frac{a}{1 - (\omega(\vec{q})/\Omega)^2}\right)^2 + \frac{a'^2 - a^2}{\epsilon^2}\right] + a^2\right\}\ \delta(e - \hbar\Omega) \tag{5}$$

Here a and α are the coherent and incoherent scattering amplitudes for the host atoms and a' and α' the corresponding quantities for the impurity atoms. The scattering vector $\vec{\kappa}$ is the difference between the incoming and outgoing neutron wavevectors, $\vec{k}_0$ and $\vec{k}$ respectively. The energy transfer e equals $\hbar^2(k_0^2 - k^2)/2m$, and $\omega(\vec{q})$ denotes the frequency of the band-mode phonon with wavevector $\vec{q}$, which is related to $\vec{\kappa}$ through $\vec{\kappa} = \vec{q} + \vec{\tau}$, $\vec{\tau}$ being a reciprocal lattice vector. Finally $B(\Omega)$ is related to the host lattice frequency distribution $\nu(\omega)$ by

$$B(\Omega) = \int \nu(\omega)\,\omega^2(\Omega^2 - \omega^2)^{-2}\,d\omega \tag{6}$$

The localized mode frequency Ω has been evaluated numerically from Eq. (1) using the frequency distribution given by Woods [2], see

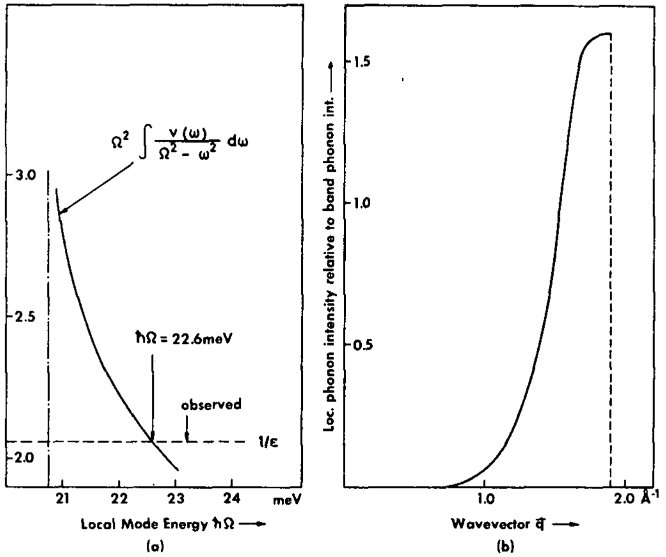

FIG. 1. (a) Calculation of the localized phonon mode energy using Eq.(1). The result is approximately proportional to the maximum frequency in the band mode frequency spectrum for the pure crystal; (b) the scattering cross-section for excitation of a localized phonon of wavevector $\vec{q}$ relative to that for a band phonon of the same wavevector. The width of the peak indicates the spatial extent of the localized vibration.

Fig. 1(a). The scattering cross-section for excitation of a localized phonon relative to that for a band phonon with the same wavevector has also been evaluated and is shown in Fig. 1 (b). It should be noted that instrumental resolution effects have been neglected in Fig. 1(b). The dispersion relation for the transverse (q, 0, 0) mode in Ta [2] is shown in Fig. 2. For comparison Fig. 2 also shows the equivalent dispersion relation for Nb [3] which, scaled with a factor of 0. 71, would coincide with the Ta curve if the interatomic forces in these materials were identical. In the upper part of Fig. 2 is shown the calculated energy shift $\hbar\Delta(\vec{q})$ of the band modes and the phonon widths $\hbar\Gamma(q)$ for a Ta_{88}-Nb_{12} alloy.

3. EXPERIMENTAL RESULTS

The inelastic neutron scattering was investigated using a triple-axis spectrometer. The sample consisted of two single-crystal rods 5 cm long and with a diameter of 0. 6 cm. Their orientations were aligned within an accuracy of 0. 1° so the (2, 0, 0) and (0, 2, 2) reciprocal lattice vectors were in the horizontal scattering plane. It follows from Eq. (5) that the intensity from a localized phonon excitation is maximum for that wavevector where the band modes have maximum frequency. Consequently, we confined the investigations to transverse (q, 0, 0) phonons near the zone boundary. It is essential to minimize the experimental broadening of the phonon peaks in attempting to resolve the localized phonon peak from the band phonon peak in a constant-q,

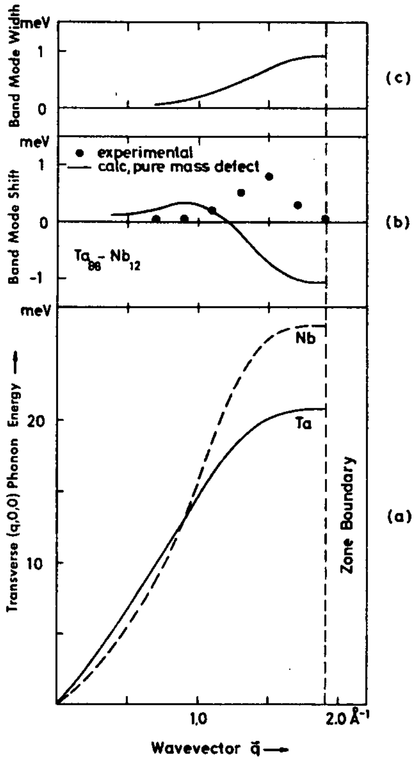

FIG.2. (a) Dispersion relations for pure Ta [2] and Nb [3] for the transverse (q, 0, 0) mode; (b) calculated shift of band phonon energies in a Ta_{88}-Nb_{12} alloy assuming unchanged force constants only, experimental points are also shown; (c) calculated band-phonon widths or inverse life-time due to light mass defects in a Ta_{88}-Nb_{12} alloy.

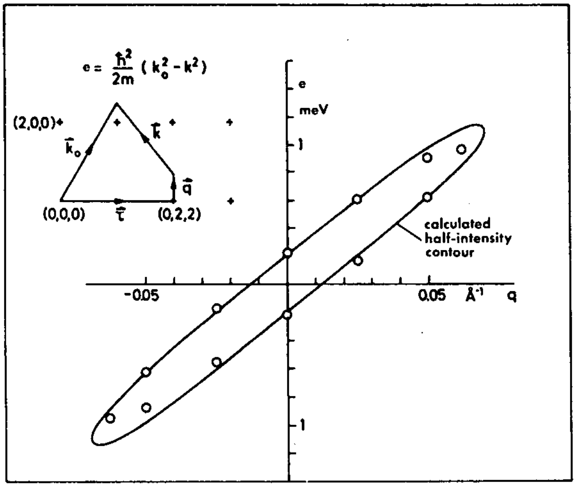

FIG.3. Comparison between measured and calculated experimental resolution function. The correlation between q and e gives rise to the focussing effect in triple-axis spectrometry.

variable-ω scan. It is not possible to take advantage of the focussing effect in this problem. because the phonon frequencies do not depend on the wavevector near the zone boundary.

The optimal compromise between the demands for sufficient intensity and narrow resolution was obtained with the scattering vector $\vec{k}_0 - \vec{k} = (q, 2, 2)$, k_0 being fixed to 4.66 Å^{-1}, and using Be in the (0, 0, 2) orientation as monochromator and analyser crystals. The resolution function $R(\vec{q}, \omega)$ was determined experimentally by the surfaces of constant intensity around the (0, 2, 2) Bragg reflection. Figure 3 shows a cut through the half-peak intensity surface in the (q, 0, 0, ω) plane. Cooper and Nathans [7] have derived a very useful analytical expression for the resolution function in terms of scattering angles, collimations and mosaic spreads of the monochromator and analyser crystals. The calculated resolution is shown as the full line in Fig. 3. The agreement is satisfactory and gives confidence in the accuracy of the calculation of the experimental broadening of phonon peaks[1]. The phonon energies for

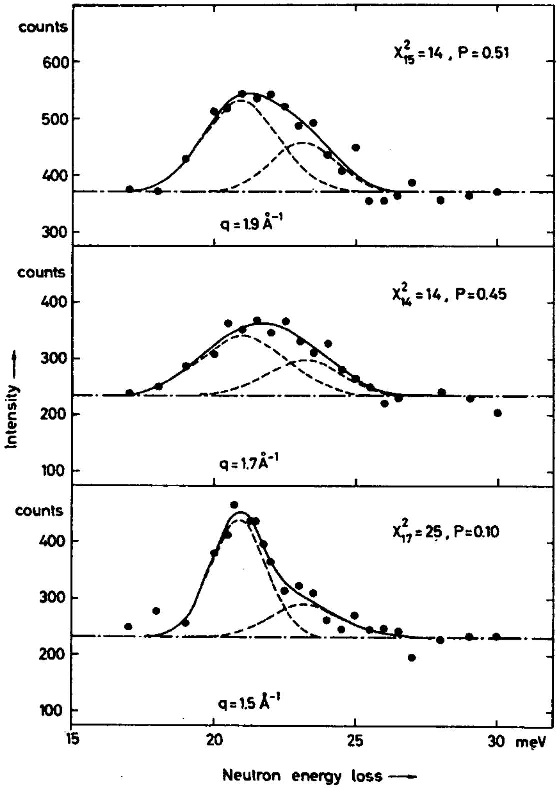

FIG.4. Intensity versus neutron energy loss in constant-q scans. The dashed curves are the band-phonon peaks and the localized phonon peaks which are derived from a least-squares fit. The total counting time for q = 1.9 Å^{-1} was 50% greater than that for q = 1.7 Å^{-1} and q = 1.5 Å^{-1}.

---

[1] It should be noted that there is a misprint in Ref. [7] in Eq. (67d) for the phonon width; Eq. (67d) should read: $G_3^2 = M_{44} - G_1 (M_{14} - \text{etc.})$.

$q \leq 1.3$ Å^{-1} were measured for $\vec{k}_0 - \vec{k} = (q, 2, 2)$ and $\vec{k}_0 - \vec{k} = (q, 3, 3)$, and consistent results were obtained (Table I). The measured widths Γ_e were also consistent, but they are systematically slightly greater than the calculated widths Γ_r due to the resolution. This may be due to a finite life-time for the low-energy band phonons.

For $q \geq 1.5$ Å^{-1} the neutron intensity peaks in a constant-q, variable-ω scan are shown in Fig. 4. The effect of the curvature of the dispersion curve at $q = 1.5$ Å^{-1} within the extension of the resolution function would be a tail on the low-energy side of the peak, whereas a tail on the high-energy side was observed. It is therefore almost certain that this tail must derive from the excitation of a localized phonon. A weighted least-squares fit of two Gaussian peaks with adjustable positions, heights and widths gave the results listed in Table I and drawn as dashed curves in Fig. 4.

The background level was determined by the count rate at $q = 0.5$ Å^{-1} and the plotted intensities were accumulated in four repetitions for each setting of the spectrometer. The statistical quality of the fit is given by the χ^2 test. χ^2 is the sum of the squared deviations of the measured intensities from the calculated Gaussian peaks, relative to the standard deviation expected from Poisson statistics. From the value of χ^2, the number of measured points, and the number of fitted parameters, the probability P that a repetition would give a higher value of χ^2 is found from standard tables.

TABLE I. TRANSVERSE (q, 0, 0) VIBRATIONAL MODES IN Ta_{88}-Nb_{12} ALLOY

Position and widths of intensity peaks in constant-q, variable-ω scans with the scattering vector $\vec{\kappa} = (q, 2, 2)$ or $(q, 3, 3)$. The widths Γ_r due to instrumental resolution were calculated using the results obtained by Cooper and Nathans [7]. $\Gamma = (\Gamma_e^2 - \Gamma_r^2)^{1/2}$ is also listed.

	$\vec{\kappa}$	q (Å^{-1})	$\hbar\omega$ (meV)	Width (meV)		
				Γ_e	Γ_r	Γ
Band modes	(q, 3, 3)	0.7	9.80	1.0 ± 0.15	0.86	0 < 0.5 < 0.8
	(q, 2, 2)	0.7	9.80	0.95 ± 0.10	0.50	0.7 < 0.8 < 0.9
	(q, 2, 2)	0.9	13.25	1.10 ± 0.15	0.62	0.7 < 0.9 < 1.1
	(q, 3, 3)	1.1	16.30	1.3 ± 0.2	0.95	0.6 < 0.9 < 1.2
	(q, 2, 2)	1.1	16.40	1.3 ± 0.2	0.84	0.7 < 1.0 < 1.2
	(q, 3, 3)	1.3	19.25	2.0 ± 0.3	1.5	0.8 < 1.3 < 1.8
	(q, 2, 2)	1.5	20.85	2.25 ± 0.2	2.0	0 < 1.0 < 2.0
	(q, 2, 2)	1.7	21.0	3.6 ± 0.2	2.6	2.2 < 2.5 < 2.8
	(q, 2, 2)	1.9	20.9	3.0 ± 0.2	2.6	1.1 < 1.5 < 1.8
Local. mode	(q, 2, 2)	1.5	23.2	2.9 ± 0.2	2.5	1.1 < 1.5 < 1.8
	(q, 2, 2)	1.7	23.2	3.0 ± 0.2	2.5	1.2 < 1.7 < 2
	(q, 2, 2)	1.9	23.2	2.7 ± 0.2	2.5	0 < 0.9 < 1.4

A similar analysis was carried out for the results obtained at $q = 1.7$ Å^{-1} and $q = 1.9$ Å^{-1}. The band phonon and the localized phonon peaks have nearly equal heights and widths (because the dispersion relation is flat). The resulting intensity curve is therefore one broad peak, which is approximately twice as broad as the calculated width due to instrumental resolution. In view of the agreement between the measured and calculated resolution at $q = 0$ and of the relatively small differences between the calculated and measured phonon widths for $q \leq 1.5$ Å^{-1}, the anomalous broadening of the experimental widths for $q \geq 1.7$ Å^{-1} indicates very strongly that the broad peak is a superposition of a band phonon peak and a localized phonon peak.

4. DISCUSSION

The results obtained in constant-q, variable-ω scans, the scattering vector co-ordinates being (q, 2, 2), demonstrate the existence of a localized mode of vibration, although it has not been possible to resolve the localized phonon peak from the band phonon peak. The overlap reduces the accuracy in the determination of the position, height and width of the two peaks; however, the localized phonon energy is found to be 23.2 meV with an estimated accuracy of ± 0.2 meV. This result is not far from the theoretical prediction of 22.55 meV based on Woods' data for pure Ta metal [2].

The band phonon peaks show a tendency to an increasing natural width with increasing q and to a flat or even decreasing dispersion relation for $q > 1.5$ Å^{-1}. These features are qualitatively in agreement with theoretical expectations (Fig. 2).

The quantitative comparison between theory and experiment is very sensitive to a small systematic error in the determination of the phonon energies for the alloy or for the pure Ta metal. It would therefore simplify the discussion considerably if identical measurements were carried out on the pure Ta crystal and the alloy on the same instrument. This comparison would also give more accurate information about the band phonon widths in the alloy. Measurements of this kind are planned for the immediate future.

ACKNOWLEDGEMENTS

The author is indebted to Professor A. R. Mackintosh who suggested the experiment and gave his time to discussions throughout the investigation. Dr. M. J. Cooper is acknowledged for discussions on his calculation of the triple-axis spectrometer resolution function. I am grateful to Dr. A. D. B. Woods for arranging the loan of the Chalk River Ta sample for a future comparison with the Ta-Nb alloy.

REFERENCES

[1] BÜCKLE, H., Z. Metallk. 37 (1946) 53.
[2] WOODS, A.D.B., Phys. Rev. 136 (1964) A781.
[3] NAKAGAWA, Y., WOODS, A.D.B., in Lattice Dynamics, Pergamon Press, Oxford (1965) 39; Phys. Rev. Lett. 11 (1963) 271.
[4] Van HOVE, L., Phys. Rev. 95 (1954) 1374.
[5] MARADUDIN, A.A., in Solid State Physics 18, Academic Press Inc., New York (1966).
[6] ELLIOTT, R.J., in Symp. Inelastic Scattering of Neutrons in Condensed Systems, Rep. BNL 940(C-45) (1965) 23.
[7] COOPER, M.J., NATHANS, R., Acta Crystallogr. 23 (1967) 357.

NORMAL MODES OF VIBRATION OF MIXED KBr/RbBr CRYSTALS

W.J.L. BUYERS and R.A. COWLEY
ATOMIC ENERGY OF CANADA LTD,
CHALK RIVER, ONT., CANADA

Abstract

NORMAL MODES OF VIBRATION OF MIXED KBr/RbBr CRYSTALS. Normal modes of vibration of crystals of KBr/RbBr containing 50 and 20 at.% of RbBr have been compared by neutron scattering with normal modes in KBr. In both the 20 and 50% crystals, normal modes were well defined. For the [111] LA branch, the decrease in frequency in going from pure KBr to both mixed crystals exhibited a dependence on wavevector characteristic of a resonance mode of frequency approximately 2.1 (10^{12} cps). The widths of the neutron groups were larger in the resonance region. Other modes did not show resonance behaviour. The frequencies of the [111] TA, [111] TO and [110] TA branches in the 50% crystal were less than those in KBr by an approximately constant small amount; the shifts are 0.11 ± 0.06, 0.5 ± 0.1 and 0.16 ± 0.04 (10^{12}cps) respectively. There were no appreciable increases in the widths of the neutron groups from these modes. These results are compared with theoretical calculations based on mass defects from the mean lattice approximation.

There have been a number of neutron scattering experiments to determine the effect of defects on the lattice vibrations of crystals. Both resonance and localized modes have now been detected [1,2,3], in systems containing a few percent of heavy or light impurities. In the experiments described below we have studied the normal modes of vibration of mixed KBr/RbBr crystals containing 22% and 45% of RbBr in order to determine the nature of the normal modes in systems with a large concentration of defects. These experiments are in contrast to those on metal alloys [4,5] in which the electronic structure is intermediate between that of the two pure materials, but nevertheless is well defined. In our case there is little doubt that the rubidium behaves as a defect and is present in large concentration in these crystals.

The experiments were conducted on a triple axis crystal spectrometer at Chalk River with the incident energy fixed at 18.2 milli eV. The constant '$\vec{Q}$' mode of operation was used throughout to study the two mixed crystals and pure KBr at room temperature. Measurements have so far been completed for the transverse optic and both acoustic modes propagating in the [111] direction and for the transverse acoustic mode propagating in the [110] direction and polarized in the ($1\bar{1}0$) plane.

The results show that there is surprisingly little change in the phonon spectrum as the RbBr concentration is increased. The transverse acoustic modes show no detectable broadening and only a slight decrease in frequency with increasing RbBr concentration. Similar results were obtained for the transverse optic branch although the instrumental resolution was not sufficiently good that we might well have missed some broadening of the neutron groups. The results for the longitudinal acoustic branch were more dramatic and showed a marked increase in width in the region around 70% of the zone boundary wave-vector and an associated behaviour in the change of phonon frequency which is characteristic of a resonance mode. These results are summarized in Fig. 1, which shows the difference between the centres of the neutron groups of the mixed crystals as compared with pure potassium bromide for all the branches and the widths observed for the longitudinal acoustic branch.

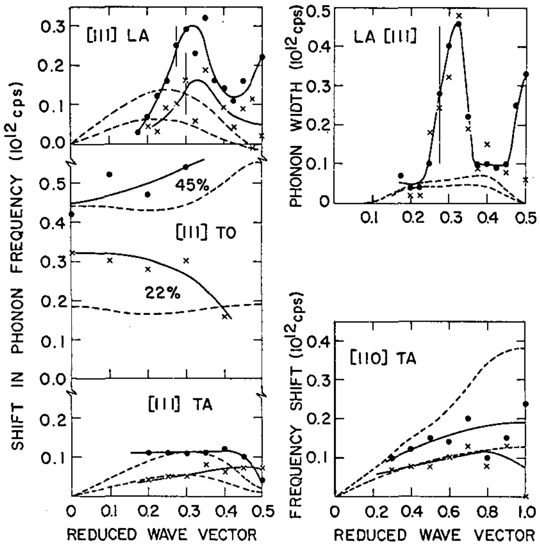

FIG. 1. The changes in the frequencies and widths of some of the normal modes of mixed KBr/RbBr crystals from those of pure KBr (solid lines) as compared with theoretical calculations (dotted lines). The experimental points for crystals containing 22% and 45% of RbBr are shown as crosses and circles respectively. Only one experimental line is shown for the width of the LA [111] modes as the results for the two concentrations are similar.

Most of the theories of the normal modes of vibration in crystals containing defects are only applicable to small concentrations of defects. Recently Taylor [6] has extended these theories to large concentrations by use of a mean lattice which is obtained self-consistently. Unfortunately his theory is only readily applicable to a mass defect in a cubic Bravais lattice. Consequently we have used a mean lattice theory in which the mean lattice is taken to be harmonic but has lattice constants, masses and force constants which are the appropriate average of those of the pure crystals.

In table I we list the parameters of simple shell models [7] for KBr and RbBr as deduced from their elastic and dielectric constants. Clearly the nearest neighbour short-range forces and electrical polarizability are unchanged, while the short-range polarizability, d, is only moderately altered from going from KBr to RbBr. The parameters of the mean lattice approximation for the mixed crystals are also listed in table I.

TABLE I

Parameters of the simple shell models. The notation is described in [7].

	M_+	M_-	R	A	B	Z	α	d
	atomic	masses	Å	$\frac{e^2}{v}$	$\frac{e^2}{v}$	e		e
KBr	39.1	79.9	3.293	12.18	-1.165	1	0.072	0.24
RbBr	85.5	79.9	3.427	12.70	-1.165	1	0.072	0.16
$KBr_{78}RbBr_{22}$	49.2	79.9	3.32	12.30	-1.165	1	0.072	0.22
$KBr_{55}RbBr_{45}$	60	79.9	3.35	12.42	-1.165	1	0.072	0.205

In the mixed crystals the K and Rb atoms are regarded as defects from the mean lattice. The comparatively small changes for the short-range forces and polarizabilities, table I, suggest that it is a reasonable approximation to treat the defects as mass defects. The change in the self-energy of the mode $(\vec{q}j)$ for a concentration c of Rb ions may then be evaluated by the usual method [8]. The lowest approximation is to consider the multiple scattering of the normal modes from each individual defect, but to add the total scattering from all the defects by linear superposition. The result for the self-energy of the mode $(\vec{q}j)$ is then

$$\sum(\vec{q}j,\omega) = \sum_{\alpha} \frac{e_\alpha(+|\vec{q}j)^2}{2\omega(\vec{q}j)} \left[(1-c)\, T_K + c\, T_{Rb}\right] \qquad (1)$$

where $e_\alpha(+|\vec{q}j)$ is the mean lattice eigenvector of the positive ion in the $(\vec{q}j)^{th}$ mode and $\omega(\vec{q}j)$ its frequency, and T_K and T_{Rb} are the T matrices for the potassium and rubidium mass defects from the mean lattice. For example

$$T_K = \frac{(M_{Rb} - M_K)\, c}{1 - \omega^2\, (M_{Rb} - M_K)\, c\, P(\omega)} \qquad (2)$$

where $P(\omega)$ is the function

$$P(\omega) = \frac{1}{N} \sum_{\vec{q}j} \frac{e_\alpha(+|\vec{q}j)^2}{\omega^2 - \omega(\vec{q}j)^2} \qquad (3)$$

Eqns. (1 - 3) now enable the change in the frequencies, $Re(\sum)$ added to the change in mean lattice frequency, and the width, $Im(\sum)$ to be calculated. The results are compared with experiment in Fig. 1.

The agreement between the calculations and experiment shown in Fig. 1 is not at all good. By and large the changes in the frequency, which result largely from the change in mean lattice, are of the right order of magnitude, but the widths of the longitudinal acoustic branch are far too small, although qualitatively they do have the correct shape. It appears as if Eqn. 1 considerably underestimates the influence of the defects. This could be because we have neglected terms arising from the scattering by pairs of defects and this certainly cannot be justified rigourously. However it is equally certain that their inclusion is very difficult. Another possibility for the discrepancy is that the mixed crystals are not completely uniform in concentration throughout or completely random. If this was the case the observed groups might be in error because they would average over many different concentrations and configurations. Further experiments are planned to investigate these points and to determine the properties of other branches of the dispersion curves.

REFERENCES

[1] SVENSSON, E.C., BROCKHOUSE, B.N., ROWE, J.M., Solid State Commun. 3 (1965) 245.

[2] MØLLER, H.B., MACKINTOSH, A.R., Phys. Rev. Lett. 15 (1965) 633.

[3] NICKLOW, R.M., VIJAYARAGHAVEN, P.R., (this conference)

[4] WOODS, A.D.B., POWELL, B.M., Phys. Rev. Lett. 15 (1965) 778.

[5] NG, S.C., BROCKHOUSE, B.N., Solid State Commun. 5 (1967) 79.

[6] TAYLOR, D.W., Phys. Rev. 156 (1967) 1017.

[7] WOODS, A.D.B., COCHRAN, W., BROCKHOUSE, B.N. Phys. Rev. 119 (1960) 980.

[8] ELLIOTT, R.J., TAYLOR, D.W., Proc. Roy. Soc. 296 (1967) 161.

COHERENT INELASTIC SCATTERING STUDY OF LOCAL AND IN-BAND MODES IN Cua$_{1-x}$Al$_x$ CRYSTALS*

R.M. NICKLOW, P.R. VIJAYARAGHAVAN, H.G. SMITH, G. DOLLING**
AND M.K. WILKINSON
SOLID STATE DIVISION,
OAK RIDGE NATIONAL LABORATORY,
OAK RIDGE, TENN., UNITED STATES OF AMERICA

Abstract

COHERENT INELASTIC SCATTERING STUDY OF LOCAL AND IN-BAND MODES IN Cu$_{1-x}$Al$_x$ CRYSTALS. To investigate the influence of light-mass substitutional defects on the lattice dynamics of a crystal, the normal mode frequencies in copper crystals containing 4.1 and 10.0 atomic % aluminium have been measured by coherent inelastic neutron scattering experiments on a triple-axis neutron spectrometer located at the Oak Ridge High Flux Isotope Reactor (HFIR). The results for these crystals differ markedly in at least two respects from the results for pure copper. The dispersion curves $\nu(\vec{q})$ for the in-band modes fall significantly below those for pure copper, and an additional vibrational mode has been observed with a frequency ν_L ($8.8 \pm 0.1 \times 10^{12}$ cps) which is higher than the maximum frequency in pure copper. This additional mode is interpreted as a local mode that corresponds to the vibrations of the light aluminium atom in the heavier copper matrix. To our knowledge this is the first observation of a local mode in a coherent neutron scattering experiment. Both the value of ν_L and the measured $\vec{q}$ dependence of the neutron scattering cross-section for the local mode are in good agreement with calculations based on a simple mass-defect theory which assumes a low defect concentration and no force constant changes. However, the same theory fails to predict the measured changes of the in-band modes: significant decreases in $\nu(\vec{q})$ are observed rather than the small increases that are predicted.

INTRODUCTION

The dynamics of crystal lattices with dilute concentrations of mass defects has been studied theoretically for a number of years [1]. The theory of inelastic scattering by such imperfect lattices has been discussed in considerable detail by Elliott and Maradudin [2], who emphasized the advantages of the coherent scattering experiments for studying the dynamics of these lattices. Recent coherent inelastic scattering experiments on the resonant in-band modes of crystals containing heavy substitutional impurities [3-5] show results in qualitative, though not always in quantitative, accord with theory. No comparable investigation of single crystals containing light impurities has been reported, although localized vibrational modes have been observed in neutron scattering experiments on polycrystalline metal samples [6-8].

In this paper we report some results of coherent inelastic neutron scattering measurements on copper single crystals containing 4.1 and 10.0 atomic % of aluminum atoms as substitutional, light-mass impurities. Both the in-band and localized modes have been examined. On the basis of the predictions of the mass-defect theory (assuming no force constant changes) one would expect the Cu-Al alloys to have interesting vibrational properties. The mass of aluminum is sufficiently low for a localized mode to

---

* Research sponsored by the US Atomic Energy Commission under contract with the Union Carbide Corporation.

** On leave from Chalk River Nuclear Laboratories, Chalk River, Ont., Canada, now returned.

exist above the band of copper, but the predicted frequency of the mode is near the band edge, resulting in a significant perturbation of the band modes.

On the other hand, it is not expected that the theory would be strictly applicable to an analysis of the present experiments. The aluminum concentrations in the crystals studied are not particularly dilute, and since the Cu-16% Al alloy exhibits measurable short range order [9], effects of short range order and/or force constant changes could be anticipated. Nevertheless, the mass-defect theory, as presented by Elliott and Maradudin [2], predicts many of the qualitative features of the present observations.

EXPERIMENTAL DETAILS AND OBSERVATIONS

The experiments were carried out at room temperature on a triple-axis neutron spectrometer located at the Oak Ridge HFIR [10], and the constant-$\vec{Q}$ method was used to measure neutron energy loss processes [11]. In all the measurements, the scattered neutron energy, E', was held fixed at 18.9 meV (4.5×10^{12} cps), using the (111) planes of a Ge analyzer, which had been squeezed at high temperature to increase the mosaic spread [12]. The (00.2) planes of a Be crystal were used as the monochromator.

The crystal samples were cylinders about 2 in. long. The Cu-4% Al crystal was 3/4 in. in diamter, and the Cu-10% Al crystal was 1 in. in diameter. In both samples a $(1\bar{1}0)$ crystallographic direction was within 20-30° of the cylinder axis and during the measurements this direction was oriented perpendicular to the plane containing the incident and scattered neutron beams. The mosaic spreads of the crystals were in the 0.2° - 0.3° range. The room temperature lattice parameters for Cu, Cu-4% Al, and Cu-10% Al are 3.615 Å, 3.625 Å, and 3.642 Å, respectively. Photoelectric analyses of samples taken from the Cu-Al crystals were used to determine the Al concentrations and to verify that the concentrations were satisfactorily uniform throughout the crystals.

Since the in-band frequencies of the Cu-Al alloys were to be critically compared with those of pure copper, a number of phonons, measured previously in copper on our ORR spectrometer [13], were remeasured on the HFIR spectrometer to check possible systematic differences in the results obtained on the two instruments. All such remeasurements agreed quite satisfactorily with the earlier data. In particular, the $L(\zeta\zeta\zeta)$ phonon frequencies used in some calculations discussed below agreed within 1/2%, except at the zone boundary, $\zeta = 0.50$, where the newer data give a frequency of $7.36 \pm 0.08 \times 10^{12}$ cps compared to the earlier measurement of 7.29 ± 0.20.

In Fig. 1 the results for identical constant-Q scans at the $\zeta\zeta\zeta$ zone boundary for Cu and for the Cu-Al crystals are compared. The scan for Cu shows only the expected peak from the coherent neutron scattering by the $L(\zeta\zeta\zeta)$ mode, and this zone boundary mode is the highest frequency mode observed in Cu. The results for the Cu-4% Al crystal are considerably different: the frequency of the $L(\zeta\zeta\zeta)$ zone boundary mode has decreased significantly and an additional peak has appeared at a frequency slightly above the band edge. The additional peak is interpreted as coherent inelastic neutron scattering by the vibrational modes that are localized near the Al sites. The results for the Cu-10% Al crystal show that increasing the Al concentration has decreased further the frequency of the $L(\zeta\zeta\zeta)$ zone boundary mode, while not affecting appreciably the peak position of the local mode scattering. Although no accurate comparison of the in-

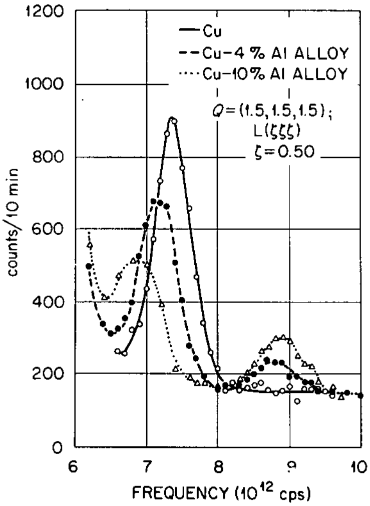

FIG.1. Constant $\vec{Q}$ scans obtained for Cu and two Cu-Al alloys showing peaks from scattering by both in-band and local modes. The $\vec{Q}$ components are in units of $2\pi/a$, where a is the lattice parameter.

tensity of the two Cu-Al samples has been attempted, the intensity of the local mode scattering at $\zeta = 0.50$ appears to have increased in rough proportion with the increase in the Al concentration. The high intensity at the low frequency end of these scans is the contamination resulting from high order diffraction processes in the monochromator and analyzer $(4E_0 - 9E' \simeq 0)$ simultaneous with $2\vec{k}_0 - 3\vec{k}' \simeq (442)$ in the sample.

The $\vec{Q}$-dependence for the local mode scattering intensity in the Cu-4% Al crystal has been reported recently [14] for $\vec{Q}$ in the [111] direction. It was found that the intensity observed in the constant-$\vec{Q}$ measurements was a maximum at the zone boundary and decreased as $|\vec{Q}|$ was varied (increased or decreased) to move away from the boundary. A selection of similar constant-$\vec{Q}$ measurements with the Cu-10% Al crystal is illustrated in Fig. 2. The fact that incoherent inelastic scattering makes a negligible contribution to the local mode peaks observed in the present work, is shown by the complete absence of a peak at $a\vec{Q}/2\pi = (2.1,2.1,2.1)$ in Fig. 2.

The intensity variation of the peaks with $\vec{Q}$ shown in Fig. 2 is qualitatively the same as that observed in Cu-4% Al. In addition, nearly all of the local mode peaks observed in the Cu-10% Al crystal seem to possess a "shoulder" on the high frequency side. Although, at present, these shoulders are barely outside counting statistics, there is a suggestion in these data that increasing the Al concentration has produced either a splitting of the previously triply degenerate local mode frequency or an impurity band which is asymmetric with respect to the original local mode frequency. The frequency width of the local mode scattering by the Cu-4% Al crystal was not significantly larger than that resulting from the instrumental resolution. Higher resolution experiments are planned to examine better the widths and shapes of the local mode peaks.

The results of measurements of the in-band modes in the Cu-Al crystals are more conveniently discussed in the next section where they are compared with theory.

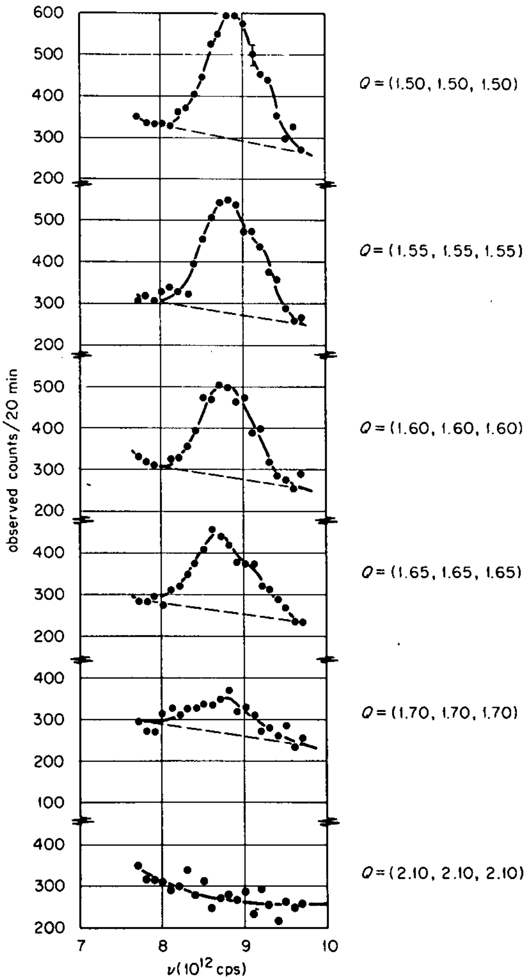

FIG. 2. Constant $\vec{Q}$ scans obtained for Cu-10% Al showing the $\vec{Q}$ dependence of the local-mode scattering intensity.

THEORETICAL DISCUSSION

The cross-section for coherent inelastic neutron scattering by the localized vibrational modes associated with a concentration, c, of isolated light-mass defects is, for neutron energy loss $E_0 - E' = h\nu$ [2, 15],

$$\frac{d^2\sigma}{d\Omega dE} = \frac{k'}{2k_0}(n_\ell + 1)\,\delta(\nu-\nu_\ell)\,\frac{c\nu_\ell b^2 \exp(-2W)}{M\,B(\nu_\ell)} \times$$

$$\sum_j (\vec{Q}\cdot\vec{e}_j(\vec{q})]^2 \left[\frac{b'/b-1}{\epsilon\nu_\ell^2} + \frac{1}{\nu_\ell^2-\nu_j^2(\vec{q})}\right]^2 \qquad (1)$$

where n_ℓ is the equilibrium number of phonons with frequency ν_ℓ, $\exp(-2W)$ is the Debye-Waller factor, b' and b are the scattering lengths of the impurity and host respectively, $\vec{Q}$ is the wave vector change $\vec{k}_0 - \vec{k}'$ of the neutron, $\vec{e}_j(\vec{q})$ and $\nu_j(\vec{q})$ are the polarization vector and frequency of the normal mode in the unperturbed crystal with wave vector $\vec{q}$ and branch index j; $\varepsilon = 1-(M'/M)$ where M' is the impurity mass and M is the host mass, and ν_ℓ is given by the solution of

$$\varepsilon\nu_\ell^2 \int \frac{g(\nu)d\nu}{\nu_\ell^2 - \nu^2} = 1 \qquad (2)$$

and

$$B(\nu_\ell) = \int \frac{\nu^2 g(\nu)d\nu}{(\nu_\ell^2-\nu^2)^2}$$

In these equations $g(\nu)$ is the frequency distribution function of the unperturbed host lattice.

The local mode frequency predicted by Equation (2) and the $g(\nu)$ for Cu [13] is 8.48×10^{12} cps, which is in good agreement with the experimental value of $8.8 \pm 0.1 \times 10^{12}$ cps deduced from measurements on Cu-4% Al [14]. The results for Cu-10% Al shown in Fig. 2 are consistent with those for Cu-4% Al. The close agreement between the measured and calculated values for ν_ℓ indicate that no large changes in the force constants have occurred. Consideration of concentration effects as discussed by Elliott and Taylor [16] qualitatively would tend to increase the calculated ν_ℓ and bring it into even closer agreement with experiment. On the other hand, one must not overlook the fact that the Cu lattice has expanded upon the addition of the Al impurities. It would be expected that an expansion of the unperturbed lattice would lower the force constants and, hence, lower the frequencies of the in-band modes and the ν_ℓ calculated with Equation (2).

In Fig. 3 the $\vec{Q}$ dependence in the [111] direction of the relative intensity of the local mode scattering is compared with that calculated using Equation (1) and the measured values of ν_ℓ and $\nu_j(\vec{q})$. Because $\vec{Q}$ lies along the [111] direction in these measurements, only the longitudinal $L(\zeta\zeta\zeta)$ branch contributes to the sum over j. The calculated curve and the experimental results have been adjusted to agree at $a\vec{Q}/2\pi = (1.55,1.55,1.55)$, and the indicated experimental errors are based on counting statistics only. The shaded region around the calculated curve is an estimate of the uncertainty in the calculations arising from the experimental errors in $\nu_j(\vec{q})$ and ν_ℓ. The Cu-4% Al results are in excellent agreement with the theory. The Cu-10% Al results are in poorer agreement, although if an impurity band exists in this crystal, Eq. (1) might not be expected to apply. Nevertheless, it is interesting to note that Eq. (1) can be brought into better agreement with the Cu-10% Al results if the values of $\nu_j(\vec{q})$ for the perturbed lattice are used in the calculation.

The $\vec{Q}$ dependence of the neutron cross section can be related to the spatial distribution of the vibrational displacements in the vicinity of the impurity atom. The second term in the square brackets in Eq. (1) is proportional to the Fourier transform of the classical Greens-function for the lattice which describes the response of the lattice to the displacements of an impurity [15]. Since the theory is in satisfactory agreement with the measured $\vec{Q}$-dependence of the cross section, the response of the Cu lattice to the displacements of the Al impurities may be estimated as sug-

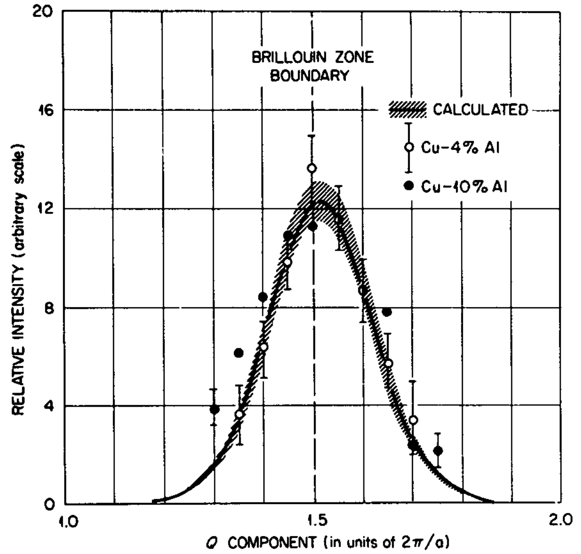

FIG.3. Comparison of the $\vec{Q}$ dependence of the measured relative intensity of the local-mode scattering in Cu-Al with that calculated using Eq.(1).

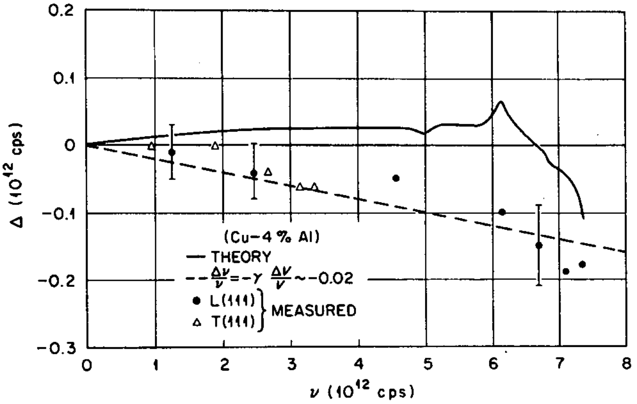

FIG.4. Experimental frequency shifts for Cu-4% Al compared to calculations.

gested by Maradudin [15]. For the range of $\vec{Q}$ studied in the present experiments the results obtained for the Cu-4% Al crystal indicate that the displacements of the Cu lattice decay exponentially with distance from the impurity atom with an inverse decay length in the [111] direction of 2.6/a, where a is the lattice parameter [14]. Thus, the impurity vibrational modes apparently are well localized; however, this result pertains to the asymptotic (distances greater than ∿ a) behavior of the displacements. To determine the behavior of the displacements very near the impurity site, the measurements and/or the theoretical calculations must be extended to values of $\vec{Q}$ further from the zone boundary.

The predictions of the theory with regard to the in-band modes is less satisfactory than for the local modes. In Fig. 4 is shown a comparison of the frequency shifts theoretically predicted [2] with those measured for the T($\zeta\zeta\zeta$) and L($\zeta\zeta\zeta$) modes in the Cu-4% Al crystal. Although the negative frequency shift, predicted for modes near the band edge, is in qualitative agreement with the experiment, the observed shifts for the lower frequency modes are also negative, whereas the theory predicts small positive shifts. Not unexpectedly, the disagreement between theory and experiment is even greater for the Cu-10% Al crystal as shown in Fig. 5, but at least some positive shifts for low frequency modes were observed in this crystal.

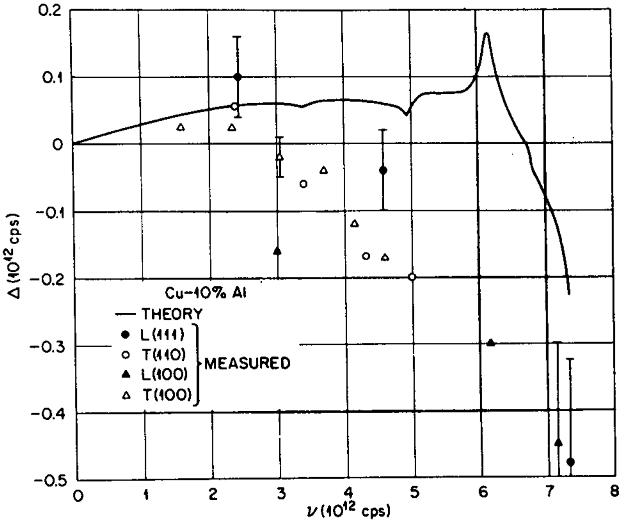

FIG.5. Experimental frequency shifts for Cu-10% Al compared to calculations.

As mentioned previously the addition of Al to Cu results in an expansion of the Cu lattice. One might argue that regardless of the fundamental mechanism that has caused the lattice to expand, if there are no large differences between the Al-Cu and Cu-Cu force constants, the total shift of the normal mode frequencies could be estimated by first considering the influence of the expansion of the lattice and then applying the mass-defect theory to the normal modes of the expanded lattice. For Cu-4% Al the increase in the volume of the unit cell over that of Cu is about 1%. The relative frequency change $\Delta\nu/\nu$ induced by the volume change $\Delta V/V$ may be estimated from $\Delta\nu/\nu \simeq -\gamma(\Delta V/V)$, where γ is an average Grüneisen parameter obtainable from thermodynamic properties [13]. For Cu, $\gamma \cong 2$, and as seen in Fig. 4 the observed frequency shifts, relative to the line $\Delta\nu \simeq -0.02\ \nu$, tend to be positive at low frequencies and negative only near the band edge. For Cu-10% Al similar qualitative arguments might apply, but concentration effects are probably beginning to be important in this crystal.

ACKNOWLEDGMENTS

The help of C. J. Sparks in obtaining the Cu-Al samples is gratefully acknowledged. We also thank R. C. Tseng and J. A. Krumhansl for helpful discussions.

REFERENCES

[1] MARADUDIN, A.A., in Astrophysics and the Many Body Problem, W.A. Benjamin, Inc., New York (1963), and references therein.

[2] ELLIOTT, R.J., MARADUDIN, A.A., Inelastic Scattering of Neutrons (Proc. Symp. Bombay, 1964) 1, IAEA, Vienna (1965) 231.

[3] SVENSSON, E.C., BROCKHOUSE, B.N., ROWE, J.M., Solid State Commun. 3 (1965) 245.

[4] MØLLER, H.B., MACKINTOSH, A.R., Phys. Rev. Lett. 15 (1965) 623.

[5] SVENSSON, E.C., BROCKHOUSE, B.N., Phys. Rev. Lett. 18 (1967) 858.

[6] MOZER, B., OTNES, K., THAPER, C., Phys. Rev. 152 (1966) 535.

[7] NATKANIEC, I., PARLINSKI, K., BAJOREK, A., SUDNIK-HRYNKIEWICZ, M., Phys. Lett. 24A (1967) 517.

[8] ZEMLYANOV, M.G., SOMENKOV, V.A., CHERNOPLENKOV, N.A., Soviet Phys. JETP 25 (1967) 436.

[9] BORIE, B., SPARKS, C.J.,Jr., Acta crystallgr. 17 (1964) 827.

[10] WILKINSON, M.K., SMITH, H.G., KOEHLER, W.C., NICKLOW, R.M., MOON, R.M., On-line computer-controlled triple-axis neutron spectrometers at the HFIR, these Proceedings, SM-104/83.

[11] BROCKHOUSE, B.N., Inelastic Scattering of Neutrons in Solids and Liquids (Proc. Symp. Vienna, 1960), IAEA, Vienna (1961) 113.

[12] DOLLING, G., NEIMAN, H., Nucl. Instrum. Meth. 49 (1967) 117.

[13] NICKLOW, R.M., GILAT, G., SMITH, H.G., RAUBENHEIMER, L.J., WILKINSON, M.K., Phys. Rev. 164 (1967) 922.

[14] NICKLOW, R.M., VIJAYARAGHAVAN, P.R., SMITH, H.G., WILKINSON, M.K., to be published.

[15] MARADUDIN, A.A., Solid State Physics (SEITZ, F., TURNBULL, D., Eds) 18, Academic Press, New York (1966) 18.

[16] ELLIOTT, R.J., TAYLOR, D.W., Proc. Roy. Soc. 296 (1967) 161.

LOCALIZED MODES, RESONANT MODES AND IMPURITY VIBRATIONAL BANDS IN VANADIUM ALLOYS

B. MOZER
NATIONAL BUREAU OF STANDARDS,
WASHINGTON, D.C.,
UNITED STATES OF AMERICA

Abstract

LOCALIZED MODES, RESONANT MODES AND IMPURITY VIBRATIONAL BANDS IN VANADIUM ALLOYS. Inelastic neutron scattering data have been obtained on several vanadium alloys using time-of-flight techniques. Localized impurity modes of vibration and a split impurity band have been observed in Be_xV_{1-x} alloys for $0.75 < x < 3.3$ at.%. The frequency of the localized mode observed in the lower concentration alloys occurs at about 0.047 eV, in agreement with the frequency predicted for a single isotopic impurity of the same mass ratio of beryllium to vanadium and using the experimental vanadium frequency distribution cut-off at 0.031 eV. As the concentration of beryllium is increased, the localized mode peak broadens and finally splits into two peaks at 3.3 at.% concentration of beryllium. Several theories of vibrational spectra of disordered alloys indicate structure in the impurity band; the theory favoured here for the explanation of our experiments is one that includes correlation of pairs of impurities. Assuming the observed splitting is caused by the proximity of another impurity, one finds the decay constant of the localized mode to be $2.5\ a_0^{-1}$.

Heavy mass atoms have been alloyed with vanadium to observe resonant modes of vibration and changes in the over-all frequency distribution. Inelastic neutron data were obtained on Ta_xV_{1-x}, W_xV_{1-x} and $Pt_{0.05}V_{0.95}$ alloys. None of the data for these alloys show peaks at the resonant mode frequencies expected for a single impurity or for resonant mode structure for a measurable concentration of impurities. Estimates of the effect expected for heavy solute atoms based on a single impurity calculation or an approximate theory of many impurities indicate resonant mode structure 20 to 50% above background for the alloys used when instrumental resolution is included. Such a large effect is easily observable within the accuracy of our experiments, yet no peaks were observed and even very little structure was observed in the ratio of the alloy data to pure vanadium data. An absence of resonant mode structure in our experiments and the small effects observed in experiments of other researchers indicate a more sophisticated theory is required which includes pair correlation of impurities and perhaps anharmonic effects.

Experiments have been initiated on alloys when the solute atoms have very different charge configurations than vanadium. Measurements of Cr, $Cr_{0.25}V_{0.75}$; and $Ni_{0.05}V_{0.95}$ have been made and frequency distributions estimated. Comparison of the high-frequency part of the spectrum for the pure metals and the $Ni_{0.05}-V_{0.95}$ alloy with $Cr_{0.25}V_{0.75}$ spectrum indicates that Ni atoms contribute 10 electrons to the electron bands. The additional Coulomb attraction of the +10 nickel ion is not strong enough to form bound states for the extra electrons and we have indirect proof that localized electron states do not exist in this alloy.

INTRODUCTION

Incoherent inelastic neutron scattering measurements have been used to determine the vibrational properties of pure vanadium. Incoherent inelastic scattering on vanadium alloys yields information about the "self-part" of the van Hove correlation function [1] for alloys or approximately the "self-part" of the displacement-displacement correlation function for the sum of the atoms in the alloy. Thus the frequency response of the square of the displacement of each atom in the alloy is probed and direct evidence obtained for any new defect modes of vibration that occur upon alloying.

It is extremely important in the study of vibrational properties of alloys to determine the basic structural properties of the alloys under investigation. Under certain conditions x-ray, neutron, or metallographic examinations can yield information about the alloys. Since many of the experiments have been chosen for the most part to investigate the vibrational properties of disordered alloys, one needs the assurance that the alloys are indeed disordered. Vanadium alloys are extremely convenient in this respect since many metals with widely varying properties can be alloyed with vanadium and the solubility of the metal (or the disorder) determined from an examination of the Bragg reflections obtained in neutron diffraction. A comparison between various analytical techniques can yield information about the properties of the disordered alloys.

EXPERIMENTAL EQUIPMENT AND ALLOY PREPARATION

The inelastic neutron scattering data were taken on the slow-chopper facility at the Brookhaven Graphite Research Reactor [2]. The resolution of this instrument and the incoming beryllium filtered beam is such that vibrational excitations less than 0.025 eV are broadened by the spread in the incoming filtered beam (0.0025 eV) and have a spectral shape determined by a combination of the vibrational excitation spectrum and triangular incoming beam. The resolution for vibrational excitations between 0.025 and 0.050 eV is broadened by a combination of the incoming filtered beam and resolution of the instrument yielding an approximately symmetrical resolution function of 0.004 eV width and the spectral shape dependent more on the spectrum of vibrational excitation.

Alloys were prepared by arc melting pure solute materials with 99.7% pure vanadium which is first melted to eliminate oxide impurities. Arc melted buttons of 10 gram size are formed of the alloy which can be cut into smaller pieces and powdered when necessary. Chemical analysis was obtained on each button and the powders to ascertain composition and x-ray and neutron diffraction patterns obtained on the powders. All concentrations reported upon here with respect to the alloys are atomic concentration.

RESULTS AND DISCUSSION

Neutron diffraction data were taken on the alloys reported here. An examination of the (110) reflection of pure vanadium and of the alloys was made, and from a comparison of the intensities of the (110) lines the impurity concentration in solution was determined. The patterns were also closely checked for non-vanadium lines to see if another phase was present. Solubilities determined from neutron diffraction data agreed with the concentration of solute determined chemically and it was established that the alloys were single phase and disordered.

All inelastic neutron scattering measurements were taken at room temperature to insure sufficient population of the vibrational modes and at a number of scattering angles to observe any angular dependence. A typical example of data of one scattering experiment is shown in Fig. 1 for the 3.3% Be alloy taken at 90° scattering angle with a flat background subtracted. The impurity band (.040 to .060 eV) is quite evident in this data and shows structure that has been observed in all measurements on this alloy. Changes in the impurity band with concentration are shown in Fig. 2 for .75%, 2.2%, 3.3% Be alloys, and pure vanadium in the region of the impurity band and with only a flat background subtracted from the raw data. Figure 3 shows reduced data which includes correction factors for chopper transmission, thermal occupation number, detector efficiency <u>and</u> a subtraction of the spectrum of pure vanadium in the impurity band region. The impurity band at lowest concentration represents essentially the localized vibrations of isolated beryllium atoms; the frequency of the localized mode measured (.047 eV) is in close agreement with the frequency predicted where one

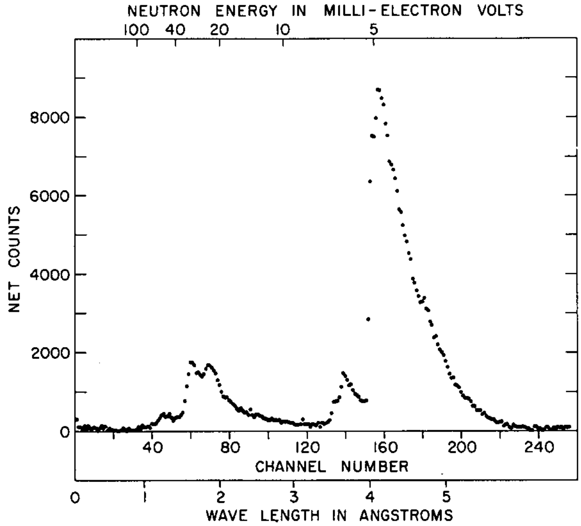

FIG.1. Time-of-flight spectrum of neutrons scattered 90° from $Be_{0.033}V_{0.967}$ at room temperature. Statistical errors are the size of the dots.

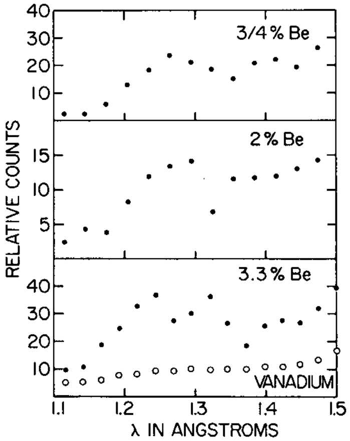

FIG.2. Neutron time-of-flight spectrum in region of the impurity band obtained on Be-V alloys and vanadium. Scattering angle was 90° and the samples at room temperature.

considers the Be atom to differ only in mass from vanadium and one uses the measured vanadium frequency distribution cut-off at .031 eV. As the concentration increases, the localized vibrations overlap and interact, causing a broadening and finally a splitting. Several theoretical explanations for this behavior are possible. Lifshitz [3] calculated the behavior of an isolated impurity band and noted that, when pair correlations were taken into account, an asymmetrical split peak was produced. Montroll calculated the splitting of the local mode peak into two symmetrical peaks for two impurities close together and suggests an asymmetry appears when his calculation is refined [4]. Evidence for asymmetrical splitting attributable

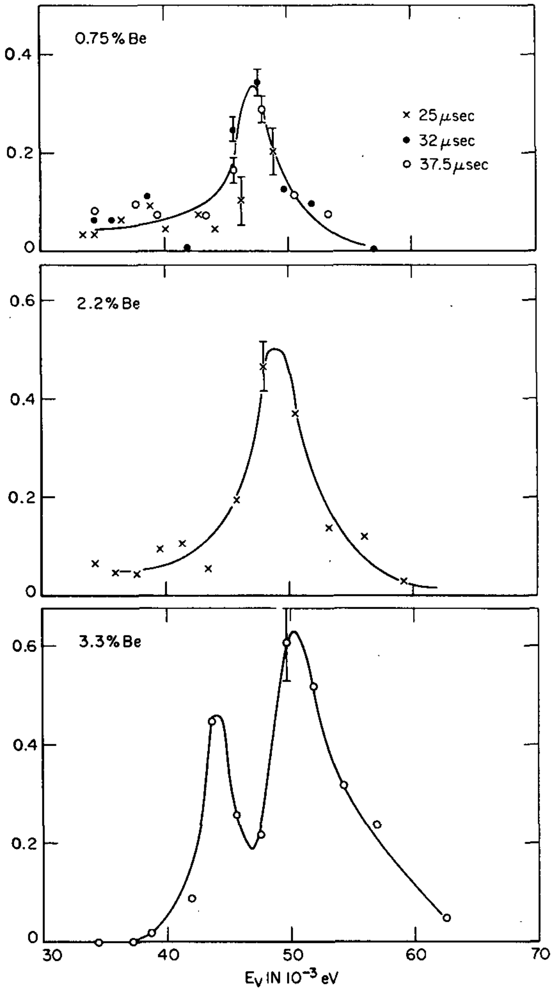

FIG. 3. Impurity band intensity for three Be-V alloys versus vibrational energy. Figures are a composite of many runs such as shown in Fig. 2 and with the pure vanadium spectrum subtracted from the data.

to pairs of impurities was noted in calculations of Dean [5] and Payton and Visscher [6], but more refined calculations are necessary for direct comparison. On the other hand, the Green's function technique of Langer [7], Maradudin [8], and Taylor [9] also indicate an asymmetric splitting of the impurity band. In these latter calculations any structure in the impurity band is only a reflection of the structure in the host lattice frequency distribution. Taylor's calculation is closest to reproducing the location and shape of the impurity band, but his attempt to add improvements by a self-consistent calculation causes a smearing of the spectra and a loss of structure. Here again no interaction between pairs is taken into account and no structure of the impurity band would occur for a structureless host spectrum. If the splitting is caused by the presence of another neighboring impurity, then the splitting could be estimated from the behavior of the amplitude of the localized mode. Figure 4 shows the exponential fall-off of the wave vector amplitude with distance of neighboring shells of atoms in <111> and <100> directions [10] using Fine's force constant model [11] for a b.c.c. lattice. We find the measured splitting agrees well with the splitting caused by two impurities a distance $\sqrt{11/4}\ a_0$ apart using the decay constant in Fig. 4 for the observed localized mode frequency. This distance is close to the average distance between impurities and we conclude that the splitting is indeed caused by the presence of neighboring impurities and that a calculated impurity band must include correlation between pairs. The asymmetry in the intensity is obtained from more refined calculations such as those of Lifshitz [3]. We note that the decay constant used in the calculation is $K \approx 2.5\ a_0^{-1}$.

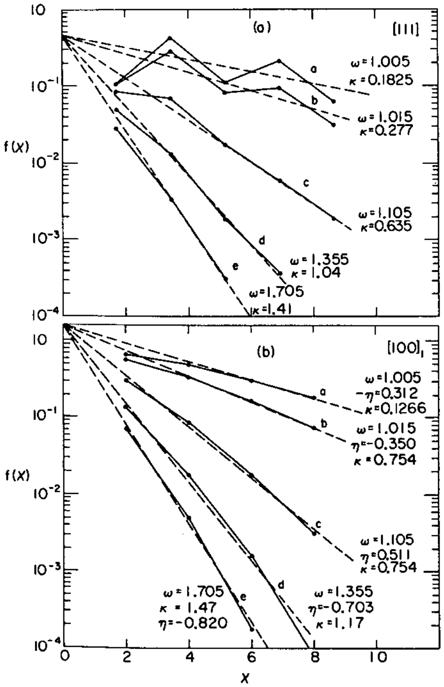

FIG.4. Vibrational amplitude for a localized mode for a single isotopic impurity in a bcc lattice using nearest and next-nearest neighbour central force constants [unpublished work of Leath and Mozer]. $\eta = (M'-M)/M$, κ is the exponential decay constant in units $2/a_0$, and χ the distance out to neighbouring shells of atoms.

A search for resonant modes of vibration associated with heavy mass atoms in vanadium was attempted on $Pt_{.05}V_{.95}$ [12], $Ta_{.02}V_{.98}$, $Ta_{.05}V_{.95}$, $W_{.02}V_{.98}$, and $W_{.05}V_{.95}$ alloys. The large cores (and charge differences) of these heavy ions will produce force constant changes. The changes observed in the spectra are very small except for the $Pt_{.05}V_{.95}$ alloy. The other four alloys have spectra exceedingly similar to the spectrum of pure vanadium and any differences arising from mass effects should be observable in the neutron wavelength region 2 to 3.5 angstroms or .007 - .025 eV neutron energy. Figure 5 shows the data for vanadium and for 5% alloys of Ta or W, the highest concentration of these alloys studied. The data has been averaged over three time-of-flight channels to yield the best statistics

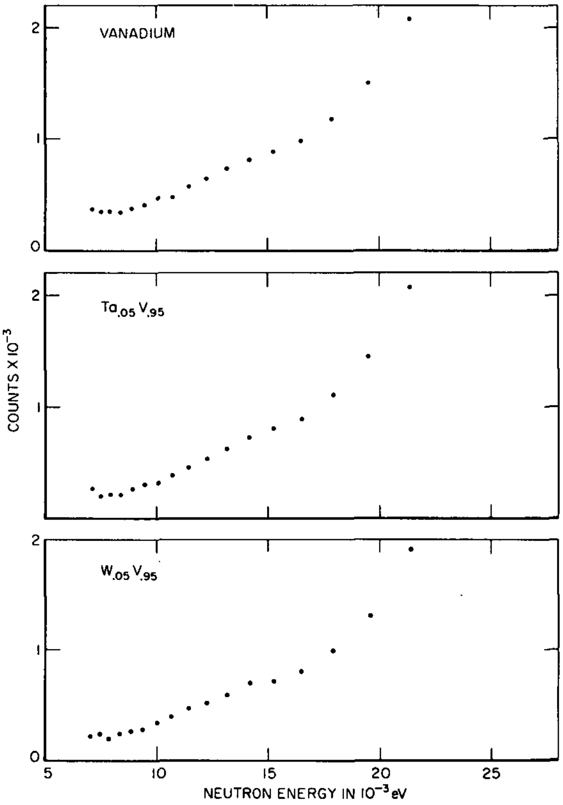

FIG. 5. Neutron time-of-flight spectrum in region of resonant mode frequency for vanadium and two alloys. Data was taken at 90° scattering angle and room temperature. The statistical errors are the size of the dots. Raw data minus a flat background is presented and three time-of-flight channels added together to improve statistics.

(2-3%), yet this averaging will not spoil the resolution in this region of the spectrum. One notes an absence of any large changes in the spectrum of the alloys compared to the spectrum of pure vanadium. In the $Pt_{.05}V_{.95}$ data, an indication of a broad band corresponding to a 5 to 10% change was observed [12] with a hint of a peak at 0.015 and 0.018 eV neutron energy. The other alloys yield even less an effect as noted in Fig. 5, except perhaps for the $W_{.05}V_{.95}$data where again one sees a hint of peaks at 0.0115 and 0.014 eV neutron energy. The $Ta_{.05}V_{.95}$ data and other TaV alloys show essentially no change in this region. The vibrational frequency midway between the small peaks agrees with calculation for a mass defect in vanadium. The appearance of the two small peaks is puzzling. It is worthwhile to consider at this point what theory indicates concerning the resonant modes of an alloy. First, for simplicity we assume the defects are dilute enough to examine the behavior of the impurity and a few shells of neighbors. The impurity itself has a Green's function frequency response which is of resonance shape, peaked at .010 eV and a width 0.003 eV according to the calculation of Leath and Mozer [10] using Fine's force constant model [11]. This peak would be 12% above the vanadium background for a 2% alloy and 30% above for a 5% alloy when one includes the additional broadening from the incoming beam. If we consider the nearest-neighbor shell of vanadium atoms, we find a resonance behavior in the same frequency region with a 20% effect for a 2% alloy and a 50% effect for a 5% alloy. Thus we expect a single resonant peak with a signal above vanadium scattering of about 100% for a 5% alloy and shape determined by the beryllium filtered beam. Looking now at the many-body Green's function techniques [8] or [9], we find the peak for the Green's function of the alloy to be of resonance shape and again 100% above the vanadium background. The single peak is expected because this latter calculation does not include correlations between pairs of impurities explicitly. The machine calculations on crystallites [6] indicate an enhanced response for the alloy over the pure material. A direct comparison with this calculation must await further refinements. Thus we can conclude that according to theory we should have seen a single large signal corresponding to resonant modes whereas one would not hesitate to say we see no change. What we see at best is two minute peaks in only two of the alloys studied. If these peaks are significant, we have demonstrated in the resonant mode behavior of the alloy the need for including correlation between pairs in the theory of resonant mode structure. The two peaks are again the splitting of a single peak when two impurities are sufficiently close to one another to interfere. It is possible to measure the amplitude of vibration of the resonant mode from this splitting, but we leave this for another occasion and for more convincing data. Our arguments about the resonant mode behavior can be extended to other measurements [13] where the observed structure in the alloy scattering is of weaker intensity than present calculations indicate. A final point must be made concerning possible mechanisms that broaden any structure and increase the difficulty of measurement of these modes. Phonon-phonon interactions and electron-phonon interactions would broaden the structure, but no evidence has been seen of such strong broadening mechanisms in single crystal measurements on similar alloys [14].

Frequency distributions of pure vanadium, pure chromium, $Cr_{.25}V_{.75}$ and $Ni_{.05}V_{.95}$ alloys were derived from neutron time-of-flight data. The pure chromium spectrum was obtained on a sample of pellets small enough to be considered a powder for this measurement. The incoherent approximation was used to derive the frequency distribution from the raw data and should be valid because of the small coherent cross-section of chromium relative to the large incoherent cross-section. The two alloys are essentially incoherent scatterers and yield the frequency distributions. Figure 6 shows the derived frequency distributions of pure vanadium and pure chromium. The chromium vibrational frequencies are much higher than those of vanadium, yet the over-all spectrum has a similar shape within our resolution. Additional van Hove singularities are present in the chromium data as well as some structure in the low frequency part of the spectrum. The latter structure could be spurious, does not change with angle, and could come from aluminum construction material in the scattered beam. The higher frequencies of chromium could be accounted for by attributing them to the increased coulomb interaction between higher charged chromium ion cores compared to lesser charged vanadium ion cores such as one expects for the bare ion plasma frequency. The ratio of the two frequencies at the upper end of the spectrum would be $(6/5)(a_V/a_{Cr})^{3/2} = 1.31$ which agrees with the maximum frequency and the frequency of the critical point near the high frequency end of the spectrum. We consider the number of band electrons to be 5 for vanadium and 6 for chromium. The vibrational spectrum of $Ni_{.05}V_{.95}$ has been previously reported [12]. We conjectured that nickel contributes 10 electrons to the conduction band and that its vibrational spectrum should be similar to a chromium-vanadium alloy of equal electron concentration. Figure 7 shows the frequency distribution for the two alloys where certain similarities and differences are observed. At the high frequency end of the spectra the features of the two alloys are

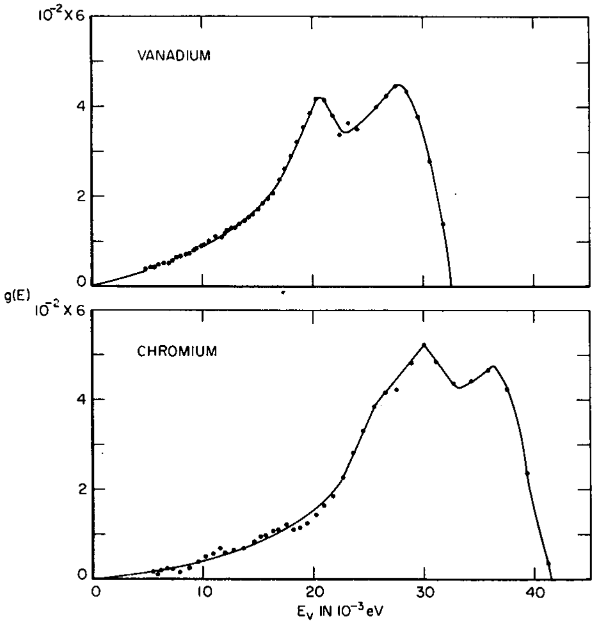

FIG. 6. Vibrational frequency distributions of pure vanadium and pure chromium obtained from incoherent neutron scattering on powder samples at 90° scattering angle and room temperature.

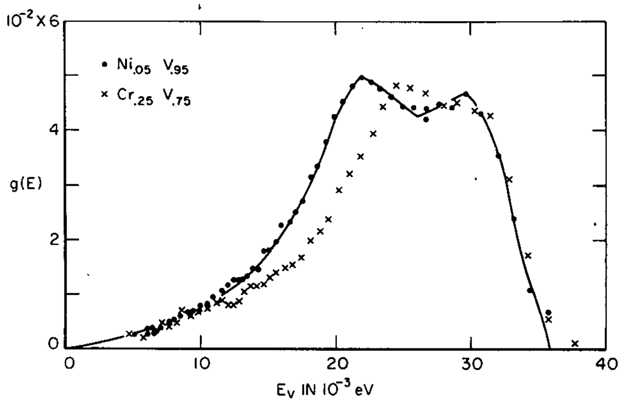

FIG. 7. Vibrational frequency distribution of $Ni_{0.05}V_{0.95}$ and $Cr_{0.25}$ $V_{0.75}$ alloys obtained from incoherent neutron scattering experiments at 90° scattering angle and room temperature.

similar; at the low frequency end the Ni-V spectrum resembles more the pure vanadium spectrum, especially the prominent low frequency critical point. The high frequencies of these alloys can be scaled from vanadium using the arguments presented above. On the other hand, one could imagine that the attractive coulomb potential of the +10 nickel ion core was large enough to produce bound electron impurity states and the effective inter-atomic potential thereby reduced. The vibrational spectrum of this alloy with the screened nickel ion cores would be even more like pure vanadium; the higher frequencies would be reduced in value. It is interesting to note that one can use the lattice dynamics of alloys to indirectly probe the electron properties of the alloy systems and we can state that the +5 extra coulomb attraction of the nickel ion core is not strong enough to produce a bound (local) electron impurity state.

ACKNOWLEDGEMENTS

The author would like to thank A. Cinquepalma for his help with many aspects of the experiment, and H. Palevsky for making the slow chopper available to the author and for continued interest and encouragement.

This research was substantially supported by the United States Atomic Energy Commission. The experiments were performed while the author was employed by Associated Universities, Inc., at Brookhaven National Laboratory.

REFERENCES

[1] VAN HOVE, L., Phys. Rev. 89 (1953) 1189.
[2] EISENHAUER, C.M., PELAH, I., HUGHES, D.J., and PALEVSKY, H., Phys. Rev. 109 (1958) 1046; MOZER, B., OTNES, K., and PALEVSKY, H., Lattice Dynamics, Pergamon Press, Oxford (1964), p. 63.
[3] LIFSHITZ, I.M., Advan. Phys. 13 (1964) 483.
[4] MONTROLL, E., private communication.
[5] DEAN, P., and BACON, M.D., Proc. Roy. Soc. (London) A283 (1965) 64.
[6] PAYTON, D.N., and VISSCHER, W.M., Phys. Rev. 156 (1967) 1032.
[7] LANGER, J.S., J. Math. Phys. 2 (1961) 548.
[8] MARADUDIN, A.A., Solid State Physics 18 (1966) 316.
[9] TAYLOR, D.W., Phys. Rev. 156 (1967) 1017.
[10] LEATH, P.L., and MOZER, B., unpublished.
[11] FINE, P.C., Phys. Rev. 56 (1939) 355.
[12] MOZER, B., OTNES, K., and THAPER, C., Phys. Rev. 152 (1966) 535.
[13] CHERNOPLEKOV, N.A., and ZEMLYANOV, M.G., Zh. Eksperim. i Teor. Fiz. 49 (1965) 449 [English transl.: Soviet Phys.--JETP 22 (1966) 315]; CHERNOPLEKOV, N.A., et al., Phys. Stat. Sol. 20 (1967) 767.
[14] MØLLER, H.B., and MACKINTOSH, A.R., Phys. Rev. Letters 15 (1965) 623.

LOCAL VIBRATIONS OF IMPURITY ATOMS IN COPPER AND LEAD

I. NATKANIEC, K. PARLIŃSKI, J.A. JANIK*,
A. BAJOREK AND M. SUDNIK-HRYNKIEWICZ
JOINT INSTITUTE FOR NUCLEAR RESEARCH,
DUBNA, USSR, AND
*INSTITUTE OF NUCLEAR PHYSICS,
CRACOW, POLAND

Abstract

LOCAL VIBRATIONS OF IMPURITY ATOMS IN COPPER AND LEAD. The inelastic neutron scattering technique was applied in the determination of the energy of the local vibrations of light impurity atoms in the alloys: Cu-Be (42 ± 2 meV), Cu-Mg (34.5 ± 2 meV), Pb-Na (17 ± 1 meV), and Pb-Mg (16 ± 1 meV). The structure of the samples examined was checked simultaneously by means of the elastic Bragg neutron scattering technique. For all alloys the energies of the local vibrations are lower than the values calculated assuming that the force constants of the impurity atom are equal to those of the host crystal. On the basis of the experimental values of the local vibration energy, the change in the force constants for the impurity atoms was estimated.

1. INTRODUCTION

The insertion into a crystal lattice site of an impurity atom of smaller mass than that of the matrix atom may give rise to local vibrations of a frequency higher than the maximum of the vibrations of the crystal [1, 2]. Experimental determination of the parameters of the local vibrations of light impurity atoms in the crystal lattice makes it possible to estimate directly the values of the impurity atom force constants and in alloys to estimate indirectly the variation in the conduction electron density. The results of these studies [3-6] show that the method of inelastic scattering may be particularly useful here. The purpose of this work, a continuation of that reported in Ref. [7], is to determine the energy of the local vibrations in binary alloys of copper and lead with light metals. A further aim of the work was to find samples for which the scattered neutron intensity would be high enough to allow subsequent determination of such paramaters as the width, shift and shape of the local vibration peak, which describe the anharmonicity introduced by the impurity atom.

2. THEORETICAL REMARKS

The interaction potential of the atoms in a pure metal (and thus its force constants) consists of the Coulomb potential of the bare ionic cores and the potential of interaction via the conduction electrons, in which the interaction of electrons with an ionic core is described by a pseudopotential and the screening interaction is described by the dielectric constant of the metal. By means of a potential defined thus, it is possible to calculate the dispersion curves of pure metals with satisfactory accuracy [8, 9].

The presence of the impurity atom introduces another local pseudopotential characteristic of a given atom and when the valencies differ, it also gives rise to a change in the density of the conduction electrons around the impurity atoms (Friedel oscillations) [10].

The frequencies of the local vibrations are given by the solutions to the equation

$$\left| \bar{G}(\omega^2)\delta\bar{L} - \bar{1} \right| = 0 \tag{1}$$

where $\bar{G}(\omega^2)$ is the Green function of the pure crystal [1], and $\delta\bar{L}$ is the matrix defining the perturbation caused by the presence of the impurity atom. Its elements depend on differences between the force constants of the impuritiy atoms and the host atoms. If we assume that the force constants of the impurity atom are identical to those of the host atoms, then the frequency of the local vibrations, ω_ℓ, for a cubic crystal is given by the solution to the equation

$$\epsilon\omega^2 \int_0^{\omega_{max}} \frac{g(\omega_0)\,d\omega_0}{\omega^2 - \omega_0^2} = 1 \tag{2}$$

where $\epsilon = 1 - (m'/m_0)$, m' is the mass of the impurity atom, m_0 is the mass of the host atom, $g(\omega_0)$ is the frequency spectrum of the host lattice, and ω_{max} is the maximum frequency of the host crystal vibrations.

The local vibrations can be observed by means of inelastic neutron scattering. The cross-section for the interaction between the neutron and the impurity atom and the lattice distortion caused by it is entirely incoherent. Assuming that there is no change in the force constants, this is expressed for a polycrystal of cubic symmetry by the formula [4]

$$\frac{d^2\sigma}{d\Omega dE} = c\,\frac{k}{k_0}\,e^{-W}\,\frac{\kappa^2}{2m_0}\,\frac{1}{\omega_\ell}\left(D\frac{d\ln\omega_\ell^2}{d\epsilon} + C\right) n_\ell\,\delta(\Delta E - \omega_\ell) \tag{3}$$

where

$$D = [(1-\epsilon)\bar{A} - A_0]^2 + C_0 - (1-\epsilon)C \tag{4}$$

$$\frac{d\ln\omega_\ell^2}{d\epsilon} = \left\{\epsilon^2\omega_\ell^4 \int_0^{\omega_{max}} \frac{g(\omega_0)\,d\omega_0}{(\omega_\ell^2 - \omega_0^2)^2} - \epsilon\right\}^{-1}, \quad n_\ell = \frac{1}{1 - e^{\omega_\ell/kT}} \tag{5}$$

c is the impurity concentration, k, k_0, E and E_0 are the wave numbers and energies of the scattered and incident neutrons, respectively, $\vec{\kappa} = \vec{k}_0 - \vec{k}$, $\Delta E = E_0 - E$, $\bar{A}$ and A_0 are the coherent neutron scattering lengths for the atoms of the host lattice and the impurity, and $4\pi C$ and $4\pi C_0$ are the incoherent cross-section of the atoms of the host lattice and the impurity.

The neutron scattering cross-section increases with increasing frequency of the local vibrations since function (5) grows rapidly when ϵ tends to unity. When there is a change in the force constants of the impurity atom with respect to the host atoms, the value of the cross-section also changes. Nevertheless, Eq.(3) is in general sufficient for estimating the intensity of the local vibration peak. Table I gives a com-

TABLE I. PROPERTIES OF THE ALLOYS STUDIED

Alloy	$\frac{m'}{m_0}$	ϵ	$4\pi\bar{A}^2$	$4\pi D$	$\frac{r_{host}-r_{imp.}}{r_{host}}$	Max. solubility c_{max} (at.%)	Temp. of max. solubility (°C)
Cu-Be	0.142	0.858	7.0	4.5	+ 0.133	16.4	866
Cu-Mg	0.383	0.617	7.0	1.3	- 0.250	7	722
Pb-Na	0.111	0.889	11.58	2.66	- 0.063	12	300
Pb-Mg	0.117	0.883	11.58	2.40	+ 0.086	6	253
Pb-Li	0.096	0.904	11.58	1.77	+ 0.131	3	235

parison of the cross-section for neutron scattering on atoms of the host lattice and the impurity atoms.

3. EXPERIMENTAL TECHNIQUE AND SAMPLE PREPARATION

The measurements were performed in the time-of-flight spectrometer operating in inverted-filter geometry at the IBR pulsed reactor (Fig. 1). Details of the spectrometer for inelastic incoherent neutron scattering (arm I) have been presented in Refs [11, 12]. In accordance with the concept presented in Ref. [13], arm II of the spectrometer was used for simultaneous measurement of the neutron diffraction patterns in order to check the sample structure.

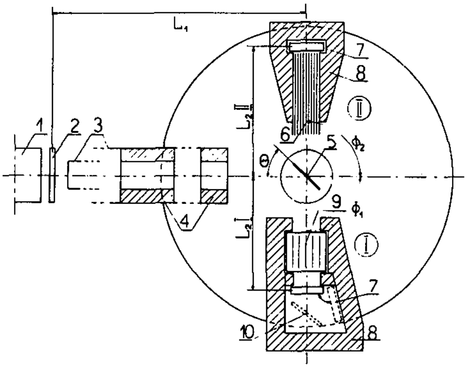

FIG. 1. Diagram of the IBR pulsed reactor facility: 1. reactor core, 2. moderator, 3. vacuum tubes, 4. collimators for incoming beam, 5. sample in low-temperature cryostat, 6. collimator for diffraction study, 7. detectors (trays of BF_3 counters), 8. shielding, 9. beryllium filter with collimating cadmium inserts, 10. zinc single crystal.

The duration of the thermal neutron pulse was approximately 200 μsec and the moderator-to-sample distance, L_1, was 20.4 m. Other spectrometer parameters during the measurements were:

I. Inelastic neutron scattering (arm I)
Energy analyser: Be filter,
Sample-to-detector distance: L_2I = 0.94 m
Mean scattered energy: 4.08 meV
Resolution: $\Delta\lambda/\lambda \approx 8\%$ for an energy transfer of 10 to 130 meV
Scattering angle: $\phi_1 = 90°$.

II. Elastic neutron scattering (arm II)
Sample-to-detector distance: L_2II = 0.95 m
Resolution $\Delta\lambda/\lambda$ = 1.5 to 2% for λ = 5 to 1 Å
Scattering angle: $\phi_2 = 90°$.

The distribution of inelastic neutron scattering for all the samples presented here displays a strong peak at a neutron energy transfer of approximately 60 meV. A similar peak is also observed in the distribution of neutrons scattered inelastically on beryllium with large momentum transfer. In our case this kind of scattering takes place in the beryllium filter, in which only vertical layers of absorbing material spaced every 40 mm were inserted in order to obtain higher transmission. Neutrons which are removed from the beam due to Bragg scattering in the Be filter may become scattered inelastically on the beryllium and be recorded by the detector before reaching the absorbing layer. Similar effects in the sample, namely, elastic Bragg scattering in the plane of the sample and subsequent inelastic multiphonon scattering of these neutrons in the direction of the detector, give rise to a certain structure of the phonon peak of beryllium. The position of these weaker peaks in the scale of the scattered energy depends on the angle θ of sample alignment with respect to the incident beam direction.

These effects are negligibly small in the case of thin samples (from 0.1 to 1 mm) of substances containing hydrogen which scatter neutrons inelastically. This is the primary subject of the work done with this spectrometer. For metal samples, yielding primarily elastic scattering and whose thickness is larger by an order of magnitude at the same transmission, the effects of multiple scattering (of the elastic-inelastic type) both in the sample and the Be filter become quite important. The effect due to the filter can be reduced considerably by the use of a grid of absorbing material, the spacings of which are shorter than the mean free path for a neutron scattered inelastically in beryllium ($\approx$ 1.35 cm). However, this would greatly decrease the transmission of the filter because of the double collimation. Another way of abating this effect is to shift the incident neutron spectrum towards the lower energies. The sample effect can be eliminated by the use of an absorbing grid in the sample (which would also lower the intensity considerably) or, as mentioned, by making an appropriate choice of the angle θ.

The metals Li, Be, Na, and Mg introduced as admixtures into copper or lead form with them solid substitutional solutions of limited solubility [14]. Some of the data characterizing this solubility are given in Table I. It decreases rapidly with lower temperatures and at room temperature did not exceed 1% for the alloys examined. Owing to the low value of the cross-section for neutron scattering with excitation of local vibrations of the impurity atoms (see Table I), samples of impurity concentrations higher than 1 at.% had to be used. The samples were prepared by melting the two metals in an argon atmosphere in a weight ratio appropriate for the given concentration. The copper-based alloys were annealed in vacuum at approximately 700°C (Cu-Mg) and 800°C (Cu-Be) in order to homogenize the composition in the solid state, and then hardened. To obtain samples of the required dimensions ($\emptyset \approx$ 20 cm), shavings were made which were then pressed in a special mould and placed in aluminium containers. The lead-based alloys, after homogenization in the liquid phase, were poured into a mould, rapidly solidified and hardened. Following this, the samples were worked down to an identical thickness of approximately 6 mm by cutting off the upper and lower sides of the ingot. The lead alloys of concentrations near maximum solubilities were measured some three hours after preparation. The pure metal samples of copper and lead were made under the same conditions as the alloy samples. During the measurements the samples were placed in a cryostat and cooled down to the temperature of liquid nitrogen, i.e. 77°K. The transmission of the samples was about 85%.

4. RESULTS OF MEASUREMENTS

Copper alloys

We had investigated the dynamics of $Cu_{0.98}$-$Be_{0.02}$ and $Cu_{0.95}$-$Be_{0.05}$ alloys about a year and a half previously [7], soon after the samples had been prepared. A check of the sample structure made then did not reveal the presence of the other phase in these samples. In the distribution of the neutrons scattered inelastically by these alloys we observed an additional peak at an energy of approximately 42 meV, which was interpreted as corresponding to the excitation of local vibrations of Be atoms in the Cu lattice. Since in the early stages of the aging process of supersaturated Cu-Be solid solutions precipitation of linear and two-dimensional distortions in the uniform structure of the solid solution (fcc as for Cu) called the α phase was observed, in the present measurements we attempted to determine whether the peak observed is perhaps due to the aging effects of the alloys.

The aging process of supersaturated Cu-Be solid solutions was studied by the anomalous X-ray scattering technique [15]. Aging proceeds slowly at room temperature (some 5.5 years are needed for phase equilibrium to be achieved) but at aging temperatures of up to about 170°C there is a characteristic precipitation of linear and, subsequently, two-dimensional regions approximately 25 Å thick and with a β'-phase structure (ordered alloy of CsCl structure, $a \approx 2.70$ Å). At higher aging temperatures the anomalous effects of linear and two-dimensional diffraction vanish and at temperatures around 400°C equilibrium between the α and β' phases is reached within some hours. Samples annealed at temperatures higher than 800°C for several hours and then hardened did not reveal any traces of anomalous scattering.

In our experiment the $Cu_{0.98}$-$Be_{0.02}$ sample aged naturally at room temperature for about $1\frac{1}{2}$ years and the $Cu_{0.95}$-$Be_{0.05}$ sample was annealed further in a vacuum furnace at 400°C for about 48 hours before being measured. According to Elistratov [15], in the $Cu_{0.98}$-$Be_{0.02}$ sample we should expect only linear and planar precipitates of β'-phase structure, whereas in the $Cu_{0.95}$-$Be_{0.05}$ sample there should be separate blocks of β'-phase crystallites in quantities corresponding to the state of α and β'-phase equilibrium at 400°C.

The diffraction patterns of the samples examined, a section of one of which is presented in Fig. 2, confirms these expectations. The diffraction pattern of the $Cu_{0.98}$-$Be_{0.02}$ alloy sample (curve 3) is identical with that of the pure copper sample (curve 1). The slight broadening of the peaks corresponding to the Bragg reflections from the α-phase fcc structure, as compared with the analogous peaks for pure copper, can be explained by the effect of anomalous scattering on the precipitates distorting this structure, as described above. In the diffraction pattern of the $Cu_{0.95}$-$Be_{0.05}$ sample (curve 4) we see distinct peaks corresponding to the β'-phase structure, while the peaks corresponding to the α-phase structure are shifted somewhat. This enables us to estimate that the lattice parameter is contracted by 1 to 2% relative to the lattice parameter of pure copper.

Figure 3 shows the distributions of neutrons scattered inelastically by the samples of copper alloys examined. The background has been subtracted and the measurement time and sample transmission have been normalized, but not the incident neutron beam itensity. Curves 3 and 4,

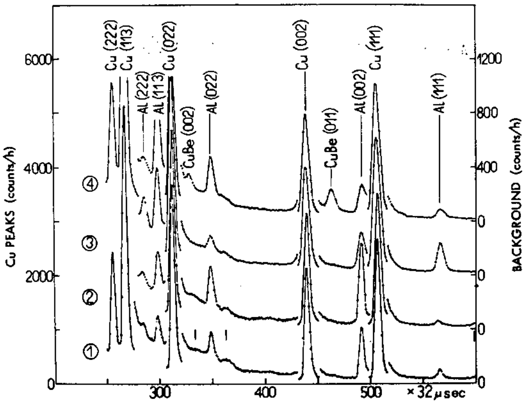

FIG.2. Section of the diffraction pattern for the investigated copper-based alloy samples: 1. Cu, 2. $Cu_{0.97}$-$Mg_{0.03}$, 3. $Cu_{0.98}$-$Be_{0.02}$, 4. $Cu_{0.95}$-$Be_{0.05}$.

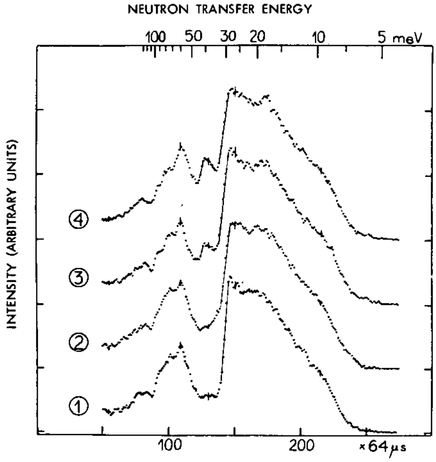

FIG.3. Inelastic neutron scattering distributions for the investigated copper-based alloy samples: 1. Cu, 2. $Cu_{0.97}$-$Mg_{0.03}$, 3. $Cu_{0.98}$-$Be_{0.02}$, 4. $Cu_{0.95}$-$Be_{0.05}$.

corresponding to the $Cu_{0.98}$-$Be_{0.02}$ and $Cu_{0.95}$-$Be_{0.05}$ alloys respectively, show an additional peak at a neutron energy transfer of approximately 42 meV which is not observed in the distribution of pure copper (curve 1). Comparison of the relative heights of this peak in the measurements presented here and those performed $1\frac{1}{2}$ years earlier [7] show that it has dropped by an estimated 30% for the $Cu_{0.98}$-$Be_{0.02}$ sample and by approximately 15% for the $Cu_{0.95}$-$Be_{0.05}$ sample. According to formula (3), the Be atom concentration in the Cu lattice should decrease in the same ratio. This corresponds to the precipitation of approximately 0.2% of the Be atoms from the α phase for the $Cu_{0.98}$-$Be_{0.02}$ sample and about 1.5% for the $Cu_{0.95}$-$Be_{0.05}$ sample.

These facts imply that the peak at 42 meV in the distributions of inelastic neutron scattering by Cu-Be alloys corresponds to the α-phase structure and hence to local vibrations of the Be atoms in the crystal lattice of copper. The dynamics of the β' phase may be revealed by a slight broadening of the observed peaks, relative to the measurements made earlier. An explanation of this problem requires measurements with a much better resolution and also measurements of the inelastic neutron scattering distribution for a sample of uniform β'-phase structure.

Curve 2 of Figs 2 and 3 corresponds to the $Cu_{0.97}$-$Mg_{0.03}$ alloy. The diffraction pattern of this alloys reveals small traces of a Cu_2Mg type structure. More substantial, however, is the fact that the peaks corresponding to the α-phase structure (fcc as for Cu) are shifted, indicating dilatation of the crystal lattice parameter by 1 to 2% as compared with that of pure copper. As the radius of the magnesium atom is larger than that of copper (see Table I), this is evidence that the Mg atoms occupy atom sites in the crystal lattice of copper.

In the distribution of the neutrons scattered inelastically by this sample we observe only an increase in the scattered intensity within the region of the maximum frequencies of the copper lattice vibrations. The shape of this distribution suggests that in the sample there are vibrations of frequencies higher than the maximum frequency of atomic vibrations in copper. Dividing this distribution by that for copper, we get a curve whose maximum corresponds to a neutron energy transfer of approximately 34.5 meV. This value was assumed to be the energy of the local vibrations of Mg atoms in the copper lattice. An alloy with the composition $Cu_{0.99}$-$Mg_{0.01}$ was also examined. No difference between this sample and the copper sample was found within the accuracy of the measurements.

The copper sample, to which curve 1 of Figs 2 and 3 corresponds, was produced from 99.9% pure electrolytic copper under conditions identical to those for the Cu-Mg alloys. The diffraction patterns for this sample and those Cu-Mg samples show insignificant traces of oxidation. The positions of the observed peaks corresponding to the CuO structure are indicated by arrows in Fig. 2. The traces of oxidation in the Cu-Be alloys are still smaller.

Lead alloys

Among the light metals which form solid solutions with lead, sodium, whose atoms bear the closest resemblance to those of Pb in their dimensions, has the highest solubility (see Table I). The Pb-Na solid solution (α phase) has a fcc structure, and the lattice parameter of lead ($a = 4.9497$ Å) is contracted with increased sodium concentration [14], even though Na atoms have a greater radius than Pb atoms do. When the sodium concentration exceeds maximum solubility, a β phase of the fcc structure of the Cu_3Au type ordered alloy ($a \approx 4.88$ Å) is precipitated. The range of homogeneity of this phase lies within 26.5 to 35 at.% Na and hence it does not include the Pb_3Na composition [16].

We examined the Pb-Na alloys in the 1 to 10 at.% Na concentration range. The neutron diffraction data of samples of concentrations lower than 5 at.% Na measured less than two months after sample preparation did not reveal any traces of the β phase. The diffraction pattern of samples with ~ 10 at.% Na taken immediately after the samples had been prepared had traces of peaks corresponding to the β-phase structure. These peaks appeared much more distinctly after this sample was aged for one month at a temperature of about 40°C. If we compare the intensities of the peaks corresponding to the α and β phases, we can estimate that the β-phase content in the aged sample does not exceed 5% (95% of the α phase would correspond to a $Pb_{0.91}$-$Na_{0.09}$ composition). Differences between the inelastic neutron scattering distributions measured under identical conditions did not exceed the accuracy of the measurements. With increased sodium concentration in the alloy we can also observe a slight shift of the peaks corresponding to the α-phase structure. This corresponds for the $Pb_{0.90}$-$Na_{0.10}$ sample to a contraction of the lattice parameter of approximately 1%. These facts imply that the effects observed in the inelastic neutron scattering distribution correspond to the phase structure in which the Na atoms occupy isolated sites in the crystal lattice of lead.

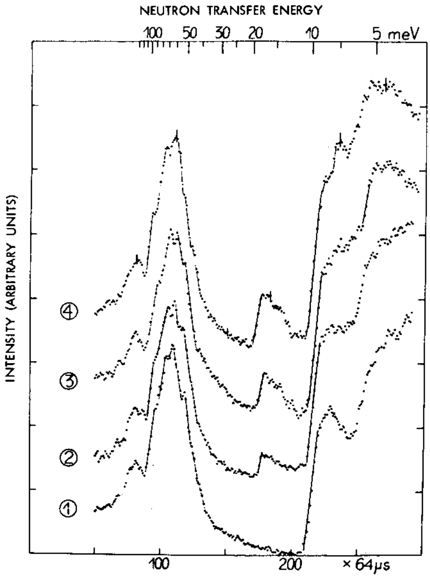

FIG.4. Inelastic neutron scattering distributions for the investigated lead-sodium alloy samples: 1. Pb, 2. $Pb_{0.98}$-$Na_{0.02}$, 3. $Pb_{0.95}$-$Na_{0.05}$, 4. $Pb_{0.90}$-$Na_{0.10}$.

In Fig.4 we have a comparison of the distributions of neutrons scattered inelastically by lead and some Pb-Na samples of different concentrations. In the lead distribution (curve 1) we can distinguish peaks at neutron energy transfers of about 5 meV and about 8.5 meV, which stand in good agreement with the maxima in the frequency spectra of lead [17, 18]. The severe drop in neutron intensity at the energy transfer of approximately 10 meV corresponds to the limit of the lead frequency spectrum. The reason for the peak at approximately 60 meV is discussed in section 3. In the distributions of the alloy we see an additional peak beyond the limit of the lead frequency spectrum, the amplitude of which is proportional to the concentration of Na atoms in the sample. This peak corresponds to a neutron energy transfer of about 17 meV and, in accordance with what has been said about the sample structure, is interpreted as due to the excitation of local vibrations of the Na atoms in the crystal lattice of lead. The width of this peak, being approximately 9%, is in conformity with the spectrometer resolution at this energy [11]. By comparing the distribution shown in Fig.4 in the range of the normal vibrations for lead, we see that with increasing concentration of Na atoms there is a rise in the scattered intensity at the limit of the frequency spectrum. This implies that in the region of the normal vibrations of lead there is an increased probability of excitation of high-frequency vibrations.

The solubility of magnesium in the solid phase of lead is much more limited than that of sodium (despite similar ratios of atomic radii), as the Mg atoms form with Pb an electronic bond, Mg_2Pb, of metallic properties. The structure of this compound is of the CaF_2 type (a = 6.85 Å).

We examined the Pb - Mg alloy in the concentration range from 1 to 5 at.% Mg. In the $Pb_{0.99}$-$Mg_{0.01}$ and $Pb_{0.97}$-$Mg_{0.03}$ samples, without hardening after moulding and measured some two months after preparation, there was no additional peak beyond the limit of the natural vibrations of lead. Only a slight rise in the intensity of the scattered neutrons was observed in the region of the maximum frequencies of the lead vibrations. The diffraction patterns of these samples revealed the presence of an Mg_2Pb type structure. In the $Pb_{0.95}$-$Mg_{0.05}$ sample, hardened immediately after solidification and cooled to the temperature of liquid nitrogen some two hours after preparation, we observed an additional peak at a neutron energy transfer of approximately 16 meV, which was assigned to the excitation of the local vibrations of the Mg atoms. A strong rise in the scattered intensity was observed in the high-frequency region of the normal vibrations of lead. The diffraction pattern of the sample showed traces of a Mg_2Pb structure in quantities not higher than for the $Pb_{0.97}$-$Mg_{0.03}$ sample.

The region of lithium solubility in solid lead is even more restricted owing to the considerable difference in the atomic radii and valencies. The diffraction patterns of the samples examined with $Pb_{0.99}$-$Li_{0.01}$ and $Pb_{0.97}$-$Li_{0.03}$ compositions and hardened after solidification, show the presence of a PbLi phase of bcc structure of the CsCl type (a ≈ 5.25 Å). In the distributions of neutrons scattered inelastically by these samples only the effects of neutron absorption by Li atoms are observed. No effects of neutron scattering on Li atoms exceeding the accuracy of the measurements were found. To observe them, the effect-to-background ratio would have to be improved by increasing the incident beam intensity and the effect of the Be filter would have to be eliminated.

5. DISCUSSION

In all the alloys examined the experimentally determined energy of the local vibrations of light impurity atoms is lower than the value calculated with the assumption that the force constants around the impurity atom remain unchanged (Eq.(2)). Table II gives a comparison of the local vibration energies calculated for different frequency spectra of copper and lead. The greatest effect on the calculated values of the local vibration energy is borne by the high-frequency vibrations of the host crystal lattice. This fact is illustrated by the differences in the results calculated for the Sinha and Debye spectra, in which the Debye limit frequency for copper was taken to be equal to that of the Sinha spectrum. The assumed limit frequency of the Debye spectrum for lead corresponds to 88°K. The most realistic frequency spectra are the Sinha spectrum for copper [21] and the

TABLE II. COMPARISON OF THE LOCAL VIBRATION ENERGIES CALCULATED FOR DIFFERENT FREQUENCY SPECTRA AND THE DERIVED CHANGES IN FORCE CONSTANTS

Alloy	Local vibration energy		$\frac{E_{th} - E_{exp}}{E_{th}}$ (%)	Change in force constants from Eq.(6)	References for $g(\omega_0)$
	Experimental value (meV)	Calculated from Eq.(2) (meV)			
Cu-Be	42 ± 2	54.0	22	0.43	[19]
		56.1	25	0.50	[20]
		57.9	28	0.56	[21]
		61.5	31	0.60	Debye spectrum
Cu-Mg	34.5 ± 2	34.2	0	0.00	[19]
		35.9	3	0.10	[20]
		37.5	8	0.22	[21]
		38.7	11	0.27	Debye spectrum
Pb-Na	17 ± 1	18.75	9	0.16	Debye spectrum
		19.25	12	0.23	[18]
		19.70	14	0.27	[17]
Pb-Mg	16 ± 1	17.9	11	0.20	Debye spectrum
		18.7	14	0.30	[18]
		19.2	17	0.34	[17]

Stedman spectrum for lead [18] calculated from the experimentally determined dispersion curves for these metals.

To assess the change in the force constants from the experimentally determined energy for the local vibrations of the impurity atom, we shall make use of the approximation of an extremely light impurity. With this assumption the non-diagonal elements of the $\bar{G}(\omega^2)\delta\bar{L}$ matrix are negligible. The local frequency will be given in the following integral equation (for cubic crystals):

$$\left[\epsilon\omega^2 - p\int_0^{\omega_{max}} \omega_0^2 g(\omega_0)\, d\omega_0\right] \int_0^{\omega_{max}} \frac{g(\omega_0)\, d\omega_0}{\omega^2 - \omega_0^2} = 1 \qquad (6)$$

where

$$p = 1 - \frac{\phi(00)}{\phi^0(00)}\ , \quad \phi^0(00) = m_0 \int_0^{\omega_{max}} \omega_0^2\, g(\omega_0) d\omega_0$$

$\phi^0(00)$ and $\phi(00)$ are the force constants of the host atoms and impurity atoms, respectively. The impurity atom is at the site $\ell = 0$. The parameter p defines the magnitude of the change in the force constants of the impurity atom in the zeroth co-ordination sphere. Its value for various frequency spectra are given in Table II.

This approximation can also be applied for rather heavier impurities, but the perturbation caused by the impurity should spread out to larger distances and at the same time the change of the force constants of the first co-ordination spheres should be negligible, i.e.

$$|\Delta\phi(0\ell)| < |\Delta\phi(00)| \qquad \text{where } \ell > 0$$

The force constants of the zeroth co-ordination sphere are associated with the remaining ones by the relationship

$$\phi(00) = -\sum_{\ell} \phi(0\ell) \qquad (7)$$

A better approximation would be obtained with a model in which only the force constants of the zeroth and first co-ordination spheres become changed. Their change can be determined from the experimental value of the local vibration energy and the dispersion curves of the host crystal [22]. For beryllium atoms in copper the result of such calculations is

$$p = \frac{\Delta|\phi(00)|}{|\phi(00)|} \approx \frac{\Delta|\phi(01)|}{|\phi(01)|} \approx 70\%$$

The estimation of the contribution of the long-range forces of Coulomb, ion-electron, and electron-electron interactions (causing a change in the force constants in the higher-order co-ordination spheres) gives the following assessment of the changes in the force constants for this alloy [22]

$$\frac{\Delta|\phi(00)|}{|\phi(00)|} = 65\%, \qquad \frac{\Delta|\phi(01)|}{|\phi(01)|} = 55\%$$

A comparison of these results with the values of the parameter p for Cu - Be in Table II shows the differences in the estimate of p in dependence on the model assumed. Unfortunately, a complete solution of Eq.(1) which would give an exact value for the local frequency is impossible and a simplifying model must be used.

Determination of the energy of the vibrations of light atoms in ordered phases of the alloys investigated should enable us to assess the effect of the force constants change of the higher-order co-ordination spheres on the local vibration energy, and also facilitate the choice of a model corresponding more close to the actual situation in a crystal. No changes exceeding the measurement accuracy were observed in the local vibration energy as a function of impurity atom concentration within the range of the solid solution phase.

To get more precise and complete information on the dynamics and interaction of atoms in the crystals of metals, measurements with much better resolution should be made. Of the alloys discussed here, the Cu-Be and Pb-Na alloys are best suited for this type of research, owing to the high intensity of neutron scattering and the structure of the solid phase. The time-of-flight technique and inverted-filter geometry are convenient for this type of research, as they permit simultaneous measurement of the structure and the dynamics of the sample.

ACKNOWLEDGEMENTS

The authors express their gratitude to Professor H. Niewodniczański and Professor F.L. Shapiro for their interest in this work, and to Professor B. Buras for discussions concerning the methods of checking the sample structure.

REFERENCES

[1] MARADUDIN, A.A., Solid State Physics 18 (1966) 274; 19 (1967) 2.
[2] LIFSHITS, I.M., Usp.fiz.Nauk 83 (1964) 617.
[3] KAGAN, Yu.M., IOSILEVSKY, Ya., Zh. èksp.teor.Fiz. 44 (1963) 1375.
[4] KRIVOGLAZ, M.A., Zh.èksp.teor.Fiz. 40 (1961) 567.
[5] ELLIOTT, R.J., MARADUDIN, A.A., Inelastic Scattering of Neutrons (Proc.Symp.Bombay, 1964) 1, IAEA, Vienna (1965) 231.
[6] PARLIŃSKI, K., Postępy Fiz. 16 (1965) 667.
[7] NATKANIEC, I., PARLIŃSKI, K., BAJOREK, A., SUDNIK-HRYNKIEWICZ, M., Phys. Lett. 25A (1967) 517.
[8] BROVMAN, E.G., KAGAN, Yu.M., Zh.èksp.teor.Fiz. 52 (1967) 557.
[9] ANIMALU, A.O.E., BONSIGNORI, F., BORTOLANI, V., Nuovo Cim. 64B (1966) 159.
[10] FRIEDEL, J., Phil. Mag., Suppl. 3 (1954) 496; Nuovo Cim. Suppl. 7 (1958) 287.
[11] BAJOREK, A., MACHEKHINA, T.A., PARLIŃSKI, K., SHAPIRO, F.L., Inelastic Scattering of Neutrons (Proc.Symp.Bombay, 1964) 2, IAEA, Vienna (1965) 519.
[12] PARLIŃSKI, K., SUDNIK-HRYNKIEWICZ, M., BAJOREK, A., JANIK, J.A., OLEJARCZYK, W., Research Applications of Nuclear Pulsed Systems (Proc.Panel Dubna, 1966), IAEA, Vienna (1967) 179.
[13] BURAS, B., Institute of Nuclear Research, Świerk, Rep.702/II/PS (1966); Research Applications of Nuclear Pulsed Systems (Proc.Panel Dubna, 1966), IAEA, Vienna (1967) 17.

[14] HANSEN, M., ANDERKO, K., Constitution of Binary Alloys, McGraw-Hill Book Co., New York, Toronto, London (1958).

[15] ELISTRATOV, A.M., FINKELSHTEIN, S.D., PASHILOV, A.I., Dokl.Akad. Nauk SSSR 68 (1949) 1017; ELISTRATOV, A.M., FINKELSHTEIN, S.D., GOLDSHTEIN, T.Yu., Dokl.Akad.Nauk SSSR, 88 (1953) 669; ELISTRATOV, A.M., Dokl.Akad Nauk SSSR 101 (1955) 69.

[16] MAKAROV, E.S., POPOVA, Z.V., Izv.Akad.Nauk SSSR, Otdel.khim.Nauk (1951) 337.

[17] GILAT, G., Solid State Comm. 3 (1965) 101.

[18] STEDMAN, R., ALMQUIST, L., NILSON, G., Phys. Rev. 162 (1967) 549.

[19] JACOBSEN, E.H., Phys. Rev. 97 (1955) 654.

[20] LEIGHTON, R.B., Rev.Mod. Phys. 20 (1948) 165.

[21] SINHA, S.K., Phys. Rev. 143 (1966) 422.

[22] PRIEZZHEV, V.B., Dubna Preprint 3746 (1968).

ИССЛЕДОВАНИЕ ПРИМЕСНЫХ СОСТОЯНИЙ В СПЛАВАХ НА ОСНОВЕ ВАНАДИЯ

М.Г.ЗЕМЛЯНОВ, С.П.МИРОНОВ
Г.Ф.СЫРЫХ
ИНСТИТУТ АТОМНОЙ ЭНЕРГИИ
им.И.В.КУРЧАТОВА, МОСКВА,
СССР

Abstract — Аннотация

INVESTIGATION OF ADMIXED STATES IN VANADIUM ALLOYS. The results are given of research into quasi-local states caused by the introduction of different substitutional atoms of impurities into a vanadium metal crystal lattice.

The results obtained are compared with theoretical calculations carried out using different model assumptions, and with results of experimental work done at other scientific centres.

Research into inelastic scattering of cold neutrons is being done on an assembly at the IRT-M reactor at the Kurchatov Institute of Atomic Energy. The spectral line of incident neutrons is established using a beryllium filter cooled by liquid nitrogen and a mechanical chopper. The energies of neutrons scattered at an angle of 90° are analysed at a distance of 4.5 m by the time-of-flight method. The excitation spectra for the systems studied, derived from the experimental results, are established with allowance for all necessary instrument corrections.

ИССЛЕДОВАНИЕ ПРИМЕСНЫХ СОСТОЯНИЙ В СПЛАВАХ НА ОСНОВЕ ВАНАДИЯ. Приводятся результаты исследования квазилокальных состояний, обусловленных введением различных примесных атомов замещения в кристаллическую решетку металлического ванадия.

Полученные результаты сравниваются с данными теоретических расчетов, проведенных в различных модельных предположениях, а также с результатами экспериментальных исследований, выполненных в других научных центрах.

Исследования по неупругому рассеянию холодных нейтронов проведены на установке, смонтированной на реакторе ИРТ-М в ИАЭ им.И.В.Курчатова. Формирование спектральной линии падающих нейтронов обеспечивается с помощью Ве-фильтра, охлаждаемого жидким азотом, и механического прерывателя. Энергетический анализ нейтронов, рассеянных под углом 90°, осуществляется на расстоянии 4,5 м по времени пролета. Восстановление спектров возбуждения исследованных систем из экспериментальных результатов проводится с учетом всех необходимых аппаратурных поправок.

Твердые растворы замещения представляют собой системы, обладающие простейшим типом дефектов – дефектами замещения. При этом примесные атомы, находящиеся в узлах кристаллической решетки, отличаются от атомов матрицы величиной массы, строением электронной оболочки и значениями атомных радиусов. Различие размеров атомов растворителя и растворенного элемента приводит к искажению кристаллической решетки. Как правило, при растворении элементов с меньшим атомным радиусом, чем атомный радиус растворителя, период решетки уменьшается, а при растворении элементов с большим атомным радиусом период решетки возрастает. Средние значения искажений кристаллической решетки в сплавах превышают разность атомных радиусов сплавляемых металлов. Следовательно, эти искажения нельзя рассматривать как результат несовпадения размеров ионов металла. Здесь, несомненно, проявляется перераспределение электронной плотности в решетке растворителя под действием атомов растворенного металла.

Различие в электронной структуре атомов матрицы и атомов примесного элемента должно приводить к различию в характере или величине взаимодействия между атомами примеси и атомами матрицы, по сравнению с межатомным взаимодействием в исходной матрице.

Таким образом, все три упомянутых фактора приводят в результате к деформации спектра колебаний исходной матрицы при введении в нее примесных атомов.

Наиболее детальная информация о колебаниях кристаллической решетки металла с введенными в нее примесями может быть получена из экспериментов по неупругому рассеянию нейтронов.

К настоящему времени уже выполнены исследования с помощью рассеяния нейтронов для целого ряда сплавов [1 – 5]. Однако, большой интерес представляет проведение исследований для сплавов, полученных на основе одной и той же матрицы.

Среди некогерентно рассеивающих систем наиболее приемлемыми являются твердые растворы на основе металлического ванадия. Ванадий образует, хотя и в ограниченной области концентраций, твердые растворы с целым рядом элементов, отличающихся как атомным радиусом, так и электронной структурой и массой [6]. Ванадий является элементом полностью некогерентно рассеивающим нейтроны, и в этом случае не возникает вопрос о влиянии когерентных эффектов при изучении неупругого рассеяния нейтронов.

Кроме того, ванадий является одним из двух элементов [7], для которых проведено строгое, безмодельное восстановление колебательного спектра из экспериментальных данных по рассеянию нейтронов. Наличие такой информации о фононном спектре дает возможность провести более корректное сравнение экспериментальных данных, получаемых для сплавов на основе ванадия, с различными теоретическими предположениями.

В связи с этим нами начаты исследования для целого ряда сплавов на основе ванадия и к настоящему времени выполнены экспериментальные измерения для сплавов ванадия с примесью тантала (3% ат) и вольфрама (3% ат).

ИЗМЕРЕНИЕ, РЕЗУЛЬТАТЫ И ОБСУЖДЕНИЕ

Все исследования ванадиевых сплавов проводятся на установке по рассеянию холодных нейтронов, смонтированной на реакторе ИРТ-М в ИАЭ им.И.В.Курчатова.

Для монохроматизации падающих нейтронов используется поликристаллический фильтр из металлического бериллия (длина 50 см), охлаждаемый до температуры жидкого азота, и механический прерыватель с параболической формой щели.

На рис.1 приведен вид спектральной линии нейтронов, падающих на исследуемый образец. Для сравнения на рис.1 дана спектральная линия, получаемая непосредственно после бериллиевого фильтра.

Применение механического прерывателя позволяет значительно уменьшить размытие падающей спектральной линии, что очень существенно для исследований при малых передачах энергии.

Как следует из наклона бериллиевого скачка, разрешение спектрометра по времени пролета составляет 1,8%.

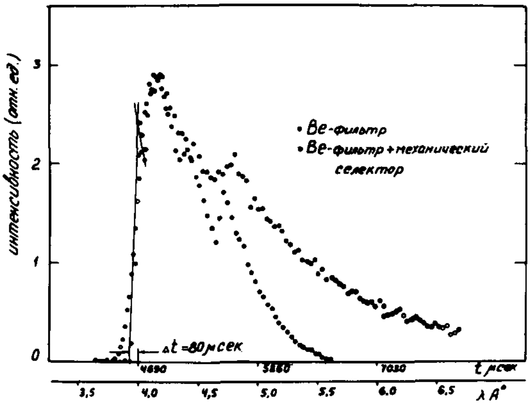

Рис.1. Спектральная линия падающих нейтронов.

Образец исследуемого сплава располагался на расстоянии 29 см от центра ротора прерывателя, под углом 45°, в отражающем положении.

Неупруго рассеянные нейтроны исследовались по времени пролета под углом 90° к направлению падающих нейтронов. Регистрация рассеянных нейтронов осуществлялась на расстоянии 4,5 м от образца с помощью детектора, состоящего из 25 пропорциональных счетчиков, наполненных обогащенным BF_3 до давления в одну атмосферу. На установке имеется возможность проводить исследования с регистрацией рассеянных нейтронов детектором аналогичной конструкции, но заполненным гелием-3 до давления 8 атм. Однако, при исследовании рассеяния с малыми изменениями энергии, как это имеет место при изучении ванадиевых сплавов с тяжелыми примесными атомами, использование счетчиков с гелием-3 под давлением становится нецелесообразным из-за относительно более высокого фона, по сравнению с фоном у детекторов BF_3. Были исследованы сплавы $V_{0,97}$ $Ta_{0,03}$ и $V_{0,97}$ $W_{0,03}$.

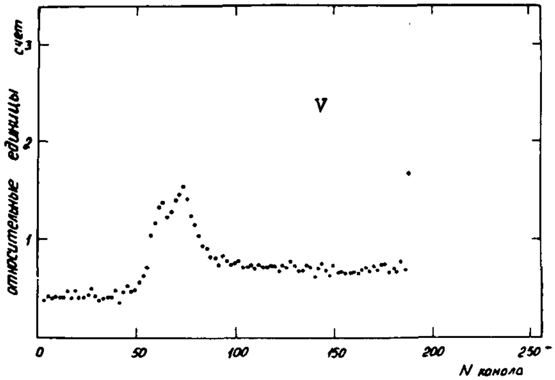

Рис.2. Спектр неупруго рассеянных нейтронов ванадием.

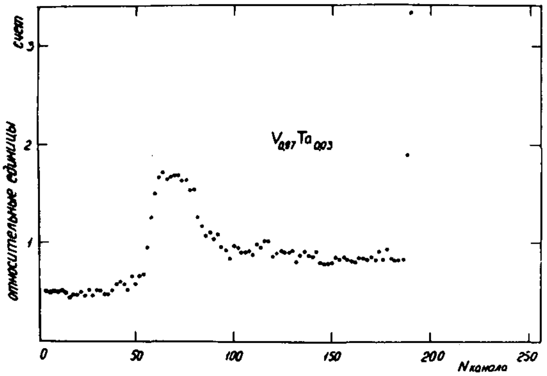

Рис.3. Спектр неупруго рассеянных нейтронов сплавом ванадий-тантал.

Используемые образцы представляли собой диски или порошки, помещаемые в тонкостенные алюминиевые контейнеры. Эффективная толщина всех образцов составляла $<\frac{1}{4}$ длины упругого рассеяния падающих нейтронов, что позволяло не учитывать влияния процессов многократного рассеяния на окончательные результаты.

На рис.2 приведены исходные экспериментальные результаты для ванадия, а на рис.3 и рис.4, соответственно, – для сплавов $V_{0,97}$ $Ta_{0,03}$ и $V_{0,97}$ $W_{0,03}$.

Введение всех необходимых аппаратурных поправок (фон быстрых и тепловых нейтронов, рассеяние на воздухе, энергетическая зависимость эффективности детектора) дает возможность получить из приведенных данных дважды дифференциальное сечение рассеяния нейтронов ($d^2\sigma/d\Omega d\epsilon$). Величина фона определялась в независимых экспериментах с пустыми держателями образцов.

Для некогерентно рассеивающих систем, какими являются и сплавы на основе ванадия, измеряемое экспериментально дважды дифференци-

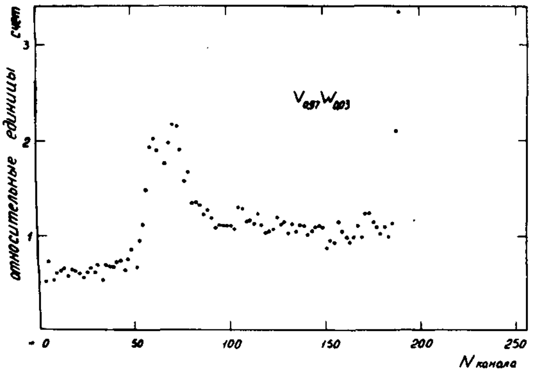

Рис.4. Спектр неупруго рассеянных нейтронов сплавом ванадий-вольфрам.

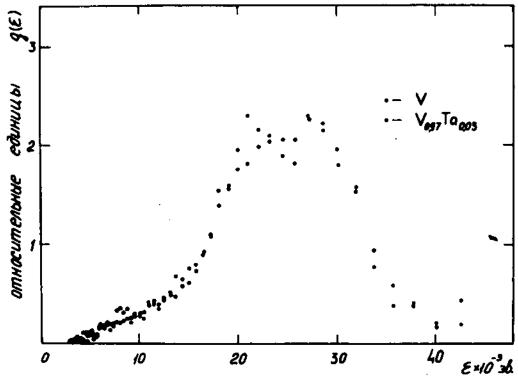

Рис.5. Фононный спектр для сплава ванадий-тантал.

альное сечение рассеяния нейтронов, связано линейно с функцией распределения частот нормальных колебаний g(ε) следующим соотношением:

$$g(\epsilon) = \mathrm{Const}\frac{d^2\sigma}{d\Omega d\epsilon}\left(\frac{E_0}{E}\right)^{\frac{1}{2}}\frac{(e^{\epsilon/kT}-1)\epsilon}{E+E_0}$$

где используемые величины имеют общепринятое значение.

На рис.5 ($V_{0,97}$ $Ta_{0,03}$) и рис.6 ($V_{0,97}$ $W_{0,03}$) приведены значения g(ε), восстановленные из полученных данных. Для сравнения на рис.5 и 6 приведен также спектр g(ε) для исходной матрицы металлического ванадия.

Из сравнения кривых g(ε) для ванадия и сплавов следует, что введение одинакового количества примесных атомов (3% ат) тантала и вольфрама приводят к различным деформациям колебательного спектра кристаллической решетки ванадия. Для сплава $V_{0,97}$ $Ta_{0,03}$ энергетическое положение основных особенностей спектра g(ε) полностью совпадает с положением аналогичных особенностей спектра решетки

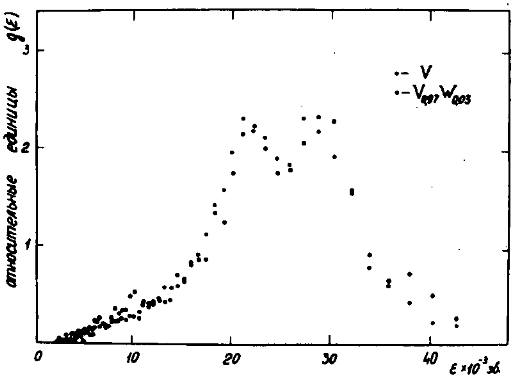

Рис.6. Фононный спектр для сплава ванадий-вольфрам.

ванадия. Однако, наблюдается очень существенное размытие максимумов спектра, особенно низкоэнергетического. В области низких энергий (~8,5 мэв) в спектре $g(\epsilon)$ для сплава $V_{0,97}$ $Ta_{0,03}$ наблюдается дополнительная особенность, которая не проявляется в спектре ванадия.

Для сплава $V_{0,97}$ $W_{0,03}$ наблюдается смещение всего спектра $g(\epsilon)$ в целом в область более высоких частот. Никакого размытия основных максимумов спектра не наблюдается. В области низких энергий, как и для сплава $V_{0,97}$ $Ta_{0,03}$, наблюдается дополнительная особенность. Однако, энергетическое положение отмеченной особенности для сплава $V_{0,97}$ $W_{0,03}$ ($\epsilon \approx 10$ мэв), по сравнению со сплавом $V_{0,97}$ $Ta_{0,03}$ ($\epsilon = 8{,}5$ мэв), оказывается смещенным в сторону больших частот.

В ряде теоретических работ [8 – 10] было показано, что введение изолированной тяжелой примеси в более легкую матрицу должно приводить к образованию квазилокальной частоты, расположенной в пределах интервала частот, отвечающих решетке исходной матрицы. Положение возникающей квазилокальной частоты определяется следующим соотношением [10]:

$$\omega^2 = \omega_0^2 \left\{ |\epsilon| \langle \omega^2/\omega_0^2 \rangle^{-1} \left[1 - \frac{2\tau}{1-\tau} \frac{1-\epsilon}{\epsilon} \langle \omega^2/\omega_0^2 \rangle^{-1} \right] \right\}^{-1}$$

где ω_0 – граничная частота решетки матрицы, $\epsilon = 1 - \frac{M_1}{M}$, $\tau = 1 - \frac{\gamma_1}{\gamma}$, M_1 и γ_1 – масса и силовые постоянные примесного атома, M и γ – масса и силовые постоянные исходной решетки.

Если предположить, что силовые постоянные не изменяются, т.е. $\tau = 0$, то:

$$\omega^2 = \omega_0^2 \{ |\epsilon| \langle \omega^2/\omega_0^2 \rangle^{-1} \}^{-1}$$

Для сплавов $V_{0,97}$ $Ta_{0,03}$ и $V_{0,97}$ $W_{0,03}$, предполагая неизменность силовых постоянных, квазилокальная частота должна быть локализована при $\epsilon = 10{,}3$ мэв (приближение Дебая). С учетом величины разрешения в этом интервале энергий можно сказать, что наблюдается удовлетворительное согласие между расчетным и экспериментальным положением квазилокальной частоты.

Для определения характера спектрального распределения в районе квазилокальной частоты, его ширины, необходимо проведение этих исследований с более высокой статистической точностью и более высоким энергетическим разрешением. Такие исследования нами проводятся в настоящее время. Обращает на себя внимание смещение всего спектра ванадия при введении в него лишь 3% ат W.

Аналогичное смещение всего спектра наблюдалось при введении в ванадий платины (5% ат) [11].

Введение тантала, обладающего тем же количеством валентных электронов, что и ванадиевая матрица, не приводит к такому резкому смещению спектра, т.е. в этом случае мы имеем дело с чисто изотопическим замещением.

В связи с этим представляет интерес исследования сплавов ванадия с примесью атомов, обладающих различным числом валентных электронов, а также установление концентрационной зависимости смещения всего спектра.

В заключение выражаем благодарность Н.А.Черноплекову, В.А.Соменкову, С.Ш.Шильштейну за участие в дискуссии; Ю.Л.Шитикову, А.Е.Головину, М.Д.Давыдову, Ю.В.Середе, В.Г.Федорову и А.С.Игнашову – за помощь в измерениях и обработке результатов; Л.С.Гузею – за предоставление образцов исследуемых сплавов.

ЛИТЕРАТУРА

[1] Inelastic Scat. of Neutr. in Solids and Liquids, IAEA, Vienna 1 (1963) 167.
[2] SVENSSON, E.C., BROCKHOUSE, B.N., ROWE, J.M., Solid State Commun 3 (1965) 245.
[3] MOLLER, H.B., MACKINTOSH, A.R., Phys. Rev. Lett. 15 (1965) 623.
[4] ЧЕРНОПЛЕКОВ, Н.А., ЗЕМЛЯНОВ, М.Г., ЖЭТФ, 49, в. 2 (1965).
[5] ЧЕРНОПЛЕКОВ, Н.А., ПАНОВА, Г.Х., ЗЕМЛЯНОВ, М.Г., САМОЙЛОВ, Б.Н., КУТАЙЦЕВ, В.И., Phys. Stat. Sol. 20(1967) 767.
[6] ХАНСЕН, М., АНДЕРКО, К., Структура двойных сплавов, 1962.
[7] Inelastic Scat. of Neutr. in Solids and Liquids IAEA, Vienna 1 (1963) 125, 159.
[8] КАГАН, Ю., ИОСИЛЕВСКИЙ, С., ЖЭТФ, 42 (1962) 259.
[9] BRONT, B., VISSCHER, W., Phys. Rev. Lett. (1962) 954.
[10] ЖЕРНОВ, А., АУГСТ, Г., ФТТ. 9, в. 8 (1967).
[11] MOZER, B., OTNES, K., THAPER, C., Phys. Rev. (1966) 152, 535.

DISCUSSION

Yu. M. KAGAN: I should like to ask Mr. Mozer how the concentration broadening of the local level was calculated in paper SM-104/78. With pair interaction between the impurities only, it seems to me that symmetrical splitting of the level is obtained, and further averaging with respect to the distance between the two impurities leads to a symmetrical impurity band. The asymmetry arises when the interaction of three or more impurities is considered simultaneously.

B. MOZER: I did not attempt to obtain the band shape; what I did was to see whether the observed splitting could be accounted for by considering only a pair of impurities. Using results for the exponential decay presented in Fig. 4 of my paper, I calculated the splitting of the localized mode when the second impurity is in the first shell around the other impurity, in the second shell, etc. The splittings were then averaged over the probability of finding another impurity in these shells for the measured concentration of beryllium. This average splitting agrees quite closely with the observed value and is larger than that calculated for the average distance between impurities at this concentration. The shift of the levels about the single impurity level is symmetric, as it is in the measurement. I have not tried to calculate the intensities expected for neutron scattering but am probably in a position to do so since I have the perturbed amplitudes for the pair. I agree that one should also consider the possibility of three impurities close together; I consider that this leads to a small effect for the low concentration used in the experiment, but it could certainly result in asymmetry in intensity. It is interesting to note that if the splitting arises from pairs, then one has another way of measuring the spatial exponential decay of the local mode amplitude.

R. RUBIN: In connection with the splitting of the localized peak in V with 3.3% Be observed by Mr. Mozer, I may say that we detected a splitting of the localized mode likewise in the case of single crystals of niobium and vanadium with some percentage of hydrogen. This can be explained by the tetrahedral symmetry of the hydrogen sites. As a consequence one expects two modes, of which one is doubly degenerated.

B. MOZER: Beryllium in vanadium is in solution and is not interstitial, and in the low concentration case has cubic symmetry. The splitting of the observed spectra comes from the proximity of two beryllium atoms whose wave functions overlap; it is thus a consequence of pair interactions.

While I am speaking I will take the opportunity of putting a question to Mr. Zemlyanov about his paper (SM-104/144). I understand that you calculated the position of the resonant mode of tungsten in vanadium. Did you also calculate the width of this mode? My calculations yield a width of 3-4 meV, and when your instrumental resolution is added the result is a very broad line of the order 4-6 meV. Your data, on the other hand, show a very sharp line. Can you explain this discrepancy?

M.G. ZEMLYANOV: We evaluated the expected width of the band in the isotopic model approximation. This width proved to be 2.5 meV. Overall resolution in these experiments is governed mainly by the smearing out of the spectral line of the incident neutrons, and this smearing was a good deal less in our case than in your experiments. In this connection the smearing out of the resonance band through resolution in our experiments did not appear so large: the width of the band is of the order of that of the resolution function for $V_{0.97}Ta_{0.03}$ and is somewhat more for $V_{0.97}W_{0.03}$.

It is possible that in the case of alloys such as those of vanadium with heavy impurities, measurement by the usual method of monochromatization of the incident neutrons by means of a polycrystalline filter fails completely to reveal any resonance oscillations in the low-frequency region, owing to the substantial smearing out of their resolution functions.

B. MOZER: The full width at half maximum of your incident beam is 1.25 meV. The full width at half maximum of our incoming beam is 2.5 meV. The total width of the resonant mode plus instrumental resolution is not very different in the two cases (ours is perhaps 30% greater). I suggest we compare results again after more measurements on these alloys. The main point I wish to emphasize is that in no sample measured yet by incoherent methods does the intensity of the observed structure agree at all with any simple theories applied in your paper or in mine. The intensity is far too small.

B.N. BROCKHOUSE: I should like to offer a comment on the beautiful work on the local modes of aluminium in copper described in the paper of Nicklow et al. (SM-104/85). It is obvious that a light atom in a crystal composed of heavy atoms will vibrate at a high frequency; the interest resides largely in the locality of the vibration, and Elliott and Maradudin have provided the key by which the degree of locality of the local mode can be assessed. This assessment has now for the first time been carried out experimentally in the paper to which I am referring.

I would add that the shift in the longitudinal modes with increasing aluminium content is almost quantitatively in agreement with some unpublished work of Hallman on the shifts in the frequencies for copper as zinc is added (when considered as a function of the number of additional electrons). Thus the local mode is a true local mode, but has modified force constants due to change in electron concentration.

B. MOZER: I have a question for anyone doing single-crystal measurements of impurity modes. When one considers a general formulation of the many-impurity problem, or when one is measuring the square of the Fourier transform of the amplitudes of vibration for the perturbed system, one notices a dependence of the shift or width on the polarization index of the lattice waves. Has anyone considered the possibility of measuring this dependence? I believe that the results would be very interesting to the theorists.

A.R. MACKINTOSH: Such effects have been observed in different transverse phonon branches in Cr with 3% W impurities where both the position and the frequency shift over the resonance differ between the branches. However, this behaviour was ascribed in this case to force constant changes rather than to finite concentration effects.

Yu.M. KAGAN: Turning to paper SM-104/42, I consider that the linear concentration theory used for describing the high-concentration alloys must inevitably lead to erroneous results, and hence the large discrepancy between the experimental and the theoretical values is not surprising.

Incidentally, it can be shown that in the case of heavy impurities the effects of non-linearity in concentration begin to play an important role at a relatively low concentration. The results of Brockhouse and his co-workers for a Cu-Au alloy can probably be explained in this way. Perhaps Mr. Cowley and Mr. Brockhouse would care to comment.

R.A. COWLEY: Mr. Kagan is quite correct when he says that it is not surprising that our results disagree with the linear concentration theory. However, the object of the experiments was to study the large concentration limit, and what is surprising is that the phonons are still quite good excitations.

B.N. BROCKHOUSE: With reference to Mr. Kagan's remarks on our results for alloys of small concentrations of gold in copper, I should point out that recent work by Kamitakahara, continuing that of Svensson et al., indicates that the deviations from theory probably arise from force constant changes as well as from excessive concentrations of defect atoms. Kamitakahara has also performed some calculations which have a bearing on the paper of Buyers and Cowley (SM-104/42), to which Mr. Kagan was primarily referring. These calculations relating to a PdNi disordered alloy were made on the basis of the theory expounded by Ng and myself in paper SM-104/53. Rather broad phonons are indicated for this alloy of about a 2:1 mass ratio. For many of the phonons in KBr/RbBr the effective mass ratio would be much less than 2:1 (particularly for acoustic modes) and quite reasonable phonon groups should occur.

R. RUBIN: We have also observed a shift of phonon energy due to impurities in a single crystal of niobium containing 5% hydrogen.

APPLICATION OF THE KREBS MODEL TO THE STUDY OF THE LATTICE DYNAMICS OF HEXAGONAL CLOSE - PACKED METALS

S. HAUTECLER AND M. NEVE de MEVERGNIES
CENTRE D'ETUDE DE L'ENERGIE NUCLEAIRE,
MOL, BELGIUM

Abstract

APPLICATION OF THE KREBS MODEL TO THE STUDY OF THE LATTICE DYNAMICS OF HEXAGONAL CLOSE-PACKED METALS. The physical content of the Krebs model, which was originally formulated for bcc and fcc metals, has been applied to hexagonal close-packed metals. The metal is considered as a set of spherical ions, of uniform charge distribution, embedded in an electron sea. The elements of the dynamical matrix have been deduced by assuming central spring interactions extending up to the sixth neighbours, and a screened Coulomb interaction between all ions. Six relations between the eight parameters introduced in the model and the five elastic constants have been obtained by the method of long waves. It is found that the lattice equilibrium condition obtained by equating the two expressions for C_{44} requires that the long-range interaction cancels out. It is concluded that the Krebs force model does not describe a crystal in equilibrium. If one wants to keep to the long-range term, the lattice is no longer elastically consistent, which means that the calculated long wavelength limit for some branches of the dispersion relation in some directions is not correct.

1. INTRODUCTION

KREBS [1] has recently proposed a force model from which the lattice dynamics of metals can be derived. A metal is considered as a lattice of spherical ions, of uniform charge distribution, embedded in an electron sea. The elements of the dynamical matrix were given for bcc and fcc crystals assuming central spring interactions between first and second neighbours upon which is superposed a screened Coulomb interaction between all ions. This simple model contains a very small number of parameters which are chosen so as to give correct values for the elastic constants. The screening parameter λ was written as

$$\lambda = C \left(\frac{3}{4\pi n a_o^3}\right)^{1/6} k_F \qquad (1)$$

where n is the electron density, a_o the Bohr radius, and $\vec{k}_F$ the electron wave vector at the Fermi surface. The value of the constant C is not well defined; in the Thomas-Fermi theory it takes the value 0.814, while only a value of 0.353 is obtained from the plasma theory of Bohm and Pines (more exactly, this theory gives a maximum value of 0.47).

Krebs calculated the dispersion curves for Li, Na and K, by chosing the Pines C - coefficient, assuming one free electron per atom, and determining k_F in the free electron approximation; in the case of Na, for which experimental dispersion relations are available, an excellent fit to the data is obtained. On the same basis, SHUKLA [2] has shown that for Cu also good agreement with the experimental dispersion curves is obtained.

Later, SHUKLA [3] and MAHESH and DAYAL [4] calculated respectively the heat capacities of noble metals (Cu, Au) and of alkali metals (Na, K, Rb, Cs) by means of frequency spectra deduced from the Krebs model. An excellent agreement with the experimental data could be obtained when the factor C appearing in the expression for the electronic screening parameter was treated as an adjustable parameter. The best-fit values ranged between the Pines and the Thomas-Fermi C-values.

MAHESH and DAYAL [5] and SHUKLA and DAYAL [6] have slightly modified the Krebs model by including the third-neighbour central interaction; the additional parameter is obtained with the help of one of the experimentally observed vibration frequencies at the Brillouin zone boundary. For α-Fe, Mo, W and Al, the theoretical phonon dispersion curves and specific heats exhibit a good agreement with the experimental data.

In view of the preceding successes, we thought it would be very interesting to extend the formulation of the Krebs model to hexagonal close-packed metals. Only the mathematical developments are given here, the results of compution being not yet available.

2. SECULAR EQUATION

The unit cell of the hexagonal close-packed lattice is shown in Fig. 1; it is characterized by the lattice constants a and c. The Cartesian system of coordinates, x_1, x_2 and x_3, which we use is also shown in this figure.

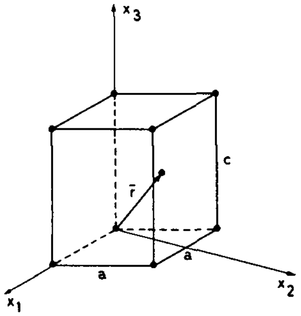

FIG.1. Unit cell of the hexagonal close-packed lattice.

The matrix equation which determines the dispersion relations of the lattice is given by

$$\left| D(\vec{q}) - 4\pi^2 \nu^2 I \right| = 0 \qquad (2)$$

where I is a unit matrix, ν and $\vec{q}$ the frequency and the wave vector of a normal mode of vibration. The dynamical matrix D $(\vec{q})$ can be written in this model in the form

$$D\,(\vec{q}) = \begin{pmatrix} A & B \\ B^{*} & A^{*} \end{pmatrix} \tag{3}$$

A and B being 3 x 3 submatrices and A^{*} (B^{*}) the complex conjugate of A (B).

According to the physical content of the Krebs model, each element of D $(\vec{q})$ is split up into two parts : a short-range part which takes into account central spring interactions between a limited number of neighbours, and a long-range part corresponding to the screened Coulomb interaction between ions. Thus we have

$$\begin{aligned} A_{\alpha\alpha'} &= S_{\alpha\alpha'} + V_{\alpha\alpha'} \\ B_{\alpha\alpha'} &= T_{\alpha\alpha'} + W_{\alpha\alpha'} \end{aligned} \tag{4}$$

2.1. The central spring interaction force constant matrices

As the ordered sequence of the neighbouring atoms is depending on the c/a ratio, we found preferable to include in the mathematical formulation a relatively large number of neighbours. In each specific case, only the appropriate first few neighbour interactions have to be conserved. The force constant matrices [7] for the representative atoms are given in Table I, where :

$$\beta' = \beta/(\frac{a^2}{3} + \frac{c^2}{4})$$

$$\gamma' = \gamma/(\frac{4a^2}{3} + \frac{c^2}{4})$$

$$\varepsilon' = \varepsilon/(\frac{7a^2}{3} + \frac{c^2}{4})$$

2.2. The short range part of the dynamical matrix

By including the 6 sets of neighbours generated by the atoms given in Table I, we found the following expressions :

$$S_{11} = M^{-1}\left\{\alpha(2\;C_{21} + C_1\;C_2 - 3) + \zeta(3\;C_{31}\;C_2 - 3) - a^2\;E\right\}$$

$$S_{22} = M^{-1}\left\{\alpha(3\;C_1\;C_2 - 3) + \zeta(C_{31}\;C_2 + 2\;C_{22} - 3) - a^2\;E\right\}$$

$$S_{33} = M^{-1}\left\{\delta(2\;C_{33} - 2) - \frac{3\,c^2}{2}\;F\right\}$$

TABLE I. FORCE CONSTANT MATRICES FOR THE CENTRAL SPRING INTERACTIONS

Representative atom	Force constant matrix	Representative atom	Force constant matrix
(a, 0, 0)	$\begin{pmatrix} \alpha & 0 & 0 \\ 0 & 0 & 0 \\ 0 & 0 & 0 \end{pmatrix}$	(0, 0, c)	$\begin{pmatrix} 0 & 0 & 0 \\ 0 & 0 & 0 \\ 0 & 0 & 0 \end{pmatrix}$
$\left(0, \frac{a}{\sqrt{3}}, \frac{c}{2}\right)$	$\beta' \begin{pmatrix} 0 & 0 & 0 \\ 0 & \frac{a^2}{3} & \frac{ac}{2\sqrt{3}} \\ 0 & \frac{ac}{2\sqrt{3}} & \frac{c^2}{4} \end{pmatrix}$	$(0, a\sqrt{3}, 0)$	$\begin{pmatrix} 0 & 0 & 0 \\ 0 & \zeta & 0 \\ 0 & 0 & 0 \end{pmatrix}$
$\left(0, \frac{-2a}{\sqrt{3}}, \frac{c}{2}\right)$	$\gamma' \begin{pmatrix} 0 & 0 & 0 \\ 0 & \frac{4a^2}{3} & -\frac{ac}{\sqrt{3}} \\ 0 & \frac{-ac}{\sqrt{3}} & \frac{c^2}{4} \end{pmatrix}$	$\left(\frac{a}{2}, \frac{5a}{2\sqrt{3}}, \frac{c}{2}\right)$	$\frac{\epsilon'}{4} \begin{pmatrix} a^2 & \frac{5a^2}{\sqrt{3}} & ac \\ \frac{5a^2}{\sqrt{3}} & \frac{25a^2}{3} & \frac{5ac}{\sqrt{3}} \\ ac & \frac{5ac}{\sqrt{3}} & c^2 \end{pmatrix}$

$$S_{12} = S_{21} = - M^{-1} \sqrt{3}\, S_2 \,(\alpha\, S_1 + \zeta\, S_{31})$$

$$S_{13} = S_{31} = S_{23} = S_{32} = 0$$

$$T_{11} = M^{-1}\, a^2\, C_3 \exp(im_3) \Big\{ \beta' C_1 \exp(im_2) + 4\gamma' C_{21}$$

$$+ \varepsilon' \Big[C_1 \exp(-im_2) + 9\, C_{31} \exp(im_2) + 4\, C_{21} \exp(i\, 2m_2) \Big] \Big\}$$

$$T_{22} = M^{-1} \frac{a^2}{3} C_3 \exp(im_3) \Big\{ \beta' \Big[2 + C_1 \exp(im_2) \Big] + 4\gamma' \Big[2\exp(i2m_2) + C_{21} \Big]$$

$$+ \varepsilon' \Big[25 C_1 \exp(-im_2) + C_{31} \exp(im_2) + 16 C_{21} \exp(i2m_2) \Big] \Big\}$$

$$T_{33} = M^{-1} \frac{c^2}{2} C_3 \exp(im_3) \Big\{ \beta' \Big[1 + 2C_1 \exp(im_2) \Big] + \gamma' \Big[\exp(i2m_2) + 2C_{21} \Big]$$

$$+ 2\varepsilon' \Big[C_1 \exp(-im_2) + C_{31} \exp(im_2) + C_{21} \exp(i2m_2) \Big] \Big\}$$

$$T_{12} = T_{21} = i\ M^{-1}\ \frac{a^2}{\sqrt{3}}\ C_3\ \exp\ (im_3)\Big\{\beta' S_1\ \exp\ (im_2)\ -\ 4\gamma' S_{21}$$

$$+\ \varepsilon'\Big[-\ 5\ S_1\ \exp(-im_2) +\ 3\ S_{31}\ \exp\ (im_2)\ +\ 8\ S_{21}\ \exp\ (i2m_2)\Big]\Big\}$$

$$T_{13} = T_{31} = -\ M^{-1}\ a\ c\ S_3\ \exp\ (im_3)\ \Big\{\beta'\ S_1\ \exp\ (im_2)\ +\ 2\gamma' S_{21}$$

$$+\ \varepsilon'\Big[S_1\ \exp\ (-im_2)\ +\ 3\ S_{31}\ \exp\ (im_2)\ +\ 2\ S_{21}\ \exp\ (i2m_2)\Big]\Big\}$$

$$T_{32} = T_{23} = i\ M^{-1}\ \frac{ac}{\sqrt{3}}\ S_3\ \exp\ (im_3)\Big\{\beta'\Big[C_1\ \exp\ (im_2)\ -\ 1\Big]$$

$$+\ 2\gamma'\Big[\exp\ (i2m_2) -\ C_{21}\Big] +\ \varepsilon'\Big[-5\ C_1\ \exp(-im_2)\ +\ C_{31}\ \exp(im_2) +\ 4C_{21}\exp(i2m_2)\Big]\Big\}$$

where

$E\ = \beta' + 4\gamma' + 14\varepsilon'$

$F\ = \beta' + \gamma' + 2\varepsilon'$

$i\ = \sqrt{-1}$

$C_1 = \cos\ q_1\ \frac{a}{2}$ $\qquad S_1 = \sin\ q_1\ \frac{a}{2}$

$C_2 = \cos\ q_2\ \frac{a\sqrt{3}}{2}$ $\qquad S_2 = \sin\ q_2\ \frac{a\sqrt{3}}{2}$

$C_3 = \cos\ q_3\ \frac{c}{2}$ $\qquad S_3 = \sin\ q_3\ \frac{c}{2}$

$C_{21} = \cos\ q_1\ a$ $\qquad S_{21} = \sin\ q_1\ a$

$C_{22} = \cos\ q_2\ a\sqrt{3}$ $\qquad S_{22} = \sin\ q_2\ a\sqrt{3}$

$C_{31} = \cos\ q_1\ \frac{a3}{2}$ $\qquad S_{31} = \sin\ q_1\ \frac{a3}{2}$

$C_{33} = \cos\ q_3\ c$ $\qquad S_{33} = \sin\ q_3\ c$

$m_2 = q_2\ \frac{a\sqrt{3}}{2}$ $\qquad m_3 = q_3\ \frac{c}{2}$

M being the mass of an atom and q_1, q_2, q_3 the Cartesian components of the wave vector $\vec{q}$.

2.3. The long-range part of the dynamical matrix

This part arises from the screened Coulomb interaction between spherical ions of uniform charge distribution. If λ is the screening parameter, and A a parameter depending on the total charge of an ion, we get

$$V_{\alpha\alpha'} = M^{-1} A \sum_{\vec{y}} \left\{ \frac{(q_\alpha + y_\alpha)(q_{\alpha'} + y_{\alpha'})}{|\vec{q} + \vec{y}|^2 + \lambda^2} G^2 (u_1) - \frac{y_\alpha \, y_{\alpha'}}{y^2 + \lambda^2} G^2 (u_2) \left[1 + \exp (i \, \vec{y}.\vec{r})\right] \right\}$$

$$W_{\alpha\alpha'} = M^{-1} A \sum_{\vec{y}} \frac{(q_\alpha + y_\alpha) \, (q_{\alpha'} + y_{\alpha'})}{|\vec{q} + \vec{y}|^2 + \lambda^2} G^2 (u_1) \exp \left[i(\vec{q}+\vec{y}).\vec{r} \right]$$

Here we have defined

$$G (u) = 3 (\sin u - u \cos u)/u^3$$

$$u_1 = r_o \left|\vec{q} + \vec{y}\right| \qquad\qquad u_2 = r_o \left|\vec{y}\right|$$

where r_o is the radius of the ions; the vector $\vec{r}$ is shown in fig. 1, so that

$$\vec{r} = (0, \frac{a}{\sqrt{3}} , \frac{c}{2})$$

The vector $\vec{y}$ is a reciprocal lattice vector whose Cartesian components are

$$\vec{y} = (\frac{2\pi \, h_1}{a} , \frac{2\pi(h_1 + 2h_2)}{a\sqrt{3}} , \frac{2\pi \, h_3}{c})$$

where h_1, h_2, h_3 are any three integers, positive, negative, or zero. Due to the presence of the G^2 function, the summations are converging rapidly with increasing $|\vec{y}|$.

It is again possible to make the screening parameter λ dependent of the electron wave vector by multiplying it by the function $f^{1/2}$ (t) given by Krebs.

3. RELATIONSHIPS BETWEEN ELASTIC CONSTANTS AND PARAMETERS

By means of the method of long waves of BORN and HUANG [8], we obtained the following relations between parameters and elastic constants

$$C_{11} = B \left\{ \frac{\mathcal{K}^2}{\mathcal{A}} - \frac{9a^2}{4} (\alpha + 3\zeta) - \frac{a^4}{4} (\beta' + 16\gamma' + 98\varepsilon') + A \sum_{\vec{y}} \left[2 F_o + 5y_1^2 P + y_1^4 Q\right]\left[1 + \exp (i \, \vec{y}.\vec{r})\right] \right\}$$

$$C_{44} = B\left\{ - \frac{a^2c^2\,E}{4} + A\sum_{\vec{y}}\left[y_1^2\;P + y_1^2\;y_3^2\;Q\right]\left[1 + \exp\;(i\;\vec{y}.\vec{r})\right]\right\}$$

$$C_{44} = B\left\{ - \frac{a^2c^2\,E}{4} + A\sum_{\vec{y}}\left[y_3^2\;P + y_1^2\;y_3^2\;Q\right]\left[1 + \exp\;(i\;\vec{y}.\vec{r})\right]\right\}$$

$$C_{33} = B\left\{ - 2c^2\delta - \frac{3c^4\;F}{8} + A\sum_{\vec{y}}\left[2\;F_o + 5y_3^2P + y_3^4Q\right]\left[1 + \exp\;(i\;\vec{y}.\vec{r})\right]\right\}$$

$$C_{44} + C_{13} = B\left\{ - \frac{a^2c^2\,E}{2} + 2\;A\sum_{\vec{y}}\left[F_o + (y_1^2 + y_3^2)\;P + y_1^2\;y_3^2\;Q\right]\;x\right.$$
$$\left.\left[1 + \exp\;(i\;\vec{y}.\vec{r})\right]\right\}$$

$$C_{11} + C_{12} = B\left\{ - 3\;a^2\;(\alpha + 3\zeta) - \frac{a^4}{3}\;(\beta' + 16\gamma' + 98\varepsilon')\right.$$
$$\left. + 4\;A\sum_{\vec{y}}\left[F_o + 2y_1^2\;P + \frac{1}{3}\;y_1^4\;Q\right]\left[1 + \exp\;(i\;\vec{y}.\vec{r})\right]\right\}$$

where we have put

$$B = \frac{2}{a^2\;c\sqrt{3}}$$

$$\mathcal{H} = \frac{a^3}{2\sqrt{3}}\;(\beta' - 8\gamma' + 20\varepsilon') - i\;A\sum_{\vec{y}}\;y_1^2\;y_2\;P\;\exp\;(i\;\vec{y}.\vec{r})$$

$$\mathcal{A} = a^2\;E + A\sum_{\vec{y}}\;y_1^2\;F_o\;\exp\;(i\;\vec{y}.\vec{r})$$

$$F_o = \frac{G^2\;(u_2)}{T}$$

$$P = \frac{r_o\;G_1\;(u_2)}{yT} - \frac{2\;G^2(u_2)}{T^2}$$

$$Q = - \frac{r_o\left[y^{-1}\;G_1\;(u_2) - r_oG_2\;(u_2)\right]}{y^2\;T} - \frac{4r_oG_1\;(u_2)}{y\;T^2} + \frac{8\;G^2\;(u_2)}{T^3}$$

$$T = y^2 + \lambda^2$$

$$G_1\;(u) = 6u^{-1}\;G(u)\left[u^{-1}\;\sin\;u - G(u)\right]$$

$$G_2(u) = -24u^{-2}G(u)\left[u^{-1}\sin u - G(u)\right] - 2G^2(u)$$

$$+ 18u^{-2}\left[u^{-1}\sin u - G(u)\right]^2$$

It is seen that F_o, P and Q are only depending on the modulus y of the reciprocal lattice vector.

4. DISCUSSION

One has to solve the secular equation (2) in order to calculate the dispersion curves for the normal modes of vibration. Before that the parameter values must be obtained from the values of the five elastic constants. However, an arbitrary set of values of five parameters does not give a unique set of elastic constants since we have obtained in the preceding section two different expressions for C_{44}. We can indeed introduce six non zero parameters which have to satisfy a condition deduced from equating the two expressions. This gives

$$A\left\{\sum_{\vec{y}} y_1^2\, P\left[1 + \exp(i\,\vec{y}.\vec{r})\right] - \sum_{\vec{y}} y_3^2\, P\left[1 + \exp(i\,\vec{y}.\vec{r})\right]\right\} = 0 \qquad (4)$$

This condition leads to A = 0 so that from our developments we draw the disappointing conclusion that, in order for the lattice to be elastically consistent, the long range screened Coulomb interaction must cancel.

The interrelation between the force constants obtained from the two different expressions for C_{44} is generally called the lattice equilibrium condition [9]. We thus arrive at the important conclusion that the Krebs force model does not describe a crystal in equilibrium . An identical conclusion could already have been drawn previously from the fact that for cubic lattices Krebs got a deviation from the Cauchy relation $C_{12} = C_{44}$. According to ZENER [10] and LEIBFRIED [11] the conditions for the validity of the Cauchy relations are :

1. All forces must be central
2. Every atom must be at a center of symmetry
3. The crystal should be initially under no stress.

As in the Krebs model all forces are central, and since in a cubic metal each atom is at a center of symmetry, the deviation obtained reveals that the crystal must be under stress. Some additional conditions on the parameters such as to the requirement that the configuration corresponds to vanishing internal stress [12] have probably been neglected.

If in spite of all, one wants to keep the long range term which is characteristic of the Krebs model, it is possible to proceed as follows: to determine five parameters from the above expressions for C_{11}, C_{33}, $C_{44} + C_{13}$, $C_{11} + C_{12}$, and from a last equation obtained by adding the two different expressions for C_{44}

$$2\,C_{44} = B\left\{-\frac{a^2c^2\,E}{2} + A\sum_{\vec{y}}\left[(y_1^2 + y_3^2)\,P + 2y_1^2\,y_3^2\,Q\right]\left[1 + \exp(i\,\vec{y}.\vec{r})\right]\right\}$$

and then to solve the secular equation. The degree of elastic consistency of the crystal will be given by the deviation from zero of eq. (4). The non-fulfilment of this condition gives rise to wrong slopes for the long wavelength limit of the degenerate transversal acoustical branch of the dispersion relation in the [0001] direction and for that transversal acoustical branch in the [01$\bar{1}$0] direction whose polarization is along the c-axis. Some calculations along these lines are in progress for Mg, Be and Zn.

REFERENCES

[1] KREBS, K., Phys. Letters, 10 (1964) 12; Phys. Rev. 138 (1965) A 143.

[2] SHUKLA, M.M., Phys. Stat. Sol. 7 (1964) K 11.

[3] SHUKLA, M.M., Phys. Stat. Sol. 8 (1965) 475.

[4] MAHESH, P.S. and DAYAL, B., Phys. Stat. Sol. 9 (1965) 351.

[5] MAHESH, P.S. and DAYAL, B., Phys. Rev. 143 (1966) 443.

[6] SHUKLA, M.M. and DAYAL, B., Phys. Stat. Sol. 16 (1966) 513.

[7] LEHMAN, G., WOLFRAM, T. and DE WAMES, R., Phys. Rev. 128 (1962) 1593.

[8] BORN, M. and HUANG, K., "Dynamical theory of crystal lattices", § 26, Oxford University Press, London (1956).

[9] BEGBIE, G.H., Proc. Roy. Soc. A 188 (1947) 189;
COLLINS, M.F., Proc. Phys. Soc. 80 (1962) 362;
IYENGAR, P.K., VENKATARAMAN, G., VIJAYARAGHAVAN, P.R. and ROY, A.P., "Lattice Dynamics" p. 223 (WALLIS, R.F., Ed.), Pergamon Press, Oxford (1965);
GUPTA, R.P. and DAYAL, B., Phys. Stat. Sol. 13 (1966) 519.

[10] ZENER, C., Phys. Rev. 71 (1947) 323.

[11] LEIBFRIED, G., Z. Physik 129 (1951) 307.

[12] HUANG, K., Proc. Roy. Soc. A 203 (1950) 178.

LATTICE DYNAMICS AND ELECTRONIC STRUCTURE OF SODIUM, MAGNESIUM AND ALUMINIUM

T. SCHNEIDER AND E. STOLL
DELEGATION FUR AUSBILDUNG UND HOCHSCHULFORSCHUNG,
SWISS FEDERAL INSTITUTE FOR REACTOR RESEARCH,
WÜRENLINGEN, SWITZERLAND

Abstract

LATTICE DYNAMICS AND ELECTRONIC STRUCTURE OF SODIUM, MAGNESIUM AND ALUMINIUM. The actual interaction between ions in a metal is divided into the direct interaction of the ion cores and the ion-electron-ion interaction. The ion-electron-ion interaction is treated according to the Hartree-Fock approximation, modified by a screened exchange potential. Since until now the bare ion potential has not been known very accurately, the observed phonon frequencies were used to determine a model pseudo-potential with the least-squares method. Using this model pseudo-potential, the electronic band structure, the Fermi surface, the cohesive energy, the crystal stability, the interactomic potential and the electrical resistivity were calculated. The method described enables us to relate the measured phonon dispersions with the electronic structure and the electrical properties of simple metals.

1. INTRODUCTION

The neutron scattering technique has now been developed to yield detailed information on phonon dispersion curves. The interpretation of the experimental data is normally based on a force constant model. This model does not provide the best physically sound interpretation, but seems to be the best available interpolation scheme for fitting the observed frequencies and for use in the derivation of a frequency distribution.

The first attempt to calculate dispersion curves for simple metals by a satisfactory method was made by Toya [1]. These calculations, which preceded the experimental measurements by some years, proved to be in rather good agreement with them. Toya divided the interactions between the ions in a metal into three parts: the exchange or overlap potential between the ion cores, the Coulomb potential between the ions, and the potential induced by the electron-phonon interaction including electron-electron interactions.

In the present paper the potential induced by the electron-phonon interaction is formulated by the pseudo-potential method. If we know the pseudo-potential, we can calculate the electronic, electrical and some dynamical properties in both the solid and liquid states [2]. It is still a difficult problem to calculate this potential from first principles with any degree of precision. Consequently, the potential is generally presented in a model form, which includes in a simple parametric way all the features dictated by the physics of the situation. In the model potential method of Heine and Abarenkov [3] the information on the pseudo-potential is obtained from spectroscopic data pertinent to the free atom. Another approach consists of determining a model potential from the measured phonon dispersion curves.

Following Harrison [2] and our earlier work [4-6], we shall show that the measured phonon dispersion curves can be used to determine a model pseudo-potential over the whole range in momentum space. Using this model pseudo-potential, we shall discuss the electronic band structure, the Fermi surface, the cohesive energy, the crystal stability, the interatomic potential and the electrical conductivity of sodium, magnesium and aluminium.

2. GENERAL FORMULATION

The problem considered is that of finding the total energy of a simple metal in the Born-Oppenheimer adiabatic approximation. The Hamiltonian can be written symbolically as

$$H = T_I + \Phi(\vec{R}), \qquad \Phi = E_c(\vec{R}) + E_e(\vec{R}) \tag{1}$$

where $\Phi(\vec{R})$ is the total potential energy of the crystal, T_I the kinetic energy of the ions, $E_c(\vec{R})$ the Coulomb energy of the ions embedded in a uniform negative background and $E_e(\vec{R})$ is the total energy of the electrons, immersed in a uniform background of positive charge. The exchange overlap force in sodium, magnesium and aluminium is negligible [4].

The calculation of the Coulomb term E_c for the ideal and distorted lattice presents no difficulty using Ewald's method [7]. We may now proceed to the evaluation of the total electronic energy. Here, we present a simple calculation, based on perturbation theory, starting from free electrons. Assuming that the electron-ion potential is the sum of individual ionic potentials, the total electronic energy per ion becomes [8]

$$E_e = \frac{3}{5} Z E_F - \frac{3Ze^2}{4\pi} k_F + Z(0.678 \ln r_0 - 2.505) 10^{-12} \text{erg}$$
$$+ \sum_{\vec{k} \le k_F} \langle \vec{k} | V_I - V_P | \vec{k} \rangle + E_b \tag{2}$$

where

$$E_F = \frac{\hbar^2}{2m} k_F^2 \qquad k_F = (3\pi^2 n Z)^{1/3}$$

$$r_0 = \frac{r_s}{a_0 Z^{1/3}} \qquad r_s = \left(\frac{3}{4\pi n}\right)^{1/3}$$

$$E_b = \frac{1}{2} \sum_{Q \neq 0} |F(\vec{Q})|^2 U_e(\vec{Q}) \tag{3}$$

$$F(\vec{Q}) = \frac{1}{N} \sum_{l} e^{i\vec{Q}\cdot\vec{R}_l}$$

$$U_e(\vec{Q}) = -\sum_{\vec{k}\leq k_F} \frac{U_I(\vec{k}+\vec{Q},\vec{k})\,V_I(\vec{k}+\vec{Q},\vec{k}) + U_I(\vec{k},\vec{k}+\vec{Q})\,V_I(\vec{k},\vec{k}+\vec{Q})}{E_{\vec{k}+\vec{Q}} - E_{\vec{k}}}$$

$$U_I(\vec{k}+\vec{Q},\vec{k}) = n\int e^{-i(\vec{k}+\vec{Q})\cdot\vec{X}}\, U_I(\vec{X})\, e^{i\vec{k}\cdot\vec{X}}\, d\vec{X}$$

k_F : Fermi wave number
E_F : Fermi energy
Z : Valence
r_s : Atomic radius
n : Ions per unit volume
N : Number of ions in the crystal
$F(Q)$: Structure factor
V_P : $V_p = -Ze^2/R$
$U_I(\vec{Q})$: Self-consistent or screened pseudo-potential
$V_I(\vec{Q})$: Unscreened or bare pseudo-potential
$U_e(\vec{Q})$: Fourier transform of the electronic contribution to the effective ion-ion potential

The first three terms of Eq.(2) are, respectively, the kinetic, exchange, and correlation energies, and erg units are used throughout. For the latter we used the Nozières-Pines form [9]. The fourth term arises from the first-order contribution to the perturbation expansion. The last term comes from the second-order contribution and describes the electronic band-structure effects. This contribution depends on the detailed configuration of the ions.

When the ions disturb the uniform Fermi sea, the electrons undergo a change in potential. They redistribute themselves under the influence of the bare pseudo-potential and screen this potential. This effect has been considered by several authors [10-13]. If we make the assumption that V_I is a local pseudo-potential, Eq.(4), the relation between the bare and screened pseudo-potential reduces to Eq.(5) where we have used the modified static dielectric function of the Fermi sea introduced by Sham [13] in the manner suggested by Hubbard:

$$V_I(\vec{k}+\vec{Q},\vec{k}) = V_I(Q) \tag{4}$$

$$U_I(Q) = \frac{V_I(Q)}{1+S(Q)} \tag{5}$$

$$S(Q) = \frac{4\pi n e^2}{Q^2}[1 - C(Q)]X(Q) \qquad X(Q) = \frac{3Z}{2E_F}\, f(Q/2k_F)$$

$$f(t) = \frac{1}{2} + \frac{1-t^2}{4t}\ln\left|\frac{1+t}{1-t}\right| \qquad C(Q) = \frac{1}{2}\,\frac{Q^2}{Q^2+pk_F^2}$$

C(Q) represents a correction for the effect of exchange and correlation as suggested by Sham. Following Geldart and Vosko [14], we have chosen p such that we get for $Q = 0$ the compressibility of the Fermi sea, determined from the first three terms in Eq.(2). This leads to

$$P \cong \frac{2}{1+0.153\left(\frac{1}{\pi a_0 k_F}\right)} \tag{6}$$

where a_0 is the Bohr radius. The band structure energy, Eq. (3), now becomes

$$E_b = \frac{1}{2} \sum_{Q \neq 0} |F(\vec{Q})|^2 \, U_e(Q) \tag{7}$$

where

$$U_e(Q) = -\frac{V_I^2(Q)}{1 + S(Q)} X(Q) \tag{8}$$

The adiabatic principle enables us to expand the total potential energy $\Phi(\vec{R})$ of the crystal in powers of the ionic displacements $\vec{u}(\overset{l}{\kappa})$ as follows:

$$\Phi(\vec{R}) = \Phi(\vec{R}^0) + \sum_{l,\kappa,i} \Phi_i(\overset{l}{\kappa})\, u_i(\overset{l}{\kappa}) + \frac{1}{2} \sum_{\substack{l,\kappa,i \\ l',\kappa',j}} \Phi_{ij}(\overset{l\,l'}{\kappa\kappa'})\, u_j(\overset{l'}{\kappa'}) \tag{9}$$

where $\Phi(\vec{R}^0)$ is the static equilibrium energy and

$$\begin{aligned} \Phi_i(\overset{l}{\kappa}) &= \left. \frac{\partial \Phi(\vec{R})}{\partial u_i(\overset{l}{\kappa})} \right|_{u_i(\overset{l}{\kappa}) = 0} \\ \Phi_{ij}(\overset{l\,l'}{\kappa\kappa'}) &= \left. \frac{\partial^2 \Phi(\vec{R})}{\partial u_i(\overset{l}{\kappa})\, \partial u_j(\overset{l'}{\kappa'})} \right|_{u_i(\overset{l}{\kappa}) = u_j(\overset{l}{\kappa'}) = 0} \end{aligned} \tag{10}$$

In the equilibrium configuration $\vec{R}^0$ the force on any ion must vanish, therefore $\Phi_i(\overset{l}{\kappa})$ is zero. The equilibrium position of the κ^{th} ion in the l^{th} unit cell is denoted by $\vec{R}^0(\overset{l}{\kappa})$.

From Eqs (1), (2), (3) and (7) we obtain the following expression for the static equilibrium energy:

$$\begin{aligned} \Phi(\vec{R}^0) = {} & \frac{3}{5} Z E_F - \frac{3Ze^2}{4\pi} k_F + Z(0.678 \ln r_0 - 2.505)\, 10^{-12} \\ & + \sum_{\vec{k} \leq k_F} \langle \vec{k} | V_I - V_P | \vec{k} \rangle + E_b(\vec{R}^0) + E_c(\vec{R}^0) \end{aligned} \tag{11}$$

where

$$E_b(\vec{R}^0) = \frac{1}{2} \sum_{h \neq 0} |F(\vec{h})|^2 \, U_e(h) \tag{12}$$

$\vec{h}$ is a reciprocal lattice vector. $E_c(\vec{R}^0)$ is the electrostatic energy of point ions of valence Z, immersed in a uniform compensating background of electrons. $E_c(\vec{R}^0)$ is calculated according to the Ewald-Fuchs method [7]:

$$E_c(\vec{R}^0) = \frac{1}{2r_s} (Ze)^2 \alpha \tag{13}$$

where

$$\alpha = \sum_{l,\kappa,\kappa'} \frac{1}{r} \frac{G[X\binom{l\ 0}{\kappa\kappa'}]}{X\binom{l\ 0}{\kappa\kappa'}} - \frac{2}{\sqrt{\pi}} + 3\left[\sum_{\vec{h}'\neq 0} |F(\vec{h}')|^2 \frac{e^{-\vec{h}'^2/4}}{\vec{h}'^2} \frac{|F(0)|^2}{4}\right]$$

$$G(Y) = \frac{2}{\sqrt{\pi}} \int_Y^\infty e^{-X^2}\,dX, \qquad \vec{h}' = \vec{h}\,r_s, \qquad \vec{X}\binom{l\ l'}{\kappa\kappa'} = \frac{1}{r_s}[\vec{R}^0\binom{l}{\kappa} - \vec{R}^0\binom{l'}{\kappa'}]$$

Here r is the number of atoms per unit cell.

The energy contribution belonging to the dynamic term of the potential energy (9) is due to the Bose-Einstein gas of phonons arising from the quantized modes of vibration of the ions. Even at 0°K, the ions execute zero-point vibrations. The zero-point energy is given by

$$E_N = \frac{1}{2} \sum_{\vec{q},\alpha} \hbar\omega_\alpha(\vec{q}) \tag{14}$$

Here $\omega_\alpha(\vec{q})$ is the phonon frequency, $\vec{q}$ the phonon wavevector and α the polarization index. From the static equilibrium energy (11) and the zero-point energy we obtain the free energy per ion at 0°K

$$F_0 = E_G = \Phi(\vec{R}^0) + E_N \tag{15}$$

The phonon frequencies must be determined from the Hamiltonian (1, 9)

$$H - \Phi(\vec{R}^0) = H_L = T_I + \frac{1}{2} \sum_{\substack{l,\kappa,i\\ l',\kappa',j}} \Phi_{ij}\binom{l\ l'}{\kappa\kappa'} u_i\binom{l}{\kappa} u_j\binom{l'}{\kappa'} \tag{16}$$

Using Eqs (2), (7), (10) and (16) the phonon frequencies are obtained from the eigenvalue equation for the polarization vectors $\vec{e}(\kappa,\vec{q})$

$$\sum_{\kappa',j} [D_{ij}\binom{\vec{q}}{\kappa\kappa'} - \delta_{ij}\,\delta_{\kappa\kappa'}\,M\omega^2(\vec{q})]\; e_j(\kappa',\vec{q}) = 0 \tag{17}$$

where

$$D_{ij}\binom{\vec{q}}{\kappa\kappa'} = \sum_{l} \Phi_{ij}\binom{0\ l}{\kappa\kappa'} \cdot e^{-i\vec{q}[\vec{R}^0\binom{0}{\kappa} - \vec{R}^0\binom{l}{\kappa'}]}$$

Since the potential energy (2) is a sum of two-body potentials which depend only on the magnitude of the separation between ions, we obtain from Eqs (2) and (7)

$$D_{ij}\binom{\vec{q}}{\kappa\kappa'} = C_{ij}\binom{\vec{q}}{\kappa\kappa'} + E_{ij}\binom{\vec{q}}{\kappa\kappa'} \tag{18}$$

where

$$E_{ij}\binom{\vec q}{\kappa\kappa'} = \frac{1}{r}\Big[\sum_{\vec h}(\vec q+\vec h)_i(\vec q+\vec h)_j U_e(|\vec q+\vec h|)\, e^{i\vec q\cdot[\vec R^0\binom{0}{\kappa}-\vec R^0\binom{0}{\kappa'}]} - \delta_{\kappa\kappa'}\sum_{\vec h\neq 0}(\vec h)_i\,(\vec h)_j\, U_e(h)\cdot L(\vec h)\Big] \tag{19}$$

$$L(\vec h) = \sum_{\kappa}\cos\vec h\cdot\vec R^0\binom{0}{\kappa}$$

$$C_{ij}\binom{\vec q}{\kappa\kappa'} = M\omega_p^2\, C'_{ij}\binom{\vec q\,'}{\kappa\kappa'} \qquad \omega_p^2 = \frac{4\pi n(Ze)^2}{M},\quad \vec q\,' = \vec q\, r_s \tag{20}$$

$$\vec h' = \vec h r_s \qquad \vec X\binom{l\;l'}{\kappa\kappa'} = \frac{1}{r_s}\Big[\vec R^0\binom{l}{\kappa} - \vec R^0\binom{l'}{\kappa'}\Big]$$

$$\begin{aligned}
C'_{ij}\binom{\vec q\,'}{\kappa\kappa'} = -\frac{1}{3}\Bigg\{&\sum_{l=0}\frac{1}{\vec X^2\binom{l\,0}{\kappa\kappa'}}\Bigg[\left(\frac{3X_i\binom{l\,0}{\kappa\kappa'}X_j\binom{l\,0}{\kappa\kappa'}}{X^2\binom{l\,0}{\kappa\kappa'}} - \delta_{ij}\right)\\
&\times\left(\frac{G[X\binom{l\,0}{\kappa\kappa'}]}{X\binom{l\,0}{\kappa\kappa'}} + \frac{2e^{-\vec X^2\binom{l\,0}{\kappa\kappa'}}}{\sqrt{\pi}}\right) + \frac{4}{\sqrt{\pi}}X_i\binom{l\,0}{\kappa\kappa'}X_j\binom{l\,0}{\kappa\kappa'}e^{-\vec X^2\binom{l\,0}{\kappa\kappa'}}\Bigg]\\
&\times e^{-i\vec q\,'\vec X\binom{l\,0}{\kappa\kappa'}} - \delta_{\kappa\kappa'}\sum_{l,\kappa_1}\frac{1}{\vec X^2\binom{l\;0}{\kappa_1 0}}\Bigg[\left(\frac{3X_i\binom{l\;0}{\kappa_1 0}X_j\binom{l\;0}{\kappa_1 0}}{\vec X^2\binom{l\;0}{\kappa_1 0}} - \delta_{ij}\right)\\
&\times\left(\frac{G[X\binom{l\;0}{\kappa_1 0}]}{X\binom{l\;0}{\kappa_1 0}} + \frac{2e^{-\vec X^2\binom{l\;0}{\kappa_1 0}}}{\sqrt{\pi}}\right) + \frac{4}{\sqrt{\pi}}X_i\binom{l\;0}{\kappa_1 0}X_j\binom{l\;0}{\kappa_1 0}e^{-X^2\binom{l\;0}{\kappa_1 0}}\Bigg]\Bigg\}\\
&+\frac{1}{r}\Bigg[\sum_{\vec h'}\frac{(\vec h'+\vec q\,')_i\,(\vec h'+\vec q\,')_j}{(\vec h'+\vec q\,')^2}\,e^{-\frac{(\vec h'+\vec q\,')^2}{4}}\;e^{i\vec h'\vec X\binom{00}{\kappa\kappa'}}\\
&-\delta_{\kappa\kappa'}\sum_{\vec h'\neq 0}\frac{(\vec h')_i\,(\vec h')_j}{(\vec h')^2}\,e^{-\frac{\vec h'^2}{4}}\;L(\vec h')\Bigg]
\end{aligned}$$

ω_p^2 is the plasma frequency of the ions, C'_{ij} depends only on the crystal structure. In cubic and hexagonal lattices Eq. (17) factors for $\vec q$ parallel to the crystallographic directions [100], [110], [111] and [0001], and can be reduced to the form

$$\Omega^2(\vec q,\alpha) = \Omega_e^2(\vec q,\alpha) + \Omega_c^2(\vec q,\alpha) \tag{21}$$

where

$$\Omega^2(\vec{q},\alpha) = \frac{\omega^2(\vec{q},\alpha)}{\omega_p^2}$$

From Eq.(21) we see that certain phonon frequencies can be separated into two parts, the direct Coulomb interaction between rigid ions with uniform neutralizing but non-responsive background, and the ion-electron-ion interaction. Since Ω_c^2 depends only on the crystal structure (20), a number of important observations about the strength of the electron-ion coupling can be made, when the experimental $\omega^2(\vec{q},\alpha)$ are expressed in units of ω_p^2 (see Refs [15, 25]).

It is of some physical interest to deduce from the dynamic part of the potential energy (9) an effective two-body interaction which depends only on the magnitude of the separation between ions. From Eqs (18), (19) and (20) we obtain

$$U(Q) = U_c(Q) + U_e(Q) \tag{22}$$

where

$$U_c(Q) = \frac{4\pi n(Ze)^2}{Q^2}$$

U(Q) is the Fourier transform of the effective ion-ion interaction U(R) so that

$$U(R) = \frac{1}{(2\pi)^3 n}\int U(Q)\,e^{-i\vec{Q}\cdot\vec{R}}\,d^3Q = \frac{(Ze)^2}{R} + \frac{1}{(2\pi)^3 n}\int U_e(Q)e^{-i\vec{Q}\cdot\vec{R}}\,d^3Q \tag{23}$$

The discontinuity of $U_e(Q)$ (4, 8) at $Q = 2k_F$ leads to an oscillating behaviour of U(R) at large values of R. Using the form of $U_e(Q)$ given in Eq.(8), we obtain

$$U_\infty(R) = \lim_{R\to\infty} U(R) = B(2k_F)\frac{\cos 2k_F R}{(2k_F R)^3} \tag{24}$$

where

$$B(2k_F) = \frac{9\pi^2 V_I^2(2k_F)Z^2}{\left[1+\frac{1}{2\pi a_0 k_F}\left(1-\frac{2}{4+p}\right)\right]^2 E_F} \tag{25}$$

The origin of these Friedel oscillations [14] and that of the Kohn anomalies in the phonon dispersions are the same, namely, the singular behaviour of the first derivative of the static dielectric function, Eq.(5).

3. LATTICE DYNAMICS AND MODEL POTENTIAL

We turn now to the main problem: how is the bare ion potential to be calculated? Various methods have been used to determine $V_I(Q)$, including the pseudo-potential and model-potential approach [2]. Lin and Phillips [16] pointed out that there is always an important quantity, the core shift, which greatly affects the first-principle calculations. This shift arises from one-electron and many-electron effects, which make the zero of energy in the crystal different from that in the free atom.

From Eqs (19) and (21) we see that the phonon frequencies are very sensitive to $U_I(Q)$ or $V_I(Q)$. This raises the possibility of obtaining a model potential for a large and continuous range of Q in contrast to the electronic and electrical properties which give $U_I(Q)$ for Q only equal to a few lattice vectors or $2k_F$ respectively. Hence, it may be better to treat this potential as a function which is to be found from the measured phonon dispersions. The first attempt was made by Cochran [17]. He assumed that $U_I(Q)$ falls to very small values for $Q > \sqrt{2} \cdot 2\pi/a$. This assumption is based on Bardeen's [10] expression for $U_I(Q)$ on the basis of which the contribution of the Umklapp - processes to Ω_e^2, Eq.(21), is underestimated.

By using the arguments of Hellman and Kassatotschkin [18] and of the pseudo-potential method [2] we expressed the bare model potential in the following form [4, 8]:

$$V_I(Q) = -\frac{4\pi n Z e^2}{Q^2} + \sum_n \gamma_n H_n(Qr_n) \tag{26}$$

where

$$H_1(Q) = \frac{1}{[1+(Qr_1)^2]^2} \qquad\qquad H_2(Q) = \frac{Qr_2}{[1+(Qr_2)^2]^3}$$

γ_n and r_n are the model parameters. The first part of Eq.(26) represents the attractive forces coming from the long-range Coulomb field of the net ion charge Ze. The second term is an expansion of all other contributions, including the repulsive part of the pseudo-potential, in terms of hydrogen-like wave functions.

Using Eqs (8), (17), (19), (20) and (26), the model parameters are readily determined from the experimental data by means of the least-squares method. To ensure that the phonon frequencies satisfy the symmetry of the Brillouin zone, the sum over the reciprocal lattice included the following number of nearest neighbour shells: Na: 16, Al: 20, Mg: 60. The physical constants and the results are listed in Table I. The sources of the experimental results are as follows: Na, Woods et al. [19], Al: Yarnell et al. [20] and Walker [21], Mg: Iyengar et al. [22]. The fitted and experimental results are compared in Figs 1, 2 and 3. For a quantitative comparison we use the root-mean-square deviation (RMD) of the fit expressed in the form

$$\mathrm{RMD} = \left(\frac{\sum_i g_i \{[\omega_i^2 - \omega_{0i}^2]^2 - [\Delta\omega_i^2]^2\}}{\sum_i g_i (\omega_i^4 - [\Delta\omega_i^2]^2)} \right)^{\frac{1}{2}}$$

TABLE I. PHYSICAL CONSTANTS AND MODEL POTENTIAL PARAMETERS

		Na	Mg	Al
k_F	Å^{-1}	0.923	1.369	1.750
p		1.860	2.120	2.390
r_1	Å	0.34 ± 0.03	0.18 ± 0.03	0.17 ± 0.01
r_2	Å	0.20 × 0.01	0.18 ± 0.04	0.16 ± 0.01
γ_1	10^{-12} erg	2.70 ± 0.07	5.27 ± 0.42	7.37 ± 0.16
γ_2	10^{-12} erg	3.77 ± 0.23	4.27 ± 2.14	3.55 ± 1.39
RMD	%	4.92	3.33	3.8

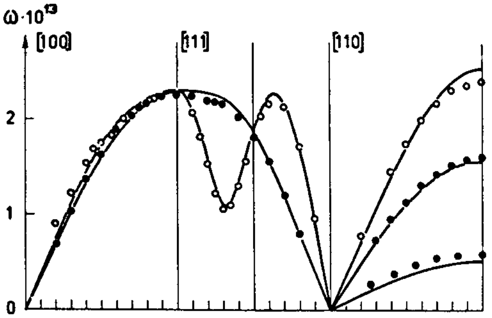

FIG. 1. Phonon dispersion curves for bcc Na. The circles show some of the experimental points of Woods et al. [19]. The lines represent the four parameter fit. ω in units of $\sec^{-1}$.

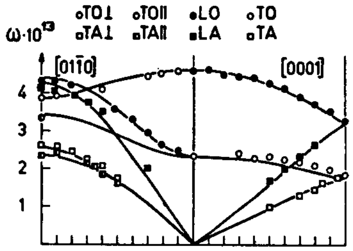

FIG. 2. Phonon dispersion curves for hcp Mg. The circles show some of the experimental points of Iyengar et al. [22]. The lines represent the four parameter fit. ω in units of $\sec^{-1}$.

where $g_i = [\Delta\omega_i^2]^2\omega_i$ are the observed phonon frequencies, $\Delta\omega_i$ the experimental errors and ω_{0i} the calculated frequencies. The numerical RMD values are listed in Table I. The values of Ω_c^2 and Ω_e^2 (21) for hexagonal Na, Mg and Al are given in Table II. It is known that the

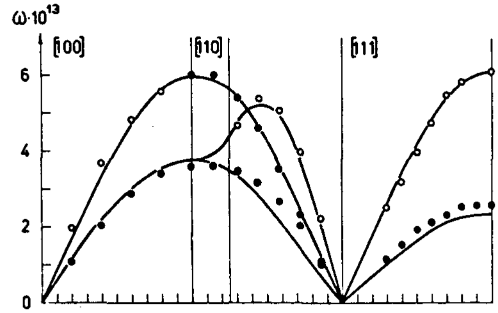

FIG.3. Phonon dispersion curves for fcc Al. The circles show some of the experimental points of Yarnell et al. [20] and Walker [21]. The lines represent the four parameter fit. ω in units of $\sec^{-1}$.

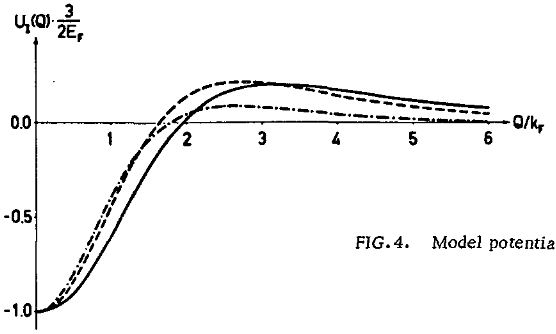

FIG.4. Model potential for Na ——, Mg - - - - and Al —·—·—.

TABLE II. CONTRIBUTION TO Ω^2 FOR hcp Na, Mg AND Al IN THE [0001] DIRECTION

	q/q_{max}	Ω_c^2	Ω_e^2		
			Na	Mg	Al
LA:	0.2	0.9978	- 0.9916	- 0.9950	- 0.9955
	0.4	0.9915	- 0.9663	- 0.9795	- 0.9824
	0.6	0.9815	- 0.9252	- 0.9510	- 0.9615
	0.8	0.9689	- 0.8716	- 0.9146	- 0.9347
	1.0	0.9549	- 0.8100	- 0.8763	- 0.9046
LO:	0.0	0.9087	- 0.5944	- 0.7422	- 0.8033
	0.2	0.9110	- 0.6077	- 0.7490	- 0.8084
	0.4	0.9176	- 0.6377	- 0.7686	- 0.8233
	0.6	0.9279	- 0.6865	- 0.7984	- 0.8489
	0.8	0.9407	- 0.7463	- 0.8353	- 0.8741
	1.0	0.9549	- 0.8100	- 0.8763	- 0.9046

strengths of the electron-phonon interaction in Na, Mg and Al are different, i.e. very weak, weak, intermediate. This difference manifests itself in many of their properties, e.g. their electronic contribution to the specific heat which is influenced by the electron-phonon interaction [9]. (Na: $C/C_0 = 1.27$, Mg: 1.31 and Al: 1.45, where C_0 is the free electron value.) The distinction is even more striking when one compares Ω_e^2 (Table II). Since Ω_e^2 represents an important contribution to Ω^2, it is clear that phonon dispersion curves can be used to obtain information about the model potential for a large continuous range of Q. Figure 4 shows the screened model potentials $U_I(Q)$ for Na, Mg and Al, derived from the observed phonon frequencies.

4. EFFECTIVE ION-ION INTERACTION

Using Eqs (8), (23), (25), (26) and Table I we calculated the effective ion interaction U(R) and the amplitudes of the Friedel oscillations $B(2k_F)$. Figure 5 shows the results we have obtained for Na, Mg and Al. As expected (Table III), the Friedel oscillations in Na are too small to produce a visible effect. With regard to Al, Yarnell et al. [20] have pointed out that their data indicates interactions up to 15 neighbours. This agrees with our findings for the more pronounced Friedel oscillations in this metal (Table III, Fig. 5).

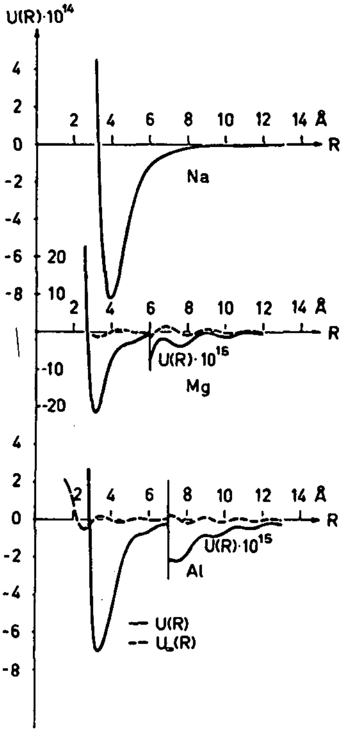

FIG. 5. Effective ion-ion interaction in Na, Mg and Al. U_∞ (R) is the asymptotic form given by Eq. (24). U(R) in units of erg.

TABLE III. AMPLITUDES OF THE FRIEDEL OSCILLATIONS IN UNITS OF 10^{-12} erg

	Na	Mg	Al
$B(2k_F)$	0.03	10.32	13.99

5. BAND STRUCTURE AND FERMI SURFACE

We computed the energy shifts of electron states by the perturbation theory, Eq. (2). In simple metals the matrix elements are small, but the computed shifts are not always small since the energy denominators $E_{\vec{k}+\vec{Q}} - E_{\vec{k}}$, which enter the perturbation expansion, can become zero near the Bragg planes $\vec{Q} = \vec{h}/2$. To improve upon this approach, it is necessary to use perturbation theory for degenerate systems. One uses a few-plane-wave basis set for the expansion of the electron wave function. The plane-wave expansion (27) may be substituted into the one-electron Schrödinger equation (28). This leads in the usual way to a set of coupled equations (29):

$$|\vec{k}) = \sum_{\vec{h}} a_{\vec{h}\vec{k}} e^{i(\vec{k}-\vec{h})\vec{r}} \tag{27}$$

$$[T + U_I(\vec{r})]|\vec{k}) = E_k|\vec{k}) \tag{28}$$

$$\left[\frac{\hbar^2}{2m}(\vec{k}-\vec{h})^2 - E(\vec{k},\vec{h})\right] a_{\vec{k}\vec{h}} + \sum_{\vec{h}'} F(\vec{h}-\vec{h}')\, U_I(|\vec{h}-\vec{h}'|)\, a_{\vec{h}\vec{h}'} = 0 \tag{29}$$

For a consistent solution the determinant (29) must vanish:

$$\det\left|\left[\frac{\hbar^2}{2m}(\vec{k}-\vec{h})^2 - E(\vec{k},\vec{h})\right]\delta_{\vec{h}\vec{h}'} + F(\vec{h}-\vec{h}')U_I(|\vec{h}-\vec{h}'|)\right| = 0 \tag{30}$$

For each $\vec{k}$ there are many solutions of the secular equation; these solutions correspond to the many-band energies.

From the Fermi energy defined by

$$\int_0^{E_F} N(E)\, dE = Z \tag{31}$$

where

$$N(E) = \frac{2}{(2\pi)^3 n} \int \frac{d\sigma_E}{|\mathrm{grad}\, E(k)|_E}$$

and the secular equation (30), it is now possible to calculate the shape of the Fermi surface

$$E(\vec{k}_F) = E_F \tag{32}$$

TABLE IV. FERMI ENERGY. E_F^0 IS THE FREE ELECTRON AND E_F THE EFFECTIVE FERMI ENERGY IN UNITS OF 10^{-12} erg

	E_F^0	E_F
Na	5.193	5.133
Mg	11.434	11.166
Al	18.679	18.629

Using Eqs (30), (31), (32) and Table I, we calculated the Fermi energy and the radial distortion of the Fermi surface. The Fermi energies are listed in Table IV. The calculated angular distortions of the Fermi surface in sodium are shown in Fig. 6. For comparison we have also plotted the experimental results of Lee [23]. The agreement between the calculated and measured distortions is satisfactory. The band structure and the Fermi surface for Mg will be published elsewhere [24].

6. LATTICE ENERGY AND CRYSTAL STABILITY

The lattice energy, Eq. (15), provides a wealth of information including the relative stability of different phases, their lattice constants and the cohesive energy. Therefore this is one of the central problems in understanding the nature of simple metals. Harrison [2] and the authors [6] have applied the pseudo-potential approach to problems

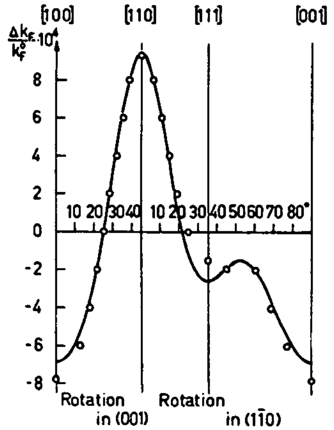

FIG. 6. Deviation of the Fermi surface from sphericity in Na. The circles show some experimental data from Ref. [23].

TABLE V. CONTRIBUTIONS TO THE LATTICE ENERGY E_G (11, 33) IN UNITS OF 10^{-12} erg

	r_0/a_0	$3/5 \cdot E_F$	E_{ex}	E_{corr}	γ_1	E_c	E_b	Φ_0	Φ_0 (exp)
Na	3.917	3.12	- 5.08	- 1.58	2.70	- 9.93	- 0.29	- 11.12	- 10.04
Mg	2.650	6.86	- 7.54	- 1.85	5.27	- 23.39	- 1.51	- 22.16	- 19.43
Al	2.073	11.21	- 8.63	- 2.01	7.37	- 39.18	- 0.76	- 33.00	- 30.22

$\gamma_1 = \frac{1}{Z} \sum_{\vec{k}} \langle \vec{k} | V_I - V_P | \vec{k} \rangle$, $E_{ex} = -\frac{3e^2}{4\pi} k_F$, $E_{corr} = (0.678 \cdot \ln r_0 - 2.505)$

such as the relative stability of different lattices. These effects are expected to be insensitive to errors arising from the little-known absolute energy. Kleinman [26], however, has claimed that a proper accounting of the energy contributions can lead to reasonable values of the cohesive energy in the OPW-pseudo-potential method.

Here we examine a simple model for the lattice energy based on perturbation theory. Using Eqs (11), (13), (15) and Table I we calculated the free energy per electron at 0°K. This energy is the sum of the sublimation heat E_S and the magnitude of the first Z ionization energies per electron I

$$E_G = \Phi(R^0) + E_N = E_S + |I| \tag{33}$$

In these calculations we neglected the zero-point energy. The results are listed in Table V. The agreement with the experimental values is reasonable.

In spite of these uncertainties, there are other properties which we may reasonably treat. These are properties which involve rearrangements at constant volume, such as the energy difference between different structures. In the following we specify the volume of the metal and examine the relative energies of different structures at that volume. We have done this for the three simple metallic structures bcc, fcc and hcp, the latter as a function of the c/a ratio. Table VI gives these values at constant volume and 0°K relative to the most stable structure. From experiment [27] it is known that Na undergoes partial transition to the hcp structure below 35°K. The correct structure is therefore obtained for Na, Mg and Al. Also, the computed axial ratios are close to those observed. To investigate the microscopic stability [28], we calculated the phonon dispersion curves of each metal in all three structures. Some results are listed in Table II. We have found that in all cases, except bcc Al, $\omega^2(\alpha, \vec{q}) > 0$ so that the microscopic stability condition is fulfilled. Judging from our limited results, it is unlikely that the martensitic transformation of Na could be caused by instability of phonons. Our calculations indicate that the lowest transverse branch is higher in the fcc and hcp than in the bcc phase. This is consistent with a temperature-induced phase transition.

TABLE VI. RELATIVE ENERGIES OF THE CRYSTAL STRUCTURES IN UNITS OF 10^{-16} erg PER ION

	Na	Mg	Al
bcc	13.9	548	410
fcc	1.2	189	0
hcp	0	0	4.2
c/a	1.633	1.633	1.633
$c/a)_{exp}$	1.634	1.622	-

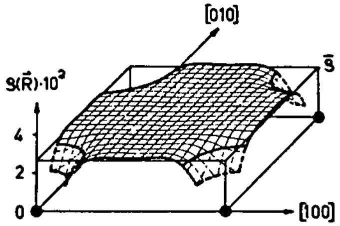

FIG.7. Calculated valence-charge density on a [001] plane in Na. $\bar{\rho}$ is the charge density of the free electron model. $\rho(\vec{R})$ in units of $Å^{-3}$.

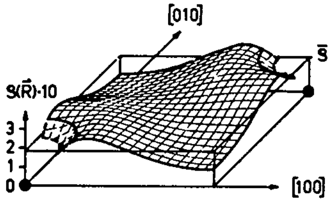

FIG.8. Calculated valence-charge density on a [001] plane in Al. $\bar{\rho}$ is the charge density of the free electron model. $\rho(\vec{R})$ in units of $Å^{-3}$.

We will now consider one further property which sheds some light on the metallic binding. Since we have computed the valence wave functions to first order, we may also obtain the valence-electron charge density for any crystal structure of interest. Figure 7 shows the calculated charge density on a [001] plane in Na and Fig.8 the charge density on a [001] plane in Al. For Na we find a nearly uniform density between the ions, whereas Al shows moderate non-uniformity. This partially explains the deviations between the experimental and calculated lattice energies.

7. ELECTRICAL RESISTIVITY

The variational expression for the electrical resistivity obtained, using the simplest trial function, is given in the first Born approximation by Ref.[29]:

$$\rho = \frac{9}{2\hbar k_B T e^2 k_F^2 \sigma^2} \iiint \frac{d\sigma\, d\sigma'}{\vec{V}_k \vec{V}_{k'}} Q_i^2 |\langle \varphi_{\vec{k}'} | U_I | \varphi_{\vec{k}} \rangle|^2 \frac{S(\vec{Q},\omega)}{1 - e^{-\beta\omega}}\, d\omega \tag{34}$$

where $\varphi_{\vec{k}}$, $\varphi_{\vec{k}'}$ are electron states, $\vec{Q} = \vec{k} - \vec{k}'$, σ the area of the Fermi surface, $\vec{V}_k$ the electron velocity in state $\varphi_{\vec{k}}$, $\langle \varphi_{\vec{k}} | U_I | \varphi_{\vec{k}'} \rangle$ is the matrix element of the screened electron-phonon interaction, Q_i is the component of $\vec{Q}$ in the direction of the applied field, and β is equal to $\hbar/k_B T$. Lastly, $S(\vec{Q},\omega)$ is the dynamic structure factor. For the solid phase, in the one-phonon approximation, and with the further assumption that the phonons are in thermal equilibrium

$$S(\vec{Q},\omega) = \frac{\pi\hbar}{M} \sum_{\alpha} \frac{[\vec{e}_\alpha(\vec{Q})\vec{Q}]^2}{[e^{\beta\omega_\alpha(\vec{Q})} - 1]\,\omega_\alpha(\vec{Q})} \{\delta(\omega - \omega_\alpha(Q)) + \delta(\omega + \omega_\alpha(Q))\}$$

In the case of spherical Fermi surfaces, a local pseudo-potential and cubic symmetry, expression (34) is reduced to

$$\rho = \frac{3m^2\pi}{4\hbar^3 e^2 k_F^6 n} \int_0^{2k_F} Q^3 U_I(Q)\, S(Q)\, dQ \tag{35}$$

where

$$S(Q) = \frac{1}{4\pi} \int S(\vec{Q})\, d\Omega$$

$$S(\vec{Q}) = \frac{1}{2\pi} \int_{-\infty}^{+\infty} \frac{\beta\omega}{1 - e^{-\beta\omega}}\, S(Q,\omega)\, d\omega = \frac{\beta\hbar}{M} \sum_{\alpha} \frac{[\vec{e}_{\alpha}(\vec{Q})\,\vec{Q}]^2}{[e^{\beta\omega_{\alpha}(\vec{Q})} - 1][1 - e^{-\beta\omega_{\alpha}(\vec{Q})}]} \tag{36}$$

To perform the integrals, we had to know the phonon dispersions and the polarization vectors over the irreducible part of the Brillouin zone. We used the measured phonon dispersion curves, a force constant model, and an interpolation method. With the help of this data and the model potential, we calculated the electrical resistivity at constant volume as a function of temperature. The results are plotted in Fig. 9 and compared with the experimental data of Dugdale and Gugan [30]. The agreement is very satisfactory. The deviations are 0.03% at 50°K and 14% at 293°K. The discrepancy at 293°K can be explained in terms of the neglected anharmonic contributions. For Al we obtained the following result: $T = 77°\text{K}$, $\rho/T = 2.40 \times 10^{-9}$ Ω cm/°K, compared with the experimental value of 2.9×10^{-9} Ωcm/°K. The agreement is good and indicates clearly that one can reasonably expect to get just as good agreement in the solid as is found in the liquid phase [3, 5]. Similar calculations have been extended to other materials [31]. In the liquid phase, as $\beta\omega/(1 - e^{-\beta\omega}) \cong 1$, S(Q) is the static structure factor, which can be obtained from X-ray or neutron diffraction.

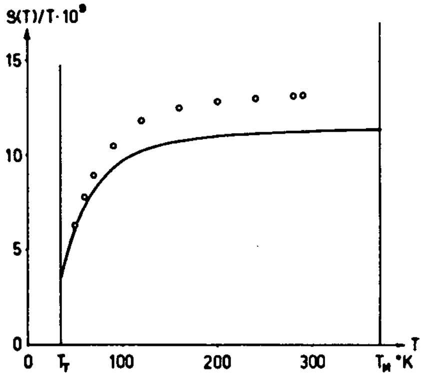

FIG. 9. ρ/T plotted against degrees K for Na. ——— calculated, o experimental. T_T is the phase transition temperature and T_M is the melting point. ρ/T in units of $\Omega\,\text{cm}\,°\text{K}^{-1}$.

REFERENCES

[1] TOYA, T., J. Res. Inst. Catalysis 6 (1958) 183.
[2] HARRISON, W.A., Pseudopotential in the Theory of Metals, Benjamin, New York (1966).
[3] HEINE, V., ABARENKOV, I., Phil. Mag. 9 (1964) 457.
[4] SCHNEIDER, T., STOLL, E., Phys. Kondens. Materie 5 (1966) 331, 364; 6 (1967) 135.
[5] SCHNEIDER, T., STOLL, E., Adv. Phys. 16 (1967) 731.
[6] SCHNEIDER, T., STOLL, E., Phys. Letters 24A (1967) 258.
[7] FUCHS, K., Proc. Roy. Soc. A151 (1935) 585.
[8] SCHNEIDER, T., EIR-Rep. No. AF-SSP-15, Würenlingen (1967).
[9] PINES, D., NOZIERES, P., The Theory of Quantum Liquids 1, Benjamin, Inc., New York (1966).
[10] BARDEEN, J., Phys. Rev. 52 (1937) 668.
[11] HONE, D., Phys. Rev. 120 (1960) 1600.
[12] BAILYN, M., Phys. Rev. 117 (1960) 974.
[13] SHAM, L.J., Proc. Roy. Soc. A283 (1965) 33.
[14] FRIEDEL, J., Phil. Mag. 43 (1952) 153.
[15] NG, S.C., BROCKHOUSE, B.N., Solid State Commun. 5 (1967) 79.
[16] LIN, P.J., PHILLIPS, J.C., Adv. Phys. 14 (1965) 257.
[17] COCHRAN, W., Proc. Roy. Soc. A276 (1963) 308.
[18] HELLMAN, H., KASSATOTSCHKIN, W., J. Chem. Phys. 4 (1936) 324.
[19] WOODS, A.D.B., BROCKHOUSE, B.N., MARCH, R.H., STEWART, A.T., BOWERS, R., Phys. Rev. 128 (1962) 1112.
[20] YARNELL, J.L., WARREN, J.L., KOENIG, S.H., Lattice Dynamics, Pergamon Press, London (1965) 57.
[21] WALKER, C.B., Phys. Rev. 103 (1956) 547.
[22] IYENGAR, P.K., VENKATARAMAN, G., VIJAYARAGHAVAN, P.R., ROY, A.P., Inelastic Scattering of Neutrons (Proc. Symp. Bombay, 1964) 1, IAEA, Vienna (1965) 153.
[23] LEE, M.J.G., Proc. Roy. Soc. A295 (1966) 440.
[24] STOLL, E., SCHNEIDER, T., Phys. Kondens. Materie, to be published.
[25] VOSKO, S.H., TAYLOR, R., KEECH, G.H., Can. J. Phys. 43 (1965) 1187.
[26] KLEINMAN, L., Phys. Rev. 146 (1967) 472.
[27] BARRET, C.S., Acta Cryst. 9 (1956) 671.
[28] TOSI, M., ARAI, T., Advances in Highpressure Research 1, Academic Press, Inc., New York (1966) 277.
[29] GREENE, M.P., KOHN, W., Phys. Rev. 137A (1965) 513.
[30] DUGDALE, J.S., GUGAN, D., Proc. Roy. Soc. A270 (1962) 186.
[31] BUHRER, W., SCHNEIDER, T., STOLL, E., Helv. Phys. Acta 40 (1967) 813.

MICROSCOPIC THEORY OF FORCE CONSTANTS IN SOLIDS*

M.H. COHEN, R.M. MARTIN** AND R.M. PICK†
THE JAMES FRANCK INSTITUTE,
CHICAGO UNIVERSITY,
UNITED STATES OF AMERICA

Abstract

MICROSCOPIC THEORY OF FORCE CONSTANTS IN SOLIDS. The expressions of the force constants are derived from the energy of a neutral system of interacting nuclei and electrons. These force constants depend only on the nuclear charges and the inverse dielectric function of the electronic system. We verify that they fulfil the general symmetry, translational and rotational invariance properties required by the Born-von Kármán theory. When the role of the core electrons is neglected, these force constants can be evaluated in metals from the bare ionic potentials. In insulators, the existence of long-wavelength acoustical phonons implies that the inverse dielectric function satisfies a certain number of sum rules. The method becomes more difficult to apply, which explains the general use of phenomenological models.

1. INTRODUCTION

The theory of lattice dynamics is based on the concept of the Born-von Kármán force constants. In the classical theory, these are introduced as disposable parameters, subject only to a few restrictive conditions imposed either by the periodicity of the lattice or the invariance of the energy of the crystal under any displacement. In practice these coefficients are nowadays determined by the comparison between the measured phonon spectrum and the one computed with the help of a given model of the solid under study. Unfortunately, such models depend not only on the nature of the solid (e.g. molecular, ionic, covalent or metallic crystal) but also on various physical assumptions which make any comparison between their predictions often meaningless. The aim of this paper is to offer a link between such models by presenting a general theory of the force constants independent of the nature of the crystal. The basic differences between various types of forces in solids will then appear in a natural way.

There is no difficulty in formulating such a theory in the many-body language, which will be done elsewhere [1]. The presentation we shall give here will nevertheless be done within the Hartree (or self-consistent field, SCF) approximation. In this form, many expressions we shall derive in section 2 closely parallel those obtained by Sham [2] and Sham and Ziman [3]. Our motivation for such an exposition is that some properties we wish to discuss in later sections are more evident in this language. Let us stress anyhow that the expressions we shall derive and the properties we shall exhibit do not depend on the Hartree approximation. On the other hand, they are not general because we have neglected a certain number of effects we want to discuss now.

First of all, we have essentially derived 0°K force constants, because we restricted ourselves to a perturbation theory which is second order in nuclear displacements and have not considered any renormalization effect due to the phonon-phonon interaction. Thus the entropy term we shall use in section 2 simply represents the blurring of the Fermi surface in the metallic case; we used the free energy and not the total energy only because it allowed for a more compact presentation of the theory.

Secondly, we have restricted ourselves to a Born-Oppenheimer approximation, i.e. we have assumed that the electrons are always in equilibrium with respect to the nuclei. This implies that the plasma frequency is higher than that of any phonon. Our treatment is basically incorrect for low carrier concentration semiconductors [4] or semimetals.

Within such approximations, we shall first derive the expression for the force constants and show that it depends only on the charge of the nuclei and the complete dielectric function of the system.

The third section will be devoted to a short study of this dielectric function, which reveals the basic difference between insulators and metals.

In section 4 we shall look at the problems raised by the application of this theory to metals. We shall see that an unphysical weight has been given to the core electrons which rigidly move with the nuclei and that they represent the major obstacle to its straightforward application. This can be remedied by the use of pseudo-potentials. We rapidly discuss the further simplifications which make this approach very useful in simple metals, and end by a brief comment on the Kohn anomaly in any metal.

Finally, section 5 is devoted to insulators. We first point out why all the models used in such materials are very far from the general theory. We then discuss a possibility of actually using it by making an approximation originally due to Sinha [5] and show the type of forces which appear in such a model.

2. THE GENERAL FORMALISM

2.1. Free energy and force constants

Let us consider a neutral system composed of nuclei and electrons. The nuclei charge density of this system is

$$\sum_a Z_a \, \delta(r - R_a)$$

where the index a labels a given nucleus, while α will stand at the same time for a and for a co-ordinate axis index. For any given set of R_a, we can express the energy of our system as the interaction energy of the nuclei, plus the free energy of the electronic system in the presence of the nuclear charges

$$F(R_a) = \tfrac{1}{2} \sum_{a,b}{}' \frac{Z_a Z_b}{R_{ab}} + F_e(R_a) \tag{2.1}$$

Let R_a^0 represent the rest position of R_a. When the nuclei make small excursions from their equilibrium positions, one can write

$$F(R_a) = F^0 + \tfrac{1}{2} \sum_{\alpha,\beta} \delta R_\alpha \, \delta R_\beta \, \frac{\partial^2 F_0}{\partial R_\alpha \, \partial R_\beta} \tag{2.2}$$

where F^0 is the equilibrium value of F, and the δR_α are the nuclear displacements. The Born-von Kármán force constants $C^{\alpha\beta}$ are simply $\partial^2 F_0/\partial R_\alpha \partial R_\beta$ which need now to be expressed more specifically.

In the SCF approximation the Hamiltonian of the electronic system is

$$H = -\frac{\nabla^2}{2} + V(r) + V_S(r) \tag{2.3}$$

where

$$V(r) = \sum_a \frac{-Z_a}{|r - R_a|} \tag{2.4}$$

and $V_S(r)$ is the self-consistent potential. If $N\bar{Z}$ is the total number of electrons of the system, the Fermi energy E_F and $V_S(r)$ are self-consistently determined by the system of equations

$$N\bar{Z} = \mathrm{Tr}\left\{f(H)\right\} \tag{2.5a}$$

$$V_S(r) = \int d^3r \frac{1}{|r - r'|} \rho e(r') = \int d^3r' \frac{1}{|r - r'|} \mathrm{Tr}\left\{f(H(r_1))\, \delta(r' - r_1)\right\} \tag{2.5b}$$

$$f(H) = \frac{1}{e^{\beta(H-E_F)} + 1} \tag{2.5c}$$

In such a picture, each electron moves independently in the mean field of the other electrons so that if

$$H\,|\varphi_k\rangle = E_k\,|\varphi_k\rangle$$

the mean occupation of the state k is

$$n_k = \langle\varphi_k\,|f(H)|\,\varphi_k\rangle = f(E_k) \tag{2.6}$$

and the free energy of the system is given by, [6]

$$F_e = \mathrm{Tr}\left\{f(H)\left(H - \frac{1}{2} V_S\right)\right\} - \frac{1}{\beta}\sum_k [n_k \log n_k + (1 - n_k)\log(n - n_k)] \tag{2.7}$$

The $-\frac{1}{2}V_S$ term prevents the electron-electron energy from being counted twice, while the second term is just the entropy of an independent gas of fermions.

Replacing in Eq. (2.7) the sum over k by a Trace operator, and n_k by its expression as a function of H gives

$$F_e = \mathrm{Tr}\left\{f(H)(E_F - \frac{1}{2} V_S) - \frac{1}{\beta}\log(1 - f(H))\right\} \tag{2.8}$$

This expression leads to an easy evaluation of $\partial^2 F_e / \partial R_\alpha \partial R_\beta$. Indeed we have

$$\frac{\partial F_e}{\partial R_\alpha} = E_F \frac{\partial}{\partial R_\alpha} \mathrm{Tr}\left\{f(H)\right\} + N\bar{Z} \frac{\partial E_F}{\partial R_\alpha} - \frac{1}{2} \frac{\partial}{\partial R_\alpha} \int \mathrm{Tr}\left\{f(H)\,\delta(r)\right\} \frac{1}{|r-r'|}$$

$$\times \mathrm{Tr}\left\{f(H)\,\delta(r')\right\} d^3r\, d^3r' - \frac{1}{\beta}(-\beta)\, \mathrm{Tr}\left\{f(H) \frac{\partial}{\partial R_\alpha}(H - E_F)\right\} \tag{2.9}$$

Because of Eq. (2.5a), the first term of expression (2.9) is equal to zero.

The second cancels against the last one while the third term is just equal to

$$-\mathrm{Tr}\left\{f(H) \frac{\partial V_S}{\partial R_\alpha}\right\}$$

(see Eq. 2.5b). Thus

$$\frac{\partial F_e}{\partial R_\alpha} = \mathrm{Tr}\left\{f(H) \frac{\partial}{\partial R_\alpha} (H - V_S)\right\}$$

$$= \mathrm{Tr}\left\{f(H) \frac{\partial V}{\partial R_\alpha}\right\} \tag{2.10}$$

and

$$\frac{\partial^2 F_e}{\partial R_\alpha \partial R_\beta} = \mathrm{Tr}\left\{f(H) \frac{\partial^2 V}{\partial R_\alpha \partial R_\beta}\right\} + \mathrm{Tr}\left\{\frac{\partial f(H)}{\partial R_\beta} \frac{\partial V}{\partial R_\alpha}\right\} \tag{2.11}$$

Differentiating twice the nucleus-nucleus interaction and noting that $\partial V / \partial R_\alpha$ does not depend on R_b if $R_b \neq R_a$ gives

$$C^{\alpha\beta} = \mathrm{Tr}\left\{\frac{\partial f(H)}{\partial R_\beta} \frac{\partial V}{\partial R_\alpha}\right\} + (1 - \delta_{ab}) \frac{\partial^2}{\partial R_\alpha \partial R_\beta} \frac{Z_a Z_b}{R_{ab}}$$

$$+ \delta_{ab} \left[\mathrm{Tr}\left\{f(H) \frac{\partial^2 V}{\partial R_\alpha \partial R_\beta}\right\} + \sum_c{}' \frac{\partial^2}{\partial R_\alpha \partial R_{\alpha'}} \frac{Z_a Z_c}{R_{ac}}\right] \tag{2.12}$$

where $\delta / \delta R_{\alpha'}$ means that the derivation is taken with respect to the same variable R_a.

2.2. The dielectric function and the final form of the force constants

Let us now interpret the first term of Eq. (2.12). Expressing (2.5b) as the potential created by the total electronic density ρ_e (r) we have

$$\mathrm{Tr}\left\{\frac{\delta f(H)}{\partial R_\beta} \frac{\partial V}{\partial R_\alpha}\right\} \equiv \int \frac{\partial V(r)}{\partial R_\alpha} \mathrm{Tr}\left\{\frac{\partial f(H(r_1))}{\partial R_\beta} \delta(r_1 - r)\right\} d^3r$$

$$= \int \frac{\partial V(r)}{\partial R_\alpha} \frac{\partial}{\partial R_\beta} \rho_e(r)\, d^3r \tag{2.13}$$

Let us define the function $\tilde{v}(r, r')$ such that

$$\int \tilde{v}(r, r') \frac{1}{|r'-r''|} d^3r' = \delta(r - r'') \tag{2.14}$$

With the help of Eq. (2.14) we can express $\frac{\partial \rho_e(r)}{\partial R_\beta}$ as

$$\frac{\partial \rho_e(r)}{\partial R_\beta} = \int \tilde{v}(r, r_1) \frac{1}{|r_1 - r_2|} \frac{\partial \rho_e(r_2)}{\partial R_\beta} d^3r_1 \, d^3r_2$$

$$= \int \tilde{v}(r, r_1) \frac{\partial V_S(r_1)}{\partial R_\beta} d^3r_1 \tag{2.15}$$

By analogy with the usual Maxwell theory we define now the function $\epsilon^{-1}(r, r')$ which relates the small external potential $\delta V_{ext}(r')$ imposed to the system to the variation of the total potential felt by an electron at the point r

$$\delta V_{tot}(r) = \delta V_{ext}(r) + \int \frac{\partial V_S(r)}{\partial V_{ext}(r')} \delta V_{ext}(r') \, d^3r' = \int \epsilon^{-1}(r, r') \, \delta V_{ext}(r') \, d^3r' \tag{2.16}$$

We recall in Appendix A that the inverse function $\epsilon(r, r')$ has the following expression

$$\epsilon(r, r') = \delta(r-r') - \int \frac{1}{|r-r''|} \sum_{1,2}{}' \frac{f(E_1) - f(E_2)}{E_1 - E_2} \langle 1 | \delta(r'') | 2 \rangle \langle 2 | \delta(r') | 1 \rangle \, d^3r'' \tag{2.17}$$

where E_i ($|i\rangle$) are the eigenvalues (functions) of the unperturbed Hamiltonian (2.3). As the external potential imposed here is $(\partial V(r)/\partial R_\alpha)\delta R_\alpha$, we obtain from Eq. (2.16)

$$\frac{\partial V_S(r)}{\partial R_\beta} = \int [\epsilon^{-1}(r, r') - \delta(r-r') \frac{\partial V(r')}{\partial R_\beta} d^3r' \tag{2.18}$$

Then we find

$$\int \frac{\partial V(r)}{\partial R_\alpha} \frac{\partial}{\partial R_\beta} \rho_e(r) \, d^3r$$

$$= \int \frac{\partial V(r)}{\partial R_\alpha} \tilde{v}(r, r') \, [\epsilon^{-1}(r', r'') - \delta(r'-r'')] \frac{\partial V(r'')}{\partial R_\beta} d^3r d^3r' d^3r''$$

$$= Z_a Z_b \frac{\partial^2}{\partial R_\alpha \partial R_\beta} \int \delta(r'-R_a) [\epsilon^{-1}(r'r'') - \delta(r'-r'')] \frac{1}{|r''-R_b|} d^3r' d^3r'' \tag{2.19}$$

For a + b the second term in Eq. (2.19) just cancels the second term of Eq. (2.12) and the expression for $C^{\alpha\beta}$ finally reads

$$C^{\alpha\beta} = (1-\delta_{ab})\; Z_a Z_b \frac{\partial^2}{\partial R_\alpha \partial R_\beta} \int \epsilon^{-1}(R_a, r)\, \frac{1}{|r-R_b|}\, d^3r + \delta_{ab}\; Z_a \frac{\partial^2}{\partial R_\alpha \partial R_{\alpha'}} \times$$
$$\left[\int [\epsilon^{-1}(R_a, r) - \delta(R_a - r)]\, \frac{Z_a}{|r-R_a|}\, d^3r - \mathrm{Tr}\left\{ f(H(r_1))\, \frac{1}{|r_1 - R_a|} \right\} + {\sum_c}' \frac{Z_c}{R_{ac}} \right] \tag{2.20}$$

where the derivation symbols mean that the derivation must be taken with respect to the explicit variable (e.g. $\frac{\partial}{\partial R_a} \mathrm{Tr}\left\{ f(H(r))\, \frac{1}{|r-R_\alpha|} \right.$

$\left. \equiv \mathrm{Tr}\left\{ f(H(r))\, \frac{\partial}{\partial R_\alpha}\, \frac{1}{|r-R_a|} \right\} \right).$

2.3. Symmetry and invariance properties of the $C^{\alpha\beta}$

We shall now prove briefly that some of the usual properties of the force constants derived from the phenomenological theory are actually fulfilled.

2.3.1. Symmetry

$\int \epsilon^{-1}(r, r'')\, \frac{1}{|r''-r'|}\, d^3r''$ is a symmetrical function of r and r' because its inverse is $\int \tilde{v}(r, r'')\epsilon(r''r')\, d^3r''$ which is symmetrical (see Eq. 2.17). Thus $C^{\alpha\beta} = C^{\beta\alpha}$.

2.3.2. Translation invariance

The energy of the system must be invariant under any translation of the whole system. This gives the condition

$$\sum_b C^{\alpha\beta} = 0 \tag{2.21}$$

for any given and fixed direction j of β. This property is easily proven by considering expression (2.12):

(a) For the nucleus-nucleus part because $\frac{\partial^2}{\partial R_\alpha \partial R_\beta} \frac{1}{R_{ab}} = -\frac{\partial^2}{\partial R_\alpha \partial R_{\alpha'}} \frac{1}{R_{ab}}$

(b) For the electronic part we have by partial integration

$$\mathrm{Tr}\left\{ f(H(r))\, \frac{\partial^2 V(r)}{\partial R_\alpha \partial R_\beta} \right\} = \mathrm{Tr}\left\{ \frac{\partial f(H(r))}{\partial r_j}\, \frac{\partial V(r)}{\partial R_\alpha} \right\} \tag{2.22}$$

but $\frac{\partial H(r)}{\partial r_j} = [\nabla_{r_j}, H] = [\nabla_{r_j}, (V(r) + V_S(r)] = \frac{\partial}{\partial r_j}(V(r) + V_S(r))$ (2.23) where the second equality of Eq. (2.23) holds because ∇_{r_j} commutes with the $-\nabla^2/2$ term of H.

The last term of Eq. (2.23) is the derivative of the total potential at r. By the equality of action and reaction, it is self-evident that it is equal to minus the change of total potential due to a global displacement of all the nuclei, i.e.

$$\frac{\partial}{\partial r_j} V_{tot}(r) = -\sum_b \frac{\partial V_{tot}(r)}{\partial R_\beta} \quad (\beta = b, j) \tag{2.24}$$

In fact the last statement is another way of invoking the translational invariance, and equality (2.24) is rigorously proven in Appendix B. With the help of Eq. (2.24) one can work backward to Eq. (2.22) which now reads

$$\mathrm{Tr}\left\{f(H(r_1)\ \frac{\partial^2 V(r_1)}{\partial R_\alpha \partial R_\beta}\right\} = -\sum_b \mathrm{Tr}\left\{\frac{\partial f(H(r_1))}{\partial R_\beta}\ \frac{\partial V(r_1)}{\partial R_\alpha}\right\} \tag{2.25}$$

which proves equality (2.21).

2.3.3. Rotational invariance

The energy of the system must also be invariant under an arbitrary infinitesimal rotation of the crystal, i.e. $\delta R_\beta = \omega \Lambda R_\beta$. This leads to the condition

$$\sum_b C^{ab}_{ij} R^b_k - C^{ab}_{ik} R^b_j = 0 \tag{2.26}$$

whatever be i, j, k (we have here explained the splitting of (a) and (b) in their position and Cartesian co-ordinate indices). We shall not demonstrate here this property, which can be proven by exactly the same technique as used above. Let us just mention that when j (or k) equals i, one finds that

$$\sum_b (C^{ab}_{ij} R^b_k - C^{ab}_{ik} R^b_j) = Z_a \sum_b \left[Z_b \frac{\partial}{\partial R_\alpha} \frac{1}{R_{ab}} + \mathrm{Tr}\left\{f(H)\ \frac{\partial V}{\partial R_\alpha}\right\}\right] \tag{2.27}$$

Each term in the right-hand side of Eq. (2.27) is just $\partial F/\partial R_\alpha$ (see Eqs (2.1) and (2.11)) and Eq. (2.27) is equal to zero because each nuclei is in equilibrium.

2.3.4. Lattice case - periodicity

If the nuclei form a regular lattice of periodicity L, then clearly

$$C^{ab}_{ij} = C^{a+L\ b+L}_{i\ \ j}$$

This last property is true because the same periodicity holds for $\epsilon(r, r')$ (see Eq. (2.17)).

2.4. Conclusion

In conclusion, we see that we have derived microscopic force constants which are entirely expressed with the help of the complete set of wave functions of the unperturbed system in a formally simple way. We have then verified that they are bound by the usual relations which hold for the phenomenological Born-von Kārmān force constants. The formulae given above are so far completely general, and we shall see in later sections how the actual $C^{\alpha\beta}$ differ from one type of substance to another.

3. METALS AND INSULATORS: THE ACOUSTICAL SUM RULES

3.1. Introduction

Up to now our formulation has been completely general and did not take into account any particular property of the electronic eigenfunctions and eigenvalues. Nevertheless, on physical grounds, the properties of the inverse dielectric function are very different in metals and insulators. Such a difference will appear in the study of the long-wavelength acoustical branches. We shall show that such phonons can exist in insulators only if a certain number of sum rules are fulfilled, while no such conditions exist in metals.

To show the necessity of such sum rules, we shall first briefly recall how is usually shown the existence of acoustical branches. We shall then discuss some properties of the dielectric function and afterwards apply the results found to the propagation of acoustical phonons. A brief discussion on the physical origin of those sum rules will end this section.

3.2. Acoustical branches in phenomenological theory

Let us split index a which specifies the position of a nucleus between a cell index L and a position in the cell index A. In classical notations, the phonon frequencies ω are the solutions of the equation

$$D(\vec{q}) = \left\| D_{ij}^{AB}(\vec{q}) \right\| = \left\| C_{ij}^{AB}(\vec{q}) - M_A\,\omega^2\,\delta_{A,B}\,\delta_{ij} \right\| = 0 \qquad (3.1)$$

where

$$C_{ij}^{AB}(\vec{q}) = \frac{1}{N^2}\sum_{L,L'} C_{ij}^{AB\,LL'}\; e^{-i\vec{q}\cdot(\vec{R}_L+\vec{R}_A-\vec{R}_{L'}-\vec{R}_{A'})} \qquad (3.2)$$

and M_A is the mass of the nucleus at point $\vec{R}_L + \vec{R}_A$.

In the phenomenological theory of lattice vibrations, one proves the existence of acoustical branches by noting that $D(\vec{q})$ is equal to the determinant $\left\| \mathbb{D}_{ij}^{AB}(\vec{q}) \right\|$ whose elements are formed in the following manner:
for any A_0 let

$$\mathbb{D}_{ij}^{AB}(\vec{q}) = D_{ij}^{AB}(\vec{q}) \qquad A,\ B \neq A_0$$

$$\mathbb{D}_{ij}^{A_0B}(\vec{q}) = \sum_{A} D_{ij}^{AB}(\vec{q}) \qquad A = A_0$$

$$(3.3)$$

$$\mathbb{D}_{ij}^{AA_0}(\vec{q}) = \sum_{B} D_{ij}^{AB}(\vec{q}) \qquad B = A_0$$

$$\mathbb{D}_{ij}^{A_0A_0}(\vec{q}) = \sum_{A,B} D_{ij}^{AB}(\vec{q}) \qquad A = B = A_0$$

Writing $\vec{q} = |q|\vec{e}$ one expands $\mathbb{D}_{ij}^{AB}(\vec{q})$ in powers of q. Due to the translational invariance relation (2.21)

$$\mathbb{D}_{ij}^{AB}(0) = 0 \tag{3.4}$$

if A or $B = A_0$.
If we assume that ω^2 is proportional to $|q|^2$, both $\mathbb{D}_{ij}^{A_0B}(\vec{q})$ and $\mathbb{D}_{ij}^{AA_0}(\vec{q})$ are proportional to $|q|$ and $\mathbb{D}_{ij}^{A_0A_0}$ is proportional to $|q|^2$ while the remaining terms are finite. Thus Eq. (3.1) has three solutions proportional to q^2.

This demonstration shows that a condition for the existence of acoustical phonons is that $\mathbb{D}_{ij}^{AB}(\vec{q})$ has a well-defined 0 limit when $|q|$ goes to zero, if A, or B, or both are equal to A_0.

3.3. Properties of the dielectric function

As the $C^{\alpha\beta}$ are expressed as functions of $\epsilon^{-1}(r, r')$, let us first study some properties of its Fourier transform. $\epsilon(q_1, q_2)$ is given by

$$\epsilon(q_1, q_2) = \delta(q_1 - q_2) - \frac{4\pi}{q_1^2} \sum_{1,2} \langle 1 | e^{-iq_1r_1} | 2 \rangle \langle 2 | e^{iq_2r_2} | 1 \rangle \frac{f(E_1) - f(E_2)}{E_1 - E_2} \tag{3.5}$$

$f(E_1) - f(E_2)$ restricts the summations in Eq. (3.5) to the case where one state is occupied and the other empty. Furthermore, due to the periodicity of the lattice, $\epsilon(e_1, q_2)$ is different from zero only when

$$q_1 = q_2 + K$$

where K is any vector of the reciprocal lattice. Then q_1 and q_2 do not tend independently to zero, which is the limit of ϵ we want to study in detail.

When $|1\rangle$ and $|2\rangle$ do not belong to the same band, in the $q \to 0$ limit

$$\langle 1 | e^{iqr} | 2 \rangle \simeq \vec{q} \cdot \vec{A}_{1,2} \tag{3.6}$$

where $\vec{A}_{1,2}$ is finite.

This is the only situation which happens in insulators, so that, inserting (3.6) in Eq. (3.5), one obtains

$$\left.\begin{aligned} &\epsilon(q, q+K) = -\frac{4\pi}{q^2}\, \vec{q} \cdot \vec{A}_{q+K} \\ &\epsilon(q+K, q) = -\frac{4\pi}{|q+K|^2} \vec{A}^{*}_{q+K} \cdot \vec{q} \end{aligned}\right\} K \neq 0 \qquad K \neq 0 \tag{3.7}$$

$$\epsilon(q, q) = 1 - \frac{4\pi}{q^2} [\vec{q} \cdot \vec{A}_q]^2$$

where lim $\vec{A}_{q+K}$ is finite.

In metals on the other hand $|1\rangle$ and $|2\rangle$ can belong to the same band, in which case $\langle 1 | e^{iqr} | 2\rangle$ remains finite when q goes to zero. The energy denominator then becomes proportional to $q\,(E_2 = E_1 + \vec{q} \cdot \frac{\partial E_1}{\partial \vec{q}})$ but so is the number of terms involved in the summation. We see that the states close to the Fermi surface govern the dependence of ϵ for $q \to 0$ in metals and that

$$\begin{aligned} &\epsilon(q+K, q) \text{ remains finite, } K \neq 0 \\ &\epsilon(q, q+K) \text{ is } \propto \text{ to } \frac{1}{q^2} \text{ whatever be } K \end{aligned} \tag{3.8}$$

Let us close this paragraph by remarking that the last line of (3.8) simply expresses the perfect screening properties of a metal.

3.4. Properties of the dynamical matrix in the $q \to 0$ limit

We can now study easily the properties of the transformed dynamical matrix $\mathbb{D}^{AB}_{ij}(\vec{q})$ for small $\vec{q}$. Replacing $C^{\alpha\beta}$ by its value gives

$$C^{AB}_{ij}(\vec{q}) = Z_A A_B \sum_{K,K'} (q+K)_i\, \epsilon^{-1}(q+K, q+K')\, \frac{(q+K')_j}{|q+K'|^2}\, e^{i[(q+K)R_A - (q+K')R_B]} + g^A_{ij}\, \delta_{AB} \tag{3.9}$$

where $\vec{q}$ is restricted to be in the first Brillouin zone. The last term in Eq. (3.9) comes from the $\delta_{a,b}$ term of $C^{\alpha\beta}$, and does not depend on $\vec{q}$.

3.4.1. The metallic case

For metals it follows from (3.8) that $q_1^2 \epsilon(q_1, q_2)$ is finite in the $q_0 \to 0$ limit[1] and so is the inverse matrix $\epsilon^{-1}(q_1, q_2)\,(1/q_2^2)$ in the same limit; $q_1^i\, \epsilon^{-1}(q_1, q_2)\, q_2^j (1/q_2^2)$ then always tends to zero in this limit, and any term of the sum of the right-hand side of Eq. (3.9) has a well-defined limit when q tends to zero.

The requirement that $\mathbb{D}^{A_0 B}_{ij}(q)$ should be proportional to q for small q can then be fulfilled by

$$g^A_{ij} = -\sum_B \sum_{KK'}{}' Z_A Z_B K_i\, \epsilon^{-1}(K, K')\, \frac{K'_j}{|K'|^2} e^{i(KR_A - K'R_B)} \tag{3.10}$$

where $\sum'$ means that the summation is restricted to $|K|$ and $|K'| \neq 0$. The hermiticity of $\mathbb{D}^{AB}_{ij}(q)$ automatically ensures that $D^{AA_0}_{ij}(0)$ is also equal to zero.

3.4.2. The insulator case

For insulators we see from Eq. (3.7) that the quantity $(1/q_1^j)\, q_1^2\, \epsilon(q_1, q_2)\,(1/q_2^i)$ never tends to zero in the $q_0 \to 0$ limit. In the

---

[1] We shall here write in short $q_0 \to 0$ limit for any of the three possibilities: $q_1 \to 0$, $q_2 \neq 0$; $q_2 \to 0$, $q_1 \neq 0$; $q_1 = q_2 \to 0$

same limit, the inverse matrix $q_1^i \epsilon^{-1}(q_1, q_2)(q_1^j/q_2^2)$ will always remain finite, but this limit clearly depends on the direction of $\vec{q}$ because, e.g., it can be equal to zero if $q_1^i = 0$. Then in the right-hand side of Eq.(3.9) exist a certain number of terms whose limit depends on the direction of $\vec{q}$. So that g_{ij}^A can be defined whatever this direction, we must impose that the sum of all those terms is a well-behaved quantity. Due to the symmetry of $\epsilon^{-1}(q_1, q_2)(1/q_2^2)$ this means that

$$\lim_{q\to 0} \sum_B \left\{ q_i \epsilon^{-1}(q,q) \frac{q_j}{q^2} + \sum_K{}' \epsilon^{-1}(q+K,q) \frac{1}{q^2} \times \left[(q+K)_i q_j e^{iKR_A} + q_i (q+K)_j e^{-iKR_B} \right] \right\} Z_B e^{-iqR_B} = 0 \qquad (3.11)$$

As the determinant $\mathbb{D}_{ij}^{AB}$ is Hermitian, there will exist in general 3n such sum rules to be satisfied. Symmetry considerations may very well reduce this number. For instance, in the case of the diamond structure, from cubic symmetry arguments alone, this relation is always fulfilled for i ≠ j. Furthermore, the existence of a centre of symmetry shows that the relations for the two atoms are complex conjugates one of the other. But symmetry considerations cannot apply any further and we remain with one sum rule. The existence of this sum rule is thus an intrinsic property of insulators.

Equation (3.11) takes into account all values of K. One then needs in general very good accuracy in $\epsilon(q_1, q_2)$ for large values of q_1 and q_2 to ensure the correctness of this equation. The difficulty of obtaining this accuracy will make necessary the use of suitable approximation schemes like the one discussed in section 5.

Before closing this sub-section, we can briefly comment on the origin of this sum rule. In an insulator the Coulomb field is not perfectly screened at large distances. Thus when two nuclei far apart from one another move with respect to the rest of the lattice, this mutual interaction is a dipole-dipole one. Similarly, $C_{ij}^{AB}(\vec{q})$ represents the interaction of the two sub-lattices A and B when their nuclei have a periodic displacement. Neglecting all other contributions to C_{ij}^{AB}, we can say, for example, that any dipole associated with a nucleus on sub-lattice A interacts with the field due to the whole array of dipoles associated with nuclei on sub-lattice B. It is well known that, even when $\vec{q}$ goes to zero, such a field does not depend on the direction of the dipoles only, but also on their relative angle with vector $\vec{q}$. $C_{ij}^{AB}(\vec{q})$ cannot have, then, a definite limit when $\vec{q}$ goes to zero. Equation (3.11) means that, in the limit of long acoustical waves, the sum of the dipole fields associated with all the nuclei and electrons disappears at each nuclear site.

4. GENERAL REMARKS AND APPLICATIONS TO METALS

4.1. The core electron problem

In the two preceding sections we have shown that a general dielectric function formalism enables one to express in a simple way the dynamical matrix and that the lowest eigenvalues of this matrix always behave as acoustical branches in metals.

The preceding formalism is, of course, difficult to apply as such because it requires the inversion of an infinite matrix, already very long to compute. It would also be extremely awkward to do because in the general expression (2.20) it is the nuclear charge Z_a which appears. By working with a general formalism, we let all the electrons of our system play an equivalent role which is physically absurd. In the actual case, most of the core electrons do move bodily with the nuclei, while the electrons which are responsible for the interatomic forces have energy comparable with the Fermi energy.

Our last statement is mathematically apparent from the very form of $\epsilon(q_1, q_2)$: the $(E_1 - E_2)^{-1}$ factor gives a prominent weight to those states, compared to the inner core ones.

It is less easy to understand how the core electrons play their role in the general theory. To see it, let us study a matrix element $\langle 1 | e^{iqr} | 2 \rangle$, where state $|1\rangle$ is occupied and state $|2\rangle$ empty. We can write

$$\langle 1 | e^{i\vec{q}\cdot\vec{r}} | 2 \rangle = \int d^3\vec{q}_1 \, 1^*(\vec{q}_1) \int e^{-(\vec{q}-\vec{q}_1)\cdot\vec{r}} \, 2(\vec{r}) \, d^3\vec{r} \tag{4.1}$$

where

$$1(\vec{r}) = \int d^3\vec{q} \; 1(\vec{q}) \, e^{i\vec{q}\cdot\vec{r}} \tag{4.2}$$

The function $1(\vec{r})$ being well localized in the vicinity of the nucleus, its Fourier transform $1(\vec{q})$ will not decrease rapidly with $|q|$ until $|q| r_0 \simeq 1$, where r_0 is of the order of the spatial extension of this function. The effect of such a matrix element is thus to spread out the dependence of $\epsilon(q_1, q_2)$ over values of q_1 or q_2 which are much larger than r_0^{-1}, and the lower the energy E_1, the larger is r_0^{-1}. Then, by letting the core electrons play a role in the calculation, two complementary difficulties occur at the same time:

(a) The matrix we need to invert must have, in q space, a size much larger than the largest possible r_0^{-1}. The inversion problem is thus formidable.

(b) Any element of the dynamical matrix is proportional to $Z_a Z_b$, while, on physical grounds, we expect it to depend on the product $z_a z_b$ of the ionic charges.

It is clear that the above-mentioned difficulties may be overcome by making use of a theory which emphasizes the sole role of the valence electronic states. This is the aim of the pseudo-potential theory. By doing so, one neglects the distortion of the core electron wave functions under the influence of the nuclear displacements and of the corresponding reorganization of the valence electrons. Such an effect is small and presumably negligible in view of the other approximations usually made at the same time in actual calculations.

4.2. Pseudo-potentials and simple metals

The mathematical transcription of the pseudo-potential technique consists in writing that there exists a Hamiltonian H_M of the form

$$H_M = -\frac{\nabla^2}{2} + \sum_a W_{R_a}(r) + V_S(r) \tag{4.3}$$

where W_{R_a} (r) is a pseudo-potential operator which represents the bare potential seen by a valence electron when there is a nucleus of charge Z_A at point R_A. One assumes that W_{R_a} (r) moves rigidly with R_a, and that V_S (r) is the self-consistent potential created by the valence electrons only. It is physically evident that for large values of $|r-R_a|$, W_{R_A} (r) behaves as a simple Coulomb potential of the form $z_a/|r-R_a|$, where z_a is the ionic charge. From electrical neutrality we have

$$\sum_a z_a = \int \rho_e(r)\, d^3r = \int \tilde{v}(r, r')\ V_S(r')\ d^3r d^3r' \tag{4.4}$$

The basic assumption of Eq. (4.3) is that its eigenfunctions and eigenvalues are, at least for the occupied valence states and the empty states corresponding to the first empty bands, identical to those of the Hamiltonian (2.3). Such an assumption is rigorously correct when H_M is not a Hermitian operator and W_{R_a} (r) a pseudo-potential of the form described by Austin, Heine and Sham [7]. But in most cases, the conditions for the validity of Eq. (4.3) are only approximately satisfied.

Actually the models used have generally made one or two more simplifying assumptions.

4.2.1. Local potential

The bare potential is a local potential of the form $W_{R_a}(r) = w(r-R_a)$. A simple repetition of the argument given in section 2 shows that, for $a \neq b$, one has:

$$C^{\alpha\beta} = \frac{\partial^2}{\partial R_\alpha \partial R_\beta} \Big[\int w(r_1 - R_a) \tilde{v}(r_1, r_2)\, \epsilon_M^{-1}(r_2, r_3)\, w(r_3 - R_b) d^3r_1\, d^3r_2\, d^3r_3$$

$$+ \frac{z_a z_b}{R_{ab}} - \int w(r_1 - R_a) \tilde{v}(r_1, r_2) w(r_2 - R_b) d^3r_1\, d^3r_2 \Big] \tag{4.5}$$

where $\epsilon_M^{-1}(r, r')$ is the inverse of the dielectric function constructed with the help of all the eigenfunctions of Eq. (4.3).

The two last terms of expression (4.5) describe a direct core-core interaction, which does not take into account any valence electron. Due to the long-distance asymptotic form of $w(r-R_a)$, those two terms completely cancel for large values of $|R_a - R_b|$, and the form of $C^{\alpha\beta}$ is dominated by its first term.

4.2.2. Free electron gas dielectric function

Instead of using the complete inverse function $\epsilon_M^{-1}(q_1, q_2)$, one takes as an approximation for it, the inverse dielectric function of a free electron gas of the same density. It has the well-known form

$$\bar{\epsilon}^{-1}_{(q_1, q_2)} = \delta(q_1 - q_2) \frac{1}{1 + 2\, \dfrac{k_F}{\pi q_1^2} \left[1 + \dfrac{(4k_F^2 - q_1^2)}{q_1 k_F} \log \left| \dfrac{q_1 + 2k_F}{q_1 - 2k_F} \right| \right]} \tag{4.5a}$$

This last approximation has been extensively made in all recent phonons calculations, whether or not a local pseudo-potential was used. Such an approximation short-circuits many calculations; it implies that all the conduction electrons are s-like and rules out the transitions and noble metals. Even in this case, it is the lowest order one. It has frequently been improved upon by adding corrections related to the exchange and correlations effects in the free electron gas. In principle, those depending on the more precise determination of the eigenfunctions and values could be added by writing

$$\epsilon_M(q_1, q_2) = \bar{\epsilon}(q_1, q_2) + \Delta(q_1, q_2) \tag{4.6}$$

and considering $\Delta(q_1, q_2)$ as a small quantity compared to $\bar{\epsilon}(q_1, q_2)$.

4.3. Transition and noble metals

Though identical in principle, the situation is in fact more difficult in such metals. A simple way of finding the eigenvalues of Eq. (4.3) does not exist and the actual $\epsilon_M^{-1}(q_1, q_2)$ is very far from Eq. (4.5a). A numerical resolution of Eq. (4.3) based on a realistic and simple form of $W_{R_a}(r)$ has been only done in a few metals [8, 9], and these results have not been applied yet to phonons problems.

4.4. The Kohn anomaly

We can simply note here that the analytical singularity which appears in $\bar{\epsilon}^{-1}(q_1, q_2)$ for $q = 2k_F$ is only related to the existence of a sharp Fermi surface. When the actual wave functions are used to compute $\chi(q_1, q_2)$ this singularity will appear at $\vec{q}_1$, whenever there exists a vector $\vec{K}$ such that $\vec{q}_1 + \vec{K}$ is a diameter of the Fermi surface [10]. Such a singularity then exists simultaneously on every term of $\epsilon(q_1, q_2)$ and, by inversion, of $\epsilon^{-1}(q_1, q_2)$. One deduces that $C^{\alpha\beta}$ has a slowly decreasing oscillatory behaviour for large nuclei separation. This behaviour is reflected on the phonon spectrum by an infinite derivative of the dispersion curve for such values of q_1. In practice the Kohn anomaly may be more visible with some transition metals [W, Ta, Mo...] than with normal metals, where this effect is difficult to see, except in lead, and possibly in lithium.

5. INSULATORS

5.1. General remarks

In the preceding section we emphasized that the difficult problem of inverting $\epsilon(q_1, q_2)$ when all the core electrons are taken into account could be reduced without making any appreciable error by using the pseudopotential technique. It is hoped that a similar scheme will work in insulators and the only occupied electronic states one need consider in detail are those of the last full band. But such simplifications which, in simple metals, enable one to perform easy calculations leave unsettled many difficulties when one deals with insulators. For the sake of exposition we can divide them in two different classes.

(a) The actual electronic wave functions are extremely different from plane waves, or orthogonal plane waves. Their computation is then difficult and requires a large amount of computer work. This also means that a leading term equivalent to the inverse dielectric function of the free electron gas does not exist in $\epsilon^{-1}(q_1, q_2)$. The inversion of $\epsilon(q_1, q_2)$ is thus again long and difficult.

(b) This inversion problem is also delicate because the acoustical sum rules force us to take into account the off-diagonal terms of $\epsilon^{-1}(q_1, q_2)$ for q_1 or q_2 tending to zero. This means that, in every specific case, a detailed asymptotic form of $\epsilon^{-1}(q_1, q_2)$ for large values of q_1 or q_2 has to be derived.

These difficulties explain why this approach has not been used up to now and are clearly related to two different and complementary aspects of the problem:

Point (b) reflects the infinite range of the electrostatic forces in an insulator, while point (a) expresses the important localization of the valence electrons in the vicinity of the ions and, in covalent systems, along the direction of the bonds. In the phenomenological approaches which are used to describe the phonon spectra of such systems, these two aspects are completely separated out. One assumes the existence of point ionic charges, forming electrically neutral atomic cells and interacting by a purely Coulombic potential to deal with point (b) and the effect of the localized electrons are represented by short-range forces between those ions. In the more sophisticated shell model [11-13] those electrons are taken into account in a more physical way by rigid electronic shells moving with respect to the ions. A net effect is to reduce the range of the non-Coulombic ion-ion forces necessary to explain a given spectrum. As has been shown by G. and M.S. Dresselhaus [14] in the case of germanium and silicon, this effect is self-evident in the sense that a shell_1-ion_1-ion_2-shell_2 interaction is mathematically equivalent to an interaction between more distant ions.

Despite the good results given by the above-mentioned models, the next developments of the general theory presented in sections 2 and 3 can be seen in two different ways.

As a mathematical tool, this theory enables one to give expressions for macroscopic quantities related to nuclear displacements. For instance, a microscopic derivation of the zero-frequency dielectric constant has been given by Adler [15] and Wiser [16]. Their expression does not take into account such displacements and is thus invalid for most systems. Its extension to 'ionic' crystals can be readily obtained with techniques similar to those presented here, and will be published elsewhere [17]. In the same way one can express the piezoelectric tensor, or the effective charge related to the splitting of the zero frequency optical modes in the Lyddane-Sachs-Teller formula [17].

The general method can offer also new and more realistic models to be compared with experiments. We shall now emphasize this last aspect by discussing, in this last sub-section, some properties of an approximation recently proposed by Sinha [5].

5.2. The Sinha model and force constants in insulators

5.2.1. The dielectric matrix approximate inversion technique

The difficult problem of inverting matrix $\epsilon(q_1, q_2)$ can be greatly simplified by the following procedure. Let us consider a given complete (not necessarily orthonormal), set of one variable functions $f_n(\vec{q})$. For any such set, there exists an infinite number of ways of writing

$$\chi(q_1, q_2) = \sum_{n,m} E_{nm} \, f_n(q_1) \, f^*_m(q_2) \tag{5.1}$$

(the E_{nm} are not unique because, though the left-hand side of Eq. (5.1) is defined only for $q_2 = q_1 + K$, its right-hand side is mathematically defined for any value of q_1 and q_2).

Moreover, the set of functions $f_n(q)$ is itself arbitrary. It is then perfectly reasonable to assume that there exists a development of $\chi(q_1, q_2)$ of the form of Eq. (5.1) which is rapidly enough convergent so that one can approximate $\chi(q_1, q_2)$ by its first few terms

$$\chi(q_1, q_2) \simeq \sum_{m=1}^{P} \sum_{n=1}^{P} E_{nm} \, f_n(q_1) \, f^*_m(q_2) \tag{5.2}$$

From the analysis made in section 3, it is clear that, in the limit $q \to 0$, $f_m(q)$ must be proportional to qA_m where $\lim_{q\to 0} A_m$ is finite. We can thus write that, for every value of q, $f_m(q)$ has the form

$$f_m(q) = \sum_{i=1}^{3} q_i \, f^i_m(q) \tag{5.3a}$$

where

$$\lim_{q\to 0} f^i_m(q) = \mathrm{cte} \neq 0 \tag{5.3b}$$

In the same manner, we shall let $E_{n,m}$ depend also on i and j. With such a form, the inversion of

$$\epsilon(q_1, q_2) = \delta(q_1 - q_2) - \frac{4\pi}{q_1^2} \sum_{i,j=1}^{3} \sum_{n,m=1}^{P} E^{ij}_{nm} \, q_{1i} \, f^i_n(q_1) f^{*j}_m(q_2) q_{2j} \tag{5.4}$$

is straightforward. By simply writing the definition of $\epsilon^{-1}(q_1, q_2)$:

$$\sum_K \epsilon^{-1}(q_1, q_1 + K) \, \epsilon(q_1 + K, q_1 + K') = \delta_{K',0} \tag{5.5}$$

one finds:

$$\epsilon^{-1}(q_1, q_2) = \delta(q_1 - q_2) + \frac{4\pi}{q_1^2} \sum_{i,j=1}^{3} \sum_{n,m=1}^{P} E^{-1\,ij}_{nm}(q_1) q_{1i} \, f^i_n(q_1) f^{*j}_m(q_2) q_{2j} \tag{5.6}$$

where

$$E^{-1\,ij}_{nm}(q) = \sum_{k=1}^{3} \sum_{\ell=1}^{P} E^{ik}_{n\ell} \, F^{-1\,kj}_{\ell m}(q) \tag{5.7a}$$

$$F^{\ell j}_{nm}(q) = \delta_{nm} \, \delta_{ij} - \sum_K \sum_{k=1}^{3} \sum_{\ell=1}^{P} \frac{4\pi}{|q+K|^2} \tag{5.7b}$$

$$\times (q+K)_i \, f^{*i}_n(q+K) \, f^k_\ell(q+K) (q+K)^k \, E^{kj}_{\ell m}$$

The inversion matrix problem is thus reduced to that of a $3p \times 3p$ matrix. This matrix depends on q and, due to the summation on K in Eq. (5.7b) is periodical in q with a period K.

5.2.2. The acoustical sum rules

Equation (5.5) enables one to fulfil more easily the acoustical sum rules (3.11). The direct calculation of $\chi(q_1, q_2)$ does not allow for a precise determination of the asymptotic form of $f^i_m(q)$ for large values of q. *One can then assume a parametric expansion of this asymptotic form;* the sum rules then become numerical equations between those parameters, which represents a much simpler procedure to apply. The form of $\epsilon(q_1, q_2)$ as given in Eq. (5.4) and first proposed in a very similar form by Sinha [5] seems then to be a possible approach for the use of the general theory.

5.2.3. The asymptotic form for force constants

We can now use Eq. (5.5) to get an explicit expression of the force constants $C^{\alpha\beta}$ for $a \neq b$. As we are interested here in some of their general properties, we shall suppose that we can make here the point-charge pseudo-potential approximation. This means that the $\chi(q_1, q_2)$ used in Eq. (5.2) has been computed by taking into account the last full electronic band only, and that at the same time the corresponding pseudo-potentials were simple Coulomb potentials with effective charges $z^1_A\ z^1_B \ldots$ With such hypotheses, we obtain with the help of Eqs (2.19) and (2.20) for $(1-\delta_{a,b}) \neq 0$

$$C^{\alpha\beta} = z^1_a z^1_b \frac{\partial^2}{\partial R_\alpha \partial R_\beta}$$

$$\times \left[\frac{1}{R_{ab}} + \int \delta(r_1 - R_a) \left\{ \epsilon^{-1}(r_1, r_2) - \delta(r_1 - r_2) \right\} \frac{1}{|r_2 - R_b|} d^3r_1\, d^3r_2 \right] \tag{5.8}$$

By Fourier transforming Eq. (5.6) we get

$$C^{\alpha\beta} = z^1_a z^1_b \frac{\partial^2}{\partial R_\alpha \partial R_\beta} \left[\frac{1}{R_{ab}} + \sum_{\substack{i,j\\n,m}} \sum_{N,M} \int f^i_\ell(R_a - r) \frac{\partial}{\partial r_i} \frac{1}{|r-N-M|} E^{-1\,ij}_{nm}(M) \right.$$

$$\left. \times \frac{\partial}{\partial r'_j} f^{*j}_m(N-r') \frac{1}{|r'-R_b|} d^3r\ d^3r' \right] \tag{5.9}$$

where

$$f^i_\ell(r) = \int f^i_\ell(q)\, e^{iqr}\, d^3q \tag{5.10a}$$

$$E^{-1}_{nm}{}^{ij}(R) = \sum_K E^{-1\,ij}_{nm}(K)\, e^{iKR} \tag{5.10b}$$

N, M being points of the direct lattice.

The first term of Eq. (5.9) is the direct interaction between the two dipoles $z_a^1\ \delta R_\alpha$ and $z_b^1\ \delta R_\beta$. To understand its second term, let us consider $f_\ell^i(r)$ as a charge distribution corresponding to a net non-zero charge (its Fourier transform $f_\ell^i(0)$ is different from zero). This charge distribution has no physical existence; it is just a mathematical artefact to express that if a dipole p exists at the origin, it induces at point r a charge variation equal to $p(\partial f_\ell^i/\partial r)(-r)$.

Any term of the second part of Eq. (5.9) can now be interpreted as follows. The dipole $z_a^1\ \delta R_\alpha$ at point R_a creates a charge distribution $z_a^1\ \delta R_\alpha(\partial f_\ell^i/\partial r)(R_A - r)$ to which corresponds an electrical field at N + M. This field polarizes the whole medium so that a net dipole moment exists at point N. Finally this dipole creates, via the charge distribution f_m^{*j}, a field at R_b which interacts with the dipole $z_b^1\ \delta R_\beta$.

This interpretation which, as noted by Sinha [5], parallels that of the shell model, is nevertheless purely formal because the relation between the field at N + M and the dipole moment at N depends on the indices 1 and m, which is not physically reasonable. The second term of expression (5.9) describes, then, a certain generalization of the shell model.

We can finally remark that the second term of Eq. (4.9) behaves as a dipole-dipole interaction. If we assume that $E^{-1}(M)$ decreases rapidly with M, in a first-order approximation, one can neglect all values of M such that $|M| > R_0$. A direct dipole-dipole term comes from $|N-R_a|$ or $|N-R_b| > R_0$. But the summation on all the other values of N also leads to a $|R_a - R_b|^{-3}$ term. This dipole-dipole interaction will not cancel completely against the first term of Eq. (5.9) and their difference is the origin of the dynamical effective charge which exists in insulators. The other forces between a and b will strongly depend on the variation of $E^{-1}(M)$ on M, thus on the detailed calculation of $\chi(q_1, q_2)$.

APPENDIX A

THE INVERSE DIELECTRIC FUNCTION

Let us add to the Hamiltonian H a small external potential $\delta V_{ext}(r)$. The corresponding variations of the self-consistent potential and of the Fermi energy will be denoted $\delta V_S(r)$ and δE_F respectively.

The electronic Hamiltonian, the density operator and the electronic density are now given by

$$H_1 \equiv H + \delta H = H + \delta V_{ext}(r) + \delta V_S(r) \tag{A.1}$$

$$f(H_1 - \delta E_F) \equiv \frac{1}{1 + e^{\beta[(H + \delta H - \delta E_F) - E_F]}} \tag{A.2}$$

$$\rho_e^1(r) = \mathrm{Tr}\left\{ \delta(r - r_1)\ f(H_1 - \delta E_F) \right\} \tag{A.3}$$

By integrating along a contour which includes every pole of $f(H_1-(E_F+\delta E_F))$, the charge density can also be written as

$$\rho_e^1(r) = \frac{1}{2\pi i}\oint \mathrm{Tr}\left\{\delta(r-r_1)\,\frac{1}{x-H_1+\delta E_F}\right\} f(x)\,dx \tag{A.4}$$

One can now expand the denominator of the right-hand side in powers of δH and δE_F. By considering the first-order terms on both sides of Eq. (A.4), we obtain

$$\delta\rho_e(r) = \int \left. \frac{1}{2\pi i}\oint \mathrm{Tr}\left\{\delta(r-r_1)\frac{1}{x-H}\,\delta(r'-r_2)\frac{1}{x-H}\right\} f(x)dx\,\right]\left(\delta H(r') - \delta E_F\right)d^3r' \tag{A.5a}$$

$$\equiv \int \chi(r,r')\,(\delta V_{ext}(r') + \delta V_S(r') - \delta E_F)\,d^3r' \tag{A.5b}$$

We can now use Eq. (2.15) which relates $\delta\rho_e(r)$ and $\delta V_S(r)$. Solving for $\delta V_S(r)$ this gives

$$\int \left(\delta(r-r') - \left[\int \frac{1}{|r-r''|}\,\chi(r'',r')d^3r''\right]\right)\delta V_S(r')\,d^3r'$$

$$= \int \frac{1}{|r-r''|}\,\chi(r'',r')\left(\delta V_{ext}(r') - \delta E_F\right)d^3r''\,d^3r' \tag{A.6}$$

Both sides of Eq. (A.6) can also be written with the help of the dielectric function $\epsilon(r,r')$ by taking as a definition

$$\epsilon(r,r') = \delta(r-r') - \int \frac{1}{|r-r''|}\,\chi(r'',r')\,d^3r'' \tag{A.7}$$

Multiplying both sides of Eq. (A.6) by $\epsilon^{-1}(r_1,r)$ and summing over r, we obtain

$$\delta V_S(r_1) = \int \left[\epsilon^{-1}(r_1,r') - \delta(r_1-r')\right]\left(\delta V_{ext}(r') - \delta E_F\right)d^3r' \tag{A.8}$$

Finally, since both systems represented by H and H_1 are electrically neutral, the net charge associated with $\delta V_{ext}(r)$ is equal to zero and the Fourier transform of δH and $\delta\rho_e$ are continuous functions of q. From the properties of $\epsilon^{-1}(q_1,q_2)$ when q_1, q_2 go to zero (see section 3), Eq. (A.8) imposes that $\delta E_F = 0$.

The exact expression of $\chi(r,r')$ has to be derived from Eq. (A.5a). If we compute the trace with the help of the complete set of functions which are the eigenfunctions of H ($H|1\rangle = E_1|1\rangle$), we have

$$\chi(r,r') = \frac{1}{2\pi i}\oint \sum_{1,2}\langle 1|\delta(r)|2\rangle\,\frac{1}{x-E_2}\,\langle 2|\delta(r')|1\rangle\,\frac{1}{x-E_1}\,f(x)dx \tag{A.9}$$

The poles of the integrand are simply $x = E_i$ and the contour integral gives

$$\chi(r, r') = \sum_{1,2} \langle 1 | \delta(r) | 2 \rangle \langle 2 | \delta(r') | 1 \rangle \frac{f(E_1)-f(E_2)}{E_1 - E_2} \qquad (A.10)$$

APPENDIX B

We justify here the equality (2.24) which proves the translation invariance of $C^{\alpha\beta}$. We have

$$\frac{\partial}{\partial r_{1j}} V_T(r_1) = \frac{\partial V(r_1)}{\partial r_{1j}} + \frac{\partial V_S(r_1)}{\partial r_{1j}} \qquad (B.1)$$

From expression (2.5b) we can write

$$\frac{\partial V_S(r_1)}{\partial r_{1j}} = \frac{\partial}{\partial r_{1j}} \int \frac{1}{|r_1 - r'|} \rho_e(r') \, d^3r' = - \int \frac{\partial}{\partial r'_j} \frac{1}{|r_1 - r'|} \rho_e(r') \, d^3r'$$

$$= \int \frac{1}{|r_1 - r'|} \frac{\partial}{\partial r'_j} \rho_e(r') \, d^3r' \qquad (B.2)$$

We can use for the evaluation of $\frac{\partial}{\partial r'_j} \rho_e(r')$ the same technique as in Eq. (2.22), namely

$$\frac{\partial}{\partial r'_j} \rho_e(r') = \frac{\partial}{\partial r'_j} \mathrm{Tr}\left\{ f(H(r_2)) \, \delta(r' - r_2) \right\} = - \mathrm{Tr}\left\{ f(H(r_2)) \frac{\partial}{\partial r_{2j}} \delta(r' - r_2) \right\}$$

$$= \mathrm{Tr}\left\{ \frac{\partial f(H(r_2))}{\partial r_{2j}} \delta(r' - r_2) \right\} \qquad (B.3)$$

From Eq. (A.5a) we have

$$\frac{\partial \rho_e(r')}{\partial r'_j} = \frac{1}{2\pi i} \oint \mathrm{Tr}\left\{ \delta(r' - r_2) \frac{1}{x - H} \frac{\partial(H - E_F)}{\partial r_{2j}} \frac{1}{x - H} \right\} f(x) \, dx$$

$$= \frac{1}{2\pi i} \oint \mathrm{Tr}\left\{ \delta(r' - r_2) \frac{1}{x - H} \frac{\partial(V(r_2) + V_S(r_2))}{\partial r_{2j}} \frac{1}{x - H} \right\} f(x) \, dx \qquad (B.4)$$

Using the definition of $\chi(r, r')$ (Eq. (A.5b)) and Eq. (2.15) we obtain

$$\frac{\partial V_T(r_1)}{\partial r_{1j}} = \frac{\partial V(r_1)}{\partial r_{1j}} + \int \frac{1}{|r_1 - r'|} \chi(r', r_2) \frac{\partial V_T(r_2)}{\partial r_{2j}} \, d^3r' d^3r_2 \qquad (B.5)$$

This equation can be expressed with the help of Eq. (A.6), which gives by inversion

$$\begin{aligned}\frac{\partial V_T(r_1)}{\partial r_{1j}} &= \int \epsilon^{-1}(r_1, r_2)\, \frac{\partial V(r_2)}{\partial r_{2j}}\, d^3r_2 \\ &= -\int \epsilon^{-1}(r_1, r_2) \sum_b \frac{\partial V(r_2)}{\partial R_\beta}\, d^3r_1\end{aligned} \qquad (B.6)$$

The last equality holds because of the definition of V(r) (see Eq. (2.4)). Multiplying both sides of Eq. (B.6) by an arbitrary infinitesimal vector $\vec{a}$, we see that any term of the right-hand side of Eq. (B.6) is, by definition of $\epsilon^{-1}(r, r')$, the variation of the total potential at r_1 due to the imposed external potential $-(\partial V(r_2)/\partial R_\beta)\cdot\vec{a}$. This can be written as

$$\frac{\partial V_T(r_1)}{\partial r_{1j}} = -\sum_b \frac{\partial V_T(r_1)}{\partial R_\beta}$$

which is Eq. (2.24).

REFERENCES

[1] COHEN, M.H., PICK, R.M., to be published.
[2] SHAM, L.J., Proc. R. Soc. Ser. A 283 (1965) 33.
[3] SHAM, L.J., ZIMAN, J., Adv. Phys. 15 (1963) 221.
[4] MOORADIAN, A., WRIGHT, G.B., Phys. Rev. Lett. 16 (1966) 999.
[5] SINHA, S., to be published.
[6] HORWITZ, G., BROUT, R., ENGLERT, F., Phys. Rev. 130 (1963) 409.
[7] AUSTIN, B.J., HEINE, V., SHAM, L.J., Phys. Rev. 127 (1962) 276.
[8] MUELLER, F.M., Phys. Rev. 153 (1967) 659.
[9] MUELLER, F.M., to be published.
[10] KOHN, W., Phys. Rev. Lett. 2 (1959) 393.
[11] MASHKEVITCH, V.S., TOLPYGO, K.B., Soviet Phys. JETP 5 (1957) 435.
[12] COCHRAN, W., Phil. Mag. 4 (1959) 1082.
[13] HARDY, J.R., Phil. Mag. 6 (1961) 27.
[14] DRESSELHAUS, G., DRESSELHAUS, M.S., Phys. Rev., to be published.
[15] ADLER, S.L., Phys. Rev. 126 (1962) 413.
[16] WISER, N., Phys. Rev. 129 (1963) 62.
[17] MARTIN, R.M., PICK, R.M., to be published.

NEUTRONS, FREE ELECTRONS AND HIGH MAGNETIC FIELDS

R.A. COWLEY
LABORATORY OF ATOMIC AND SOLID STATE PHYSICS,
CORNELL UNIVERSITY, ITHACA, N.Y.,
UNITED STATES OF AMERICA,
AND
ATOMIC ENERGY OF CANADA LTD.,
CHALK RIVER, ONTARIO, CANADA

Abstract

NEUTRONS, FREE ELECTRONS AND HIGH MAGNETIC FIELDS. The application of high magnetic fields to a material containing free electrons leads to a quantization into highly degenerate Landau levels. Blank and Kaner have shown that neutron scattering techniques can be used to study these levels through their influence on the phonon spectrum. When the phonon wavevector, $\vec{q}$, is parallel to the magnetic field, $\vec{H}$, a simple 'jellium' model shows logarithmic singularities in the phonon dispersion curves. However, it seems unlikely that these can be observed with presently available resolutions and magnetic fields. When $\vec{q}$ is perpendicular to $\vec{H}$, the model yields anomalies in the phonon dispersion curves at the cyclotron resonance frequencies; these anomalies should be observable. Calculations are presented for the case of potassium. Neutron scattering techniques may also be used to study the magnetic scattering. The form factor for the elastic scattering is very dependent on the Fermi surface diameter. The inelastic scattering shows anomalies similar to those of the phonon spectrum. Calculations are presented for a free electron model of a nearly ferromagnetic material.

1. INTRODUCTION

One of the most fruitful ways of studying the electronic properties of metals is to study their properties while applying a large magnetic field. It was therefore considered worthwhile to examine the effect of applying a large magnetic field on the neutron scattering by a metal. The next section reviews the results obtained [1] for the polarizability of a free electron gas in the presence of a magnetic field. The change of the polarizability manifests itself in a change in the details of the phonon spectrum [1]. In section 3 we emphasize those results which are most relevant to the neutron scattering by the phonons and illustrate the results by a calculation for potassium metal. In a final section we examine the modification of the magnetic scattering by the conduction electrons. This is largest for nearly ferromagnetic metals and we use the same model as Doniach [2] in his treatment of the magnetic scattering in the absence of magnetic fields.

2. THE POLARIZABILITY

If the electrons in a gas of free electrons do not interact with one another their response to a probe of wavelength, $\vec{q}$, and frequency, ω, may be calculated by second-order perturbation theory as:

$$\chi(\vec{q},\omega) = \frac{1}{N} \sum_{\vec{p}} \frac{n(\vec{p}) - n(\vec{p}+\vec{q})}{\varepsilon(\vec{p}+\vec{q}) - \varepsilon(\vec{p}) - \omega} \tag{1}$$

where $n(\vec{p})$ and $\epsilon(\vec{p})$ are the occupation number and energy of the electron described by wavevector $\vec{p}$. In the case of free electrons the susceptibility is isotropic and the sum over $\vec{p}$ can be performed analytically to obtain the well-known expression first obtained by Lindhard [3]

$$\mathrm{Re}[\chi(q,\omega)] = \rho_F \left[\frac{1}{2} + \frac{k_F}{4q} \left\{ (1 - x_-^2) \log \left| \frac{1 - x_-}{1 + x_-} \right| - (1 - x_+^2) \log \left| \frac{1 - x_+}{1 + x_+} \right| \right\} \right]$$

$$\mathrm{Im}[\chi(q,\omega)] = \pi \rho_F \frac{k_F}{4q} \left\{ (1 - x_-^2)\, \theta(x_-^2 - 1) - (1 - x_+^2)\, \theta(x_+^2 - 1) \right\} \tag{2}$$

where ρ_F is the density of states at the Fermi surface, k_F is the Fermi radius, and

$$x_\pm = \frac{2m\omega \pm q^2}{2q\, k_F}$$

while $\theta(x)$ is 1 when x less than one and zero otherwise.

It is well known when a strong magnetic field is applied along the z axis that the electrons become quantised into Landau levels. The energy is then specified by two quantum numbers; n the Landau level number, and p_z the momentum along the field direction. The energy of the electron is [4]

$$\epsilon_n(p_z) = (n + \tfrac{1}{2})\, \omega_c + \frac{p_z^2}{2m}$$

where ω_c is the cyclotron frequency, $\frac{eH}{mc}$.

The calculation of the polarizability is now more complex than in the field free case but the result is given by Blank and Kaner [1]. We shall not need to display their result in full generality but restrict our attention to two simplifications. One arises if the probe wavevector is parallel to the magnetic field. The susceptibility is then given by

$$\mathrm{Re}[\chi(q,\omega)] = \frac{\omega_c\, m^2}{2\pi^2\, q} \sum_{n=o}^{N} \log \left| \frac{(-\,2T_n\, q + q^2)^2 - 4m^2\, \omega^2}{(2T_n\, q + q^2) - 4m^2\, \omega^2} \right| \tag{3}$$

where

$$T_n{}^2 = k_F{}^2 - 2m\, \omega_c\, (n + \tfrac{1}{2})$$

and N is the maximum value of n for which T_n is real.

The corresponding imaginary part is

$$\mathrm{Im}[\chi(q,\omega)] = \frac{\omega_c m^2}{2\pi q} \alpha \tag{4}$$

where α is the number of integers which lie between

$$\frac{1}{2m\,\omega_c} \left(k_F^2 - \left(\frac{m\omega}{q} - \frac{q}{2}\right)^2\right) \text{ and } \frac{1}{2m\,\omega_c} \left(k_F^2 - \left(\frac{m\omega}{q} + \frac{q}{2}\right)^2\right)$$

These results are clearly very different from those of eqn. 2. In particular the nature and position of the singularities is very different . It is well known that the singularity in the field free response is the logarithmic singularity in the derivative, as given by eqn. 2. By contrast eqn. 3 exhibits logarithmic singularities where $(2T_N q + q^2)^2 = 4m^2 \omega^2$. The location of these singularities is shown schematically in Fig. 1. It is interesting to note that the position of the singularities also determines the value of α in eqn. 4 as shown in Fig. 1.

The other case of interest is when the probe wavevector is perpendicular to the magnetic field. Under these conditions the susceptibility is

$$\mathrm{Re}[\chi(q,\omega)] = \frac{m\omega_c}{2\pi^2} \sum_{n_1=0}^{\infty} \sum_{n_2=0}^{N} |M_{n_1 n_2}(y)|^2 \, T_{n_2} \left(\frac{1}{(n_1-n_2)\omega_c - \omega} + \frac{1}{(n_1-n_2)\omega_c + \omega} \right)$$

while

$$\mathrm{Im}[\chi(q,\omega)] = \frac{m\omega_c}{2\pi} \sum_{n_1=0}^{\infty} \sum_{n_2=0}^{N} |M_{n_1 n_2}(y)|^2 \, T_{n_2} \Big(\delta(\omega - \omega_c(n_1-n_2)) - \delta(\omega + \omega_c(n_1-n_2)) \Big) \tag{5}$$

where if $n_1 > n_2$,

$$M_{n_1 n_2}(y) = \exp\left(-\frac{y}{2}\right) y^{(n_1 - n_2)/2} \, L_{n_1}^{n_1 - n_2}(y)$$

and $y = \frac{c}{2eH} q^2$ and $L_n^{\alpha}(y)$ is a generalized Laguarre polynomial.

These results show a very different behaviour from those for q parallel to H. The singularities occur at the cyclotron

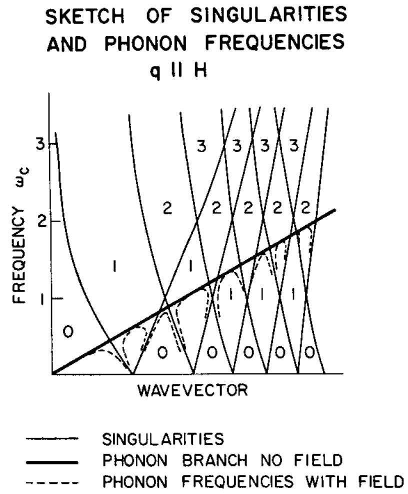

FIG. 1. The position of the singularities in the electronic polarizability when the wavevector is parallel to the magnetic field. These singularities cause a change in the phonon spectrum from the solid line to the dotted lines. The imaginary part of the electronic polarizability is proportional to α, which is the number associated with different regions in the diagrams.

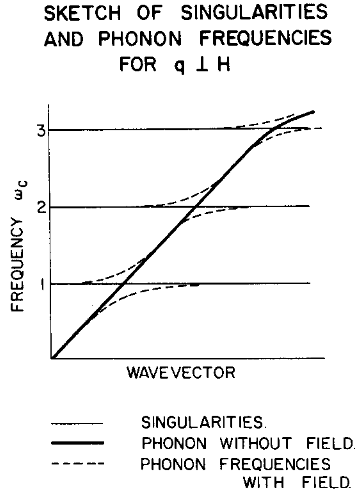

FIG. 2. The position of the singularities in the electronic polarizability when the wavevector is perpendicular to the magnetic field. The change in phonon spectrum from the field free (solid line) to field applied (dotted line) is also shown.

resonance frequencies independently of the wavevector, as shown in Fig. 2. It is therefore of interest that at small frequencies the Im$[\chi(q,\omega)]$ is concentrated into particular regions of $\vec{q}$ space by a longitudinal magnetic field and into particular regions of ω space by a transverse field.

3. THE PHONON SPECTRUM

The calculation of the phonon spectrum of the nearly free electron metals is made comparatively simply by the use of the pseudo-potential formalism [5]. The frequencies of the normal modes of vibration of a longitudinal mode are given by

$$\omega(\vec{q}j)^2 = \omega_p(\vec{q})^2 + \frac{1}{M} V(\vec{q})^2 \left(\frac{1}{\varepsilon(q)} - 1\right) \qquad (6)$$

where $\omega_p(\vec{q})$ is the plasma frequency, $V(\vec{q})$ the pseudo-potential and $\varepsilon(\vec{q})$ the dielectric constant of the free electron gas. We have neglected Umklapp processes since at least for sodium and potassium these are negligible for longitudinal modes with wavevectors less than 80% of the Brillouin zone boundary. In the self-consistent Hartree field approximation the dielectric constant is given in terms of the polarizability as

$$\varepsilon(\vec{q},\omega) = 1 + \frac{4\pi e^2}{q^2} \chi(\vec{q},\omega) \qquad (7)$$

We may then use eqn. 6 to deduce the change in the frequencies with applied magnetic field by replacing the field free $\chi(\vec{q},\omega)$ with the field dependent expressions. The qualitative shape of the dispersion curves are illustrated in Figs. 1 and 2 for longitudinal and transverse fields.

At first sight the phenomena described above seem very large and extremely interesting. It is now necessary to evaluate the magnitude of the effects in detail to assess the extent to which the theory is applicable to present experimental conditions. These calculations were for potassium for which a pseudo-potential was readily available [6]. In a field of 100,000 gauss the cyclotron frequency is 0.28 (10^{12} cps) which is comparable to neutron scattering energies. With a transverse magnetic field the anomalies occur at these frequencies and might well be observed in a neutron scattering experiment. The calculated widths and shifts of the neutron groups are shown in Fig. 3. The anomalies obtained with a longitudinal magnetic field occur over so small a region of the wavevector that they are not directly observable. The widths and shifts averaged over a small region of the wavevector are shown in Fig. 3, where it is seen that the differences between the field-free and longitudinal field results are quite small.

The other conditions for the observation of these effects are that the electrons should have a collision time which is much longer than the cyclotron frequency. This means using reasonably low temperatures, below 10°K, and reasonably although not exceptionally pure materials. In the calculations described above we have assumed the lifetime to be 10 cyclotron periods.

In more complex metals than the alkalis it is necessary to take account of Umklampp processes and the real band structure. The former causes the resonances for $\vec{q} \parallel \vec{H}$ and $\vec{q} \perp \vec{H}$ to occur for all wavevectors, while the latter gives rise to an anisotropic polarizability and possibly many different

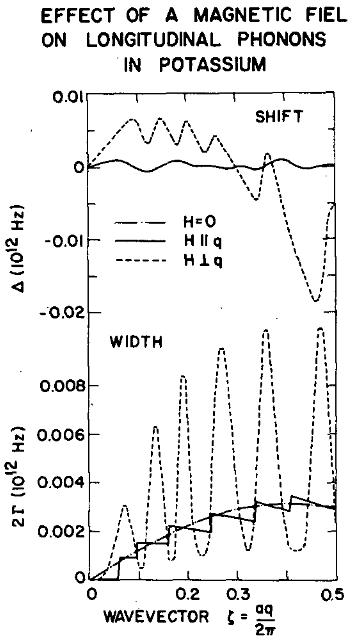

FIG.3. The change in phonon frequency and the width of the normal modes of the small ζ end of the [100] L branch in potassium. The applied field is 100,000 gauss.

resonance corresponding to the different pieces of the Fermi surface.

4. THE MAGNETIC SCATTERING

Under an applied magnetic field a metal becomes magnetized and there will be a magnetic component of the Bragg scattering. This arises because there is one more Landau level present with 'up' spin than with 'down' spin. Consequently the form factor of the magnetic Bragg scattering is given by the wavefunctions of the Landau levels. In the direction of $\vec{q}$ parallel to $\vec{H}$ this is a constant proportional to $\vec{H}$ until $\vec{q} = \vec{k}_F$, when it falls to zero. Unfortunately we are not able to suggest a way of measuring this.

The inelastic scattering can be calculated as first discussed by Elliott [7]. However it it known to be very small unless the susceptibility is enhanced, as for example in palladium. A simple model to describe this situation has been put forward by Doniach [2]. The enhancement of the spin fluctuations is included by the random phase approximation to give a susceptibility $P(\vec{q},\omega)$ as

$$P(\vec{q},\omega) = \frac{\chi(\vec{q},\omega)}{1-I\,\chi(\vec{q},\omega)}$$

where $\chi(\vec{q},\omega)$ is calculated for free electrons. I is the electron-electron Coulomb repulsion between electrons on the same site. The neutron scattering is then proportional to

$$\frac{1}{1 - \exp(-\beta\omega)} \operatorname{Im}[P(\vec{q},\omega)]$$

This expression clearly shows that the resonance discussed above will give rise to anomalies in the magnetic neutron scattering. As in the case of the phonon spectrum the resonances with a longitudinal field likely cannot be observed but those with a transverse field may be. Numerical calculations have been made for a free electron model but with I chosen to give an enhancement factor of 0.99. The results are shown in Fig. 4.

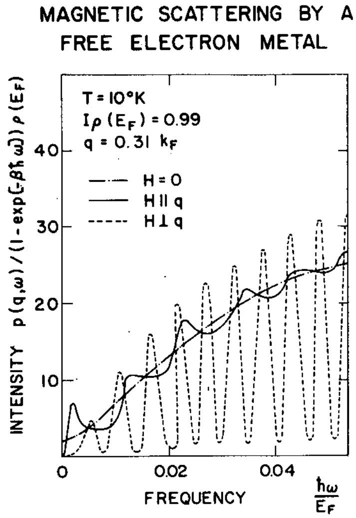

FIG.4. The magnetic neutron scattering cross-section for low frequencies and a momentum transfer of 0.31 k_F. The Stoner enhancement of a factor is 100, and the applied magnetic field is 100,000 gauss.

5. DISCUSSION

The neutron scattering from metals in high magnetic fields has been calculated with very simple models. The experiments to confirm these predictions appear in many cases to be extremely difficult even with very high magnetic fields. It may be wondered what information can be obtained from these experiments and whether they have any advantages over other magnetic resonance experiments.

The experiments in a transverse field enable the cyclotron resonance frequency to be measured, while in principle at least those in longitudinal fields yield information about Fermi-surface diameters. They are then exactly the same phenomena as the cyclotron resonance and de Haas-van Alpen effect normally studied by magnetic resonance. The same technique may then be used to separate out the different bands and complex Fermi surface structure. The only advantage of using neutrons would seem to be that the magnetic field can and must be much larger. This means that there are far less stringent requirements on the purity and temperature of the specimen. This might enable experiments to be done in some materials which cannot be prepared pure or have phase transitions which prevent the usual techniques from being used. The neutron scattering also has the advantage that by doing measurements at different wavevectors and magnetic fields it is possible to vary the magnitude of the pseudo-potential and hence the coupling with different bands of the electronic structure. This then gives further information to assist with the identification of different pieces of the Fermi surface.

ACKNOWLEDGEMENTS

The author is grateful for the hospitality of the Laboratory of Atomic and Solid State Physics at Cornell University where he was pleased to be a visitor for 4 months.

REFERENCES

[1] BLANK, A. Ya, KANER, E.A., J. Exptl. Theoret. Phys. (U.S.S.R. 50 (1966) 1013. Translation - Soviet Physics JETP 23 (1966) 673.
[2] DONIACH, S., Proc. Phys. Soc. 91 (1967) 86.
[3] LINDHARD, J., Kgl. Danske Videnskab., Mat-Phys. Medd 28 (1954) 8.
[4] KITTEL, C., "Quantum Theory of Solids", Wiley, New York (1963) 217.
[5] HARRISON, W.A., "Pseudo-potentials in the Theory of Metals", W.A. Benjamin Inc., New York (1966) Ch. 7.
[6] COWLEY, R.A., WOODS, A.D.B., DOLLING, G., Phys. Rev. 150 (1966) 487.
[7] ELLIOTT, R.J., Proc. Roy. Soc. A235 (1956) 289.

PHONON DISPERSION CURVES IN LITHIUM*

H.G. SMITH, G. DOLLING**, R.M. NICKLOW,
P.R. VIJAYARAGHAVAN AND M.K. WILKINSON
SOLID STATE DIVISION,
OAK RIDGE NATIONAL LABORATORY,
OAK RIDGE, TENN., UNITED STATES OF AMERICA

Abstract

PHONON DISPERSION CURVES IN LITHIUM. Phonons have been measured in several high-symmetry directions in Li^7 metal by coherent inelastic neutron scattering. Most of the measurements were made at 98°K (well above the Martensitic transition at 78°K) on the triple-axis spectrometer at the HFIR. The results indicate that the interatomic forces in lithium are of a longer range than in sodium or potassium; for example, the sixth-neighbor force constants based on a general model are 12% of the first neighbor force constants. The frequency distribution and Θ versus T relation have been calculated.

The measurement of phonon dispersion curves by the method of coherent inelastic neutron scattering is an increasingly useful tool for a possible understanding of the theory of metals. The results of recent neutron scattering investigations of metals have emphasized the long-range nature of the interatomic forces which exist in the solid state. Phonon dispersion curves for the alkali metals, sodium [1] and potassium [2], indicate that the interatomic forces are not negligible out to fifth neighbors. Frequency calculations with a Born-von Kármán general or central force model are in excellent agreement with the observed data; however, satisfactory results [3-4] have been obtained using the psuedo-potential method. Since lithium is, in principle, the simplest of all metals, a knowledge of its lattice dynamics is of fundamental importance to any theory of metals. We report here the results of a preliminary investigation of the phonon spectra in lithium as measured by coherent inelastic neutron scattering.

The sample, grown from 99.993% lithium-7 metal, measured 0.5 inches in diameter by 2.5 inches in length. Unfortunately, the sample is essentially a bicrystal and the two crystals are separated by about one degree. This is reflected in the width of the measured phonon peaks. In addition, a large grain of about 4° misorientation also exists in the specimen. There did occur a number of extraneous peaks in the phonon spectrum, and, although some could be identified with higher-order and multiple scattering effects, others that could not be so identified are undoubtedly due to the presence of this grain. Many of the phonon measurements were repeated under different experimental conditions in order to eliminate these effects as much as possible. Measured frequencies are listed in Table I and several phonons are shown in Fig. 1. Attempts over the past 18 months to grow or purchase a Li^7 crystal of good quality have been unsuccessful. However, we have recently obtained a crystal of more desirable quality containing natural lithium (7.5% Li^6) and preliminary measurements with this crystal confirm the present results.

---

* Research sponsored by the US Atomic Energy Commission under contract with the Union Carbide Corporation.

** On leave from Chalk River Nuclear Laboratories, Chalk River, Ont., Canada, now returned.

Table I. Measured frequencies (10^{12} c/s) of the normal modes in lithium-7 at 98°K

ζ	ν $[00\zeta]\Delta_1$	ζ	ν $[00\zeta]\Delta_5$	ζ	ν $[\zeta\zeta\zeta]\Lambda_3, F_3$	ζ	ν $[\zeta\zeta\zeta]\Lambda_1, F_1$
0.125	2.00 ± 0.15	0.198	2.50 ± 0.25	0.10	1.50 ± 0.20	0.108	3.50 ± 0.10
0.195	3.00 ± 0.15	0.242	3.00 ± 0.20	0.30	4.04 ± 0.10	0.208	6.50 ± 0.20
0.264	4.00 ± 0.15	0.275	3.50 ± 0.20	0.40	5.60 ± 0.18	0.350	8.37 ± 0.30
0.345	5.00 ± 0.15	0.310	4.00 ± 0.25	0.60	8.10 ± 0.20	0.545	6.50 ± 0.20
0.46	6.00 ± 0.18	0.346	4.50 ± 0.15	0.70	8.45 ± 0.20	0.700	3.60 ± 0.10
0.62	7.00 ± 0.20	0.380	5.00 ± 0.12	0.80	8.60 ± 0.20	0.830	6.50 ± 0.30
0.70	7.60 ± 0.20	0.442	6.00 ± 0.15	0.90	8.80 ± 0.20		
0.77	8.00 ± 0.30	0.540	7.00 ± 0.10				
0.80	8.30 ± 0.30	0.660	8.00 ± 0.10				
0.90	8.76 ± 0.30	0.700	8.30 ± 0.20				
1.00	8.82 ± 0.40	0.800	8.74 ± 0.20				
		0.900	8.70 ± 0.30				

ζ	ν $[\zeta\zeta 0]\Sigma_1$	ζ	ν $[\zeta\zeta 0]\Sigma_4$	ζ	ν $[\zeta\zeta 0]\Sigma_3$
0.10	2.60 ± 0.10	0.15	0.97 ± 0.10	0.10	1.88 ± 0.10
0.15	3.92 ± 0.10	0.20	1.20 ± 0.10	0.15	2.60 ± 0.15
0.25	6.40 ± 0.15	0.25	1.40 ± 0.10	0.20	3.48 ± 0.20
0.30	7.35 ± 0.20	0.30	1.55 ± 0.10	0.30	4.54 ± 0.10
0.35	8.15 ± 0.15	0.35	1.70 ± 0.10	0.40	5.35 ± 0.10
0.40	8.70 ± 0.20	0.40	1.80 ± 0.10	0.50	5.70 ± 0.20
0.45	8.87 ± 0.20	0.45	1.90 ± 0.10		
0.50	9.00 ± 0.40	0.50	1.90 ± 0.10		

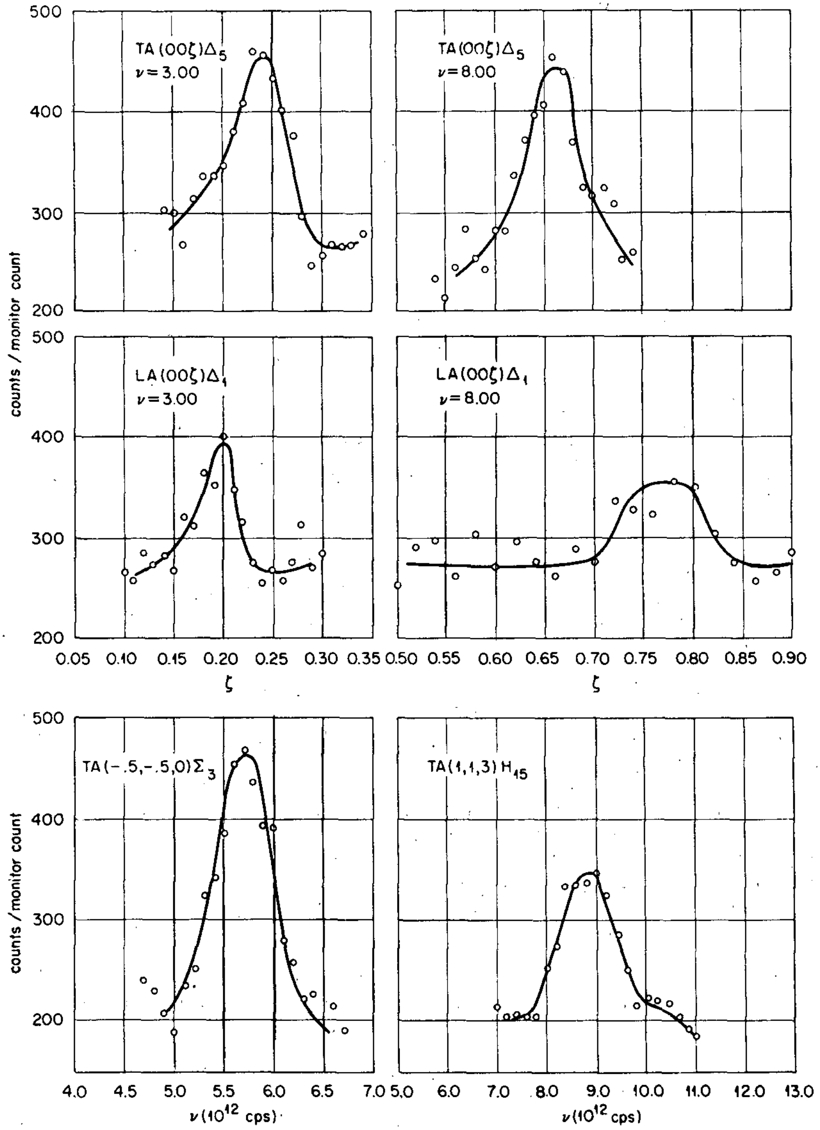

FIG. 1. Selected phonons in lithium. The crossover of the L(00ζ) branch below the T(00ζ) branch is illustrated.

The phonon measurements were made on the computer-controlled-triple-axis spectrometer [5] at the High Flux Isotope Reactor (HFIR) at a temperature of 98° ± 1°K. (Lithium undergoes a Martensitic transition at 78°K.) Most of the phonons were measured in the [1$\bar{1}$0] zone, while a few were measured in the [001] zone. The dispersion curves for the high symmetry directions are shown in Fig. 2. The pronounced behavior of the L(00ζ) branch indicates that the interatomic forces are, indeed, of long range. The crossover of this branch below the T(00ζ) branch is illustrated in

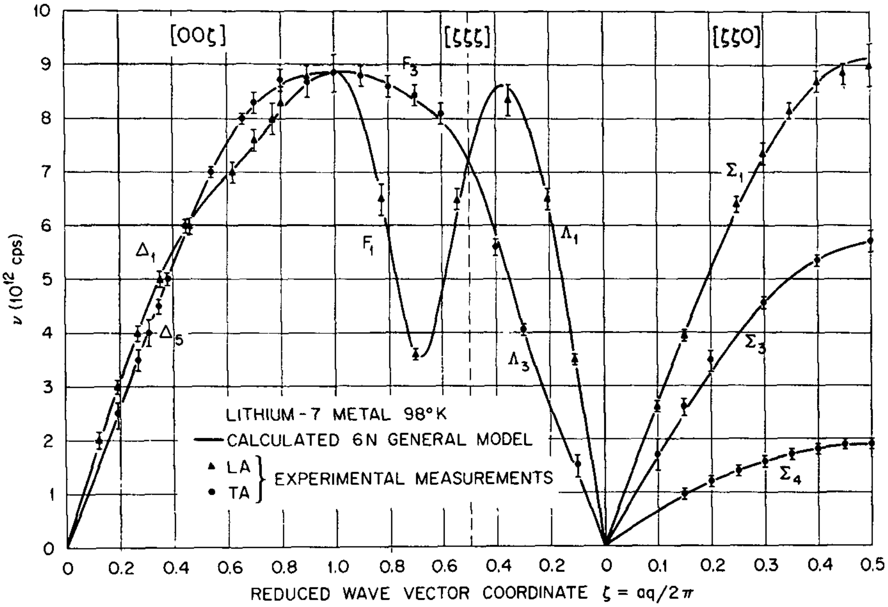

FIG. 2. Dispersion curves in lithium. The solid lines are calculated from a sixth-neighbour Born-von Kármán general force model.

Fig. 1. The solid lines in Fig. 2 are calculated on the basis of a sixth-neighbor (15 parameters) Born-von Kármán general force model. The force constants for several models are listed in Table II. It is observed that the sixth-neighbor general force constants are approximately 12% of the first neighbor force constants. The seventh-neighbor force constants based on a 19-parameter model are negligible. An axially-symmetric model [6] involving eighth-neighbors (16 parameters) did not give quite as good a fit as the general model although the differences may not be too significant. However, unlike sodium [1], the force constants in lithium based on the general force model are not compatible with those of an axially-symmetric model, i.e., $\beta_3^{220} \neq \alpha_1^{220} - \alpha_2^{220}$, etc.

The frequency distribution based on the sixth-neighbor general force model is shown in Fig. 3. From this g(ν) a Debye Θ vs temperature was calculated and compared to the Θ values determined by Martin [7] from specific heat measurements (Fig. 4a). At intermediate temperatures (100° - 200°K) the agreement is, perhaps, not unreasonable. At low temperatures the specific heat measurements were made on partially transformed lithium and at the higher temperatures anharmonic effects may be important, whereas, the calculations based on the neutron data are in the harmonic approximation. The total mean square displacement as a function of temperature is shown in Fig. 4b. It is apparent that most of the motion of the lithium atoms at 98°K is due to zero-point motion.

The isothermal elastic constants determined by ultrasonic methods [8] were used in the least squares analysis but with relatively low weight. They agree within 10% or less with the calculated elastic constants. Recently, phonon dispersion curves [4, 9] and elastic constants [10] have been calculated for lithium by the method of the psuedo-potential, but they are in poor agreement with the present results; however, the calculations of Animalu, et al.,[4] do predict a crossover of the L(00ζ) branch below the T(00ζ) branch, as observed experimentally.

Table II. Force constants for Li^7 (dyn/cm)

n		Sixth-Neighbor General Model	Seventh-Neighbor General Model	Eighth-Neighbor Axially-Symm. Model	
1	α_1	2336 ± 29	2320 ± 32	2355 ± 38	
	β_1	2462 ± 38	2520 ± 58	2489 ± 48	
2	α_2	694 ± 66	678 ± 71	631 ± 103	
	β_2	140 ± 46	153 ± 48	50 ± 57	
3	α_3	−277 ± 26	−285 ± 28	−205 ± 30	
	β_3	125 ± 34	110 ± 40	122 ± 38	
	γ_3	−158 ± 38	−152 ± 46	−327	$\gamma_3 = \alpha_3 - \beta_3$
4	α_4	171 ± 26	185 ± 33	152 ± 37	
	β_4	−126 ± 17	−116 ± 22	−141 ± 27	
	γ_4	−122 ± 34	−113 ± 34	37	$\gamma_4 = (\alpha_4 - \beta_4)/8$
	δ_4	11 ± 26	22 ± 27	110	$\delta_4 = 3\gamma_4$
5	α_5	148 ± 17	158 ± 20	130 ± 22	
	β_5	−38 ± 41	−89 ± 57	−136 ± 32	
6	α_6	−282 ± 60	−266 ± 63	−298 ± 136	
	β_6	12 ± 36	8 ± 38	15 ± 96	
7	α_7		−3 ± 18	9 ± 25	
	β_7		−8 ± 12	1 ± 13	
	γ_7		−22 ± 13	−9	$\gamma_7 = 3\delta_7$
	δ_7		30 ± 27	−3	$\delta_7 = 3(\alpha_7 - \beta_7)/8$
8	α_8			4 ± 30	
	β_8			6 ± 20	
	γ_8			6	$\gamma_8 = (4\beta_8 - \alpha_8)/3$
	δ_8			−1	$\delta_8 = 2(\alpha_8 - \beta_8)/3$
	χ^2	0.60	0.59	0.75	

Although one may expect to observe Kohn anomalies near such points as TA(0,0,0.25) and LA(0,0,0.75), the low experimental resolution precluded observation of any modest deviations from a smooth curve in these regions. This is primarily due to the poor quality of the specimen. A detailed investigation into the presence of Kohn anomalies will be attempted with the natural-lithium crystal if the adverse effects of absorption (due to Li^6) are not too severe.

A study of the temperature dependence of the phonon spectra is also planned for the near future.

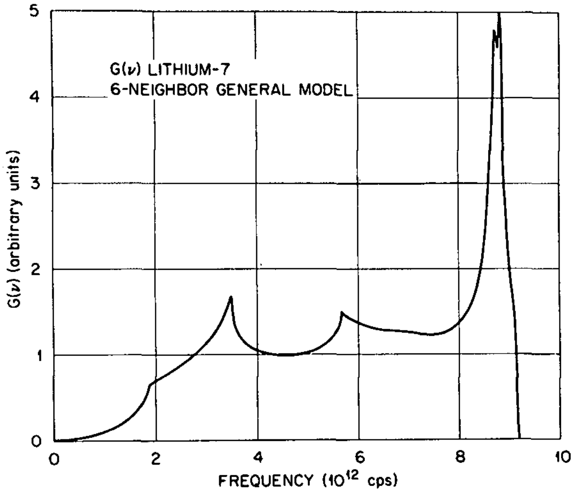

FIG.3. Frequency distribution based on the sixth-neighbour general force model.

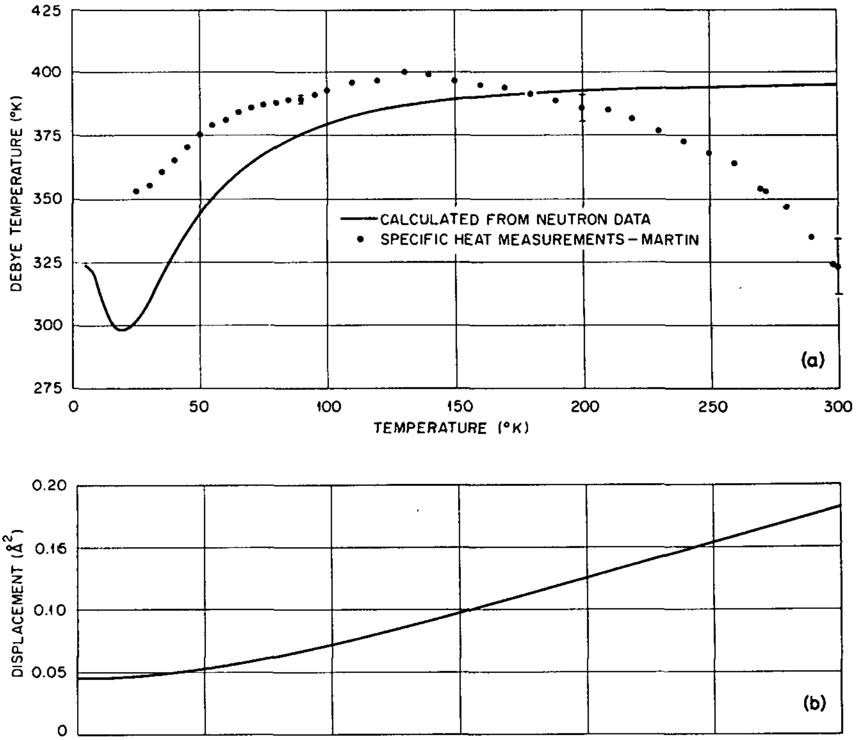

FIG.4. a) Debye θ versus T. The solid line is based on the neutron results and the open circles were determined from specific heat measurements [7]. (b) Total mean square displacement versus temperature.

REFERENCES

[1] WOODS, A. D. B., BROCKHOUSE, B. N., MARCH, R. H., and STEWART, A. T., Phys. Rev. 128 (1962) 1112.

[2] COWLEY, R. A., WOODS, A. D. B., and DOLLING, G., Phys. Rev. 150 (1966) 487.

[3] COCHRAN, W., Proc. Roy. Soc. (London) A276 (1963) 308; COCHRAN, W. in Inelastic Scattering of Neutrons in Solids and Liquids (International Atomic Energy Agency, Vienna, 1965) Vol. I, p. 3.

[4] ANIMALU, A. O. E., BONSIGNORI, F., and BORTOLANI, V., Nuovo Cimento 44 (1966) 159.

[5] WILKINSON, M. K., SMITH, H. G., KOEHLER, W. C., NICKLOW, R. M., and MOON, R. M. These Proceedings.

[6] WOLFRAM, T., LEHMAN, G. W., and DE WAMES, R. E., Phys. Rev. 129 (1963) 2483.

[7] MARTIN, D. L., Physica 25 (1959) 1193.

[8] NASH, H. C. and SMITH, C. S., J. Phys. Chem. Solids 9 (1959) 113.

[9] KREBS, K., Phys. Rev. 138 (1965) A143.

[10] SHYU, W. and GASPARI, G. D., Phys. Rev. 163 (1967) 667.

NOTE ADDED IN PROOF

Additional data in several symmetry directions have been obtained with the better quality crystal (rocking curve ~ 0.30°) containing natural lithium. Although the intensities of the phonons were down slightly from the previous crystal, the signal to background was improved and the phonon peak shapes were also improved. In general, the previous measurements were confirmed and the error bars for many of the phonons shown on the dispersion curves were reduced; in addition, a number of unexplained peaks were no longer observed. With fine slits (0.3° FWHM) before and after the sample, and good focusing conditions, a detailed study of the $T(00\zeta)$ branch in the region $\zeta = 0.2 - 0.5$ was made. A sharp increase in the widths between 0.24 and 0.26 ($Q = 2k_F$ at $\zeta = 0.25$) was observed and the widths remained broad until $\zeta \simeq 0.5$. In the $T(\zeta\zeta\zeta)$ branch between 0.1 and 0.5 the phonons appear to consist of two unequal peaks, (observed in both constant-Q and constant-E scans). This branch was very poorly determined with the original Li^7 crystal. Several low-energy peaks in the $L(00\zeta)$ branch also remain unexplained and it appears that a more thorough study of the phonon dispersion relation will be necessary to clear up some of these anomalies. It is hoped that a larger crystal will become available.

PHONON DISPERSION RELATIONS IN BISMUTH

J. SOSNOWSKI, S. BEDNARSKI AND A. CZACHOR
INSTITUTE OF NUCLEAR RESEARCH,
ŚWIERK, POLAND

Abstract

PHONON DISPERSION RELATIONS IN BISMUTH. Phonon dispersion relations in bismuth at room temperature have been studied by neutron inelastic scattering using a triple-axis neutron crystal spectrometer and the constant-Q method. The fixed wavelength $\lambda_0 = 1.50$ Å was used, K_0 was kept fixed and K_1, the scattering angle φ and the crystal orientation were varied to realize the 'constant-Q' mode of operation. The principles of focusing were used throughout the measurements. The plane of the experiment was the (01$\bar{1}$) plane. The phonon dispersion relations for the [100], [110], and [$\bar{2}$11] and [111] directions have been obtained. The dispersion relations for the [111] direction are compared with those obtained by Yarnell et al. Special care was devoted to the study of dispersion relation for the [100] direction where, according to Ovchinnikov's calculations, an anomaly connected with electron-phonon interaction can be expected. The experimental curves are compared with the calculated ones based on the Born-von Kármán theory.

1. INTRODUCTION

Bismuth is a metal belonging to group V of the periodic table and crystallizes in the trigonal system (space group R^- 3 m) with two atoms per unit cell. Geometrically its lattice resembles a primitive cubic lattice, slightly distorted along the diagonal of the cube. Figure 1 shows several sets of nearest neighbours for every atom in this structure. The symmetry points in the reciprocal space can be seen in Fig. 2, taken from Cohen's paper [1].

The electronic structure of elements belonging to group V has been investigated by several authors [1-3], however, only few papers deal with the lattice dynamics of these elements. Fouret [4] investigated the phonon spectra of antimony using the diffuse scattering of X-rays. The phonon dispersion relations for bismuth were first measured using the neutron scattering methods by Koenig and Yarnell [5], followed by Yarnell et al. [6]. Some measurements have also been performed by Sosnowski et al. [7, 8]. These papers (particularly Ref. [6]) contain a complete set of phonon curves for the trigonal direction and two longitudinal branches for the binary axis direction.

In the present work the investigation of phonon dispersion relations for bismuth have been carried out using the constant-Q method. A complete pattern of acoustic branches and also some optical branches for phonons with polarization vectors parallel to the mirror plane along four non-equivalent directions in the Brillouin zone is presented.

2. EXPERIMENT

The three-axis neutron spectrometer at the EWA reactor of the Institute of Nuclear Research at Świerk was used and the constant-Q method [9] with fixed neutron wavelength $\lambda_0 = 1.50$ Å was applied. The calculations

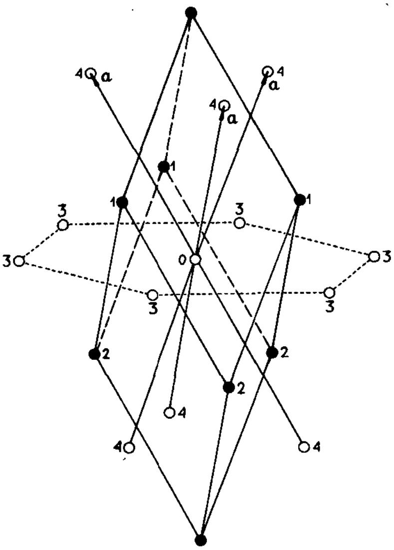

FIG. 1. Rhombohedral unit cell of bismuth. The numbers designate the appropriate co-ordination spheres.

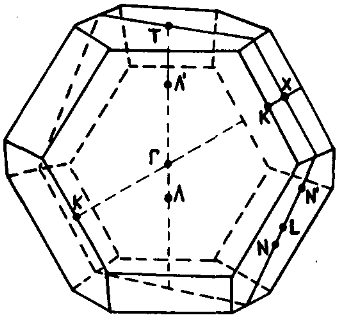

FIG. 2. The Brillouin zone for bismuth, notation according to Cohen [1].

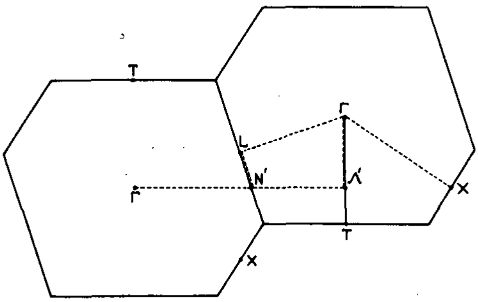

FIG. 3. Mirror plane section of the Brillouin zone for bismuth, present results have been carried out along directions marked by dashed lines.

for the proper orientation of the sample, the direction of the wavevector of the inelastically scattered neutrons and the orientation of the analysing crystal were carried out with a special ALGOL programme for the GIER computer.

The single-crystal bismuth sample was grown and prepared in this laboratory [10], using a special method that accounts for the expansion of bismuth in the course of transition from the liquid to the solid phase. The sample had the form of a cylinder 60 mm in diameter and 120 mm long. The cylinder axis was perpendicular to the crystallographic mirror plane, which was the plane of experiment. The measurements were carried out at room temperature, using 'focusing' as described by Peckham et al.[11].

Dispersion curves for the acoustic branches have been obtained for the following directions: [100], i.e. Γ-L; [011], i.e. Γ-X; [$\bar{2}$11], i.e. Γ-N'-Λ'-X; [111], i.e. Γ-T; and along the Brillouin zone boundary, N'-L, as shown in Fig.3. For convenience two additional points (as compared with Cohen [1]), namely N' and Λ', have been distinguished in the reciprocal space.

The random errors in the observed frequencies are approximately 3-4%, as estimated from the width of the phonon peaks.

3. RESULTS AND DISCUSSION

Phonon dispersion curves are presented in Figs 4, 5 and 6.

According to the theory of elasticity [12, 13] the velocities of sound-wave propagation in the various directions of the crystal can be found from the eigenvalues of a 3 × 3 matrix, the elements of which are linear combinations of the elastic constants. There are six independent elastic constants for the bismuth structure: c_{11}, c_{33}, c_{44}, c_{12}, c_{13}, c_{14}. For sound waves propagating parallelly to the mirror plane the matrix has a simple block diagonal form and its eigenvalues can be found easily. Using the elastic constants for room temperature [14], the velocities of sound for all the directions being studied have been evaluated. The slopes of the heavy lines seen in Figs 4 and 5 indicate the respective velocities of sounds. They coincide with the experimental points.

For the Γ-T direction the present results are in good agreement with the results of Yarnell et al.[6], as shown in Fig.4, and also with the early data obtained by Sosnowski et al.[7].

A careful search for the Ovchinnikov [15] anomalies has been carried out in the neighbourhood of the point L. The experimental data (Fig.5) show no evidence of the theoretically expected anomaly.

The frequencies of the upper acoustic branches for Γ-L, Γ-N'-Λ'-X and Γ-X directions do not approach the region of optical frequencies. This seems to suggest that an energy gap occurs in the frequency spectrum of bismuth, in accordance with some theoretical predictions [16].

Most of the measurements were carried out in the neighbourhood of the $|1, 2, 2|$, $|3, 2, 2|$, $|2, 2, 2|$ reciprocal lattice points. In these cases some well-defined neutron peaks, suggesting the presence of longitudinal phonons, were observed, in spite of the fact that they should not have been observed because of the polarization factor. The corresponding 'dispersion relations' were of the form $\omega = s|\vec{q}|$ over a whole Brillouin zone, with s equal to the

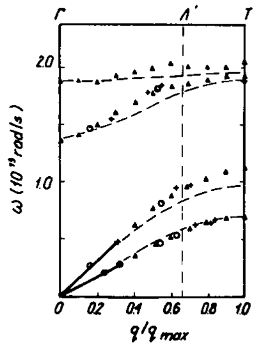

FIG.4. Phonon dispersion relations in bismuth for the Γ- T direction. O present results; + Sosnowski et al.[8]; ▲ Yarnell et al. [6] ; – – – phonon frequencies calculated with Brovman's model [16] .

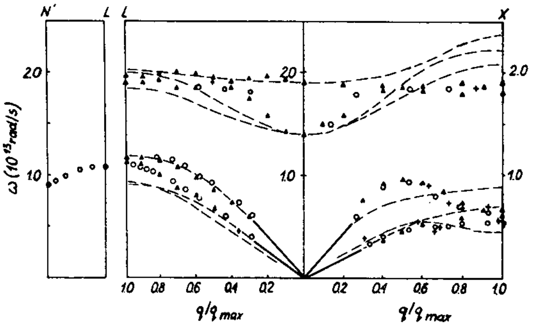

FIG.5. Phonon dispersion relations in bismuth for the L - Γ- X and N'-L directions. Symbols as in Fig.4.

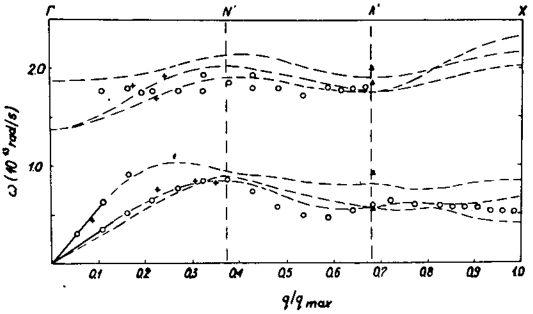

FIG.6. Phonon dispersion relations in bismuth for the Γ-N'-Λ'-X directions. Symbols as in Fig.4.

appropriate longitudinal sound velocity. However, the measurements at other reciprocal lattice points[1] did not confirm the evidence of such phonon branches.

---

[1] Such measurements were suggested to us by Dr. J. L. Yarnell. We are grateful to him for providing us with the results obtained at Los Alamos [17]. For the directions Γ-L and Γ-X our results are close to the results of D. Smith obtained at 75° K.

To compare the dispersion relations found experimentally with the calculated ones, several models of interactions in bismuth were used. The model given by Fouret [4] was obviously over simplified, so we turned to the more realistic models of Yarnell et al. [6] and Brovman [16]. However, Yarnells' model is appropriate only for phonons propagating along the trigonal direction and cannot be used for other directions.

In Brovman's model [16] every atom interacts with its four nearest neighbours. The force constants of this model have been calculated using the equations for elastic constants, the invariance Huang relations and two optical frequencies at point Γ taken from Yarnell et al. [6].

The present results are in a good agreement with both models for the trigonal direction Γ-T. For the lower acoustic branch in the direction Γ-L a comparatively good agreement with the curve given by Brovman is observed. No explicit results for the directions Γ-L and Γ-X were presented in Brovman's paper. Using the force constants given in this paper, we calculated the phonon frequencies for these directions. We found a qualitative agreement for the upper acoustic and optical branches for the direction Γ-L and for the lower acoustic branch for the direction Γ-X.

In this situation an effort has been made to construct another four-nearest-neighbours model of the Born-von Kármán type with parameters (force constants) calculated from neutron data, without relating to the elastic constants. Beside the usual invariance and Huang relations, the phonon frequencies at Γ, T and X were used. The values of these frequencies were taken from Ref. [6] and from the present measurements. The interaction with third and fourth neighbours was assumed to be of the axial symmetry type [16]. The following models have been checked:

(1) The interactions with first and second neighbours are described by tensor forces (in this case it was necessary to introduce in addition the elastic constant c_{13} and omit, to obtain a consistent set of equations, the equation for one frequency at X);

(2) The interaction with the first neighbours is given by tensor forces and with the second neighbours by axial symmetry forces;

(3) The interaction with the first neighbours is given by axial symmetry forces and with the second neighbours by tensor forces;

(4) The interaction with the first neighbours is given by tensor forces and with the second neighbours by quasi-axial symmetry forces (i.e. three independent constants describe the force matrix, whereas in the axial symmetry case the number of independent constants is only two);

(5) The interaction with the first neighbours is given by quasi-central forces ($\phi_{xx} = 0$ for an atom in the mirror plane; the remaining force constants are arbitrary) and the interactions with second neighbours by tensor forces.

In all cases it was possible to obtain linear equations for the force constants. The force constants obtained for the third and fourth neighbours were not very sensitive to the choice of the particular model. In all cases it was quite simple to fit the calculated phonon frequencies to the experimental ones for the trigonal direction. However, for other directions all models lead to non-physical imaginary frequencies.

Taking this all into account together with the results of Brovman, it seems reasonable to conclude that a four-nearest-neighbours model can describe the lattice dynamics of bismuth at most qualitatively. It would seem necessary to develop a more sophisticated model.

Further experimental and theoretical work is in progress.

ACKNOWLEDGEMENTS

The authors would like to express their gratitude to Professor B. Buras for his advice and stimulating discussions. They are grateful to Mr. A. Pindor, Mr. A. Holas and Mr. A. Rajca for valuable discussions and help in computations. Thanks are also due to Mr. H. Kępa for help in carrying out the experiment.

REFERENCES

[1] COHEN, M.H., Phys. Rev. 121 (1961) 387.
[2] FALICOW, L.M., GOLIN, S., Phys. Rev. 137 (1965) 871.
[3] PRIESTLEY, M.G., WINDMILLER, L.R., KETTERSON, I.B., ECKSTEIN, Y., Phys. Rev. 154 (1967) 671.
[4] FOURET, R., Ann. Phys. 8 (1963) 611.
[5] KOENIG, S.H., YARNELL, J., Bull. Am. Phys. Soc. 5 (1960) 198.
[6] YARNELL, J.L., WARREN, J.L., WENZEL, R.G., KOENIG, S.H., I.B.M. J. Res. Dev. 8 (1964) 234.
[7] NITZ, W.W., SOSNOWSKA, I., SOSNOWSKI, J., JINR-Dubna, Rep. R-1847 (1964).
[8] SOSNOWSKI, J., SOSNOWSKA, I., JINR Dubna, Rep. 2409 (1965).
[9] BROCKHOUSE, B.M., Inelastic Scattering of Neutrons in Solids and Liquids (Proc. Symp. Vienna, 1960), IAEA, Vienna (1961) 113.
[10] BEDNARSKI, S., Phys. Stat. Sol. 9 (1965) 839.
[11] PECKHAM, G.E., SAUNDERSON, D.H., SHARP, R.I., Brit. J. appl. Phys. 18 (1967) 473.
[12] HUNTINGTON, H.B., "The Elastic Constants of Crystals ", in Academic Press, Solid State Physics 7 (1958).
[13] BEGBIE, G.H., BORN, M., Proc. roy. Soc. A 188 (1947) 179.
[14] ECKSTEIN, Y., LAWSON, A.W., RENECKER, D.H., J. appl. Phys. 31 (1960) 1534.
[15] OVCHINNIKOV, A.A., Sol. Phys. 7 (1965) 1183 (in Russian).
[16] BROVMAN, E.G., Kurchatov Institute Rep. 1456, Moscow (1967).
[17] SMITH, D., Thesis, University of New Mexico (Los Alamos Scientific Laboratory Rep. LA-3773, unpublished) (1967).

DISCUSSION

G. CAGLIOTI: Did the authors of paper SM-104/86 find any anomalous behaviour of the phonon lines (shifts, widths, etc.) in the region of the accidental degeneracy of the phonon branches along the (00ζ) direction?

R.M. NICKLOW: No anomalous behaviour was noticed at that point with the resolution being used. However, more measurements in that region are needed to determine definitely whether such behaviour exists or not.

R.M. PICK: I would just remark that the calculation of the lithium phonon spectrum which we performed several years ago using a pseudopotential derived from first principles (cf. HARRISON, W., Phys. Rev. 129 (1963) 2503) is certainly in much better agreement with experiment than that of Animalu et al.

B.N. BROCKHOUSE: Did this calculation suggest the system of extraordinarily long-range forces which seems to exist here?

R.M. PICK: Although the range of the forces is not as long as in the case of aluminium, the pair interaction extends much further in lithium than in sodium or aluminium.

B.N. BROCKHOUSE: The evidence for the long-range forces in lithium comes solely from the anomalous behaviour of the L (00ζ) branch, does it not? Quite simple arguments suggest that this branch should be especially sensitive to anharmonic effects. The line shapes observed in measurements for this branch at temperatures of ~ 100°K in sodium and rubidium were quite anomalous, though this effect may yet be shown to be spurious. For potassium at 9°K, I understand that the line shapes have proved to be quite normal. These facts suggest to me that the apparent long range may arise from anharmonicity.

R.M. NICKLOW: The long-range character of the forces in lithium deduced from these measurements is consistent with theoretical pseudopotential calculations and apparently is not solely a result of anharmonic effects. As indicated in the paper, the calculations of Animalu et al. do predict a crossing of the $T(00\zeta)$ and $L(00\zeta)$ branches. Mr. Pick's calculations also show this crossing.

R.M. PICK: I have a comment on paper SM-104/1. The only forces in the model which do not automatically maintain the equilibrium of the system are the long-range ones. By retaining the pair interactions only, it is possible to establish the equilibrium conditions of the crystal. These will be more numerous than those found by the authors of the paper. The latter conditions can be obtained by writing the equation in such a way that the crystal is in equilibrium under the action of these forces and of isotropic pressure. The equivalence of the two coefficients C_{44} may, in their model, be reflected in a $\sin\lambda$ condition, the Fermi screening parameter. By taking a pair potential with a larger number of free parameters (arbitrary pseudopotential method), good agreement with experiment may perhaps be obtained.

K.H. KREBS: It would be possible to avoid the C_{44} difficulty by using tangential force constants in the first part of the model.

In this same paper there is a statement that in the cubic case the model is under stress. This statement is made in order to explain the fact that the Cauchy relation is not fulfilled. I myself think that it would be more accurate to say that in the cubic case the Cauchy relation is not valid because of the presence of purely volume-dependent terms in the dielectric constant.

Yu. M. KAGAN (Chairman): The principal inference derived from this work (SM-104/1) - the disappearance of the long-range interaction in the Krebs model when hexagonal metals are involved - is in fact a result of the Born-Huang condition, to the importance of which in connection with non-cubic metals I made particular reference in my review paper (SM-104/203) earlier. A centrally-symmetric force matrix is used in the Krebs model for interaction with the nearest co-ordination spheres, and for this the Born-Huang condition is automatically fulfilled. The screened Coulomb interaction leads to an axially-symmetric model, for which the Born-Huang condition is not fulfilled even in the general case. Therefore, if fulfilment of the condition is a requirement, the results described by the authors then ensue.

I also have a comment to make on paper SM-104/4. It seems to me that the use of a generalized Harrison model pseudo-potential results in a picture of electron-ion interaction which is far from the truth. Thus, in the case of magnesium the authors find a characteristic ion radius which is about four times smaller than the real one. At the same time the tails of the Fourier component of the pseudo-potential are very much stretched in the high-pulse region, which must inevitably result in substantial overestimation of the contribution from the distant points of the reciprocal lattice.

R. M. PICK: I should like to ask the authors of paper SM-104/4 whether they get such good agreement for the Fermi surface of potassium.

T. SCHNEIDER: The agreement was fairly good for potassium, and in this connection I would suggest that you consult Ref. [4] of the paper.

ТЕОРИЯ КОЛЕБАТЕЛЬНОГО СПЕКТРА ГЕКСАГОНАЛЬНЫХ МЕТАЛЛОВ

Е.Г.БРОВМАН, Ю.КАГАН, А.ХОЛАС
ИНСТИТУТ АТОМНОЙ ЭНЕРГИИ
им.И.В.КУРЧАТОВА, МОСКВА,
СССР*

Abstract — Аннотация

THEORY OF VIBRATIONAL SPECTRUM IN HEXAGONAL METALS. The previously developed general theory of vibrational spectrum in metals, based on separation of the long and short-range interionic interactions in the electron-ion system, is applied to the analysis of the phonon spectrum in the hexagonal metals Be, Mg and Zn. The long-range interaction is demonstrated with help of the concrete form of the pseudo-potentials in these metals, while the parameters of the short-range interaction are determined from some experimental quantities. The essential role of the short-range interaction is demonstrated. A detailed comparison of theory with experiment is given.

ТЕОРИЯ КОЛЕБАТЕЛЬНОГО СПЕКТРА ГЕКСАГОНАЛЬНЫХ МЕТАЛЛОВ. Развитая ранее общая схема рассмотрения колебательного спектра металлов, основанная на выделении дальнодействующей и короткодействующей части межионного взаимодействия в электронной системе [5], применяется для анализа фононного спектра гексагональных металлов Be, Mg, Zn. Для описания дальнодействующего взаимодействия используется конкретный вид псевдопотенциала для этих металлов, а параметры короткодействия находятся в рамках обратной задачи.

Демонстрируется существенная роль короткодействующего взаимодействия.

Проводится подробное сравнение теории с экспериментом.

I. ВВЕДЕНИЕ

В последние годы стало очевидно, что в формировании фононного спектра металлов существенную роль играют электроны проводимости. Это сделало заманчивым определение фононного спектра из "первых принципов", опираясь на знание эффективного потенциала электрон-ионного взаимодействия.

Исследования такого типа были проведены в работах Тойи [1], Шама [2], Воско и др. [3], Бровмана и Кагана [4], [5]. Во всех этих работах, кроме последней, косвенное взаимодействие между ионами через электроны учитывалось во втором порядке теории возмущения по электрон-ионному потенциалу, что приводило к появлению парного межионного взаимодействия центрального типа. При этом для прямого межионного взаимодействия сохранялась лишь обычная кулоновская часть, ибо короткодействующее взаимодействие за счёт непосредственного перекрытия ионов в металлах в большинстве случаев мало [6].

---

* Работа выполнена совместно с Объединенным Институтом Ядерных Исследований (Дубна, СССР), сотрудником которого является А.Холас.

В работах [4] , [5] было проведено последовательное рассмотрение задачи о формировании фононного спектра в металлах, основанное на регулярном разложении адиабатической электронной энергии в ряд по степеням электрон-ионного псевдопотенциала.

При этом был получен существенный результат, согласно которому в электрон-ионной плазме металла, наряду с обычным парным взаимодействием существует межионное взаимодействие через электроны непарного типа. Физически такое взаимодействие связано с рассеянием электронов одновременно на трёх или более ионах металла.

Как показывает непосредственный анализ [4] , [5] , это взаимодействие обладает симметрией решётки и носит короткодействующий характер.

Таким образом, в металле возникают межионные взаимодействия, ковалентные по своей структуре.

Если говорить о величине таких непарных сил, то в то время как парный межионный потенциал определяется выражением квадратичным по псевдопотенциалу, каждый из следующих членов разложения содержит лишний параметр $V_{\vec{K}}/\varepsilon_F$, где $V_{\vec{K}}$ – значение псевдопотенциала в точках обратной решётки $\vec{K} \neq 0$. Как правило, этот параметр невелик, что фактически и определило успех модели свободных электронов при описании электронного спектра металлов. Например, в случае щелочных металлов $V_{\vec{K}}/\varepsilon_F$ очень мал для всех $\vec{K}$ (ближайшие $\vec{K}$ расположены так, что $|\vec{K}| > 2k_F$). Аналогичная картина наблюдается в случае металлов типа Al и Pb . Именно по этой причине расчёты, учитывающие только парное межионное взаимодействие в существенной степени схватывали основные черты фононного спектра этих металлов ([1] - [3]), что и создало иллюзию верификации простого варианта теории.

Однако положение радикально меняется, когда мы переходим к металлам с более сложной структурой, например, обладающим двумя атомами в элементарной ячейке. Так, в случае металлического олова оказалось, что параметр $V_{\vec{K}}/\varepsilon_F$ уже не пренебрежимо мал и, естественно, роль непарных сил весьма существенна (без их учёта решётка олова вообще не была бы устойчивой [4] , [5]).

Хотя структура всех членов ряда разложения по степеням псевдопотенциала, соответствующих непарному взаимодействию, совершенно ясна, непосредственное количественное вычисление их весьма громоздко (оно проводится в настоящее время).

Поэтому, в связи с короткодействующим характером непарного взаимодействия, возникла идея вернуться для его описания к обычному пространству и считать, что оно распространяется лишь до ближайших соседей.

Такая программа разделения дальнодействующих и короткодействующих сил была реализована на примере олова. Три независимых константы, отвечающие полному учёту взаимодействия с ближайшей координационной сферой, могли быть определены из значений модулей упругости или из нескольких частот спектра. В результате был найден устойчивый фононный спектр, близкий к экспериментально измеренному.

В связи со сказанным представляло большой интерес провести анализ картины формирования фононного спектра на примере целой группы металлов со сложной структурой и с разными значениями характерных параметров $V_{\vec{K}}/\varepsilon_F$. Наиболее удобной для этого оказалась группа гексагональных металлов Be, Mg, Zn, для которых произведены подробные измерения фононных спектров с помощью неупругого рассеяния нейтронов [7] - [12]. Действительно, как будет показано ниже, значения $V_{\vec{K}}/\varepsilon_F$ для существенных векторов обратной решётки сильно меняются в этой группе от металла к металлу, что приводит к резко различной роли непарного взаимодействия. Заметим, в заключение, что анализ традиционного типа, основанный на тензорной модели Борна-Кармана проводился для Be, Mg, Zn весьма подробно (см., например, работы [8], [9], [13] и ссылки, содержащиеся в них).

2. ОБЩИЕ СООБРАЖЕНИЯ

Кристаллографическая структура семейства гексагональных металлов второй группы хорошо известна, и мы на ней не останавливаемся (см., например, [8], [13]).

Наш анализ будет проводиться главным образом в обратном пространстве. На рис. I изображено несколько важнейших узлов обратной решётки. Пунктиром показаны границы первой зоны Бриллюэна. Специально выделены симметричные направления и точки, для которых возможно в настоящее время сравнение с экспериментом.

Если воспользоваться соображениями теории групп [8], [14], то для этих направлений можно факторизовать динамическую матрицу $\mathcal{D}^{\alpha\beta}_{ss'}(\vec{q})$ при произвольном характере взаимодействия между ионами и найти явные выражения для закона дисперсии всех ветвей фононного спектра. Получающиеся результаты совпадают с приведенными в работе [8 (см. таблицу III)] за исключением направления T, для которого в матрицах второго порядка представлений T_1 и T_4 для исправления необходимо произвести замену:

$$\operatorname{Im} \mathcal{D}^{xy}_{12}(\vec{q}) \to \operatorname{Im} \mathcal{D}^{xy}_{12}(\vec{q}) \mp \operatorname{Im} \mathcal{D}^{xy}_{11}(\vec{q}) \tag{I}$$

(- для T_I и + для T_4)

Для того чтобы в явном виде определить динамическую матрицу

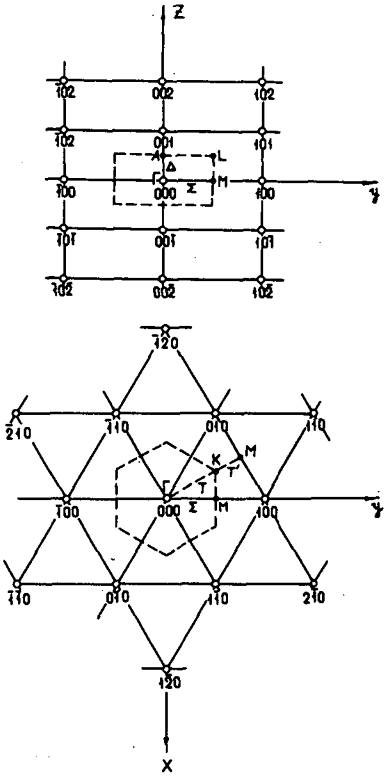

Рис. I.

колебаний, воспользуемся результатами работы [5], согласно которой динамическая матрица представляется в виде:

$$\mathcal{D}^{\alpha\beta}_{ss'}(\vec q) = \mathcal{D}^{\alpha\beta}_{1ss'}(\vec q) + \mathcal{D}^{\alpha\beta}_{2ss'}(\vec q) \tag{2}$$

Здесь матрица $\mathcal{D}_1$ соответствует парному взаимодействию между ионами, включающему в себя как прямое кулоновское взаимодействие, так и косвенное взаимодействие через электроны проводимости. В решётке из n одинаковых атомов в элементарной ячейке эта матрица имеет вид:

$$\mathcal{D}^{\alpha\beta}_{1ss'}(\vec q) = \frac{\omega_0^2}{n}\left\{\sum_{\vec K}\frac{(\vec q+\vec K)^\alpha(\vec q+\vec K)^\beta}{|\vec q+\vec K|^2}\left[1-\psi(\vec q+\vec K)\right]e^{i\vec K(\vec\rho_s-\vec\rho_{s'})}\right.$$
$$\left. - \delta_{ss'}\sum_{s''}\sum_{\vec K\neq 0}\frac{\vec K^\alpha\vec K^\beta}{|\vec K|^2}\left[1-\psi(\vec K)\right]e^{i\vec K(\vec\rho_s-\vec\rho_{s''})}\right\} \tag{3}$$

где $\omega_0^2 = \dfrac{4\pi Z^2e^2}{MV_0}\cdot n$; $\psi(\vec q) = \dfrac{V_{\vec q}\,\tilde\pi_{\vec q}|\vec q|^2}{\varepsilon(\vec q)}\cdot\dfrac{V_0}{4\pi Z^2e^2}$ (4)

а остальные обозначения совпадают с принятыми в [5].

Матрица $\mathcal{D}_2$ описывает косвенное взаимодействие между ионами через электроны многочастичного типа. В соответствии с короткодействующим характером этого взаимодействия мы будем считать, как уже указывалось во введении, что оно локализовано на ближайших координационных сферах. В случае рассматриваемых гексагональных металлов расстояния до ближайших двух координационных сфер мало отличаются друг от друга. В силу этого, в отличие от олова, мы не считали возможным ограничиться только одной координационной сферой.

Однако, чтобы сделать анализ максимально простым, мы использовали для описания взаимодействия с каждой из двух координационных сфер аксиально симметричную модель в виде $\mathcal{D}^{\alpha\beta}(R) = f_R \frac{R_\alpha R_\beta}{R^2} + G_R \delta_{\alpha\beta}$. Интересно, что ограничение такой моделью, вместо полной тензорной, как видно из дальнейшего, вообще не сказывается на ряде основных результатов и слабо сказывается на остальных.

Отметим далее следующее важное обстоятельство. Как известно, правильно построенная динамическая матрица должна удовлетворять условию отсутствия анизотропных напряжений (т.н. условия Борна-Хуанга) (см. [15]). Очень существенно, что это условие не выполняется автоматически для матрицы $\mathcal{D}_1$. Это связано с тем, что при произвольном парном взаимодействии между ионами $\varphi(R)$ в частности и при взаимодействии, описываемом $\mathcal{D}_1$, тензор сил $\left(\frac{\partial^2 \varphi}{\partial R_\alpha \partial R_\beta}\right)_{R=R_0}$ имеет вид $\varphi'_{R_0} \delta_{\alpha\beta} + \left(\varphi'' - \frac{\varphi'}{R}\right)_{R_0} \frac{R_0^\alpha R_0^\beta}{R_0^2}$. Условие равновесия для всего кристалла отнюдь не приводит к условию $\varphi'_{R_0} = 0$, т.е. каждая координационная сфера не обязана находиться в минимуме парного потенциала. Нетрудно проследить, что именно существование члена пропорционального $\delta_{\alpha\beta}$ в достаточно несимметричном кристалле приводит к нарушению соотношений Борна-Хуанга. Поэтому, в частности, модель, опирающаяся только на учёт матрицы $\mathcal{D}_1$ в общем случае, была бы внутренне противоречивой.

В соответствии со сказанным, условие Борна-Хуанга должно накладываться на динамическую матрицу в целом.

Для рассматриваемых гексагональных кристаллов оно оказывается эквивалентным требованию равенства скоростей поперечного звука (соответствующих модулю упругости C_{44}), определенных из направлений ГМ и ГК в обратном пространстве. Это приводит, естественно, к уменьшению числа независимых параметров короткодействия с четырёх (f_c, f_a, G_c, G_a) до трёх.

3. ФОНОННЫЙ СПЕКТР МАГНИЯ

Анализ фононного спектра гексагональных металлов мы начали с магния, что в первую очередь связано с тем, что он наиболее полно изучен с экспериментальной точки зрения [8], [9]

При использовании псевдопотенциала для описания дальнодействующей части взаимодействия можно различать прямую и обратную постановки задачи. В рамках прямой задачи мы должны воспользоваться значениями псевдопотенциала, полученного из непосредственных расчётов. Для обратной задачи псевдопотенциал заменяется модельным и параметры его определяются из анализа самого фононного спектра.

Для магния задача рассматривалась нами в обоих аспектах.

В первом случае мы воспользовались для псевдопотенциала значениями, полученными в работах Абаренкова, Хейне и Анималу [16], [17], [18]. Этот псевдопотенциал успешно верифицировался по измерениям формы ферми-поверхности магния [19] и оценке энергии связи [20].

Элементы динамической матрицы, соответствующие прямому кулоновскому взаимодействию, вычислялись обычным образом, путём приведения к быстро сходящимся рядам Эвальда (подробные формулы см. в [4]).

Элементы матрицы $\mathcal{D}_2$ находились с помощью частот фононного спектра, измеренных экспериментально [8], [9]. При этом для определения двух констант f_c и G_c использовались значения двух оптических частот при $\vec{q} = 0$. Третья константа f_a определялась для достижения лучшего описания ветвей Σ_1 и Σ_4 в точке M. Четвёртая константа G_a не является независимой и находилась из соотношения Борна-Хуанга. В результате были получены следующие численные значения для констант:

$$f_c = -7{,}05 \cdot 10^3 \text{ дин/см},$$
$$f_a = -7{,}55 \cdot 10^3 \text{ дин/см},$$
$$G_c = 0{,}46 \cdot 10^3 \text{ дин/см},$$
$$G_a = 0{,}43 \cdot 10^3 \text{ дин/см}.$$

Эти значения ясно указывают на изотропность взаимодействия в магнии ($f_c \approx f_a$; $G_c \approx G_a$).

На рис.2 приводятся полученные нами дисперсионные кривые для Mg и экспериментальные точки из работ [8], [9]. Отметим, что для всех рассмотренных симметричных направлений ветви колебаний с поляризациями вдоль оси Z отделяются и поэтому изображены нами отдельно. На рис. 3 изображены те же дисперсионные кривые, но без учёта короткодействующего взаимодействия. Из сравнения видно, что дальнодействующее парное взаимодействие схватывает основные черты спектра, однако количественно хорошее соответствие теории с экспериментом достигается лишь при учёте короткодействия.

Естественно, что псевдопотенциал электрон-ионного взаимодействия вычисляется с ограниченной точностью, причём неточность

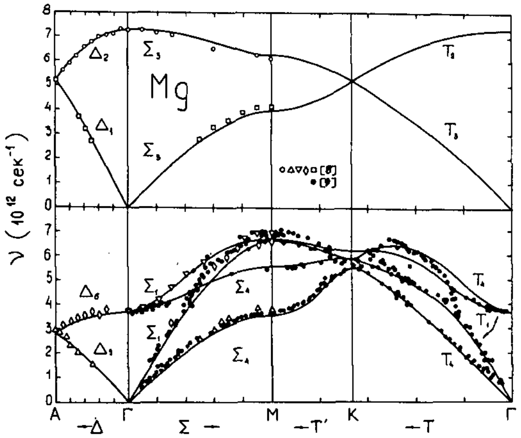

Рис. 2

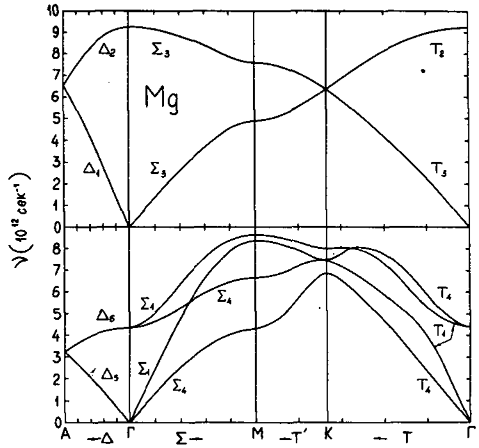

Рис. 3

часто велика в той области q, которая не была важна для определения электронных свойств, однако важна для фононов. Поэтому является разумной постановка обратной задачи с модельным потенциалом и свободными параметрами. В качестве такого модельного псевдопотенциала мы приняли потенциал вида:

$$V(r) = \begin{cases} V_0 & r < r_0 \\ -\dfrac{Ze^2}{r} & r > r_0 \end{cases} \tag{5}$$

который представляется естественным для всей концепции псевдопотенциала. Параметры V_0 и r_0 являются свободными. В импульсном пространстве фурье-компонента этого потенциала следующая:

$$V(q) = -\frac{4\pi Ze^2}{q^2\Omega}\cos q r_0 + 4\pi\left(\frac{r_0^3}{\Omega}\right)V_0\,\frac{\sin q r_0 - q r_0 \cos q r_0}{(q r_0)^3} \tag{6}$$

Здесь Ω - объём, приходящийся на один атом.

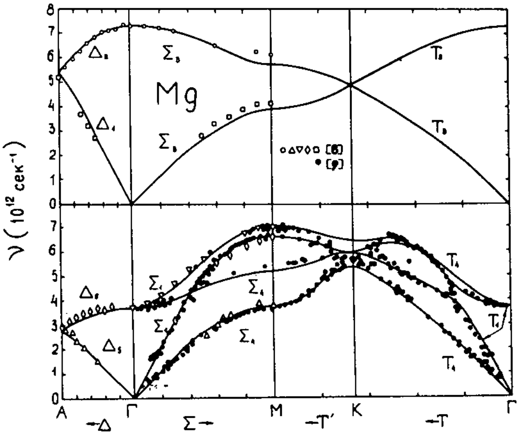

Рис. 4.

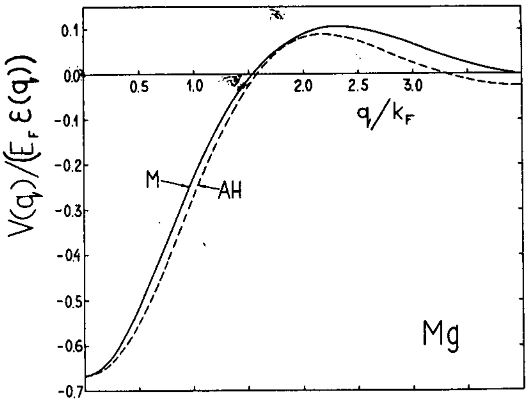

Рис. 5.

Диэлектрическая постоянная и поляризационный оператор в (4) выбирались так же, как в случае расчёта фононного спектра олова [4], [5].

Несколько слов о схеме, по которой решалась обратная задача. Задаётся пара значений (V_0 r_0). Тем самым полностью определяется дальнодействующая часть взаимодействия, а остальные параметры, описывающие короткодействие, могут быть найдены в точности как для прямой постановки задачи. В результате можно найти значения модулей упругости $C_{33}(V_0 r_0)$ и $C_{44}(V_0 r_0)$. Теперь линия пересечения кривых $C_{33}(V_0 r_0) = C_{33}^{(\text{эксп})}$ и $C_{44}(V_0 r_0) = C_{44}(\text{эксп})$ определяет искомые электронные параметры $V_0 r_0$.

Описанный выше способ решения обратной задачи с помощью модулей упругости C_{33} и C_{44} имеет следующее важное преимущество: если учесть короткодействующие взаимодействия атома со всеми соседями в плоскости $Z = 0$ и со всеми соседями в плоскостях $Z = \pm \frac{c}{2}$, причём в полной тензорной модели, электронные параметры V_0 r_0 получаются прежними. Поэтому приближённость выбранной модели для описания короткодействия абсолютно не сказывается на значениях V_0 r_0 (а также и на ветвях колебаний $\Delta_1, \Delta_2, \Sigma_3$).

Заметим ещё, что с точки зрения обратной задачи более удобными являются независимые электронные параметры q_0 r_0 , где q_0 определяет первый ноль псевдопотенциала ($V(q_0) = 0$).

В результате применения описанной схемы были найдены следующие параметры (пять независимых):

$r_0 =$ $0{,}88.10^{-8}$ см,
$q_0 =$ $1{,}54 \cdot k_F$ ($V_0 = -1.65\ \mathcal{E}_F$),
$f_c =$ $-16{,}3.10^3$ дин/см,
$f_a =$ $-15{,}3.10^3$ дин/см,
$G_c =$ $2{,}18.10^3$ дин/см,
$G_a =$ $2{,}08.10^3$ дин/см.

На рис. 4 изображен фононный спектр,найденный с помощью приведенных параметров. Видно, что наблюдается хорошее согласие теории с экспериментом. В таблице I приводятся данные относительно модулей упругости, из которых можно сравнить с экспериментом результаты прямой и обратной задачи для Mg , а также относительный вклад дальнодействующего и короткодействующего взаимодействия. Модуль C_{13} не может быть найден из рассматриваемых высокосимметричных направлений и определялся из направления $\vec{q}$, лежащего в несимметричном направлении.

Экспериментальные данные взяты из работы [21].

Таблица I. (Модули упругости даны в единицах $10^{11}\frac{дин}{см^2}$)

	Псевдопотенциал Х.А.	Псевдопотенциал Х.А. + короткодействие	Обратная задача	Эксперимент
c_{11}	7,20	4,29	6,63	5,97
c_{33}	8,95	5,03	6,17	6,17
c_{44}	1,95	1,50	1,64	1,64
c_{66}	2,0	1,32	1,82	1,67
c_{13}	-	0,76	2,54	2,17

Интересно также сравнить найденный модельный псевдопотенциал с вычисленным в работе [17] . На рис. 5 приводятся соответствующие кривые для фурье-компонент. Они весьма близки друг к другу, в частности близки значения q_0 ($V(q_0) = 0$). Отметим кстати, что найденный параметр r_0 оказался близким к величине радиуса иона Mg^{++}(0,78Å [17]), что полностью соответствует исходной концепции псевдопотенциала. В заключение этого раздела обратим внимание на следующее важное обстоятельство. Как показывает общий групповой анализ в точке K (см.рис.I), значения фононных частот определяются выражениями:

$$\left.\begin{aligned} \omega_1^2 &= \operatorname{Re} \mathcal{D}_{11}^{xx} + \operatorname{Im} \mathcal{D}_{11}^{xy} \\ \omega_2^2 &= \operatorname{Re} \mathcal{D}_{11}^{xx} - \operatorname{Im} \mathcal{D}_{11}^{xy} + 2 \operatorname{Re} \mathcal{D}_{12}^{xx} \end{aligned}\right\} K_1$$
$$\left.\begin{aligned} \omega_3^2 &= \operatorname{Re} \mathcal{D}_{11}^{xx} + \operatorname{Im} \mathcal{D}_{11}^{xy} \\ \omega_4^2 &= \operatorname{Re} \mathcal{D}_{11}^{xx} - \operatorname{Im} \mathcal{D}_{11}^{xy} - 2 \operatorname{Re} \mathcal{D}_{12}^{xx} \end{aligned}\right\} K_4 \qquad (7)$$

Если бы непарное взаимодействие отсутствовало, то, как легко показать, $\operatorname{Im} \mathcal{D}_{11}^{xy} = 0$. В этом случае значения частот ω_2^2 и ω_4^2 отделены на равное расстояние от вырожденных частот $\omega_1^2 = \omega_3^2$. При наличии непарных сил картина меняется. Теперь вырожденный уровень $\omega_1^2 = \omega_3^2$ смещён относительно центра $\frac{\omega_2^2 + \omega_4^2}{2}$ на величину $2 \operatorname{Im} \mathcal{D}_{11}^{xy}$. Таким образом, появляется интересная возможность прямого определения масштаба непарного взаимодействия.

К сожалению, имеющиеся пока экспериментальные данные [9] не дают возможности сколько-нибудь однозначно оценить эту величину.

4. ФОНОННЫЙ СПЕКТР ГЕКСАГОНАЛЬНЫХ МЕТАЛЛОВ (Be, Mg, Zn) И РОЛЬ КОВАЛЕНТНОСТИ

Хотя гексагональные металлы образуют во многих отношениях родственную группу, они тем не менее значительно отличаются друг от друга по физическим свойствам. Как нам представляется, это в решающей степени связано с различием в конкретном виде псевдопотенциалов для соответствующих ионов.

Такое различие чётко можно проследить на примере поведения функций $\Psi(q)$ (см. (4)), построенных с помощью значений, взятых из работы [18]. На рис. 6 приводятся эти кривые вместе с расположением ближайших узлов обратной решётки. (Части кривых для $q/k_F \gtrsim 1.2$ приводятся в увеличенном масштабе).

Нетрудно заметить резкое различие в поведении "хвоста" функции $\Psi(q)$. Оно отражает тот факт, что параметр $V_{\vec{K}}/\varepsilon_F$ для узлов обратной решётки $|\vec{K}| \gtrsim 2k_F$ оказывается существенно больше в случае Be и Zn, чем в Mg. Но именно эта область определяет короткодействующее взаимодействие ковалентного типа [4], [5]. Это сразу заставляет думать, что эффекты ковалентности в Be и Zn должны быть выражены

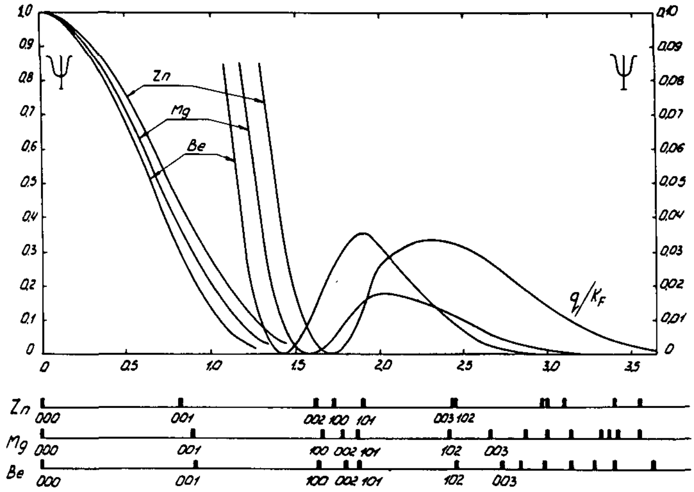

Рис. 6.

значительно ярче, и поэтому фононный спектр во всех трёх случаях должен существенно различаться.

Для того чтобы выявить получающуюся картину в наиболее чёткой форме, мы воспользовались для вычисления фононного спектра для всего ряда металлов значениями псевдопотенциала, найденными в рамках одного приближения [16] , [17] , [18] .

При этом для определения трёх параметров короткодействующего взаимодействия использовалась та же схема, что и в случае магния.

Для бериллия получаются следующие значения параметров (из них только три независимых):

$$f_c = -89{,}5.10^3 \text{ дин/см},$$

$$f_a = -78.10^3 \text{ дин/см},$$

$$G_c = 11{,}7.10^3 \text{ дин/см},$$

$$G_a = 8{,}73.10^3 \text{ дин/см}.$$

На рис. 7 приведены окончательные результаты расчёта для Be и экспериментальные значения, полученные в работе [7] . (В этой работе не были произведены измерения для двух ветвей вдоль ГМ). Видно, что получается неплохое согласие между теорией и экспериментом, особенно если учесть простоту использованной схемы.

На рис. 8 изображены дисперсионные кривые для Be при учёте лишь парного дальнодействующего взаимодействия. Из сравнения видно, что непарное взаимодействие играет в Be чрезвычайно большую роль. Интересно, что даже при варьировании псевдопотенциала в широких пределах роль ковалентности сохраняется. Следует думать, что именно по этой причине в работе Кёппеля и Марадудина [22] , где впервые для описания динамики

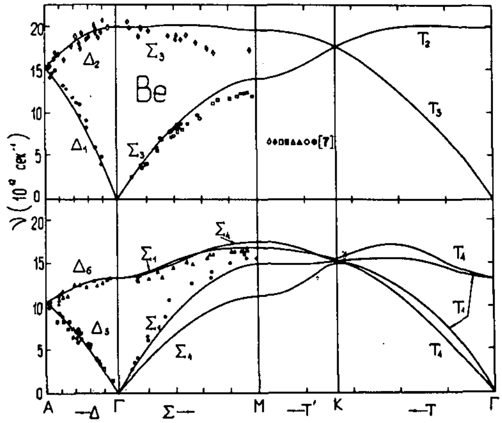

Рис. 7.

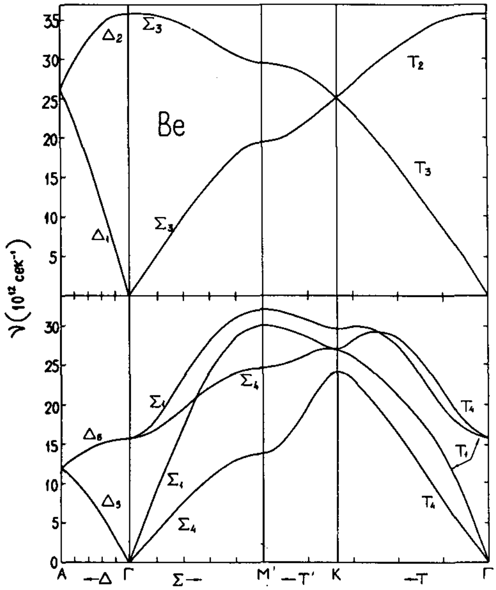

Рис. 8.

Be учитывалась роль электронов, но только в парном приближении, не удалось достичь хорошего согласия с экспериментом.

Перейдём теперь к анализу цинка. Если провести рассмотрение, аналогичное Mg и Be, то для констант, описывающих короткодействие, получим следующие значения (как и раньше, только три параметра независимы):

f_c = $14{,}85 \cdot 10^3$ дин/см,

f_a = $13{,}82 \cdot 10^3$ дин/см,

G_c = $-1{,}57 \cdot 10^3$ дин/см,

G_a = $-2{,}61 \cdot 10^3$ дин/см.

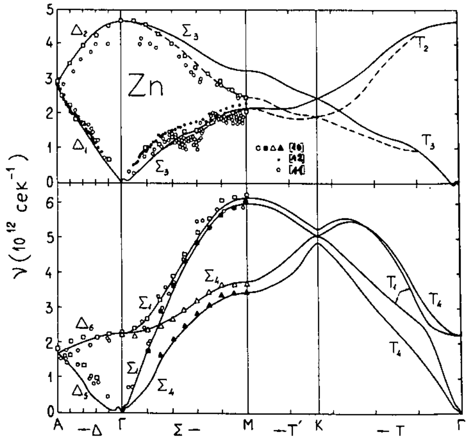

Рис. 9.

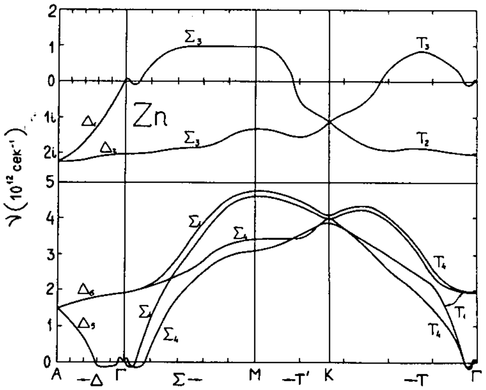

Рис. 10.

Результаты расчёта фононного спектра и экспериментальные точки, полученные в работах [10], [11], [12], приведены на рис. 9.

Бросается в глаза различие в величине щели между двумя ветвями Σ_3 в точке M. Оно не может быть устранено за счёт использования общей тензорной модели для взаимодействия с ближайшими координационными сферами. С другой стороны, как мы уже отмечали, параметр $V^{\vec{k}}/\varepsilon_f$ для существенных узлов обратной решётки в Zn не очень мал, и поэтому непарное взаимодействие в прямом пространстве может оказаться затянутым на большее расстояние (см. [4]). В этой связи мы провели расчёт, включив взаимодействие со следующей (третьей) координационной сферой. При этом, поскольку нас интересовали только ветви колебаний с поляризацией вдоль Z, мы выбрали простейший вид взаимодействия с единственным параметром, отличным от нуля $\mathcal{D}^{zz}=1.18\cdot10^{3}$ дин/см. Измененные дисперсионные кривые обозначены на рис. 9 пунктиром (остальные ветви изменяются незначительно или вовсе не изменяются). Согласие теории с экспериментом существенно улучшается.

На рис. 10 приводится фононный спектр в Zn, соответствующий учёту только парного дальнодействующего взаимодействия. Существенно, что спектр колебаний в этом случае в отличие от Mg и Be оказывается неустойчивым. Лишь наличие сильного ковалентного взаимодействия в существенной степени стабилизирует решётку. Однако даже в окончательном спектре (рис. 9) сохраняется аномальный характер поведения дисперсионных кривых при малых $\vec q$. Такие аномалии, как и неустойчивость спектра при учёте лишь парного взаимодействия, являются прямым следствием специфического характера зависимости $V(\vec q)$ для цинка.

Для того чтобы проанализировать это, рассмотрим для примера поведение оптической частоты при $\vec q = 0$ с поляризацией вдоль z. Используя (3), можно получить для неё следующее выражение:

$$\omega_z^2(0) = \omega_0^2\left[\left(\frac{\omega_{z\,\text{ион}}(0)}{\omega_0}\right)^2 + \sum_{\vec K\neq 0}\frac{K_z^2}{K^2}\cos\vec K\vec\rho\,\Psi(\vec K)\right] \qquad (8)$$

Здесь первый член описывает вклад от чисто ионной решётки, а второй - вклад парного взаимодействия через электроны. Как нетрудно видеть, основной вклад в сумму (8) дают эквивалентные узлы обратной решётки $\vec K$ = 001,00-1. Используя далее, что для этих узлов $\cos\vec K\vec\rho = -1$, получим:

$$\omega_z^2(0) \simeq \omega_0^2\left[\left(\frac{\omega_{z\,\text{ион}}(0)}{\omega_0}\right)^2 - 2\Psi(001)\right] \qquad (9)$$

Для Zn $\left(\frac{\omega_{z\,\text{ион}}(0)}{\omega_0}\right)^2 \simeq 0.95$, а $2\Psi(001) \simeq 0.91$

Мы видим, что происходит почти полная взаимная компенсация электронного и ионного вкладов. Это совершенно особая ситуация, свойственная лишь Zn, и отсутствующая в Be и Mg (в Be, используя (9) получим $\omega_z^2(0) \simeq 0.44\,\omega_0^2$, а в Mg $\omega_z^2(0) \simeq 0.30\,\omega_0^2$). При такой компенсации фононный спектр становится очень чувствительным к особенностям псевдопотенциала в широкой области q. По-видимому, аномалии, наблюдавшиеся экспериментально в Zn, именно такого происхождения.

Интересно далее, что область псевдопотенциала вблизи = 001, столь важная для фононного спектра рассматриваемых металлов, абсолютно не даёт вклада в электронные свойства из-за обращения в нуль структурного фактора статической решётки и поэтому не может быть верифицирована из экспериментов, относящихся к электронам.

В этой связи особую роль приобретает обратная задача. Однако большая чувствительность к конкретному ходу псевдопотенциала $V(\vec q)$ делает необходимым использование модельного потенциала в более гибкой форме, нежели простая форма (6) или аналогичные двухпараметрические выражения других авторов. Модельный потенциал должен допускать сравнительно независимые изменения в областях $q<q_0$ и $q>q_0$. Такая задача делается в настоящее время.

Заметим в заключение, что, в силу сказанного, цинк является весьма чувствительным объектом также для анализа строгой обратной задачи, при которой должен быть использован явный вид для непарной части взаимодействия как функционала $V(\vec{q})$ (см. [4], [5]). В этом случае в задаче, естественно, не остаётся никаких свободных параметров, кроме вида амплитуды электрон-ионного рассеяния.

ЛИТЕРАТУРА

[1] TOYA, T., J. Res. Ist. Catal. 6 (1958) 161, 183.
[2] SHAM, L.J., Proc. R. Soc. Ser. A 283 (1965) 33.
[3] VOSKO, S.H., ROGER, T., KEECH, G.H., Can. J. Phys. 43 (1965) 1187.
[4] БРОВМАН, Е.Г., КАГАН, Ю., Тезисы LT-10, Москва (1966). Препринт ИАЭ-1186 (1966).
[5] БРОВМАН, Е.Г., КАГАН, Ю., ЖЭТФ 52 (1967) 557.
[6] VOSKO, S.H., Phys. Lett. 13 (1964) 97.
[7] SCHMUNK, R.E., BRUGGER, R.M., RANDOLPH, P.D., STRONG, K.A., Phys. Rev. 128 (1962) 562.
[8] IYENGAR, P.K., VENKATAMARAN, G., VIJAYARAGHAVAN, P.R., ROY, A.P., Inelastic Scattering of Neutrons (Proc. Symp. Bombay, 1964) 1, IAEA, Vienna (1965) 153.
[9] SQUIRES, G.L., Proc. phys. Soc. 88 (1966) 919.
[10] BORGONOVI, G., CAGLIOTI, G., ANTAL, J.J., Phys. Rev. 132 (1963) 683.
[11] MALISZEWSKI, E., SOSNOWSKI, J., BLINOWSKI, K., KOZUBAWSKI, J., PADŁO, I., SLEDZIEWSKA, D., Inelastic Scattering of Neutrons in Solids and Liquids (Proc. Symp. Chalk River, 1962) 2, IAEA, Vienna (1963) 87; MALISZEWSKI, E., частное сообщение.
[12] IYENGAR, P.K., частное сообщение.
[13] CZACHOR, A., Inelastic Scattering of Neutrons (Proc. Symp. Bombay, 1964) 1, IAEA, Vienna (1965) 181.
[14] БРОВМАН, Е.Г., Препринт ИАЭ-1456 (1967).
[15] БОРН, М., ХУАН КУНЬ, Динамическая теория кристаллических решеток. И.Л. (1958).
[16] HEINE, V., ABARENKOV, I., Phil. Mag. 9 (1964) 451.
[17] ANIMALU, A.O.E., HEINE, V., Phil. Mag. 12 (1965) 1249.
[18] ANIMALU, A.O.E., Proc. R. Soc. Ser. A 294 (1966) 376.
[19] KIMBALL, J.C., STARK, R.W., MUELLER, F.H., Phys. Rev. 162 (1967) 603.
[20] HEINE, V., WEAIRE, D., Phys. Rev. 152 (1966) 603.
[21] LONG, T., SMITH, C., Acta metall. 5 (1957) 200.
[22] KOPPEL, J.U., MARADUDIN, A.A., Phys. Lett. 24 A (1967) 224.

LATTICE DYNAMICS OF Cu_{1-x} - Ni_x

M. SAKAMOTO AND Y. HAMAGUCHI
JAPAN ATOMIC ENERGY RESEARCH INSTITUTE,
TOKAI, IBARAKI, JAPAN

Abstract

LATTICE DYNAMICS OF Cu_{1-x}-Ni_x. The phonon dispersion relations for the (110) direction in the alloy $Cu_{0.9}$ -$Ni_{0.1}$ and pure copper have been measured by the method of inelastic scattering of slow neutrons using the time-of-flight spectrometer at the 10-MW research reactor JRR-2 in Tokai. The measurements were made at room temperature. There are significant differences in the shapes of the dispersion curves for $Cu_{0.9}$-$Ni_{0.1}$, as compared with the results for Cu. Those of $Cu_{0.9}$-$Ni_{0.1}$ show large anomalies in the range of reduced wave number q = 0.5 to 1.1 for both l and T_2 branches. This is in contrast to the very smooth behaviour on the dispersion curves for copper and also for nickel. The range of the forces of interactions was determined by performing least-squares fits of the experimental dispersion relations for Cu and $Cu_{0.9}$-$Ni_{0.1}$ to Fourier series of the form $4\pi^2 M\nu^2 = \sum_n A_n(1 - \cos n\pi q/q_m)$, where A_n represent the interplanar force constants for the n^{th} neighbour's plane. For $Cu_{0.9}$-$Ni_{0.1}$ seven planes at least are needed to fit the observed dispersion curves in both branches, as compared with three planes needed to obtain a reasonable fit for Cu. This fact indicates that the force constants between distant neighbours for alloys are larger than those for Cu.

1. INTRODUCTION

The Tokai Laboratory time-of-flight spectrometer was put into operation in the fall of 1965 and the conversion of the usual neutron diffractometer to the tripe-axis neutron spectrometer was completed in the spring of last year (1967). Since then neutron spectroscopy studies on lattice vibrations, magnons and so on have been started. This report describes that part of the results which concerns the lattice vibration of alloy systems.

It has been recognized that in the lattice dynamics of metals the deformation of the electron density within the ions plays an essential role through electron-phonon interactions. In the case of nickel the electronic band structure and the Fermi surface are believed to be similar to those of copper, whereas there are holes in the d-electron shell. The overall dispersion relations for the normal mode of copper [1-8] and nickel [9-10] show very similar behaviour. They are generally rather smooth and do not show Kohn anomalies. The ratio of the frequencies in nickel and those in copper is almost constant at about 1.24 [1] in the full range of the phonon wavevector. This should be attributed to the difference of the force system through the electronic structure in two metals, because the masses of these metals are not very different. The Fermi surface and the electronic structure primarily depend on the electron concentration. The effect of different electron concentrations could be studied in the disordered alloys. The alloys of copper-nickel system form a complete series of substantial solid solutions, all having a face-centered cubic structure. The study of the lattice dynamics of those alloys was undertaken in the hope that some pattern in the correlation between the electron concentration and the lattice vibration could emerge.

2. APPARATUS

The measurements of the dispersion curves were done with two kinds of spectrometer, a time-of-flight spectrometer and a triple-axis spectrometer. These spectrometers are at the 10-MW research reactor JRR-2 in Tokai. The time-of-flight spectrometer is composed of three rotors which are connected electronically with one motor each. Their rotational axes are parallel to the neutron beam. The speed of rotations and the relative phases between each rotor are controlled by a digital control system [11]. The rotor controls are in multiples of 0.6° in phase and 0.1 rev/sec in rotational speed. The distance between the first rotor and the third rotor is 3 m and the flight path between the sample and the detector is 2 m.

In the triple-axis crystal spectrometer the single crystal for a monochromater and an analyser are usually Cu (111) and Al (200) respectively. Spectrometer movements in the scattered, sample and analyser angle are in multiples of a 0.01° step and controlled by a program tape. The normal mode of operation is constant-Q.

The single crystals of the pure copper and the alloys were grown by the modified Bridgeman method. The crystals used for the measurements were about 3 cm in diameter and 4 cm long. The mosaic widths of these crystals were about 1/3°. The lattice constants were measured by X-ray diffraction. They are in agreement with those given in the literature [12].

3. EXPERIMENTAL RESULTS

The measurements of the frequency wavevector dispersion relations for the normal modes of vibrations propagating in the [110] direction were made at room temperature for Cu, $Cu_{0.95}$ -$Ni_{0.05}$ and $Cu_{0.9}$ -$Ni_{0.1}$. The dispersion curves obtained by the time-of-flight method for [110] L, T, and T_2 branches in Cu are shown in Fig. 1. The errors estimated with regard to the counting statistics and the shape of the neutron group are about 4% in frequency. The dispersion curves of the lattice vibrations in Cu have been studied by several authors. The present results are in satisfactory agreement with the results of Sinha [1], and Svensson, Brockhouse and Rowe [7] for the three branches in the [110] direction.

Figures 2 and 3 show the dispersion curves for the [110] L branches in $Cu_{0.9}$ -$Ni_{0.1}$ and for the [110] T_2 branch in $Cu_{0.95}$ -$Ni_{0.05}$ and $Cu_{0.9}$ - $Ni_{0.1}$ compared with the curves for Cu, shown as a broken line. The results for $Cu_{0.9}$ -$Ni_{0.1}$ have been obtained by using the time-of-flight and constant-Q methods, and those for $Cu_{0.95}$ -$Ni_{0.05}$ by the constant-Q method only. As compared with the results for Cu, there are significant differences in the shape of the dispersion curves for the alloys. The errors estimated for the results obtained by constant-Q operation of the triple-axis spectrometer are about 2% in the low frequency region. In the region where the anomalous features of the dispersion curves are observed, however, the errors estimated with regard to the counting statistics and the shapes of the neutron groups are larger than 5% in frequency. This is because, in the alloys, it has become rather difficult to observe the well-defined neutron peak in the good statistics in the anomalous region. This phenomenon should be attributed to the change of the focussing conditions in the

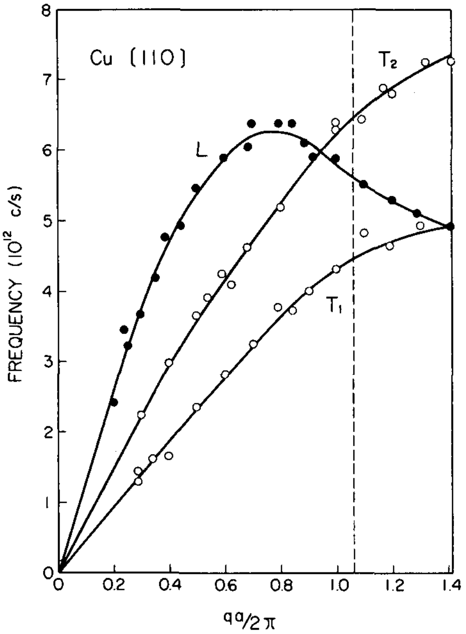

FIG. 1. The dispersion curves for Cu in the [110] L, T_1 and T_2 branches. The solid lines are the results of Fourier fitting for $\kappa = 7$.

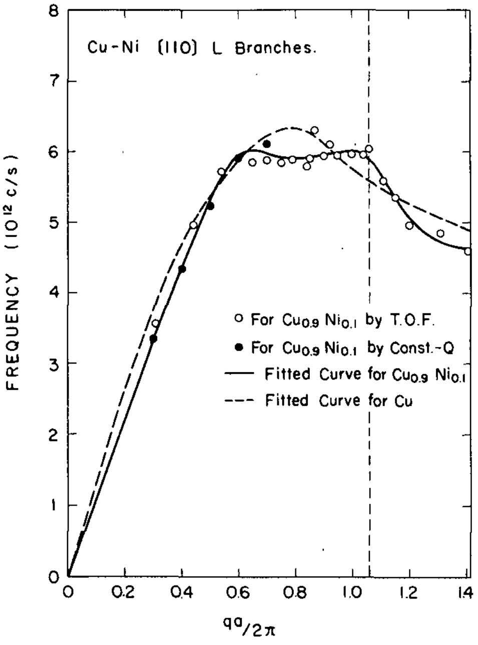

FIG. 2. The dispersion curve for $Cu_{0.9}$-$Ni_{0.1}$ in the [110] L branch, compared with the curve for Cu. The lines through the points are result of Fourier fitting for $\kappa = 7$.

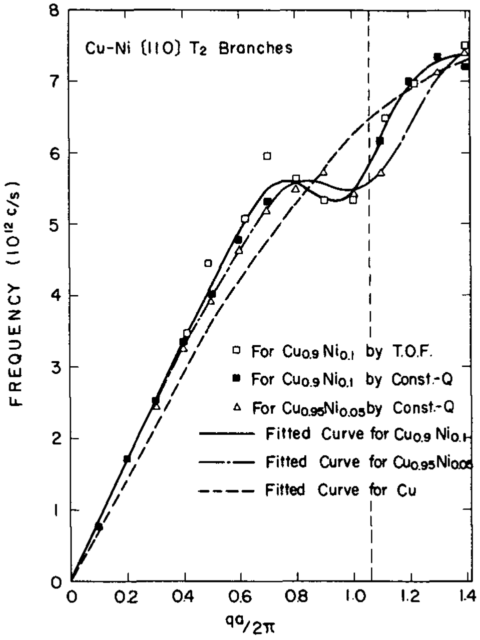

FIG.3. The dispersion curves for $Cu_{0.9}$-$Ni_{0.1}$ and $Cu_{0.95}$-$Ni_{0.05}$ in the [110] T branch, compared with the curve for Cu. The lines through the points are the results of Fourier fitting for $\kappa = 7$.

triple-axis spectrometer, due to the change of the slope on the dispersion curves in the alloys.

The dispersion curves for the alloys show large anomalies beyond the reduced wavevector q = 0.6. In the [110] T_2 branch the local minimum and maximum of the dispersion curves in the alloys moved to small q as the concentration of nickel atom increased. In the [110] L branch of the alloys $Cu_{0.9}$ -$Ni_{0.1}$ the flat part was observed in the range of the reduced wavevector q = 0.6 to 1.1. These features of the dispersion curves in the alloys are in contrast to the very smooth behaviour of the dispersion curves for Cu and Ni.

Following Foreman and Lomer [13], the range of the forces of interactions was determined by performing a least-squares fits of the experimental dispersion curves to Fourier series of the form

$$4\pi^2 M\nu^2 = \sum_n A_n[1-\cos(n\pi q/q_M)]$$

where A_n represents the interplanar force constants for the n^{th} neighbour plane and q_M is one half the distance from the origin to the nearest reciprocal lattice point in a certain direction. M is an average atomic mass and ν is the frequency corresponding to the wavevector q. For the alloys seven planes at least are needed to reproduce the qualitative features of the observed dispersion curves in every branch, as compared with three planes needed to obtain a reasonable fit for Cu. The results of the Fourier fits taking n = 7 for every branch on the dispersion curves in Cu and the alloys are shown in the figures as the line through the measured points.

TABLE I. COMPARISON OF INTERPLANAR FORCE CONSTANTS FOR THE [110] T_2 BRANCH IN CU, $Cu_{0.95}$ -$Ni_{0.05}$ AND $Cu_{0.9}$ -$Ni_{0.1}$ (Units 10^4 dyn/cm)

[110] T_2	A_1	A_2	A_3	A_4	A_5	A_6	A_7
Cu	10.62	-0.65	0.32	0.03	0.08	-0.31	0.11
$Cu_{0.95}$ -$Ni_{0.05}$	9.17	0.19	1.62	-1.65	0.88	-0.81	-0.22
$Cu_{0.9}$ -$Ni_{0.1}$	9.63	0.03	1.95	-1.46	0.01	0.69	-0.45

The interplanar force constants obtained from the fits, taking n = 7 for the [110] T_2 branch in Cu and the alloys, are given in Table I. It can be seen that the signs of the force constants are changed as the nickel concentrations increase. The magnitudes of the force constants for the alloys are smaller than those of Cu for the first and second neighbours. However, the force constants for the distant neighbours in the alloys are larger than those of Cu.

4. CONCLUSION

If there were differences in the force constants between pairs of atoms in the disordered alloys, even though the masses of Cu and Ni are similar, the neutron groups observed would show a broadening in the energy distributions of neutrons scattered by coherent and one-phonon processes from the single crystals of alloys. A similar situation could be considered if strong coupling between the phonons and the electrons in the Cu-Ni alloys exists. It was difficult to investigate the width of the neutron group in detail in the present experimental arrangements. However, the observed neutron groups for the Cu-Ni alloys do not show strong evidence of the increases in width. This is similar to the features observed for Mo-Nb [14] and Bi-Pb-Ti [15] alloy systems. From this fact the electronic structures and the general appearance of the phonon dispersion curves in the alloy Cu-Ni could be considered substantially analogous to the pure metal. In addition, it appears that the dispersion curves are systematically dependent on the electron concentration. Therefore, the anomalous features for the dispersion curves in the Cu-Ni alloys imply that the long-range forces through the electron-phonon interaction increase as the concentration of nickel increases.

If the rigid band model is reasonable for Cu-Ni alloys, the phonon dispersion curves might be similar in shape and slightly larger in frequency than those in Cu. Therefore the large anomalies observed in Cu-Ni should be attributed to the electron-phonon interactions taking into account the α-electron holes of nickel atom, and probably suggest the breakdown of the simple rigid band model. However, no attempt has been made to correlate the observed anomalies with the actual Fermi surface for the Cu-Ni alloys.

ACKNOWLEDGEMENTS

The authors would like to express their appreciation to Mr. M. Iizumi for providing the computer programs for the constant-Q operation and the least-squares fits, and to Mr. H. Motohashi and Mr. N. Minakawa for their technical assistance.

REFERENCES

[1] SINHA, S.K., Phys. Rev. 143 (1966) 422.
[2] SINHA, S.K., SQUIRES, G.L., Lattice Dynamics (WALLIS, R.F., Ed.) Pergamon Press, London (1965) 53.
[3] CRIBIER, D., JACROT, B., SAINT-JAMES, D., Inelastic Scattering of Neutrons in Solids and Liquids, IAEA, Vienna (1961) 549.
[4] MALISZEWSKI, E., SOSNOWSKI, T., BLINOWSKI, K., KOZUBOWSKI, T., PADLO, I., SLEDZIEWSKA, T., Inelastic Scattering of Neutrons in Solids and Liquids, (Proc. Conf. Chalk River, 1962) 2, IAEA, Vienna (1963) 87.
[5] VINTAINKIN, E.Z., GORBACHEV, V.V., GRUZIN, P.L., Soviet Phys.-Solid State, 7 (1965) 296.
[6] SCHNEIDER, T., STOLL, E., Solid State Commun. 4 (1966) 79.
[7] SVENSSON, E.C., BROCKHOUSE, B.N., ROWE, T.M., Phys. Rev. 155 (1967) 619.
[8] BUEHER, W., SCHNEIDER, T., GLAESER, W., Solid State Commun. 4 (1966) 443.
[9] HAUTECLER, S., YAN DINGENER, J.W., J. Phys. Radium 25 (1964) 653.
[10] BIRGENEAU, R.J., CORDES, J., DOLLING, G., WOODS, A.D.B., Phys. Rev. 136 (1964) A1359.
[11] OHNO, E., KAWABATA, T., Nuclear Instrum Meth. 39 (1966) 109.
[12] PEARSON, W.B., Handbook of Lattice Spacing and Structure of Metals, Pergamon Press (1958).
[13] FOREMAN, A.T.E., LOMER, W.M., Proc. Phys. Soc. B70 (1957) 1143.
[14] WOODS, A.D.B., POWELL, B.M., Phys. Rev. Lett. 15 (1965) 778.
[15] NG, S.C., BROCKHOUSE, B.N., Solid State Commun. 5 (1967) 79.

OBSERVATIONS OF THE KOHN EFFECT IN COPPER

G. NILSSON
AB ATOMENERGI,
STUDSVIK, SWEDEN

Abstract

OBSERVATIONS OF THE KOHN EFFECT IN COPPER. The dispersion relations for phonons in copper have been investigated by neutron spectrometry in regions where the Kohn anomalies are expected to be large, and where simultaneously the phonon frequencies can be determined with good instrumental resolution. Phonon frequencies are obtained with estimated errors of 0.2%, apart from a possible systematic error. Anomalies have been observed, and they may be interpreted in terms of several points in the central (2, 2, 0) section of the Fermi surface, in agreement with determinations by other methods. As is expected from earlier experiments and theoretical predictions, the Kohn effect in copper is weak and very careful measurements and analysis are necessary to make the anomalies observable with the techniques now available.

INTRODUCTION

In 1959 Kohn [1] predicted that an image of the Fermi surface should be present in the phonon spectra of metals. This image results from the screening of the lattice vibrations of the ions in metals by the conduction electrons, which reduce the interionic forces and lower the phonon frequencies. This screening decreases abruptly at certain phonon wavevectors that can be said to lie on a Kohn anomaly surface, and this is in principle related in a very simple way to the shape of the Fermi surface. If the phonon dispersion surfaces in a metal can be determined with sufficient accuracy for the Kohn anomalies to be observed, one has a very direct method for determination of the Fermi surface. In lead [2] this method has already been used for an extensive study, and in many other metals (with three or more conduction electrons), among them niobium, molybdenum [3] and aluminium [4], Kohn anomalies have been studied. In other metals, e.g. sodium [3] and copper [5], and other metals with only one valence electron, it has not been possible to see the effect in measurements with an accuracy of about 1%.

The shapes, magnitudes, and positions of the Kohn anomalies play a prominent role in a comparison between theory and experiment and an experimental determination of the Kohn effect is of interest even for this reason.

For copper the Fermi surface [6] is rather well understood from other experiments and calculations, very good single crystals are commercially obtainable and the neutron coherent scattering properties are favourable. Thus, from the experimental point of view, this metal seems suitable for precise measurements of phonon dispersion relations.

We have made a series of measurements at 80° K in order to investigate the strength of the Kohn effect in copper. A triple-axis crystal spectrometer [7] at the R2 reactor at Studsvik has been used. The same instrument and similar technique have earlier proved successful in the same kind of measurements in aluminium [8].

THEORY FOR KOHN ANOMALIES

In his first paper, where he pointed out the effect, Kohn treated only a completely convex Fermi surface [1] containing non-interacting electrons. It was considered possible for the phonons to cause virtual excitations of the electrons with conservation of momentum for phonon wavevectors $q < 2K_F$ but not for $q > 2K_F$, where K_F is a radius of the Fermi surface. The Kohn anomaly surfaces in phonon q-vector space are in a general case given by

$$\vec{q} + \vec{G} = \vec{K}_2 - \vec{K}_1 \tag{1}$$

where $\vec{K}_1$ and $\vec{K}_2$ are two diametrical points on the Fermi surface, $\vec{q}$ is the phonon wavevector and $\vec{G}$ is any reciprocal lattice vector. It was thought that there should be an anomalous change in $\omega(q)$ at these q values (ω = phonon frequency) and the magnitude of the anomalies was expected to be of the order of per cent.

The Kohn anomaly surfaces are easily constructed by drawing the surface with radius $2K_F$ around every reciprocal lattice point. The sign of the anomalies is given by considering where electron scattering is possible or not. On the side where it is possible there is a negative contribution to the frequency [9].

A semi-quantitative estimate of the magnitude of the anomalies was later (1961) made by Woll and Kohn [10] when the effect had been observed by Brockhouse et al. [11]. According to Woll and Kohn's treatment for Bloch electrons the magnitude of the effect ought to be very small, and they could not explain why the effect could be seen at all within the experimental accuracy. Harrison [12] has suggested that the anomalies come from the energy-wave number relation for electrons, but this seems now to be a less probable explanation.

Taylor [13] has treated various factors affecting the magnitude of the anomalies. He considers not only Fermi surfaces that are completely convex, but also multiply connected surfaces, which are in better accordance with real conditions. This gives rise to new Kohn anomaly surfaces for which formula (1) is still valid, but $\vec{K}_2 - \vec{K}_1$ need no longer be a diameter of the Fermi surface, but is just a chord between two points on the surface with parallel tangent planes, and the interpretation of the Kohn anomaly surfaces in terms of Fermi surfaces becomes in this general case much more complicated. According to Taylor the anomalies come mainly from an 'energy denominator' where the phonon frequency plays an important role. This seems to be at variance with other treatments [12]. In a comparison of the magnitude of the Kohn effect in different metals, Taylor finds that the dominating factor is the valence, which enters in the third power in his formulas, and accordingly he concludes that the Kohn effect should not be observable in copper or sodium, with only one valence electron per atom. Somewhat different results, especially for non-diametral transitions, have been obtained by Roth et al. [14], who consider some of the anomalies which Taylor says are strong to be non-existent on account of cancellation when inversion symmetry is taken into account.

Vosko et al. [15] have made an extensive calculation of phonon dispersion curves in sodium, aluminium and lead. According to their calculations, the relative smallness of the Kohn anomalies in sodium are due mainly to the structure (bcc in sodium and fcc in lead, aluminium and copper) and in a less degree to the valence. This supports the idea that it should be possible to see the Kohn effect in copper at 80°K with a somewhat better resolution than that used by Svensson et al. [5], but it should be considerably more difficult in sodium.

Stedman et al. [2] have given an account of the interpretation of experimental Kohn anomalies in terms of points on the Fermi surface, and the method has been applied to lead.

PREVIOUS MEASUREMENTS

There have been several determinations of phonon dispersion curves in copper, of which the most recent was at room temperature by Svensson et al. [5]. They reported that no Kohn anomalies could be seen, "though they probably exist and might be seen at lower temperature and/or under very high resolution". From one point of view the Kohn anomalies result from long-range atomic forces, and an analysis of their results also showed that there are forces out to at least sixth-nearest neighbours.

EXPERIMENTAL DETAILS

The measurements were made on a triple-axis spectrometer [7] at the R2 reactor at Studsvik. The sample was a plate 1 cm × 5 cm × 6 cm kept at 80°K in a cryostat cooled with liquid nitrogen. The monochromator and analyser were copper crystals with the [220] reflection. The constant-Q method [16] was used all the time. The setting of the angles of the instrument are given by a computer which calculates the positions for the arms and tables of the spectrometer for specified energy and momentum transfers when the ingoing wavevector $\vec{k}_1$ or outgoing wavevector $\vec{k}_2$ is given. All movements are punched on a tape which is used to control the spectrometer. For every phonon peak the same program produces a table of estimated instrumental energy and momentum resolution for a given value of the slope m of the phonon dispersion curve. A list is also produced which shows individual contributions to the resolutions from the collimators before and after the sample as well as the individual contributions from the analyser and monochromator mosaic widths. Some of these contributions are dependent on the four possible beam paths, and for them all the possible values are given, as a check that the best possible conditions have been chosen. Furthermore, there is a list of the variation of the energy resolution with m for ten values around the one given. And finally there is a table showing the variation of the resolution with k_2 (in order to show if 'focusing', i.e. the best possible resolution with a certain intensity [17, 18], is obtained or not). Either k_1 or k_2 can be chosen as desired within reasonable limits.

Every phonon peak is measured with k_2 fixed to avoid variation of the analyser efficiency, but for every new phonon in most series where a Kohn anomaly has been sought for, k_1 has swept over the same values to avoid influence from possible spectral variation in an extended k_1 range or a possible change in the background. (Change in k_1 means that the sample is moved around and some of the shielding must then also be moved, which can cause variation in the background.)

Figure 1 shows a possible shape of the intersection of the [110] plane with the Fermi surface (the outline is reproduced from Segall [6]). In the [200] direction, phonons of wavevectors corresponding to, e.g.,

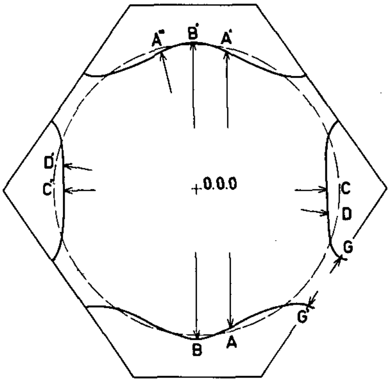

FIG.1. An outline of an equi-energy surface for conduction electrons in copper for an energy near the Fermi energy (reproduced from Segall [6]). Arrows indicate the electron transitions considered in the search for Kohn anomalies.

AA' can scatter electrons across the Fermi surface and so also can phonons with wavevectors somewhat longer. But when the phonon wavevector has increased to a length corresponding to BB', it is not possible for longer wavevectors to scatter electrons with energy and momentum conservation. There ought thus to be a sudden increase in phonon frequency $\omega(Q)$ in the [200] direction for longitudinal phonons, when the unreduced phonon wavevector Q exceeds a length corresponding to BB'. This corresponds to a decrease in $\omega(q)$ for increasing q at the reduced phonon wavevector q equal to 0.45 in the 200 L branch. As may be seen from Fig. 2, the 200 branch is very smooth even in this range, but it is obviously difficult in such a diagram to see irregularities where in many cases deviations exceeding 0.2% are significant. The plot of $\Delta\omega/\Delta q$ in Fig. 3 indicates that a sudden decrease in the slope sets in at $q = 0.45 \pm 0.05$. For comparison a similar measurement was made for [ζ 0.14 0.14] L to see if the anomaly corresponding to an unreduced phonon wavevector of length AA'' in Fig. 1 could be seen. The corresponding results are also shown in Figs 2 and 3. An anomaly which can be attributed to AA'' is seen in Fig. 3 at $q = 0.475 \pm 0.05$.

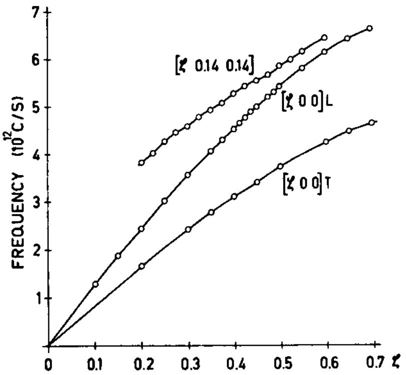

FIG.2. Phonon dispersion curves for [ζ 0.14 0.14] L, [ζ 0 0] L and [ζ 0 0] T directions.

In the region 0.20 <q> 0.43 there are two anomalies, which can be identified as points on the necks and bodies of Kohn anomaly surfaces that have their centres outside the 220 plane; they are not considered further here. The limits of error in our measurements are somewhat more uncertain in this region. A plot of dω/dq (not shown) for measurements in the [ζ 0.47 ζ 0.47 ζ] direction for longitudinal vibrations (where we have looked for an anomaly corresponding to transition across the neck (GG' in Fig. 1)) shows an anomaly at ζ = 0.24 ± 0.03. In deriving Δω/Δq it is necessary to have the same Δq all the time to avoid false discontinuities. The limits of error become large when dq is small and when the measured points are close together, it may be preferable to take Δq as the distance between, for instance, every second or every third point.

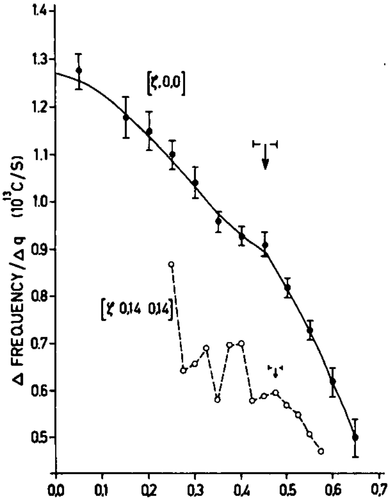

FIG.3. The slope of the dispersion curves in Fig.2.

For measurements corresponding to electron transitions across the diameters at CC' and DD' in Fig. 1 it was possible to plot the measured results directly as is seen in Fig. 4 (the curves correspond to transverse vibrations in the [220] plane, q_x is in the [200] direction and q_y is in the [220] direction).

The strongest anomaly is anticipated at $q_x = 1$, but a better experimental resolution is obtained for $q_x = 0.8$. An anomaly can be traced near $q_y = 0.1$ for $q_x = 1$, 0.8 and 0.6 but not for $q_x = 0.5$. The variation is striking when the individual phonon peaks for a definite q_x are plotted together in the same diagram (not shown). This is in this case easily

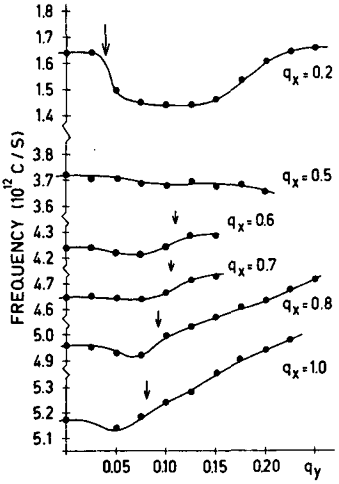

FIG. 4. Phonon dispersion curves for the T_1 branch. q_x is in the [200] direction, q_y is in the [220] direction ($q_{x\,max} = 1$; $q_{y\,max} = 1.414$. Polarization is in the [220] plane).

done because of the small variation in energy. Where the slope of the dispersion curves is large, this method is not applicable. We have in these cases tried to fit parts of the curves with polynomials and considered the deviation from this fitted curve. This gives a test for which points deviate most from the smooth curve (they can then even be redetermined).

At $q_x = 0.2$ there is a rapid decrease in energy at $q_y = 0.05$. This was not foreseen and the effect can probably not be explained from the anticipation that there is in the Fermi surface a chord of the corresponding length between two points with parallel tangent planes. But it still seems that the origin for this rapid variation is to be found in a rapid change in the electron-phonon interaction, although further measurements are considered necessary before an interpretation is possible. It should be observed that the decrease in frequency is very pronounced when one moves from the [200] direction. (The effect is also observed for $q_x = 0.3$, 0.35, and 0.4, but is most pronounced for small q_x.) This should cause an error in the frequency distribution, if this is derived from measurements in the symmetry directions only.

In Fig. 5 the anomalies are interpreted in terms of points on the Fermi surface. The equi-energy surface as given by Segall is slightly modified to fit the experimental points. There is good agreement with values given by Segall's theoretical calculations, which in turn are reported by him to be in agreement with de Haas-van Alphen experiments.

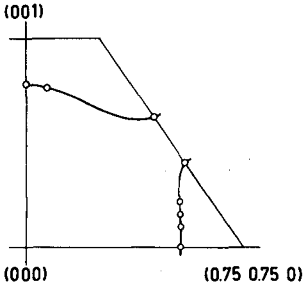

FIG. 5. Kohn anomalies in this experiment interpreted as points on the Fermi surface.

LINE WIDTH

One of the effects predicted by Kohn and Woll is a change in the phonon line width due to a change in phonon life-times at the anomaly surfaces. No such effect was observed in these measurements. The peaks observed were in many cases not broader than the computed instrumental resolution, which was 1.5% at best.

SUMMARY

Kohn anomalies can be observed in copper at 80°K, when the phonons are determined with a relative accuracy of about 0.2%. Therefore the theory by Taylor overestimates the importance of the number of conduction electrons [13]. There is for small q values a pronounced anisosymmetry in the isofrequency surfaces for the T_1 branch (polarization in the [220] plane).

ACKNOWLEDGEMENTS

The author wishes to thank Dr. R. Stedman for many valuable suggestions, Mr. K.O. Isaxon for his technical assistance, and Mr. R. Lindh, who wrote the computer program.

REFERENCES

[1] KOHN, W., Phys. Rev. Lett. 2 (1959) 393.

[2] STEDMAN, R., ALMQVIST, L., NILSSON, G., RAUNIO, G., Phys. Rev. 163 (1967) 567.

[3] DOLLING, G., WOODS, A.D.B., in Thermal Neutron Scattering (EGELSTAFF, P.A., Ed.), Academic Press, London (1965) 209, 212.

[4] STEDMAN, R., NILSSON, G., Phys. Rev. Lett. 15 (1965) 634.

[5] SVENSSON, E.C., BROCKHOUSE, B.N., ROWE, J.M., Phys. Rev. 155 (1967) 619.

[6] SEGALL, B., Phys. Rev. 125 (1962) 109.

[7] STEDMAN, R., NILSSON, G., Rev. scient. Instrum., to be published.

[8] STEDMAN, R., NILSSON, G., Phys. Rev. Lett. 15 (1965) 634.

[9] HARRISON, W.A., in Phonons in Perfect Lattices and in Lattices with Point Imperfections (STEVENSON, R.W.H., Ed.), Oliver & Boyd, Edinburgh and London (1966) 102.

[10] WOLL, E.J., Jr., KOHN, W., Phys. Rev. 126 (1962) 1693.

[11] BROCKHOUSE, B.N., ARASE, T., CAGLIOTI, G., RAO, K.R., WOODS, A.D.B., Phys. Rev. 128 (1962) 1099.

[12] HARRISON, W.A., Phys. Rev. 129 (1963) 2512.

[13] TAYLOR, P.L., Phys. Rev. 131 (1963) 1995.

[14] ROTH, L.M., ZEIGER, H.J., KAPLAN, T.A., Phys. Rev. 149 (1966) 519.

[15] VOSKO, S.H., TAYLOR, R., KEECH, G.H., Can. J. Phys. 43 (1965) 1187.

[16] BROCKHOUSE, B.N., in Phonons in Perfect Lattices and in Lattices with Point Imperfections (STEVENSON, R.W.H., Ed.), Oliver & Boyd, Edinburgh and London (1966) 122.

[17] STEDMAN, R., Rev. scient. Instrum., to be published.

[18] STEDMAN, R., NILSSON, G., Inelastic Scattering of Neutrons in Solids and Liquids (Proc. Conf. Bombay, 1964) 1, IAEA, Vienna (1965) 213.

KOHN ANOMALIES IN ZINC

P.K. IYENGAR, G. VENKATARAMAN, Y.H. GAMEEL*
AND K.R.RAO
NUCLEAR PHYSICS DIVISION,
BHABHA ATOMIC RESEARCH CENTRE,
BOMBAY, INDIA

Abstract

KOHN ANOMALIES IN ZINC. The dispersion relations in zinc have been measured along two symmetry directions. The phonon frequencies are in qualitative agreement with those of Borgonovi et al. Screening effects of the conduction electrons on the frequencies of normal vibrations of zinc are known to be large and hence electron phonon interaction is strong in this metal. The frequencies of lattice modes are fairly low, hence one could expect to see the images of the Fermi surface in the dispersion relations even at room temperature. The results are in agreement with these predictions. An interpretation of the observed Kohn anomalies is made on the basis of the geometry of the Fermi surface in zinc.

1. INTRODUCTION

Zinc is a divalent element belonging to group II of the periodic table. It has a hexagonal close-packed structure with a c/a ratio of 1.855 far removed from the ideal close-packing ratio of 1.633. In this paper we present an account of our experimental investigations of the lattice dynamics of zinc by neutron inelastic scattering. From the theory of lattice dynamics of this metal, it is known [1] that many of the branches of the dispersion curves are greatly influenced by the conduction electrons. Secondly, from the experimental work of other groups [2, 3], the phonon frequencies are known to be relatively low compared to those in other metals like magnesium [4] or beryllium [5] possessing similar structure. Based on these two considerations, zinc would appear to be one of the most favourable substances to study the effect of conduction electron scattering on the dispersion curves. Our aim is to present evidence for observation of such effects in the form of anomalies in the dispersion curves, the 'Kohn anomalies'[6], in zinc. The measurements were all carried out at room temperature and details are given in section 2. A discussion of the Kohn anomalies in terms of the Fermi surface of the metal is presented in section 3.

2. EXPERIMENT

2.1. Measurements

The experiments were conducted at room temperature using the multi-arm crystal spectrometer [7] at the CIRUS reactor at Trombay.

---

* Visiting scientist from Atomic Energy Estabishment, Cairo, UAR.

The single crystal of zinc which had an irregular shape was aligned with the [2$\bar{1}\bar{1}$0] axis vertical. Neutrons of 1.67 Å wavelength were incident on the crystal and the scattered neutrons were analysed using the constant-momentum transfer technique [8]. At each setting of this mode of measurement, counts were accumulated for a fixed number of counts on a thin BF_3 counter placed in the monochromatic beam. The monitor setting was such as to accumulate not less than about 1000 neutron counts at the peak of the scattered neutron group over and above the background. Typical peaks are shown in Fig. 1.

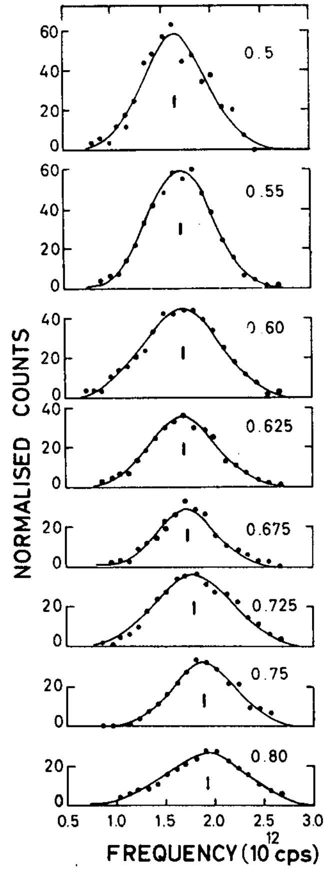

FIG.1. A few typical neutron groups measured in the TA branch along the [0ξ$\bar{ξ}$0] direction in the range of ξ from 0.5 to 0.8. The intensities measured are corrected for the background and normalized to the same preset monitor counts. The line through the points is the Gaussian fit to the measured intensity to derive the phonon frequency.

Measurements were carried out to study the longitudinal acoustic branch along the [0001] direction (the LA branch) and the transverse acoustic branch polarized perpendicular to the hexagonal plane of the reciprocal lattice along the [01$\bar{1}$0] direction (the TA branch). Experiments were conducted mostly around the (0004) and (0002) reciprocal lattice points. These two reciprocal lattice points are equivalent in the repetitive enlarged reciprocal space as far as the structure factor for neutron scattering is concerned. In Fig. 2 we have plotted the results of all measurements.

2.2. Analysis

The scattered neutron spectrum consisted generally of a well-defined peak riding over a sloping background. The background under the peak was obtained by interpolating between the wings and was used to isolate the peak. The wings of the spectra corresponding to different q values of phonons measured around the same lattice point, when plotted as a function of the analyser angle, gave a smooth curve which was used as a guide in deriving the interpolated background.

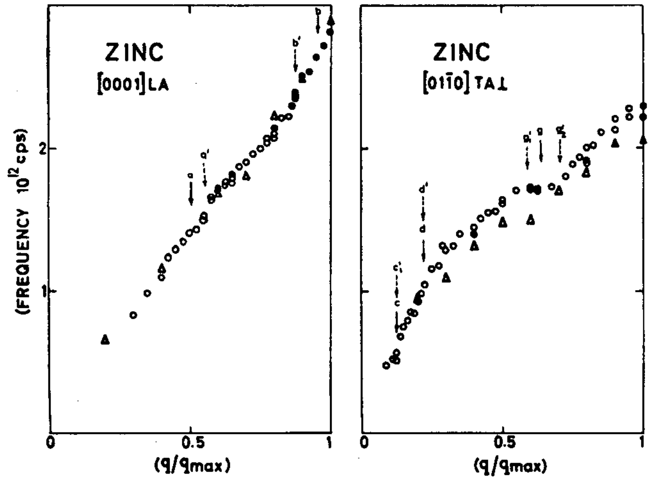

FIG. 2. The dispersion relations of phonons for the LA branch along the [000ξ] direction and for the TA branch along the [0ξξ̄0] direction. The open circles refer to phonons studied around the (0004) reciprocal lattice point and filled circles to those around the (0002) reciprocal lattice point. The triangles are results of measurements by Borgonovi et al. The full arrows refer to positions of anomalies expected on the basis of Kohn construction (see Fig. 3) and dashed arrows correspond to the positions assigned on the basis of these measurements.

The peak thus isolated from the background was fitted to a Gaussian in energy using a computer program and the frequency corresponding to the peak deduced by a least-squares technique. The error in the frequency corresponding to the peak, due to the counting statistics, was typically of the order of 10% of the full width at half maximum of the neutron group. This resulted in estimated errors in the phonon frequencies in the range of 1–2%. In Fig. 2 these errors are of the size of the circles. In the same figure we have also shown the results of the earlier measurements of Borgonovi et al. [2] by triangles. These measurements were performed at large intervals of ξ ($\xi = q/q_{max}$, where q is the wavevector of the phonon, q_{max} being that of the phonon at the Brillouin zone boundary) and estimated errors in the frequency were of the order of 10%. It can be easily seen that whereas there is good agreement between our measurements and those of Borgonovi et al. [2] for the LA branch, there is a systematic difference of about 10% for the TA branch, although the general trend of the dispersion relation is the same. The reason for this discrepancy could not be ascertained. A few measurements for selected phonons carried out at the other lattice points, however, have confirmed our results. It should be noted that no evidence is found in our measurements for the large oscillations reported by Maliszewski et al. [3] in the TA-branch.

3. KOHN ANOMALIES

3.1. Kohn construction

The positions of Kohn anomalies in the dispersion curves of a metal can be estimated by a 'Kohn construction' based on the relation

$$2\,\vec{k}_F = 2\pi\,\vec{G} + \vec{q} \tag{1}$$

where $2\pi\,\vec{G}$ is a reciprocal lattice vector and $\vec{k}_F$ the Fermi wavevector. This relation is a result of singularities which occur in the matrix element for the electron-phonon interaction in metals. Anomalies corresponding to these singularities occur in the dispersion relations of phonons in the metal. Hence, to look for these anomalies one draws spheres of radius $2k_F$ from each reciprocal lattice point. The surfaces of these spheres represent the required loci of the position of Kohn anomalies and one can derive the q values by reference to the nearest reciprocal lattice subjected to the condition given by Eq. (1).

Figure 3 corresponds to the section of such spheres drawn from the reciprocal lattice points in and out of the Γ ALM plane of the reciprocal lattice of zinc. The construction has been restricted so as to show mainly the anomalies that may be expected in one quarter of the central Brillouin zone. We have used in this construction a value of 1.573 $Å^{-1}$ for k_F, the radius of the Fermi surface in the free electron approximation. The lattice parameters are a = 2.6649 Å and c = 4.9468 Å [9]. The pattern of Kohn lines is symmetric about the ΓA and ΓM lines and the same geometry repeats in any Brillouin zone constructed around any other reciprocal lattice point. The solid lines in Fig. 3 represent the intersection of the spheres of radius $2k_F$ drawn from the different reciprocal lattice points in the Γ ALM plane, while the dashed lines arise from the intersection of spheres drawn from the out-of-plane reciprocal lattice points with the Γ ALM plane. The anomalies are likely to be pronounced at those points where two or more spheres intersect. The expected positions will be different when the effects of the periodic potential on electrons in the metal are considered.

3.2. Discussion

We have examined our experimental results in the light of the Kohn construction described earlier. In the Γ A direction referring to Fig. 2, two anomalies marked a and b are expected to be observed at ξ equal to 0.5 and 0.95 respectively. In the experimental measurements (see Fig. 2) two anomalies are observed at ξ equal to 0.55 and 0.87. Both the anomalies are upward [10], indicating increasing frequency as q increases, corresponding to crossing the Fermi surface from inside to outside. This is also seen to be so from the construction in Fig. 2.

Considering the Γ M direction, five anomalies marked c, d, e, f and g are expected at values of ξ equal to 0.12, 0.217, 0.314, 0.53 and 0.63, respectively. Of these, anomalies e and f are not expected to be observed in the TA branch since the polarization vector of the phonon in the branch is normal to $2\pi\vec{G}$, the associated reciprocal lattice vector [11]. Referring now to Fig. 2, we observe that there is a change in slope at wavevectors corresponding to c and d, though the evidence is not very clear. A prominent anomaly is, however, seen around ξ in the range of 0.6 to 0.7 which should be compared with the value of $\xi = 0.63$ expected on the basis of the free electron sphere. The anomaly is not sharp and is rather spread out. This is discussed in detail later.

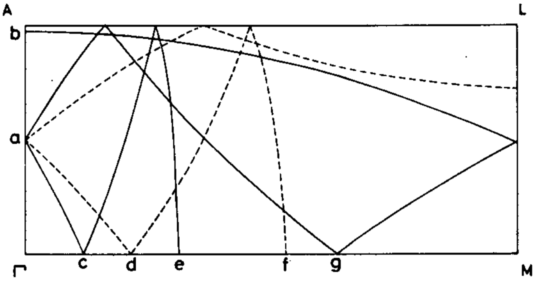

FIG.3. Kohn construction in the ΓALM plane of the reciprocal lattice. The continuous arcs are drawn from reciprocal lattice points lying in the plane and dashed arcs from those lying off the plane. The radius of arcs is $2k_F$. Points a, b, c, d, e, f and g are the positions where anomalies are expected.

We shall now discuss the results of these measurements in relation to the free electron Fermi surface and possible qualitative modifications of this surface due to zone edges. Figure 4 shows the cross-section of the Fermi surface in the Γ ALM plane, drawn around the origin of the reciprocal space. We have denoted by open circles marked a', b', c', e' and g' the points on the Fermi surface corresponding to the position of anomalies a, b, c, e and g (see Fig. 3) expected by the Kohn construction. The points corresponding to d and f cannot be shown in this section as they correspond to points lying on a great circle of the Fermi surface in a plane inclined to the Γ ALM plane. We have shown in Fig. 4 by filled circles the anomalies as observed from the measured dispersion relations, the points corresponding to the dashed arrows in Fig. 2.

If the anomalies observed represent the true Fermi surface, the following distortions to the Fermi surface from the spherical shape are indicated. At b' the surface is pulled slightly inwards, whereas at a' the distortion is outwards. The open and closed circles coincide at c', indicating no distortion but the evidence for c' is not strong. At g' we have shown two filled circles corresponding to two dashed arrows in Fig. 2. We believe that anomaly g is broadened as a result of the splitting of the anomaly into two anomalies corresponding to the ones shown by the dashed arrows, as this region is influenced strongly by Bragg reflections. Hence these two closed circles at g' give an estimate of maximum distortion of the Fermi surface in this region due to Bragg reflection. There is no filled circle corresponding to the open circle at e' as this anomaly is not observable in the TA branch, as already mentioned. The possible distortions of the Fermi surface at other regions are also shown by dotted lines in Fig. 4. Measurements of dispersion curves along the off-symmetry directions should be carried out to locate these distortions. This has not been done in this series of measurements.

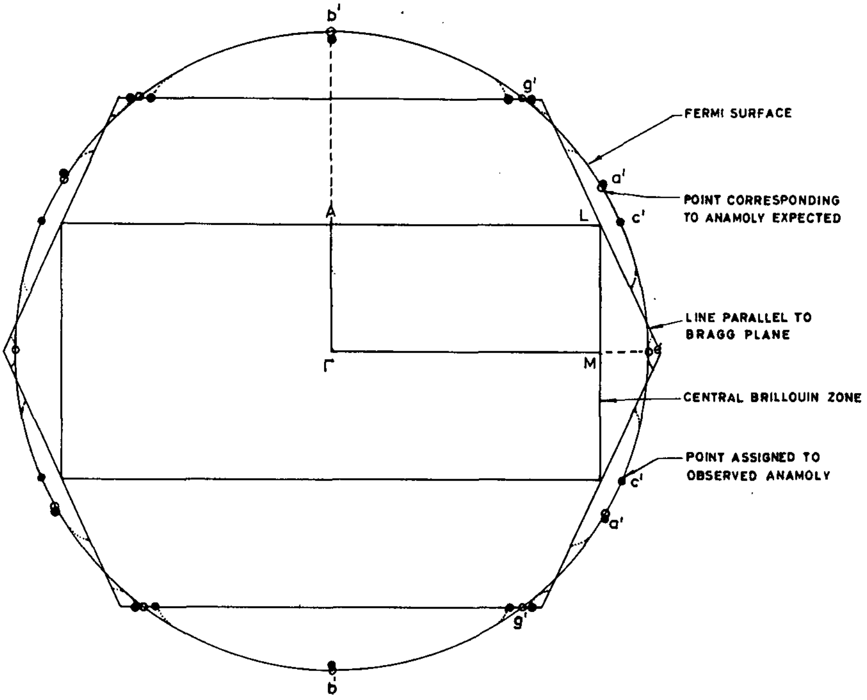

FIG. 4. The cross-section of the Fermi surface in the ΓALM plane of the reciprocal space. The possible qualitative distortions of the Fermi surface at the zone boundaries is indicated by dotted lines. The open circles and filled circles correspond to the positions expected on the basis of the Kohn construction (full arrows in Fig. 2), and assigned on the basis of our measurements (dashed arrows in Fig. 2) respectively.

Recently Stark and Falicov [12] have reported band structure calculations for metallic zinc using a non-local pseudo-potential approach which included spin-orbit effects. The results of these calculations agree within a few per cent with results of de Haas-Van Alphen frequency measurements. We cannot compare the results of this calculation with our measurements straightaway. The de Haas-Van Alphen frequencies reported by these authors are related to the extreme areas of the cross-section of the interesting regions of the Fermi surface of zinc. But the anisotropic dimensions of the Fermi surface in different directions obtained by calculations are not yet available to make a comparison with results of our 'caliper' measurements.

4. CONCLUSION

Our measurements have shown that Kohn anomalies may be observed rather easily in zinc even at room temperature, as anticipated. Secondly, the results obtained in this study indicate small distortions of the Fermi surface along certain directions. It appears worth while undertaking similar and more detailed measurements at low temperature to obtain finer details of the Fermi surface.

ACKNOWLEDGEMENTS

The authors wish to thank Mr. V. C. Sahni for many helpful discussions.

REFERENCES

[1] HARRISON, W., Pseudopotentials in the Theory of Metals, Benjamin, New York (1966).
[2] BORGONOVI, G., CAGLIOTTI, C., ANTAL, J.J., Phys. Rev. 132 (1963) 683.
[3] MALISZEWSKI, E., ROSOLOWSKI, J., SLEDZIEWSKA, D., CZACHOR, A., Lattice Dynamics, Pergamon Press, New York (1965) 33.
[4] IYENGAR, P.K., VENKATARAMAN, G., VIJAYARAGHAVAN, P.R., ROY, A.P., Inelastic Scattering of Neutrons (Proc. Symp. Bombay, 1964) 1, IAEA, Vienna (1965) 153.
[5] SCHMUNK, R.E., BRUGGER, R.M., RANDOLPH, P.D., STRONG, K.A., Phys. Rev. 128 (1962) 562.
[6] KOHN, W., Phys. Rev. Lett. 2 (1958) 393.
[7] IYENGAR, P.K., Symp. Inelastic Scattering of Neutrons by Condensed Systems, Brookhaven National Laboratory, New York (1966).
[8] BROCKHOUSE, B.N., Inelastic Scattering of Neutrons in Solids and Liquids (Proc. Symp. Vienna, 1960), IAEA, Vienna (1961) 113.
[9] International Tables of X-ray Crystallography (LONDSDALE, K., Ed.) 3, The Kynoch Press, Birmingham, England (1962) 228.
[10] WOLL, E.J., KOHN, W., Phys. Rev. 126 (1962) 1963.
[11] STEDMAN, R., NILSSON, G., Phys. Rev. Lett. 16 (1965) 634.
[12] STARK, R.W., FALICOV, L.M., Phys. Rev. Lett. 19 (1967) 795.

LATTICE DYNAMICS OF PLATINUM

R. OHRLICH AND W. DREXEL
INSTITUT FÜR ANGEWANDTE KERNPHYSIK,
KERNFORSCHUNGSZENTRUM KARLSRUHE,
FEDERAL REPUBLIC OF GERMANY

Abstract

LATTICE DYNAMICS OF PLATINUM. The energy/wavevector relations of phonons in the 100 and 110 planes of the reciprocal lattice of platinum have been determined by inelastic neutron scattering at room temperature. The measurements have been performed by the time-of-flight technique using the rotating crystal spectrometer and the pseudo-statistical chopper at the FR2 in Karlsruhe. The measured dispersion relations have been fitted with a Born-von Kármán model using up to fifth-nearest neighbours. From these data the frequency distribution has been generated with the sampling technique and used for the calculation of various thermodynamic quantities.

1. EXPERIMENTAL TECHNIQUE

The experimentally determined phonon dispersion data of platinum at room temperature described in this paper are results of coherent inelastic neutron scattering from a platinum single crystal. The crystal was in the form of a 1.4 cm × 5 cm cylinder. The measurements have been performed with the rotating crystal time-of-flight spectrometer and the pseudo-statistical chopper at the reactor FR2 [1, 2].

Parts of the scattering surfaces have been measured for different angles between incident and scattered neutrons in the (100) and (110) planes of the lattice. Scattered neutrons are counted in 6 time-of-flight detectors positioned one degree apart from one another at a distance of 2 m from the sample. The principle of the technique which resembles the method of successive approximation but allows the successive steps to be done in one run is demonstrated schematically in Fig. 1.

In this way about 400 phonons have been collected in the (100) and (110) planes essentially around the directions of high symmetry: [100], [110] and [111]. By interpolating or extrapolating the data, phonons in these directions could be determined.

All measurements have been performed with an incident energy of 42 ± 0.8 meV. Because a crystal was used as a pulsing monochromator, focusing techniques known from triple-axis spectrometry could be applied.

The principal difficulty in the experiment is caused by the high absorption cross-section of Pt of 9 barns for thermal neutrons compared to a coherent scattering cross-section of 11.2 ± 0.7 b. This especially aggravates the identification of phonons at high q values.

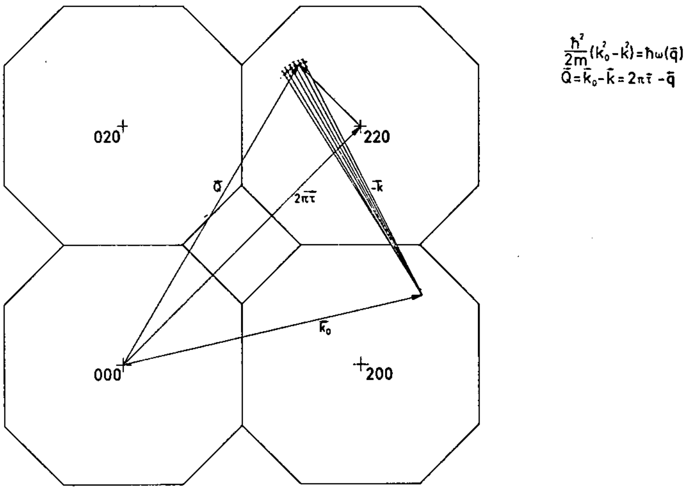

FIG. 1. (100)-plane of the reciprocal lattice of Pt. Experimental determination of a transverse phonon in [110] direction.

2. RESULTS

2.1. Experimental phonon data

Figure 2 shows the experimentally determined normal mode frequencies in face-centred platinum at room-temperature propagating along the high symmetry lines [100], [110] and [111]. In addition the frequency values including experimental errors are given in Table I.

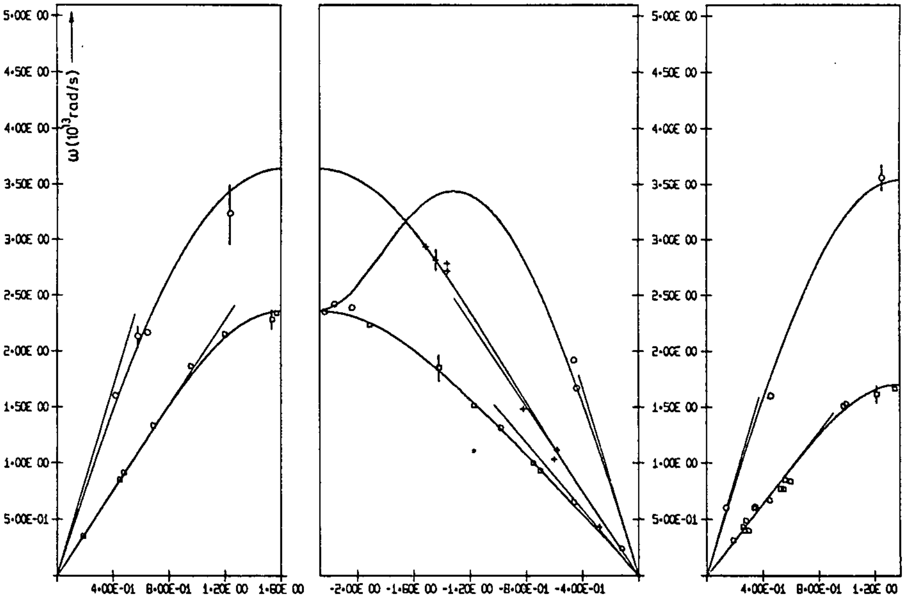

FIG. 2. Phonon dispersion relations in platinum.

TABLE I. ANGULAR FREQUENCIES (units 10^{13} rad/s) OF THE LATTICE VIBRATIONS IN PLATINUM AT 300°K PROPAGATING IN [100], [111] AND [110] DIRECTIONS

q[A^{-1}]	[100]		[111]	
	ω_T	ω_L	ω_T	ω_L
0.14				0.6 ± 0.08
0.19	0.35 ± 0.06		0.31 ± 0.09	
0.26			0.43 ± 0.08	
0.27			0.40 ± 0.08	
0.28			0.49 ± 0.08	
0.30			0.40 ± 0.09	
0.34			0.60 ± 0.07	
0.35			0.61 ± 0.07	
0.42		1.6 ± 0.05		
0.45	0.85 ± 0.01		0.67 ± 0.09	
0.46				1.6 ± 0.05
0.48	0.91 ± 0.05			
0.53			0.77 ± 0.05	
0.55			0.77 ± 0.07	
0.56			0.85 ± 0.06	
0.58		2.13 ± 0.05		
0.60			0.84 ± 0.05	
0.65		2.16 ± 0.08		
0.69	1.33 ± 0.06			
0.96	1.86 ± 0.05			
0.98			1.51 ± 0.02	
1.00			1.53 ± 0.04	
1.20	2.15 ± 0.03			
1.22			1.62 ± 0.04	
1.24		3.23 ± 0.16		
1.26				3.57 ± 0.07
1.35			1.67 ± 0.04	
1.54	2.28 ± 0.03			
1.57	2.34 ± 0.07			

TABLE I. (cont.)

$q[A^{-1}]$	[110]		
	ω_{T_1}	ω_{T_2}	ω_L
0.12	0.24 ± 0.08		
0.28		0.43 ± 0.1	
0.44			1.67 ± 0.07
0.46	0.65 ± 0.04		1.92 ± 0.07
0.58		1.11 ± 0.15	
0.60		1.03 ± 0.08	
0.70	0.93 ± 0.05		
0.75	1.00 ± 0.04		
0.82		1.48 ± 0.08	
0.98	1.31 ± 0.05		
1.17	1.51 ± 0.06		
1.36		2.71 ± 0.04	
1.42	1.85 ± 0.06		
1.44		2.81 ± 0.05	
1.51		2.93 ± 0.02	
1.91	2.23 ± 0.2		
2.06			2.46 ± 0.07
2.16			2.42 ± 0.05
2.23			2.35 ± 0.05

The transverse branches in the symmetry directions have been covered with experimental points nearly up to the zone boundary. Therefore, we discussed these branches especially and compared them with analogous phonons in palladium adjacent to Pt in the periodic table. Using the square root of the mass ratio as the scaling factor yields an agreement within about 10%. Similar relations have been found for other elements [3] and are therefore not unexpected.

2.2. Born-von Kármán analysis

Although the number of experimental points in the symmetry directions is rather limited so far, we made a preliminary analysis in terms of the Born-von Kármán model. The well-known expressions for the dynamical equations of the fcc lattice were used and the interatomic force constants were directly determined in a least-squares fit.

TABLE II. INTERATOMIC FORCE CONSTANTS FROM THE BORN-VON KÁRMÁN FIT WITH THIRD NEIGHBOURS
(units 10^3 dyn/cm)

α_1^{110}	26.68 ± 1.1
α_3^{110}	- 0.8 ± 1.28
β_3^{110}	31.76 ± 1.94
α_1^{200}	10.45 ± 2.47
α_2^{200}	- 5.02 ± 1.8
α_1^{211}	- 1.92 ± 1.2
α_2^{211}	0.23 ± 0.47
β_1^{211}	2.68 ± 0.52
β_2^{211}	- 1.0 ± 0.44

In the evaluations third and fifth neighbours were taken into account. From the increase in uncertainty in the force constants we concluded that only the third neighbour set was reasonable. The resulting force constants are quoted in Table II.

The full lines in Fig. 2 show the corresponding dispersion curves. A great number of phonons which have been measured outside the symmetry directions have been used as an additional check by comparing calculated values with the measured ones. Evaluations including part of the off-symmetry phonons already in the least-squares fit of the interatomic constants are underway.

The elastic constants derived from the force constants in Table II have been compared with those derived from acoustic measurements [4]. The results are given in Table III.

TABLE III. COMPARISON OF ELASTIC CONSTANTS
(units 10^{12} dyn/cm^2)

Elastic constants	Acoustic m.	Neutron m.
c_{11}	3.467	3.066
c_{44}	0.765	0.731
$c_{12} + c_{44}$	3.272	2.993

Using the third-neighbour interatomic force constant model, the spectral density of phonons f(V) has been determined. The calculations have been done by an improved root-sampling technique [5], solving the dynamical equations for 2750 q values of an irreducible part of the first Brillouin zone. f(V) is plotted in Fig. 3.

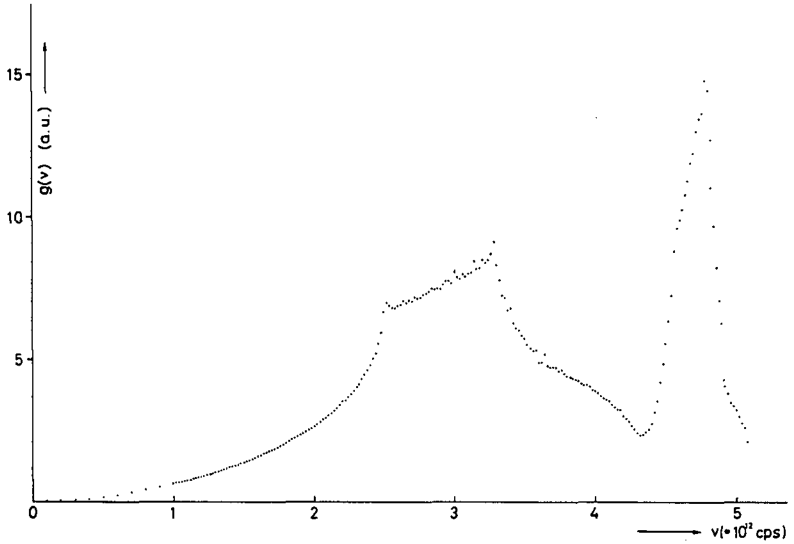

FIG. 3. Frequency distribution f(V) of platinum.

The dispersion curves measured contain, in principle, useful information on the electronic properties of platinum. For simple metals several models based on the pseudo-potential idea [6] have been successful in explaining the phonon dispersion on physical grounds, especially when free-electron-like behaviour of the conducting electrons can be assumed. For platinum this concept probably breaks down. Nevertheless, the fit of such a pseudo-potential model including unknown parameters may give hints for improving the theory. As a first step in this direction we are at present analysing our data with the Krebs model [7].

REFERENCES

[1] GLÄSER, W., EHRET, G., Rep. KFK 261, (1964).

[2] GOMPF, F., REICHARDT, W., GLÄSER, W., BECKURTS, K.H., The Use of a Pseudo-statistical Chopper for Time-of-Flight Measurements, these Proceedings, SM-104/67.

[3] BROCKHOUSE, B.N., "Phonons", Ch. 4, Neutron Scattering by Phonons (STEVENSON, R.W.H., Ed.), Oliver and Boyd, Edinburgh and London (1966).

[4] MACFARLANE, R.E. et al., Phys. Lett. 18 (1965) 91.

[5] GILAT, G., DOLLING, G., Phys. Lett. 8 (1964) 304.

[6] HARRISON, W.A., Pseudopotentials in the Theory of Metals, Benjamin, Inc., New York (1966).

[7] KREBS, K., HÖLZL, K., Inelastic Neutron Scattering and Lattice Dynamics of Metals in Quasi-Ion Approximation, Rep. EUR 3621e (1967).

LATTICE DYNAMICS OF RUBIDIUM

J.R.D. COPLEY AND B.N. BROCKHOUSE
McMASTER UNIVERSITY,
HAMILTON, ONT.,
AND
S.H. CHEN
UNIVERSITY OF WATERLOO,
WATERLOO, ONT., CANADA

Abstract

LATTICE DYNAMICS OF RUBIDIUM. The frequency/wave-vector dispersion relation for the normal modes of vibration in the major symmetry directions of body-centred cubic rubidium has been measured at 120°K. The large (~ 75 cm^3) single crystal was aligned with either a [110] or a [100] axis vertical, and constant incident frequencies between 3.8 and 5.5 × 10^{12} c/s were employed. The measurements were taken with the McMaster University triple-axis spectrometer at Chalk River in the constant-$\vec{Q}$ mode of operation. The dispersion curves are similar in shape to those of sodium and potassium. The ratio $<\nu(K, 9°K)/\nu(Rb, 120°K)>$ for a set of 104 values of $\vec{q}$ common to both sets of data, is 1.667 ± 0.005 with a standard deviation for an individual ratio from the mean of 0.05. The homology of the lattice vibrations for Na and Rb is poorer than for K and Rb. A Born-von Kármán analysis of the measurements has been made, and it is found that third nearest neighbour forces must be included to obtain reasonable agreement. More distant neighbour forces improve the fit relatively little. Axially symmetric constraints do not change the force constants significantly. As expected, the force constant 1XY is larger than 1XX, which suggests that the forces between nearest neighbours are repulsive. The initial slopes of the dispersion curves are considerably larger than the slopes deduced from ultrasonic measurements. The errors, mainly in the ultrasonic measurements, are barely sufficient to account for the differences.

Introduction

The frequency/wave-vector dispersion relation for metallic rubidium at 120°K has been studied by inelastic neutron scattering. The crystal, purchased from Research Crystals Inc., Richmond, Va., was a cylinder approximately 3" long and 1-1/2" in diameter, with a [110] axis close to the cylindrical axis. The mosaic width of the crystal was 0.4°(f.w.h.m.). Protective grease was removed from the surface which was then cleaned with xylene. The crystal was placed in a close-fitting aluminium can fitted with an indium O-ring.

The measurements were made on the McMaster University triple-axis spectrometer at Chalk River [1] in the Constant $\vec{Q}$ mode, with fixed incident frequencies between 3.8 and 5.5 x 10^{12} c/s, in the $(1\bar{1}0)$ and (100) planes.

Results and comparison with sodium and potassium

The dispersion curves are shown in Fig. 1; a partial list of the observed phonons is given in Table I. Considerable difficulty was experienced in measuring the $[00\zeta]$L branch. The groups for this branch were poorly defined; occasionally peaks at smaller energy transfer were observed which did not correspond in energy to possible contributions from the [00ζ]T branch. Similar difficulties have been reported for measurements of this branch in sodium [2].

The dispersion curves resemble closely those of sodium [2] and potassium [3]. The mean frequency ratios $R = \langle \nu_A(\vec{q}_i)/\nu_B(\vec{q}_i) \rangle$ for pairs (A,B) of elements (Na,K), (K,Rb), and (Na,Rb) are given in Table II. N is the number of values of $\vec{q}_i$ common to both sets of data, σ is the standard deviation of an individual ratio from the mean, and δ is the mean error in an individual ratio obtained from the experimental errors. There appears to be a definite departure from homology of the lattice vibrations especially for Na and Rb. Direct comparison of the dispersion curves supports this view.

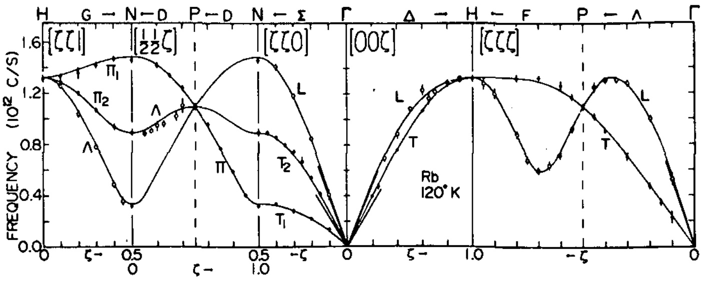

FIG. 1. Measured dispersion curves of rubidium at 120°K. The solid lines represent a third-neighbour Born-von Kármán fit. The straight lines from the points Γ represent the appropriate velocities of sound, calculated from the ultrasonic measurements [6].

Born-von Kármán analysis

A Born-von Kármán analysis of 132 phonons (elastic constants not included), indicates that forces extending to third nearest neighbours must be included in order to obtain a reasonable fit. The weighted r.m.s. value of $(\nu_{EXP}^2 - \nu_{CALC}^2)$, ($\Delta_4$ in [4], p. 630), is 0.038, 0.013, 0.009 and 0.008 for fits extending to 1st, 2nd, 3rd and 8th neighbours respectively. The third neighbour fit is shown in Fig. 1. The [½½ζ] branch is significantly worse fitted than the other branches. Measurements of this branch were taken on two occasions, with different incident frequencies, so it is unlikely that the discrepancy arises from errors in alignment. The fit to this branch improves considerably when six neighbours are included in the fit.

Models calculated with and without axially symmetric constraints give force constants which agree to well within the errors. In Table III force constants for Na, K and Rb are compared; all were obtained from sixth neighbour axially symmetric fits, with no elastic constants included. The force constants 1XX and 1XY decrease with increasing atomic weight, but 2XX and 3XX remain relatively constant. Thus second (and third)

TABLE I

Normal mode frequencies (units 10^{12} c/s) in Rubidium at 120°K

ξ	ν	Δν	ξ	ν	Δν	ζ	ν	Δν
	[00ζ]L			[00ζ]T			$[\frac{1}{2}\frac{1}{2}\zeta]\Lambda$	
0.3	0.69	0.03	0.2	0.39_5	0.01	0.1	0.88_5	0.02_5
0.4	0.88	0.04	0.4	0.75_5	0.01	0.2	0.94_5	0.04
0.6	1.22_5	0.04	0.6	1.06_5	0.01	0.35	1.02	0.03_5
0.8	1.31_5	0.03	0.8	1.27_5	0.02	0.4	1.10_5	0.06
1.0	1.31_5	0.03	1.0	1.31_5	0.03	0.5	1.09_5	0.03
	[ζζζ]L			[ζζζ]T			$[\frac{1}{2}\frac{1}{2}\zeta]\pi$	
0.1	0.52_5	0.05	0.1	0.22_5	0.05	0.1	....	
0.2	1.00	0.03	0.2	0.47	0.03	0.2	1.42	0.02_5
0.3	1.28	0.03	0.3	0.70_5	0.03_5	0.3	1.34	0.02
0.4	1.30_5	0.03	0.4	0.91	0.02	0.4	1.24_5	0.02_5
0.5	1.09_5	0.03	0.5	1.09_5	0.03	0.5	1.09_5	0.03
0.6	0.72	0.03_5	0.6	1.26	0.04	0.6	0.96	0.01_5
0.7	0.60	0.03	0.7	1.32_5	0.02	0.7	0.77	0.01_5
0.8	0.88	0.03	0.8	1.32	0.03	0.8	0.59	0.01_5
0.9	1.19_5	0.04_5	0.9	....		0.9	0.40_5	0.01_5
1.0	1.31_5	0.03	1.0	1.31_5	0.03	1.0	0.32	0.02
	[ζζ0]L			[ζζ0]T1			[ζζ0]T2	
0.1	0.41	0.04	0.1	0.13_5	0.02	0.15	0.41_5	0.02
0.2	0.85	0.02_5	0.2	0.22	0.01_5	0.2	0.54	0.02
0.3	1.18_5	0.01_5	0.3	0.28_5	0.02	0.3	0.74_5	0.02
0.4	1.41	0.02_5	0.4	0.33_5	0.01_5	0.4	0.86	0.02
0.5	1.46	0.02_5	0.5	0.32	0.02	0.5	0.90	0.03
	[ζζ1]Λ			[ζζ1]π1			[ζζ1]π2	
0.1	1.26	0.02_5	0.1	1.33_5	0.02	0.1	1.29	0.02_5
0.2	1.04	0.03	0.2	1.36	0.05	0.2	1.20_5	0.02
0.3	0.78	0.02	0.3	1.42	0.03	0.3	1.07	0.02
0.4	0.49	0.02_5	0.4	1.47	0.02_5	0.4	0.94	0.03
0.5	0.32	0.02	0.5	1.46	0.02_5	0.5	0.90	0.03

TABLE II

Mean frequency ratios

	R	N	σ	δ
Na/K	1.635 ± 0.005	82	0.04	0.06
K/Rb	1.667 ± 0.005	104	0.05	0.07
Na/Rb	$2.73_4 \pm 0.01_3$	88	0.12	0.09

TABLE III

Atomic force constants for alkali metals in dynes/cm.

The notation is that of refs. [4,5].

	1XX	1XY	2XX	2YY	3XX	3ZZ
Na	1172±11	1345±14	472±33	86±18	-35±8	7±10
K	762± 7	882± 9	417±19	5±11	-37±5	-4± 7
Rb	614± 8	741± 9	455±19	1±12	-33±6	6± 7

neighbours are relatively more important for the heavier members of the series. 2YY is appreciable only for Na. For first neighbours, 1XY is larger than 1XX, which indicates that forces between nearest neighbours in the alkali metals are repulsive, a result which conforms to the rule [5] that, for metals, forces between first neighbours are repulsive except for B.C.C. transition elements, for which they are attractive.

Initial slopes of the dispersion curves

In Fig. 1, the slopes of the straight lines drawn from the points Γ represent velocities of sound obtained from the elastic constants measured by Roberts and Meister [6]. These workers measured five wave velocities at 80°K but were unable to measure shear velocities at 293°K, allowing evaluation of C_{11}, but not C_{12} or C_{44}, at this temperature. Using the measured elastic constants for potassium [7], and making the approximation:

$$[(dc/dT)_K/(dc/dT)_{Rb}] = [(dc_{11}/dT)_K/(dc_{11}/dT/_{Rb}] \ ,$$

we have obtained values of 2.86 ± 0.20, 2.38 ± 0.40, and 1.38 ± 0.19 (in units of 10^{10} dynes/cm.), for C_{11}, C_{12} and C_{44} respectively, for Rb at 120°K. The slopes were calculated using these values and the lattice constant a = 5.628 Å.

No initial slope is shown for the [ζζo]T1 or the [ζζζ]T branches , since the errors were > 20%. For the other branches the errors are ± 7% or less. The slopes are considerably smaller than those of the neutron measurements (e.g. ~ 15% smaller for the [00ζ]T branch). A possible error of ± 10° in the orientation of the crystal used in the ultrasonic measurements [6] is barely sufficient to account for the differences.

The Debye-Waller factor

If the same normal mode is measured at several equivalent points in reciprocal space, the dependence of the intensity of the group on $\vec{Q}$ may be investigated. This dependence is given by

$$I(\vec{Q}) \propto (\vec{Q}.\vec{\xi})^2 \ \exp-[\vec{Q}.\vec{u}]^2$$

where, for a given material, $\vec{u}$ (the r.m.s. nuclear displacement) is a function of temperature only : ξ is the polarization vector. In favourable cases it is likely that the Debye-Waller parameter $[\vec{Q}.\vec{u}]^2$ can be directly determined in this way. The method may offer some advantages over the use of elastic scattering intensities, because of the absence of extinction.

In order to obtain intensity measurements at a number of different values of $\vec{Q}$, a specimen with a large lattice constant is required, and short wavelengths are desirable. The choice of a zone boundary phonon has the advantage that there are no focussing effects involved, but second order Bragg reflections can cause trouble. It is likely that the most suitable choice is a phonon near to the zone boundary. Preliminary measurements of the $[0\zeta\zeta]T1$ zone boundary phonon and the $[\frac{1}{2}\frac{1}{2}\zeta]\pi$ phonon at $\zeta = 0.9$, have given encouraging results.

Conclusion

We intend to investigate the temperature dependence of the frequencies and widths of the neutron groups in rubidium, in order to study the anharmonic properties of the lattice vibrations. We plan also to investigate the $[00\zeta]L$ branch in more detail; to look for evidence of zero sound [8] in rubidium; to study the Debye-Waller factor as described above; and to make a comparison of our results with the theoretical calculations of Animalu et al.[9] and of Schneider and Stoll [10].

ACKNOWLEDGEMENTS

We are grateful to the staff of Atomic Energy of Canada Limited for cooperation and encouragement and to our colleagues in the Neutron and Solid State Physics Group at McMaster for helpful discussions. The work was supported by a National Research Council of Canada grant and one of us (JRDC) was supported by an N.R.C. Studentship.

REFERENCES

[1] BROCKHOUSE, B.N., DEWIT, G.A., HALLMAN, E.D., and ROWE, J.M., "McMaster University Neutron Crystal Spectrometers", these Proceedings, SM-104/52 .
[2] WOODS, A.D.B., BROCKHOUSE, B.N., MARCH, R.H., STEWART, A.T., and BOWERS, R., Phys. Rev. 128 (1962) 1112.
[3] COWLEY, R.A., WOODS, A.D.B., and DOLLING, G., Phys. Rev. 150 (1966) 487.
[4] SVENSSON, E.C., BROCKHOUSE, B.N., and ROWE, J.M., Phys. Rev. 155 (1967) 619.
[5] BROCKHOUSE, B.N., ABOU-HELAL, H.E., and HALLMAN, E.D., Solid State Communications 5 (1967) 211.
[6] ROBERTS, C.A., and MEISTER, R., J. Phys. Chem. Solids 27 (1966) 1401.
[7] MARQUARDT, W.R., and TRIVISONNO, J., J. Phys. Chem. Solids 26 (1965) 273.

[8] SVENSSON, E.C., and BUYERS, W.J.L., Bull. Am. Phys. Soc. 12 (1967) 708, and COWLEY, R.A., BUYERS, W.J.L., SVENSSON, E.C., and PAUL, G.L., "Neutron scattering and elastic constants", these Proceedings, SM-104/46 .

[9] ANIMALU, A.O.E ., BONSIGNORI, F., and BORTOLANI, V., Nuovo Cimento B 44 1 (1966) 159.

[10] SCHNEIDER, T., and STOLL, E., Phys. Kondens. Materie 5 (1966) 364.

MEASUREMENTS OF FREQUENCIES OF NORMAL MODES OF MAGNESIUM

R. PYNN AND G.L. SQUIRES
CAVENDISH LABORATORY,
CAMBRIDGE, ENGLAND

Abstract

MEASUREMENTS OF FREQUENCIES OF NORMAL MODES OF MAGNESIUM. The investigation of the phonon dispersion relations in magnesium has been continued and the frequencies of over 1 500 phonons with wave-vectors in the (10$\bar{1}$0) plane have been measured on the DIDO reactor at Harwell. The velocity spectra of inelastically scattered slow neutrons have been analysed by the time-of-flight method. The wave-vectors of the measured phonons are distributed throughout the plane and an interpolation method has been used to obtain the dispersion relations in several directions, including those principal symmetry axes which lie in the plane. The results are compared with a simple theoretical model.

1. Introduction

Experiments with slow neutrons to determine the frequencies of phonons in magnesium at room temperature, previously reported by Squires [1,2], have been continued. This paper presents a survey of recent results. The majority of the phonon frequencies have been determined by time-of-flight measurements - the rest by constant-q measurements on a triple-axis spectrometer.

2. Experimental method

The time-of-flight apparatus has been described in detail by Harris et al [3] and Squires [2]. The apparatus is shown schematically in Fig. 1. Neutrons from the DIDO reactor at Harwell pass through a curved-slot rotor, strike a magnesium crystal and are scattered into a ring of 24 scintillator-detectors arranged in a vertical plane - termed the scattering plane.

The frequency ν and wave-vector $\underset{\sim}{q}$ of a phonon which gives rise to a coherent one-phonon scattering process are determined from a knowledge of the wave-vectors of the incident and scattered neutrons. These wave-vectors are determined by time-of-flight analysis.

The wavelength of the incident neutrons was 4.12 Å with a r.m.s. spread of 0.15 Å. The distance from the crystal to the counters was 2.28 m, and the channel width in the time-of-flight analysis was 8μs. The crystal used in the present measurements was in the form of a cylinder 35 mm in diameter and 75 mm long, with one of the basal-plane diads along its length.

3. Results

In the previous experiment [2], the orientation of the crystal was such that the hexad was kept perpendicular to the scattering plane. Thus the phonons measured had wave-vectors lying in the q_x q_y plane - see Fig. 2. In the present experiment, the diad along the length of the cylinder was kept perpendicular to the scattering plane, thus ensuring that the wave-vectors of the measured phonons were in the q_x q_z plane. Measurements were made at 40 orientations of the crystal with respect to the direction of the incident neutrons.

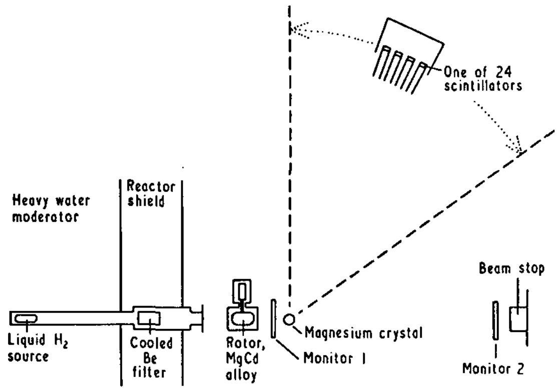

FIG.1. Diagram of time-of-flight apparatus.

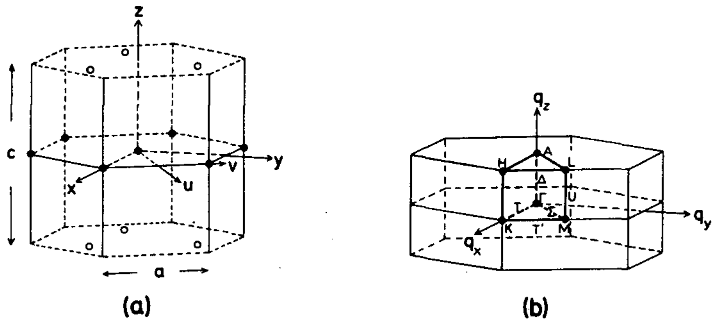

(a) (b)

FIG.2. Hexagonal close-packed structure: (a) space lattice; (b) reciprocal lattice — first Brillouin zone.

The experimental data were analysed by an interpolation method similar to that described by Squires [2]. Dispersion relations have been obtained in a number of directions in the q_x q_z plane. The results for some special directions are shown in Fig. 3 (T, T' axes), Fig. 4 (Δ axis) and Fig. 5 (U axis). (It may be noted that the area LHKM in Fig. 2b is, by symmetry, equivalent to an area in the q_x q_z plane outside the first Brillouin zone.) The T and T' axes also lie in the q_x q_y plane, and the previous results are included in Fig. 3. Iyengar et al [4] have measured the frequencies of phonons with wave-vectors along the Δ and Σ axes, using a triple-axis spectrometer, and their results are included in the figures.

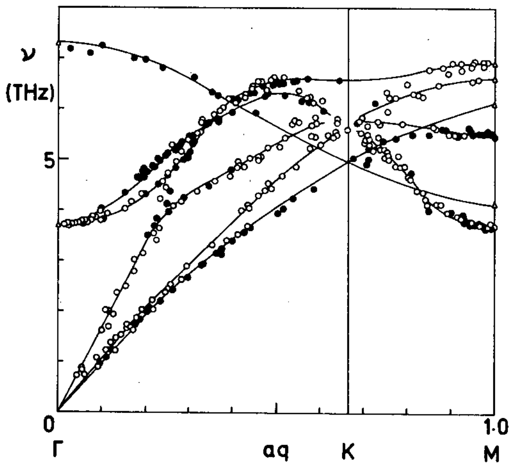

FIG. 3. Experimental dispersion relations for $\vec{q}$ along T and T' axes.

- ● T-O-F
- ○ T-O-F results from Ref. [2]
- ⊕ Triple-axis spectrometer
- Δ Iyengar et al.

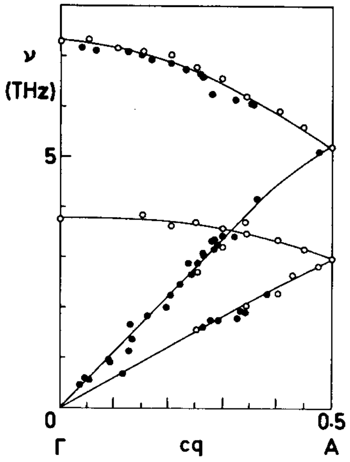

FIG. 4. Experimental dispersion relations for $\vec{q}$ along Δ axis.

- ● T-O-F
- ○ Iyengar et al.

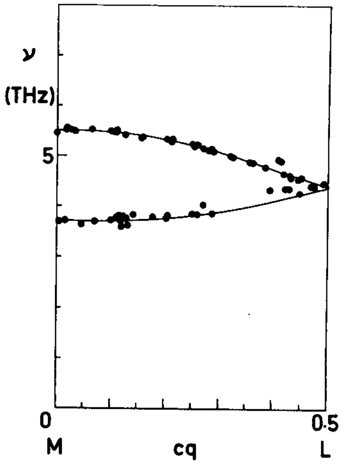

FIG. 5. Experimental dispersion relations for $\vec{q}$ along U axis.

- ● T-O-F
- ⊕ T-A S

TABLE I. MOTION OF ATOMS

Irreducible representation	Direction of atomic vibration(a)	Phase between sub-lattices (in units of π)
Γ_6^- , Γ_5^+	(b)	0 , 1
Γ_2^- , Γ_3^+	z	0 , 1
T_1 and T_1'	x y plane : E	
T_4 and T_4'	x y plane : E	
T_2 and T_2'	z	1
T_3 and T_3'	z	0
M_2^- , M_1^+	u	0 , 1
M_3^- , M_4^+	v	0 , 1
M_4^- , M_3^+	z	0 , 1
Δ_1 , Δ_2	z	$q_z c$, $(1+q_z c)$
Δ_6 , Δ_5	(b)	$q_z c$, $(1+q_z c)$
U_1 , U_2	u z plane : E	
U_3 , U_4	v	$q_z c$, $(1+q_z c)$

(a) The modes are linearly polarised, except those marked E which are elliptically polarised. In the latter case, the relative phases depend on the magnitude of the interatomic forces.

(b) Eigenvalues of dynamical matrix doubly degenerate: polarisation vector anywhere in x y plane.

In addition to time-of-flight measurements, we have also measured some frequencies of phonons with wave-vectors along the T and Σ axes, using the DIDO triple-axis spectrometer [5]. The results along T are included in Fig. 3.

4. Discussion

One difficulty of deducing the dispersion relations from the experimental results is the correct assignment of a measured phonon of wave-vector $\underset{\sim}{q}$ to its polarisation branch. To do this unambig-

TABLE II. FORCE CONSTANTS USED TO CALCULATE THE FREQUENCIES SHOWN IN FIGS 6-8 (UNITS 10^3 dyn/cm)

$\alpha_1 = 0.01$	$\alpha_2 = 10.12$	$\alpha_3 = -0.90$
$\beta_1 = 3.91$	$\beta_2 = 0.59$	$\beta_3 = 0.61$
$\gamma_1 = 7.34$	$\gamma_2 = 0.19$	$\gamma_3 = -0.27$
	$\rho_2 = -1.03$	

TABLE III. MEASURED FREQUENCIES OF SOME SPECIAL MODES

Irreducible representation	Frequencies given in ref [2]. (THz)	Frequencies used in this paper. (THz)
Γ_5^+	3.70	3.70
K_5	5.65	5.80
M_1^+	6.88	6.88
M_2^-	6.58	6.58
M_3^-	5.32	5.45
M_4^+	3.70	3.70
Γ_3^+	-	7.25
T_2 ($q = 0.2/a$)	-	7.05

uously, a knowledge of the eigenvectors of the dynamical matrix for the given wave-vector is required. For each eigenvector, the neutron scattering cross-section could then be calculated, and comparison with the experimental value would allow the polarisation branch to be identified. Since the interatomic forces are not known, the eigenvectors are in general inaccessible. However, along many special directions in the Brillouin zone, the phonon eigenvectors belonging to each irreducible representation are known and are independent of the interatomic forces. These considerations have been used to identify the polarisation branches of the majority of the phonons.

Table I gives the direction of the atomic vibrations and the phase difference between the motions of the two sublattices - the convention used is given in ref [2] - for each of the irreducible representations considered. The notation used to identify the representations is one of those given by Altmann and Bradley [6].

A simple three-neighbour tensor force model has been found, whose phonon frequencies are in good qualitative agreement with the

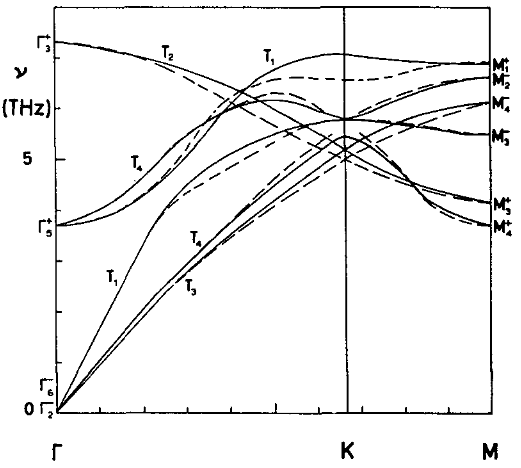

FIG. 6. Comparison of experimental and theoretical results for $\vec{q}$ along T and T' axes.

------ Experimental results from Fig.3

——— Three neighbour tensor force model.

FIG. 7. Comparison of experimental and theoretical results for $\vec{q}$ along Δ axis.

------ Experimental results from Fig.4

——— Three neighbour tensor force model.

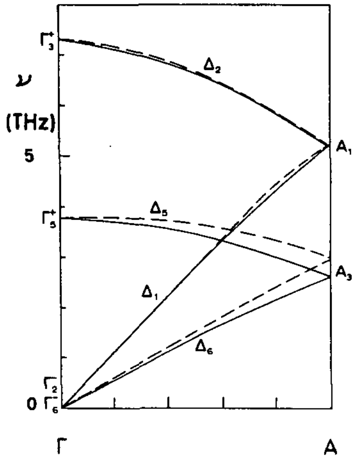

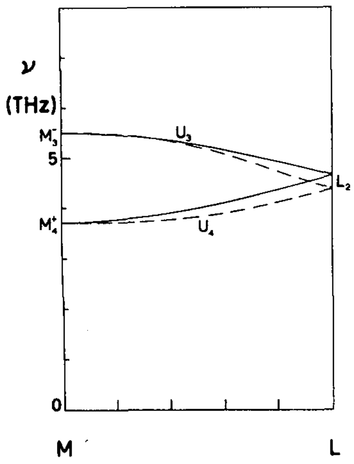

FIG. 8. Comparison of experimental and theoretical results for $\vec{q}$ along U axis.

------ Experimental results from Fig.5

——— Three neighbour tensor force model.

measured dispersion relations, and which gives the correct polarisation vectors along symmetry axes. The values of the force constants are listed in Table II in the notation of ref [2]. They were obtained by fitting the measured frequencies given in Table III and the elastic constants c_{11}, c_{66}, c_{33} [7]. (The first seven force constants are practically identical to those deduced in [2], the differences being due to the small changes in the measured frequencies of the M_3^- and K_5 modes.)

The dispersion relations given by this model are shown as solid lines in Fig. 6 (T, T' axes), Fig. 7 (Δ axis) and Fig. 8 (U axis). For comparison, the curves drawn through the experimental points on Figs. 3 to 5 are shown as broken lines.

The model should not be regarded as highly significant physically. However, a Born-von Karman model of the type used here is useful in predicting polarisation vectors and for generating frequencies. But it should be noted that the present model does not include values for the force constants δ_1 and δ_3 and is therefore applicable only if $\underset{\sim}{q}$ lies in certain planes and directions in the Brillouin zone.

5. Conclusion

The results given in this paper are a preliminary survey of recent experiments, but, even so, it can be seen from Figs. 3 to 5 that many of the dispersion relations in magnesium are now well-established. We intend to continue these investigations and to make measurements at other temperatures.

ACKNOWLEDGEMENTS

We would like to thank Messrs. G. Clarke, C. Duffill, V. Rainey, D. H. Saunderson and other members of the Slow Neutron Physics Group at Harwell for invaluable assistance with the running of the apparatus. We would also like to thank the staff of the Atlas Computer Laboratory at Chilton for their help in processing the experimental data. One of us (R.P.) would like to acknowledge a Science Research Council studentship during the tenure of which this work has been performed.

REFERENCES

[1] Squires, G. L., Symposium on Inelastic Scattering of Neutrons by Condensed Systems, p. 78, Brookhaven National Laboratory (1965).

[2] Squires, G. L., Proc. Phys. Soc. 88 (1966) 919.

[3] Harris, D., Cocking, S. J., Egelstaff, P. A., and Webb, F. J., "Inelastic Scattering of Neutrons in Solids and Liquids" Vol I, p. 107, IAEA Vienna (1961).

[4] Iyengar, P. K., Venkataraman, G., Vijayaraghavan, P. R., and Roy, A. P., "Inelastic Scattering of Neutrons in Solids and Liquids" Vol I, p.153, IAEA Vienna (1965).

[5] Duffill, C., Saunderson, D. H., Sharp, R. I., UKAEA Report AERE-R 4895 (1965).

[6] Altmann, S. L., and Bradley, C. J., Rev. Mod. Phys. 37 1 (1965) 33.

[7] Slutsky, L. J., and Garland, C. W., Phys. Rev. 107 4 (1957) 972.

THE DYNAMICS OF HYDROGEN IMPURITIES IN NIOBIUM AND VANADIUM

G. VERDAN, R. RUBIN AND W. KLEY
DIVISION OF EXPERIMENTAL NEUTRON PHYSICS,
DEPARTMENT OF REACTOR PHYSICS,
EURATOM,CCR — ISPRA (VARESE), ITALY

Abstract

THE DYNAMICS OF HYDROGEN IMPURITIES IN NIOBIUM AND VANADIUM. The inelastic scattering of cold neutrons in single crystals of vanadium hydride and niobium hydride revealed local modes at $E_1^V = 167 \pm 6$ meV, $E_2^V = 123 \pm 6$ meV and $E_1^{Nb} = 177 \pm 6$ meV, $E_2^{Nb} = 114 \pm 6$ meV. From a measurement of the width function of hydrogen in polycrystalline niobium, the diffusion constant D(200°C) = 2×10^{-15} cm²/sec and the time between diffusive jumps $\tau = 1.3 \times 10^{-12}$ sec could be determined.

1. INTRODUCTION

Scattering experiments on cold neutrons from polycrystalline samples of VH_n, NbH_n and PdH_n systems [1-3] have revealed the existence of local and band modes as well as the diffusive motion of hydrogen in the host lattices. The possible sites for the hydrogen are either of the tetrahedral or octahedral type, therefore, the localized states of the hydrogen in V and Nb are only two-fold degenerate: $\omega_1 = \omega_2 = \omega_3\sqrt{2}$. Contrary to this symmetry condition, only one broad local peak was observed in the earlier scattering experiments with polycrystalline samples. The present study shows that this is due to the spatial averaging of $\langle \vec{\kappa} \cdot \vec{u} \rangle_\Omega$, where $\vec{\kappa}$ stands *for the momentum transfer and* $\vec{u}$ for the amplitude of the local mode, which leads to a strong overlap of the local peaks, producing one broad peak in the scattered neutron spectrum. Using single crystals of V and Nb, this effect can be avoided and the two local peaks can be observed since even for an incoherent scatterer the inelastic scattering intensity is directly proportional to $\langle \vec{\kappa} \cdot \vec{u} \rangle$ and therefore strongly direction dependent. Modes with amplitude vectors $\vec{u}$ perpendicular to $\vec{\kappa}$ have zero inelastic cross-section.

The quasi-elastic scattering of cold neutrons from polycrystalline samples can be used for the study of the microscopic diffusion process and in particular to determine in which site the hydrogen is located and if it jumps from tetrahedral to tetrahedral or from octahedral to octahedral or even from tetrahedral to octahedral sites, as was first demonstrated by Sköld and Nelin [3]. Although polycrystalline samples give pertinent information, in certain cases single-crystal measurements should give additional information on the microscopic diffusion process. This is particularly true for a 'lattice' of interstitial sites that form a simple Bravais lattice. In this case the anisotropic diffusion constant can be measured by varying the position of $\vec{\kappa}$ with respect to the principal axes of the lattice. In a bcc lattice, the 'lattices' of the tetrahedral, the octrahedral and even of all the interstitial sites, tetrahedral and octahedral together, do not form a simple lattice that can be built up through translation of a 'unit cell'. The lattices can only be built up through translation and rotation of a 'unit cell'. In spite of these difficulties, we assume that for bcc lattices, for which proton tunnelling or channelling along the three directions [100] have been proposed [2], a cubic lattice of interstitial sites is a reasonable approximation to the actual situation. For such a lattice, the quasi-elastic peak should be truly Lorentzian and the width of this Lorentzian will be sensitive on the relative position of $\vec{\kappa}$ with respect to the three directions [100]. In this respect single-crystal measurements are meaningful also for the study of the diffusion process. If proton tunnelling should occur, it can be expected that there will be a large difference in the diffusion constant of hydrogen and deuterium. To prove this point of view, which was suggested by our neutron results, internal friction measurements have been carried out by Schiller [4] at Ispra which show that the diffusion constant for hydrogen in Nb is 300 times larger than for deuterium.

For the various reasons mentioned above, the present study has been carried out with polycrystalline and single-crystal samples of vanadium and niobium.

2. THEORY

We know from the earlier neutron scattering experiments [2] that cold neutrons are scattered quasi-elastically by hydrogen and that local and band modes are generated by hydrogen in V and Nb. Therefore, hydrogen vibrates for a certain time τ in a certain interstitial position that may be taken as the origin, and then it jumps to an adjacent site at position $\vec{\ell}$. There may be n such adjacent sites, where it may vibrate for a time τ.

Under the assumption that the origin and the adjacent sites form a 'unit cell' and that the lattice of interstitial sites can be obtained by simple translation of this 'unit cell', and assuming further that the diffusive and oscillatory motions are not correlated and that the diffusive jumps take place instantaneously, Chudley and Elliott [5] have derived the incoherent double-differential cross-section. This theory does not cover the actual situation in the bcc lattice and leads to imaginary cross-sections by applying it to tetrahedral or octahedral sites. Since there are certain reasons to believe in proton tunnelling or channelling along the principal axes of the crystal, a cubic lattice of interstitial sites with a lattice constant of a/4 seems to be a reasonable first approximation to the real situation. Therefore, we use the Chudley and Elliott formalism as a first approximation to our problem:

$$\frac{d^2\sigma}{d\Omega\, d\epsilon} = \frac{a^2 k_f}{h k_i}\, \Gamma(\vec{\kappa}, \omega) \tag{1}$$

The scattering law $\Gamma(\vec{\kappa}, \omega)$ for the zero-phonon contributions is given by

$$\Gamma_s^0(\vec{\kappa}, \omega) = e^{-2W}\, \frac{2\cdot f(\vec{\kappa})}{\left[\omega^2 + \{f(\vec{\kappa})\}^2\right]} \tag{2}$$

and the one-phonon destruction process

$$\Gamma_s^{(-1)}(\vec{\kappa}, \omega) = \frac{\hbar\kappa^2}{2\pi M} e^{-2W} \int \frac{g(\nu)\, d\nu}{\nu\left[\exp\left(\frac{h\nu}{kT}\right) - 1\right]}\quad \frac{f(\vec{\kappa})}{(\omega-\nu)^2 + [f(\vec{\kappa})]^2} \tag{3}$$

where a is the incoherent scattering length; $\vec{k}_i$, $\vec{k}_f$ are the initial and final neutron wavevectors, $\hbar\vec{\kappa} = \hbar(\vec{k}_i - \vec{k}_f)$ is the momentum transfer; and W is the Debye-Waller exponent.

The width function is defined by

$$f(\vec{\kappa}) = -\frac{1}{n\tau}\sum_{\vec{\ell}_i=1}^{n}\left[\exp\{i\vec{\kappa}\vec{\ell}_i\} - 1\right] \tag{4}$$

where $\vec{\ell}_i$ is the position vector; τ is the time between jumps; and n is the number of nearest neighbours.

For the case of a cubic lattice, with lattice constant (9/4), the averaged cross-section over all possible orientations of the crystallites with respect to $\vec{\kappa}$ can easily be obtained and is described by a Lorentzian, whose width is given by

$$f(\kappa) = \frac{1}{\tau}\left[1 - \cos\left(\frac{9}{4}\kappa\right)\right] \tag{5}$$

This function is plotted together with the experimental results in Fig. 1.

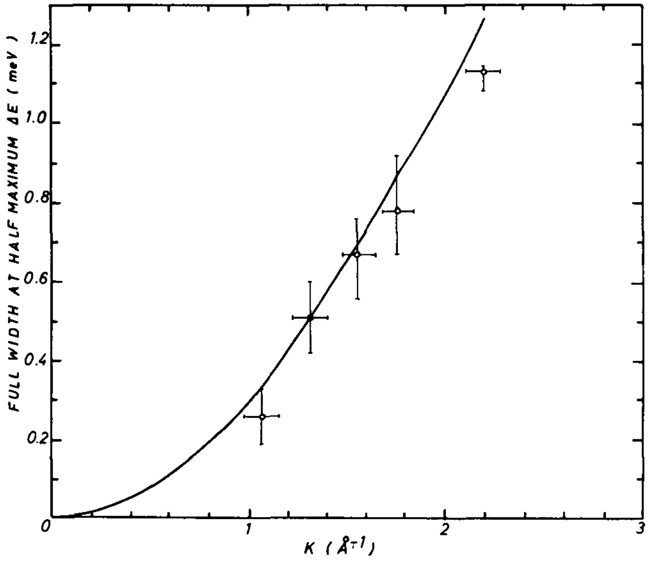

FIG. 1. The width function $\Delta E(\vec{\kappa})$ for hydrogen in niobium at 200°C. The solid line gives the theoretical width function $\Delta E = 2\hbar \cdot f(\kappa) = (2\hbar/\tau)[1 - \cos(\kappa a/4)]$.

3. EXPERIMENTAL RESULTS AND DISCUSSION

The samples have been prepared in the usual manner, as discussed in Ref. [2]. The neutron measurements were carried out at the Ispra-I cold neutron facility. Two flight paths of 3 and 4.5 m have been used.

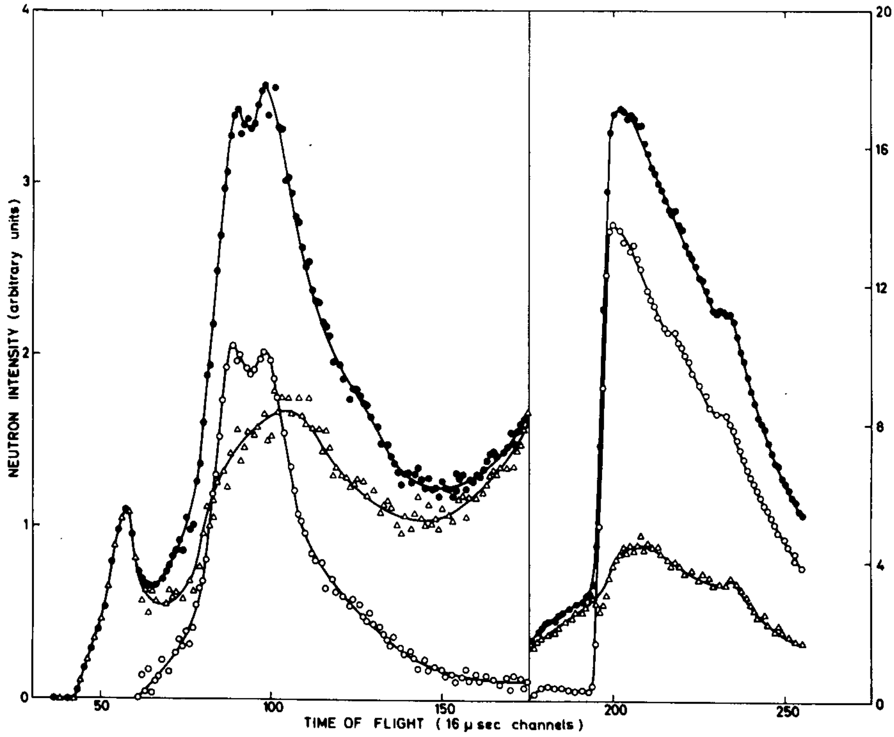

FIG.2. Neutron time-of-flight spectrum of inelastically scattered cold neutrons on $VH_{0.04}$(●) and V (O) at a temperature of 50°C and a scattering angle of 90°. The difference of the two measurements $VH_{0.04}$-V is marked by (Δ).

3.1. The VH_x-results

Figure 2 shows the time-of-flight spectrum of cold neutrons inelastically scattered by a polycrystalline sample of $VH_{0.04}$ (●) at 50° C and 90° scattering angle. The spectrum of pure vanadium (o) and the difference $VH_{0.04}$-V = H(Δ) is also plotted. The difference of the intensity reveals the hydrogen motions in vanadium, showing clearly the existence of local and band modes and the zero-phonon contribution is broadened (quasi-elastic scattering). Figure 3 shows the TOF spectrum of neutrons scattered from a single crystal of $VH_{0.04}$ at 200° C and a scattering angle of 90°. The spectrum shows clearly two local peaks as expected from symmetry conditions. Because of symmetry conditions, unfortunately, one cannot align $\vec{\kappa}$ and $\vec{u}_1$ and make at the same time $\vec{\kappa}$ and $\vec{u}_2$ perpendicular in order to measure only one mode at a time. But, as can be seen from Figs 1 and 2, the spatial averaging is avoided and the two peaks can be separated. In Fig.4(a) the generalized frequency distribution function for the local peaks is plotted and the energy of the two peaks determined as $E_1 = 167 \pm 6$ meV and $E_2 = 123 \pm 6$ meV. Within the errors of this experiment, the ratio of $E_1/E_2 = \sqrt{2}$.

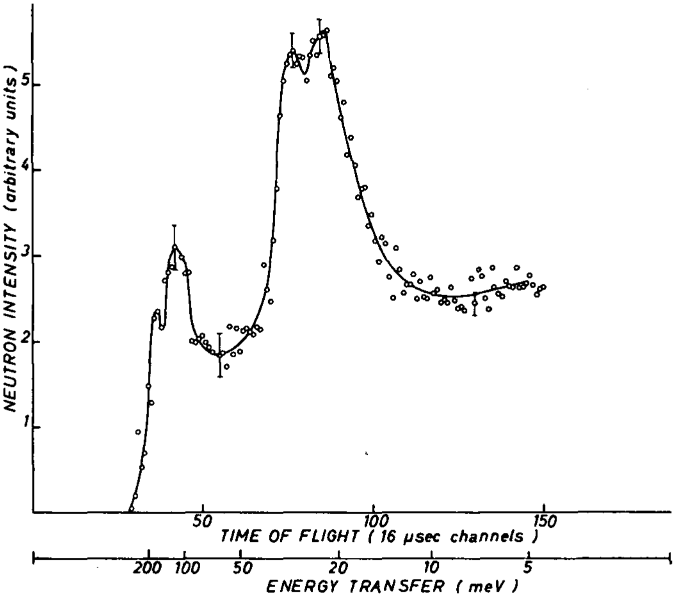

FIG.3. Time-of-flight spectrum of neutrons scattered by a single crystal of $VH_{0.04}$ by 90°. The sample was kept at a temperature of 200°C.

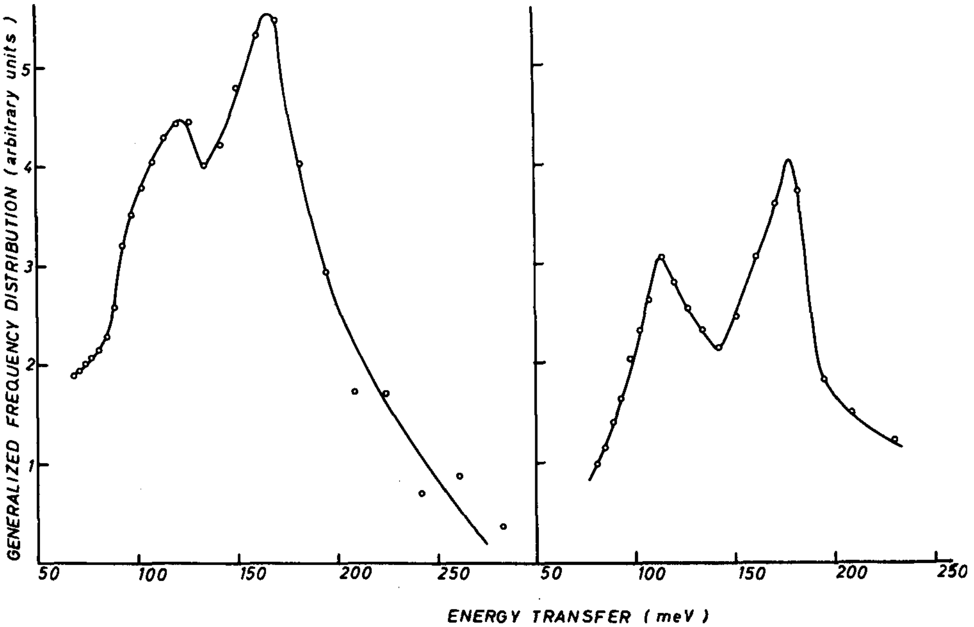

FIG.4. (a) The generalized frequency distribution function in the region of the local peaks of $VH_{0.04}$;
(b) The generalized frequency distribution function in the region of the local peak of $NbH_{0.05}$.

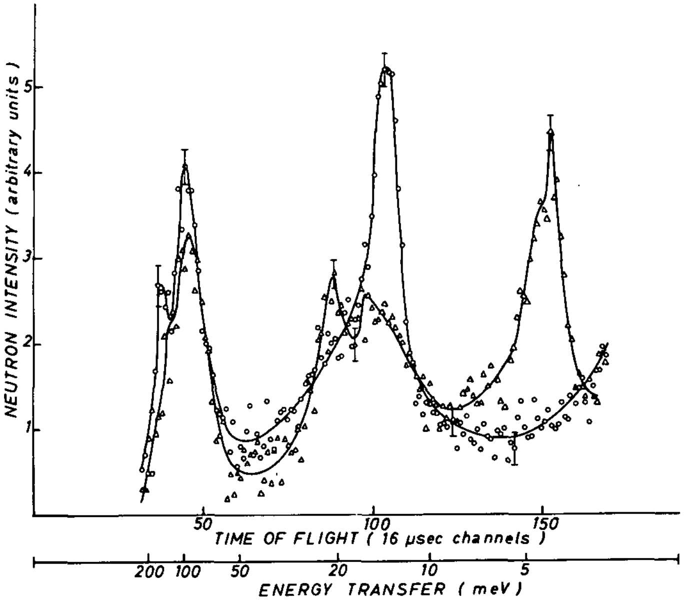

FIG.5. Time-of-flight spectra of neutrons scattered by a single crystal of $NbH_{0.05}$ by 90°. The sample was kept at a temperature of 200°C. The sample was oriented in a manner that $\kappa_{elastic}$ was parallel to the [100] direction (○) and parallel to the [110] direction (△).

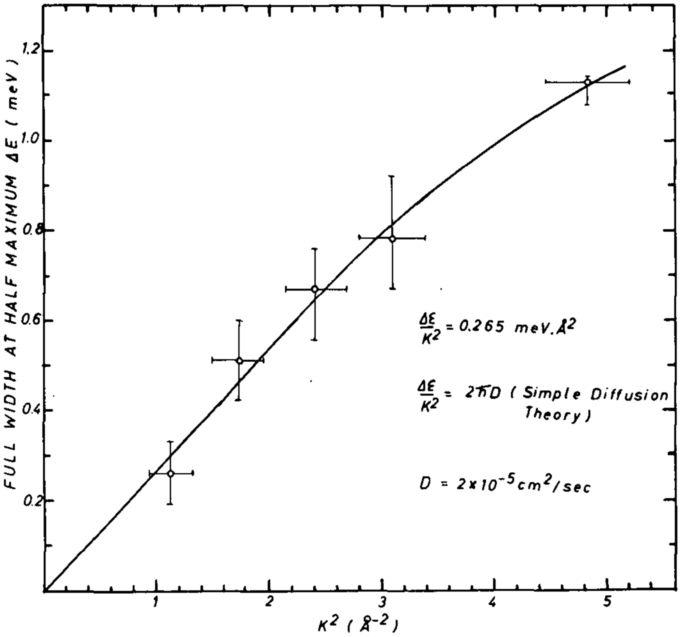

FIG. 6. The width function ΔE is plotted against κ^2 and the diffusion coefficient for hydrogen in niobium is derived to $D = 2 \times 10^{-5}$ cm²/sec at 200°C.

3.2. The NbH_x-results

In Fig. 5 the time-of-flight spectrum of neutrons scattered from a single crystal of $NbH_{0.05}$ is plotted. The sample was kept at a temperature of 200° C and the results are given for $\vec{\kappa}_{elastic}$ parallel to the [100] and [110] directions. Again two local peaks can be observed, as expected from symmetry conditions. Figure 4(b) gives the generalized frequency distribution function for the range of the local peaks and their energies are determined as $E_1 = 177 \pm 6$ meV, $E_2 = 144 \pm 6$ meV.

3.3. Diffusion of hydrogen in niobium

To measure the diffusion constant D of hydrogen in niobium and the time between jumps τ, the width function was measured using a polycrystalline sample of $NbH_{0.09}$ at 200° C and 5 different scattering angles. In Fig. 1 the width function is plotted as a function of κ. As can be seen, this agrees quite well with the assumption of a cubic lattice for the interstitial sites. Unfortunately, we could not measure yet beyond the maximum of the width function which would be a more convincing proof of this approximation. From the fit we deduce a value $\tau = 1.3 \times 10^{-12}$ sec. Figure 6 shows the quasi-elastic broadening as function of κ^2. Since we are obviously in the small κ region, a continuous diffusion model may be applied to determine the macroscopic diffusion constant. Using Vineyard's formula [6], we obtain $D_{200°C} = 2 \times 10^{-5}$ cm^2/sec for hydrogen in niobium. It is interesting to note that the value of τ derived in this manner does not agree at all with the one derived from the width of the local peak. The width of the local peak is about 25 meV and would give a value $\tau = 2.7 \times 10^{-14}$ sec. This result suggests very strongly that a band model is much more appropriate to explain the width of the local peak. A further extension of this experimental work to higher κ values is being prepared. An improved Chudley and Elliott model might then allow also the assignment of the site configuration in which the hydrogen is moving. Figure 7 shows the results of the quasi-elastically scattered cold neutrons in the [100] and [110] directions. Because of an experimental difficulty, only a qualitative statement can be made about this result. It confirms the assumption of a cubic lattice for the interstitial sites accessible to the hydrogen.

Table I shows the results from internal friction measurements, as obtained by Schiller [4] at Ispra and by Cannelli and Verdini [7]. From their results we can extrapolate the diffusion constant for jumps in the tetrahedral sites at 200° C to $D_{I.F.} = 7.55 \times 10^{-5}$ cm^2/sec. Considering the extrapolation over 7 orders of magnitude, reasonable agreement is obtained with the neutron data. The measurements of the diffusion constant for deuterium in niobium give a value 300 times smaller than the one for hydrogen.

ACKNOWLEDGEMENTS

We would like to thank Dr. J. Peretti (Ispra), Dr. I. Pelah (Israel) and Dr. G. Blässer (Ispra) for many enlightening discussions. The technical assistance of Mr. P. Dominke and Mr. Y. Claesen is particularly acknowledged.

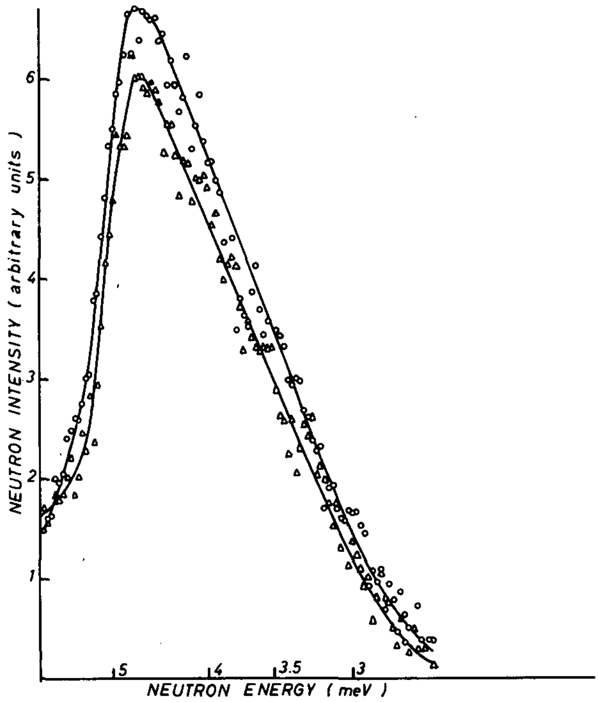

FIG.7. The spectra of quasi-elastic scattered cold neutrons from a 'single crystal' of $NbH_{0.05}$ at 200°C for two orientations of $\vec{\kappa}$ with respect to the crystal axes. The results for $\vec{\kappa}$ parallel to the [100] are marked (○) and the one for $\vec{\kappa}$ parallel to the [110] direction are marked (△).

TABLE I. JUMP FREQUENCIES AND ACTIVATION ENERGIES FROM INTERNAL FRICTION MEASUREMENTS

	T_m (°K)	f_m (c/sec)	Activation energy (meV)
Cannelli			NbH_n
and	97 ± 0.5	17.300	
Verdini [7]	100 ± 0.5	30.700	
	103 ± 0.5	60.000	W = 180
	106 ± 0.5	95.200	
	107 ± 1.0	127.900	
Schiller [4]			NbH_n
	100	30.000	
	107	130.000	W_H = 185
			NbD_n
	110	750	
	129	10.000	W_D = 160

REFERENCES

[1] RUBIN, R., PERETTI, J., VERDAN, G., KLEY, W., Phys. Lett. 14 (1965) 100.
[2] KLEY, W., PERETTI, J., RUBIN, R., VERDAN, G., Symp. Inelastic Scattering of Neutrons by Condensed Systems, Brookhaven National Laboratory, September 1965, Rep. BNL 940 (C-45).
[3] SKÖLD, K., NELIN, G., J. Phys. Chem. Solids 28 (1967) 2369-80.
[4] SCHILLER, P., Ispra, private communication (1967).
[5] CHUDLEY, C.T., ELLIOTT, R.J., Proc. Phys. Soc. 77 (1960) 353-61.
[6] VINEYARD, G.H., Phys. Rev. 110 (1958) 999.
[7] CANNELLI, G., VERDINI, L., Ricerca scient. 36 2 (1966) 98.

LATTICE DYNAMICS OF α-Fe AND Fe_3Al

C. VAN DIJK AND J. BERGSMA
REACTOR CENTRUM NEDERLAND,
PETTEN (N.H.), THE NETHERLANDS

Abstract

LATTICE DYNAMICS OF α-Fe AND Fe_3Al. Detailed measurements of the phonon dispersion relations in alpha-iron have been made at room temperature using the triple-axis crystal spectrometer at the HFR reactor at Petten. Over 200 modes, observed at regular distances in the $[\zeta 00]$, $[\zeta\zeta 0]$, $[\zeta\zeta\zeta]$, $[\zeta\zeta 1]$ and $[\frac{1}{2}\frac{1}{2}\zeta]$ directions, are presented. An analysis in terms of the Born-von Kármán theory, using a linear least-squares method, shows that for getting qualitative agreement with experiment it is sufficient to take into account forces out to third neighbours only, but for reproducing the details of the dispersion relations forces out to fourth and fifth neighbours have also to be included. An interesting feature, also confirmed by other recent measurements on α-Fe, is the attractive force between first neighbours manifested in $\alpha_1 > \beta_1$. This has been found so far for all bcc transition metals. Based on this model the phonon frequency distribution has been calculated. An attempt to include the effect of the conduction electrons according to the Krebs' model, was not very successful.

In addition, phonon measurements on the closely related iron-aluminium alloy Fe_3Al in the ordered phase are reported. The structure of Fe_3Al consists of four interpenetrating fcc lattices and can be derived from the α-Fe structure by replacing every fourth atom along the [111] direction by aluminium. The close relation between the lattice dynamics of α-Fe and Fe_3Al becomes much more clear, when the α-Fe data are described according to the Fe_3Al lattice. The different mass of the aluminium atom and the different interaction with its neighbours, and a possible change in the iron-iron interaction as compared to that in the iron lattice, cause the marked differences in the dispersion relations of the two specimens.

1. INTRODUCTION

Investigations of the lattice dynamics of α-iron, reported earlier [1], have been extended. By means of inelastic neutron scattering using a triple-axis crystal spectrometer, the phonon dispersion relations have been determined for the principal symmetry directions and for directions at the zone boundary where the dynamical matrix factorizes. Since the previous report [1], experimental work on α-iron, carried out independently at other laboratories, has been published [2-5], enabling the results to be compared.

The interest in the dynamics of α-iron originates, among other reasons, in its complicated electric band structure. It is hoped that the information desired can be extracted from the phonon dispersion relations either by fitting them to a physically realistic model or by comparing them with the relations of other systems. As regards the latter aspect, the study of the dynamical behaviour of the alloy Fe_3Al could provide an interesting comparison with the results for iron. In the ordered phase Fe_3Al has a fcc structure and contains two species of iron atoms. Those of type I are surrounded by 8 atoms of type II in a spatial configuration similar to that of the atom in α-Fe, whereas atoms of type II are surrounded by 4 atoms of type I and by 4 aluminium

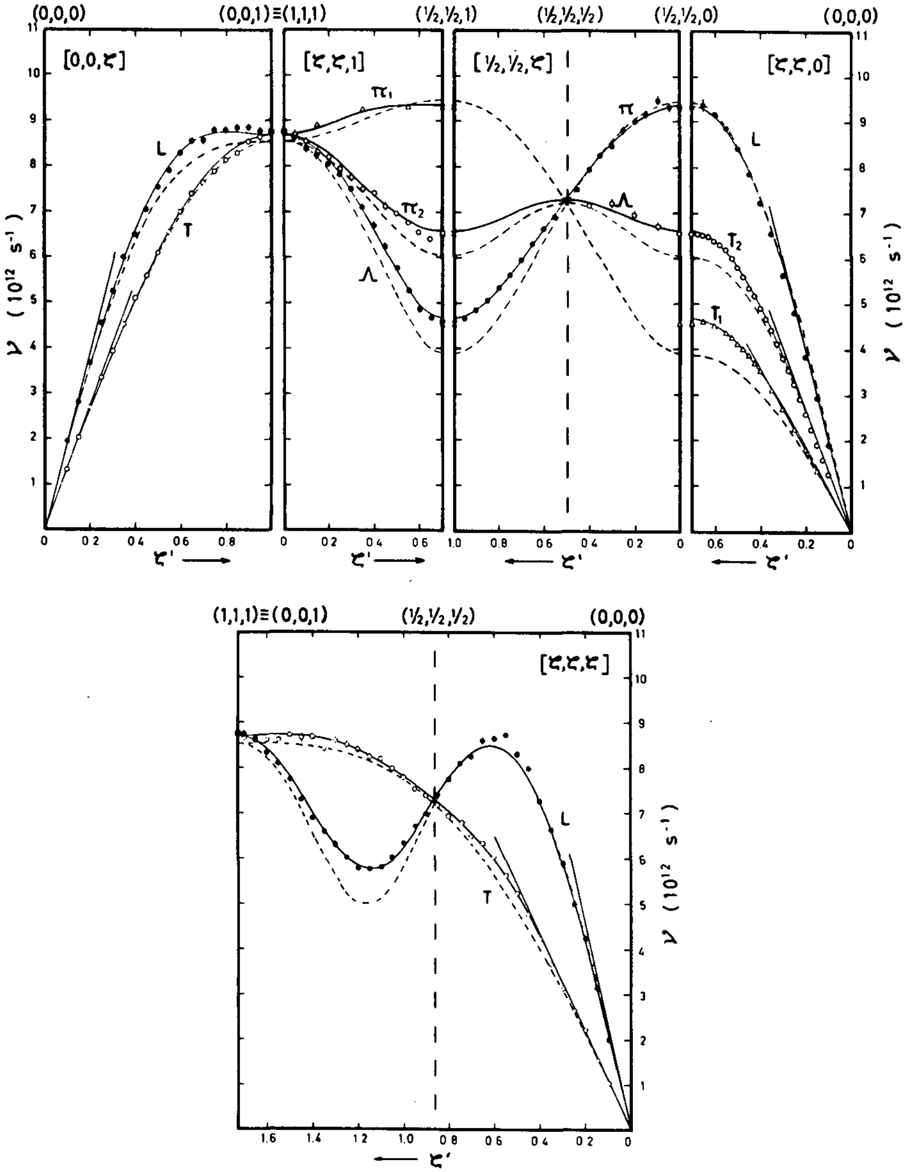

FIG.1. Dispersion relations for α-iron: solid lines: 5th neighbour Born-von Kármán model; dashed lines: Krebs' model.

atoms. A neutron diffraction study by Pickart and Nathans [6] showed that the type I atoms possess a magnetic moment much the same as in iron, whereas that for type II is lower by roughly 25%.

In this paper the result of the analysis for α-iron with all new data included is reported. In addition experimental data on Fe_3Al in the ordered phase, obtained with the same technique, are given. It is shown that the general behaviour of the dispersion relations can be understood from the dynamics of α-Fe when this is described on the Fe_3Al structure.

2. LATTICE DYNAMICS OF α-Fe

Since the previous publication [1] on the inelastic neutron scattering by phonons in iron the experimental work has been extended, in particular to branches at the zone boundary. Comparison with the results of Van Dingenen and Hautecler [2] obtained on an iron crystal with 3.5% silicon suggested appreciable differences in the dynamics of the two specimens. Therefore, part of the experiments were repeated on the same iron-silicon crystal, obtained through the courtesy of Dr. Hautecler.

TABLE I. INTERATOMIC FORCE CONSTANTS FOR IRON (10^2 dyn/cm)

	Present results	Minkiewicz et al. [5]	Brockhouse et al. [4]
α_1 (1XX)	178.6 ± 1.0	168.8	162.8
β_1 (1XY)	149.1 ± 1.3	150.1	148.5
α_2 (2XX)	149.2 ± 2.5	146.3	155.2
β_2 (2XY)	3.6 ± 1.4	5.5	5.4
α_3 (3XX)	12.4 ± 0.8	9.2	11.8
β_3 (3ZZ)	-10.9 ± 1.3	-5.7	-8.8
γ_3 (3XY)	3.0 ± 1.2	6.9	12.7
α_4 (4XX)	-6.0 ± 0.8	-1.2	-2.3
β_4 (4YY)	-0.6 ± 0.4	0.3	2.4
γ_4 (4YZ)	2.8 ± 0.8	5.2	3.9
δ_4 (4XZ)	1.0 ± 0.5	0.07	0.7
α_5 (5XX)	-2.3 ± 0.7	-2.9	-4.6
β_5 (5XY)	-2.4 ± 1.0	3.2	-3.0

The differences in the results turned out to be small and never exceeded 2%. Because of the larger size of the Fe(Si) crystal, the observed intensities were higher than for pure iron and consequently provided the possibility of improving the experimental data for the longitudinal branch in the [ζζ0] direction near the zone boundary.

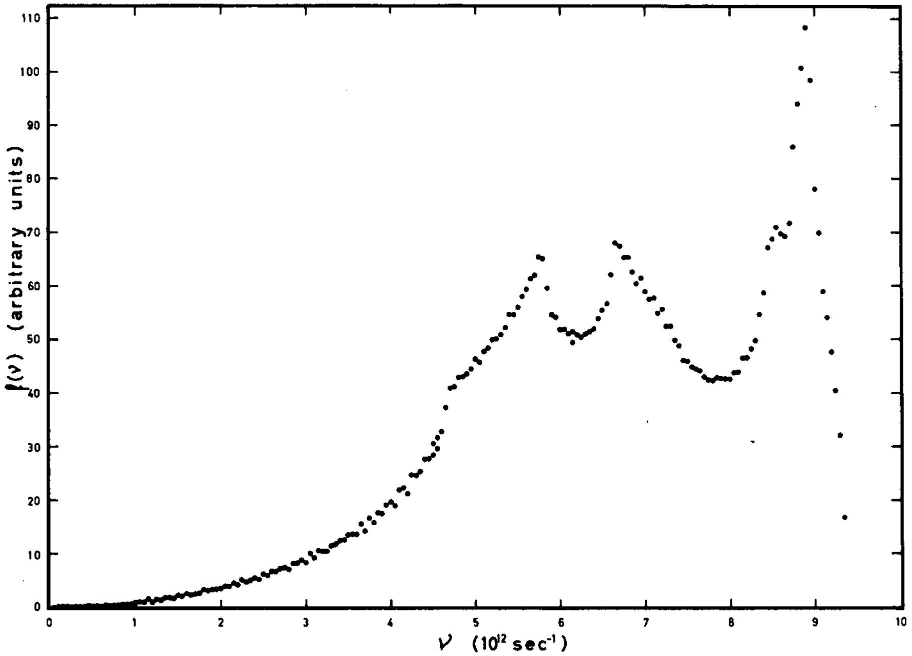

FIG. 2. Phonon frequency distribution calculated from interatomic force constants.

The whole set of experimental data is displayed in Fig. 1. The least-squares analysis in terms of the Born-von Kármán general forces model taking into account interactions out to fifth neighbours resulted in the set of interatomic force constants given in Table I. These results differ only slightly from those given previously [1], as could be expected since all new measurements were predicted quite well by the calculations using the old force constants. The disagreement with the earlier data for the longitudinal branch in the [ζζ0] direction and close to the zone boundary concerns a very small region only and has hardly any effect on the frequency distribution. Table I also gives the equivalent sets of force constants given by Minkiewicz et al. [5] and by Brockhouse et al. [4]. The agreement with the present results is rather good. The most significant differences between the three sets can be seen in the force constant α_1, mainly reflecting a small overall frequency shift with respect to each other, the largest α_1 giving the largest frequencies. The three sets agree with respect to the relation $\alpha_1 > \beta_1$, a fact which suggests that bonding occurs between nearest neighbours as pointed out by Brockhouse.

In Fig. 2 the phonon frequency distribution is shown; it has been calculated from the interatomic force constants by means of a sampling method. It is interesting to note that the highest peak in this distribution occurs for a frequency which is approximately 3% higher than the zone boundary frequency of the [ξ00] modes, which point according to Gilat [7] should give rise to a logarithmic singularity in the distribution. A similar tendency can be observed in the phonon frequency distribution of Minkiewicz et al. [5].

The attempt to describe the lattice dynamics of α-Fe by means of the Krebs' model [8] has already been reported. The dashed curves in Fig. 1 corresponding to that model show the failure of such a description.

3. LATTICE DYNAMICS OF Fe_3Al

The structure of Fe_3Al in the ordered phase can be described as four interpenetrating fcc lattices, one of aluminium and three of iron, each with a lattice spacing approximately twice that of iron. Compared to the bcc iron structure every fourth atom position along the [111] direction is occupied by an aluminium atom. There is much similarity between the dynamical behaviour of Fe_3Al and that of α-Fe, which is almost completely obscured when the dynamics of both specimens are described each on its own reciprocal lattice. In α-Fe one has, generally speaking, three acoustical branches, while in Fe_3Al with four atoms per primitive unit cell one has three acoustical plus nine optical branches. It is, therefore, very illuminating to describe iron according to the Fe_3Al lattice. In Fig. 3 the dashed lines indicate the zone boundaries in the $(1\bar{1}0)$ section of the normal iron reciprocal lattice, while the solid lines denote the corresponding section of the reciprocal lattice for Fe_3Al. For Fe_3Al points A, D and C are equivalent except for their structure factors. When iron is described on this lattice the parts AB, CB and DE should, for example, each fully contain the information of the [00ξ] direction which in the iron lattice is to be found by combining them. In Fig. 4(a) dispersion relations of α-Fe in the [00ξ] direction, described on the Fe_3Al lattice, are displayed. These data have been

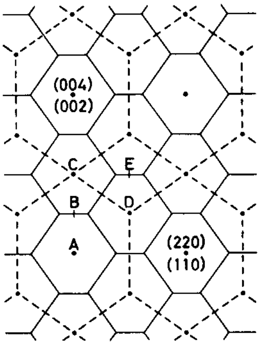

FIG. 3. $(1\bar{1}0)$ planes of the reciprocal lattices of the body-centred and face-centred cubic lattices with Brillouin zone boundaries indicated.

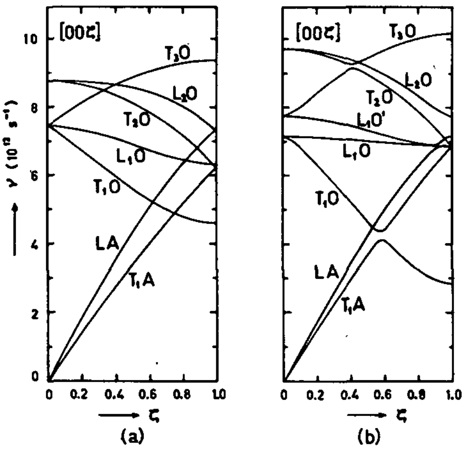

FIG.4. (a) Calculated dispersion relations for α-Fe in the [00ζ] direction described on the fcc lattice; (b) calculated dispersion relations for Fe_3Al in the [00ζ] direction.

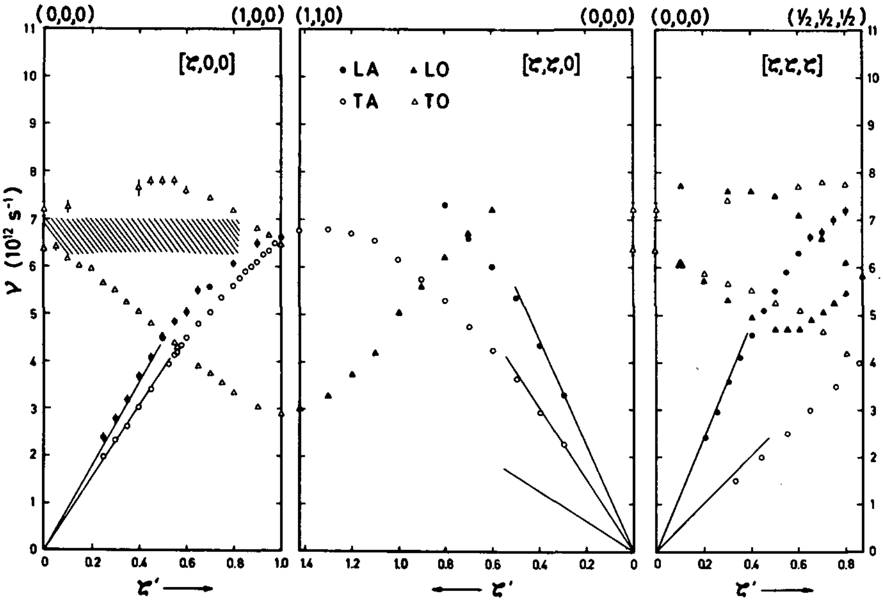

FIG.5. Experimental dispersion relations for Fe_3Al.

obtained from a Born-vonKármán model using forces out to second neighbours only. As in iron, the structure factor is known from simple symmetry considerations, approximate values for Fe_3Al are obtained by assuming equal structure factors for corresponding modes at corresponding points. This assumption is not unreasonable, and has served at least as a very useful guide for the phonon measurements carried out so far.

In Fig. 5 the experimental data obtained from a single crystal of ordered Fe_3Al, 6 cm in length and 2.5 cm in diameter, are displayed. The set is still far from complete, yet it shows some features which are of importance for the evaluation of the interatomic force constants. Force matrices and coefficients of the dynamical matrix have been used as evaluated by Borgonovi et al. [9], corrected for some obvious slight errors. In the present paper their notation of force constants is used.

A general forces Born-von Kármán model with second neighbour interactions contains 8 independent parameters. This number is reduced by 3 on introducing the elastic stiffness constants. These have recently been measured [10] for Fe_3Al and have the values: $c_{11} = 17.48 \times 10^{11}$ dyn/cm, $c_{12} = 13.00 \times 10^{11}$ dyn/cm and $c_{44} = 12.82 \times 10^{11}$ dyn/cm. These data show that the Cauchy relation $c_{12} = c_{44}$ is satisfied within 1.4%. It is, therefore, worthwhile trying a model with central forces, which leaves only 2 independent force constants. The ratio of the force constants γ and α describing the first neighbour iron-iron and iron-aluminium interactions determines to a large extent the degree in which dispersion relations of the same symmetry type are deflected away from each other at places where the iron dispersion relations (Fig. 4(a)) cross, when described with respect to the Fe_3Al lattice. The experimental data of Fig. 5 do not show any of these deflections in the dispersion curves, which suggests an iron-like behaviour. Therefore the assumption is made that $\alpha/\gamma = \surd(m/M)$, in close analogy with the iron model. Here M and m are the masses of iron and aluminium, respectively. Taking the same ratio for the force constants A and D of the second neighbour interactions, the iron-type behaviour is complete in that no gaps appear at the origin and zone boundaries where the iron dispersion relations are degenerate by symmetry. However, from the experimental data it is clear that a gap occurs at the origin between approximately 6.3×10^{12} and 6.9×10^{12} sec^{-1}.

There is also strong experimental evidence that in the $[00\zeta]$ direction the longitudinal mode, denoted as $L_1 0$ in Fig. 4(a), is split up. The measured phonons of this branch had much larger line widths than usual. This branch has been indicated in Fig. 5 by a shaded band, which probably consists of two separate modes.

Variation of the ratio of A and D gave a crude value for A, which would lead in the applied model to a splitting of the proper size. The set of interatomic force constants obtained in this way is:

$\alpha = \beta = 150 \times 10^2$ dyn/cm $\qquad \gamma = \delta = 215 \times 10^2$ dyn/cm
A = 25×10^2 dyn/cm $\qquad$ D = 117×10^2 dyn/cm $\qquad$ B = E = 0

In Fig. 4(b) the dispersion relations calculated with these constants are given. The agreement with the experimental data of Fig. 5 is rather poor for the optical modes. However, in the applied model, the elastic constants play a dominating role, and probably only an analysis with interactions out to more than second neighbours can improve the fit. Such an analysis will be undertaken in the near future, when more experimental results on the high energy optical modes will be available.

From the present analysis it seems very probable that in Fe_3Al the ratio between second and first neighbour interactions of iron atoms is much smaller than in α-Fe. More definite conclusions cannot be drawn at the present stage of this investigation.

ACKNOWLEDGEMENT

The authors wish to acknowledge Dr. D. Tocchetti, who participated during the first stage of this investigation.

REFERENCES

[1] BERGSMA, J., Van DIJK, C., TOCCHETTI, D., Phys. Lett. 24A (1967) 270.
[2] Van DINGENEN, W., HAUTECLER, S., Physica 37 (1967) 603.
[3] SCHWEISS, P., FURRER, A., BÜHRER, W., Helv. phys. Acta 40 (1967) 378.
[4] BROCKHOUSE, B.N., ABOU-HELAL, H.E., HALLMAN, E.D., Solid State Commun. 5 (1967) 211.
[5] MINKIEWICZ, V.J., SHIRANE, G., NATHANS, R., Phys. Rev. 162 (1967) 528.
[6] PICKART, S.J., NATHANS, R., Phys. Rev. 123 (1961) 1163.
[7] GILAT, G., Phys. Rev. 157 (1967) 540.
[8] KREBS, K., Phys. Rev. 138 (1965) 143.
[9] BORGONOVI, G., LOGIUDICE, G., TOCCHETTI, D., J. Phys. Chem. Solids 28 (1967) 467.
[10] LEAMY, H.J., GIBSON, E.D., KAYSER, F.X., Acta Met. 15 (1967) 1827.

DISCUSSION

R.I. SHARP: May I ask the author of paper SM-104/40 a question about his copper results? Bearing in mind the discrete angular steps through which triple-axis machines move, are the peak positions corrected for the efficiency of the counter and the actual energy at which the spectrometer 'looks'? Alternatively, was any correction made for incident spectrum?

G. NILSSON: There is no need for any such correction in this experiment. Every phonon was measured with the outgoing wavevector κ_2 fixed, and thus there was no change in the efficiency of the counter or analyser. Between two phonon measurements in a series where an anomaly was sought, κ_2 was changed in order to make it possible to use the same incident spectrum when the next phonon was measured. Furthermore a 1/v-sensitive monitor was used, and the monochromator was programmed to move in equal steps as regards energy and not as regards angle.

R.M. PICK: Could anybody explain the strong distortion in the $Cu_{0.9}Ni_{0.1}$ phonon spectrum? As far as I remember, the ratio of the Cu/Ni phonon is more or less constant for any frequency and wavelength.

B. MOZER: We have demonstrated conclusively that Cu/Ni is not an ideal solid solution. Diffraction data on $Cu_{52.5}{}^{62}Ni_{47.5}$ show short-range order of the clustering type, with nickel preferring to have more nickel surrounding it than would be expected from a random probability distribution. Clustering is bound to affect the electron states, phonon states, etc., and the electron bands for these alloys would not behave as rigid bands.

J.J. RUSH: I have a comment and a question on paper SM-104/128. In my opinion the statement that, due to spatial averaging, two separate peaks of the optical hydrogen vibrations cannot be observed in scattering from polycrystalline samples of NbH and VH is not correct. We have recently published a cold-neutron study of polycrystalline vanadium hydride in three crystal phases. We do observe double maxima in good agreement with the results given in paper SM-104/128, although they are not too well resolved. In addition, Pan et al. at Rensselaer Polytechnic Institute have recently reported the observation of a well-resolved double hydrogen peak in niobium hydride, which they obtained by energy-loss measurements on a polycrystal.

Could the authors say something more about the interpretation of the significant inelastic scattering intensity in the region of 5-meV energy transfer in $V_{99.96}\,H_{0.04}$?

R. RUBIN: In reply to your comment I would announce that in recent measurements in NbH, performed with the same resolution as that used for an NbH single crystal, we ourselves have detected the existence of the second peak. However, it was significantly smaller than in the single-crystal sample.

As regards your question, the inelastic intensity observed at very small transfer energies can be interpreted as quasi-elastic scattering due to a high mobility of the hydrogen atoms, a mobility which seems to exist only in the α-phase. The experimental results, especially from internal friction measurements, indicate the existence of tunnelling. In such a case the resulting energy bands would give rise to the low-energy intensity.

W. GISSLER: The theory of Chudley and Elliott predicts a deflection of the quasi-elastic line width dependent on κ^2. I imagine the κ region covered in the experiment described in this paper is too small to permit observation of this deflection. Could you say what value of κ would be required for this purpose?

R. RUBIN: Under the assumptions which we made, the value of κ for maximum ΔE should, according to the Chudley-Elliott model, be about 3 $\mathring{A}^{-1}$.

M.G. ZEMLYANOV: I also have one or two questions for Mr. Rubin. First, has he done experiments to determine the structure of metal hydrides using neutron diffraction? And secondly, what was the reason for choosing a temperature of 200°C for performing the measurements on niobium and vanadium hydrides?

R. RUBIN: We performed no diffraction measurements, but we did study the relative intensities of the localized peaks of vanadium hydride in the α- and β-phase over the temperature range 50-250°C and at concentrations ranging from 4 to 20%. Further data on the phase diagrams at lower temperatures (100-150°K) were obtained from internal friction measurements. We selected a temperature of 200°C, firstly to have a sufficiently high localized peak population in connection with the energy gain measurements, and secondly to obtain a large broadening of the quasi-elastic spectrum.

M.G. ZEMLYANOV: We have ourselves carried out neutron diffraction studies of niobium and vanadium hydrides, giving our attention both to the structure and to the dynamics of cold neutron scattering. These studies showed that in niobium hydride the order-disorder transition occurs at about 100°C, while in vanadium hydride the transition takes place at about -50°C. In the ordered state the hydrogen atoms occupy tetrahedral sites and form a sub-lattice. In niobium hydride the order-disorder transition is accompanied by an increase in quasi-elastic scattering. Evaluation of the coefficient of diffraction gave a value of 5×10^{-5}. In vanadium hydride no quasi-elastic broadening was observed at room temperature.

J.J. RUSH: May I ask Mr. Zemlyanov a question about his neutron diffraction results for vanadium hydride? Our inelastic scattering data on the tetragonal phase suggest that two types of lattice site, presumably octahedral and tetrahedral, are occupied by hydrogen atoms in this phase. How does this compare with the structural information from his diffraction data?

M.G. ZEMLYANOV: The neutron structure investigations on vanadium hydride showed that the hydrogen atoms are located in the tetrahedral sites.

J.J. RUSH: At what concentrations were the diffraction patterns measured?

M.G. ZEMLYANOV: The polycrystalline samples we first used had a near-stoichiometric composition of vanadium hydride, while the single crystals which we later employed contained about 3% hydrogen ($VH_{0.03}$).

W. GLÄSER: On the subject of the Fe_3Al system described in paper SM-104/137, do the authors of the paper hope, after completing and fully analysing their data, to obtain accurate information on the change in interatomic potential or in electronic density around an iron site, as a function of the additional aluminium atoms? This is of interest for Mössbauer effect studies on such systems, which are notoriously difficult to interpret.

An accurate calculation of the mean square displacement of the different atoms would likewise be of assistance.

C.van DIJK: First I would state that our investigations are still in a preliminary stage, and we are therefore somewhat reluctant to predict the amount of information which will be obtained from this experiment. But because of the close relationship between the α-Fe and the ordered Fe_3Al systems, which becomes clear when both systems are described with reference to the same lattice (as shown during the presentation of the paper), differences in the relevant force constants in α-Fe and Fe_3Al will reflect the difference in interatomic potential around the iron site. If the important role the electrons play in lattice dynamics were better understood, the change in this potential due to the aluminium atoms could probably be interpreted in terms of the electron density around the iron site.

INELASTIC NEUTRON SCATTERING ON SOLID AND LIQUID TELLURIUM AND SELENIUM

W. GISSLER, A. AXMANN AND T. SPRINGER
INSTITUT FÜR FESTKÖRPER- UND NEUTRONENPHYSIK,
KERNFORSCHUNGSANLAGE JÜLICH,
FEDERAL REPUBLIC OF GERMANY

Abstract

INELASTIC NEUTRON SCATTERING ON SOLID AND LIQUID TELLURIUM AND SELENIUM. The lattice dynamics of tellurium and selenium are of interest with regard to the relatively strong deformations of the valence electron shells and the asymmetric lattice structure of the crystal which consists of spiral chains in a hexagonal array. Inelastic scattering experiments have been performed on crystalline and liquid selenium and tellurium and on amorphous selenium using a rotating crystal and a triple-axis spectrometer. The experiments on selenium polycrystals and tellurium poly- and single crystals show high-energy modes which can be identified as intra-chain bond stretching modes with a pronounced molecular vibrational character. There are further optical modes at lower energies due to bond-shearing vibrations and to torsional modes of the chains against each other. The results are consistent with infrared experiments. No reliable check of the existing theories has been possible, but a rough agreement was found.

Comparing the spectra of polycrystalline, amorphous, and liquid selenium, there is no appreciable shift or broadening of the peaks ascribed to optical intra-chain modes in the amorphous and liquid phase. The influence of small admixtures of iodine has been studied which reduces the length of the chains. For liquid tellurium at 470 °C there are no peaks at all in the spectrum which results from a breakdown of the polymeric structure. The change of the quasi-elastic line width with the chain length was found to be considerably smaller than the change of the reciprocal viscosity.

1. INTRODUCTION

Crystalline selenium and tellurium have in common a structure [1] which consists of helical chains in a hexagonal array with 3 atoms per unit cell (Fig.1). The atoms are bound tightly to their next neighbours within the chains, whereas the interaction with the neighbours in adjacent chains is weaker. The difference [2] between the Se and Te structures is that the first neighbour distances within the chains are smaller for Se relative to the inter-chain distances because the covalent bonding is stronger. The pronounced 'individuality' of the chains in the case of Se is even maintained after melting.

Part of the optical lattice vibrations of Se and Te is infrared active with relatively low frequencies. This is due to appreciable deformations of the valence electron shells and to the low crystal symmetry. The interaction between these vibrations and the charge carriers has an important influence on the semiconductor properties [3]. For this reason and because of the highly asymmetric lattice structure, there is considerable theoretical interest in the lattice dynamics of these elements. Dispersion curves have been calculated by Hulin [4] on the basis of a model with three force constants. An improved model with seven force constants has been worked out by Geick et al.[5]. This uses general

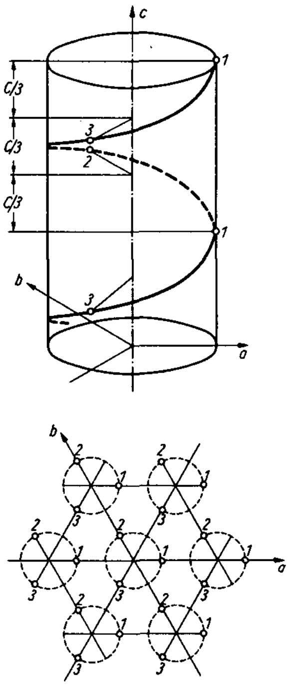

FIG. 1. Lattice structure of Se and Te.

forces between neighbours within a chain and central forces between adjacent chains.

The optical frequencies at wavevectors $q \simeq 0$ have been determined by a number of infrared experiments [3, 5-7]. Neutron spectroscopic measurements on Se and Te were performed previously by us [8] and on Se by Kotov et al. [9].

In both the vitreous and the liquid states Se is assumed to consist of chains (several 10 to 10^3 atoms long) mixed with a considerable amount of smaller rings (probably of the Se_8 type); Te is also considered to have a chain structure in liquid [10, 11]. The polymeric ring structure prevents immediate crystallization after solidification. The addition of small amounts of alkalides or halogens reduces the viscosity greatly and facilitates crystallization considerably. Te, on the other hand, crystallizes easily and relatively big single crystals can be grown.

Section 2 of our paper discusses neutron spectroscopic experiments on crystalline Se and Te in connection with the theory and with infrared experiments. In section 3 experiments on amorphous and liquid Se and Te are presented. The typical differences between both elements are discussed, as well as the influence of small amounts of admixtures in liquid Se.

2. EXPERIMENTS AND DISCUSSION OF THE RESULTS IN THE CRYSTALLINE PHASE

The measurements were performed with the rotating crystal spectrometer at the FRJ-2 (DIDO) reactor [12]. Its resolution is about

25 μsec/m. Part of the single crystal work was carried out with the triple-axis spectrometer at the FRJ-2. In this case eight Te single crystals (1 cm diam., 5 cm high) were fixed together and aligned by X-ray diffraction. For the polycrystalline samples the probability of both multiple scattering (combining two inelastic events) and two-phonon scattering has been estimated. The contribution of both is sufficiently small to avoid any spurious peaks.

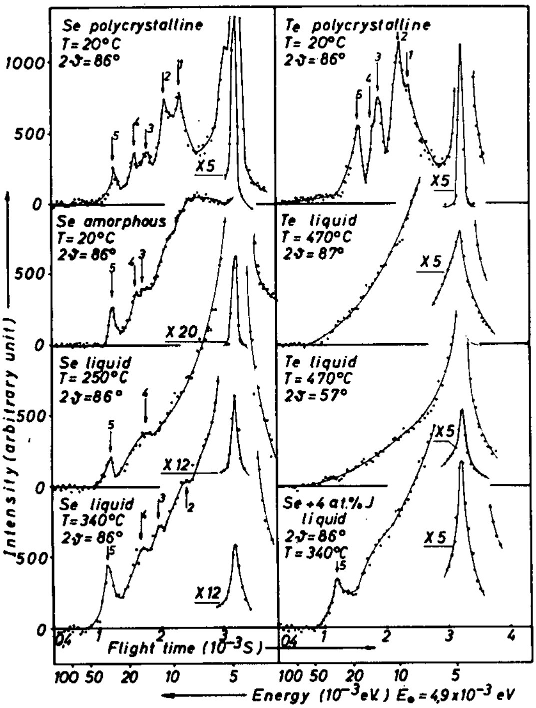

FIG. 2. Time-of-flight spectra on Se and Te at different temperatures. 2ϑ = scattering angle.

Figure 2 shows spectra from Se and Te polycrystals together with the results from the liquid and amorphous phase (see section 3). In the energy region corresponding to peaks 3, 4, 5 the shape of the spectra is not essentially affected by the condition of momentum conservation for coherent scattering because contributions from many different reciprocal lattice vectors come into play. A change of the scattering angle did not shift the position of these peaks. Therefore, we conclude that the peaks mark the energies for which the density of normal vibrations is high.

Figure 3 represents dispersion curves in the [100] direction of Te, as calculated by Geick and Schröder [5]. The force constants were found by an optimum fit using the elastic constants and the existing infrared data (squares at q = 0 in Fig. 3). Arrows show the peak positions taken from Fig. 2. A series of phonons has been measured on Te single crystals with the time-of-flight and the triple-axis instrument. Those in [100] direction are also shown in Fig. 3. Further measurements are in progress.

TABLE I. SPECTROSCOPIC RESULTS FOR SELENIUM AND TELLURIUM

Element			Selenium						Tellurium					
Vibration type			acoust.		O_1	O_2O_3	O_1'	$O_2'O_3'$	acoust.		O_1	O_2O_3	O_1'	$O_2'O_3'$
N	this work	cryst	4.6	7.1	11.7	16.2	31.5		4.8	6.0	10.0	10.5	18.5	
		amorph	-	-	-	15.3	32.4							
		liquid[a]	-	-	12.8	-	34		-	-	-	-	-	-
IR	[7]	cryst			-	17.5	-	34			11	13	-	-
		amorph			-	14.6	-	31						
	[5]	cryst			12.8	17.3	-	28.8			-	12.5	-	-
	[6]	cryst									10.7	11.4	-	17.6
	[3]	cryst			12.6	17.7		27.7			11.1	11.3	-	17.7
		amorph	many peaks betw. 6.2 and 31.4											
Th	[4]	cryst									9.2	15.2		20.1

N: Line energies (in units of 10^{-3} eV) from neutron spectroscopy (maxima of the states density). IR: infrared spectroscopy ($q \simeq 0$); [a] at 350 °C.
Th: Theory.

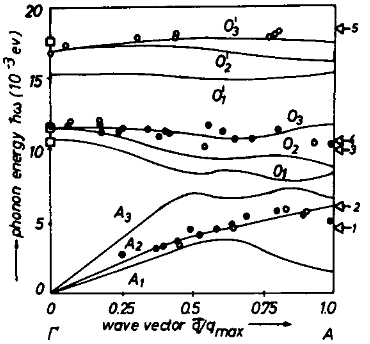

FIG. 3. Wavevector q and frequency $\omega/2\pi$ for Te in [100] direction. Solid curves: theory [5]. O time-of-flight, ● triple-axis experiments. Squares at $q = 0$: infrared experiments [6]. Arrows: position of neutronic intensity peaks from Fig. 2.

The three highest branches (0') in Fig. 3 are primarily due to stretching modes of the rather stiff intra-chain bonds. For a scattering vector $\vec{\kappa}$ parallel as well as perpendicular to the hexagonal axis the experiment did not resolve these three branches. Therefore, the splitting of the 0' modes must be much smaller than predicted by theory.

The calculated lower optical branches are attributed to intra-chain bond shearing modes (O_2, O_3) and torsions of the chains against each other (O_1) for $q \simeq 0$. Branch O_3 falls into the region of the experimental points. O_1 and O_2 might have been missed in the experiment due to a small dynamical structure factor. Consistency exists between the neutron data at $q \simeq 0$ and the infrared lines at 17 and 11×10^{-3} eV. The agreement between the rather sharp peak energies from the polycrystal (arrows) and the energies of the high optical branches in Fig. 3 is an indication of the isotropy and the relatively small slope of $\omega(q)$ for these phonons. Table I compares all available data.

The frequency ratio $\nu(Se)/\nu(Te)$ is smaller than $(M_{Te}/M_{Se})^{\frac{1}{2}} = 1.27$ for the O_1 mode (1.17), and considerably greater for the O' modes (1.7) and for the modes O_2 and O_3 (1.5). This indicates nearly two times higher coupling constants within the chains for Se than for Te, and naturally an even more pronounced 'molecular' character of the modes O', O_3 and O_2.

3. AMORPHOUS AND LIQUID PHASE

Comparing the spectra of crystalline, amorphous and liquid Se (Fig. 2; Table I), there is no relevant shift or broadening of the high-energy peak 5 which we identify by the intra-chain bond stretching mode (like O' in the crystal) of the polymeric chains in liquid and amorphous Se. Peak 5 might also contain stretching vibrations within Se_8 rings. They will not be very different from those in the (more or less) straight chains because the nearest neighbour arrangement is approximately the same. Peaks 3 and 4 in the amorphous phase correspond to peaks 3 and 4 in the crystal (O_1 and O_2O_3). Peak 4 in the liquid is assumed to correspond to peak 3 in the amorphous phase (explained by torsional motions). Surprisingly, this peak seems to be more pronounced in the liquid than in

TABLE II. EFFECTIVE DIFFUSION CONSTANTS AND VISCOSITY OF LIQUID SELENIUM AND TELLURIUM

Sample	Deff (cm^2/sec)	Viscosity (poise)	Estimated chain length (atoms)
Se (340 °C, pure)	0.9×10^{-5}	1.7	85-100
Se (340 °C + 4% J)	1.4×10^{-5}	~0.5	~50
Te (450 °C)	2.6×10^{-5}		-

the amorphous phase; this might result from a greater flexibility of the chains to rearrange with their neighbours. Peaks 2 and 3 do not coincide with the peaks in the polycrystal.

The addition of halogens, as iodine, reduces the chain length, presumably by forming J-Se...Se-J complexes such that the average chain length is just $n = 2/p$, where p is the atomic fraction of the iodine admixture [10]. This helps to increase the disorder amongst the chains which could explain the disappearance of peak 4, whereas peak 5 appears to become less intense.

In Te the spectral structure has disappeared completely above the melting temperature (450°C). This could be assumed to result from a rather complete breakdown of the chain structure. On the other hand, X-ray patterns of liquid Se and Te are not drastically different [14]. The observed amount of smearing of the Te spectrum could not be interpreted merely by a stronger contribution of multiphonon scattering (this is infered from a comparison of the spectra of Te at 20°, and 350°C).

The loss of the peak structure in the spectra is connected with an increase of the quasi-elastic line width Γ. We define an effective diffusion constant D_{eff} by[1] $\Gamma = 2\hbar\kappa^2 D_{eff}$ (in a somewhat similar sense as in Ref.[13]). This describes the combined diffusive motion of individual atoms, namely the parallel motion of the chains, torsional jumps, and the diffusion of the Se_8 rings. Table II shows the viscosity η, D_{eff}, and estimated chain lengths [10] using for pure Se the relation $\ln \eta = \text{const}\ n^{\frac{1}{2}}$ [16]. The viscosity increases stronger than $1/D_{eff}$. This could be explained by assuming that η is mainly determined by the mobility of large fragments of the chains, whereas D_{eff} is given by the motion of single atoms within the chains, and of small atomic groups, as Se_8. More detailed studies on the relation between the quantities of Table II are in preparation.

---

[1] The influence of the line narrowing effect [15] on the κ^2 dependency of Γ was shown to be safely below 20% by a series of measurements on liquid Se [8].

ACKNOWLEDGEMENTS

The authors are indebted to Prof. H. Krebs for stimulating discussions connected with the chemical aspects of the problem, Dr. P. Grosse for the preparation of the Te single crystals and for helpful discussions, and Dr. B. Dorner and Dr. H.H. Stiller for their support and co-operation at the triple-axis spectrometer. Finally, we thank Dr. G. Wolff for the chemical preparation of the samples.

REFERENCES

[1] GMELIN, L., Hdb. Anorg. Chemie A (Selen), Weinheim (1953); WYCKHOFF, R.W., Crystal Structures, New York (1963).

[2] KREBS, H., Angew. Chem. 70 (1958) 615.

[3] LUCOVSKY, G., KEEZER, R.C., Solid State Comm. 5 (1967) 439.

[4] HULIN, M., Annls Phys. 8 (1963) 647.

[5] GEICK, R., SCHRÖDER, U., STUKE, J., Proc. 1st Int. Symp. Physics of Se and Te, Montreal, 1967 (to be published); GEICK, R., SCHRÖDER, U., to be published (1968).

[6] GEICK, R., GROSSE, P., RICHTER, W., Proc. 1st Int. Symp. Physics of Se and Te, Montreal, 1967 (to be published).

[7] CALDWELL, R.C., FAN, H.J., Phys. Rev. 114 (1959) 664.

[8] AXMANN, A., GISSLER, W., Phys. Stat. Sol. 19 (1967) 721; AXMANN, A., GISSLER, W., SPRINGER, T., Proc. 1st Int. Symp. Physics of Se and Te, Montreal, 1967 (to be published).

[9] KOTOV, B.A., OKUNEVA, N.M., REGEL, A.R., Sov. Phys. Sol. State 9 (1967) 955.

[10] KREBS, H., MORSCH, W., Z. anorg. allg. Chem. 263 (1950) 305.

[11] EPSTEIN, A.S., FRITZSCHE, H., LARK-HOROWITZ, K., Phys. Rev. 107 (1957) 412; KREBS, H., Z. anorg. allg. Chem. 265 (1951) 156.

[12] AXMANN, A., GISSLER, W., Rep. JÜL-338 NP (1965); AXMANN, A., Thesis T.H. Aachen (1967).

[13] LARSSON, K.-E., DO AMARAL, L.Q., IVANCHEV, N., RIPEANU, S., BERGSTEDT, L., DAHLBORG, U., Phys. Rev. 151 (1966) 126.

[14] BUSCHERT, R., GEIB, I.G., LARK-HOROWITZ, K., Phys.Rev. 98 (1955) 1157.

[15] SINGWI, K.S., Physica 31 (1965) 1257.

[16] FLORY, P.J., J. Am. chem. Soc. 62 (1940) 1057.

DISCUSSION

L.A. de GRAAF: How do the measured effective diffusion coefficients compare with the macroscopic data?

T. SPRINGER: No macroscopic self-diffusion data were available.

G.S. PAWLEY: This is really a point of nomenclature. Mr. Springer mentioned that he had a branch on his dispersion curves which was very nearly flat, and he described this as having practically no dispersion. Now, a phonon branch with no dispersion is really a straight line from the origin of the dispersion curves. I feel, therefore, that some alternative terminology is necessary to describe flat optical mode branches in which the frequency is independent of wavevector. To say that these branches have no dispersion may well be confusing to the uninitiated!

T. SPRINGER: At all events I meant optical branches of a highly 'molecular' character where the change of ω as a function of q is very small, as is the case with the highest branches shown in my figures.

B.M. POWELL: The model used to interpret your single-crystal measurements was obtained by fitting to four optical frequencies and two elastic constants. Can you tell me how good this fit was when applied to the optical frequencies for tellurium, and how the fit compared with that for selenium?

W. GISSLER: The fit for tellurium was good, with an error of about 10%, while for selenium it was poorer (error about 25%), owing to the more pronounced anisotropy in the case of the latter element.

ATOMIC VIBRATIONS IN FACE-CENTRED-CUBIC ALLOYS OF Bi, Pb AND Tl

S.C. NG* AND B.N BROCKHOUSE
DEPARTMENT OF PHYSICS,
McMASTER UNIVERSITY,
HAMILTON, ONT., CANADA

Abstract

ATOMIC VIBRATIONS IN FACE-CENTRED-CUBIC ALLOYS OF Bi, Pb AND Tl. The atomic vibrations in the alloy systems Bi-Pb-Tl have been studied at 100°K, over a wide range of electron concentrations (3.2-4.15 electrons per atom), by inelastic neutron scattering. Six binary alloys and one ternary have been investigated. The dispersion curves for these alloys show a progressive change with electron concentration. The main features of the dispersion curves for pairs of alloys having the same electron concentrations (3.4 and 4.0 electrons/atom) are quite similar. The variation of the frequencies with electron concentration indicates that the electron-phonon coupling strength increases with increasing electron concentration. This result correlates well with the superconducting properties of the alloys.

Analysis of the dispersion curves based on Born-von Kármán theory shows that long-range forces extending beyond the eight neighbour exist for these materials. However, distant neighbour interactions appear to become smaller as the electron concentration in the alloy systems is reduced. The dispersion curves for some of the alloys are believed to show Kohn anomalies similar to those observed in Pb. The anomalies in the alloys have moved and grown weaker with respect to those in Pb. From these anomalies, diameters of the Fermi surface along the [110] and [111] directions have been deduced for the Pb-Tl alloys. The results are consistent with the rigid band model.

The neutron groups observed in the alloys are in general reasonably sharp and well-formed. They are, however, somewhat broader than those observed in Pb, particularly those in the ternary alloy ($Bi_{0.2}Pb_{0.6}Tl_{0.2}$). The broadening of the neutron groups has been attributed to the force constant disorder in the alloys. A theoretical discussion based on perturbation theory is given. The widths involve products of pairs of deviations (of the force constants from their mean values) and hence are relatively insensitive to force constant order.

I. INTRODUCTION

Considerable effort has been devoted in recent years to determination of phonon dispersion relations for pure metals by neutron inelastic scattering. The motivation behind the work is largely interest in the interatomic forces, the electron-phonon interaction, and the electronic structure of metals. Similar studies on alloy systems have recently been undertaken [1,2,3,4]. In addition to the interest in alloys *per se*, such experiments offer the possibility to study *specific* features of the crystal dynamics of metals in a controlled way; in particular effects of smooth variations in the atomic force constants, of changes in conduction electron concentration and of changes in the relative concentrations of 3d and

---

* Now at Clarendon Laboratory, Oxford, England. This work forms part of a Ph. D. thesis submitted to McMaster University (1967).

4s electrons may be studied. By proper choice of alloy system, it is possible to separate, to a large extent, these various effects,

The present work on Bi-Pb-Tl alloy systems was designed to study the effects of atomic force constant variation and of changes in conduction electron concentration. Bi-Pb-Tl alloy systems are favourable for these studies for several reasons:

(i) Bi, Pb and Tl are neighbouring elements in the periodic table; differences in the masses can be completely neglected (see § 4).

(ii) The ion cores are small and thus the interatomic forces are almost completely metallic. Overlap interaction between the core electrons can be neglected.

(iii) Disordered substitutional alloys of Bi, Pb and Tl having a face-centred-cubic structure exist for binary compositions of Bi-Pb(0-18 at. % Bi), Bi-Tl (4-27 at.% Bi) and Pb-Tl (13-100 at.% Pb). It is thus possible to change the conduction electron concentration from about 3.1 to 4.18 electrons per atom.

(iv) The alloys are superconductors with relatively high transition temperatures. This indicates that the electron-phonon interaction is rather large, so that effects of conduction electrons on the crystal dynamics are observable.

(v) Neutron properties of the elements are good, in that the capture and incoherent scattering cross sections are small. The coherent cross sections are almost identical (Tl-10b; Pb-11.5b; Bi-9.35b), a fact favorable from the point of the phonon experiments, though not from the point of view of detecting order in the alloys.

Six binary alloys ($\mathrm{Bi_{0.15}Pb_{0.85}}$, $\mathrm{Bi_{0.1}Tl_{0.9}}$, $\mathrm{Bi_{0.2}Tl_{0.8}}$, $\mathrm{Pb_{0.4}Tl_{0.6}}$, $\mathrm{Pb_{0.6}Tl_{0.4}}$, and $\mathrm{Pb_{0.8}Tl_{0.2}}$), and one ternary ($\mathrm{Bi_{0.2}Pb_{0.6}Tl_{0.2}}$), have been investigated at 100°K. The electron concentration ranges from 3.2 to 4.15 electrons per atom. The alloy crystals used were grown by Research Crystals Inc. of Richmond, Virginia, using the Bridgman method; they were cylindrical, 3.1 cm in diameter x 9 cm long. It is desirable to know the compositions and homogeneities of the alloy crystals, as well as the lattice constants and mosaic widths. We have used neutron diffraction to obtain these characterizations [5]. Because the large neutron beam takes in and penetrates almost the whole ingot, the lattice constants obtained by this method characterize the mean composition of the ingot, and the spreads in lattice constant characterize its homogeneity. Results indicated that the measured mean compositions were in good agreement with the nominal compositions. With the exceptions of $\mathrm{Bi_{0.15}Pb_{0.85}}$ and $\mathrm{Bi_{0.2}Pb_{0.6}Tl_{0.2}}$, the alloy crystals were of good quality. The degrees of inhomogeneity range from 1 to 5% (in composition) and the mosaic widths range from 0.4° to 0.8° (F.W.H.M.).

2. DISPERSION CURVES AND FORCE CONSTANT MODELS

The frequency-wave vector dispersion relations for the lattice vibrations in the seven crystals were measured, mainly along the four major symmetry directions. The measurements were made on two different triple axis crystal spectrometers - the Chalk River (C5) spectrometer [6] and the McMaster University spectrometer [7] at Chalk River. The measurements were made usually in the 'Constant $\underset{\sim}{Q}$' mode of operation [6], and in neutron energy loss. In order to reduce the occurrence of spurious neutron groups arising from higher order reflections of the monochromator and of the analyzer, a 15 cm. quartz single crystal filter was normally used in the incoming beam. In several cases the same normal mode was studied in two planes of the reciprocal lattice, (100) and $(1\bar{1}0)$, and with both spectrometers. In all cases agreement was well within the assigned errors.

The results indicate that marked regularities exist. The dispersion curves for the alloys show a progressive change, both in general frequency level and in shape, with electron concentration. Alloys in different systems which have the same electron concentration, have similar dispersion curves.

According to recent theories of crystal dynamics of metals, the interatomic forces can be considered to consist of three parts: (1) Coulomb force between the bare ion, (2) interatomic forces acting via the conduction electrons and (3) exchange repulsive force arising from the overlap of ion cores (which can be neglected in these materials). The frequencies of the lattice vibrations can be separated into two parts [8],

$$\omega^2 = \omega_d^2 - \omega_e^2 = \omega_p^2 \; (I_d - I_e) \quad ,$$

where ω_d^2 is the contribution from the direct Coulomb interaction, ω_e^2 is the contribution from the indirect interaction via the conduction electrons, ω_p is the plasma frequency for the ions, given by the expression

$$\omega_p^2 = 16\pi \frac{(Ze)^2}{Ma^3} \quad .$$

I_d depends only on the crystal structure and I_e depends on the electron-phonon coupling strength. The average mass (M) and charge (Ze) for the ions in the alloys were used to calculate ω_p^2 . If the phonon frequencies were dominated by the direct Coulomb interaction between the ions, then ω^2/ω_p^2 would be similar for equivalent modes. In fact, they vary quite drastically, and depend on the conduction electron concentration as well as on the particular mode considered. In general ω^2/ω_p^2 decreases with increasing conduction electron concentration;

see, for example, Fig. 2 of ref. [3]. That is to say, the contribution from the indirect interaction increases with increasing electron concentration, which in turn indicates that the electron-phonon coupling increases with electron concentration.

The overall shapes of the dispersion curves are quite different for alloys with different electron concentrations. Fig. 1 shows a comparison between the dispersion curves for the alloy $Pb_{0.4}Tl_{0.6}$ (3.4 electrons per atom) and for pure Pb (4 electrons per atom). (The results for

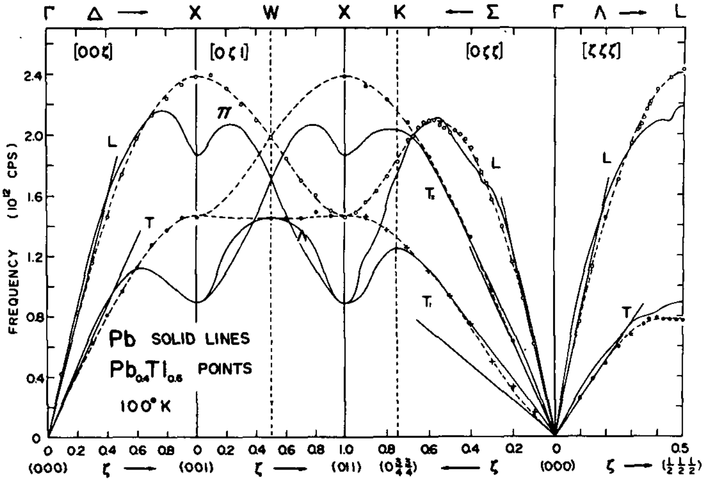

FIG. 1. Dispersion curves of fcc lead [9] and of a fcc lead-thallium alloy for the major symmetry directions. To avoid confusion no experimental points are shown for lead. The dashed curves represent a Born-von Kármán fit to the measurements for the alloy. The slopes of the straight segments of line through the origin represent the velocities of sound of the alloy.

Pb were taken from the literature [9]; to avoid confusion, the experimental points for Pb are omitted). Striking differences exist in the two sets of dispersion curves. In particular, the local minima observed for Pb near the points X(100) disappear for the alloy. However, the main features of the dispersion curve for pairs of alloys having the same electron concentration are quite similar. Fig. 2 compares the results for two alloys ($Pb_{0.4}Tl_{0.6}$ and $Bi_{0.2}Tl_{0.8}$) which have the <u>same</u> number (3.4) of conduction electrons per atom. In fact, the mean frequency ratio $\langle\nu(Pb_{0.4}Tl_{0.6})/\nu(Bi_{0.2}Tl_{0.8})\rangle$ is 1.033 ± 0.005 with a standard deviation of a single ratio from the mean of 0.027. The standard deviation expected from the estimated errors is 0.05; thus the curves for the two materials are almost identical except for a 3% scale change.

The ternary alloy, $Bi_{0.2}Pb_{0.6}Tl_{0.2}$, and Pb comprise another pair of analogous materials with 4 conduction electrons per atom; the mean ratio $<\nu(Bi_{0.2}Pb_{0.6}Tl_{0.2})/\nu(Pb)>$ is 0.963 ± 0.006 with a standard deviation of 0.050. Again the homology of the lattice vibrations [10] is quite pronounced, though less so than for the preceding pair. The results indicate that the lattice dynamics of these alloys are principally determined by the number of conduction electrons per atom.

An analysis of the dispersion curves has been carried out on the basis of Born-von Kármán theory. From previous work [9] on Pb, it is obvious that the Born-von Kármán model is not very useful for purposes of detailed analysis, because of the long-range nature of the interatomic forces.

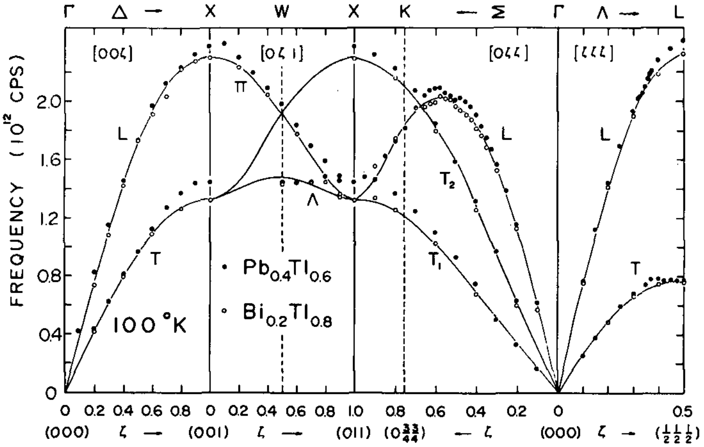

FIG. 2. Dispersion curves for two alloys having the same number of electrons per atom (n_e = 3.4).

Nevertheless, approximate fits to the measurements are obtainable and the resultant models may be adequate for some purposes.

We have carried out the analyses using the programs of SVENSSON et al.[11]. The results are tabulated in Table 1. Reasonably good fits were obtained using 8th neighbour models, with forces from fifth to eighth neighbours constrained to be axially symmetric. Better fits were obtained for alloys with small electron concentrations than for those with large. It was possible to fit the observed frequencies for $Bi_{0.1}Tl_{0.9}$ with a mean deviation of 1.2%, about the same as the expected deviation due to experimental error. However, the best fit for Pb has a deviation of 2.8%, about twice the expected experimental deviation. The goodness of fit for the other alloys lies between these two extremes. Examples of the results are shown by dashed lines in Fig. 1 for $Pb_{0.4}Tl_{0.6}$ and by solid lines in Fig. 2 for $Bi_{0.2}Tl_{0.8}$. Measure-

TABLE I. ATOMIC FORCE CONSTANTS FOR Bi-Pb-Tl ALLOYS AT 100°K IN UNITS OF dyne/cm

AFC	$Bi_{0.15}Pb_{0.85}$	$Bi_{0.2}Pb_{0.6}Tl_{0.2}$	Pb	$Pb_{0.8}Tl_{0.2}$	AFC	$Pb_{0.6}Tl_{0.6}$	$Pb_{0.4}Tl_{0.6}$	$Bi_{0.2}Tl_{0.8}$	$Bi_{0.1}Tl_{0.9}$
1XX	3564 ± 88	3687 ± 75	3933 ± 65	4055 ± 78	1XX	4603 ± 90	4944 ± 63	4679 ± 99	4984 ± 82
1ZZ	-1426 ± 178	-1574 ± 152	-1280 ± 133	-1111 ± 182	1ZZ	-1333 ± 194	-1532 ± 142	-1448 ± 213	-1485 ± 164
1XY	5170 ± 118	5037 ± 118	4929 ± 98	5270 ± 128	1XY	5445 ± 141	5540 ± 120	5198 ± 164	6161 ± 172
2XX	1922 ± 111	1532 ± 100	1617 ± 92	976 ± 101	2XX	407 ± 108	43 ± 82	151 ± 130	65 ± 130
2YY	-23 ± 76	-15 ± 71	309 ± 60	103 ± 82	2YY	-128 ± 82	-148 ± 65	-129 ± 102	107 ± 91
3XX	-499 ± 122	-312 ± 96	-266 ± 90	-252 ± 117	3XX	-97 ± 133	193 ± 88	104 ± 139	-26 ± 105
3YY	170 ± 57	71 ± 46	41 ± 46	59 ± 51	3YY	-92 ± 62	-150 ± 40	-133 ± 66	-44 ± 52
3YZ	349 ± 61	233 ± 60	349 ± 52	147 ± 59	3YZ	53 ± 59	-4 ± 53	-37 ± 73	-72 ± 86
3XZ	35 ± 34	40 ± 32	-58 ± 27	-4 ± 30	3XZ	45 ± 33	-8 ± 22	-61 ± 36	-66 ± 42
4XX	763 ± 40	572 ± 37	757 ± 31	566 ± 39	4XX	382 ± 40	141 ± 32	251 ± 51	-3 ± 46
4ZZ	136 ± 58	25 ± 51	105 ± 51	-68 ± 57	4ZZ	-9 ± 61	-6 ± 47	-60 ± 72	-74 ± 69
4XY	265 ± 133	176 ± 143	376 ± 124	-51 ± 152	4XY	-100 ± 164	123 ± 124	337 ± 188	12 ± 164
5XX	74 ± 99	-4 ± 86	-288 ± 75	-35 ± 103	5XX	-64 ± 116	-142 ± 75	-156 ± 115	12 ± 97
5YY	-293 ± 42	-221 ± 43	-341 ± 41	-217 ± 54	5YY	-26 ± 59	67 ± 41	40 ± 62	-7 ± 52
5ZZ	-339 ± 56	-248 ± 56	-347 ± 54	-240 ± 70	5ZZ	-21 ± 77	93 ± 53	64 ± 80	-10 ± 68
5XY	138 ± 48	81 ± 47	20 ± 41	68 ± 55	5XY	-14 ± 62	-79 ± 41	-73 ± 61	7 ± 52
6XX	53 ± 29	-6 ± 26	34 ± 26	50 ± 28	6XX	-25 ± 30	-81 ± 24	1 ± 36	11 ± 35
6YZ	-213 ± 83	-88 ± 77	-177 ± 70	8 ± 82	6YZ	43 ± 84	23 ± 63	117 ± 107	15 ± 87
7XX	-81 ± 49	-32 ± 46	-59 ± 42	-97 ± 54	7XX	-10 ± 62	97 ± 42	51 ± 63	38 ± 54
7YY	143 ± 54	84 ± 47	133 ± 44	101 ± 59	7YY	31 ± 68	-38 ± 43	-81 ± 69	17 ± 55
7ZZ	-9 ± 22	-1 ± 21	30 ± 21	40 ± 28	7ZZ	26 ± 28	-5 ± 19	20 ± 33	-25 ± 25
7YZ	25 ± 15	12 ± 14	33 ± 14	13 ± 14	7YZ	9 ± 14	10 ± 13	-7 ± 15	4 ± 15
7XZ	37 ± 22	18 ± 22	50 ± 20	20 ± 21	7XZ	14 ± 20	14 ± 20	-10 ± 22	7 ± 20
7XY	74 ± 21	37 ± 20	100 ± 14	39 ± 16	7XY	27 ± 17	29 ± 10	-21 ± 23	13 ± 22
8XX	85 ± 115	144 ± 107	679 ± 77	197 ± 70	8XX	44 ± 83	-114 ± 77	-34 ± 130	-131 ± 82
8YY	263 ± 78	267 ± 73	185 ± 51	88 ± 57	8YY	-35 ± 55	-7 ± 47	39 ± 93	78 ± 64

Force constant matrix $\begin{pmatrix} nXX & nXY & nXZ \\ nXY & nYY & nYZ \\ nXZ & nYZ & nZZ \end{pmatrix}$

Reference atoms

$\frac{a}{2}(h k \ell)$, $h \geq k \geq \ell \geq 0$

ments have been carried out on a number of off-symmetry modes at q-values uniformly distributed in the $(1\bar{1}0)$ plane for some of the alloys, in an attempt to test the goodness of the models for predicting the off-symmetry properties. The mean frequency ratios $\langle\nu(\text{calculated})/\nu(\text{measured})\rangle$, for the alloys examined are as follows:

$Pb_{0.4}Tl_{0.6}$	0.99 ± 0.007	for 11 phonons
$Bi_{0.2}Tl_{0.8}$	1.01 ± 0.01	for 11 phonons
$Bi_{0.2}Pb_{0.6}Tl_{0.2}$	0.99 ± 0.02	for 10 phonons
$Bi_{0.15}Pb_{0.85}$	1.04 ± 0.02	for 9 phonons

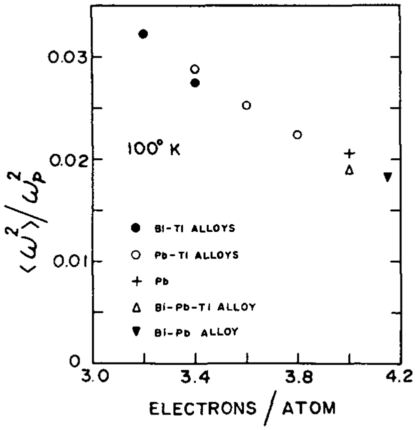

FIG.3. The second moments of the frequency distributions for some Bi-Pb-Tl alloys (in units of the plasma frequency for the ions), plotted as a function of the conduction electron concentration.

The above results indicate that, on the average, the measured frequencies of off-symmetry phonons differ from those predicted by the model by less than 2% (including errors) for the first three materials. For the last material, the difference is somewhat larger than desirable. This shows that the models are reasonably good for alloys having small electron concentrations, but less reliable for alloys with large concentrations. This result agrees with recent work of STEDMAN et al.[12] on Pb.

The results of the analysis indicate that long-range forces extending beyond eighth neighbours exist for all the materials. The interactions with distant neighbours appear to become weaker as the electron concentration in the alloy systems is reduced; for this reason better fits were obtained with the low concentration alloys.

The force constant models have been used to calculate the second moment of the frequency distributions (the average of ω^2 over the whole frequency distribution); the second moments (in units of the ion plasma frequency) are plotted as a function of electron concentration in Fig. 3.

The conclusion about the electron-phonon interaction is the same as stated previously, namely that the coupling strength increases with electron concentration. The superconducting transition temperatures, T_c, of Pb-Tl and Bi-Tl alloys have been measured by CLAESON [13]. His results show that T_c increases with electron concentration, indicating again an increase in the electron-phonon interaction with electron concentration.

3. KOHN ANOMALIES

As was demonstrated in the previous section, the conduction electrons have pronounced effects on the crystal dynamics of these alloy systems. Anomalies of the type predicted by KOHN [14] should therefore be observable. Kohn anomalies manifest themselves as logarithmic singularities in the gradient of the phonon dispersion curves. These singularities correspond to an abrupt change in the ability of the electrons to screen out the ion motions; they occur wherever the phonon wave vector is equal to an extremal distance across the Fermi surface. The existence of Kohn anomalies has been well established experimentally in Pb [9]. We think that we have observed in the Bi-Pb-Tl alloy anomalies corresponding to those observed for Pb in the L[ζζ0] and L[ζζζ] branches. The results for Pb-Tl alloys are shown in Fig. 4. (On the same figure, the behaviour of the dispersion curves in the L[ζ00] branch is also illustrated.) The arrows indicate the nature (upward or downward) of the anomalies. It can be seen that the anomalies in the alloys have moved and grown weaker compared with those in Pb. The positions of the anomalies give the Fermi diameters along the face

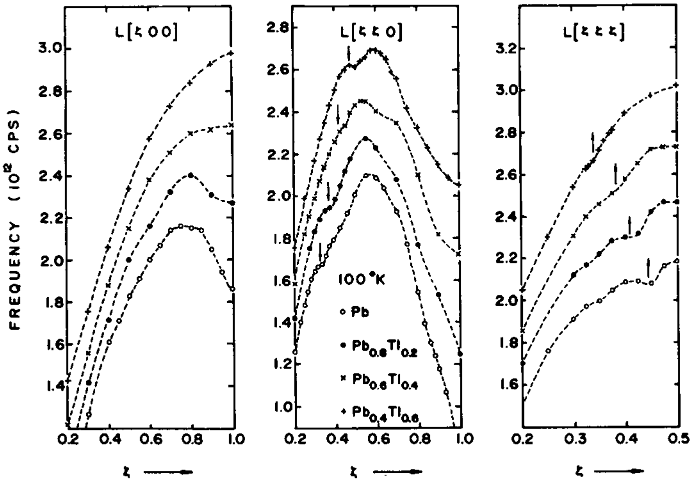

FIG.4. Dispersion curves for longitudinal modes in three symmetry directions for Pb and three Pb-Tl alloys, with arrows indicating the positions of suspected Kohn anomalies. The curves are displaced vertically by 0.2 × 10^{12} cps.

TABLE II. FERMI SURFACE DIAMETERS (units $2\pi/a$)

Alloys	Face diameter ± 0.02	Body diameter ± 0.02	Free electron diameter
Pb	2.38[a]	2.50[a]	2.48
$Pb_{0.8}Tl_{0.2}$	2.28	2.44	2.44
$Pb_{0.6}Tl_{0.2}$	2.21	2.39	2.40
$Pb_{0.4}Tl_{0.6}$	2.16	2.34	2.34

[a] Taken from Brockhouse et al. [9]; Stedman et al. [12] give values of 2.38 and 2.53 respectively.

diagonal [110], and body diagonal [111] as tabulated in Table II. It can be seen that the Fermi diameters along [110] are smaller than the free electron predictions; the percentage difference increases from about 4% for Pb to about 8% for $Pb_{0.4}Tl_{0.6}$. The latter result indicates that, for $Pb_{0.4}Tl_{0.6}$, only a very small piece of the Fermi surface in the third zone remains. However, the Fermi diameters along the [111] direction are almost identical with those of the free electron model. These results may be interpreted from the point of view of the rigid band model. According to this model, the band structure of Pb will be unchanged on adding Tl to Pb to form the alloy, the only effect being to lower the Fermi level by an amount determined by the electron concentration. The above results correlate well with the Fermi surfaces deduced from the band structure of Pb determined by ANDERSON and GOLD [15], using the rigid band model. This model has also been shown to give a satisfactory explanation of the transport properties [16], of the elastic constants [17] and of the superconducting transition temperature [13] of Pb-Tl alloys. Similar anomalies probably appear in the dispersion curves of $Bi_{0.15}Pb_{0.85}$ and $Bi_{0.2}Pb_{0.6}Tl_{0.2}$, though they have not been very well established. The sizes of the Kohn anomalies in a pure metal are an indication of the strength of the electron-phonon interaction in the metal. In alloys it may not be so clear-cut, however, since the Fermi surface in an alloy may not be as sharp as that in a pure metal because of the lack of perfect periodicity. This could spread out the abrupt changes in the slope of the dispersion curve over a region in q-space of order $2\pi/\ell$, where ℓ is the mean free path of the electrons. (Unfortunately measurements of the M.F.P. in the alloys at the temperatures of the measurements do not appear to exist.) Nevertheless, there appears to be a correlation between the relative strengths of the anomalies in the different alloys, and the strengths of the electron-phonon interaction (Fig. 3.). It should be noted that the Kohn effect provides perhaps the only known method of studying the Fermi surface in disordered alloys.

4. NEUTRON GROUPS AND FORCE CONSTANT DISORDER

It has been found experimentally [1,3,4] that the neutron groups observed in one phonon coherent scattering from a disordered alloy crystal show no marked broadening because of the lack of perfect periodicity. This would indicate that well-defined phonons still exist in a disordered alloy crystal, and, therefore, that it is justified to use the Born-von Kármán theory as a starting point for analysis. The finite phonon lifetime arising from the scattering of phonons in an imperfect lattice may then be treated using time-dependent perturbation theory. In a disordered alloy system, the masses of the constituents are, in general, different, and hence the masses of the ions at equivalent lattice sites vary randomly over the crystal. Moreover, the interatomic forces between various pairs of atoms with the same geometrical arrangement also vary randomly through the crystal. We will treat these two random variations separately, since their effects can be largely separated experimentally by proper choice of alloy constituents and composition.

Let us assume that the total Hamiltonian for the vibrating ions in a disordered alloy crystal can be separated into two parts: H_o, the unperturbed Hamiltonian which has the periodicity of the lattice, and H, the perturbation which does not have the periodicity. From first order time-dependent perturbation theory [18], the phonon lifetime arising from the scattering of phonons in an imperfect lattice may be written as,

$$\tau = \frac{\hbar^2}{2\pi g(\omega_m)\,|H_{mn}|^2} \quad .$$

where H_{mn} is the matrix element of the perturbation between the unperturbed eigenstates m and n, and $g(\omega_m)$ is the density of the final unperturbed state m. H_{mn} and $g(\omega_m)$ are assumed to be slowly varying function of m. We expect the phonon to decay in time approximately as $\exp(-t/\tau)$ in analogy with the decay of radioactive nuclei. The Fourier transform of this is a Lorentzian line shape whose full width at half maximum $\Delta\omega = 1/\tau$ gives the spread in the frequency,

$$\Delta\omega = \frac{1}{\hbar^2}\, 2\pi g(\omega_m)\,|H_{mn}|^2 .$$

The matrix element can be evaluated on the basis of Born-von Kármán theory.

For variations in the masses of the ions on the different lattice sites ("isotope" disorder), the equations of motion of a monatomic Bravais lattice are,

$$\ddot{u}_\alpha(L) = -\frac{1}{M} \sum_{L'\beta} \Phi_{\alpha\beta}(\vec{R}_{LL'})\,u_\beta(L') - \left(\frac{1}{M_L} - \frac{1}{M}\right) \sum_{L'\beta} \Phi_{\alpha\beta}(\vec{R}_{LL'})\,u_\beta(L') , \quad (1)$$

where M_L is the isotopic mass of the atom at lattice site L(and depends explicitly on L), M is the average mass,

$\Phi_{\alpha\beta}(\vec{R}_{LL'})$ is the atomic force constant which depends only on the vector distance $\vec{R}_{LL'} = \vec{R}_{L'} - \vec{R}_L$ and α,β refer to Cartesian components. The general solution for Eq. (1) can be expanded in terms of the eigenmodes for a perfect crystal with a single constituent:

$$u_\alpha(L) = \sum_{\vec{q}j} C(\vec{q}jt)\ \xi_\alpha(\vec{q}j) \exp i(\vec{q}\cdot\vec{R}_L - \omega_j(\vec{q})t) \qquad (2)$$

where $\vec{\xi}$ denotes the polarization vector, $\vec{q}$ the phonon wave vector and j characterizes the branch. From Eqs. (1) and (2), it can be shown that the matrix element,

$$H_{q'j'\to qj} = \frac{\hbar \sum\limits_{LL'} \sum\limits_{\alpha\beta} \left(\frac{1}{M_L}-\frac{1}{M}\right) \Phi_{\alpha\beta}(\vec{R}_{LL'})\, \xi^*_\alpha(\vec{q}'j')\, \xi_\beta(\vec{q}j)\, e^{i(\vec{q}\cdot\vec{R}_{L'} - \vec{q}'\cdot\vec{R}_L)}}{2N\,\omega_{j'}(\vec{q}')}$$

and the spread in frequency,

$$\Delta\omega \simeq \frac{\pi}{2}\ \frac{\omega^2 g(\omega)}{\int g(\omega)\,d\omega} \left\langle \left| \frac{M-M_L}{M} \right|^2 \right\rangle_L$$

where $\langle\ \rangle_L$ denotes an average over L. For an average (isotopic) mass variation of 1%, $\Delta\omega/\omega \sim 0.01\%$, much too small to be observable with current instrument resolution. Even for a mass variation of 10%, $\Delta\omega/\omega$ is $\sim 1\%$, still too small to be observable.

The phonon mean face path, related to the phonon lifetime, has been discussed by MATHIS [19] for an isotopic mixture with a simple cubic lattice using essentially this method. The treatment given here is, however, more general than that of Mathis, since it is not restricted to the particular case of a simple cubic lattice and to first neighbour forces only, but applies to any monatomic Bravais lattice with arbitrary interatomic forces.

For alloys composed of elements of similar mass, it is clear from the above analysis that the small mass differences have little effect. Nevertheless, disordered alloys might be expected to exhibit broad neutron groups, because of atomic force constant disorder. The equations of motion for such a system may be written as

$$M\ddot{u}_\alpha(L) = \sum_{L'\beta} \Phi_{\alpha\beta}(\vec{R}_{LL'})\, u_\beta(L') - \sum_{L'\beta} \Delta_{\alpha\beta}(\vec{R}_{LL'},L)\, u_\beta(L') \qquad (3)$$

where $\Phi_{\alpha\beta}(\vec{R}_{LL'})$ is the average value of $\Phi_{\alpha\beta}(\vec{R}_{LL'},L)$ over L for vector distance $\vec{R}_{LL'}$. The fluctuations or deviations, $\Delta_{\alpha\beta}(\vec{R}_{LL'},L)$, of $\Phi_{\alpha\beta}(\vec{R}_{LL'},L)$ from the mean value $\Phi_{\alpha\beta}(\vec{R}_{LL'})$ depend explicitly on L. We can follow the same arguments as were used in the case of mass disorder and obtain,

$$H_{q'j'\to qj} = \frac{\hbar \sum\limits_{LL'} \sum\limits_{\alpha\beta} \Delta_{\alpha\beta}(\vec{R}_{LL'},L)\, \xi^*_\alpha(\vec{q}'j')\, \xi_\beta(\vec{q}j)\, e^{i(\vec{q}\cdot\vec{R}_{L'} - \vec{q}'\cdot\vec{R}_L)}}{2NM\omega_{j'}(\vec{q}')}$$

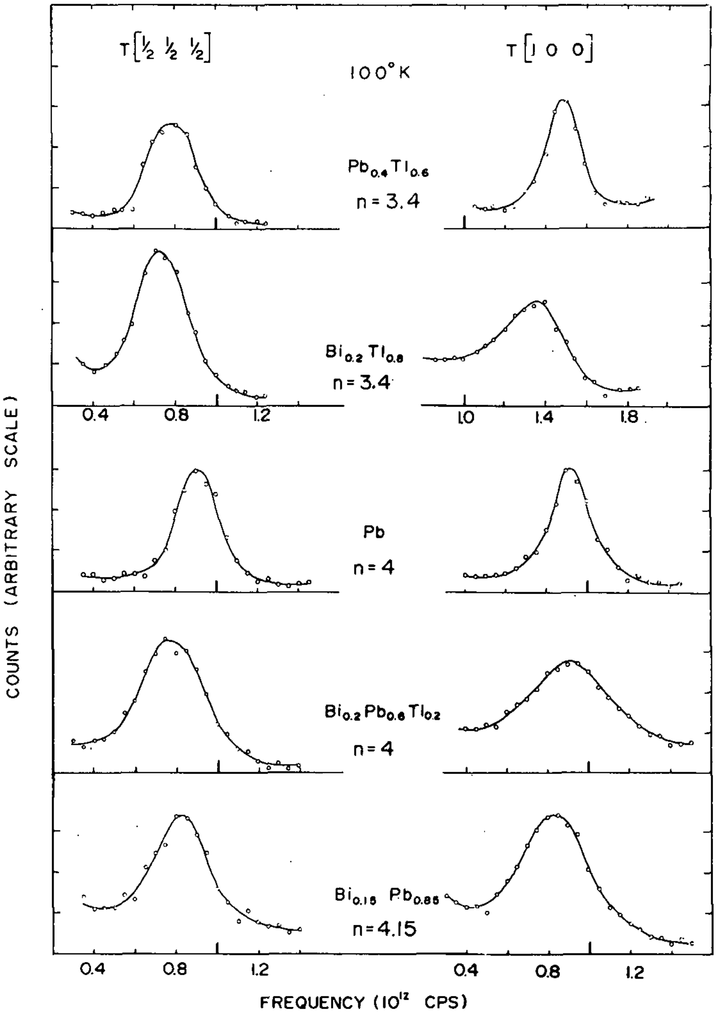

FIG.5. Neutron groups for several alloys and for pure Pb for the transverse phonons at the zone boundary in the [ζζζ] and [ζ00] directions.

Making use of the stability condition under uniform translation, $\sum_{L'} \Delta_{\alpha\beta}(\vec{R}_{LL'},L)=0$, and the relation for a function f(L),

$$\left|\sum_{L} f(L)e^{i\vec{q}\cdot\vec{R}_L}\right|^2=N(\langle|f(L)|^2\rangle-\langle f(L)\rangle^2)+\langle f(L)\rangle^2\,\frac{N(2\pi)^3}{V}\sum_{\vec{q}}\delta(\vec{q}-\vec{g}),$$

we obtain,

$$\Delta\omega = \frac{\pi}{2NM^2\omega^2}\sum_{\vec{q}j}{}'\, g(\omega_j(\vec{q}))\ \times$$

$$\left\langle\left|\sum_{\alpha\beta}\ \sum_{L'}^{L'\neq L}\ \Delta_{\alpha\beta}(\vec{R}_{LL'},L)\,\xi^{*}_{\alpha}(\vec{q},j')\,\xi_{\beta}(\vec{q}j)\,(e^{-i\vec{q}\cdot\vec{R}_{LL'}}-1)\right|^2\right\rangle_L \qquad (4)$$

where Σ' denotes summation over all the possible modes into which $\vec{q}j$ the mode ($\vec{q}'j'$) can be scattered. From Eq. (4) it can be seen that $\Delta\omega$ approaches zero as $\vec{q}$ approaches zero so that sound waves can propagate freely. We also note that $\Delta\omega$ involves products of pairs of deviations of force constants from their mean values and therefore is relatively insensitive to force constant disorder. This explains the observation that neutron groups in disordered alloy systems are usually well defined.

Even so, if the force constant disorder is large enough, broadening of neutron groups will be observed; $\Delta\omega$ may be determined experimentally from the broadening of the neutron groups beyond the instrumental resolution. However, the resolution width of a triple-axis spectrometer is difficult to calculate quantitatively; it is easier to deduce $\Delta\omega$ from comparative measurements. Fig. 5 shows some results of zone boundary phonons of the [ξξξ]T and [ξ00]T branches for a number of these materials. No focussing effect arises from the gradient of the dispersion curves for these phonons, because the gradient at the zone boundary is zero. It can be seen that the neutron groups are somewhat broader for the alloys ($Bi_{0.15}Pb_{0.85}$ and $Bi_{0.2}Pb_{0.6}Tl_{0.2}$ in particular) than for Pb, a fact which indicates short phonon lifetimes for the alloys. The "extra" widths of the group for the alloys can be attributed to the scattering of normal modes because of the presence of force constant disorder. Work is continuing on this topic and will be reported in detail elsewhere.

ACKNOWLEDGEMENTS

The authors would like to express their appreciation to the staff of the Atomic Energy of Canada Ltd. at Chalk River, especially to Dr. A.D.B. Woods, Dr. G. Dolling and Dr. R.A. Cowley, Mr. E.A. Glaser and Mr. H. Neiman; and to their colleagues at McMaster University, particularly to Dr. J.M. Rowe, Dr. E. C. Svensson, Mr. E. D. Hallman, Mr. A. P. Miiller and Mr. A. P. Roy for their cooperation. The measurements for the ternary alloy were done in collaboration with Mr. Roy. The work was supported by a grant from the National Research Council of Canada and one of us (S.C. Ng) held a National Research Council of Canada studentship.

REFERENCES

[1] WOODS, A.D.B. and POWELL, B.M., Phys. Rev. Letters 15 (1965) 778.
[2] SVENSSON, E.C. and BROCKHOUSE, B.N., Phys. Rev. Letters 18 (1967) 858, and references therein.
[3] NG, S.C. and BROCKHOUSE, B.N., Solid State Commun. 5 (1967) 79.
[4] HALLMAN, E.D. and BROCKHOUSE, B.N. to be published (1968).
[5] NG, S.C., BROCKHOUSE, B.N. and HALLMAN, E.D., Materials Research Bulletin 2 (1967) 69.

[6] BROCKHOUSE, B.N., Inelastic Scattering of Neutrons in Solids and Liquids, IAEA, Vienna (1961) 113.
[7] BROCKHOUSE, B.N., DeWIT, G.A., HALLMAN, E.D., and ROWE, J.M., these proceedings, SM-104/52.
[8] VOSKO, S.H., TAYLOR, R., and KEECH, G.H., Can. J. Phys. 43 (1965) 1187.
[9] BROCKHOUSE, B.N., ARASE, T., CAGLIOTI, G., RAO, K.R. and WOODS, A.D.B., Phys. Rev. 128 (1962) 1099.
[10] BROCKHOUSE, B.N., HALLMAN, E.D. and NG, S.C., "Atomic vibrations in metals and alloys" in Magnetic and Inelastic Scattering of Neutrons by Metals (Rowland, J.J. and Beck, P.A., Eds.), Gordon and Breach Science Publications Inc., New York (1968).
[11] SVENSSON, E.C., BROCKHOUSE, B.N. and ROWE, J.M., Phys. Rev. 155 (1967) 619.
[12] STEDMAN, R., ALMQUIST, L. and NILSSON, G., Phys. Rev. 162 (1967) 549.
[13] CLAESON. T., Phys. Rev. 147 (1966) 340.
[14] KOHN, W., Phys. Rev. Letters 2 (1959) 393.
[15] ANDERSON, J.R. and GOLD, A.V., Phys. Rev. 139 (1965) A1459.
[16] TAKANO, K. and SATO, T., J. Phys. Soc. Japan 20 (1965) 2013.
[17] SHEPARD, M.L. and SMITH, J.F., Acta Metallurgica 15 (1967) 357.
[18] SCHIFF, L.J., Quantum Mechanics, McGraw-Hill Book Company, Inc., New York (1955).
[19] MATHIS, D.C., Phys. Rev. 106 (1957) 721.

DISCUSSION

Yu. M. KAGAN: If I have understood you correctly, you believe that the changes in the phonon spectrum of the alloy in question are due entirely to changes in the electron density. Now this proposition seems strange to me, since a change in the electron-ion interaction occurs simultaneously with a change in the alloy composition. Even if we assume that the interactions inside the core do not differ very much as between the components of the alloy (they all belong to the same line of the periodic table), nevertheless they differ outside the core thanks to the different ionic charge. In view of this, I consider that your proposition has a differing validity for different parts of the phonon spectrum. Let me add that in any case your results strike me as stimulating and enlightening.

B.N. BROCKHOUSE: The fact is that the dispersion curves for $n_e = 3.4$ and for $n_e = 4.0$ are rather similar, and that the changes with n_e are smooth.

R.M. PICK: I do not think that there is any greater change of pseudo-potential in the Tl-Pb-Bi series than in Na-Mg-Al. In the latter case the position of the minimum (q_0) in the pseudo-potential is very critical, because the position of the first reciprocal lattice vectors undergoes a pronounced change in relation to q_0 as one proceeds from sodium to aluminium. In the first case there are many Langevin reciprocal lattice vectors less than q_0 and changes in the pseudo-potential then have less effect on the phonon spectrum.

NEUTRON SCATTERING NEAR THE FERROELECTRIC TRANSITION IN KD_2PO_4

W.J.L. BUYERS AND R.A. COWLEY
ATOMIC ENERGY OF CANADA LTD.,
CHALK RIVER, ONT., CANADA,
AND
G.L. PAUL AND W. COCHRAN
UNIVERSITY OF EDINBURGH,
SCOTLAND

Abstract

NEUTRON SCATTERING NEAR THE FERROELECTRIC TRANSITION IN KD_2PO_4. In the paraelectric phase of single-crystal KD_2PO_4 coherent quasi-elastic neutron scattering has been observed, the magnitude of which increases greatly as the transition temperature (-49.6°C) is approached. There is no evidence for a well-defined mode with frequency falling to zero at the transition temperature. The quasi-elastic intensity is strong near reciprocal lattice points such as (3,0,1), (3,0,3) and (2,0,4) but weak near (0,0,2), (2,0,0), (2,0,2) and (4,0,2). The structure factor is consistent with the displacements of the ions at the phase transition in KDP. The scattering is therefore associated with collective atomic fluctuations in which a dipole moment is produced along the ferroelectric axis. The energy width of the scattering from the fluctuations is less than 0.2×10^{12} cps. The intensity at (3.15,0,3), neglecting any correction for resolution, exhibits Curie law behaviour with $T_0 = -59.4$°C. In contrast, the lowest frequency phonons observed do not show any strong temperature dependence. The relevance of these results to various models for the ordering of the deuterium atoms in the phase transition will be discussed.

INTRODUCTION

The paraelectric to ferroelectric phase transition in KH_2PO_4 (abbreviated KDP) and similar compounds has been investigated for some time, but the mechanism of the transition is still unclear. The compounds are neither uniquely displacive nor order-disorder type ferroelectrics, but appear to show some characteristics of both types of behaviour. A recent article by Tokunaga and Matsubara [1] reviews the development of theories of KDP compounds. The early theory of Slater [2] and later modifications [3] were unable to explain the large isotope effect. The Curie temperature of KD_2PO_4 (DKDP) is about 90°K larger than that of KH_2PO_4. Pirenne [4] introduced the idea of protons moving in an anharmonic potential well, and after the structure of KDP had been determined [5], Blinc [6] suggested that the protons move in a double potential well perpendicular to the ferroelectric axis.

More recent developments [7] of this theory have introduced a spin formalism to describe the proton tunneling between the two possible sites and lead to a proton tunneling mode of wave vector, $\vec{q}$, and frequency $\omega_p(\vec{q})$. Above the Curie temperature, T_c, these theories predict

$$\omega_p(0)^2 \propto (T - T_c) \qquad (1)$$

which is the same temperature dependence as predicted by the theory of displacive type ferroelectrics [8]. In order to describe the spontaneous polarization, the interaction of the protons with the rest of the crystal must be introduced. A simple model [9] leads to a coupled mode whose temperature dependence is again given by Eq. (1).

The experiments described below were undertaken to attempt to find a well defined mode by coherent neutron scattering from DKDP. Calculations of the neutron scattering in references [1] and [7] suggest that the tunneling mode should be observed with neutron scattering although de Gennes [7] suggests that the mode may be over-damped.

EXPERIMENTAL RESULTS

A single crystal cylinder of DKDP with 1" diameter and 2" length was used in the experiments. The crystal is described in the body centred tetragonal unit cell, space group $I\bar{4}2d$ with $a = b = 7.468$ Å and $c = 6.974$ Å. Measurements of neutron inelastic scattering were made for temperatures between +34°C and the transition temperature -49.6°C (about 8°C above T_c) on the triple axis crystal spectrometer at the C5 facility of the NRU reactor at Chalk River, with the crystal aligned so that scattering took place in the a-c plane.

Measurements up to a frequency of 6 (10^{12} cps) of modes propagating in the a- and c-directions revealed excitations which behaved as ordinary phonons. These dispersion curves are necessarily complicated because of the structure of the crystal, and will be discussed in a later publication. The frequencies of the lowest of these excitations were found to be temperature independent. In particular, the frequencies of the lowest mode with $\vec{q}$ at the zone boundary point M, the lowest optic mode at $q = 0$ (Γ) and several low frequency acoustic modes remained constant in frequency to within a few percent between 25°C and -49.6°C. These results show that there is no well-defined elementary excitation in DKDP whose frequency $\omega \to 0$ as $T \to T_c$, such as has been found in $SrTiO_3$ [10] and $KTaO_3$ [11].

However, temperature dependent quasi-elastic scattering was detected as diffuse intensity spread throughout the reciprocal space with maxima under the Bragg peaks. The Bragg peaks were very narrow so that they could be easily subtracted. Elastic incoherent scattering which varied slowly throughout reciprocal space was also observed; it could be subtracted quite accurately to give the coherent diffuse intensity. The width in energy of this scattering was much smaller than the resolution function of the apparatus and did not exceed 0.2 (10^{12} cps). Figure 1 shows the diffuse intensity observed in the a-c plane of the Brillouin zone around the reciprocal lattice point (3,0,3). The dumbbell shaped distribution has its greatest extension in the a-direction, parallel to the deuterium bonds, but perpendicular to the ferroelectric c-axis. The temperature dependence of the intensity distribution around (3,0,3) is also shown in Fig. 1. As the temperature is decreased towards the transition temperature, T_{tr}, there is an enormous increase in the central peak intensity with an associated

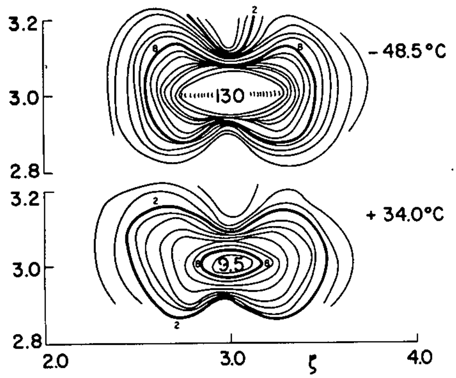

FIG. 1. Intensity contours (arbitrary units) for the critical scattering at (3, 0, 3) at -48.5° and +34°C. The contours are not equally spaced. Contours at +34°C are 0.5, 1, 1.5, 2, 2.5, 3 and then by steps of 1 to 9. Contours at -48.5°C are 1, 1.5, 2, 2.5, 3, 4, 5, 6, 8, 10, 12, 16, 20, 25, 30, 35, 40 and then by steps of 10 to 120. The figures in the centre of each distribution give the peak height. The heavy lines show how two of the contours move with temperature.

steepening of the contours, the general shape not significantly changing over the five temperatures measured between +34 °C and -49.6 °C. The intensity distribution as a function of $\vec{q}$ along the a-direction through (3,0,3) is shown for three temperatures in the left part of Fig. 2. The peak becomes narrower as the temperature is lowered to T_{tr}. Extensive data taken at (3.15,0,3) are shown in the right part of Fig. 2 as a plot of inverse intensity versus reduced temperature. This intensity has been corrected for incoherent elastic background, which was

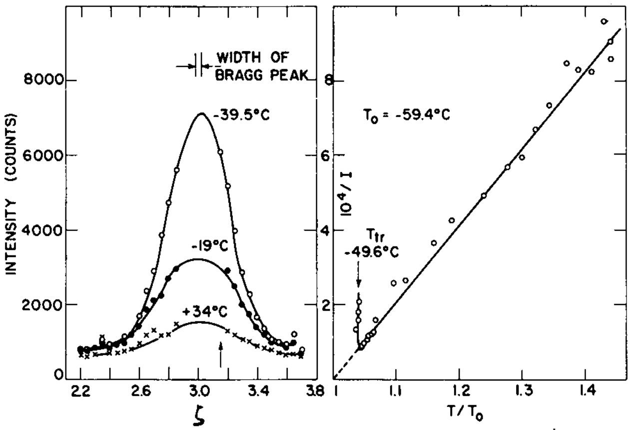

FIG. 2. Left: Intensity of critical scattering measured along the line (ζ, 0, 3) before subtraction of background. The arrow indicates the point at which the data on the right were collected. The width of the Bragg peak is also indicated. Right: The temperature variation of the inverse of the intensity of critical scattering at (3.15, 0, 3). The quantity, I, is an observed intensity such as is given on the left part of the figure less the background. Temperatures are given as fractions of T_0 (-59.4°C), which was obtained by extrapolating to zero a straight line fit to the data. The transition temperature is T_{tr}.

TABLE I. INTENSITY OF FERROELECTRIC COLLECTIVE MODE IN DKDP (ARBITRARY UNITS)

Reflection $(\zeta, 0, \eta)$	Experiment	Calculation
002	0 ± 40	0
101	100 ± 100	350
103	300 ± 100	815
200	0 ± 50	0
202	100 ± 100	12
204	1500 ± 200	14
301	1700 ± 100	6300
303	5130 ± 200	5130
402	300 ± 100	250

found to vary so slowly that it was effectively constant within any one Brillouin zone. The background was measured in the region surrounding the diffuse peak (3,0,3). The intensity of the diffuse scattering was strong in some Brillouin zones and weak in others. The diffuse intensities averaged from the points $(\zeta \pm 0.15, 0, \eta)$ are shown in Table I. It is assumed that these intensities are proportional to the diffuse intensities at the lattice points $(\zeta, 0, \eta)$.

INTERPRETATION AND ANALYSIS OF RESULTS

The rapid variation of the diffuse intensity as $T \to T_c$ from above indicates that this response of the crystal is associated with its incipient ferroelectric behaviour. Since the intensity varies considerably from one Brillouin zone to another it arises from a collective rather than an independent motion of the atoms in the crystal. Provided the displacements of the atoms are small the intensity in the different Brillouin zones are related by the structure factor

$$|F(\vec{Q})|^2 = |\sum_k (\vec{e}_k \cdot \vec{Q}) \exp (i\vec{Q} \cdot \vec{R}_k) \, b_k|^2 \qquad (2)$$

where b_k is the scattering length of the k^{th} type of atom including its Debye-Waller factor, R_k its position in the unit cell, and $\vec{Q}$ the momentum transfer. The eigenvectors, $\vec{e}_k$, describe the displacement of the atoms in the collective mode. These eigenvectors may be obtained from the measured displacements of the ions at the phase transition of KDP [5], in which case the intensities (normalized to the experimental results for (3,0,3)) are listed in Table I for several Bragg reflections. The results although not in agreement with the experimental measurements are strongly suggestive that the displacements in DKDP giving rise to the diffuse scattering are similar to those occurring at the phase transition of KDP.

The intensity depends not only on the structure factor of Eq. (2) but also on the response of the collective mode to a disturbance. By analogy with molecular field calculations for an Ising model [12], the intensity might be expected to behave as

$$I(\vec{Q}) = |F(\vec{Q})|^2 \frac{k_BT}{k_BT + J(\vec{Q})} \tag{3}$$

where $J(\vec{Q})$ is the Fourier transform of the interaction. An unusual feature of $J(\vec{Q})$ arises because the collective mode is associated with a long range dipole-dipole interaction resulting from the dipoles produced along the c-axis. The force constant $J(\vec{Q})$, or $J(\vec{q})$ since it is periodic in reciprocal space, is then of the form

$$J(\vec{q}) = J_0(\vec{q}) + \frac{4\pi P^2}{v} \frac{q_c^2}{|\vec{q}|^2} \tag{4}$$

where $J_0(\vec{q})$ is regular as $|\vec{q}| \to 0$ and P is the dipole moment for the collective mode. The dumbbell form of the scattering, shown in Fig. 1, is then a direct result of the long-range electrostatic forces through the second term in Eq. (4).

Our results shown in Figs. 1 and 2 are in qualitative agreement with the predictions of Eq. (3) as to $\vec{Q}$ dependence and temperature dependence. Some preliminary results have been obtained for $J_0(\vec{Q})$ from the experimental results, approximately corrected for experimental resolution, but these will be reported in full at a later date.

It is of interest that Eq. (3) may also be obtained from a damped simple harmonic oscillator description of the scattering. If the polarization $\vec{P}(\vec{q})$ follows the classical oscillator equation

$$\ddot{\vec{P}} + \Gamma \dot{\vec{P}} + \omega_T(\vec{q})^2 \vec{P} = 0$$

then the intensity of the scattering is given by

$$I(\vec{Q}) = |F(\vec{Q})|^2 \frac{k_BT\,\Gamma}{(\omega_T(\vec{q})^2 - \omega^2)^2 + \omega^2\Gamma^2} \tag{5}$$

Now if $\Gamma >> \omega_T(\vec{q})$ while $\omega_T(\vec{q})^2 = K(T - T(\vec{q}))$, Eq. (5) becomes for small ω

$$I(\vec{Q}) = |F(\vec{Q})|^2 \frac{k_BT\,\Gamma}{K^2(T-T(\vec{q}))^2 + \omega^2\Gamma^2}$$

The integral of this over all frequencies, ω, is then

$$|F(\vec{Q})|^2 \frac{k_BT}{K(T - T(\vec{q}))}$$

which is identical in form with Eq. (3) but with $KT(\vec{q})$ playing the role of the $J(\vec{q})$ of Eq. (3). Our experimental results do not therefore distinguish between these two descriptions of the scattering as from a very much over-damped oscillator or from an order-disorder transition.

The energy spread of the critical scattering indicates that the fluctuations have a lifetime greater than 10^{-11} sec. Nuclear magnetic resonance experiments [13] have been interpreted as showing that the deuteron spends less than 10^{-5} sec between jumps. This implies that in the tunneling models [7] in which lifetime and damping effects are neglected, ω_T should be less than 0.1 (10^{12} cps) at room temperature, which is an order of magnitude less than the values calculated for example, by Novakovic [9] and from the dielectric constant.

The energy spread is also consistent with the dielectric properties [14] of DKDP which are given approximately by a Debye relation

$$\epsilon'(\omega) - i\,\epsilon''(\omega) = \frac{\epsilon(0)}{1 + i\omega\tau}$$

with τ about 10^{-10} sec at room temperature (a range of relaxation times is required to fit the data, but this unimportant for our discussion). Since the neutron cross section at $\vec{q} = 0$ may be expected to depend on $T\,\epsilon''(\omega)/\omega$, the results for $\epsilon(\omega)$ predict that the energy spread of the scattered neutrons would not be detectable in our experiment. Also, since it has been shown [14] that $\tau \propto (T - T_C)^{-1}$, the scattering should become even more nearly elastic as $T \to T_C$ from above.

Since the energy spread of the scattering is much less than $k_B T_C/\hbar$, the properties of the transition are determined largely by the equilibrium properties rather than the dynamical properties of the crystal, as in the order-disorder transition of β-brass [15].

In tunneling models for DKDP which have a well-defined tunneling mode, its frequency must be less than 0.1 (10^{12} cps) to be consistent with our results. However this frequency is then inconsistent with the static dielectric constant. Our results then demonstrate that the simple tunneling models are unsatisfactory and that either a mechanism must be incorporated into these models by which the tunneling mode becomes greatly over-damped, or an entirely different model is needed.

The antifferoelectric transition in $NH_4H_2PO_4$ will involve the same type of behaviour as KDP, but the displacements are characteristic of a wave vector associated with the point M rather than the zone centre. Considering the magnetic analogy, this suggests that $J(\vec{q})$ is a minimum at the point M in $NH_4H_2PO_4$ instead of at $\vec{q} = 0$ for KDP. Although it is difficult to see why $J(q)$ should change greatly on substituting NH_4^+ for K^+ as suggested by Kobayashi [9], a neutron scattering experiment in $ND_4D_2PO_4$ might also exhibit quasi-elastic scattering. A neutron scattering experiment is planned for the near future to investigate this.

CONCLUSION

Quasi elastic scattering in DKDP has been observed whose variation with temperature and structure factor indicate that it is associated with the ferroelectric phase transition of DKDP. The scattering of neutrons may be described as either from fluctuations in the polarization at an order-disorder transition or from a greatly over damped oscillatory mode, but these cannot be distinguished by the experiment. The quasi-elastic nature of the scattering indicates that the transition is determined by the equilibrium rather than the dynamical properties of DKDP.

It is proposed to extend the experiments in the near future.

ACKNOWLEDGEMENTS

We are indebted to E.A. Glaser, H.F. Nieman and D.A. Betts for invaluable technical assistance.

Support by the U.K. Science Research Council (W.C. and G.L.P.) and the Royal Society (G.L.P.) while visiting Chalk River Nuclear Laboratories is gratefully acknowledged.

REFERENCES

[1] TOKUNAGA, M., MATSUBARA, T., Prog. Theor. Phys. 35 (1966) 581; 36 (1966) 857.

[2] SLATER, J.C., J. Chem. Phys. 9 (1961) 16.

[3] TAKAGI, Y., J. Phys. Soc. Jap. 3 (1948) 271;
SILSBEE, H.B., UEHLING, E.A., SCHMIDT, V.H., Phys. Rev. 133 (1964) A165.

[4] PIRENNE, J., Physica 15 (1949) 1019.

[5] BACON, G.E., PEASE, R.S., Proc. Roy. Soc. A220 (1953) 397; A230 (1955) 359.

[6] BLINC, R., J. Phys. Chem. Solids 13 (1960) 204.

[7] BLINC, R., SVETINA, S., Phys. Rev. 147 (1966) 423, 430;
DeGENNES, P.G., Solid State Comm. 1 (1964) 132;
BROUT, R., MULLER, K.A., THOMAS, H., Solid State Comm. 4 (1966) 507;
VILLAIN, J., STAMENKOVIC, J., Phys. Status Solidi 15 (1966) 585.

[8] COCHRAN, W., Adv. Phys. 9 (1960) 387; 10 (1961) 401.

[9] KOBAYASHI, K., Phys. Lett. 26A (1967) 55; J. Phys. Soc. Japan to be published;
NOVAKOVIC, L., J. Phys. Chem. Solids 27 (1966) 1469; Bull. Boris Kidrič Inst. Nuclear Sciences 18 (1967) 23.

[10] COWLEY, R.A., Phys. Rev. Lett. 9 (1962) 159.

[11] SHIRANE, G., NATHANS, R., MINKIEVICZ, V.J., Phys. Rev. 157 (1967) 369.

[12] BROUT, R., Phase Transitions, Benjamin Inc., New York (1965).

[13] BJORKSTAM, J.J., Phys. Rev. 153 (1967) 599.

[14] HILL, R.M., ICHIKI, S.K., Phys. Rev. 130 (1963) 150.

[15] ALS-NIELSEN, J., DIETRICH, O.W., Phys. Rev. 153 (1967) 706, 711.

DISCUSSION

G. CAGLIOTI: Was the intensity of the quasi-elastic scattering measured by the conventional diffraction technique or by using the triple-axis spectrometer set for elastic diffraction?

G.L. PAUL: It was measured with the triple-axis crystal spectrometer at the C5 facility of the NRU reactor at Chalk River.

H.H. STILLER: Did you observe the critical scattering likewise at Bragg reflections which do not involve deuterium atoms?

G.L. PAUL: As a matter of fact the deuterium atoms contribute to the critical scattering around all Bragg reflections, since their motion is not restricted to a symmetry direction.

A CORRELATION FUNCTION FOR PHONON EIGENVECTORS

W. COCHRAN
EDINBURGH UNIVERSITY,
SCOTLAND

Abstract

A CORRELATION FUNCTION FOR PHONON EIGENVECTORS. It was shown by van Hove that the Fourier transform of the neutron scattering intensity is a space-time correlation function of the scattering density. In the special case of a single crystal as the scattering system, the coefficients of a Fourier series can be derived from the one-phonon scattering cross-sections corresponding to a phonon of a particular frequency. Evaluation of the Fourier series gives a space correlation function involving the eigenvectors of the mode of vibration being considered. The function is a special case of the van Hove function, closely related to the Patterson function which is used in X-ray crystallography. In the special case of a phonon of wave vector zero ($\underline{q}$ = 0) the function has a sufficiently simple interpretation that it may be of practical value.

The differential scattering cross section of a crystal for thermal neutrons, for a scattering process involving a normal mode identified by a wave vector $\underline{q}$ and frequency $\omega(\underline{q}j)$, is given in standard references [1]. The cross section for a one-phonon process is directly proportional to the squared modulus of a structure factor, given by

$$|G(\underline{K}j)|^2 = \left|\underline{K}\cdot\sum_{\kappa} b_\kappa \exp(-W_\kappa(\underline{K}))\, m_\kappa^{-1/2}\, e_\kappa(\underline{q}j)\, \exp(i\underline{H}.\underline{r}_\kappa)\right|^2 \qquad (1)$$

In this expression κ identifies an atom situated in the unit cell at $\underline{r}_\kappa$, $\underline{K}$ is the scattering vector, $\underline{H}$ a vector of the reciprocal lattice and $e_\kappa(\underline{q}j)$ is an eigenvector or polarisation vector. The one-phonon cross section is non-zero only at $\underline{K}=\underline{H}-\underline{q}$, and at $\underline{K}=\underline{H}+\underline{q}$ for which the appropriate structure factor is obtained by replacing $e_\kappa(\underline{q}j)$ by $e^*_\kappa(\underline{q}j)$ in Equ (1). The structure factors and therefore the cross sections at the points $\underline{H}-\underline{q}$ and $\underline{H}+\underline{q}$ in reciprocal space are therefore unequal unless the eigenvectors are entirely real. The displacement of an atom of type κ in the ℓ^{th} unit cell, from its equilibrium position $\underline{r}_{\ell\kappa}$ is given by

$$(Nm_\kappa)^{-1/2}\sum_{\underline{q}j} e_\kappa(\underline{q}j)\, Q(\underline{q}j)\, \exp(i\,\underline{q}\cdot\underline{r}_{\ell\kappa}) \qquad (2)$$

The quantities $|G(\underline{H}-\underline{q},j)|^2$ are accessible to experimental measurement since the well defined change in energy of neutrons scattered in a one-phonon process enables this cross section to be measured against a background of multiphonon processes. The advantages of knowing the $|G(\underline{H}-\underline{q},j)|^2$ in a study of the dynamics of a crystal, and some of the points involved in making experimental measurements, have been discussed by Dolling and Woods [1]. In what follows we shall be dealing with fixed values of $\underline{q}$ and j, so these indices will be omitted whenever this can be done without causing ambiguity. It is convenient to put

$$\underline{u}_{\kappa} = m_{\kappa}^{-1/2}\, \underline{e}_{\kappa}(\underline{q}\, j) \tag{3}$$

and to refer to the $\underline{u}_{\kappa}$ also as eigenvectors. Since $G(\underline{H}-\underline{q})$ is a complex quantity it cannot be measured directly by neutron scattering, but it is convenient to begin by defining

$$D(\underline{r}) = \frac{1}{V}\sum_{\underline{H}} G(\underline{H}-\underline{q})\, \exp(-i(\underline{H}-\underline{q})\cdot\underline{r}) \tag{4}$$

It is readily shown that since $G(\underline{H}+\underline{q}) = G^{*}(-\underline{H}-\underline{q})$,

$$D^{*}(\underline{r}) = \frac{1}{V}\sum_{\underline{H}} G(\underline{H}+\underline{q})\, \exp(-i(\underline{H}+\underline{q})\cdot\underline{r}) \tag{5}$$

The function $D(\underline{r})$ is analogous to the nuclear density, which can be expressed as a Fourier series involving the structure factors for elastic scattering. A function which can be derived from a sufficient range of experimental measurements is

$$P(\underline{r}) = \frac{1}{V}\sum_{\underline{H}} |G(\underline{H}-\underline{q})|^{2}\, \exp(-i(\underline{H}-\underline{q})\cdot\underline{r}) \tag{6}$$

That is,

$$P(\underline{r}) = P_{e}(\underline{r}) - i\, P_{o}(\underline{r}) \tag{7}$$

where the real and imaginary parts have even and odd symmetry respectively. The function $P(\underline{r})$ is analogous to the Patterson function used in crystal structure analysis [2] and may be expected to give information about the eigenvectors.

To find the significance of $D(\underline{r})$ and of $P(\underline{r})$ we make use of the following properties of Fourier transforms [2]. If the scalar functions $\rho(\underline{r})$ and $f(\underline{K})$ are related by

$$\rho(\underline{r}) = \int f(\underline{K})\, \exp(-i\underline{K}\cdot\underline{r})\, d^{3}K/(2\pi)^{3} \tag{8}$$

which for conciseness we represent by

$$\rho(\underline{r}) \longleftrightarrow f(\underline{K}) \tag{8a}$$

then

$$\sum_{\ell} \rho(\underline{r}-\underline{r}_{\ell}) = \frac{1}{V}\sum_{\underline{H}} f(\underline{H})\, \exp(-i\underline{H}\cdot\underline{r})$$

and

$$\sum_{\ell} \rho(\underline{r}-\underline{r}_{\ell})\, \exp(i\underline{q}\cdot\underline{r}_{\ell}) = \frac{1}{V}\sum_{\underline{H}} f(\underline{H}-\underline{q})\, \exp(-i(\underline{H}-\underline{q})\cdot\underline{r}) \tag{9}$$

It follows from (8) that

$$\operatorname{grad} \rho(\underline{r}) \longleftrightarrow -i\, \underline{K}\, f(\underline{K}) \tag{10}$$

and therefore

$$\underline{u}\cdot\operatorname{grad} \rho(\underline{r}) \longleftrightarrow -i\,(\underline{K}\cdot\underline{u})\, f(\underline{K}) \tag{11}$$

where $\underline{u}$ is a vector in crystal space. In the same way it is found that

$$\underline{u}_2\cdot\mathrm{grad}\left(\underline{u}_1\cdot\mathrm{grad}\,\rho(\underline{r})\right)\leftrightarrow-\left(\underline{K}\cdot\underline{u}_1\right)\left(\underline{K}\cdot\underline{u}_2\right)f(\underline{K})\qquad(12)$$

Finally we note from (8) that

$$\rho(\underline{r}-\underline{r}_\kappa)\leftrightarrow f(\underline{K})\exp\left(i\underline{K}\cdot\underline{r}_\kappa\right)\qquad(13)$$

In order to apply the relations (8) to (13) to the situation in which we are interested, we rewrite Eqn (1) as

$$G(\underline{K})=i\underline{K}\cdot\sum_\kappa\underline{u}_\kappa\exp(i\underline{q}\cdot\underline{r}_\kappa)\,b_\kappa\exp\left(-W_\kappa(\underline{K})\right)\exp\left(i\underline{K}\cdot\underline{r}_\kappa\right)\qquad(14)$$

and put

$$f_\kappa(\underline{K})=b_\kappa\exp\left(-W_\kappa(\underline{K})\right)\qquad(15)$$

The Fourier transform of (15), $\rho_\kappa(\underline{r})$, is the nuclear density of an atom of type κ as modified by thermal vibration.
We identify $\underline{u}$ of Eqn (11) with $\underline{u}_\kappa\exp(i\underline{q}\cdot\underline{r}_\kappa)$ of Eqn (14) and obtain, using also Eqn (13), that

$$\sum_\kappa\left(\underline{u}_\kappa\cdot\mathrm{grad}\,\rho_\kappa(\underline{r}-\underline{r}_\kappa)\right)\exp(i\underline{q}\cdot\underline{r}_\kappa)\leftrightarrow-G(\underline{K})\qquad(16)$$

Hence by comparison with Eqn (4), and using also Eqn (9) we obtain

$$D(\underline{r})=-\sum_{l\kappa}\left(\underline{u}_\kappa\cdot\mathrm{grad}\,\rho_\kappa(\underline{r}-\underline{r}_{l\kappa})\right)\exp\left(i\underline{q}\cdot\underline{r}_{l\kappa}\right)\qquad(17)$$

This gives $D(\underline{r})$, already expressed by the Fourier series (4), in terms of the eigenvectors and the nuclear density.
In much the same way, making use of Eqn (12) and defining

$$f_{\kappa\kappa'}(\underline{K})=b_\kappa b_{\kappa'}\exp\left(-W_\kappa(\underline{K})-W_{\kappa'}(\underline{K})\right)\qquad(18)$$

and denoting the Fourier transform of $f_{\kappa\kappa'}(\underline{K})$ by $\rho_{\kappa\kappa'}(\underline{r})$, we arrive at the result

$$\sum_{\kappa\kappa'}\left(\underline{u}^*_{\kappa'}\cdot\mathrm{grad}\left(\underline{u}_\kappa\cdot\mathrm{grad}\,\rho_{\kappa\kappa'}(\underline{r}-\underline{r}_\kappa+\underline{r}_{\kappa'})\right)\right)\times$$
$$\times\exp\left(i\underline{q}\cdot(\underline{r}_\kappa-\underline{r}_{\kappa'})\right)\leftrightarrow-\left|G(\underline{K})\right|^2\qquad(19)$$

Therefore, in the same way as before

$$P(\underline{r})=-\sum_{l\kappa\kappa'}\left(\underline{u}^*_{\kappa'}\cdot\mathrm{grad}\left(\underline{u}_\kappa\cdot\mathrm{grad}\,\rho_{\kappa\kappa'}(\underline{r}-\underline{r}_{l\kappa}+\underline{r}_{\kappa'})\right)\right)\times$$
$$\times\exp\left(i\underline{q}\cdot(\underline{r}_{l\kappa}-\underline{r}_{\kappa'})\right)\qquad(20)$$

This relates the correlation function to the eigenvectors, the relation is a fairly complicated one but some further simplifications can be made.

It will usually be a good approximation to take the Debye-Waller factor $\exp(-W_\kappa(\underline{K}))$ to be isotropic and the same for every atom. Consequently, writing

$$f_\kappa(\underline{K}) = b_\kappa \exp(-K^2/4p) \tag{21}$$

we obtain

$$\rho_\kappa(\underline{r}) = b_\kappa (p/\pi)^{3/2} \exp(-pr^2) \tag{22}$$

and

$$\rho_{\kappa\kappa'}(\underline{r}) = b_\kappa b_{\kappa'} (p/2\pi)^{3/2} \exp(-\tfrac{1}{2} p r^2) \tag{23}$$

where p is a constant related to the mean square displacement of an atom. Next we consider the function

$$D_\kappa(\underline{r}) = -\underline{u}_\kappa \cdot \operatorname{grad} \rho_\kappa(\underline{r}) \tag{24}$$

where evidently

$$D(\underline{r}) = \sum_{\ell\kappa} D(\underline{r} - \underline{r}_{\ell\kappa}) \exp(i\underline{q}\cdot\underline{r}_{\ell\kappa}) \tag{25}$$

From Eqns (22) and (24),

$$D_\kappa(\underline{r}) = 2p(\underline{r}\cdot\underline{u}_\kappa)\, \rho_\kappa(\underline{r}) \tag{26}$$

Eqns (25) and (26) together give $D(\underline{r})$ in its simplest form.

Similarly defining

$$P_{\kappa\kappa'}(\underline{r}) = -\underline{u}^*_{\kappa'} \cdot \operatorname{grad}\left(\underline{u}_\kappa \cdot \operatorname{grad} \rho_{\kappa\kappa'}(\underline{r})\right) \tag{27}$$

so that

$$P(\underline{r}) = \sum_{\ell\kappa\kappa'} P_{\kappa\kappa'}(\underline{r} - \underline{r}_{\ell\kappa} + \underline{r}_{\kappa'}) \exp(i\underline{q}\cdot(\underline{r}_{\ell\kappa} - \underline{r}_{\kappa'})) \tag{28}$$

it is found on using Eqn (23) that

$$P_{\kappa\kappa'}(\underline{r}) = p\,\rho_{\kappa\kappa'}(\underline{r}) \left\{ \underline{u}^*_{\kappa'} \cdot \underline{u}_\kappa - p(\underline{r}\cdot\underline{u}^*_{\kappa'})(\underline{r}\cdot\underline{u}_\kappa) \right\} \tag{29}$$

Eqns (28) and (29) together give $P(\underline{r})$ in its simplest form.

The functions $\rho_\kappa(\underline{r})$ and $\rho_{\kappa\kappa'}(\underline{r})$ will usually be confined to regions small compared with the unit cell volume V. Consequently we can, to a good approximation, replace a function such as

$$\sum_{\ell\kappa} \rho_\kappa(\underline{r} - \underline{r}_{\ell\kappa}) \exp(i\underline{q}\cdot\underline{r}_{\ell\kappa})$$

by

$$\exp(i\underline{q}\cdot\underline{r}) \sum_{\ell\kappa} \rho_\kappa(\underline{r} - \underline{r}_{\ell\kappa})$$

Making this approximation, we find on comparing Eqns (4) and (25), that

$$D'(\underline{r}) = \frac{1}{V}\sum_{\underline{H}} G(\underline{H}-\underline{q})\exp(-i\underline{H}.\underline{r}) \simeq \sum_{\ell\kappa} D_{\kappa}(\underline{r}-\underline{r}_{\ell\kappa}) \tag{30}$$

where as before $D_{\kappa}(\underline{r})$ is given by Eqn (26). This is a very simple relationship. Similarly on comparing Eqns (6) and (28),

$$P'(\underline{r}) = \frac{1}{V}\sum_{\underline{H}} |G(\underline{H}-\underline{q})|^{2}\exp(-i\underline{H}.\underline{r}) \simeq \sum_{\ell\kappa\kappa'} P_{\kappa\kappa'}(\underline{r}-\underline{r}_{\ell\kappa}+\underline{r}_{\kappa'}) \tag{31}$$

where $P_{\kappa\kappa'}(\underline{r})$ is given by Eqn (29). This seems to be as far as one can go in simplifying the relationships in the general case. The functions $D'(\underline{r})$ and $P'(\underline{r})$ are easier to deal with because they have the periodicity of the lattice.

To visualise $D'(\underline{r})$ and $P'(\underline{r})$ we have to be able to visualise $D_{\kappa}(\underline{r})$ and $P_{\kappa\kappa'}(\underline{r})$. The former is given by Eqn (26) but it must be remembered that the eigenvector $\underline{u}_{\kappa}$ is complex and requires six components to specify it. This corresponds to the fact that the general motion of an atom in a normal mode of vibration is in an elliptic orbit. Three quantities are required to specify the magnitude and direction of the major axis, two the minor axis and one the initial phase of the motion. The motion is equally well specified by the six components of $\underline{u}_{\kappa}$. Thus one would inspect a map of the real part of $D'(\underline{r})$ in the neighbourhood of $\underline{r} = \underline{r}_{\kappa}$ to get information about the real part of $\underline{u}_{\kappa}$. The function would have locally a plane of antisymmetry passing through the point $\underline{r}_{\kappa}$, perpendicular to the real part of $\underline{u}_{\kappa}$. The height of the maximum and minimum on either side of this plane would be proportional to the magnitude of the real part of $\underline{u}_{\kappa}$. Similarly the components of the imaginary part could be determined from a map of the imaginary part of $D'(\underline{r})$. Unfortunately a map of $P'(\underline{r})$ is not so easily interpreted. A complete study of the properties of this function has not yet been made, but it is clear that it would be impossible to interpret it except for simple crystal structures. However for a crystal with all atoms on centres of symmetry the eigenvectors $\underline{u}_{\kappa}$ are entirely real, and this is also the case for any crystal structure for a few restricted values of $\underline{q}$, including $\underline{q} = 0$. In this situation each ellipse degenerates to a straight line and the initial phase is either 0 or π. The function $P_{\kappa\kappa'}(\underline{r})$ has then a simple form from which the directions $\underline{u}_{\kappa}$ and $\underline{u}_{\kappa'}$ (but not which is which) and the product $u_{\kappa}u_{\kappa'}$ can be determined. When this has been done for every pair $\kappa\kappa'$ the eigenvectors can be separately determined. In practice difficulties would arise from overlap of functions corresponding to different κ and κ' having nearly the same value of $\underline{r}_{\kappa} - \underline{r}_{\kappa'}$. The situation is very similar to the determination of the coordinates $\underline{r}_{\kappa}$ from the Patterson function. The methods used in structure analysis, such as isomorphous replacement, projection of functions on a plane or a line etc. [2] can all be adapted. When the eigenvectors have been determined approximately from $P'(r)$ they can in principle be "refined" by evaluation of $D'(r)$. The analogies with structure analysis are very close because in effect one is determining the structure of the crystal distorted by one normal mode of vibration.

REFERENCES

1 DOLLING, G., WOODS, A.D.B., "Thermal neutron scattering" Edited by EGELSTAFF, P.A., Academic Press, New York (1965) 193.

2 LIPSON, H., COCHRAN, W., "The determination of crystal structures" BELL, G., & Sons,London (1966)

DISCUSSION

G.L. SQUIRES: I understand that the direction of the 'dipole' you mention corresponds to the direction of the polarization vector. Would you please explain in a little more detail what the magnitude of the 'dipole' corresponds to?

W. COCHRAN: The magnitude of the 'dipole', i.e. the height of a peak in the Fourier transforms of $G(\vec{H}-\vec{q})$, is determined by the relative magnitude of the eigenvector $m_\kappa^{-\frac{1}{2}}\,\vec{e}(\kappa\,\vec{q}\,j)$.

R.A. COWLEY: You represent the distributions of intensity in spread-out form. Does this spreading merely reflect the Debye-Waller factor, or does it give more information?

W. COCHRAN: If the mode $\vec{q}j$ is a phonon excitation, only the Debye-Waller factor is involved. A mode involving a finite displacement of an atom would give a different distribution from the one given in the paper. Here the spread does in fact just reflect the Debye-Waller factor.

W.C. HAMILTON: You mentioned two difficulties with the application of this very interesting technique: first, the experimental difficulty of measuring the structure factors at all, and second, the difficulty in interpreting the inelastic Patterson function once it has been calculated. I wonder whether one might not solve the latter problem by procedures of the type used to interpret ordinary Patterson functions in crystal structure analysis - such as superposition techniques, image seeking, or other direct methods?

W. COCHRAN: In principle one can apply all the methods used in crystal structure analysis, such as projection on a plane, isomorphous replacement and so on, because in effect one is determining the structure of the crystal, as distorted by one normal mode of vibration.

NEUTRON SCATTERING AND ELASTIC CONSTANTS

R.A. COWLEY, W.J.L. BUYERS AND E.C. SVENSSON
ATOMIC ENERGY OF CANADA LTD.,
CHALK RIVER, ONT., CANADA,
AND
G.L. PAUL
UNIVERSITY OF EDINBURGH,
SCOTLAND

Abstract

NEUTRON SCATTERING AND ELASTIC CONSTANTS. Elastic constants of crystals obtained from neutron scattering techniques at frequencies, ω, of the order of 10^{12} cps, are frequently compared with those obtained with ultrasonic techniques for which $\omega < 10^{10}$ cps. If the normal modes of vibration of the crystal did not interact with each other or with other excitations in the crystal, these elastic constants would be identical. In a real crystal, however, interactions exist, and these lead to different behaviour, depending on whether the elastic wave propagates in a collision-free, $\omega\tau >> 1$, mode or a collision-dominated $\omega\tau << 1$, manner, where τ is the life-time of a typical phonon. In anharmonic crystals phonon-phonon interaction introduces a life-time so that elastic waves are expected to behave differently at high and low frequencies. Experiments on both KBr and $SrTiO_3$ have demonstrated this difference. In piezoelectric crystals τ is related to the time required for the electric polarization to follow the elastic wave. At frequencies so high that the electric polarization cannot follow the elastic wave, experiments on DKDP have shown that the elastic constants do not exhibit the anomaly present at low frequencies. Similar behaviour is expected to occur near many phase transitions which show anomalous elastic behaviour. Analogous, but probably smaller, effects occur through the interactions of elastic waves with conduction electrons in metals and with the spins in magnetic materials.

The purpose of this paper is to demonstrate both theoretically and experimentally that the elastic constants of a crystal as determined by neutron scattering experiments are not necessarily the same as those obtained by ultrasonic techniques. The difference [1,2] arises because of the interaction of the elastic waves with other excitations in the crystal, phonons, electrons or magnons. This interaction depends on the frequency of the elastic waves. In ultrasonic experiments the frequency ($< 10^{10}$ cps) is usually much less than the inverse collision time, Γ, of the excitations. The elastic wave, or first-sound wave, then propagates in a collision dominated mode with local thermodynamic equilibrium occuring at all times. At the higher frequencies of a neutron scattering experiment (10^{12} cps), there is insufficient time for thermodynamic equilibrium to occur in each period and the wave propagates in a collision-free or zero-sound mode.

The most common way in which an elastic wave of wave vector $\vec{Q}$ interacts with other excitations is that it destroys one excitation of type j and wave vector $\vec{q}$ and creates another of wave vector $\vec{q} + \vec{Q}$ and of type j or of a different type j'. In phonon and magnon systems where quasi-particle number is not conserved it is also possible for elastic waves to create or destroy pairs of excitations. These processes and those with

$j \neq j'$ usually give the same contribution to the elastic constants in the first- and zero-sound regions and hence will not be discussed further.

The interaction of a strain $(\alpha\beta)$ with the excitations can be written in terms of coefficients $M_{\alpha\beta}(\vec{q}j)$, which, since $|\vec{Q}| \ll |\vec{q}|$, are largely independent of $|Q|$. The contribution of these processes to the $(\alpha\beta\gamma\delta)$ elastic constant can then be expressed in terms of the susceptibility of the $(\vec{q}j)^{th}$ excitations to a probe of wave vector $\vec{Q}$ and frequency Ω as

$$- \frac{1}{V} \sum_{\vec{q}j} M_{\alpha\beta}(\vec{q}j)\, M_{\gamma\delta}(\vec{q}j)\, \chi(\vec{q}j|\vec{Q}\Omega) \qquad (1)$$

where v is the volume of the crystal.

In the collision-free regime it is relatively easy to calculate the susceptibility by second-order perturbation theory as

$$\chi(\vec{q}j,\vec{Q}\Omega) = \frac{n(\vec{q}j) - n(\vec{q} + \vec{Q}j)}{\epsilon(\vec{q}j) - \epsilon(\vec{q} + \vec{Q}j) + \hbar\Omega} \qquad (2)$$

where $n(\vec{q}j)$ is the population of the excitation $(\vec{q}j)$ and $\epsilon(\vec{q}j)$ is its energy. For bosons, in the limit as $|\vec{Q}|$ and Ω become small Eqn. (2) becomes

$$\chi(\vec{q}j,\vec{Q}\Omega) = \frac{n(\vec{q}j)(n(\vec{q}j) + 1)\ \vec{\nabla}\epsilon(\vec{q}j)\cdot\vec{Q}}{k_BT\ (\vec{\nabla}\epsilon(\vec{q}j)\cdot\vec{Q} - \hbar\Omega)} \qquad (3)$$

where $\vec{\nabla}$ is the gradient operator. This shows that there will be a quite different behaviour if the velocity of the elastic wave, $\Omega/|\vec{Q}|$, is greater or less than the group velocity, $\nabla\epsilon(\vec{q}j)/\hbar$, of the excitations. In the case of phonons the elastic wave usually has a greater velocity than the other phonons and hence Eq. (3) is small and negative, giving a small positive contribution to the elastic constant C_{11}. In the case of iron most of the magnons have a much greater velocity than the phonons, so that Eqns. (1) and (2) are given by the zero frequency or static limit;

$$- \frac{1}{Vk_BT} \sum_{\vec{q}j} M_{\alpha\beta}(\vec{q}j)\, M_{\gamma\delta}(\vec{q}j)\, n(\vec{q}j)(n(\vec{q}j) + 1) \qquad (4)$$

For other magnetic materials such as MnF_2 the magnon dispersion curves have a much smaller velocity than the elastic waves and the contribution to the elastic constant is much smaller and positive.

A further feature of this correction to the elastic constants at high frequencies is that it has only the point-group symmetry of the crystal but does not have the extra symmetry of the usual low-frequency elastic constants. For example

$\chi(\vec{q}j,\vec{Q}\Omega)$ is different for $\vec{Q}$ along [100] and [111] because the group velocities are different along these directions. This means that the elastic constants determined in a neutron scattering experiment cannot strictly be expected to show the tensor properties normally associated with elastic constants. The discrepancies in alkali halides are expected to be very small [1] however.

In the simple pseudo-potential model of a metal [3] the electron-phonon matrix element depends only on the momentum transfer, $\vec{Q}$. Hence $M_{\alpha\beta}(\vec{q}j)$ of Eq. (1) does not depend on the electron momentum $\vec{q}$. In the Hartree self-consistent field approximation the response of the electron gas is described by $\frac{Q^2}{4\pi e^2}\left[\frac{1}{\epsilon(\vec{Q},\Omega)} - 1\right]$. The dielectric constant $\epsilon(\vec{Q},\Omega)$ is isotropic and can be expressed in terms of the velocity of the probe $v = \Omega/|\vec{Q}|$ as [4]

$$\epsilon(\vec{Q},\Omega) = 1 + \frac{k_s^2}{Q^2}\left[1 + \frac{mv}{2\hbar k_F}\ln\left|\frac{mv - \hbar k_F}{mv + \hbar k_F}\right|\right]$$

This expression shows that the effective screening is dependent on the velocity of the sound wave, especially if v becomes comparable with the Fermi velocity $v_F = \hbar k_F/m$. In nearly free-electron metals (sodium, aluminum, lead) v_F is about 1000 times the velocity of the sound waves and hence the static approximation, $v = 0$, is very good for all of the elastic waves. However in transition metals and semiconductors with very flat energy bands, and large effective masses, the screening may be different for the different elastic waves and give rise to effects which are similar to those discussed above.

In the collision dominated region one part of the elastic constant is still given by Eq. (1) but now the frequency, Ω, is less than the inverse lifetime of the excitations $(\vec{q}j)$, and one can no longer ignore what happens to the excitations after they have decayed. If Ω is very small, then within one period of the elastic wave the excitations that are interacting with it can decay by collision with other excitations which themselves in turn decay. To account in detail for all these extra contributions to the susceptibility is then quite complex and involves the summing of an infinite set of ladder diagrams [5]. Fortunately, at very low frequencies sufficient collisions take place within one period of the elastic wave that the net effect may be described as a change in temperature. Thermodynamic equilibrium appropriate to the applied strain of the elastic wave is then attained, and we may use the equations developed by Guyer and Krumhansl [6].

If $\Omega \ll \Gamma(\vec{q}j)$, the susceptibility may be shown to be equivalent to the static approximation results of Eq. (4). In addition we must consider the changes in temperature which occur as a result of the strain, η. If the change in temperature is T_1 the contribution to the elastic constant $C_{\alpha\beta\gamma\delta}$ is

$$\frac{1}{V}\, F_{\alpha\beta}\, \frac{T_1}{\eta_{\gamma\delta}}$$

where $F_{\alpha\beta} = \frac{\partial^2 F}{\partial T \, \partial \eta_{\alpha\beta}}$ is a derivative of the free energy.

The equations of conservation of energy and momentum [6] can be used to deduce the ratio $T_1/\eta_{\gamma\delta}$. For a longitudinal strain in a cubic crystal the resulting change in elastic constant can be shown to be

$$\frac{1}{V} \; F_{\alpha\beta} \; \frac{(-\Omega^2 Y\tau + i\Omega)P + Q^2 \; J\tau}{(-\Omega^2 Y\tau + i\Omega)C_v + Q^2 \; H\tau} \qquad (5)$$

The relaxation time τ is the momentum collision operator introduced in Ref. [6], while P, Y, J, C_v, and H are simple sums over the phonon states. For example, the thermal conductivity is given by $H\tau$, and C_v is the specific heat.

As Ω and $\vec{Q}$ tend to 0, Eq. (5) reduces to

$$\frac{1}{V} \; F_{\alpha\beta} \; \frac{P}{C_v}$$

which is the well known difference between the adiabatic and isothermal elastic constants. At high frequencies if $Y\tau\Omega > 0$ and these equations are still applicable, a second sound mode occurs with a velocity of $(H/C_v Y)^{1/2}$.

It can be seen that the difference between the isothermal elastic constants and the zero-sound elastic constants is given by the difference between $\chi(\vec{q}j,\vec{Q}0)$ and $\chi(\vec{q}j,\vec{Q}\Omega)$. As discussed above, this will frequently be an appreciable positive quantity if the velocity of the elastic wave tends to be larger than the velocity of the excitations. One must also consider the effect of the difference between adiabatic and isothermal propagation. Numerical estimates have been made [1] of the net difference between the adiabatic and zero-sound elastic constants in alkali halides and are shown in Fig. 1.

Also shown in Fig. 1 are experimental results [2] obtained with a triple-axis neutron spectrometer. Since there is the possibility of systematic errors in the determination of the absolute elastic constants because of the finite $\vec{Q}$-space resolution of the instrument , the temperature dependence of the elastic constants was determined in order to minimize these errors. The results were obtained under several different experimental conditions and are believed to be independent of experimental resolution. The ultrasonic measurements of Haussühl [7] were used to obtain the differences shown in Fig. 1. It is seen that phonon-phonon interactions give rise to quite significant differences between the zero- and first-sound elastic constants as predicted by the theory. The magnitude of the difference is in reasonable agreement with the theoretical predictions. The theory also predicts quite different attenuations but this has not been observed.

The theory is essentially the same if the elastic wave interacts with magnons or electrons. However if the excitations

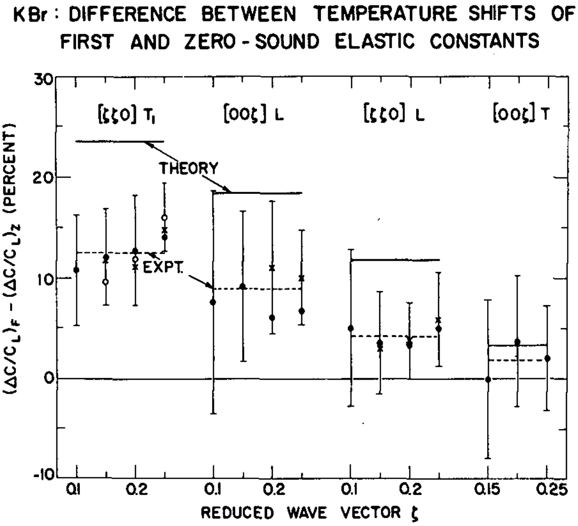

FIG.1. The difference in the temperature dependence of the first-sound and zero-sound elastic constants for four directions of wave-vector.

have much greater velocity than the elastic waves the static approximation is valid both for $\Omega \gg \Gamma$ and $\Omega \ll \Gamma$ and gives identical results in both regions. The thermodynamic effects will also be negligible if the Fermi temperature or Curie temperature is much greater than the temperature of the experiment.

There are other cases where ultrasonic measurements of elastic constants and neutron scattering measurements yield different results. Although these do not occur in all materials, they do give rise to more dramatic effects and are usually associated with phase transitions. We shall illustrate this type of behaviour with two examples.

DKDP is a ferroelectric with Curie temperature 213°K and exhibits piezoelectricity in the paraelectric phase. It is well known [8] that an elastic constant, C_{66} in this case, is anomalously temperature dependent. This temperature dependence arises because there is a coupling between the elastic waves and the electric polarization. The behaviour of the latter may be represented by a simple excitation. The elastic constant is then given by

$$-\frac{1}{V} \; M_{\alpha\beta} \, M_{\gamma\delta} \, \chi_p(\vec{Q}\Omega)$$

where χ_p is the susceptibility of the electric polarization. Suppose we write

$$\chi_p(\vec{Q}\Omega) = \frac{1}{\hbar} \; \frac{1}{\omega_p^2 - \Omega^2 + i\Omega\Gamma}$$

then, as the Curie temperature, T_c, is approached, the dielectric constant measurements show that $\omega_p^2 \to 0$ as T-T_c and

$\chi_p(0,0)$ diverges. This expression also shows that the dielectric susceptibility $\chi(\vec{Q},\Omega)$ can be determined by measuring the elastic constants at all $\vec{Q}$ and Ω as pointed out by Dvorak [9]. In DKDP $\Gamma \gg \omega_p$, and over much of the temperature range $\omega_p > \Omega$ [10]. The susceptibility is then

$$\mathrm{Re}\ \chi_p\ (\vec{Q},\Omega) = \frac{1}{\hbar}\ \frac{\omega_p{}^2}{\omega_p{}^4 + \Omega^2\Gamma^2}$$

Since $\omega_p{}^2/\Gamma < 10^{11}$ cps, there is zero contribution from this term to the elastic constant determined at high frequencies by neutron scattering. However the elastic constant determined by ultrasonic techniques should behave as $1/\omega_p{}^2$ or $1/(T-T_c)$ as is found for C_{66}. The difference between the high and low frequency elastic constants is clearly exhibited in Fig. 2 where neutron and ultrasonic results are compared.

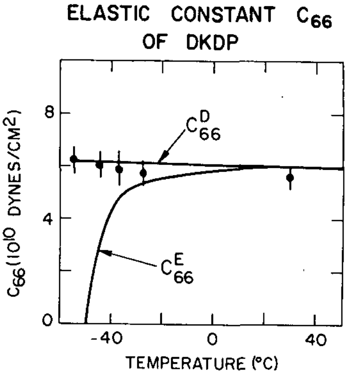

FIG.2. The difference between the temperature dependence of the high- and low-frequency elastic constants, C_{66}, in KD_2PO_4. The solid circles are the high frequency neutron measurements and the solid lines are the low frequency elastic constants for the shorted (C^E_{66}) and insulated (C^D_{66}) crystal, as deduced from the piezoelectric constants of KDP and dielectric constant of DKDP [8].

If the polarization mode was not overdamped, the elastic constant as determined by neutron scattering would differ from that obtained with ultrasonics only when $\omega_p{}^2 < \Omega^2$. This is illustrated in the experiments of Gammon and Cummins [11] on TGS.

It is worth commenting that the elastic constant obtained in DKDP is identical with the elastic constant at constant electrical displacement, C^D_{66}. This may be measured at low frequencies on the insulated crystal when the response of the polarization modes is inhibited by the surface charges but at higher frequencies when the wavelength is much shorter than the specimen, C^E_{66} is obtained by ultrasonic techniques.

A last example of the difference between first- and zero-sound elastic constants is given by $SrTiO_3$, which has a transition at 110°K associated with an anomaly in the elastic constants [12]. Figure 3 shows the behaviour as determined by ultrasonic and neutron scattering techniques [13]. Clearly the behaviour is very different in the two cases. Although the

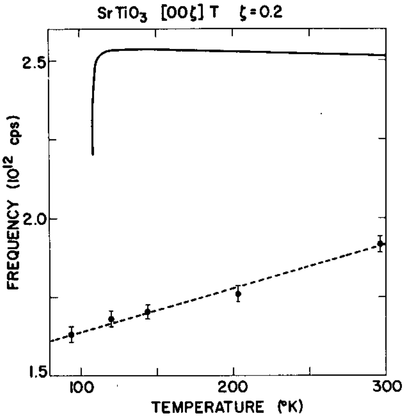

FIG.3. The frequency of a TA [100] mode of small wave-vector in $SrTiO_3$ as a function of temperature, as measured by neutron scattering [13], and by ultrasonic means [12].

theory of this transition is not yet definitely established, it may arise from an accidental degeneracy of two phonon branches. The behaviour then arises in a similar manner to that of the anharmonic interactions.

These examples illustrate the difference between elastic constants as determined by ultrasonic and neutron scattering methods. This difference arises because the mode of propagation is different at high and low frequencies. Clearly neutron scattering provides an invaluable way of studying the difference between these two different modes of propagation.

REFERENCES

[1] COWLEY, R.A., Proc. Phys. Soc. 90 (1967) 1127.

[2] SVENSSON, E.C., BUYERS, W.J.L., Phys. Rev. 165 (1968) 1063.

[3] SHAM, L.J., ZIMAN, J.M., Solid State Physics 15 (1963) 223.

[4] NOZIERES, P., PINES, D., Normal Fermi Liquids, Benjamin, New York (1966).

[5] SHAM, L.J., Phys. Rev. 156 (1967) 494.

[6] GUYER, R.A., KRUMHANSL, J.A., Phys. Rev. 148 (1966) 766 and 778.

[7] HAUSSÜHL, S., Z. Physik 159 (1960) 223.

[8] JONA, F., SHIRANE, G., "Ferroelectric Crystals" p. 18 MacMillan, New York (1962)

[9] DVORAK, V., Can. J. Phys. 45 (1967) 3903.

[10] PAUL, G.L., COCHRAN, W., BUYERS, W.J.L, COWLEY, R.A., Phys. Rev. Letters (1968) (to be published) and also this conference.

[11] GAMMON, R.W., CUMMINS, H.Z., Phys. Rev. Letters 17 (1966) 1963.

[12] BELL, R.O., RUPPRECHT, G., Phys. Rev. 129 (1963) 90.

[13] COWLEY, R.A., Phys. Rev. 134 (1964) A981.

ETUDE DE LA DYNAMIQUE DU RESEAU DE MgF_2 PAR DIFFUSION INELASTIQUE DE NEUTRONS

R. KAHN, J.P. TROTIN, D. CRIBIER et C. BENOIT*
CEA, CENTRE D'ETUDES NUCLEAIRES DE SACLAY,
FRANCE

Abstract

STUDY OF THE DYNAMICS OF THE LATTICE OF A MgF_2 MONOCRYSTAL BY INELASTIC NEUTRON SCATTERING. By analysing the inelastic neutron scattering in a MgF_2 monocrystal with a triple-axis spectrometer, the phonon dispersion relations were determined.

This study was made to prove the calculations of the two-phonon process for the i.r. and Raman spectra of MgF_2.

ETUDE DE LA DYNAMIQUE DU RESEAU DE MgF_2 PAR DIFFUSION INELASTIQUE DE NEUTRONS. Les auteurs ont déterminé, par l'analyse de la diffusion inélastique de neutrons lents d'un monocristal de fluorure de magnésium à l'aide d'un spectromètre à trois axes, des relations de dispersion de phonons.

Cette étude a pour but de fournir des renseignements pour calculer les processus à deux phonons dans les spectres infra-rouges et Raman du MgF_2.

L'interprétation des spectres infra-rouges du MgF_2, et plus particulièrement des interactions d'un photon avec deux phonons de vecteurs d'onde opposés, nécessite une bonne connaissance de la densité des états et des courbes de dispersion des phonons dans les directions de symétrie du réseau.

La théorie des groupes a permis de dénombrer et de définir l'activité de tous les modes de vibration au centre de la zone de Brillouin [1]. Deux études théoriques de la dynamique de ce réseau ont été prises parallèlement. Dans l'un des cas [2] c'est le modèle à ion rigide de Born [3] qui a été choisi, dans l'autre [4] on a pris pour base un modèle purement élastique.

Les mesures que nous avons effectuées par diffusion inélastique de neutrons lents avaient pour but de vérifier certaines conclusions de ces modèles théoriques afin de faciliter un travail de dépouillement du spectre optique actuellement en cours à la Faculté des sciences de Montpellier.

Des travaux expérimentaux antérieurs nous ont apporté des renseignements importants sur ce réseau cristallin. MgF_2 cristallise dans le groupe spatial $P4_2$ m n m avec six atomes par maille [5] (fig. 1). Les constantes élastiques ont été mesurées récemment [6]. Quelques résultats ont aussi été obtenus en infra-rouge [7] et par diffusion Raman [8]. Les sections efficaces de diffusion cohérente des noyaux de fluor et de magnésium sont sensiblement identiques et les sections efficaces de diffusion incohérente et de capture sont faibles. Ces dernières données sont particulièrement favorables pour une analyse aux neutrons thermiques.

CONDITIONS ET TECHNIQUE EXPERIMENTALES

Le cristal utilisé se présente approximativement comme un cube de quatre centimètres d'arête. Il a été obtenu par Stevenson à l'Université d'Aberdeen [9]. Les mesures dont nous rendons compte ici ont été réalisées sur le spectromètre à trois axes du réacteur EL3 à Saclay. La géométrie de cet appareil permet d'y sélectionner la longueur d'onde des neutrons incidents entre 1 et 3 Å. Nous avons mesuré celle-ci à 3,5‰ près en analysant un spectre de poudre de «nickel». Le monochromateur et l'analyseur sont des monocristaux de plomb (15 × 6 × 2 cm) et ont une mosaïcité de 20'. Les directions des faisceaux incident et diffusé par l'échantillon sont définies par deux collimateurs à fentes de Soller de 30' d'ouverture (fig. 2). Le cristal a été orienté pour que les directions [100] et [001] soient contenues dans le plan de diffusion. Nous utilisons la méthode à «Q constant» et tous nos schémas de diffusion correspondent à des créations de phonons dans le cristal.

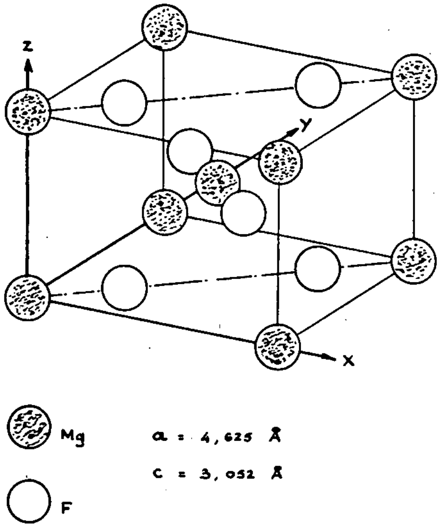

FIG.1. Structure du MgF_2.

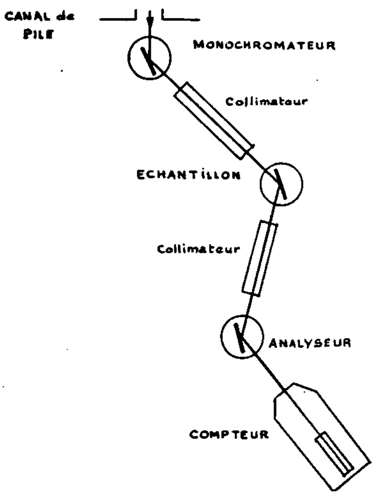

FIG.2. Géométrie du spectromètre à trois axes de EL3.

Nous avons tenté, pour chaque mesure, de réaliser les meilleures conditions de focalisation. La géométrie actuelle de notre spectromètre ne nous a pas toujours permis d'atteindre ce but. En effet la limitation de l'angle de diffusion à 100 degrés implique pour la mesure d'un phonon donné une limite supérieure dans le choix de la longueur d'onde initiale. Par ailleurs il nous est impossible de déplacer les bras de diffusion de part et d'autre de leur zéro: le seul trajet possible pour le faisceau est celui que représente la figure 2. Il semblerait d'après quelques études théoriques faites sur ce sujet que cette dernière limitation empêche dans certains cas la réalisation des conditions de focalisation optimales [10].

RESULTATS

Le choix du plan de diffusion nous a permis de tracer quelques courbes de dispersion pour les directions [100] et [001] (fig. 3). La rapide diminution de la section efficace pour les phonons de grande énergie a limité

TABLEAU I. TABLEAU COMPARATIF DES RESULTATS EXPERIMENTAUX ET THEORIQUES

Modes de vibration		Modèle théoriques ou techniques expériment.	Fréquence en 10^{12} c/s $\lvert\vec{q}_{[001]}\rvert = 0,5$	Vitesse du son dans la direction [001] en m/sec		Vitesse du son dans la direction [100] en m/sec	Fréquence en 10^{12} c/s $\lvert\vec{q}_{[100]}\rvert = 0,5$
Acoustiques Transversaux Le mode polarisé suivant [010] ne figure pas ici		Mod.ionique	6,7	4 200		3 400	4,1
		Ultrasons		4 250		4 250	
		Neutrons	6,5 ± 0,2	4 300 ± 150		4 600 ± 400	4,3 ± 0,4
Acoustiques Longitudinaux		Mod.ionique	10,4	7 200		6 400	6,4
		Ultrasons		8 000		6 700	
		Neutrons	10,4 ± 0,3	7 800 ± 600		7 400 ± 400	6,6 ± 0,2
			$\lvert\vec{q}_{001}\rvert = 0,5$		$\lvert\vec{q}\rvert = 0$		$\lvert\vec{q}_{100}\rvert = 0,5$
Optiques	1	Mod.ionique	6,6		2,75		4,1
		Mod.élast.			2,75		
		Raman			2,75		
		Neutrons	6,2 ± 0,2		2,65±0,25		4,2 ± 0,2
	2	Mod.ionique	10,4		5,4		3,65
		Mod.élast.			5,9		
		Neutrons			6,25±0,2		4,5 ± 0,2
	3	Mod.ionique	5,7		7,3		6,4
		Mod.élast.			7,5		
		Infra-rouge			7,4		
		Neutrons			7,3±0,3		6,6 ± 0,2

nos mesures à des fréquences inférieures à 8.10^{12} c/s. Les marges d'erreurs (tableau I) pourront paraître grandes dans certains cas mais les très nombreux parmètres indépendants intervenant dans ces mesures introduisent inévitablement une imprécision globale importante. Les incertitudes angulaires dans les réglages initiaux de l'appareil ont une répercussion sur les résultats des erreurs systématiques, fonction de la géométrie du diagramme de diffusion et des transferts d'énergie. D'autre part pour chaque mesure le pointage de la fréquence s'effectue avec une certaine erreur qui dépend en particulier de la largeur de la raie. Cette dernière erreur reste souvent assez faible par rapport aux incertitudes décrites plus haut. Nos mesures ne nous permettent pas de définir des dégénérescences en bout de zone dans la direction [100] pour $\nu \sim 4 \cdot 10^{12}$ c/s. Par contre, si nous trouvons bien la dégénérescence à $\nu = 6{,}6 \cdot 10^{12}$ c/s, le mode optique correspondant, donné pour transverse avec une polarisation [010] dans les études théoriques, nous semble, de par la zone où nous avons pu conduire la mesure, avoir une polarisation dans le plan de diffusion choisi et plutôt longitudinale.

Le modèle ionique [2] donne, dans l'ensemble, une bonne interprétation de nos résultats. Pourtant l'accord n'est pas aussi bon pour tous les modes de vibration et on relève en particulier un écart notable (mais constant) pour la seconde branche optique ($\nu \sim 6 \cdot 10^{12}$ c/s à $|\vec{q}| = 0$). Le modèle élastique semble plus favorable dans ce cas précis.

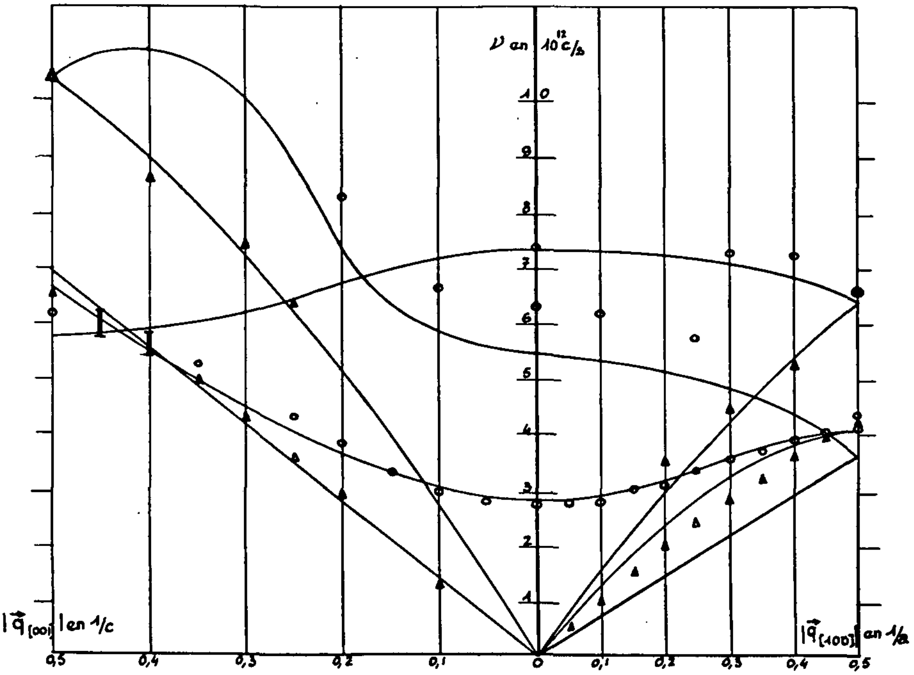

FIG.3. Courbes de dispersion dans le MgF_2 pour les directions [001] et [100]. Courbes théoriques d'après Katiyar et Krishnan [2]. Résultats expérimentaux aux neutrons: Δ phonons acoustiques, O phonons optiques.

CONCLUSION

Cette contribution expérimentale permettra sans doute d'affiner les modèles et ainsi de mieux interpréter les interactions du premier et du deuxième ordre entre le rayonnement électromagnétique et les vibrations de ce cristal.

REFERENCES

[1] NARAYANAN, P.S., J. Indian Acad. Sci. 32A (1950) 279.
BENOIT, C., VERGNOUX, A.M., J. Phys., Suppl. tome 27 (1966) C2-35.
[2] KATIYAR, R.S., KRISHNAN, R.S., Can. J. Phys. 45 (1967) 3079.
[3] BORN, M., HUANG, K., Dynamical Theory of Crystal Lattices, Oxford University Press, London (1954).
[4] BENOIT, C., VERGNOUX, A.M., Communication privée.
[5] DANAS, System of Mineralogy.
[6] WICKOFF, Tables.
FERGUSSON, J., GUGGENHEIM, H.J., KIMIMURA, H., TANABE, Y., J. chem. Phys. 42 (1965) 775.
[6] HAUSSUHL, Communication privée.
[7] BARKER, A.S., Phys. Rev. 136 (1964) 1290.
[8] PORTO, S.P.S., FLEURY, P.A., DAMEN, T.C., Phys. Rev. 154 (1967) 522.
[9] BENOIT, C., KAHN, R., TROTIN, J.P., STEVENSON, R.W.H., Comptes Rendus Séance du 4 mars 1968.
[10] PECKHAM, G.E., SAUNDERSON, D.H., SHARP, R.I., Br. J. appl. Phys. 18 (1967) 473.

PHONON DISPERSION RELATIONS IN NaCl AT 80°K

L. ALMQVIST*, G. RAUNIO* AND R. STEDMAN
AB ATOMENERGI,
STUDSVIK, NYKÖPING,
SWEDEN

Abstract

PHONON DISPERSION RELATIONS IN NaCl AT 80°K. Measurements on sodium chloride are in progress, using one of the neutron spectrometers with two-crystal monochromators which have recently begun to operate at the R2 reactor in Studsvik. Although lattice vibrations in sodium chloride might be termed one of the classical problems of solid state theory, experimental examination with neutrons is hampered by the considerable absorption and incoherent scattering and the difficulty of obtaining a large high-quality crystal. However, an almost complete set of phonon dispersion curves has now been determined, and these may be compared with the curves calculated by Karo and Hardy (1966) for their most sophisticated model (deformation dipole, next-nearest neighbours included). There are significant differences almost everywhere at the higher frequencies. The 'breathing shell' model of Schröder gives a better fit.

1. INTRODUCTION

One of the first proper applications of the Born-von Kármán theory to the calculation of phonon dispersion relations was by Kellerman [1] for NaCl, an appropriate substance for the purpose on account of the simplicity of its structure, the relative lack of complication in its ions, and the availability of good data on which to base the calculation. A glance at any list of abstracts shows that theoretical interest in NaCl has continued unabated since then; among publications containing data on phonon frequencies, calculated with successively improved models, are those of Lundqvist et al. [2], Hardy and Karo [3], Karo and Hardy [4], and Nüsslein and Schröder [5]. Experimental attention to NaCl comes rather late – neutron measurements on LiF, NaF, NaI, KBr, KI and, of course, a number of metals came earlier – and the reason is that neutron absorption in chlorine makes NaCl difficult to deal with. Buyers and Smith [6] obtained some points on the [1, 1, 1] LA, [1, 1, 1] LO and [2, 0, 0] TA dispersion curves at 295°K, using X-rays, but the difficulties of such experiments make them inferior to neutron experiments at the present time. A brief report of neutron work by Schmunk [7] (300°K) has appeared, but as yet no full account. Our measurements on NaCl at 80°K are nearing completion. They have been laborious because count rates have been low, particularly on the longitudinal optical branch – a common experience for high-frequency phonons.

2. APPARATUS AND METHOD

The measurements have been performed on a new crystal spectrometer at the reactor R2 in Studsvik (a light-water reactor with a maximum thermal

---

* From the Chalmers University of Technology, Gothenburg, Sweden.

flux of 3×10^{14} n cm^{-2} sec^{-1}). This spectrometer has a two-crystal monochromator, an arrangement with advantages that outweigh the disadvantage of intensity loss in reflection at a second crystal, at least for a high-resolution instrument operating at a reactor like R2, which delivers beams with a high proportion of fast neutrons. Figure 1 is a plan of the spectrometer, together with its twin which operates at the same beam hole. Considerable attention has been paid to shielding and this has resulted in a background level of about 7 counts per hour when thermal neutrons entering the analyser from the sample are suppressed by cadmium. A complete account of the spectrometer will be published soon.

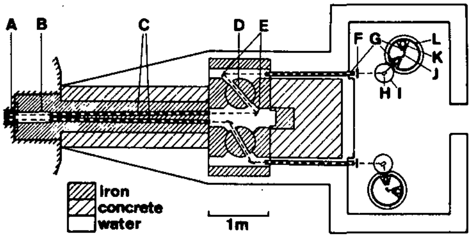

FIG.1. Plan of the twin spectrometers with two-crystal monochromators now operating in Studsvik. A – collimator plug, B – shutter housing, C – evacuated beam tubes, D – rotating collimator, E – monochromator crystals, with a rotary-translatory movement, F – monitor, G – collimators, H – sample, I – cryostat, J – analyser crystal, K – detector, L – second monitor.

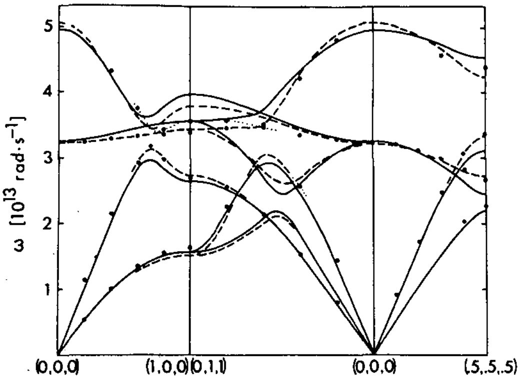

FIG.2. Dispersion curves for the principal directions in NaCl. Our data are denoted by filled circles, with dotted lines in some places to indicate the branch, calculated curves from Karo and Hardy [4] by solid lines and from Nüsslein and Schröder [5] by dashed lines (where they differ from those of Karo and Hardy).

All measurements were carried out with constant-$\vec{K}$ programmes, and applying focusing conditions to obtain as good a resolution as possible without sacrificing intensity.

A detail of some practical importance is the special difficulty of carrying out measurements on optical branches at q = 0, because this is a singular point for phonon polarizations. For instance, the longitudinal polarization vector in the neighbourhood of a reciprocal lattice point is radial with respect to that point, and the mean value of the factor $(\vec{K} \cdot \hat{e})^2$

in the cross-section for one-phonon scattering, taken over a small sphere, is at the origin one third of what it is a short distance away in the $\vec{K}$ direction. ($\vec{K}$ is the neutron's change of momentum and $\vec{e}$ the phonon's polarization vector.) In actual fact, the appropriate volume to integrate over is not a sphere but the momentum resolution ellipsoid, and since the largest dimension of this is usually perpendicular to the plane of scattering, the intensity attenuation factor is likely to be less than one third. For the transverse optical branch at $q = 0$ the attenuation factor is two thirds for the sphere, and larger in the more realistic case. Since the LO phonon at $q = 0$ is the most difficult one to carry out measurements on even without this reduction of intensity, it may be concluded that it is advisable to interpolate to this position from frequencies measured in the immediate neighbourhood, or possibly to use a special collimator arrangement to obtain a momentum resolution ellipsoid with marked elongation in the $\vec{K}$ direction.

The crystal is a slab 60 mm × 40 mm × 7 mm , with a mosaic width of about 0.1°. Several larger crystals were examined with neutrons initially and they all exhibited marked macro-structure. The present crystal is a piece cut from one of them. The crystal was mounted in a liquid nitrogen cryostat.

3. RESULTS

Figure 2 shows the results hitherto obtained, plotted together with dispersion curves calculated by Karo and Hardy [4] for a model with deformable ions and second-neighbour interactions, and by Nüsslein and Schröder [5] for their 'breathing shell' model.

Table I gives some principal values of the frequencies. The labels LO, TO, LA, TA refer to decreasing order of magnitude. Values for 300°K from Schmunk [7] are included for comparison. Our values for the (0, 0, 0) LO and TO frequencies exactly satisfy the Lyddane-Sachs-Teller relation, taking the dielectric constants quoted by Karo and Hardy [4].

TABLE I. SOME PRINCIPAL PHONON FREQUENCIES FOR NaCl

q	Branch	ω (80°K) (10^{13} rad/sec)	ω (300°K) [1] (10^{13} rad/sec)
(0, 0, 0)	LO	4.92 ± 0.04	
	TO	3.25 ± 0.02	2.96
(1, 0, 0)	LO	3.64 ± 0.01	3.40
	TO	3.40 ± 0.01	3.19
	LA	2.66 ± 0.02	2.58
	TA	1.65 ± 0.01	1.45
(0.5, 0.5, 0.5)	LO	4.33 ± 0.06	
	TO	3.37 ± 0.01	3.16
	LA	2.69 ± 0.02	
	TA	2.28 ± 0.01	2.13

Errors increase with frequency in the way indicated in Table I, although the errors there tend to be higher than elsewhere since they are for points where the gradient of the dispersion function is zero and focusing cannot be applied.

Only very approximate data on phonon widths have been obtained, but even upper limits may be of some value. The largest observed width is about 0.2×10^{13} rad/sec, for a frequency near the highest, while for the many phonons with frequencies in the range 2.5 to 3.5×10^{13} rad/sec the widths are not greater than about 0.1×10^{13} rad/sec. Most resolution widths were between 0.05 and 0.15×10^{13} rad/sec, and the peaks were therefore seldom properly resolved.

4. COMMENTS

The input data of Karo and Hardy [4] include the sound velocities, the frequency of the TO branch at (0, 0, 0) and, through $(\epsilon_0/\epsilon_\infty)^{\frac{1}{2}}$, the LO frequency at the same point. So good agreement with experimental phonon frequencies out to about q = 0.5 for all branches can be expected. This applies even to the relatively simple rigid-ion model that Kellermann in pre-computer days was obliged to adopt (though Kellermann's actual results, shown by Karo and Hardy in their Fig. 2, were based on incomplete input data). The inclusion of ion deformability in the model (see Karo and Hardy's 'DD' results [4]) introduces maxima and minima in the [1, 0, 0] and [1, 1, 0] directions which are evidently an essential part of the dispersion picture. We are not in a position to say whether the appreciable discrepancies between calculated and measured values, e. g. in the neighbourhood of (1, 0, 0) LO, are due to basic deficiencies of the model used by Karo and Hardy or whether they could be removed by an adjustment of the parameters used in the calculation. Also, of course, the comparison of theory and experiment suffers from the present incompleteness of the experimental data.

In Fig. 2 the calculated curves of Karo and Hardy for acoustic phonons lie significantly below the experimental frequencies for small values of q. The discrepancy disappears if more recent values of the elastic constants [8] are used to calculate sound velocities.

The curves calculated by Nüsslein and Schröder [5], without any adjustment of parameters to fit neutron data, agree on the whole astonishingly well with experiment – consider, for instance, the whole of the TO (ω_2) and LA (ω_4) branches.

Woods et al. [9] made measurements on KBr at 90 and 400°K, and found shifts of frequency which were largest for the TO branch (where they averaged 8%) and elsewhere considerably smaller. The general magnitudes of phonon frequencies in KBr are only about 0.4 of what they are in NaCl, so the change from 90 to 400°K there is relatively much larger than the change from 80 to 300°K in NaCl, and it is accordingly rather unexpected that the difference between our results and those of Schmunk [7] shown in Table I are so large in most cases. There is nothing in the thermal expansion coefficients and Grüneisen parameters of NaCl and KBr to indicate any marked difference in properties dependent on the third-order anharmonic term, but a relatively large fourth-order anharmonic effect in KBr (with a corresponding partial tendency for phonon frequencies to shift upward as the temperature rises) could account for a difference between

NaCl and KBr in this respect. However, reliable values of frequency shifts require the same spectrometer arrangement to eliminate possible systematic errors, so we cannot base any definite conclusions on the present comparison.

ACKNOWLEDGEMENTS

We thank Mr. K.-O. Isaxon for his technical assistance during the preparation and performance of these measurements. Drs Hardy and Karo kindly sent us their calculated data on phonon frequencies in sodium chloride. Two of us, L. Almqvist and G. Raunio, gratefully acknowledge the research grants and other financial support we have received from the Swedish Council for Atomic Research.

REFERENCES

[1] KELLERMANN, E.W., Phil. Trans. Roy. Soc., London A238 (1940) 513.
[2] LUNDQVIST, S.O. et al., Arkiv Fysik 15 16 (1959) 193.
[3] HARDY, J.R., KARO, A.M., Phil. Mag. 5 (1960) 859.
[4] KARO, A.M., HARDY, J.R., Phys. Rev. 141 2 (1966) 696.
[5] NÜSSLEIN, V., SCHRÖDER, V., Phys. Stat. Sol. 21 (1967) 309.
[6] BUYERS, W.J.L., SMITH, T., Phys. Rev. 150 2 (1966) 758.
[7] SCHMUNK, R.E., Bull. Am. Phys. Soc. 12 (1967) 281.
[8] FUGATE, R.Q., SCHUELE, D.E., J. Phys. Chem. Solids 27 3 (1966) 493.
[9] WOODS, A.D.B. et al., Phys. Rev. 131 3 (1963) 1025.

LATTICE DYNAMICS
OF GALLIUM PHOSPHIDE*

J.L. YARNELL, J.L. WARREN AND R.G.WENZEL
LOS ALAMOS SCIENTIFIC LABORATORY
OF THE UNIVERSITY OF CALIFORNIA,
LOS ALAMOS, N. MEX.,
AND
P.J. DEAN
BELL TELEPHONE LABORATORIES,
MURRAY HILL, N.J.,
UNITED STATES OF AMERICA

Abstract

LATTICE DYNAMICS OF GALLIUM PHOSPHIDE. Dispersion curves for phonons propagating in the [100], [110], and [111] directions in gallium phosphide have been measured using a triple-axis neutron diffraction spectrometer operating in the constant-Q mode. The sample was a pseudo-single crystal which was prepared by gluing together 36 single crystal plates of gallium phosphide 1 to 2.5 cm in diameter and ~0.07 cm thick. The plates were grown epitaxially on substrates of gallium arsenide or gallium phosphide, and aligned individually by neutron diffraction. Rocking curves for eight reflections symmetrically distributed in the plane of the experiment had full widths at half maximum in the range 0.52° - 0.58° and were approximately Gaussian in shape. Gallium phosphide crystallizes in the zinc blende structure. A group theoretic analysis of the lattice dynamics of this structure and a shell model fit to the measured dispersion curves are presented. Various optical properties of gallium phosphide are discussed in terms of the phonon dispersion curves. In particular, the phonons which assist indirect electronic transitions are identified as those at the zone boundary in the [100] direction (symmetry point X) in agreement with theoretical and experimental indications that the extrema of the conduction and valence bands are at X and Γ (center of the zone), respectively. The LO branches lie above the TO branches throughout the Brillouin zone in contradiction to the predictions of Keyes and Mitra. The shell model fit indicates that the charge on the gallium atom is negative.

1. INTRODUCTION

Gallium phosphide is a III - V semiconductor with an indirect energy gap. It crystallizes in the cubic zinc blende structure. The atomic arrangement is similar to that of diamond in that each atom lies at the center of a tetrahedron formed by its four nearest neighbors. In contrast to diamond, each pair of nearest neighbors is composed of different elements, and there is no center of inversion. The reciprocal lattice and Brillouin zone are the same as those for the face-centered cubic lattice. The tetrahedral coordination in the direct lattice suggests covalent bonding similar to that of the Group IV diamond structure elements. However, since the atoms in the lattice are not identical, the bonding is expected to be a mixture of covalent and ionic.

Considerable information on the lattice vibrations of gallium phosphide has been obtained from optical measurements. Kleinman and Spitzer [1] have made transmission and reflectivity measurements in the wavelength region 1 to 40 μm. They obtain zone center optical phonon frequencies from an analysis of the fundamental reflection band and propose an assignment scheme involving five phonon frequencies to explain the combination bands.

---

* Work supported in part by the US Atomic Energy Commission.

Hobden and Russell [2] have measured the first and second order Raman spectra of gallium phosphide using a helium-neon laser. Their values for the zone center phonon frequencies are in agreement with those of Kleinman and Spitzer. To explain the second order Raman spectrum and the infrared combination bands, they propose an assignment scheme involving four phonon frequencies at each of two critical points. Using the same data, Krishnan and Krishnamurthy [3] propose a different scheme based on Raman supercell modes. Russell [4] has reported a revised assignment scheme based on additional Raman data. Barker [5] has recently reported zone center phonon frequencies obtained from a detailed examination of infrared and Raman spectra. His values are the most precise presently available, and are consistant with the earlier determinations.

For compounds having an indirect energy gap, such as gallium phosphide, those phonons whose wave vector joins the extrema of the valence and conduction bands accompany many electronic transitions. Frequencies of these "momentum conserving" phonons have been determined from an analysis of the structure of the intrinsic absorption edge by Dean and Thomas [6] and from absorption and luminescence of bound excitons by Dean [7].

Theoretical [8,9] and experimental [10,11] considerations suggest that the maximum of the valence band occurs at the zone center (symmetry point Γ) and the minima of the conduction band are at the zone boundaries in the (100) directions (symmetry points X). If these assignments are assumed to be valid, the wave vector of the momentum conserving phonons corresponds to the symmetry point X.

Some regularities in the phonon frequencies of the III - V compounds have been noted by Keyes [12] and Mitra [13]. These are based on critical point frequencies inferred from analysis of combination bands. They find that it is possible to choose the polarization assignments so that certain critical point phonon frequency ratios are correlated with atomic mass ratio and effective ionic charge. These correlations, when applied to gallium phosphide, predict that the frequency of the transverse optical phonon is higher than that of the longitudinal optical phonon in the outer region of the Brillouin zone. To achieve this result, these authors were forced to interchange the LO and TO assignments originally proposed by Kleinman and Spitzer.

Only one III - V compound, the direct gap semiconductor gallium arsenide, has been studied by neutron spectroscopy [14]. This experiment was undertaken to provide additional information on the lattice dynamics of III - V compounds, and to assist in the interpretation of the optical properties of gallium phosphide.

2. EXPERIMENTAL

The sample used in these measurements was a composite prepared by gluing together 36 single crystal plates of gallium phosphide. The individual plates were ~ 0.07 cm thick, and had irregular shapes with maximum dimensions in the range 1 to 2.5 cm. The total volume of gallium phosphide in the sample was ~ 9 cm^3. The plates were grown epitaxially on substrates of gallium arsenide or gallium phosphide. The plate normals were within ± 1.5° of a (111) direction.

Neutron diffraction was used to align the individual plates, as shown in Figure 1. The indicated method of alignment assumes the full point group symmetry of the reciprocal lattice, which is the symmetry of the dispersion relation. Actually, since the zinc blende structure does not possess a center of symmetry, the (111) axes are polar. In the composite crystal, the sign of the (111) axis normal to the plates alternates randomly along the stack. It can be shown, by arguments similar to those used in deriving Friedel's law, that this alternation does not effect the measurement of phonon dispersion curves.

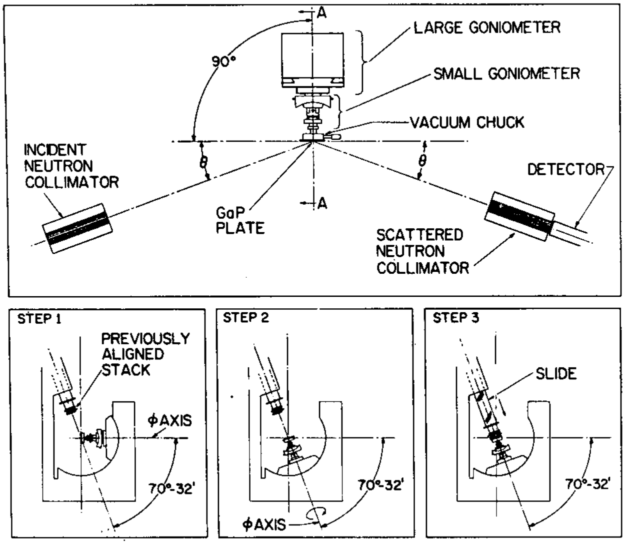

FIG.1. Method of aligning the composite sample. The upper portion of the figure shows a plan view of the apparatus, while the lower views are of the vertical plane A-A. The angle θ is set equal to the Bragg angle for the (111) reflection in GaP. An individual plate of GaP is held in the apparatus by means of a vacuum chuck. In step 1, the small goniometer is used to align a (111) plane normal to the ϕ axis of the large goniometer. In step 2, the ϕ axis is turned through 70° 32' (the angle between (111) planes in a cubic crystal) and the angle ϕ is varied until a second (111) plane is brought into the reflecting position. The orientation of the plate is now completely determined. In step 3, the previously aligned stack is moved parallel to itself by means of a slide until it just touches the plate on the goniometer. This plate is then glued to the stack, using aluminium wedges in the joint, if necessary, to avoid an excessive quantity of glue. After the glue has dried, the plate is released from the chuck, the stack is retracted, and the process repeated.

The plates were glued together with Duco Cement[1], a cellulose acetate-based adhesive. Care was taken to keep the quantity of glue to a minimum. A preliminary experiment showed that the increase in background due to the glue was negligible.

Rocking curves for the composite crystal had full widths at half maximum in the range 0.52° - 0.58°. Such curves for four reflections in the $(0\ 1\ \bar{1})$ plane used in the phonon measurements are shown in Figure 2.

The experiment was carried out on a three-axis neutron diffraction spectrometer located at the 8 Megawatt Los Alamos Omega West Reactor.

The spectrometer was operated in the constant momentum transfer mode with fixed incident energy and energy loss on scattering. The sample temperature was ~ 300° K.

---

[1] Manufactured by E. I. duPont de Nemours and Co., Inc., Wilmington, Del., USA.

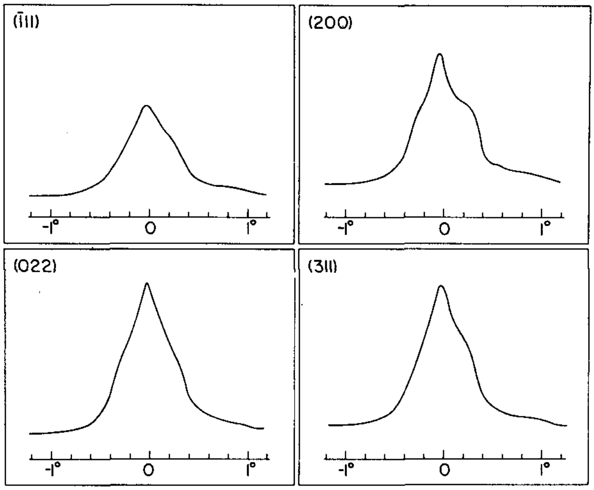

FIG. 2. Rocking curves for the composite GaP crystal.

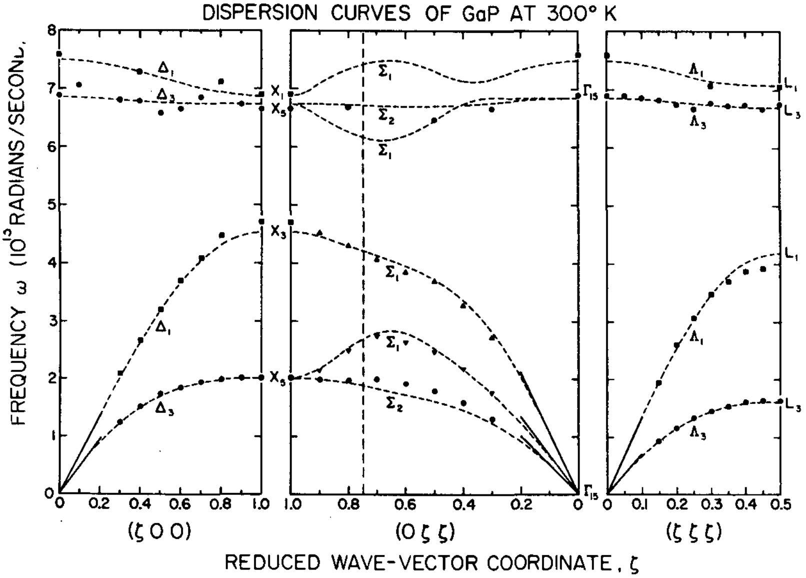

FIG. 3. Dispersion curves for phonons in gallium phosphide. Longitudinal modes are shown by squares, and transverse modes by circles. Modes whose polarizations are not determined by symmetry are indicated by triangles. The branches are also labelled by the irreducible representations according to which the associated polarization vectors transform the zone centre; optical frequencies were taken from the infrared and Raman data of Barker [5]. The initial slopes indicated by the solid lines were calculated from the elastic constants determined by Weil and Groves [15]. The dashed lines represent a shell model fit to the data.

3. RESULTS

The results of the neutron measurements are shown in Figure 3. Errors in the individual frequencies are estimated to be of the order of 2-3%. The largest errors are associated with the optical modes, for many of which the neutron groups were very weak and broad.

Table I lists the observed phonon frequencies at the critical points X and L (zone boundary in the (111) direction). For comparison we have also listed the frequencies of the momentum conserving phonons deduced from luminescence spectra. A typical luminescence spectrum is shown in Figure 4. Best values for the energies of the momentum conserving phonons, as determined from many spectra of this type, are $\hbar\omega_{TA}X = 13.2 \pm 0.1$ mev, $\hbar\omega_{LA}X = 31.6 \pm 0.2$ mev, and $\hbar\omega_{TO}X = 45.3 \pm 0.1$ mev. Since these data were obtained at 4.2° K, we have applied a temperature correction of -0.8% to obtain 300° K values. This correction was estimated from the temperature dependance of the Raman lines observed by Barker [5]. The estimated errors have been increased to take account of the uncertainty in the temperature correction. Table I also lists the frequencies assigned at critical points by Hobden and Russell[2], by Krishnan and Krishnamurthy[3], and by Russell [4] from analysis of the second order Raman data. The phonon frequencies deduced by Kleinman and Spitzer from infrared combination bands cannot easily be associated with particular critical point phonons since they give five frequencies but do not identify the corresponding wave vectors.

The dashed curves in Figure 3 represent a least squares fit of a fourteen parameter shell model to our data. The elastic constants of Weil and Groves were included in the data to be fitted [15]. The model was chosen to be the same as one used by Dolling and Waugh [14] to fit gallium arsenide in order that the parameters might be directly comparable. A comparison of parameters is made in Table II. Thirteen of the parameters were obtained by fitting the data along the symmetry lines Δ and Λ only.

TABLE I. Zone boundary phonon frequencies (units 10^{13} radians/sec).

Phonon	Neutron Data	Luminescence Data Corrected to 300° K	Hobden and Russell Ref [2]	Krishnan and Krishnamurthy Ref [3]	Russell Ref [4]
LO(X)	6.90 ± 0.23		6.74	3.84	6.64
TO(X)	6.66 ± 0.15	6.83 ± 0.03	7.14	6.63	7.40
LA(X)	4.70 ± 0.08	4.76 ± 0.04	3.24	5.75	5.37
TA(X)	2.01 ± 0.05	1.99 ± 0.03	1.94	1.96	1.97
LO(L)	7.04 ± 0.15		6.93	6.20	6.79
TO(L)	6.74 ± 0.15		7.36	6.76	7.12
LA(L)	4.00 ± 0.15		3.99	3.05	4.44
TA(L)	1.61 ± 0.03		1.21	1.43	1.42

TABLE II. Comparison of Shell Model parameters for GaAs and GaP derived from a least squares analysis of the experimental data on the basis of model C(ii) defined by Dolling and Waugh [14]. Short range force constants are in unit of(e^2/v). Quantities with subscript 1 refer to the group V atom and the subscript 2 refers to the Ga atom. Errors quoted are based on standard deviation computed in the analysis.

Parameter	GaAs	GaP
α_R	19.67	32.68 ± 2.4
γ_R	0.222	0.335 ± 0.064
γ_T	0.043	0.215 ± 0.055
S_R	1.267	1.173 ± 0.177
γ_S	-0.133	0.097 ± 0.049
Z_1	-0.018	0.31 ± 0.12
π_1	0.0754	0.0182 ± 0.0035
π_2	0.0142	0.0119 ± 0.0015
d_1	1.588	1.277 ± 0.355
d_2	0.714	0.990 ± 0.211
μ	-0.815	-2.35 ± 0.35
λ	-1.941	-2.76 ± 0.31
ν	0.736	-0.51 ± 0.20
δ	0.55	+2.14 ± 0.25

The parameter, δ, was chosen by trial to give a close match to the data in the Σ direction. In the least squares analysis the data were weighted on the assumption that the error in a given frequency was a constant percentage of that frequency. The computer code determined that percentage to be 1.7%. This is to be compared to the estimated 2-3% error in the data, and indicates the internal consistancy of the data.

The inadequacies of the shell model have already been noted by Dolling and Waugh in their discussion of gallium arsenide. We likewise find that there is a certain lack of uniqueness of the parameters which give a good fit to the data. The shell model is still the best all around interpolation scheme available for ionic and covalent materials. The physical significance of the parameters will be discussed in the next section.

4. DISCUSSION

Most phonon frequencies are 35-40% higher in gallium phosphide than the corresponding values for gallium arsenide. The zone boundary LO/LA

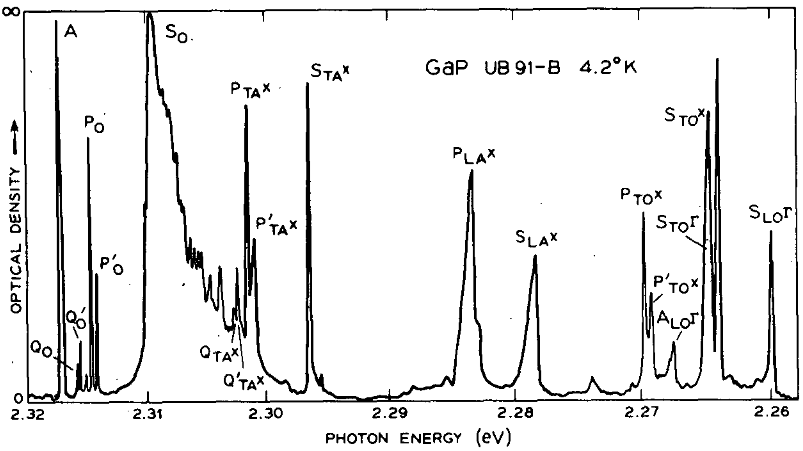

FIG.4. A portion of the low temperature luminescence spectrum of a GaP single crystal due to the recombination of indirect excitons weakly bound to impurity point defects. Line series A and S are respectively due to the recombination of excitons bound to isoelectronic nitrogen impurities and to neutral sulphur donors. Lines series P and Q have not been positively identified, though the P series is believed to involve the recombination of excitons bound to neutral silicon acceptors. No-phonon and phonon-assisted recombinations are observed, and the subscripts indicate the types of phonons. Phonons from the symmetry points X in the reduced zone, which conserve momentum in the electronic transitions at the indirect gap, are prominent in the luminescence of excitons weakly bound to neutral donors and acceptors.

ratios are also larger than in gallium arsenide, as expected from the larger atomic mass ratio. Unlike gallium arsenide, in which the LO and TO branches cross to make TO > LO at the zone boundary, the LO branch in gallium phosphide lies above the TO throughout the Brillouin zone. This ordering is opposite to that expected from the Keyes - Mitra correlation of the zone boundary LO/TO ratio with effective ionic charge [12,13]. Another example of the failure of their correlation scheme is diamond, which has zero effective charge. The predicted value of LO/TO at the zone boundary is ~ 0.85, whereas neutron spectroscopy [16] gave ~ 1.07.

Another relation which has been proposed for III - V compounds is the Brout sum rule [17,18], which states that the sum of the squares of the six frequencies at any wave vector q is independant of q. This rule is expected to be valid if the interactions are limited to first neighbor general forces plus long range electrostatic forces. In gallium phosphide, the Brout sum increases by ~ 10% from the zone center to the zone boundary. The deviation from constancy is a measure of the importance of second neighbor forces.

In Table I it may be seen that the frequencies of the momentum conserving phonons are in good agreement with the measured phonon frequencies at X, supporting the conclusions of [8,9,10,11] that the valence band maximum is at Γ and the conduction band minima are at X. Experimentally, only one momentum conserving optical phonon is observed. From neutron data, it is not possible to decide whether it is TO or LO. We favor the TO assignment, since the LO assisted transitions were very weak in diamond and not observed in silicon, whereas the TO assisted transitions were strong in both cases [19]. An alternative explanation of the observation of only one optical phonon would be the equality of the LO(X) and TO(X) frequencies to within 0.03×10^{13} rad/sec. We think that this is a less likely explanation.

Also shown in Table I are critical point phonon frequency assignments derived from analysis of second order Raman spectra. Although there are similarities, the correspondance is by no means close. This illustrates the difficulty in attempting to work backward from multiple phonon effects to specific critical point assignments via the multiple phonon density of states.

The shell model parameters for gallium arsenide and gallium phosphide are compared in Table II. The short range forces are seen to be somewhat stronger in gallium phosphide. Perhaps the most interesting feature of the parameter set for gallium phosphide is the sign of the ionic charge Z_1, which indicates that the phosphorus atom has a positive charge and the gallium atom is negative. At first glance, one might have expected the Group V atom to be negative, rather than the Group III. However, if one considers the bonding to be primarily covalent, each atom might be expected to have four electrons. This would result in the Group III atom having an extra electron and hence a negative charge. This possibility has been discussed by Slater and Koster [20] and by Hilsum [21].

5. GROUP THEORY

Group theory has three uses in this paper. The polarizations of the phonons, which enter the scattering cross section, are nearly all determined by symmetry. Group theory labels appear in Fig. 3. The dynamical matrix has been simplified by group theory in the shell model calculation.

This section summarizes information obtained from a group theoretical analysis of the lattice dynamics of the zinc-blende structure. Because of space limitations we will rely heavily on the notation and methods given in recent review articles [22,23].

The space group of GaP is $F\bar{4}3m$ or T_d^2. Atomic positions are given by the formula

$$\underset{\sim}{X}(\ell,\kappa) = \tfrac{1}{2}a_o\{[\ell_2+\ell_3+\tfrac{1}{2}(\kappa-1)]\underset{\sim}{1}_1 + [\ell_1+\ell_3+\tfrac{1}{2}(\kappa-1)]\underset{\sim}{1}_2 + [\ell_1+\ell_2+\tfrac{1}{2}(\kappa-1)]\underset{\sim}{1}_3\}$$

in the natural cubic coordinate system. The lattice constant $a_o = 5.4505$ Å is taken from Wyckoff [24]. The ℓ_i's are integers and κ is 1 or 2. The space group is symmorphic. The operations and representations of the point group of the space group can be found in Slater [25].

All sixteen elements of the dynamical matrix can be generated from only six functional forms, namely, $D_{11}(\kappa,\kappa')$ and $D_{12}(\kappa,\kappa')$ for κ,κ' = 1,1;1,2; and 2,2. Expressions for the 10 remaining matrix elements can be obtained by using Hermiticity and making cyclic permutations of the components of the wave vector in the above functional forms. A second neighbor Born-von Karman model expression for the dynamical matrix is easily obtained starting with the results of Herman [26] for the diamond structure. The only difference is that there are now two types of second neighbor interactions and the matrix elements $D_{\alpha\beta}(2,2)$ are not related to $D_{\alpha\beta}(1,1)$ by inversion symmetry although the functional forms of these elements are completely parallel[2].

---

[2] In the version of the shell model used by Dolling and Waugh, the 2nd neighbor force constants for Ga-Ga interactions and As-As interactions are made the same but the additional convention is introduced that $M_2D_{13}(22) = M_1D_{13}(11)^*$ which is really only appropriate for the diamond lattice where there is a center of inversion.

The reciprocal lattice is bcc and the Brillouin Zone is shown in Figure 5. Typical planes, lines and points of symmetry are labeled according to Parmenter [27]. Since the measurements of the dispersion curves were made along 3 symmetry lines, only these lines and their endpoints will be discussed here.

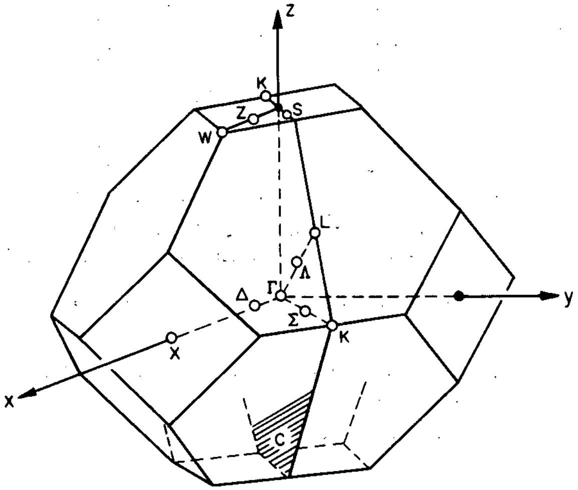

FIG.5. Brillouin zone for zinc-blende structure showing typical points, lines and planes of symmetry. The zone is the same as for diamond but the number of symmetry elements is less because of an absence of an inversion centre in the direct lattice.

Symmetry at Γ, $k_{11} = 0$.[3]

The point group of the wave vector is $G_o(k_{11}) = \bar{4}3m$. The 6 x 6 reducible representation of the point group which commutes with the dynamical matrix is called

$$T(k_{11}) = \{\underset{\sim}{T}(k_{11};\underset{\sim}{R}),\ \text{for } \underset{\sim}{R} \in G_o(k_{11})\}$$

The unitary transformation which reduces this representation into block diagonal form will also block diagonalize the dynamical matrix. We find that $T(k_{11})$ has the decomposition $T(k_{11}) = 2\Gamma_{15}$ in the notation of BSW[28]. Γ_{15} is a 3 dimensional representation and suggests three-fold degeneracy of the optical modes as well as the acoustic modes at this point. The slightly ionic character of gallium phosphide quickly breaks this symmetry as one moves away from Γ. Using symmetry relations listed in ref. [23] we find that the dynamical matrix at Γ takes the form

$$D(k_{11}) = \begin{bmatrix} A & & & C & & \\ & A & & & C & \\ & & A & & & C \\ C^* & & & B & & \\ & C^* & & & B & \\ & & C^* & & & B \end{bmatrix}$$

---

[3] The subscripted k's are a notation due to Kovalev whose tables of irreducible representations are very useful [29].

Projection operator techniques give the unitary matrix $U^{-1}(k_{11})$ which block diagonalies $D(k_{11})$ and whose columns are the symmetry adapted eigenvectors of the problem.

$$U^{-1}(k_{11}) = \begin{bmatrix} u_1 & 0 & 0 & u_2 & 0 & 0 \\ 0 & u_1 & 0 & 0 & u_2 & 0 \\ 0 & 0 & u_1 & 0 & 0 & u_2 \\ v_1 & 0 & 0 & v_2 & 0 & 0 \\ 0 & v_1 & 0 & 0 & v_2 & 0 \\ 0 & 0 & v_1 & 0 & 0 & v_2 \end{bmatrix}$$

See Ref. [23], Eq(6.36) for an evaluation of the u_i's and v_i's. It is readily established on general grounds that $AB = |C|^2$. The eigenvalues and eigenvectors for this case are discussed in the appendix of Ref. [23].

For convenience the compatibility relations at Γ are given in Table III.

TABLE III. Compatibility relations at Γ for the zinc-blende structure. Taken from Ref. [25] page 383.

	Δ	Λ	Σ
Γ_{15}	$\Delta_1 \oplus \Delta_3 \oplus \Delta_4$	$\Lambda_1 \oplus \Lambda_3$	$2\Sigma_1 \oplus \Sigma_2$

Symmetry at X, $k_{10} = 2\pi(1,0,0)/a_o$

$$G_o(k_{10}) = \bar{4}2m, \quad T(k_{10}) = X_1 \oplus X_3 \oplus 2X_5$$

X_1 and X_3 are one dimensional irreducible representations and X_5 is 2 dimensional. The dynamical matrix has the form

$$D(k_{10}) = \begin{bmatrix} A & & & & & \\ & B & & & & E \\ & & B & & E & \\ & & & C & & \\ & & E^* & & D & \\ & E^* & & & & D \end{bmatrix}$$

The matrix of eigenvectors is

$$U^{-1}(k_{10}) = \begin{bmatrix} 0 & 1 & 0 & 0 & 0 & 0 \\ 0 & 0 & 0 & u_1 & 0 & u_2 \\ 0 & 0 & u_1 & 0 & u_2 & 0 \\ 1 & 0 & 0 & 0 & 0 & 0 \\ 0 & 0 & v_1 & 0 & v_2 & 0 \\ 0 & 0 & 0 & v_1 & 0 & v_2 \end{bmatrix}$$

TABLE IV. Compatibility relations at X taken from Ref. [25] page 383.

	Δ	Σ
X_1	Δ_1	Σ_1
X_3	Δ_1	Σ_1
X_5	$\Delta_3 \oplus \Delta_4$	$\Sigma_1 \oplus \Sigma_2$

The compatibility relations are given in Table IV. Using the trial eigenvectors, one finds the eigenvalues of $D(k_{10})$ to be $\omega_1^2 = C$, $\omega_3^2 = A$

and $\omega_5^2 = \frac{1}{2}\{[B+D] \pm \sqrt{[(B+D)^2 - 4(BD-|E|^2)]}\}$

Intuitively the solutions belonging to X_5 are associated with the end-points of the transverse branches in the Δ direction. If $C > A$, then the symmetry of the point terminating the LO mode in the Δ direction is X_1. The eigenvector for this mode has the first atom in the unit cell standing still.

Symmetry at L, $k_9 = \pi(1,1,1)/a_o$ and along Λ, $k_5 = \pi(\zeta,\zeta,\zeta)/a_o$.

$$G_o(k_9) = G_o(k_5) = 3m$$

$$T(k_9) = T(k_5) = 2\Lambda_1 \oplus 2\Lambda_3$$

Λ_1 is one dimensional and Λ_3 is two dimensional.

$$D(k_5) = \begin{bmatrix} A & B & B & E & F & F \\ B & A & B & F & E & F \\ B & B & A & F & F & E \\ E^* & F^* & F^* & C & D & D \\ F^* & E^* & F^* & D & C & D \\ F^* & F^* & E^* & D & D & C \end{bmatrix}$$

$$U^{-1}(k_5) = \begin{bmatrix} u_1 & u_2 & 2u_1' & 0 & 2u_2' & 0 \\ u_1 & u_2 & -u_1' & u_1' & -u_2' & u_2' \\ u_1 & u_2 & -u_1' & -u_1' & -u_2' & -u_2' \\ v_1 & v_2 & 2v_1' & 0 & 2v_2' & 0 \\ v_1 & v_2 & -v_1' & v_1' & -v_2' & v_2' \\ v_1 & v_2 & -v_1' & -v_1' & -v_2' & -v_2' \end{bmatrix}$$

A, B, C and D are real quantities. The pure longitudinal modes belong to Λ_1, and the degenerate pure transverse modes to Λ_3.

Symmetry along Δ, $k_6 = 2\pi(\zeta,0,0)/a_o$.

$$G_o(k_6) = mm2$$

$$T(k_6) = 2(\Delta_1 \oplus \Delta_3 \oplus \Delta_4)$$

All of these representations are one dimensional. It can be shown however that time reversal symmetry requires Δ_3 and Δ_4 to be associated with the same eigenvalue.

$$D(k_6) = \begin{bmatrix} A & & & E & & \\ & B & & & F & G \\ & & B & & G & F \\ E^* & & & C & & \\ & F^* & G^* & & D & \\ & G^* & F^* & & & D \end{bmatrix}$$

$$U^{-1}(k_6) = \begin{bmatrix} u_1 & u_2 & 0 & 0 & 0 & 0 \\ 0 & 0 & u_1' & u_2' & u_1'' & u_2'' \\ 0 & 0 & u_1' & u_2' & -u_1'' & -u_2'' \\ v_1 & v_2 & 0 & 0 & 0 & 0 \\ 0 & 0 & v_1' & v_2' & v_1'' & v_2'' \\ 0 & 0 & v_1' & v_2' & -v_1'' & -v_2'' \end{bmatrix}$$

The pure longitudinal mode belongs to Δ_1 and the pure transverse modes belong to Δ_3 and Δ_4 which are degenerate in this case due to time reversal symmetry.

Symmetry along Σ, $k_4 = 2\pi(\zeta,\zeta,0)/a_o$.

$$G_o(k_4) = m$$

Any point in the symmetry plane C has this same point group symmetry.

$$T(k_4) = 4\Sigma_1 \oplus 2\Sigma_2$$

These representations are again one dimensional.

$$D(k_4) = \begin{bmatrix} A & C & D & I & K & L \\ C & A & D & K & I & L \\ -D & -D & B & M & M & J \\ I^* & K^* & M^* & E & G & H \\ K^* & I^* & M^* & G & E & H \\ L^* & L^* & J^* & -H & -H & F \end{bmatrix}$$

Herman has found that out to sixth neighbors in a general Born-von Karman model L = M. We could find no symmetry argument to justify this equality in general.

$$U^{-1}(k_4) = \begin{bmatrix} u_1 & u_2 & u_3 & u_4 & u_1' & u_2' \\ u_1 & u_2 & u_3 & u_4 & -u_1' & -u_2' \\ \sqrt{2}v_1 & \sqrt{2}v_2 & \sqrt{2}v_3 & \sqrt{2}v_4 & 0 & 0 \\ w_1 & w_2 & w_3 & w_4 & v_1' & v_2' \\ w_1 & w_2 & w_3 & w_4 & -v_1' & -v_2' \\ \sqrt{2}x_1 & \sqrt{2}x_2 & \sqrt{2}x_3 & \sqrt{2}x_4 & 0 & 0 \end{bmatrix}$$

The pure transverse modes belong to Σ_2. The other four modes are of mixed polarization and belong to Σ_1.

ACKNOWLEDGEMENTS

We wish to thank C. J. Frosch, L. C. Luther, and L. Derick for the epitaxially grown gallium phosphide crystals.

REFERENCES

[1] KLEINMAN, D. A., and SPITZER, W. G., Phys. Rev. 118 1 (1960) 110.

[2] HOBDEN, M. V., and RUSSELL, J. P., Physics Letters 13 1 (1964) 41.

[3] KRISHNAN, R. S., and KRISHNAMURTHY, N., Journal de Physique 26 (1965) 630.

[4] RUSSELL, J. P., Journal de Physique 26 (1965) 620.

[5] BARKER, A. S., JR., Phys. Rev. 165 3 (1968) 917.

[6] DEAN, P. J., and THOMAS, D. G., Phys. Rev. 150 2 (1966) 690.

[7] DEAN, P. J., Phys. Rev. 157 3 (1967) 655.

[8] COHEN, M. L., and BERGSTRESSER, T. K., Phys. Rev. 141 (1966) 789.

[9] EHRENREICH, H., J. Appl. Phys. Suppl. 32 (1961) 2155.

[10] YAFET, Y., and THOMAS, D. G., Phys. Rev. 131 (1963) 2405.

[11] ZALLEN, R., and PAUL, W., Phys. Rev. 134 (1964) A1628.

[12] KEYES, R. W., J. Chem. Phys. 37 1 (1962) 72.

[13] MITRA, S. S., Phys. Rev. 132 3 (1963) 986.

[14] DOLLING, G., and WAUGH, J. L. T., in Lattice Dynamics (WALLIS, R. F. Ed.), Pergamon Press, London (1965).

[15] WEIL, R., and GROVES, W. O., Bull. Am. Phys. Soc., Series II, 11 5 (1966) 764.

[16] WARREN, J. L., YARNELL, J. L., DOLLING, G., and COWLEY, R. A., Phys. Rev. 158 3 (1967) 805.

[17] BROUT, R., Phys. Rev. 113 (1959) 43.

[18] ROSENSTOCK, H. B., Phys. Rev. 129 (1963) 1959.

[19] DEAN, P. J., in Luminescence of Inorganic Solids (GOLDBERG, P. Ed.) Academic Press (1966) New York, p 119.

[20] SLATER, J. C., and KOSTER, G. F., Phys. Rev. 94 6 (1954) 1498.

[21] HILSUM, C., in Semiconductors and Semimetals I (WILLARDSON, R. K., and BEER, A. C., Eds.) Academic Press, New York (1966) p 3.

[22] MARADUDIN, A. A., and VOSKO, S. H., Rev. Mod. Phys. 40 (1968) 1.

[23] WARREN, J. L., Rev. Mod. Phys. 40 (1968) 38.

[24] WYCKOFF, R. W. G., Crystal Structures, 2nd ed., Interscience Publishers, New York (1963). Vol. 1, 108-10.

[25] SLATER, J. C., Quantum Theory of Molecules and Solids, McGraw-Hill In. New York (1965) Vol 2, 368-84.

[26] HERMAN, F., J. Phys. Chem. Solids 8 (1959) 405.

[27] PARMENTER, R. H., Phys. Rev. 100 (1955) 573.

[28] BOUCKAERT, L. P., SMOULUCHOWSKI, R., and WIGNER, E., Phys. Rev. 50 (1936) 58.

[29] KOVALEV, O. V., Irreducible Representations of the Space Groups, Gordon and Breach, Science Publishers, New York (1965) 61.

PHONON DISPERSION RELATION OF BERYLLIUM OXIDE*

G.L. OSTHELLER**, R.E. SCHMUNK, R.M. BRUGGER
AND R.J. KEARNEY†
IDAHO NUCLEAR CORPORATION
IDAHO FALLS, IDAHO,
UNITED STATES OF AMERICA

Abstract

PHONON DISPERSION RELATION OF BERYLLIUM OXIDE. The phonon dispersion relation measurements for BeO have been extended by neutron inelastic scattering, using the MTR triple-axis spectrometer. New data include a transverse acoustic branch and an optical branch with wave propagation in the [01$\bar{1}$0] direction and in addition the transverse acoustic, longitudinal acoustic and a transverse optic branch, all with wave propagation in the [0001] direction. The two optical branches observed are degenerate at the centre of the Brillouin zone with a frequency $\omega = 6.21 \pm 0.11 \times 10^{13}$ rad/sec. This frequency is in fair agreement with the optical data of Loh which gives $\omega = 6.41 \times 10^{13}$ rad/sec for the same mode. From the neutron scattering data of this experiment and the optical data of Loh it appears that the low-lying optical branches reported previously by Brugger et al. are not single phonon data but are the result of multiphonon processes. Comparison is made between the measured branches of the dispersion relation and the results of preliminary lattice dynamics model calculations by Young and by Solbrig.

1. INTRODUCTION

In this paper we report on an extension of the phonon dispersion relation measurements for beryllium oxide. Initial measurements on this material were made previously by Brugger et al. [1] using the phased-chopper velocity selector at the Materials Testing Reactor and the time-of-flight method. Their measurements were confined to phonons propagating in the hexagonal plane and primarily to the [01$\bar{1}$0] symmetry direction in that plane. For the [01$\bar{1}$0] direction their data included two of the acoustic branches and six optical branches.

Several groups have made preliminary calculations to obtain the dispersion relation for BeO. J. A. Young [2] has followed the general formulation for ionic crystals given by Born and Huang [3] in which the lattice potential is expressed as the sum of repulsive and Coulomb contributions. Solbrig [4] has approached the problem using general quadratic valence force fields and applying symmetry coordinates to factor the secular equation. The latter approach was used quite successfully in the case of diamond [5]. In addition to the work of Young and Solbrig, recent calculations on CdS by Nusimovici and Birman [6] have been helpful to the present work, and optical measurements by Loh [7] have established frequencies at the center of the Brillouin zone for Raman and infrared active modes.

---

* Work performed under the auspices of the US Atomic Energy Commission.

** Work performed while a graduate student at the University of Idaho.

† Member of the Physics Department, University of Idaho.

In the present work, scattering measurements were confined to phonons propagating in the crystallographic plane defined by the [0001] and [01$\bar{1}$0] directions. The MTR three axis spectrometer operating in the "constant Q" mode was used for these measurements. The third acoustical branch as well as an optical branch were mapped for the [01$\bar{1}$0] direction, and in addition the acoustical branches and an optical branch were mapped for the [0001] direction. The two observed optical branches have an intercept at $\vec{q} = 0$ of 40.9 ± 0.75 meV ($\omega = 6.21 \pm 0.11 \times 10^{13}$ rad sec^{-1}) which is compared to the value of 42.2 meV (340 cm^{-1}) obtained from recent optical measurements by Loh. General aspects of the lattice dynamics of BeO are discussed in the text; comparison is made between the present data, and 1) the data of Brugger et al, 2) optical and elastic constant data, and 3) the preliminary lattice dynamics calculations of Young and Solbrig. The present data indicate that the low lying branches observed by Brugger et al. are not branches of the dispersion relations, but probably arise from multiphonon processes. Finally estimates are made of the as yet unmeasured phonon branches for the [0001] and [01$\bar{1}$0] directions.

2. LATTICE DYNAMICS

Beryllium oxide has the wurtzite type structure which is described in terms of a hexagonal lattice with a basis having Be atoms at (0, 0, 0) and (1/3, 2/3, 1/2) and oxygen atoms at (0, 0, μ) and (1/3, 2/3, 1/2 + μ). The lattice constants for BeO are taken to be $a_1 = a_2 = a = 2.698$ Å, $a_3 = c = 4.377$ Å and $\mu = 0.378$, and the c/a ratio is very close to ideal at 1.6223 [8,9,10,11]. With 4 atoms in the hexagonal primitive cell there are 12 branches in the dispersion relation.

We are concerned primarily with phonon propagation in the two symmetry directions [0001] and [01$\bar{1}$0] in BeO. Along [0001] there are 8 distinct branches for the dispersion relation, 4 longitudinal and 4 transverse (1 acoustical and 3 optical branches for each polarization) with each of the transverse branches being doubly degenerate. Along [01$\bar{1}$0] the 12 branches are divided into two groups: first, 8 Σ_1 branches which have their polarizations in the plane of the [01$\bar{1}$0] and [0001] directions, and second, 4 Σ_2 branches which have their polarization perpendicular to both [01$\bar{1}$0] and [0001] directions. Of the 8 Σ_1 branches 2 are acoustical, one predominantly transverse and one predominantly longitudinal and the other 6 are optical whereas for the 4 Σ_2 branches one is acoustical and the other 3 are optical. The Σ_2 branches have a well defined transverse polarization while the Σ_1 branches generally do not, being dependent upon the details of the interatomic force field in the BeO crystal.

Several lattice dynamics calculations have been made in the harmonic approximation in which varying assumptions have been made regarding the nature and range of the interatomic forces. Calculations which have been applied directly to BeO were made by Young [2] and by Solbrig [4]. In Young's work the potential was expressed as the sum of a long range Coulomb contribution and a short range repulsive contribution, the latter term including interactions with only nearest neighbors. He used the value for the cohesive energy and the maximum phonon energy observed by Sinclair [12] in evaluating the two disposable parameters in the model. Solbrig has approached the problem using methods developed for calculating molecular dynamics which involve general quadratic valence force fields and the use of symmetry coordinates to factor the secular equation. His force constants are all short range in character relating to specific bond stretching and angle bending constants. The work of both Young and Solbrig should be considered as preliminary due to the lack of sufficient experimental data to evaluate parameters in the models. This point is accentuated further in the work of Sullivan [13] who has attempted to apply the shell model to wurtzite structure crystals. Even limiting short range interactions to nearest neighbors Sullivan was unable to make a unique determination of the constants in his model.

The most recent and complete lattice dynamics calculation for a wurtzite structure material is that of Nusimovici and Birman [6] on CdS. These authors expressed the potential function in terms of Coulomb and short range contributions. The latter contributions are expressed in terms of bond stretching, bond angle and cross coupling constants and include interactions out to third nearest neighbors. Nusimovici and Birman were able to evaluate the constants in their model from infrared and Raman data available on CdS. Of interest are the frequency shifts of the Γ_1 and Γ_5 modes which have different frequencies when the point $\Gamma(\vec{q} = 0)$ is approached from different directions such as [0001] and $[01\bar{1}0]$. These frequency shifts are caused by the long range electric field associated with the infrared active optical modes and are discussed in detail by Loudon [14].

Following the work of Brockhouse and Iyengar [15] Solbrig has adopted the valence force model to evaluate the structure factor for BeO which has been used as a guide in the experiments [16]. His results are reported in terms of 1) the polarization factor $|\hat{Q}\cdot\hat{\beta}_j|^2$, 2) a modified structure factor γ_j^2 and 3) the product of the first two quantities. In the evaluation of the structure factor Solbrig set the Debye-Waller factor equal to unity. The dynamic structure factor and the x-ray structure factor for BeO are periodic in the hexagonal plane but not along the c axis due to the odd spacing factor (μ) between interpenetrating lattices in the structure.

3. EXPERIMENTAL METHOD

Experimental measurements were made on the BeO single crystals using a triple axis spectrometer installed at the HT-1 south beam port of the MTR [17]. A constant initial neutron energy of 54.2 meV was used throughout these measurements which employed the constant Q mode of operation. In the experiment, the single crystals used were two beryllium oxide crystals on loan from Austerman [18], each of which was less than one cubic centimeter in volume. The crystals were individually mounted on adjustable aluminum disks and adjusted so that the reciprocal lattice plane defined by the [0001] and $[01\bar{1}0]$ directions was parallel to the scattering (horizontal) plane. The two crystals were aligned by observing elastic (Bragg) scattering from (0006), $(03\bar{3}0)$ and $(02\bar{2}3)$ crystallographic planes. The collimator between sample and detector was masked so that scattering was observed from one crystal at a time and then by comparing the two and adjusting one crystal to bring the elastic peaks into coincidence, With the sample crystals mounted as described above it was possible to investigate phonon branches having $\vec{q}$ parallel to the [0001] direction and branches having $\vec{q}$ parallel to $[01\bar{1}0]$ which have their polarization in the plane of these two symmetry directions. This means that for the $[01\bar{1}0]$ direction we could observe Σ_1 modes but not Σ_2 modes, the latter having their polarization perpendicular to the scattering plane.

4. RESULTS AND DISCUSSION

Six branches of the BeO dispersion relation were measured in the present experiment. Five of these represent new information while one branch, LA[01$\bar{1}$0], duplicates a previous measurement by Brugger et al. Table I lists the observed data giving the phonon wave vector $|\vec{q}|$, phonon frequency ω as well as the energy transfer ΔE in the scattering process, peak strength and width information and the region in κ-space where the phonon was observed. The latter information can be understood recalling that the scattering was confined to the plane containing the orthogonal crystallographic directions [01$\bar{1}$0] and [0001]. Taking these directions to be coincident with y-z axes respectively we interpret R(01$\bar{1}$5) as away from the reciprocal lattice point (01$\bar{1}$5) in the direction of increasing y (to the right). L(01$\bar{1}$5) would be away from the same lattice point in the direction of decreasing y (to the left), while A(01$\bar{1}$5) and B(01$\bar{1}$5) would be in directions of increasing z (above) and decreasing z (below) respectively from the same point. The full width at half maximum (fwhm) figure given in the table should not be construed as the accuracy of the measurements because in most cases the resonance gave well defined peaks for whch the centroids of the peaks could be determined to much higher accuracy. Fig. 1 displays the dispersion relation plot of the data listed in the table. Data shown for the [01$\bar{1}$0] direction are all Σ_1 modes.

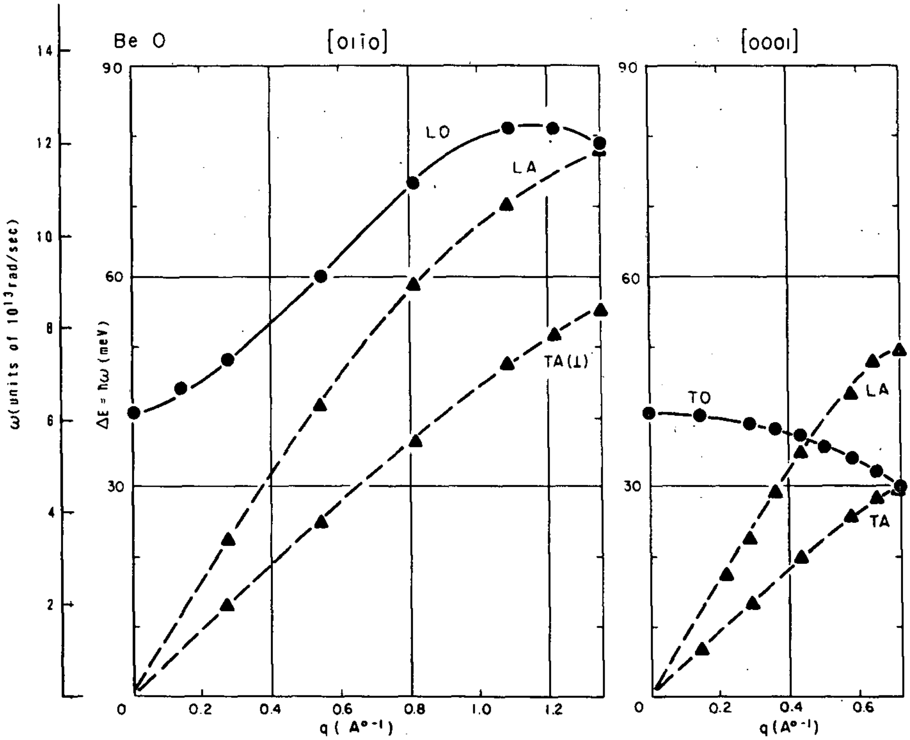

FIG.1. Dispersion relation plot of BeO phonon branches mapped in the present experiment. All branches represent new data except for the longitudinal acoustic (LA) branch for the [01$\bar{1}$0] direction.

Fig. 2 displays the data of Brugger et al. for comparison with the present data. Data for the LA[01$\bar{1}$0] branch, the only measurement repeated in the present work, are in good agreement with the previous data. Considerable effort was made to observe low lying optical branches in the range 10-20 meV which were reported in the previous experiment. It was impossible to get a good measurement at $\vec{q} = 0$ and low ΔE due to a strong background of elastic scattering. This Bragg scattering was present at lattice points for which first order Bragg scattering should be absent and was traced in every case to a double Bragg scattering from two different sets of planes which simulated the forbidden scattering. Away from the lattice points phonons were not observed, and the existence of these low lying branches is questioned. This position is supported by recent optical data which will be discussed in the following paragraphs.

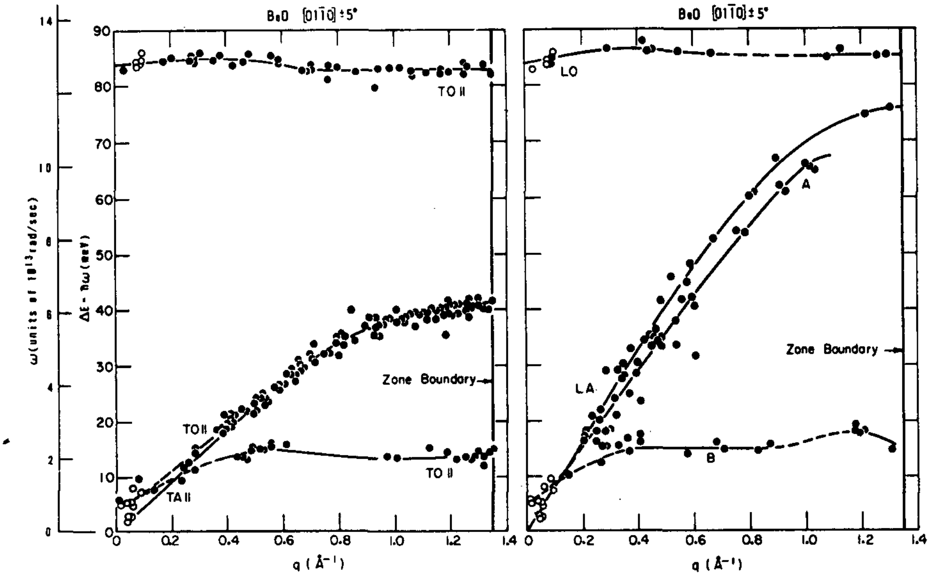

FIG. 2. BeO dispersion relation data obtained previously by Brugger et al. [1].

Other experimental data to be compared with present data include Loh's optical data and the elastic constants of Bentle [19] and of Cline et al. [20]. To put matters in proper perspective it should be noted that the series of neutron measurements reported here had been completed before Loh's optical data became available. Loh reports observing an Σ_2 mode at 340 cm^{-1} (42.2 meV) which is 3.2% higher than our optical intercept at 40.9 ± .75 meV. Although Table I indicates that the observed neutron scattering resonance at 40.9 meV was broad enough to overlap the value reported by Loh, the centroid of the observed neutron resonance was definitely lower in value than the 42.2 meV reported by Loh. Loh also reports observing another Σ_2 mode at 684 cm^{-1} (84.8 meV) which coincides with the optical branches (both Σ_1 and Σ_2 types) reported previously by Brugger et al. Our acoustical branches appear to be in agreement with both sets of elastic constant data although we have not attempted to take data at $q/q_{max} < 0.2$.

TABLE I

Listing of observed phonon data obtained by neutron scattering giving the type of mode, phonon wave vector $|\vec{q}|$, neutron energy transfer ΔE and phonon frequency ω, area of observation ($r\ell p$) in k space, peak width and signal to noise ratio.

Type	$\frac{q}{q_{max}}$	ΔE (meV)	$\lvert\vec{q}\rvert$ ($\AA^{-1}$)	ω (10^{13} rad. sec^{-1})	$r\ell p$	Peak Background	E(meV) fwhm
TA(Σ_1) [01$\bar{1}$0]	.2	12.9	.2689	1.96	R(01$\bar{1}$5)	50	3
	.4	24.7	.5378	3.75	L(01$\bar{1}$5)	31.3	3
	.6	36.3	.8067	5.51	L(01$\bar{1}$5)	21	3
	.8	47.2	1.0757	7.17	L(01$\bar{1}$5)	11	3
	.9	51.7	1.2101	7.85	L(01$\bar{1}$5)	5	3
	1.0	55.5	1.3446	8.43	L(01$\bar{1}$5)	3	3.5
LA(Σ_1) [01$\bar{1}$0]	.2	22.5	.2689	3.42	R(03$\bar{3}$0)	3	6.8
	.4	41.7	.5378	6.34	R(03$\bar{3}$0)	4	8.2
	.6	59.0	.8067	8.96	R(03$\bar{3}$0)	5	6
	.8	70.25	1.0757	10.67	R(03$\bar{3}$0)	3	2.5
	1.0	78.0	1.3446	11.85	R(0330)	2	6.8
LO(Σ_1) [01$\bar{1}$0]	.1	44.25	.1344	6.72	R(03$\bar{3}$1)	5	6.3
	.2	48.2	.2689	7.32	R(03$\bar{3}$1)	5	5
	.4	60.2	.5378	9.15	R(03$\bar{3}$1)	5	4.1
	.6	73.5	.8067	11.17	R(03$\bar{3}$1)	3	3.8
	.8	81.38	1.075	12.36	R(03$\bar{3}$1)	2	3.8
	.9	81.38	1.2101	12.36	R(03$\bar{3}$1)	1.5	3.8
	1.0	79	1.3446	12.0	R(03$\bar{3}$1)	1.2	6
TA(Δ_5) [0001]	.2	6.75	.1435	1.03	A(03$\bar{3}$0)	3	4
	.4	13.2	.2871	2.01	A(03$\bar{3}$0)	48	3
	.6	19.88	.4306	3.02	A(03$\bar{3}$0)	86	3.4
	.8	25.55	.5742	3.88	A(03$\bar{3}$0)	60	2.7
	.9	28.2	.6459	4.28	A(03$\bar{3}$0)	62	2.3
	1.0	30.15	.7177	4.58	A(03$\bar{3}$0)	77	2.4
TO(Δ_6) [0001]	0	40.9	0	6.21	B(03$\bar{3}\bar{1}$)	5	6.8
	.2	40.1	.1435	6.09	B(03$\bar{3}\bar{1}$)	6	3.8
	.4	39.0	.2871	5.92	B(03$\bar{3}\bar{1}$)	7	3
	.5	38.1	.3588	5.79	B(03$\bar{3}\bar{1}$)	11	4.2
	.6	37.3	.4306	5.67	B(03$\bar{3}\bar{1}$)	14	3.3
	.7	35.7	.5024	5.42	B(03$\bar{3}\bar{1}$)	10	2.7
	.8	34.0	.5742	5.17	B(03$\bar{3}\bar{1}$)	30	2.6
	.9	32.0	.6459	4.86	B(03$\bar{3}\bar{1}$)	30	2.3
	1.0	30.15	.7177	4.58	B(03$\bar{3}\bar{1}$)	30	2.3
LA(Δ_1) [0001]	.3	17.35	.4034	2.64	B(01$\bar{1}$3)	17	5
	.4	22.5	.5378	3.42	B(01$\bar{1}$5)	2.5	6
	.5	29.15	.6723	4.43	B(01$\bar{1}$3)	4	3.8
	.6	34.9	.8067	5.30	B(01$\bar{1}$3)	2	3.8
	.8	43.3	1.0757	6.58	A(01$\bar{1}$5)	2	9.8
	.9	48	1.2101	7.29	B(01$\bar{1}$5)	1.2	5.3
	1.0	51	1.3446	7.75	A(01$\bar{1}$5)	2	9.8

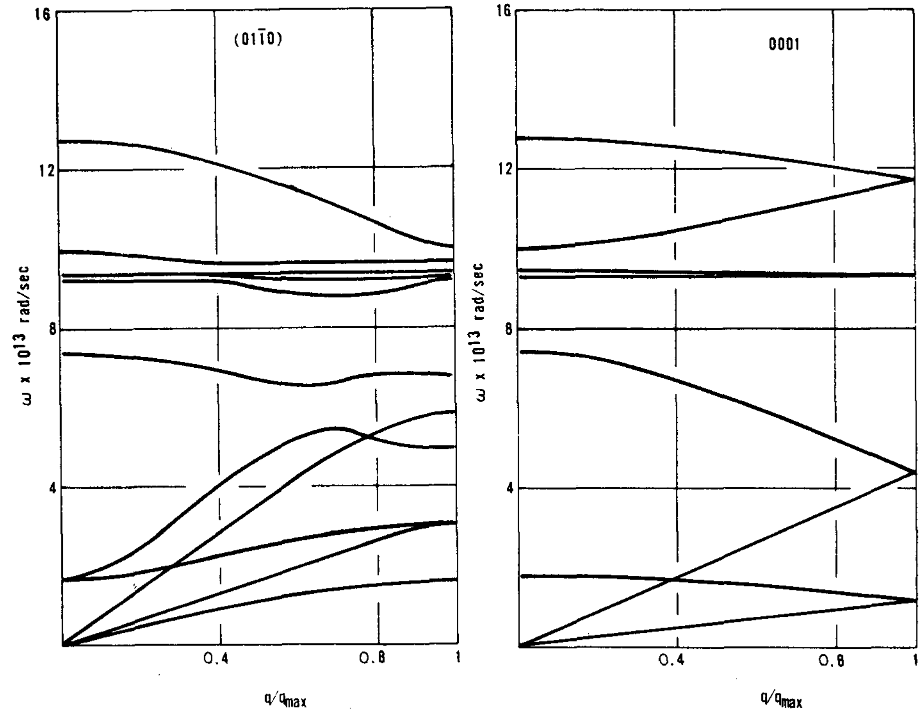

FIG.3. Dispersion relation of BeO predicted from the calculation of Young [2].

Fig. 3 and 4 give respectively the results of preliminary calculations by Young and by Solbrig. Neither of these calculations give very good agreement with the data, nor do they give the correct slopes for the acoustic branches. Solbrig has re-evaluated the constants in his model giving much improved results, however further refinements in the model are still in order [21]. Structure factor calculations based on Solbrig's model have been helpful in conducting the experiments, whether the frequencies obtained from the model are accurate or not.

In addition to the optical modes of Loh which we cited in a previous paragraph, he has also reported other infrared and Raman active modes as (in spectroscopic notation): E_1 transverse at 725 cm^{-1} (89.9 meV), E_1 longitudinal at 1095 cm^{-1} (135.8 meV) and A_1 longitudinal at 1085 cm^{-1} (134.5 meV). With these additional mode frequencies and their symmetry types we have projected what the full dispersion relation looks like for the two symmetry directions $[01\bar{1}0]$ and [0001] in Fig. 5. Branches which have been mapped by slow neutron inelastic scattering in either the present or previous experiments are displayed as solid lines. All other branches are shown as dotted lines. These unmapped branches should not be taken seriously except those intercepts at $\vec{q} = 0$ which are indicated by solid points having been established from either neutron scattering data or Loh's optical data. There remain, then, two optical intercepts at $\vec{q} = 0$ to be determined along with the mapping of 6 branches in the Σ direction and 5 branches in the Δ direction.

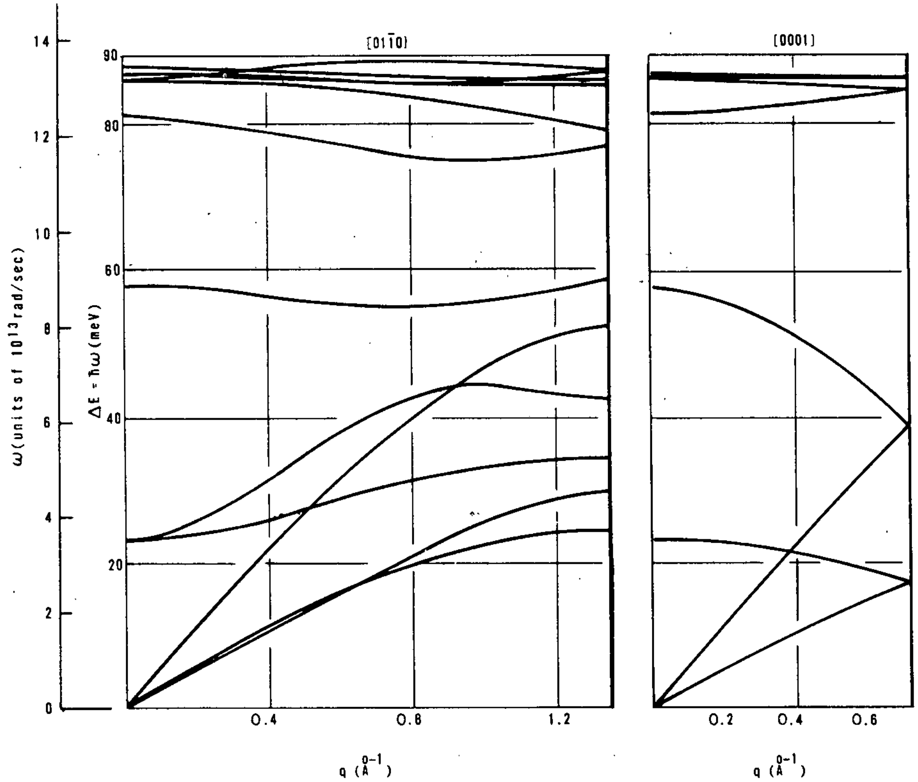

FIG.4. Dispersion relation of BeO predicted by the preliminary general valence force model calculations of Solbrig [4].

The rejection of the low lying optical branches previously reported by Brugger et al. is due to the fact that they have not been observed in this experiment or the optical work of Loh and all four Σ_2 branches required by symmetry [13] can be accounted for without including these branches.

Two Σ_2 branches can be seen clearly in Fig. 5 as having been mapped by neutron scattering (the transverse acoustic branch and a flat optical branch at approximately 85 meV); Loh has determined the intercept at $\vec{q} = 0$ for a second Σ_2 optical branch as 89.9 meV, and a third Σ_2 optical branch is required to be degenerate with the observed Σ_1 optical branch at the center of the Brillouin zone at 40.9 meV. It would seem that the low lying modes previously reported were not due to single phonon scattering but to some higher order process. While similar arguments cannot be advanced at this time to apply to the low lying Σ_1 optical branches previously reported, their existence is doubted also.

The two Σ_1 optical branches in Fig. 5 which are shown at $\vec{q} = 0$ with values of 78 meV and 98 meV are unknown .and merely estimated.

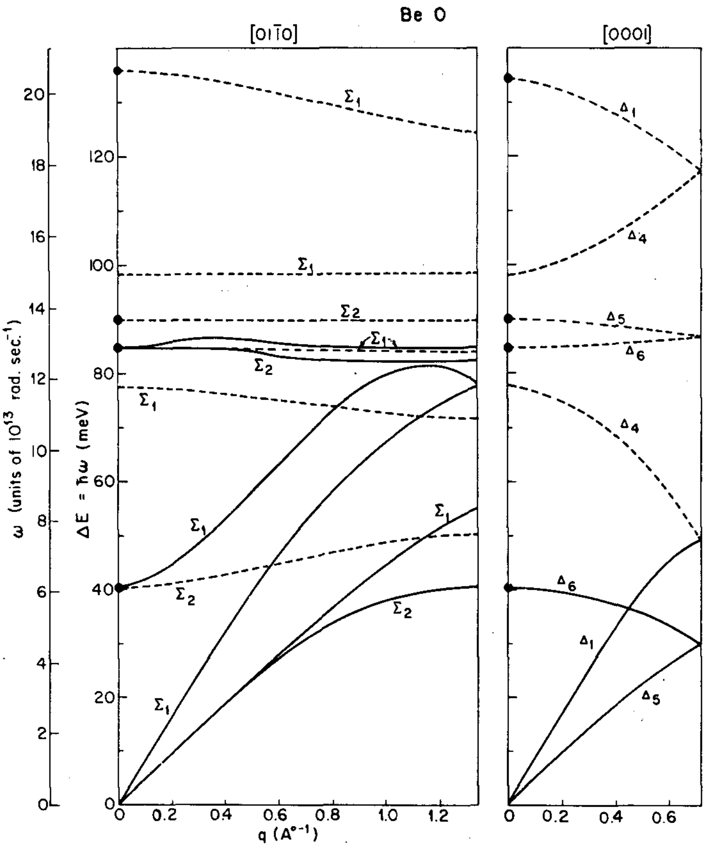

FIG. 5. Beryllium oxide dispersion relation. The solid curves represent branches which have been mapped by neutron scattering techniques while the dashed curves represent branches which have not yet been mapped. The solid points plotted at $\vec{q}$ = 0 indicate intercept frequencies which have been determined by either neutron scattering or optical measurements.

Note that the Σ_1 optical branch, which has a value of 134.5 meV at $\vec{q}$ = 0 based on Loh's data, is not degenerate with the Δ_1 branch which Loh reports as 135.8 meV at the center of the zone.

5. CONCLUSIONS

The present data completes the acoustical branches of the dispersion relation for both [01̄10] and [0001] directions. These data are in good agreement with ultrasonic data which give the initial slopes of the acoustical branches. New optical branches which were measured and which intercept at $\vec{q}$ = 0 at 40.9 meV are in fair agreement with recently reported infrared and Raman data. A search was made for low lying optical branches of the type reported by Brugger et al. with negative results. This fact together with the optical branches which have been measured and the infrared and Raman data of Loh indicate that the previously reported low lying optical branches are not the result of single phonon scattering.

The present data help to clarify the situation for the BeO dispersion relation and with the aid of Loh's data an estimate has been made of the full dispersion relation for the [01$\bar{1}$0] and [0001] directions.

ACKNOWLEDGEMENTS

The authors would like to thank Mr. S. B. Austerman for the continued loan of the BeO crystals, and Mr. E. Loh for a preprint of his work on optical measurements on BeO. Discussion with Dr. A. W. Solbrig, Jr. have been helpful and in addition he has provided us with preliminary results of his valence force model calculations in the form of dispersion relation data and structure factors, both of which have been extremely helpful to the conduct of the experiment. One of us (GLO) would like to thank the Associated Western Universities for the grant of a fellowship during the course of this work. Finally we would like to thank Dr. R. G. Fluharty for his support of this work.

REFERENCES

[1] BRUGGER, R. M., STRONG, K. A., CARPENTER, J. M., J. Phys. Chem. Solids 28 (1967) 249.
[2] YOUNG, J. A., Reactor Physics in the Resonance and Thermal Regions, I, 3-25, The MIT Press, Cambridge, Massachusetts (1966).
[3] BORN, M., HUANG, K., Dynamical Theory of Crystal Lattices, Oxford University Press, Oxford (1954) 298.
[4] SOLBRIG, A. W., Jr., Private Communication.
[5] McMURRY, H. L., SOLBRIG, A. W., Jr., BOYTER, J. K., NOBLE, C., J. Phys. Chem. Solids 28 (1967) 2359.
[6] NUSIMOVICI, M. A.. BIRMAN, J. L., Phys. Rev. 156 (1967) 925.
[7] LOH, E., Phys. Rev. 166 (1968) 673.
[8] BELLAMY, B., BAKER, T. W., LIVERY, D. T., J. Nuclear Mat. 6 (1962) 1.
[9] SMITH, D. K., NEWKIRK, H. W., KAHN, J. S., J. of Electrochemical Soc. 111 (1964) 78.
[10] MAYER, R. M., WALKER, D. G., AAEC/TM-211 (1963).
[11] JEFFREY, G. A., PARRY, G. S., MOZZI, R. L., J. Chem. Phys. 25 (1956) 1024.
[12] SINCLAIR, R. N., Proceedings of the Symposium on Inelastic Scattering of Neutrons in Solids and Liquids, Vol. 2, IAEA, Vienna (1963) 199.
[13] SULLIVAN, J. J., J. Phys. Chem. Solids 25 (1964) 1039.
[14] LOUDON, R., Advan. Phys. 13 (1964) 423.
[15] BROCKHOUSE, B. N., IYENGAR, P. K., Phys. Rev. 111 (1958) 747.
[16] NOBLE, C., SOLBRIG, A. W., Jr., McMURRY, H. L., IN-1125 (October 1967).
[17] OSTHELLER, G. L., SCHMUNK, R. E., KEARNEY, R. J., IN-1129 (April 1968).
[18] AUSTERMAN, S. B., J. Nuclear Mat. 14 (1964) 225.
[19] BENTLE, G. G., J. Am. Ceramic Soc. 49 (1966) 125.
[20] CLINE, C. E., DUNEGAN, H. L., HENDERSON, G. W., J. Appl. Phys. 38 (1967) 1944.
[21] SOLBRIG, A. W., Jr., Private Communication.

THE PHONON DISTRIBUTION OF GRAPHITE AT HIGH TEMPERATURES

D.I. PAGE
SOLID STATE PHYSICS DIVISION,
ATOMIC ENERGY RESEARCH ESTABLISHMENT,
HARWELL, DIDCOT, BERKS., ENGLAND

Abstract

THE PHONON DISTRIBUTION OF GRAPHITE AT HIGH TEMPERATURES. The phonon spectrum of graphite is notable for the high energy of some of its modes; the cut-off in the frequency distribution is about 0.22 eV (2500°K) and it is difficult to measure accurately the whole of the distribution by neutron scattering experiments on samples at room temperature. Raising the temperature of the sample, however, increases the probability of high energy gains by the neutron. Therefore the inelastic scattering of slow neutrons by graphite at 1800°K has been measured using a phased rotor spectrometer. Energy transfers covering the whole range of the frequency distribution are observed with clearly defined peaks. The results are compared with theoretical predictions and show good agreement. The incoherent approximation is shown to be reasonably valid at this high temperature and a smoothed frequency distribution is given which allows the calculation of scattering cross-sections in agreement with data measured at other temperatures.

Introduction

The scattering of neutrons by graphite has been measured several times [1] [2] [3] in attempts to derive the dispersion relations or the frequency distribution of the normal modes of vibration of the crystal lattice. Several theoretical studies [4] [5] have also been made which show the distribution extends up to an energy of 0.22 eV. It is difficult to obtain sufficient reliable experimental data at such high energy transfers owing to the Boltzmann factor. The scattering with high energy transfer can be increased by heating the sample and the experiments of Egelstaff and Cocking [3] and Egelstaff and Harris [6] on heated samples showed the presence of high energy modes in the frequency distribution.

The experiment reported here measures the neutron scattering from polycrystalline graphite at 1800°K for which comprehensive data have been obtained covering a range of energy transfer of 0-0.4 eV and momentum transfer of 1-19 Å^{-1}. The frequency distribution is calculated using the incoherent approximation of Placzek [7] after showing the contribution to the scattering from interference scattering by a polycrystalline specimen is small. The measured distribution is compared with that calculated by Young and Koppel [5]. Evidence is presented to show the frequency distribution in graphite does not change appreciably between 1300°K and 1800°K.

2. Experimental Method

2.1 Apparatus

The measurements were made at the Chalk River Nuclear Laboratories using the phased rotor spectrometer on the NRU reactor. The apparatus is fully described by Egelstaff et al. [8] and Brugger [9]. Briefly the equipment consists of four rotors in line which chop the neutron beam from the reactor and transmit pulses of monoenergetic neutrons; the chopped beam strikes a thin sample immediately after the last rotor and two arrays of LiF-ZnS scintillation counters, one in the forward direction (13 counters, 10°-90°) and one in the backward direction (9 counters, 98°-160°) detect the scattered neutrons. The experimental conditions and the detector calibration method were the same as those described by Page [10]. The energy of the incident neutrons was 0.054 eV and the probable error in the efficiencies of the detectors was estimated to be ± 3%.

2.2 Sample

The sample was a sheet (8 in. x 4 in. x 0.1 in.) of reactor grade graphite held at each end in water-cooled clamps and heated ohmically by a current of 270A at 12V. Cuts in the sheet forced the current to follow a tortuous path through the graphite to ensure almost uniform heating. Four concentric cylindrical tantalum heat shields (total thickness 0.012 in) surrounded the sheet and the whole assembly was contained in a thin windowed, water-cooled vacuum jacket. Spot temperatures over the whole of the irradiated area were constant to ± 50°C. During the experimental run, the temperature was measured and the heating controlled by a calibrated thermocouple on the inner heat shield. The design and development of the graphite furnace has been described by Bedford [11].

The sample was inclined at 45° to the neutron beam which was attenuated by 12%; the scattered neutrons were counted for periods of 16 hours followed by a background count for 8 hours. The background scattering from the heat shields was measured by cutting a hole (3 in. x 3 in.) in one end of the graphite sheet and moving the whole assembly until the neutron beam passed through the hole. A dummy run without a sample showed no variation in the scattering from different areas of the heat shields.

The total running time was 8 days and the temperature of the sample was maintained at 1800 ± 50°K. Additionally measurements were taken for 6 days with a sample temperature of 1300°K to see the effect of this temperature difference.

3. Experimental Results

3.1. Raw data

The results consisted of a time-of-flight spectrum for each detector, the set of spectra covering a momentum transfer (Q) range of 1-19Å^{-1} and an energy transfer range ($\hbar\omega$) of 0-0.4 eV. The data were corrected for background and detector efficiency and converted to partial differential cross-sections*. The data at backward angles of scattering were significantly more accurate than those at forward angles owing to the Q^2 dependence of the inelastically scattered component and the larger solid angle subtended by the detectors. Figure 1 shows the results for a single detector; the error bars show the statistical errors. The arrows along the top of the figure indicate the positions of peaks in the frequency spectrum of graphite calculated by Young and Koppel [6].

---

*The complete set of data have been tabulated by Page [12] in the form of Scattering Law S(α,β)-values.

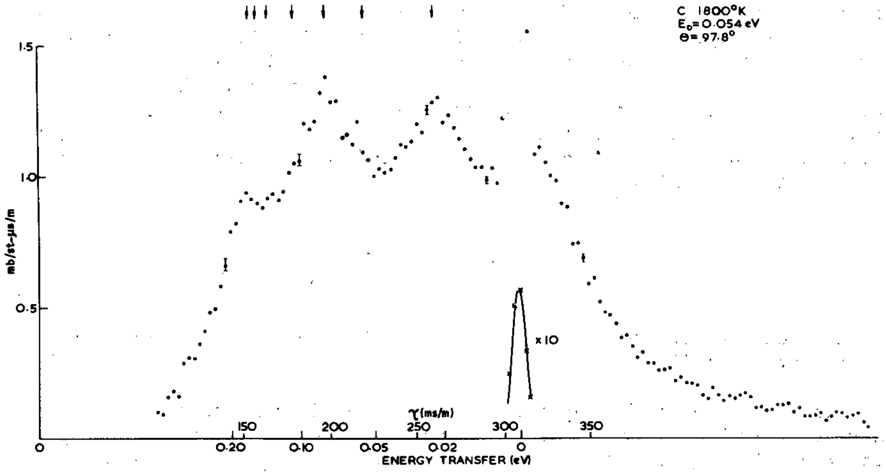

FIG.1. Time-of-flight spectrum of neutrons scattered through 97.8° by graphite at 1800°K. The arrows indicate the position of peaks calculated by Young and Koppel for graphite at room temperature.

3.2 Multiple Scattering Correction

The experimental data include contributions from one phonon and multiphonon scattering and a background due to multiple scattering of neutrons. The one phonon scattering varies as Q^2; thus the data from the low angle detectors should consist mainly of multiply scattered neutrons with a contribution from multiphonon scattering. This latter contribution would not be expected to show any structural detail and so the spectral shape in energy at low angles should be due to multiple scattering. Calculations for the Chalk River apparatus [13] show the spectrum is independent of angle and thus the low angle spectrum applies to all detectors. Calculation of the intensity of the multiple scattering is difficult and requires a knowledge of S(Q,ω) over a wide range of Q-ω space; for our purposes the

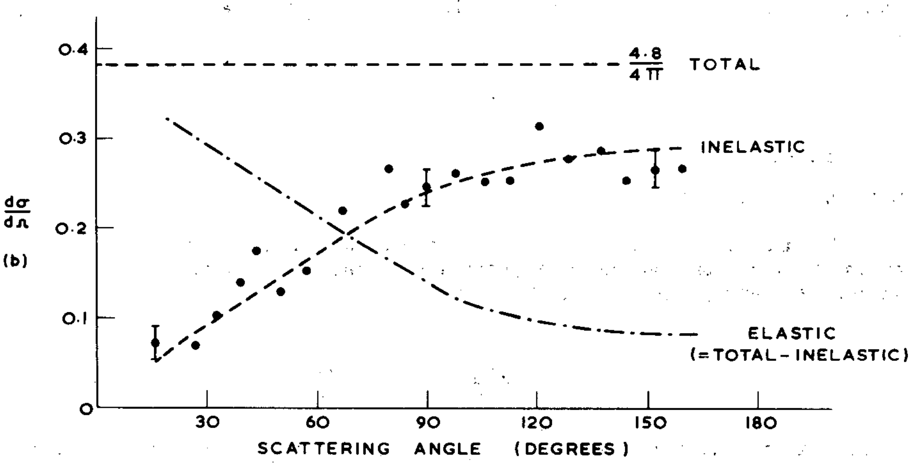

FIG.2. Elastic and inelastic differential cross-sections.

intensity can be estimated from the work of Vineyard [14]. He calculates the total multiple scattering from plane samples but in the work reported here the elastic multiply scattered neutrons cannot be separated from the elastic peak; the fraction of the multiple scattering which is non-elastic must be estimated. Figure 2 shows the integrated inelastic differential cross-section $(d\sigma/d\Omega)_{in}$ as function of scattering angle; the total scattering cross-section for graphite is 4.8b and the elastic differential cross-section is calculated from

$$\left(\frac{d\sigma}{d\Omega}\right)_{el} = \frac{4.8}{4\pi} - \left(\frac{d\sigma}{d\Omega}\right)_{in} \qquad (1)$$

which assumes an isotropic scattering distribution, i.e. any interference scattering is small.

The graph shows the rapid fall in the elastic scattering due to a large Debye-Waller factor. Within experimental error the curve is exponential when plotted as a function of Q with an exponent equal to $(-0.8\ Q^2)$. The forward peaking in the elastic scattering means the probability of a neutron being scattered through a large angle by two successive elastic collisions is small. The more likely processes are 1 large angle inelastic with 1 small angle elastic or two inelastic collisions. A simple Monte Carlo type experiment shows that for the 97.8° detector (which has the correct geometry for the Vineyard calculation), 21% of the twice scattered component is due to elastic + elastic scattering. Thus the inelastic experimental data contains only 79% of the multiple scattering calculated by the method of Vineyard which is 12% of the total scattering. Thus the multiple scattering in the inelastic region of the spectrum will be 9.5%. Vineyard's assumption that multiply scattered neutrons are isotropically distributed has been shown by Cocking [15] to be substantially correct for neutrons of high incident energy. Thus the multiple scattering is taken to be 9.5% of the total counts in the detector at 97.8° with a spectral shape given by the low angle detectors.

3.3 Resolution correction

A resolution correction was calculated by the method given by Royston [16] was applied to the data. The correction caused no significant change in the data due to it being a broad distribution with only small peaks.

4. Analysis

4.1 Outline of method

Throughout this section we follow the notation of Egelstaff [17] in which the momentum and energy transfers are measured in terms of the variables α and β which are defined by

$$\alpha = \frac{\hbar^2 Q^2}{2MkT} \qquad \beta = \frac{\hbar\omega}{kT}$$

where M is the mass of the scattering atom and T is the absolute temperature of the sample.

From the theory of Van Hove [18] it can be shown that the scattering of neutrons is described by a scattering law $S(\alpha,\beta)$ and this scattering law can be split into two terms, S_s and S_d. S_s describes the scattering due to single nuclei while S_d describes the interference term. Further the frequency distribution can be estimated from the behaviour of S_s as a function of Q - the so-called extrapolation technique.

$$(S_s/\alpha)_{\alpha \to 0} = \frac{1}{\pi} \int_0^\infty e^{i\beta t} u(t)dt + O(\alpha) \qquad (2)$$

where u(t) is a time dependent function related to the mean square displacement of an atom. Schofield [19] has shown that for a crystal u(t) has the form

$$u(t) = \int_0^\infty \frac{\cos(\beta t)\rho(\beta)d\beta}{\beta \sinh(\beta/2)} \qquad (3)$$

where $\rho(\beta)$ is the frequency distribution of the normal mode of vibration in the crystal lattice (usually written $Z(\omega)$).

Therefore
$$(S_s/\alpha)_{\alpha \to 0} = \frac{\rho(\beta)}{2\beta \sinh(\beta/2)} \qquad (4)$$

and the frequency distribution is estimated by plotting logarithmic values of S/α at fixed intervals of β and extrapolating the almost straight line to $\alpha = 0$.

To extract the frequency distribution from inelastic spectra such as shown in Figure 1, the interference term must be calculated and removed from the corrected data as the experimental data yields only values of $S(\alpha,\beta)$, (i.e. $S_s + S_d$). The extrapolation technique can then be used to estimate $\rho(\beta)$. A check on the result is made by calculating values of S_s including multiphonon terms from $\rho(\beta)$ (Egelstaff & Schofield [20]), adding in the interference and multiple scattering contributions and comparing these values with the experimental data.

4.2 Interference term

The region of (Q,ω) space covered by the experimental data is dominated by the one phonon term in the phonon expansion for crystal scattering. Egelstaff [21] has estimated the effect of the interference term from the one phonon coherent scattering cross-section for a polycrystal. He shows that for simple crystals this is a product of the self term and a type of structure factor Z, where

$$Z = \sum_{\underline{\tau}} [\pi F(\underline{\tau})/2B\tau Q_q] \qquad (5)$$

$$2\pi\tau - q \leqslant Q \leqslant 2\pi\tau + q \qquad (6)$$

where $F(\underline{\tau})$ is the usual X-ray crystal structure factor for the reciprocal lattice point $\underline{\tau}$, B is the volume per nucleus and q is the wave number of the phonon. When many values of τ are possible (i.e. at large Q) the sum produces a smooth curve but as Q decreases fewer values of τ occur and large steps can appear. Egelstaff replaces the sum in equation (5) with an integral by considering only large values of Q and many values of τ which are distributed uniformly in reciprocal space

$$Z = \frac{Q_o}{2q} \int \frac{dQ}{Q} \quad \text{(with limits } Q_o \pm q\text{)} \tag{7}$$

where Q_o is the mean value of Q and from equation (6) equals $2\pi\tau$. Carrying out the integration

$$Z = \frac{1}{2x} \log \frac{1+x}{1-x} = 1 + \frac{x^2}{3} + \frac{x^4}{5} + \ldots \tag{8}$$

where $x = \frac{q}{Q_o}$ and the sum diverges as $Q \rightarrow q$.

If we consider data collected at a fixed energy transfer, i.e. fixed phonon frequency, a suitable average q can be defined which is related to the frequency by a suitable average velocity, v. Then x can be given in terms of v:

$$x = \omega/vQ_o \tag{9}$$

Formulae (8) and (9) give the expected fractional deviation of the one phonon coherent term from the one phonon self term.

If, arbitrarily, we say that in equation (8) $x^4/5$ has to be less than 10% of $x^2/3$ for the series to converge, we can calculate a maximum value for x and hence a minimum value for Q_o which limits the validity of this approximation. For energy transfers of 0.03, 0.05 and 0.10 eV, the corresponding values of Q_o are 0.4, 1.5 and 4.8Å^{-1} respectively. Hence the treatment is valid for most of the experimental data except at low values of Q at high values of ω. Typical values are:

$$\text{At } \hbar\omega = 0.03 \text{ eV}, \quad Z = 1.04 \text{ at } Q = 6\text{Å}^{-1} \quad (\alpha = 0.04)$$
$$= 1.01 \text{ at } Q = 10 \quad (\alpha = 0.11)$$

$$\text{At } \hbar\omega = 0.01 \text{ eV}, \quad Z = 1.05 \text{ at } Q = 12 \quad (\alpha = 0.16)$$
$$= 1.01 \text{ at } Q = 20 \quad (\alpha = 0.40)$$

Generally the one phonon interference term is 5% of the self term at low values of Q falling to about 1% at the highest values of Q detected experimentally.

4.3 Derivation of Z(ω)

From equation (4)

$$(S/\alpha)_{\alpha - 0} = \frac{\rho(\beta)}{2\beta \sinh(\beta/2)} = \frac{Z(\omega)}{2\omega \sinh(\hbar\omega/2kT)} \cdot \frac{(kT)^2}{\hbar^2} \tag{10}$$

An estimate of $Z(\omega)$ is obtained by plotting values of S/α v α at fixed values of energy transfer and extrapolating the line to $\alpha = 0$. Three examples of this type of data are shown in Figure 3. To check the consistency of the results, the frequency distribution was used to generate S-values by the methods of Egelstaff and Schofield [20] which are incorporated in the computer programme LEAP [22]. The interference and multiple scattering terms (Section 3.2 and 4.2) were then added to the calculated S-values and the results compared with the experimental data.

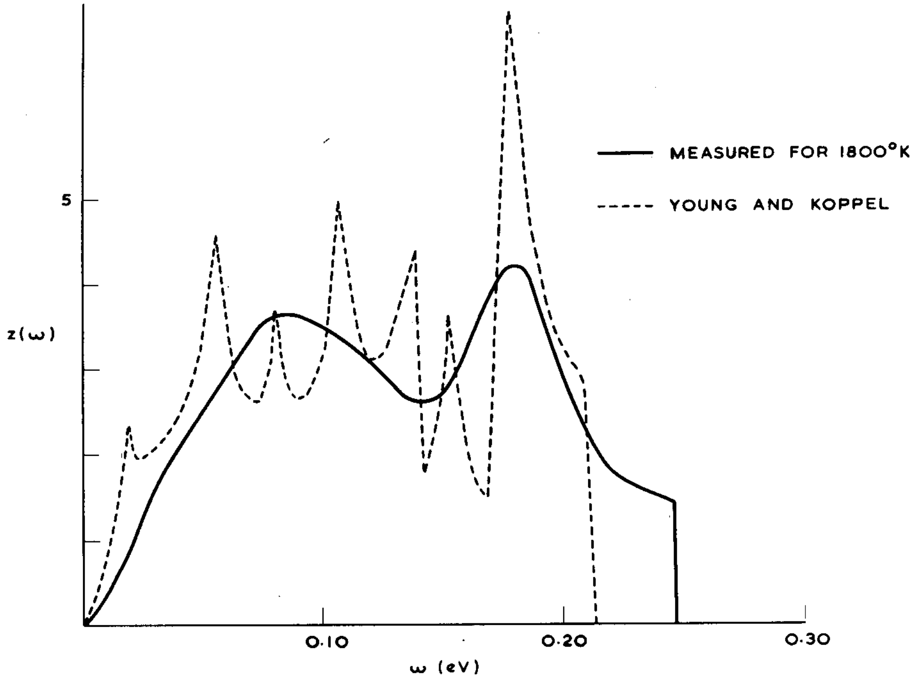

FIG.3. Phonon frequency spectrum for graphite.

Slight adjustments were made in the shape of $Z(\omega)$ to obtain the best fit over all values of energy and momentum transfer. The solid line in Figure 4 shows the final estimate of $Z(\omega)$ while the dotted line shows the calculation of Young and Koppell [5] for room temperature graphite. Both curves are normalised by the condition

$$\int_0^\infty Z(\omega)d\omega = 1 \tag{11}$$

The solid and dotted lines in Figure 3 show the contribution of the self term and the interference and multiple scattering term respectively.

5. Discussion

A comparison of the two curves in Figure 4 shows them to be in overall agreement with each other but the theoretical curve shows much more structure. The extrapolation method yields results with poor resolution as it

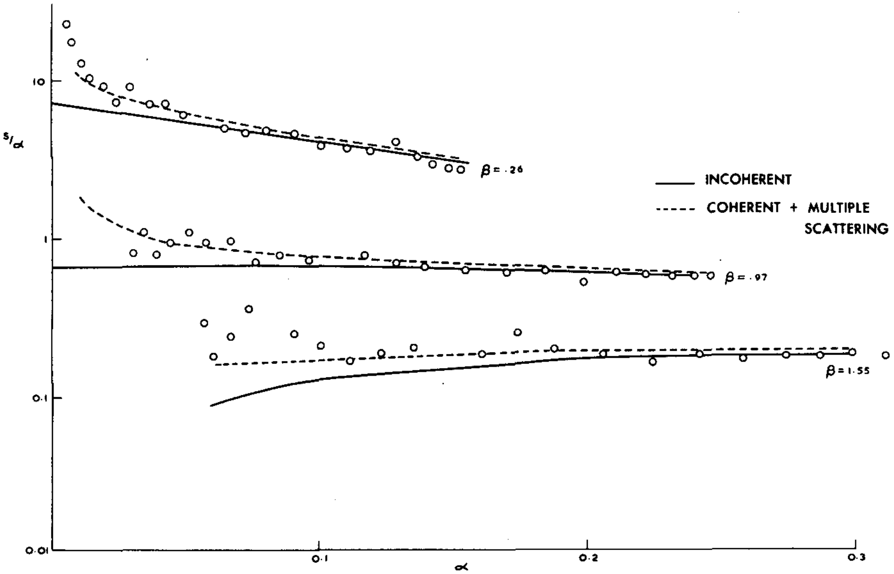

FIG.4. Calculated incoherent and coherent plus multiple scattering contributions to the neutron scattering by graphite compared with the experimental data.

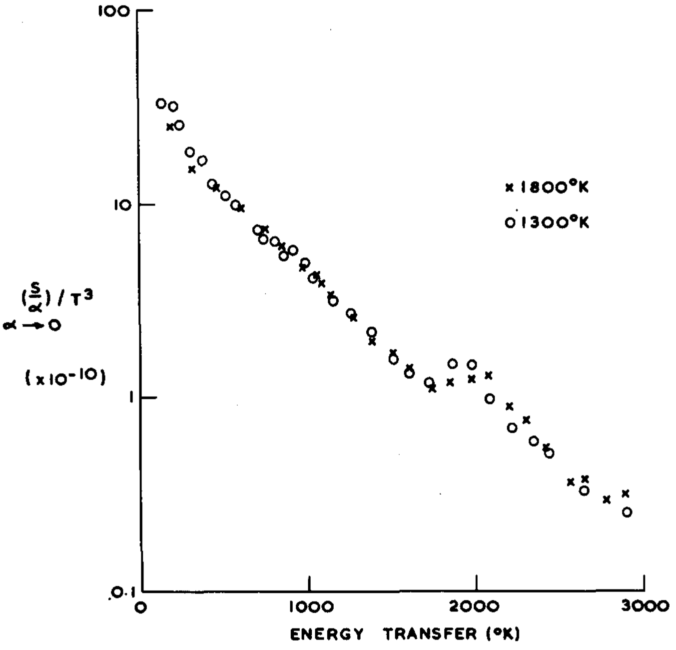

FIG.5. Comparison of $z(\omega)$ for graphite at 1300 and 1800°K.

involves interpolation between data points and fitting a smooth curve to points from different detectors. Also the experimental resolution is poor in energy gain data. Thus the lack of structure in the measured curve is not surprising. However, the broad peak at $h\omega \simeq 0.175$ eV, which is due to the strong coupling between nearest neighbour atoms in the basal planes, and the minimum at $h\omega \simeq 0.14$ eV, which marks the cut-off of the vibrational modes perpendicular to the basal planes, are quite pronounced. If the measured curve is taken as the outline of $Z(\omega)$ and looked at in conjunction with the spectrum from an individual detector (Figure 1) which shows peak positions, the agreement is very good. This agreement would be even better if the theoretical curve was resolution broadened.

The agreement between the curves implies the frequency distribution is not very temperature sensitive; small changes in frequency arising from expansion of the crystal lattice would not be observable here. Experimental evidence for this is shown in Figure 5. From equation (10),

$$(S/\alpha)_{\alpha \to 0} \propto Z(\omega)T^3 \qquad (12)$$

and Figure 5 compares $(S/\alpha)/T^3$ as a function of energy transfer for graphite at both 1300°K and 1800°K. The curves are the same within experimental error. Unfortunately there is no detailed data available at lower temperatures but the work of Egelstaff and Cocking [3] and Haywood and Thorson [2] are in qualitative agreement with Figure 5.

6. Conclusion

The frequency distribution for graphite at 1800°K has been measured and compared with the distribution calculated for room temperature graphite; the two curves are very similar. There is experimental evidence for this temperature sensitivity between 1000°C and 1500°C but there is lack of reliable data at lower temperatures.

References

[1] Dolling, G. and Brockhouse, B. N. Phys. Rev. 128 (1962) 1120.

[2] Haywood, B. C. and Thorson, I. M. A.E.C.L. Rep. 1570 (1962).

[3] Egelstaff, P. A. and Cocking, S. J. "Inelastic Scattering of Neutrons in Solids and Liquids" (I.A.E.A. Vienna 1961) 569.

[4] Yoshimori, A. and Kitano, Y. J. Phys. Soc. Japan 11 (1956) 352.

[5] Young, J. A. and Koppel, J. U. J. Chem. Phys. 42 (1965) 357.

[6] Egelstaff, P. A. and Harris, D. H. C. Phys. Lett. 7 (1963) 220.

[7] Placzek, G. Phys. Rev. 86 (1952) 377.

[8] Egelstaff, P. A., Cocking, S. J. and Alexander, T. K. A.E.C.L. Rep. 1494 (1960).

[9] Brugger, R. M. "Thermal Neutron Scattering" Ch. 2 (Academic Press, 1965).

[10] Page, D. I. Proc. Phys. Soc. 91 (1967) 76.

[11] Bedford, L. A. W. U.K.A.E.A. Rep. AERE R-5217.

[12] Page, D. I. U.K.A.E.A. Rep. AERE R-5574.

[13] Thorson, I. M. Priv. Comm. (1965).

[14] Vineyard, G. Phys. Rev. 96 (1954) 93.

[15] Cocking, S. J. Ph.D, Thesis - University of London (1967).

[16] Royston, R. J. Nuc. Inst. Meth. 30 (1964) 184.

[17] Egelstaff, P. A. "Inelastic Scattering of Neutrons in Solids and Liquids" (I.A.E.A. Vienna 1961) 25.

[18] Van Hove, L. Phys. Rev. 95 (1954) 249.

[19] Schofield, P. Phys. Rev. Lett. 4 (1960) 239.

[20] Egelstaff, P. A. and Schofield, P. Nuc. Sci. and Eng. 12 (1962) 260.

[21] Egelstaff, P. A. "Inelastic Scattering of Neutrons in Solids and Liquids" (I.A.E.A. Vienna 1963) 65.

[22] McLatchie, R. C. F. Unpublished (1962).

DISCUSSION

P.D. RANDOLPH: Regarding the double-crystal monochromator used in the NaCl experiment described in paper SM-104/41, what is the relative intensity obtained from the second crystal compared to that obtained from the first?

R. STEDMAN: If I must quote a definite figure, I would say 45%. This naturally varies with wave number, but by and large the proportion is about one half for copper crystals having the relatively narrow mosaic width – about 0.2° – which we use.

A.G. SJÖLANDER: The very interesting results presented by Cowley et al. in paper SM-104/46 bring new aspects of lattice dynamics to the attention of neutron scattering people. It is a pity, in this connection, that there are difficulties in obtaining reliable theoretical calculations, except for solid inert gases such as solid krypton and argon. We have quite a good knowledge of the interparticle interactions for these substances and detailed calculations of anharmonic energy shifts and lifetimes have recently been made. I wonder, therefore, whether anybody has the intention of carrying out these experiments in single crystals of solid krypton and argon, looking for the effects which Cowley et al. have described?

R.A. COWLEY: These calculations and experiments would be very useful. However, we ourselves do not have the crystals available, and furthermore we felt at the time that, thanks to our experience in calculating thermal expansion and so on, we could have reasonable confidence in our calculations of anharmonic effects in alkali halides.

A.R. MACKINTOSH: I should like to ask Mr. Cowley whether the discrepancy between the ultrasonically measured elastic constants and the neutron data presented by Copley, Brockhouse and Chen for rubidium (paper SM-104/54) can be explained by the mechanisms discussed in his paper.

R.A. COWLEY: Since the measurements were made at 90°K, I would estimate the discrepancy in elastic constants derived from anharmonic effects to be about 10%, with the neutron results giving the larger constant. However, it is likely to be small in the $[00\zeta]$T mode, where the experiment of Brockhouse et al. also shows a discrepancy.

W. GLÄSER: I have a comment and a question on the paper by Mr. Page (SM-104/109). We conducted scattering measurements on graphite along similar lines, using the incoherent approximation and extracting a spectral density from the experimental data. The results were presented at the Ann Arbor meeting last year[1]. There is a rough overall agreement with the distribution found by Mr. Page. More specifically, the positions of the two high-energy peaks agree quantitatively, but at low phonon energies there is a substantial deviation. Our distribution agrees fairly well with the calculations in this energy range.

Does Mr. Page have any explanation for the disagreement of his distribution with the calculations in this energy range?

D.I. PAGE: Your measurements were made at 533°K, and not at 1800°K as were those reported here. The low phonon energies will be associated with the 'out-of-plane' vibrations, which will be much more temperature-sensitive than the 'in-plane' vibrations. Perhaps the difference between our

---

[1] Neutron Thermalization and Reactor Spectra (Proc. Symp., Ann Arbor, 1967) I, IAEA, Vienna (1968) 235.

distributions is a temperature effect. If I use a frequency distribution which agrees with Young and Koppel at low ω as an input to the computer program LEAP, the computed values do not agree with the experimental data.

W. L. WHITTEMORE: First I should like to mention that we at General Atomic have completed an extensive set of measurements on graphite at room temperature, using energy loss scattering of neutrons produced by an electron Linac. Turning now to Mr. Page's paper, I have the impression that all extrapolation techniques for graphite using the scattering law give a two-hump distribution of phonons without any of the sharp peaks predicted by Young and Koppel. I should therefore like to ask Mr. Page whether he believes that his resolution explains the entire lack of these sharp peaks. It would also be interesting to hear whether, in his view, his data indicate a higher cut-off in the phonon distribution than the 0.208 eV predicted by Young and Koppel.

D. I. PAGE: The lack of resolution in the frequency distribution – to which you quite justifiably draw attention – is inherent in the extrapolation technique; spectra from individual detectors show the peaks (see Fig. 1 of the paper).

The energy resolution and statistical accuracy of the data are worst at high-energy transfers and one cannot say with certainty that the cut-off is higher than the calculated value.

J. A. YOUNG: I am going to put a question to the graphite experimentalists. Messrs. Whittemore and Gläser seem to be saying that the agreement between the calculated and measured phonon energies is quite good over the whole frequency range, whereas Mr. Page says that the differences between calculation and his experiment for the lower energy phonons are due to temperature effects. I should like an explanation of the discrepancy between theory and Page's experiment as regards the high-frequency cut-off, which is due to the in-plane vibrations and will not be temperature sensitive. Is this difference at the high-frequency end real or is it a consequence of experimental inaccuracy?

D. I. PAGE: The experimental accuracy is not good enough to say whether the effect is real or not.

K.-E. LARSSON: Mr. Page has two figures in his paper which seem to refer to related physical magnitudes: one figure (Fig. 1) shows a single-run time-of-flight spectrum, while the other (Fig. 3) shows the final frequency distribution. The two figures differ considerably, and there may be several reasons for the large discrepancy. In a single time-of-flight spectrum the coherent effects can be pronounced. In the final frequency distribution the peaks observed in a single run are smeared out. This shows, does it not, that the use of the extrapolation technique to determine the frequency distribution results in considerable uncertainty. The fact that the normalization is correctly made does not save the situation; it only guarantees that the area of f(ω) is correctly given but it does not affect the shape of f(ω).

D. I. PAGE: The extrapolated frequency distribution is merely used as a starting point in calculating the scattering function using LEAP. The iterative procedure is used to modify Z(ω) until finally the shape is quite precisely defined. Any large errors in the original Z(ω) would lead to disagreement between the computed and the experimental data.

M. S. NELKIN: One must remember, in connection with the extrapolation technique in graphite, that the data are being analysed in the incoherent approximation. Thus, some kind of smoothing of the actual (purely coherent) data is essential when one tries to extract a frequency distribution.

W. GLÄSER: I also should like to add a remark which may do something to meet Mr. Larsson's criticism. If accurate measurements are performed at high momentum transfers, where peaks wash out and the incoherent approximation may be a good one, it is possible to effect a fairly good extrapolation to zero-momentum transfer. In our measurements on graphite the area under the extrapolated points agreed to within 5% with the normalization condition. I should point out that the correction for multiple scattering was very important in this case; failure to take proper account of multiple scattering may cause large discrepancies.

J.A. YOUNG: On the other hand, I am going to buttress Mr. Larsson's comments by saying that from our calculations of both coherent inelastic scattering from polycrystals and multiple scattering effects we have concluded that extrapolations such as those performed by Mr. Page are virtually impossible to carry out with any degree of precision. In addition, graphite is not only a purely coherent scatterer, but is also not isotropic.

B. MOZER: On the subject of methods of trying to estimate frequency distributions from inelastic neutron measurements on coherent scattering powder samples, I would mention that several frequency distributions obtained from our measurements and those of others show very good agreement with distributions calculated from models fitted to dispersion curves. Discrepancies occur in the low-energy region of the spectrum in the neighbourhood of the near-zero value of the phonon wavevector, because the conservation condition regarding wavevector cannot be satisfied with very many reciprocal lattice vectors. The important point to note is that in arriving at these distributions we used data only at a large scattering angle, where the incoherent approximation works best. We do look at data at other angles and note changes in the spectrum, especially in the region where small scattering occurs because a smaller number of reciprocal lattice vectors are contributing to the conservation condition. Van Hove singularities are prominent and change slowly with angle; their observed intensities are most likely to be in error, but this depends ultimately on the dispersion curves in all κ space and not just along a few symmetry directions. If one takes into consideration instrumental resolution, one would obtain the sharp Van Hove singularities observed in the calculated distributions. If one uses the extrapolation techniques on $S(\vec{\kappa}, \omega)$, one obtains a highly smeared-out spectrum. I have not tried to explain this behaviour but suggest that the neutron data be used at one angle, preferably for large $\vec{\kappa}$, to obtain estimates of the frequency distribution, since this procedure does give very reasonable agreement in many cases.

O.K. HARLING: With further regard to the derivation of frequency spectra by means of the extrapolation technique, I would recall our own experience on this subject, particularly our work involving water and ice, the results of which I reported in paper SM-104/80. In this work we determined the frequency spectra out to much higher energy transfers than in previous studies, and we found that it was possible to obtain agreement with the experimental scattering law results with a frequency spectrum which was quite unlike the original spectral density obtained by extrapolation of the S/α curves. It is my feeling, therefore, that to whatever extent the final normalized frequency distribution agrees with the general shape of the initial estimate, then to this extent there may be physical reality in the derived spectrum. We also found that the finer structure appearing in the double-differential cross-sections at small scattering angles often disappears in the extrapolation process owing to averaging of a number of data points. It seemed justified in these cases to reintroduce at least the degree of structure seen in the cross-sections without changing the overall spectral distribution to any appreciable extent.

O.J. EDER: A few words on some recent work of ours may be of interest in connection with the incoherent approximation. At our laboratory we measured MgO single-crystal powder (size 300 - 1200 Å), and using Peckham's frequency distribution we found that the data could be fitted fairly well. The incident neutron wavelengths were around 1-2 Å and the scattering angles were large (80-90°).

Yu.M. KAGAN (Chairman): So far during the Symposium we have been repeatedly discussing the problem of finding the frequency distribution function $g(\omega)$ of the phonon spectrum, and in this connection I should like to offer the following observations. There is a simple neutron scattering procedure for directly determining $g(\omega)$, at least in simple metals. Let us assume that we are measuring scattering in single crystals and using the 'constant-q' method. Let us fix the transferred pulse $\vec{x} = \vec{\kappa}$, where $\vec{\kappa}$ is the reciprocal lattice vector multiplied by 2π. The coherent scattering will then correspond to phonons of frequency $\omega_\alpha(\vec{x} = \vec{\kappa}) = \omega_\alpha(0)$. If there is one atom in the elementary cell of the crystal, then, by measuring the cross-section as a function of the transferred energy when $|\Delta E| > 0$, we shall be measuring coherent scattering only, and consequently shall be able to determine $g(\omega)$. Where there is optical branching, the coherent scattering peaks, $\vec{a} = \vec{\kappa}$, corresponding to the optical frequencies $\omega_\alpha(0)$ where $\alpha = 4, 5 \ldots$, will be superimposed on the incoherent scattering.

W. COCHRAN: One should emphasize that, while what Mr. Kagan has just said is perfectly correct, it applies to an experiment made with a single crystal and is therefore not immediately relevant to the experiments under discussion.

Yu.M. KAGAN (Chairman): Yes, that is so.

B. DORNER: Changing the subject somewhat, may I ask the authors of paper SM-104/93 a question about the measured acoustical branches and the estimated optical branches shown in Fig. 5 of the paper? At some points these branches cross each other, and it is there that mixing of the branches and their polarizations may occur, depending on the symmetry of the system. Did the authors notice any change of polarization in the calculated dynamic structure factor or in the measured intensities?

P.D. RANDOLPH: Speaking on behalf of Mr. Schmunk, one of the authors of the paper, I can say the following. The phonon polarizations obtained in Solbrig's calculations do show variations for some of the branches. However, these variations are gradual and, when they occur, extend over the range of phonon wavevectors from the centre of the Brillouin zone to the zone boundary. Owing to the uncertainties in the calculated structure factor, it would be very difficult to obtain any meaningful information on phonon polarization from the experimental data.

LATTICE DYNAMICS OF HCP He^4 BY INELASTIC NEUTRON SCATTERING

T.O. BRUN, S.K. SINHA, C.A. SWENSON AND C.R. TILFORD
INSTITUTE FOR ATOMIC RESEARCH
AND DEPARTMENT OF PHYSICS,
IOWA STATE UNIVERSITY,
AMES, IOWA, UNITED STATES OF AMERICA

Abstract

LATTICE DYNAMICS OF HCP He^4 BY INELASTIC NEUTRON SCATTERING. Phonon dispersion curves have been measured along the c-axis of the reciprocal lattice of hcp He^4 using the triple-axis neutron spectrometer at the Ames Laboratory Research Reactor. The measurements were done on a single crystal of He^4 at a molar volume of 16.03 cm^3 and oriented in the $11\bar{2}0$ plane. The results are compared with the theoretical calculations of Gillis, Koehler and Werthamer, and with those of Morley and Kliewer. The former predict frequencies about 20% too low in comparison with experiment, while the latter are too high by about the same amount. An interesting feature of the results is that while the acoustic modes for small wave-vector show well-defined neutron groups, the modes for large wave-vector and the optic modes show considerable broadening indicating strong life-time effects.

The lattice dynamics of solid helium has been the subject of considerable theoretical and experimental interest within the last few years since helium behaves as a quantum solid in which the zero-point motion dominates the thermal energy. A considerable amount of theoretical work on this problem has been done by various authors [1-7], including predictions of the phonon dispersion relation in various phases of solid He^4 and He^3. The Debye temperatures for solid He^4 calculated from these theories are not in very good agreement with the experimental values obtained by Sample and Swenson [8] and Franck [9].

The detailed measurement of the phonon dispersion curves by inelastic neutron scattering poses considerable difficulties due to the low scattering cross-section and large Debye-Waller factors of He^4 and the problems associated with growing a reasonably large oriented single crystal. The Brookhaven group [10] has already reported preliminary measurements performed on a single crystal of hcp He^4 grown at a pressure of 27 atmospheres and having a molar volume of 21.1 cc. We wish to report here some preliminary measurements made on a single crystal of hcp He^4 grown at a pressure of 230 bars and having a molar volume of 16.03 cc.

The crystal was grown in a stainless-steel bomb having an internal diameter of 0.46 inches and a wall thickness of 0.01 inches. The bomb was pressurized to 230 bars with pure helium gas and cooled slowly from the bottom by three aluminum rods anchored to a bath of liquid helium at 4.2°K. A constriction at the bottom of the bomb was intended to ensure that only one large grain grew up from the bottom. The crystal was grown from the fluid phase at constant pressure and annealed for a period of two weeks. The cryostat was mounted in the neutron beam in such a way as to be capable of being tipped ± 25° from the vertical. The crystal orientation was determined by neutron diffraction. It was found to consist of two crystals whose c-axes almost coincided, but the b-axis of one coincided with the a-axis of the other. A

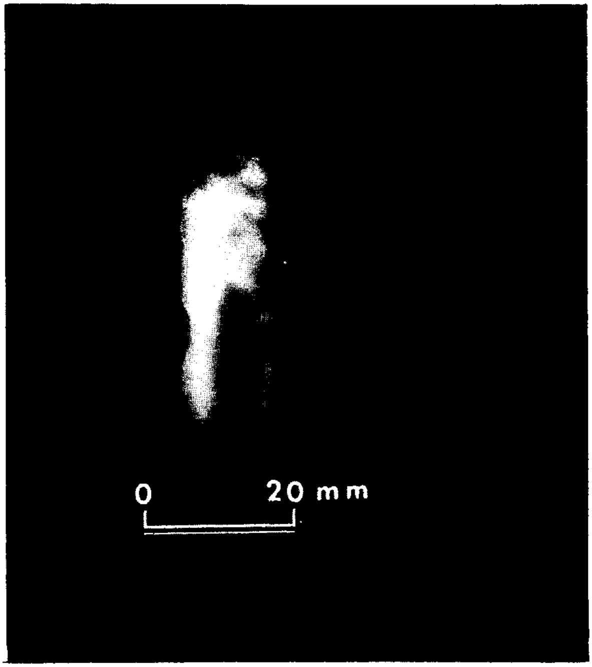

FIG. 1. Polaroid photograph of He^4 crystal seen by Bragg-reflected neutrons. The dark shadow corresponds to the crystal oriented in the $10\bar{1}0$ plane.

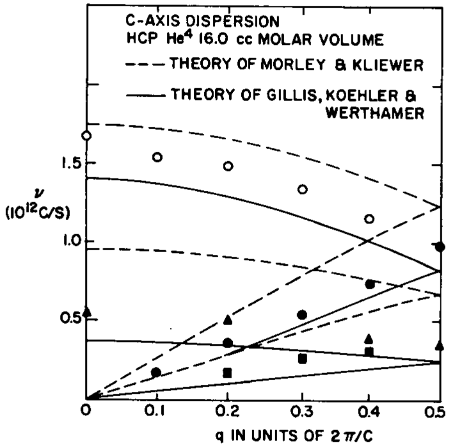

FIG. 2. Measured dispersion curves along the c-axis; open circles - LO branch; closed circles - LA branch; squares - TA branch; triangles - TO branch.

polaroid photograph of the crystal taken by Bragg-reflected neutrons is shown in Fig. 1 and illustrates the two components of the crystal. The double crystal did not affect measurements made on the longitudinal branches along the c-axis, but care had to be taken to sort out peaks for the transverse branches. The lattice constants as determined by neutron diffraction were a = 3.354 ± 0.002 Å and c = 5.463 ± 0.002 Å.

FIG.3. Observed neutron groups for longitudinal phonons along the c-axis.

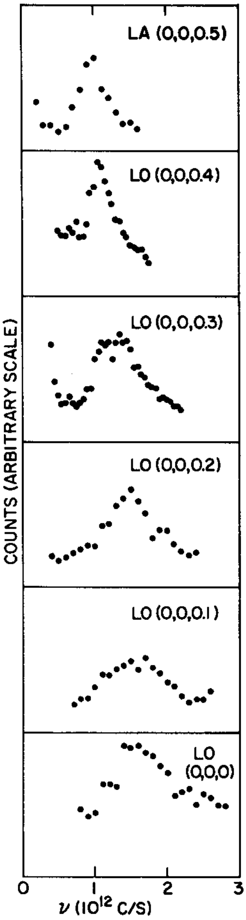

FIG.4. Phonon natural width Γ as function of q for the longitudinal branch along the c-axis in the double-zone scheme.

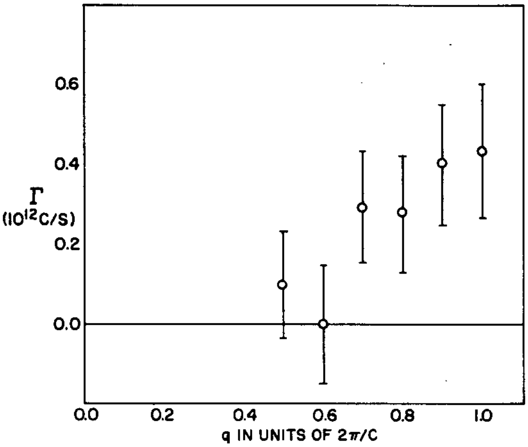

Because of the large Debye-Waller factor due to the zero-point motion, measurements had to be restricted to the first few Brillouin zones. The longitudinal branches were measured between the 002 and 003 reciprocal lattice points and the transverse in the vicinity of the 100, 002, and $10\bar{1}$ reciprocal lattice points. The measurements were made on the triple-axis spectrometer at the Ames Laboratory Research Reactor using the constant-Q technique [11] and 20.4 meV incident neutrons. The dispersion curves are illustrated in Fig. 2. Figure 3 shows some of the neutron groups scattered from the longitudinal phonons. It may be seen that in the velocity of sound region, the groups are well-defined but broaden sharply towards the zone-boundary and along the optical branch. Some structure also becomes apparent in the optical branch neutron groups. These results clearly indicate strong interaction between the normal modes so that they are not really well-defined excitations at higher frequencies. Similar effects have been observed by the Brookhaven group [10] at the larger molar volume. In all cases, the means of the scattered neutron groups have been chosen to represent the phonon frequency. Figure 4 illustrates the phonon line-width as a function of q for the longitudinal branch in the double-zone scheme after subtracting the instrumental resolution.

Figure 2 also illustrates the first-principles calculations of Gillis, Koehler and Werthamer [6] using the self-consistent "equivalent Harmonic Hamiltonian" technique devised by Koehler [5] and incorporating the short-range correlation between atoms introduced by Nosanow and Werthamer [4]. We see that the predicted frequencies are too low in comparison with experiment. This is an interesting result in view of the fact that their calculations for the molar volume studied by the Brookhaven group give frequencies too high by roughly the same order. Also shown on Fig. 2 are results of calculations by Morley and Kliewer [7] also using a version of Koehler's self-consistent phonon theory but without incorporating the short-range interatomic pair-correlation. It may be seen that their curves are too high in comparison with experiment. It would appear that the anharmonic effects so noticeably present would have to be incorporated into these theories which presently assume non-interacting normal modes, for a satisfactory description of the lattice dynamics of solid helium. Preliminary investigations of the temperature dependence of the phonon frequencies show that the frequencies do not change appreciably between 4.2° and 5°K. The melting point for the crystal used in these experiments was 5.6°K.

Further work is being continued to obtain the rest of the dispersion curves at this molar volume, and will be published in the near future.

ACKNOWLEDGEMENTS

The authors would like to acknowledge valuable discussions with R. Werthamer, T. R. Koehler, K. Kliewer, G. Shirane and V. J. Minkiewicz.

REFERENCES

1. L. H. Nosanow and G. L. Shaw, Phys. Rev. 119, 968 (1962).
2. F. W. De Wette and B. R. A. Nijboer, Phys. Letters 18, 19 (1965).
3. H. Horner, Z. Physik 205, 72 (1964).
4. L. H. Nosanow and N. R. Werthamer, Phys. Rev. Letters, 15, 618, 997 (1965).
5. T. R. Koehler, Phys. Rev. Letters 18, 656 (1967).
6. N. S. Gillis, T. R. Koehler, and N. R. Werthamer, to be published (See also Bull. Am. Phys. Soc. 13, 506 (1968)).
7. G. L. Morley and K. L. Kliewer, to be published.
8. H.H. Sample and C.A. Swenson, Phys. Rev. 158, 188 (1967).
9. J. P. Franck, Phys. Letters 11, 208 (1964).
10. F. P. Lipshultz, V. J. Minckiewicz, T. A. Kitchens, G. Shirane and R. Nathans, Phys. Rev. Letters 19, 1307 (1967).
11. B. N. Brockhouse, Inelastic Scattering of Neutrons in Solids and Liquids (International Atomic Energy Agency, Vienna, Austria, 1961), p. 113.

DISCUSSION

B.N. BROCKHOUSE: I understand that measurements on solid helium have been made at Brookhaven also. How do your results compare with theirs?

S.K. SINHA: I would like to make two points with regard to the Brookhaven results. The first is that, as mentioned in our paper, these results are for a crystal of much lower density, and for such cases the theory of Gillis, Koehler and Werthamer predicts frequencies which are about 20% too high. For our higher densities, the theory predicts frequencies which are too low by roughly the same amount. An intermediate density might have yielded spuriously good agreement with the theory. Secondly, the Brookhaven group found that their phonons became unobservable for the higher frequencies along the c^*-axis. This may be because of the rather larger Debye-Waller factors and increased phonon-phonon interaction at their densities. We certainly find phonons on the LO branch along the c^*-axis all the way back to the origin, but they are considerably broadened, and the integrated intensities of the groups do not show significant deviation from the one-phonon cross-section formula. In our b^*-axis results, however, we do find evidence for disappearance of the phonons in the region where the two $T_\perp$ branches cross, possibly due to increased phonon-phonon interaction in this region.

T. SPRINGER: In spite of the very strong anharmonicity of the binding forces in solid He, the phonon peaks shown by Mr. Sinha are quite sharp at small q values. Could this be simply explained by the fact that momentum and energy conservation prevent the decay of the phonons, because there are no suitable phonons available at this temperature?

S.K. SINHA: This is a very likely explanation, but I feel that the details should be left to a 'professional' theoretician. I should point out that even these low-frequency phonons have anharmonic effects (in the conventional sense) already built into them in a theory such as Koehler's. However, the decay of such a renormalized excitation is probably governed by the considerations you mention.

R.A. COWLEY: The theories described by Mr. Sinha cover some of the anharmonic contributions to the phonon frequencies. If these theories are applied to weakly anharmonic crystals, they result in neglect of the cubic anharmonic term, which is the largest term in these crystals. They therefore seem to be inconsistent from this point of view, and I find the agreement with the beautiful experiments somewhat surprising.

Yu.M. KAGAN (Chairman): I must say I agree with Mr. Cowley in this connection.

S.K. SINHA: This may well be the case, although I should stress that I am not qualified to comment on the neglect of the cubic anharmonic terms in the theory of Koehler et al. The agreement may, as you suggest, be spurious, a further reason being that the interactions between the 'renormalized' phonon-like excitations are not taken into account in the theory.

A.G. SJÖLANDER: Looking at higher-order anharmonic effects, one finds terms which provide a kind of self-consistent interaction between the phonons, but which apparently do not necessarily yield a significant lifetime effect. They do, however, bring about a shift of the phonons. These effects are small, except possibly in solid He and other light solids, and are very different from those resulting in 'Boltzmann collisions' between phonons and lifetime effects. There may be a link here with the treatment of Werthamer et al. for He, but the approach based on perturbation expansion cannot, it seems, be pursued in any detail.

LATTICE DYNAMICS OF HYDROGEN-BONDED CRYSTALS

S. TREVIÑO*, H. PRASK* AND T. WALL*†
EXPLOSIVES LABORATORY,
PICATINNY ARSENAL,
DOVER, N.J.,
AND
S. YIP
DEPARTMENT OF NUCLEAR ENGINEERING,
MASSACHUSETTS INSTITUTE OF TECHNOLOGY,
CAMBRIDGE, MASS.,
UNITED STATES OF AMERICA

Abstract

LATTICE DYNAMICS OF HYDROGEN-BONDED CRYSTALS. A mathematical procedure is outlined by which the dynamical equation of harmonic solids can be generally written in terms of central and non-central forces. Two systems (H_2O and HCl) are chosen for illustration. The dynamical properties of these two crystals are calculated and compared with optical and neutron spectroscopic data. A limited success is obtained in reproducing the data for ice and good results are obtained for HCl. The assignments resulting from the present investigation are discussed and further work is indicated.

1. INTRODUCTION

The general mathematical treatment used in the calculation of the lattice dynamical properties of harmonic solids is well known. The more difficult problem of choosing a suitable force field to describe the potential energy of the crystal has seen various approaches. The simplest is that of central forces between individual atoms and has been succesful in describing various systems[1]. There are crystals, however, for which a simple central force model is clearly inadequate. Such systems are those for which the bonds between particles exhibit a highly directional character so that resistance is met not only in attempts to stretch bonds but also in attempts to change their direction. This type of system lends itself to a description which includes not only the central forces but such non-central forces as angle bending, wagging and torsional forces as are used in gas phase molecular spectroscopy. In the present work we describe a method of expressing the dynamical equations in a familiar form in terms of the forces mentioned above. Two hydrogen bonded crystals (H_2O and HCl) for which both optical and neutron spectroscopic data are available have been chosen as examples.

2. THEORY

2.1 NORMAL MODE ANALYSIS

The conventional mathematical description of atomic motions in crystalline solids is based on normal mode calculations. Such analyses are well-known and are usually carried out using cartesian coordinates to express

---

* Guests at Army Materials and Mechanics Research Center, Watertown, Mass.

+ NAS Postdoctorial Fellow.

atomic displacements[2]. For complicated solids this approach gives rise to a large number of force constants which generally have to be treated as adjustable parameters. The calculations thus become unwieldy and the results less meaningful physically. In these cases it is more appropriate to consider the use of "internal" coordinates, which are well suited for describing molecular motions, such as bond stretching, angle bending, torsions, etc. The approach is admittedly somewhat less systematic, but it is considerably more tractable and is applicable to a large class of solids. The purpose of this section is to outline the normal mode calculations for subsequent applications and to establish a consistent set of notations. First, we will briefly review the formalism based on cartesian coordinates.

We begin by considering a solid consisting of N primitive cells, each with S atoms which may all be different. The position of the n^{th} cell is

$$\vec{X}_n = ha\hat{x} + kb\hat{y} + \ell c\hat{z} \tag{2.1}$$

where (x, y, z) are cartesian unit vectors, (h, k, l) are integers, and (a, b, c) are the cell dimensions. We can label this cell by the vector

$$\vec{n} = h\hat{x} + k\hat{y} + \ell\hat{z} \tag{2.2}$$

so that the displacement of an atom in the cell will be denoted $X_\alpha^{\vec{n}}$. The index α labels the particular atom as well as the cartesian components of the displacements, it can therefore take on 3S values. The potential energy of the solid, V, in the adiabatic and harmonic approximations, becomes

$$2V = \sum_{\substack{\vec{n}\vec{n}' \\ \alpha\alpha'}} \Phi_{\alpha\alpha'}^{\vec{n}\vec{n}'} X_\alpha^{\vec{n}} X_{\alpha'}^{\vec{n}'} \tag{2.3}$$

where Φ is the force constant matrix, and because of translational invariance, it depends on $\vec{n}$ and $\vec{n}'$ only through the difference $\vec{n}-\vec{n}'$ [2].

The basic quantities of interest in a normal mode calculation are the dispersion relations (eigenfrequencies $\omega_j(\vec{k})$ as a function of wave vector $\vec{k}$) and the polarization vectors $L_{\alpha j}(\vec{k})$, (cartesian eigenvectors). Both will be needed in the analysis of inelastic neutron scattering experiments[3]. One forms the dynamical matrix $D_{\alpha\alpha'}(\vec{\varphi})$ according to

$$D_{\alpha\alpha'}(\vec{\varphi}) = (M_\alpha M_{\alpha'})^{-\frac{1}{2}} \sum_{\vec{n}-\vec{n}'} \Phi_{\alpha\alpha'}^{\vec{n}-\vec{n}'} e^{i\vec{\varphi}\cdot(\vec{n}-\vec{n}')} \tag{2.4}$$

where M_α is a diagonal matrix of atomic masses and

$$\vec{\varphi} = 2\pi(ak_x\hat{x} + bk_y\hat{y} + ck_z\hat{z}) \tag{2.5}$$

is a reduced wave vector. The equations of motion to be solved are

$$\sum_{\alpha'} D_{\alpha\alpha'}(\vec{\varphi}) L_{\alpha' j}(\vec{\varphi}) = L_{\alpha j}(\vec{\varphi}) \lambda_j(\vec{\varphi}) \tag{2.6}$$

where $\lambda_j(\vec{\varphi}) = \omega_j^2(\vec{\varphi})$ and j is the branch index. The polarization vectors are chosen to satisfy the normalization conditions,[2]

$$\sum_j L^*_{\alpha j}(\vec{\varphi})\, L_{\alpha' j}(\vec{\varphi}) = \delta_{\alpha\alpha'} \tag{2.7}$$

$$\sum_\alpha L^*_{\alpha j}(\vec{\varphi})\, L_{\alpha j'}(\vec{\varphi}) = \delta_{jj'}$$

To formulate the same calculations in terms of internal coordinates[4] we denote by R_p the p^{th} coordinate which may describe a stretching, bending or any specific motion involving a particular group of atoms. The range of p values depends on the number of different types of coordinates we want to consider as well as the total number of atoms (therefore the number of bonds, angles, etc.) one uses in setting up the dynamical matrix. The range of interaction is determined by the choice of "internal" coordinates. The connection between R_p and X_α is given by

$$R_p = \sum_{\vec{n},\alpha} \left({}_pB^{\vec{n}}_\alpha\right) X^{\vec{n}}_\alpha \tag{2.8}$$

The transformation matrix B depends only on crystalline structure; it is generally not square and hence has no inverse. Corresponding to Eq. (2.3) we have

$$2V = \sum_{pp'} F_{pp'}\, R_p\, R_{p'} \tag{2.9}$$

where F is the force constant matrix for internal coordinates, and

$$\Phi^{\vec{n}\,\vec{n}'}_{\alpha\alpha'} = \sum_{pp'} F_{pp'} \left({}_pB^{\vec{n}}_\alpha\right)\left({}_{p'}B^{\vec{n}'}_{\alpha'}\right) \tag{2.10}$$

By choosing R_p appropriately one may proceed with a calculation involving a reasonable number of force constants. This also means that using internal coordinates facilitates the construction of force models and the visualization of its physical content.

For actual computations it is desirable to factor out (as much as possible) the dependence of $D_{\alpha\alpha}$ ($\vec{\varphi}$) on numerical values of the force constants. Suppose we label the different types of internal coordinates by the index r and denote the force constant as f_r; we can write

$$D_{\alpha\alpha'}(\vec{\varphi}) = \left(M_\alpha M_{\alpha'}\right)^{-1/2} \sum_r f_r\, Z^r_{\alpha\alpha'}(\vec{\varphi}) \tag{2.11}$$

where

$$Z^r_{\alpha\alpha'}(\vec{\varphi}) = \sum_{\vec{n}-\vec{n}'} S^r_{\alpha\alpha'}(\vec{n}-\vec{n}')\, e^{i\vec{\varphi}\cdot(\vec{n}-\vec{n}')} \tag{2.12}$$

$$S^r_{\alpha\alpha'}(\vec{n}-\vec{n}') = \sum_{pp'} \Delta^r_{pp'} \left({}_pB^{\vec{n}}_\alpha\right)\left({}_{p'}B^{\vec{n}'}_{\alpha'}\right) \tag{2.13}$$

and Δ^r is a matrix like F except that it has unit coupling constants for all the internal coordinates of type r and zero elsewhere. In this form the matrix Z is constructed only once in a given calculation, and it can be used repeatedly in the course of adjusting f_r. During the adjustment process it is helpful to know the relative importance of different types of internal coordinates in determining the frequency of a particular normal mode. This information is provided by the potential energy distribution

$$P_j^n(\vec{\varphi}) = f_n \lambda_j^{-1}(\vec{\varphi}) \sum_{\alpha\alpha'} (M_\alpha M_{\alpha'})^{-1/2} Z^n_{\alpha\alpha'}(-\vec{\varphi}) L_{\alpha j}(\vec{\varphi}) L^*_{\alpha' j}(\vec{\varphi}) \tag{2.14}$$

with normalizations

$$\sum_n P_j^n(\vec{\varphi}) = 1 \tag{2.15}$$

The significance of this function can be seen from the following expression for the potential energy of the solid in terms of the normal coordinates $Q_j(\vec{\varphi})$

$$2V = \sum_{jn} P_j^n(\vec{\varphi}) Q_j^*(\vec{\varphi}) Q_j(\vec{\varphi}) \tag{2.16}$$

When a set of observed eigenvalues $\lambda_j^{obs}(\vec{\varphi})$ is obtained, either from optical or neutron spectroscopic studies, a least squares refinement of the force constants is performed to bring the corresponding calculated eigenvalues $\lambda^c(\vec{\varphi})$ into agreement. This procedure is well established [5]. An initial set of force constant f_r^0 is used to obtain eigenvalues $\lambda_j^0(\vec{\varphi})$ and eigenvectors $L^0_{\alpha j}(\vec{\varphi})$. The Jacobian matrix $J_{jn}(\vec{\varphi})$ is calculated

$$J_{jn}(\vec{\varphi}) = \sum_{\substack{\alpha\alpha' \\ \vec{n}-\vec{n}'}} (M_\alpha M_{\alpha'})^{-1/2} S^n_{\alpha\alpha'}(\vec{n}-\vec{n}') e^{i\vec{\varphi}\cdot(\vec{n}-\vec{n}')} L^{0*}_{\alpha j}(\vec{\varphi}) L^0_{\alpha' j}(\vec{\varphi}) \tag{2.17}$$

Two functions A and B are then obtained as:

$$A_{nn'} = \sum_{j\vec{\varphi}} J_{jn}(\vec{\varphi}) J_{jn'}(\vec{\varphi}) P_j'(\vec{\varphi}) \tag{2.18}$$

$$B_n = \sum_{j\vec{\varphi}} J_{jn}(\vec{\varphi}) P_j'(\vec{\varphi}) \Delta\lambda_j(\vec{\varphi}) \tag{2.19}$$

where

$$\Delta\lambda_j(\vec{\varphi}) = \lambda_j^{obs.}(\vec{\varphi}) - \lambda_j^0(\vec{\varphi}) \tag{2.20}$$

and $P_j'(\vec{\varphi})$ are a set of weighting factors. The change in the force constants required to minimize $\Delta\lambda_j(\vec{\varphi})$ is then given by

$$\Delta f_{n'} = \sum_n (A_{nn'})^{-1} B_n \tag{2.21}$$

The cycle is repeated until a suitable fit is obtained if the problem converges. There are various conditions which can lead to non-convergence or very slow convergence; these have been discussed in detail elsewhere[6].

2.2 INELASTIC NEUTRON SCATTERING

The one phonon incoherent double differential scattering cross section for the crystal discussed above in powder form is

$$\frac{d^2\sigma}{d\Omega\, d\omega} = \left(\frac{E_f}{E_i}\right)^{1/2} \frac{\hbar^2 \kappa^2 e^{-\frac{\hbar\omega}{2k_B T}}}{4M\omega \sinh\left(\frac{\hbar\omega}{2k_B T}\right)} \sum_{\mu=1}^{S} a_\mu^2\, g_{eff}^{\mu}(\omega) \left(\frac{M}{M_\mu}\right) e^{-2W_\mu} \tag{2.22}$$

where

$$g_{eff}^{\mu}(\omega) = \frac{1}{3N} \sum_{\substack{j=1 \\ \vec{k}}}^{3S} \left| L_j^{\mu}(\vec{k}) \right|^2 \delta\left(\omega - \omega_j(\vec{k})\right) \tag{2.23}$$

$$2W_\mu = \frac{\hbar}{2M_\mu} \int d\omega\ \omega^{-1} \coth\left(\frac{\hbar\omega}{2k_B T}\right) g_{eff}^{\mu}(\omega) \tag{2.24}$$

and $\omega = (E_f - E_i)/\hbar$, $\kappa^2 = 2M/\hbar\,(E_i + E_f - 2\sqrt{E_i E_f}\cos\theta)$. In 2.22, a_μ is the bound-atom incoherent scattering length of the μth atom. Notice that our expression for $d^2\sigma/d\Omega\, d\omega$ is approximate because the Debye-Waller factor has been separately averaged over crystal orientations, and that moreover this averaging was carried out in the exponent.

3. HYDROGEN CHLORIDE

The crystal structure of hydrogen chloride has been investigated by various techniques[7]. A first-order phase transition at approximately 98°K has long been known from specific heat measurements[8]. The position of the chlorine atoms in the low temperature phase has been determined by x-ray diffraction[9]. These form a face-centered orthorhombic lattice whose dimensions are given in Figure 1. The positions of the hydrogen atoms were, however, not determined. Infra-red and Raman studies have shown that the molecules form a polymer of zig-zag hydrogen-bonded chains[10].

These measurements have not been able to determine, unambiguously, the manner in which the chains are packed in the crystal. The conclusions which these studies reached as to the crystalline structure of hydrogen chloride were based upon the observation of two doublets in the symmetric and antisymmetric hydrogen chlorine stretch (2758, 2748 and 2720, 2705 cm^{-1}). These four bands indicate a primitive cell containing four molecules. Such a cell could accomodate planar chains in which adjacent polymers are anti-parallel, or parallel polymers in which the hydrogen atoms are not on the plane defined by the chlorine atoms. A recent neutron diffraction study of deuterium chloride has revealed parallel planar chains in the low temperature phase[7]. The number of molecules in the primitive cell of hydrogen chloride thus depend upon whether the chains are planar, as in deuterium chloride, or not.

The lattice vibrations of hydrogen chloride in the low temperature phase have been investigated by infra-red[11] and neutron inelastic scattering[12]. Unfortunately there seems to be no Raman data available in this energy region. The infra-red observed frequencies of both hydrogen chloride and deuterium chloride have been identified as belonging to either translational or librational modes by noting their behavior due to the mass change. The attempt

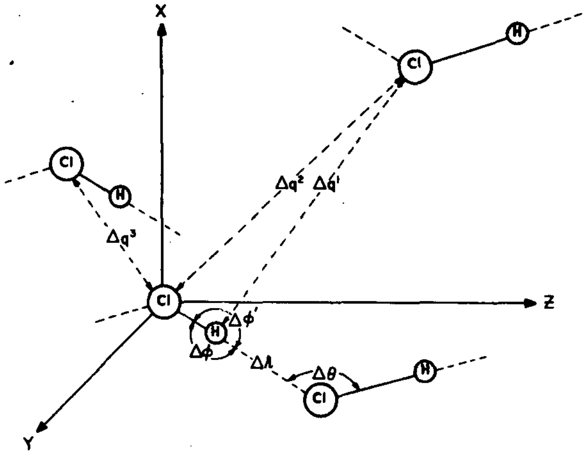

FIG. 1. The arrangement of the particles in the low-temperature phase of HCl. The Z axis is the chain axis. The dimensions of the Bravais unit cell are: a = 5.082, b = 5.41, c = 5.826 Å.

to calculate their values from a force model seems not to have been made previously.

In the present work, a force model is proposed which reasonably reproduces most of the available spectroscopic and thermodynamic data on the low temperature phase of hydrogen chloride. A crystal model consisting of parallel planar zig-zag chains was chosen and is represented in Figure 1. The planar model was used since it is consistent with the neutron diffraction study. The potential energy function includes central and non-central forces for the intrachain motions and central forces between particles in adjacent chains. Referring to the schematic of Figure 1, force constants F_R and F_r correspond to the covalent chlorine hydrogen stretch and hydrogen bond stretch respectively, H_θ to the angle bend $\Delta\theta$ defined by H---Cl-H and H_ϕ and $H_{\phi'}$ to the in plane, $\Delta\phi$, and out of plane, $\Delta\phi'$, linear angle bends defined by Cl-----H-Cl respectively.

The inter-chain force constants F_1, F_2, F_3 are due to central forces between the hydrogen in one chain and the nearest chlorine in the adjacent chains and between nearest and next nearest chlorine atoms in adjacent chains. The potential energy of the crystal is thus written as

$$2V = \sum_{\ell} \Big\{ F_R(\Delta R^{\ell})^2 + F_r(\Delta r^{\ell})^2 + (Rr)\left[H_\theta(\Delta\theta^{\ell})^2 + H_\phi(\Delta\phi^{\ell})^2 + H_{\phi'}(\Delta\phi'^{\ell})^2\right] + F_1(\Delta q_1^{\ell})^2 + F_2(\Delta q_2^{\ell})^2 + F_3(\Delta q_3^{\ell})^2 \Big\} \tag{3.1}$$

where the sum over ℓ indicates a sum over all appropriate coordinates in the crystal. The dynamical matrix in cartesian displacement coordinates is formed from the above set of internal coordinates by the method outlined above. The force model consists of eight adjustable parameters. Since our interest lies in the lattice vibrations, a value of F_R, the covalent stretch force constant, is chosen consistent with the high energy infra-red lines and held fixed. We thus have seven adjustable parameters to reproduce the observed lattice vibrations.

Table 1 contains the observed frequencies below 500 cm^{-1} for both hydrogen chloride and deuterium chloride. The two frequencies at 109 and 86 cm^{-1} in hydrogen chloride and 113 and 89 cm^{-1} in deuterium chloride can be definitely assigned to translational lattice vibrations[11]. The three remaining frequencies for hydrogen chloride and the four for deuterium chloride are assigned as either fundamental librations or combination bands. The only set of bands whose ratios are near the expected $\sqrt{2}$ are 496, 296, 217 cm^{-1}, and 328, 209, 169 cm^{-1} for hydrogen and deuterium chloride, respectively. The band at 258 cm^{-1} in DCl has no counterpart in HCl if it is assigned as a fundamental. However, if it is assumed to be a combination of 169 + 89 cm^{-1} then the corresponding combination band in HCl would lie at 303=217+86 cm^{-1}. Indeed the band centered at 296 cm^{-1} in HCl is broader than the others. For these reasons we have assigned as fundamental librational modes 496, 296, and 217 cm^{-1} in hydrogen chloride and their corresponding frequencies in deuterium chloride.

The model used in the present work belongs to the symmetry class C_{2v} and space group $Bb2_1m$. Standard group theoretical techniques[4] show that at k=o the lattice modes should consist of $2A_1$, $2A_2$, $2B_1$ and $1B_2$ non-zero frequencies. The frequencies belonging to the A_2 species are infra-red inactive, thus leaving five active fundamentals. The motions corresponding to these symmetry species and their assignment are shown in Figure 2. As a first attempt to obtain values for the force constants, only these infrared frequencies were used. For this case, the chains were considered isolated from each other, i.e., $F_1 = F_2 = F_3 = 0$, and the set of five intra-chain force constants were adjusted to obtain a fit to the five frequencies. The calculated frequencies and force constants which resulted from this refinement are given in Table 1 as set I. A model of the crystal consisting of isolated planar polymers is sufficient to explain the low frequency infra-red results except for an incomplete splitting of the 109-86 cm^{-1} band. One should turn to other sources for additional information about the forces between chains. The other spectroscopic data available is a spectrum of neutrons inelastically scattered from a sample of polycrystalline HCl at 85°K[12]. The spectrum was obtained using a beryllium filter time-of-flight spectrometer and is plotted as a function of final neutron energy in Figure 3. There is a strong peak centered at an energy transfer of 45 cm^{-1} which gives indication of being composed of a doublet with energies of approximately 40 and 50 cm^{-1}. It is difficult with the present data, to make these conclusions firm. The asymmetry of the incident line is known to have a very large effect on the shape, and therefore, resolution, of the inelastic spectrum at low energy transfers. Much better data is needed and we have plans to obtain this in the near future. For the present, we assign maxima in the density of states at 40 and 50 cm^{-1} to the transverse and longitudinal acoustic modes respectively. A second peak occurs at an energy transfer of 85 cm^{-1} and is assigned as due to the translational optic modes corresponding to the infrared frequencies of 86 and 109 cm^{-1}. A small peak at 155 cm^{-1} energy transfer can not be assigned as a fundamental, i.e., there is not expected to be a feature in the density of states at this energy with the present model. Its origin may be either a multi-phonon or multiple scattering process. Its reproducibility and behavior as a function of temperature and sample thickness should be tested. The large peak centered at an energy transfer of 215 cm^{-1} is assigned as due to the librational optic modes corresponding to the infra-red frequency of 217 cm^{-1}.

One word concerning the effect on the observed spectrum of the shape of the incident spectrum. A calculation has been performed in which the instrumental resolution and the shape of the incident spectrum has been

TABLE 1

ASSIGNMENTS AND CALCULATIONS OF I. R. FREQUENCIES FOR HCl AND DCl

HCl				DCl		
	SET I	SET II			SET II	COMB
OBS	CALC	CALC	PED	OBS	CALC	
496 a	496	496	$.74\ H_{\theta} + .26\ H_{\phi}$	328	354	
296	296	296	$.28\ H_{\theta} + .72\ H_{\phi}$	258		169 + 89
217	217	217	H_{ϕ}'	209	213	
109	103	109	$.47\ F_r + .52\ F_2$	169	156	
86	91	86	$.80\ F_r + .12\ H_{\theta} + .06 H_{\phi}$	113	108	
				89	85	

	SET I	SET II
F_r	0.0962 b	0.0641
H_{θ}	0.0428	0.0428
H_{ϕ}	0.0151	0.0151
H_{ϕ}'	0.0109	0.0109
F_1	0	0
F_2	0	0.0301
F_3	0	0.0077

(a) All frequencies in cm^{-1}.

(b) All force constant in md/Å.

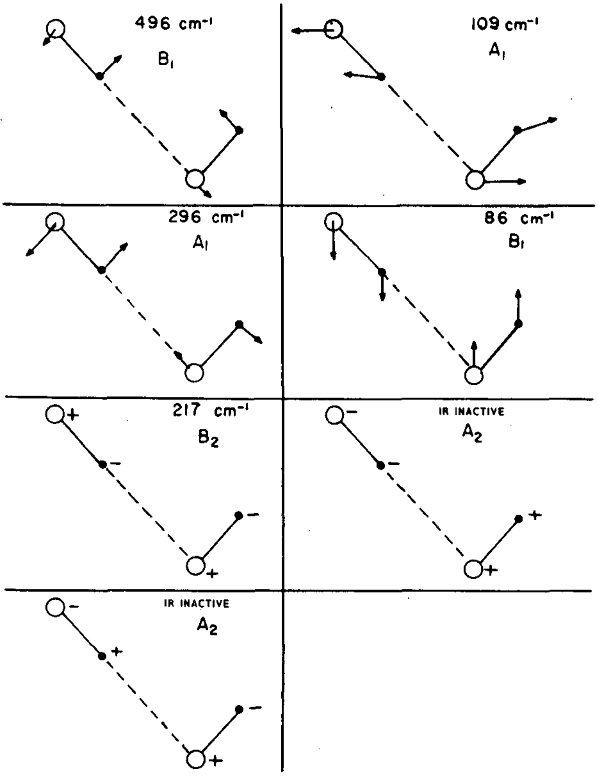

FIG. 2. The polarization vectors of the k =0 modes of the two molecules in the primitive cell of HCl. The frequency and symmetry species of each mode are indicated.

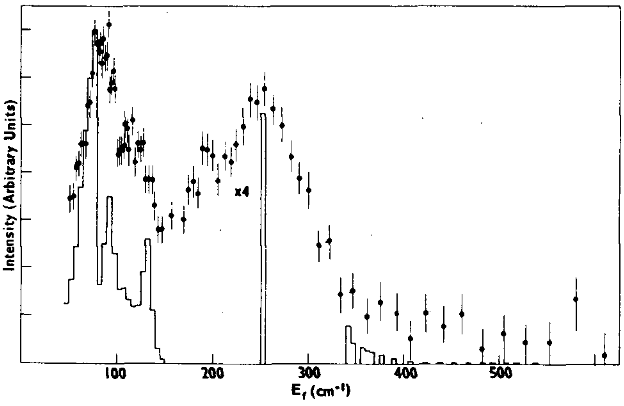

FIG. 3. The time-of-flight spectrum of inelastically scattered neutrons from a polycrystalline sample of HCl at 85°K. The histogram is the result of calculations as discussed in the text.

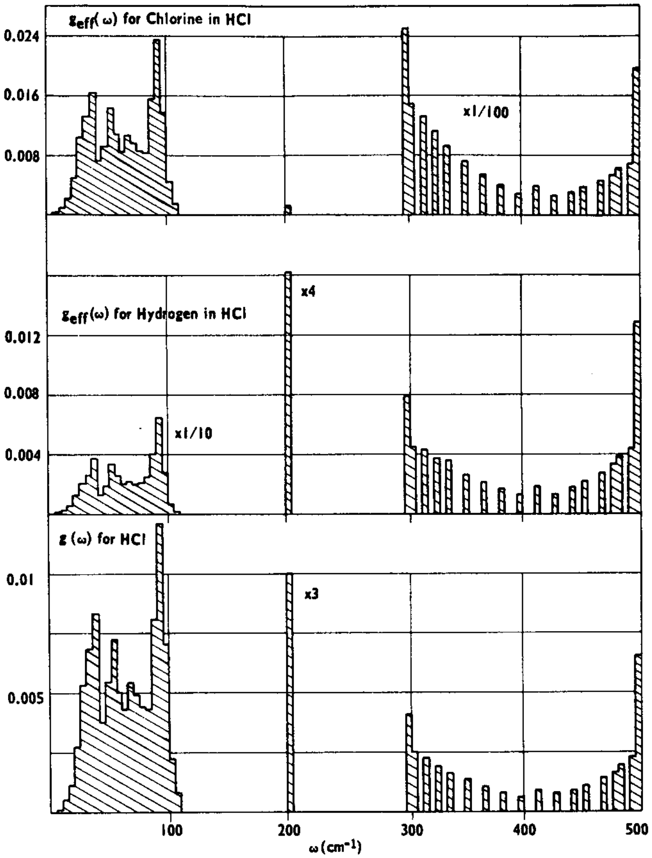

FIG.4. The frequency distribution function and effective frequency distribution functions for hydrogen and chlorine, obtained as discussed in the text, for HCl.

taken account of in reproducing a given observed spectrum[13]. The principal effect of concern here is the shift to higher frequencies which was required of peaks in the frequency distribution to reproduce the observed spectrum. All of the energy transfer assignments quoted in this work were obtained by assuming an incident energy of 40 cm^{-1} (.005 ev)and should be considered as lower limits. In the final adjustment of all the force constants, the five infra-red frequencies were assigned to $\vec{k}=0$ and the two neutron frequencies corresponding to the acoustic modes to the Brillouin Zone boundary in the [0, 0, 1] direction. This latter assignment is made in analogy with other polymers which have shown that for such an asymmetric crystal as a polymer, the dispersion relations are only weakly dependent on k_x and k_y so that maxima in the density of states can be deduced from the behavior of the dispersion relation along the k_z direction (the chain axis)[14]. With this assignment then ,the eight force constants were adjusted. It was found that if force constant F_1, which relates the interaction between the hydrogen and chlorine of adjacent polymers, was allowed to vary, a value for F_1 which was small and negative was obtained. One of the models which has been proposed for this crystal is that of parallel but non planar chains. Anderson and Savoie[10] have attempted to infer the position of the hydrogen from a measurement of the intensities of the infra-red and Raman lines in the stretching region. Their model shows the hydrogen pulled off the polymer plane toward the nearest chlorine in an adjacent chain. The above result, viz., a small and negative hydrogen chlorine force constant, therefore seems inconsistent with their model. In any case, force constant F_1 was then set to zero and held fixed in the final adjustment and set II given in Table 1 was obtained.

With these force constants, the frequency distribution and effective frequency distribution functions for the hydrogen and chlorine atoms were calculated by the root sampling technique. A total of 711 points in 1/8 of the Brillouin Zone were used in the calculation. These functions are shown in Figure 4. The neutron cross section, both one-and two-phonon, were then calculated as outlined above. The two-phonon cross-section is very small (two orders of magnitude smaller than the one-phonon cross section) so that the structure at 155 cm^{-1} can not be attributed to this effect. The Debye-Waller factor, 2W, for the hydrogen atom varied from .1 at the elastic peak to .7 at a final neutron energy of 500 cm^{-1}. The results of the calculation are shown in Figure 3. The only serious discrepancy is in the energy of the peak at 85 cm^{-1} energy transfer. Part of this could be due to the effect mentioned earlier of the asymmetric incident line. It is difficult to account for the remaining inconsistency (if any), since the infra-red frequencies are rather well known. The measurement must be repeated and the position of the peak checked. The discrete appearance of the frequency distribution for the optical modes between 300 and 500 cm^{-1} is a result of the small number of points used in the root sampling method and is not physical. The dispersion curves of the external modes using the force constants set II along the [001] direction are shown in Figure 6.

The specific heat C_V was calculated from the frequency distribution and is compared with measurements of C_p [8] in Figure 5. The agreement is quite good up to 65°K where the measurement becomes larger than the calculation. The discrepancy can have several sources, thermal expansion, anharmonic contributions and perhaps the proximity of the phase transition.

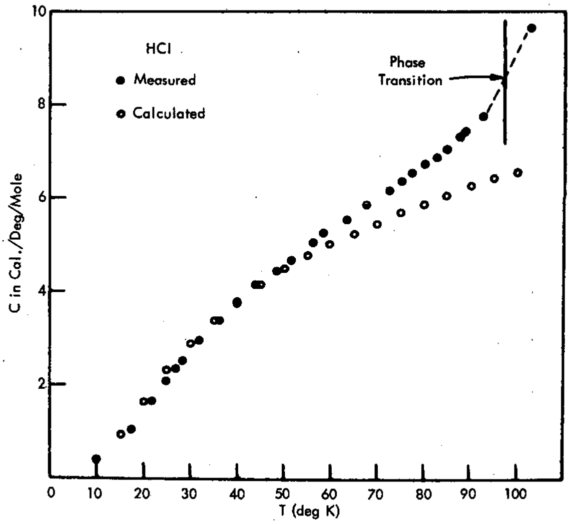

FIG.5. The calculated C_V and measured C_p of HCl.

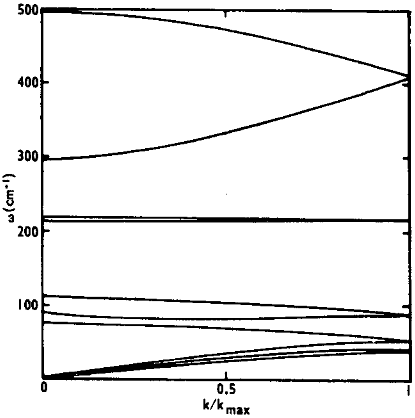

FIG. 6. The dispersion curves of HCl along the (0, 0, 1) direction.

In conclusion, the model used in the present study reasonably reproduces the available spectroscopic data and is consistent with a two molecule per primitive cell model composed of planar parallel polymers. The evidence favors the hydrogen being bound to chlorine within the common chain only, rather than to an additional chlorine in an adjacent chain and that the interchain forces are due to chlorine-chlorine interaction only.

4. CUBIC ICE

The ordinary form of ice (Ih) is hexagonal in structure with four molecules per unit cell, and has been the subject of considerable experimental study[15, 16]. Because of the complexity of the Ice Ih structure, only a few lattice dynamical calculations have been attempted and these have been approximate in nature[17 - 19]. A lower temperature form, cubic ice (Ic), having the diamond structure is also known[20]. Although the latter form has only two molecules per unit cell, Raman and infra-red spectra of Ice Ih and Ic have been found to be identical over the entire range of internal and external normal modes, 50-3500 cm^{-1}[21].

This is accounted for by the fact that the nearest neighbors in Ices Ih and Ic are identically situated, if the difference between the O-O bonds in Ice Ih that are parallel to the c-axis and those at an angle to the c-axis is ignored. In view of this it was felt that a lattice dynamical calculation for the more tractable two molecule per unit cell structure, Ice Ic, would also be a good approximation to that of Ice Ih. Both phases of Ice I are orientationally disordered[22, 23]. That is a hydrogen can occupy with equal probability either of two equilibrium positions 1Å from either oxygen on the O-O line. In the present calculation a model of cubic ice is assumed in which the hydrogens are ordered, which is to say we impose a tetragonal structure on the crystal when the hydrogen atom positions are considered.

Since the dynamical units in the translational lattice modes are essentially the oxygen atoms, the ordered hydrogen model is expected to give a good approximation to these modes. The effect of disorder on the librational and internal modes wherein the hydrogens are the principal dynamical units is not certain.

TABLE 2

FORCE MODEL FOR ICE Ic

	FORCE CONSTANT	INTERACTION	EXAMPLE (Ref. Fig. 7)
1	F_R	O - H stretch	1-4
2	H_θ	H-O-H angle bend	3-1-4
3	H_ϕ	H-libration, in-plane	1-4-2
4	$H_{\phi'}$	H-libration, out-of-plane	1-4-2
5	H_γ	non-linear wag, out-of plane	1-2-5-6
6	$H_{\gamma'}$	linear wag, out-of-plane	3-1-4-2
7	F_r	H---O stretch	4-2
8	$F_{r'}$	O---H--H---O interaction	1-7---1-8
9	$F_{r''}$	O-H---O interaction	1-4---4-2

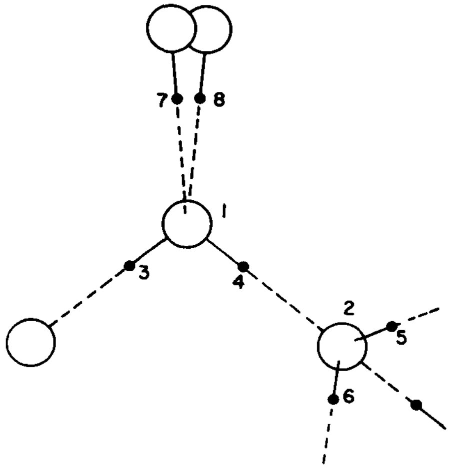

FIG. 7. The arrangement of particles in the model of cubic ice used in the present calculation $d(O_1\text{-}O_2) = 2.76$ Å, $d(O_1\text{-}H_{3,4}) = 1$ Å.

The force model chosen for cubic ice is described in Table 2 with reference to Figure 7. The potential energy of the crystal has the form

$$2V = \sum_{\ell} \Big\{ F_R (\Delta R^{\ell})^2 + F_r (\Delta r^{\ell})^2 + F_{r'} (\Delta r^{\ell})(\Delta r^{\ell'}) + F_{r''} (\Delta R^{\ell})(\Delta r^{\ell}) + R^2 H_\theta (\Delta \theta^{\ell})^2 + Rr \big[H_\phi (\Delta \phi)^2 + H_{\phi'} (\Delta \phi')^2 + H_\gamma (\Delta \gamma)^2 + H_{\gamma'} (\Delta \gamma')^2 \big] \Big\} \qquad (4.1)$$

The orientational disorder of the hydrogen in Ice I has the consequence that ordinary optical spectroscopic selection rules do not hold so that infra-red and Raman spectra show features of the density of states rather than allowed, $\vec{k}=0$ modes[21]. This is confirmed by the good agreement between the optical density/ν^2 from far-infrared measurements and recent inelastic neutron scattering results on ice Ih[13]. Conversly, the assignment of modes in ice is made more difficult in that infra-red provides essentially the same information, although with higher resolution, as that obtained from incoherent neutron scattering data.

The observed frequencies were obtained for Ice Ih at 150°K by means of a Be-filter time-of-flight spectrometer. Corrections were made for instrumental resolution and incident neutron distribution[13].

Initial assignments of the observed translational frequencies were made by assuming, as discussed above, that the approximate frequency distribution of Ice Ih obtained from incoherent neutron scattering data (Fig. 8) is also a good approximation to the frequency distribution of Ice Ic. Assignments of the observed maxima in the approximate frequency distribution to specific $\vec{k}$ values were then made in analogy with frequency distributions obtained from calculated dispersion curves for simpler diamond-like structures[24].

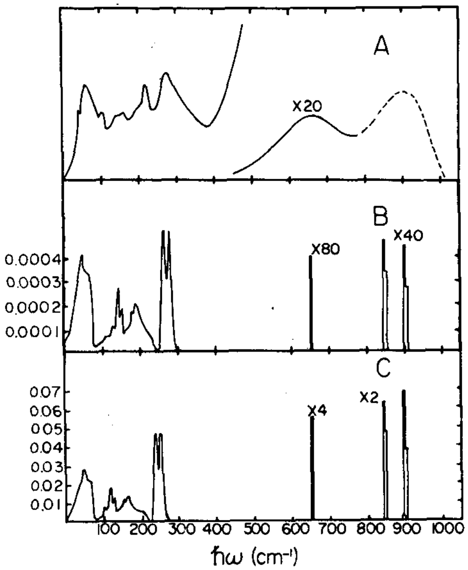

FIG.8. The calculated frequency distribution (C) and effective frequency distribution (B) for hydrogen in cubic ice from assignment 1 as discussed in the text and the effective frequency distribution derived from neutron scattering data (A).

This method of assignment presents difficulties since the comparison of dispersion curves and calculated frequency distribution for the simpler structures does not unambiguously give the $\vec{k}$ values at which high densities of states occur. Furthermore, a close correspondence between the translational lattice modes of monatomic solids such as germanium, silicon and diamond and those of Ice Ic is not necessarily to be expected. Because of these difficulties two distinct tentative assignments were made for the maxima obtained from the neutron data, and these are shown in Table 3.

TABLE 3

ASSIGNMENTS FOR ICE Ic

ASSIGNMENT I				ASSIGNMENT II			
DESCRIPTION[a]	MODE	OBSERVED FREQUENCY (cm^{-1})	CALCULATED FREQUENCY (cm^{-1})	DESCRIPTION	MODE	OBSERVED FREQUENCY (cm^{-1})	CALCULATED[b] FREQUENCY (cm^{-1})
[0, 0, 0]	H-O-H Bend	1640	1640	[1, 0, 0]	Libration	900	901
	Libration	900	900				848 (c)
	"	840	840				646 (c)
	"	650	650				
[1, 0, 0]	TO	220	259	[1, 1, 1]	TO	280	280
			255(c)				271 (c)
	TA	63	68		LO	220	213
			63(c)				
[1, 1, 0]	LO	190	201		LA	140	153
	LA	160	158		TA	63	60
							20 (c)
[1, 1, 1]	TO	280	280				
			263(c)				
	TA	45	45				
			26(c)				

(a) Frequencies assigned at B. Z. Boundary

(b) Calculation gave all 18 modes in each direction

(c) No frequency assigned

The assignment of librational frequencies at 650, 840 and 900 cm^{-1} was based on the neutron scattering data and optical spectroscopic measurement[16]. The assignments and calculated frequencies are shown in Table 3 and the corresponding force constants in Table 4.

TABLE 4

FORCE CONSTANTS FOR ICE IC

FORCE CONSTANT	ASSIGNMENT I (md/Å)	ASSIGNMENT II (md/Å)
1	5.51827 (a)	5.5182
2	.6166	.6166
3	.0566	.0566
4	.0755	.0755
5	.0057	.0066
6	.0517	.0517
7	.2485	.2733
8	-.0733	-.0385
9	0. (b)	.0251

(a) Assigned from reference 17, and held fixed.

(b) Held fixed during adjustment.

The frequency distribution and effective frequency distribution of the external modes calculated by the root sampling method for each assignment are shown in Figures 8 and 9, along with the effective frequency distribution obtained directly from the neutron data. A total of 711 points in 1/8 of the Brillouin Zone were used in each calculation. The agreement between measured and calculated effective frequency distribution is not completely satisfactory for the translational lattice modes for either assignment, however, positions of maxima are quite well reproduced, particularly in assignment II. The relative intensities of the librational modes and the effect of polarization vectors on scattered neutron intensity are clearly shown by the calculated frequency distribution and effective frequency distributions. The polarization vectors greatly enhance the relative intensity of neutrons which are scattered by librating hydrogens relative to those scattered by hydrogens undergoing translations. This enhancement has been noted previously and accounted for by proposing different rotational and translational effective masses for the scatterers[13, 25]. The present lattice dynamical calculation yields this result directly.

The present results for cubic ice represent the first lattice dynamical calculation which includes all modes of the cubic ice crystal. The incomplete agreement between calculation and experimental data is possibly due to the choice of force model. It is also possible that, contrary to the optical spectroscopic data, the frequency distribution of cubic and hexagonal ice are different. High resolution neutron scattering data on Ices Ih and Ic would be of great importance in this regard.

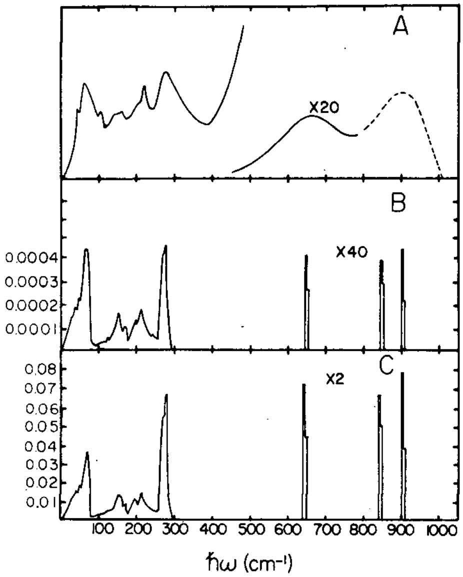

FIG.9. The calculated frequency distribution (C) and effective frequency distribution (B) for hydrogen in cubic ice from assignment 2 as discussed in the text and the effective frequency distribution derived from neutron scattering data (A).

REFERENCES

[1] Dolling, G., Woods., A. D. B., "Thermal Neutron Scattering", Ch.5, (Egelstaff, P. S., Ed.), Academic Press, New York (1965).
[2] Born, M., Huang, K., "Dynamical Theory of Crystal Lattices", Clarendon Press, Oxford (1954); Maradudin, A. A., Montroll, E. W., Weiss, G. H., Solid State Physics, Supplement 3 (1963).
[3] Lomer, W. M., Law, G. G., Ref. [1], Ch. 1.
[4] Wilson, E. B., Jr., Decius, J. C., Cross, P. C., "Molecular Vibrations", McGraw-Hill, New York (1955); McMurry, H. L., Solbrig, A. W. Jr., J. Chem. Phys. 32 (1960) 1289, 1720.
[5] Shimanouchi, T., Suzuki, I., J. Chem. Phys. 42 (1963) 296.
[6] Schachtschneider, J. H., Vibrational Analysis of Polyatomic Molecules VI, Shell Development Co., Tech. Rpt. No. 57-65; Overend, J., Scherer, J. R., J. Chem. Phys. 32 (1960) 1289, 1720.
[7] Sándor, E., Farrow, R. F. C., Nature (1967) 171, and references therein.
[8] Giaque, W. F., Wiebe, R. J. Amer. Chem. Soc. 30 (1928) 101.
[9] Natta, G., Gaz. Chem. Ital. 63 (1933) 425.
[10] Savoie, R., Anderson A., J. Chem. Phys. 44 (1966) 548.
[11] Anderson, A., Gebbie, H. A., Walmsby, S. H., Mol. Phys. 7 (1964) 401; Arnold, G. M., Heastie, R., Chem. Phys. Letters 1 (1967) 51.
[12] Boutin H., Safford, G. J., "Inelastic Scattering of Neutron in Solids and Liquids", I.A.E.A., Vienna (1965) Vol. II 393.
[13] Prask, H., Boutin, H., Yip, S., J. Chem. Phys., in press.
[14] Summerfield, G. C., J. Chem. Phys.43 (1965) 1079.
[15] Leadbetter, A. J., Proc. Roy. Soc. 287A (1965) 403 and references therein.
[16] Ockman, N., Adv. Phys. 7 (1958) 199 and references therein.
[17] Kyogoku, Y., J. Chem. Soc., Japan, Pure Chem. Sec 81 (1960) 1648.
[18] Kahane, A., C. R. Acad. Sci 250 (1960) 500; 252 (1961) 678.

[19] Forslind, E., Proc. Swedish Cement and Concrete Res. Inst. Nr. 21 (1954).
[20] Lonsdale, K., Proc. Roy. Soc. 247A (1958) 424.
[21] Bertie, J. E., and Whalley, E., J. Chem. Phys. 46 (1967) 1271 and references therein.
[22] Peterson, S. W., Levy, H.A., Acta. Cryst. 10 (1957) 70.
[23] Honjo, G., Shimaoko, K., Acta. Cryst. 10 (1957) 710.
[24] Dolling, G., Cowley, R. A., Proc. Phys. Soc. 88 (1966) 463.
[25] Hahn, H., "Inelastic Scattering of Neutrons in Solids and Liquids", I.A.E.A., Vienna (1965) Vol. II, 279.

DISCUSSION

W. COCHRAN: It is remarkable that a model which uses only short-range forces should give results in apparent agreement with observation. The molecule of HCI has a dipole moment of about one Debye unit, and certain phases of hydrogen halides are ferroelectric. It follows that Coulomb interaction must be of some importance.

H. PRASK: As you say, one would expect Coulomb interactions to be important in HCl. Fitting the limited amount of data available at present, however, did not require inclusion of long-range interactions. In this regard, better incoherent scattering data might show the force model we used to be inadequate. Ultimately, dispersion curve measurements by coherent inelastic scattering would provide the most sensitive test of any force model.

E.E. SÁNDOR: I have five observations to make on this paper:

(1) On the basis of the authors' own notation in labelling the unit cell axes in Fig. 1, the chain axis should be called y-axis and not z-axis. Furthermore, the unit cell associated with the planar chain model used in the authors' calculations is body-centred and not face-centred as stated.

(2) The claim that the present study reasonably reproduces the spectroscopic data – if taken literally – would mean that it is inconsistent, since the spectroscopic information available at present is contradictory. In particular, infrared and Raman data obtained recently in the stretching region suggest non-planar chain structure, whereas the far infrared spectra of lattice frequencies suggest planar chain structure.

(3) The authors seem to question the reliability of the inelastic neutron scattering data of HCl available at present. With this I fully agree, but I also think that they treated these data in rather an arbitrary way – I refer to their assigning the peak at 45 cm^{-1} to transverse and longitudinal modes at 40 and 50 cm^{-1} respectively and ignoring the peak at 155 cm^{-1}.

(4) It should be pointed out that another fundamental assumption of the authors' theory – the assignment of some strong peaks observed in the far infrared spectrum to pure librational modes – is still a controversial matter.

(5) The discrepancy between the measured specific heat curve of HCl and the one calculated on the basis of the authors' model starts becoming conspicuous above 50°K (Fig. 5). Since up to this temperature the specific heat curve can be approximated by a Debye function indicating that HCl up to 50°K behaves very much like a monatomic solid, one would suspect that the discrepancy is closely related to the treatment of the librational modes in the authors' model, as above 50°K these modes are expected to give the dominant contribution to the observed specific heat.

H. PRASK: I will reply to your comments in order:

(1) In the preprint the axes of the unit cell were incorrectly labelled. This has been corrected in the final version and I should have mentioned it here. With respect to the symmetry of the unit cell as used in our calculation, the chlorine atoms alone define a face-centred orthorhombic unit cell. The complete symmetry of the cell with hydrogen included is $Bb2_1m$, which is identical to that found by Sándor and Farrow.

(2) Our main interest in this work, as is clearly stated in the text, is the lattice mode spectral region of HCl, for which there are both far infrared and inelastic neutron data. These data are reasonably well reproduced. The spectroscopic information on the fundamental HCl stretch bands is internally contradictory, as is discussed in the text, and suggestions advanced to resolve the contradictions could change our model, but perhaps only slightly. For example, it has been proposed that the hydrogens may lie up to 0.02 Å off the Cl-Cl line. In view of the fact that this work was, to our knowledge, the first attempt at calculating the lattice modes of HCl, we felt that including a refinement such as this was unwarranted at present.

(3) The neutron data available at present consist of a single measurement made some years ago by Boutin and Safford using the full beryllium-filtered spectrum and samples 1-mm thick. These data were adequate for qualitative discussion of vibrational modes in HCl; however, higher-resolution data with higher statistical accuracy are needed. The assignment of acoustic mode maxima at 40 and 50 cm^{-1} is somewhat arbitrary and is discussed as such in the text. Positive assignments would be possible only if coherent inelastic scattering data were available. Because of the sample thickness the peak at 155 cm^{-1} could well be due to multiple scattering. However, this is a tentative explanation which will be easily checked when thin sample data are obtained.

(4) We have based our assignment of modes as librational and translational on the evidence presented by the optical spectroscopists as referred to in the text. This evidence consists mainly of the behaviour of the bands upon deuteration. The calculated frequencies for HCl agree with our assignment and although this does not prove the correctness of the model, the model is at least consistent with the available data. The subsequent reasonably good agreement of the observed and calculated frequencies of DCl without any change of force constants is further justification of the assignment. Whether these bands are in reality the only bands present or whether there are more unresolved peaks is not absolutely certain.

(5) I don't think the fact that the measured specific heat of HCl up to 50°K can be approximately reproduced from a Debye distribution is important here. What is of interest is that the calculated frequency distribution gives a very good absolute fit to the measured specific heat at least up to 50°K. This indicates that the force model employed to fit spectroscopic data is also reasonable for the thermodynamic data. The discrepancy above 50°K may, as you suggest, arise from an incorrect frequency distribution in the librational mode region. It might also arise because thermal expansion and anharmonicity were not taken into account.

J.J. RUSH: How accurately are the $q = 0$ lattice-mode peaks determined in the infrared measurements with which you compared your calculations?

H. PRASK: The intrinsic instrumental resolution in the far infrared measurements is, of course, considerably better than that at present obtainable in inelastic neutron scattering measurements. The infrared vibrational energies given in the paper are those quoted in the literature used as references. The accuracy of these values would have to be determined by examining the spectra, since some of the bands are quite broad. The uncertainty might be 5 cm^{-1} or larger.

W. C. HAMILTON: With regard to your treatment of ice, perhaps the fact that you used an ordered proton model – when we know it to be disordered – may be a source of error. The proton disorder tends to muddy any experimental or theoretical study of ice. I would therefore like to suggest that both theoreticians and experimentalists consider working on one of the ordered forms of ice where the structural model is clear. At Brookhaven, Kamb, Laplaca and myself have completed a study of ice II by neutron diffraction and the proton positions are thus well known. Ice II crystals, however, have a rather large mosaic spread and are subject to twinning, so they are perhaps not suitable for measurement of dispersion curves. Ice III, on the other hand, may be a suitable candidate. The spectroscopic data from the Canadian group suggest an ordered proton arrangement, although Kamb favours a disordered structure on the basis of the X-ray diffraction data. We now have a set of neutron diffraction data from a single crystal and should soon know whether ice III is ordered or not. If it is ordered, it is a very good candidate for a lattice dynamics experiment, since large single crystals with low mosaic spread can be grown. It should be noted that, although the structures are simple, there are 12 molecules per unit cell, which may be an inhibiting factor.

H. PRASK: I quite agree that a lattice dynamical study of one of the ordered forms of ice would be more realistic than our calculation, in which we assume an ordered model for ice IC. As you mentioned, however, the calculation of the normal modes might be prohibitively complicated.

It was our intention in this paper to present an initial attempt at a calculation of the normal modes, including hydrogen motions, because of the considerable interest in ice and water, and the considerable amount of spectroscopic data available. In the region of translational lattice modes it is expected that the use of an ordered model should be a reasonably good approximation (see Ref. [21] of the paper).

H. H. STILLER: We have recently carried out measurements and somewhat similar calculations for HF, from which two interesting features emerged. First, we found that we had to take account of considerable interaction between the chains in order to get agreement with the experimentally observed spectrum; the interaction between the chains has a particularly strong effect on the acoustic frequencies at the zone boundary. Secondly, as soon as one gets to larger values of q, there is considerable mixing of the modes, so much so, in fact, that the F-H stretching mode mixes into other motions and cannot be neglected.

L. J. SLUTSKY: I believe that Hornig and his co-workers have found it possible to give a satisfactory interpretation of the infrared and Raman spectra of hydrogen halides, deutero-hydrogen halides and solid solutions of the normal and the deutero halides by assuming that the (dynamic) dipole-dipole interaction is the principal mode of interaction between non-hydrogen-bonded species. In your work, however, you have elected to represent the interaction between chains exclusively as a Cl-Cl central force; this seems to be in some respects at variance with the spectroscopic situation. Could you explain further the rationale underlying your choice of model?

H. PRASK: The rationale for our choice of force model was the practical one of including only as many interactions as was found necessary to fit available infrared and neutron data. In this regard, we show in Table I that the assumed central force interaction between the hydrogens of the chain and the nearest-neighbour non-chain chlorine ($\Delta q'$) proved to be negligible in its contribution to obtaining a fit to the available data. The work of Hornig et al. has, I believe, been primarily concerned with interpreting the fundamental HCl stretching bands ($\sim 2700\ cm^{-1}$), and inferring the arrangement of the chains in HCl.

There is also more recent work which we refer to in the paper. Our main concern was to propose a force model which would give reasonable agreement with available data on lattice modes. When more extensive data are obtained, it may well be necessary to include long-range interactions to obtain this reasonable agreement.

PRESSURE DEPENDENCE OF THE FREQUENCY OF SOME PHONONS IN SODIUM IODIDE*

G. QUITTNER, S. VUKOVICH AND G. ERNST
OESTERREICHISCHE STUDIENGESELLSCHAFT
FÜR ATOMENERGIE,
REAKTORZENTRUM SEIBERSDORF,
AUSTRIA

Abstract

PRESSURE DEPENDENCE OF THE FREQUENCY OF SOME PHONONS IN SODIUM IODIDE. Results of measurements on the pressure-induced phonon frequency shifts of some phonons of the LA (00ζ) and the TA $(\zeta\zeta 0)$ branches in NaI are presented. A hydrostatic pressure of 3000 atm was applied. Some special features and problems of the measurement and of the evaluation of frequency shifts are briefly discussed. The results are compared to Grüneisen parameters calculations by E.R. and R.A. Cowley based on a shell model.

Lattice vibrations in the two alkali halides, sodium iodide and potassium bromide, have been studied extensively both experimentally [1] and theoretically [2, 3]. We present here measurements of Grüneisen parameters of a few phonons in sodium iodide, performed by the inelastic neutron scattering technique.

1. DETAILS OF THE EXPERIMENT

The measurements were done on a conventional triple-axis spectrometer in the constant-Q mode of operation. A scattering chamber described in detail in Ref. [4] was used to apply a hydrostatic pressure of 3000 atm to the sample.

The requirements for the intensity and good shape of neutron peaks are necessarily higher in phonon shift measurements than in simple dispersion relation measurements. As the magnitude of the phonon frequency changes is of the order of 1%, Grüneisen parameter determinations of even moderate accuracy (~30%) require count numbers at least an order of magnitude larger than phonon frequency determinations of good quality (~1%) do. The mean number of counts per point in the phonon peaks has to be typically several thousands as compared to several hundreds in simple phonon frequency measurements. This, together with the relatively high incoherent background in sodium iodide severely restricted the set of phonons that could be measured with reasonably good results within a reasonable time, to those where favourable experimental conditions could be found. Thus all optical phonons had to be excluded.

Phonons at Brillouin zone boundaries present considerable difficulties because of their low intensity and the high incoherent background. Only one of them, the LA (001) phonon is included in our list of results, all the others being in-zone phonons. The latter offer the advantages of higher intensity, lower background and the possibility of focusing.

---

* Research sponsored in part by the US Government under Contract 61 (052)-638.

TABLE I. PRESSURE DEPENDENCE OF PHONON FREQUENCIES IN SODIUM IODIDE

Phonon	Branch	Position of Q	Phonon energy (meV)	Phonon energy difference between 3000 atm and 0 atm	Grüneisen parameter γ
A	TA	- 0.21 - 0.21 4	2.591	0.042 ± 0.006	0.87 ± 0.13
B_1	TA	- 0.30 - 0.30 4	2.866	0.067 ± 0.007	0.92 ± 0.11
B_2	TA	- 2.30 - 2.30 4	3.865	0.079 ± 0.014	1.09 ± 0.21
C_1	TA	- 0.40 - 0.40 4	4.628	0.050 ± 0.008	0.57 ± 0.09
C_2	TA	+ 0.40 + 0.40 4	4.628	0.058 ± 0.028	0.67 ± 0.34
C_3	TA	- 2.40 - 2.40 4	4.628	0.029 ± 0.019	0.34 ± 0.22
D	TA	- 0.60 - 0.60 4	6.308	0.045 ± 0.014	0.37 ± 0.10
E	LA	2.00 2.00 2.25	4.855	0.108 ± 0.029	1.18 ± 0.31
F	LA	1.00 1.00 6.00	7.304	0.081 ± 0.108	0.59 ± 0.78

There was considerable difference in the quality and intensity of the actual phonon groups which could not always be explained by the conventional factors including structure factors [1] and focusing effects [5, 6]. Good intensities and shapes were found for the LA phonons of the (00ζ) direction and for the TA phonons of the $(\zeta\zeta 0)$ direction. The focusing diagrams [5, 6] showed very good focusing for the former and a moderately good one for the latter. On the other hand, the TA$(\zeta\zeta 0)$ phonons in the (440) zone which have similar structure factors and focusing diagrams to the TA(00ζ) phonons in the (002) zone, show rather poor phonon groups.

The good quality of the TA $(\zeta\zeta 0)$ phonons allowed additional measurements on two of them (the (0.3, 0.3, 0) and the (0.4, 0.4, 0)) in other parts of the reciprocal space. This was done to obtain an idea of the magnitude of possible systematic errors. The phonons, which are essentially the same but measured with different Q's, are given the same capital letters in Table I, B_1, B_2 and C_1, C_2, C_3.

A value for the relative change $-\Delta V/V$ must be known when evaluating the Grüneisen parameters

$$\gamma_{qj} = -\frac{\Delta\omega_{qj}/\omega_{qj}}{\Delta V/V}$$

As we were not able to find the pertinent data in the literature, we used $-\Delta V/V = 0.0188$ derived from our measurements on the shift of Bragg angle upon application of pressure. This value happens to be exactly the same as that calculated for KBr from the data of Bridgman [7].

Figure 1 shows the dispersion relations of Ref. [1]. Figures 2 and 3 show examples of phonon groups with and without pressure. The results of our measurements are summarized in Table I.

2. COMPARISON WITH THEORY

Before comparing our results with a particular theory, let us make some general remarks on the kind of theories that can be compared with Grüneisen parameter measurements. Not every model used to describe measured dispersion relations is suitable for a Grüneisen parameter calculation: the crucial point is the number and the physical meaning (if any) of the model parameters that are to be determined by fitting to experimental data. 'Spring constants', e.g., cannot be evaluated for Grüneisen parameters; hence the tradiational Born-von Kármán theory gives no information whatsoever in this respect.

A more interesting 'mixed' case is the conventional shell model where one part of the interactions, i.e. the long-range Coulomb interaction between known charges and dipoles, is in a form suitable for Grüneisen parameter evaluation, whereas another part, spring constants for field and distortion polarizability, is not. Only the non-linear interactions contribute to calculated Grüneisen parameters, whereas the consequences of possible changes of 'spring constants' must be neglected.

E.R. and R.A. Cowley have calculated Grüneisen parameters for sodium iodide and potassium bromide [3]. They used a shell model which takes into account the nearest neighbour repulsive forces, not by spring constants - as the more conventional shell models do - but by a Born-Mayer

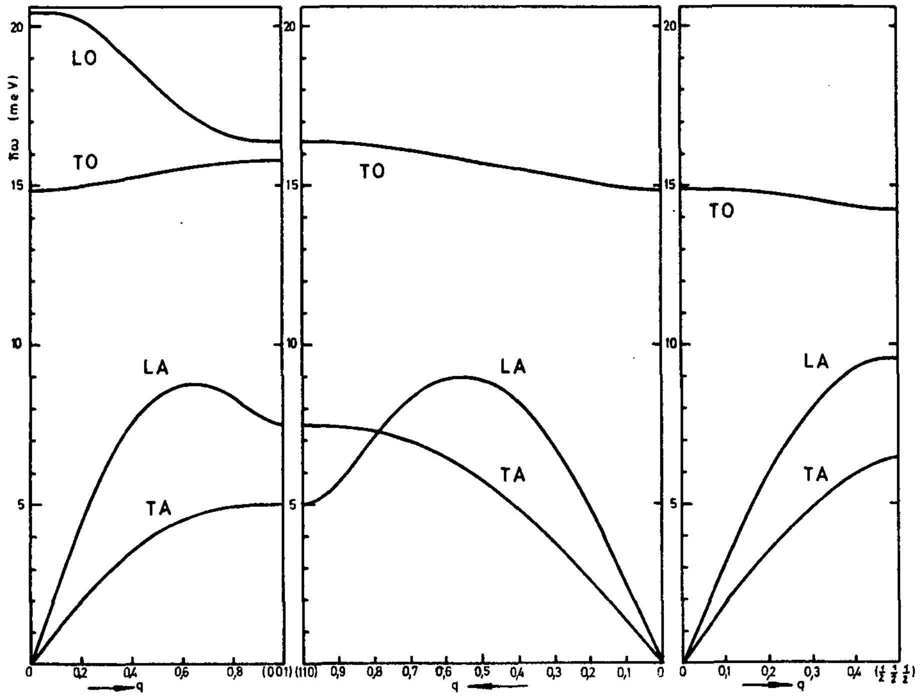

FIG. 1. Phonon dispersion relations in the main symmetry direction in NaI from Ref.[1].

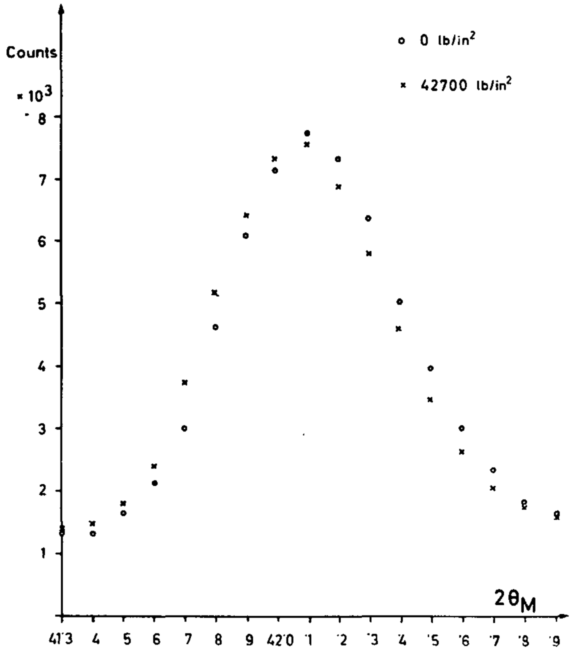

FIG. 2. Phonon groups of the phonon C_1.

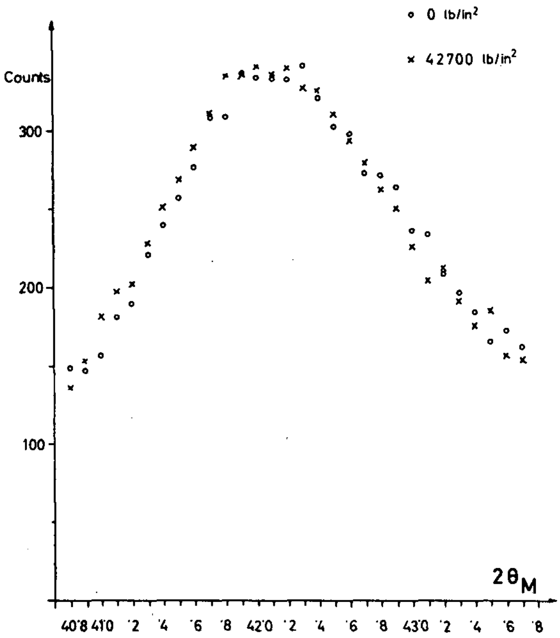

FIG.3. Phonon groups of the phonon C_2.

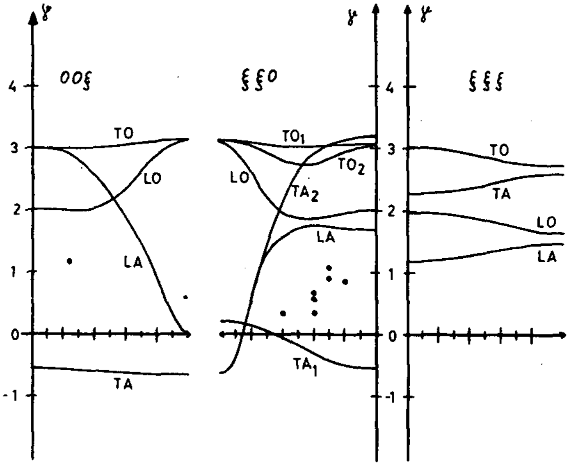

FIG.4. The complete model B Grüneisen parameters in NaI from Ref.[9]. The results of the present measurement are shown by points without error bars.

potential with two parameters D and s [2]. The numerical values of these two parameters are obtained, together with the other parameters, by fitting the model to the experimental dispersion curves at 90° K of Ref. [1].

Figure 4 shows the complete model B [3] Grüneisen parameters of sodium iodide [8] together with our results. The latter are shown here as points without error bars in order to give an indication of the scatter of Grüneisen parameters of phonons B and C as measured at different Q's.

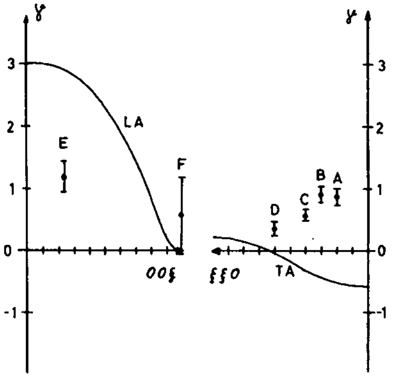

FIG 5. The results of the present measurement with their statistical errors. Only the corresponding Grüneisen parameter curves of Ref.[9], i.e. the LA (00ζ) and the TA (ζζ0), have been retained for comparison.

In Fig. 5 only those calculated Grüneisen parameter curves were retained to which our measurements refer: the LA branch of (00ζ) and the TA branch of (ζζ0). The results are shown here with error bars; in the case of phonons B and C only the best focused is shown. There is qualitative agreement with model predictions in the LA (00ζ) branch but a considerable discrepancy in the TA (ζζ0) branch: none of our measurements showed the negative Grüneisen parameters predicted by the model.

Negative Grüneisen parameters are generally expected in alkali halides and this expectation has been confirmed by acoustic measurements of the elastic constants for some of them [9], though not for NaI. E.R. and R.A. Cowley regard the observed drop of average Grüneisen parameters with temperature as an indication of the negative Grüneisen parameters of the low-frequency TA modes. Their Fig. 2, however, where the experimental temperature dependence of average Grüneisen parameters of both NaI and KBr is shown, suggests that this inference rests on weaker ground in NaI than in KBr. In any case, we are not in a position to give an explanation of the discrepancy between our results and the predictions of Refs [2] and [9].

ACKNOWLEDGEMENTS

The authors are grateful to Drs E.R. and R.A. Cowley for having made available to them their unpublished Grüneisen parameter calculations, to Prof. P. Weinzierl for his continual support of and interest in our work and to Dr. R. Lechner for his work during the early stages of this measurement series.

REFERENCES

[1] WOODS, A.D.B., COCHRAN, W., BROCKHOUSE, B.N., Phys. Rev. 119 (1960) 980.
[2] COWLEY, R.A., Adv. Phys. 12 (1963) 421.
[3] COWLEY, E.R., COWLEY, R.A., Proc. R. Soc. Ser. A 281 (1965) 259.
[4] LECHNER, R., Rev. scient. Instrum. 32 11 (1966) 1534.
[5] PECKHAM, G., Rep. AERE-R 4380 (1964).
[6] PECKHAM, G.E., SAUNDERSON, D.H., SHARP, R.J., Brit. J. appl. Phys. 18 (1967) 437.
[7] BRIDGMAN, P.W., The Physics of High Pressure, G. Bells and Sons, London, (1958).
[8] COWLEY, E.R., private communication.
[9] DANIELS, W.B., Lattice Dynamics, (WALLIS, Ed.) Pergamon Press (1965) 273.

PHONON-PHONON INTERACTIONS IN ZINC

G. CAGLIOTI AND G. RIZZI
COMITATO NAZIONALE PER L'ENERGIA NUCLEARE,
ISPRA, VARESE,
AND
G. CUBIOTTI*
ISTITUTO DI FISICA,
UNIVERSITÀ DI MESSINA,
ITALY

Abstract

PHONON-PHONON INTERACTIONS IN ZINC. Experimental results on the shape of phonon peaks in the neighbourhood of the point of accidental degeneracy of the longitudinal acoustic (LA) and transverse optic (TO//)$(0, \zeta, \bar{\zeta}, 0)$ branches polarized in the basal plane of zinc have been recently obtained with the purpose of investigating anharmonic contributions to the potential energy for the motions of the nuclei in this metal. The study has so far been limited to room temperature; particular care is being taken to get adequate instrumental resolution. At present it seems impossible to exclude a slight extra broadening of the phonon lines at ω and q values barely smaller than those corresponding to the point of degeneracy. Further work in this field is under way and will be soon extended to higher and possibly lower temperatures.

The problem of anharmonicity of interatomic forces in crystals has attracted the attention of an increasing number of physicists in view of both its challenging complexity and its intrinsic interest for an understanding at a microscopic level of several phenomena characterizing the macroscopic behaviour of real crystals [1-6].

Cubic and higher order terms in the expansion of the potential energy of the crystal in powers of the displacements of the atoms from their official positions are responsible for thermal expansion, heat conductivity of the lattice, and other important properties. At a microscopic level these terms represent phonon-phonon interactions and cause, in the field of neutron spectroscopy, broadening and frequency shift of the phonon lines [7]. Furthermore, it is conceivable that at a point of accidental degeneracy anharmonicity might produce a splitting of the frequency level, according to the non-crossing rule [5]. Evidence for a situation of this type was observed for the first time by Fermi [8] in the simple case of the molecule of carbon dioxide, whose Raman spectrum presents splittings due to the removal of the accidental degeneracy of the fundamental ν_1 and overtone $2\nu_2$ frequencies of these normal modes of vibration.

Among possible substances exhibiting accidental degeneracies of branches pertaining to different irreducible representations, we have considered zinc, a crystal having a reasonably simple structure and whose dynamical behaviour had previously been studied in our laboratory [9]. The reciprocal lattice plane $(\vec{b}_1, \vec{b}_2)$ of this crystal is presented in Fig. 1. To indicate the regions of interest for the present study, a sketch is also given in this figure of the behaviour of the structure factor as computed elsewhere [9]. Actually, along the symmetry direction

---

* Visiting scientist at the CNEN Laboratory, Ispra.

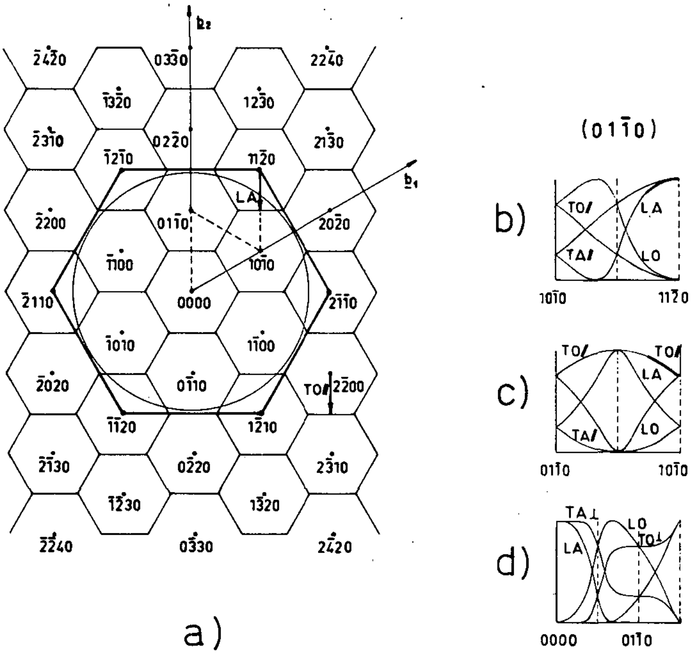

FIG.1. (a): the $(\vec{b}_1, \vec{b}_2)$ reciprocal lattice plane. The bold lines enclose the area in which the structure factor repeats. Within this area dashed lines, as far as the structure factor is concerned, are equivalent to the lines covered by the measurements, the latter being indicated by arrows. The elastic circle of radius k_0 is also indicated. (b), (c) and (d): the structure factor along the dashed lines of (a). The bold lines indicate those along which measurements were taken.

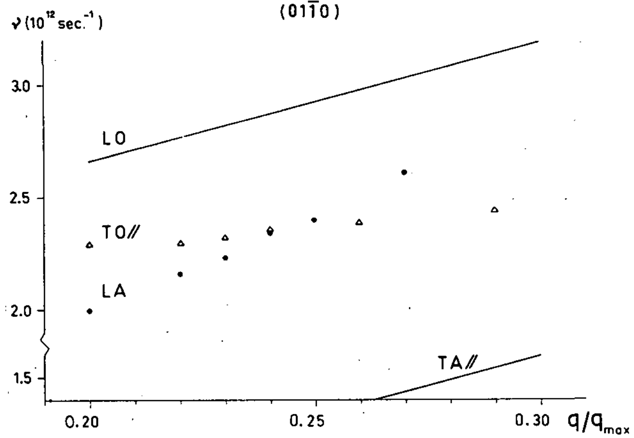

FIG.2. The dispersion relations for the $(0, \zeta, \bar{\zeta}, 0)$ LA and $(0, \zeta, \bar{\zeta}, 0)$ TO// modes in the region of accidental degeneracy. The experimental points for these two branches have been obtained in the course of the present study; segments of the LO and TA// branches in the same direction, as taken from Ref.[9], are also presented.

$(0, \zeta, \bar{\zeta}, 0)$ the LA (or Σ_1) and TO// (or Σ_4) modes tend to merge into each other in a region of wavevector transfer $q/q_{max} = 0.24$ and frequency transfer 2.37×10^{12} sec^{-1}. This region of the dispersion curves is presented in Fig. 2 where, beside the trend of other branches previously considered [9], new frequency versus wavevector data are reported for the modes under discussion.

Measurements are being taken by our three-axis spectrometer installed at the 5-MW Ispra-1 reactor utilizing the constant-Q method [10], with a fixed impinging neutron wavelength of 1.57Å. This wavelength has been selected as a compromise between the needs of reaching (by energy loss experiments) the interesting $(\omega, \vec{q})$ region ($\hbar\omega \sim 10$ meV, $\vec{q}$ around the reciprocal lattice (r.l.) points $(2\bar{2}00)$ and $(11\bar{2}0)$) and operating at high resolution [11-14]. To improve resolution, comparatively high take-off angles were used at the monochromator[1] (Ge(311)[2]) and the analysing crystal (^{220}Pb); furthermore, collimator divergences were selected as follows: in-pile 19', monochromator-to-sample 50', sample-to-analyser 35', analyser-to-counter 25'.

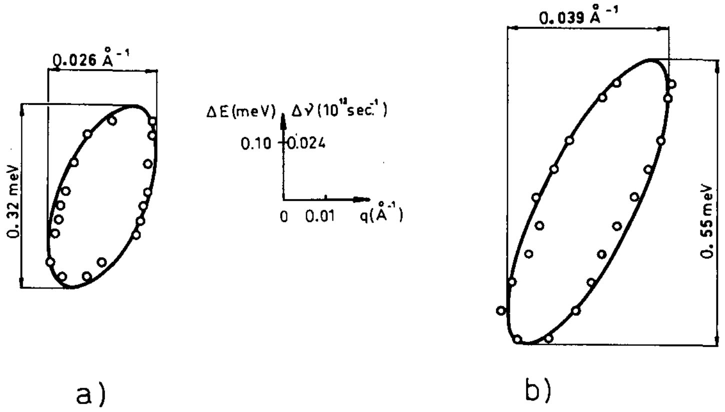

FIG.3. Resolution ellipsoids, as measured at reciprocal lattice points (a) $(11\bar{2}0)$ for LA phonons, and (b) $(02\bar{2}0)$ for TO// phonons.

The zinc sample is the same crystal utilized previously [9] (a 2-in. diam. sphere, having a mosaic spread of 6' full width at half maximum (fwhm)) kept at room temperature.

Under these conditions the resolution ellipsoids of the spectrometer, as measured at the r.l. points $(11\bar{2}0)$ and $(2\bar{2}00)$ are presented in Fig. 3. These r.l. points are very near to the end points of the wavevector $\vec{q}$ of the LA and TO// phonons under investigation. The reason for measuring these phonons in these particular regions of r.l. space comes from a consideration of the structure factor (see Fig. 1). Attempts to look at the $(0, \zeta, \bar{\zeta}, 0)$ LA branch around the most natural and previous choice [9], i.e. the r.l. point $(02\bar{2}0)$, were not so successful because of the spoiling contributions from the competing LO modes.

---

[1] The arrangement of our spectrometer does not offer the possibility of reaching Bragg angles higher than $2\theta_M = 55°$.

[2] To increase the mosaic spread of this crystal, the crystal itself was thermally treated under pressure at the Brookhaven National Laboratory, by courtesy of Doctors D.E. Cox and R. Nathans.

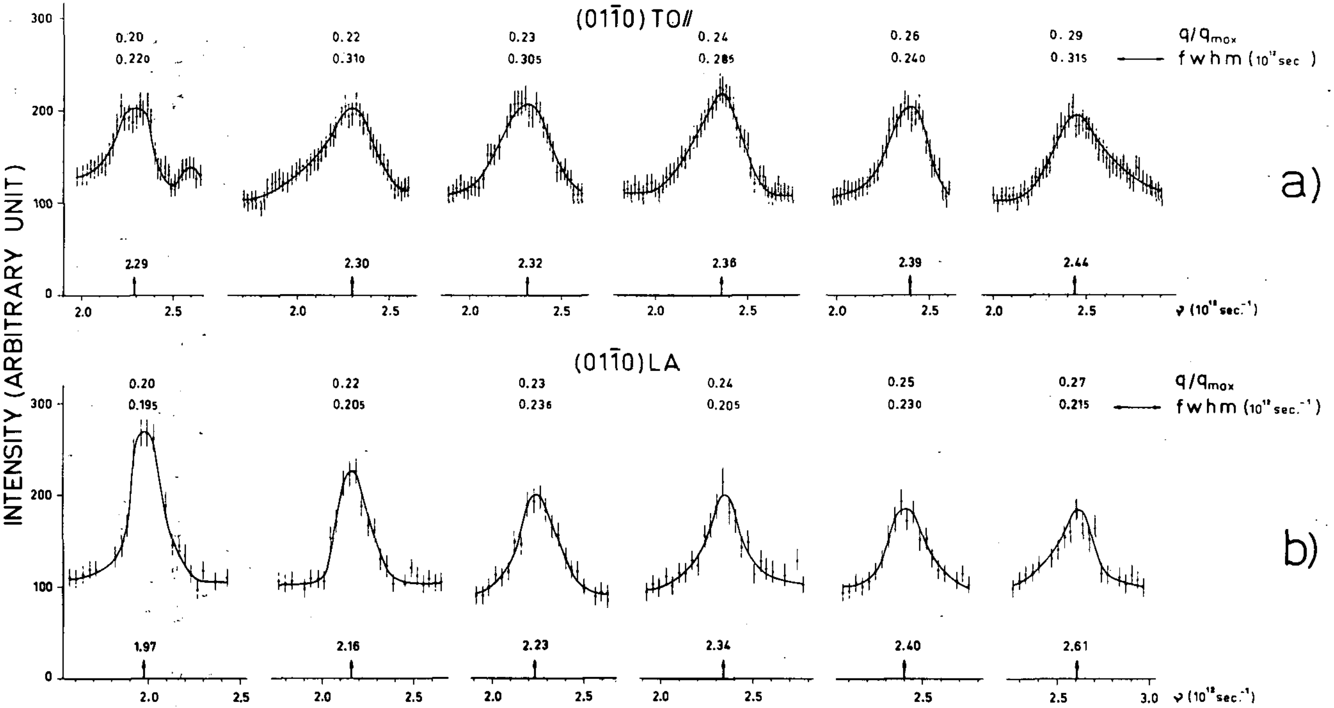

FIG. 4. Some phonon lines in the neighbourbood of the accidental degeneracy for (a) the TO// branch, and (b) the LA branch. The widths of the peaks are indicated.

A selection of the phonon lines so obtained in the neighbourhood of the accidental degeneracy, is presented in Fig. 4(a) for the TO// and in Fig. 4(b) for the LA branches. The widths of the phonon peaks are also indicated. It appears that at present it is not possible to exclude a slight extra broadening of the LA and TO// modes at values of wavevector transfers ($q/q_{max} \simeq 0.23$) barely smaller than that corresponding to the point of degeneracy ($q/q_{max} = 0.24$ (see Fig. 2)).

It seems then that anharmonic terms do not play a major role in the nature of these modes, polarized both parallel to the basal plane. In particular, the fact that, at least at room temperature, this degeneracy, within the limits of our instrumental resolution, does not appear to be strongly affected by anharmonicity could perhaps be attributed to the rather rigid structure of the basal plane in zinc, leading to its strong individuality within the crystal. We think it interesting to proceed with this study at other and especially higher temperatures, focussing our attention both on the region of the degeneracy and on other modes whose frequencies should be strongly affected by the anisotropic behaviour of this crystal.

ACKNOWLEDGEMENTS

It is a pleasure to acknowledge helpful discussions with Professor F. Bassani and Doctor S. Boffi. Messrs. F. Calza and G. De Giorgi gave valuable technical assistance.

REFERENCES

[1] NIKLASSON, G., SJÖLANDER, A., Annls Phys., to be published.
[2] MARADUDIN, A.A., FEIN, A.E., Phys. Rev. 128(1962) 2589.
[3] KOKKEDEE, J.J.J., Physica 28(1962) 374.
[4] KASHCHEEV, V.N., KRIVOGLAZ, M.A., Sov. Phys. Solid State 3(1961) 1107.
[5] KAGAN, Yu., ZHERNOV, A.P., Sov. Phys. JETP 21(1965) 646.
[6] COWLEY, R.A., in Phonons in Perfect Lattices and in Lattices with Point Imperfections (STEVENSON, R.W.H., Ed.), Oliver and Boyd, Edinburgh (1965) 170.
[7] BROCKHOUSE, B.N., ARASE, T., CAGLIOTI, G., SAKAMOTO, M., SINCLAIR, R.N., WOODS, A.D.B., Inelastic Scattering of Neutrons in Solids and Liquids (Proc. Symp. Vienna, 1960), IAEA, Vienna (1961) 531.
[8] FERMI, E., in Note e Memorie (Collected Papers) 1, Ed. Accademia Nazionale dei Lincei, Roma (1961) 472.
[9] BORGONOVI, G., CAGLIOTI, G., ANTAL, J.J., Phys. Rev. 132(1963) 683.
[10] BROCKHOUSE, B.N., Inelastic Scattering of Neutrons in Solids and Liquids (Proc. Symp. Vienna, 1960), IAEA, Vienna (1961) 113.
[11] PECKHAM, G.E., SAUNDERSON, D.H., SHARP, R.I., Brit. J. appl. Phys. 18(1967) 473.
[12] COOPER, M.J., NATHANS, R., Acta Cryst. 23(1967) 357.
[13] COLLINS, M.F., Brit. J. appl. Phys. 17(1966) 147.
[14] BJERRUM MØLLER, H., Investigation of Magnons in Rare Earth Metals by Inelastic Neutron Scattering, Internal Rep., Research Establishment, Risø.

DISCUSSION

R. A. COWLEY: I do not understand how anharmonic interactions can couple phonons belonging to different irreducible representations of the space group. Since the potential obeys the symmetry of the crystal it seems to me that modes belonging to different representations are not coupled by anharmonic effects.

G. CAGLIOTI: The situation we are facing here seems somewhat similar to that occurring in the Raman spectrum of carbon dioxide, where a cubic term in the potential energy expansion couples a bending and a stretching mode of this molecule. In that case the overtone bending frequency happens to be equal to the stretching frequency (Fermi resonance). In the present case it seems that crystal symmetry does not prevent coupling of the modes pertaining to the two $(01\bar{1}0)$ branches, at least if the anharmonic interaction term contains an even power of the transverse displacement. The experimental indications obtained so far encourage us to proceed further in this study. Meanwhile we shall, I am sure, all be very pleased if Mr. Kagan will say a few words on the theoretical aspects of the problem.

Yu.M. KAGAN (Chairman): In cases of accidental degeneration in the immediate vicinity of the intersection point, anharmonic interaction results in differing values of width, shift and temperature behaviour for the phonons of the two branches. Thus, for example, the phonon width may substantially increase in the case of one branch, and decrease in that of the other. This will occur over a narrow pulse range. An analysis of the problem is contained in the work by A.P. Zhernov and myself quoted as Ref. [5] of Mr. Caglioti's paper.

A.G. SJÖLANDER: In connection with what Mr. Kagan has just said, I would again refer to the detailed calculations of anharmonic effects in solid krypton by Mr. Högberg. In cases of accidental degeneration he obtains effects of polarization mixing and phonon line deformation.

NUCLEAR MAGNETIC RESONANCE IN LIQUIDS AND SOLIDS

J.G. POWLES
THE PHYSICS LABORATORIES, UNIVERSITY OF KENT,
CANTERBURY, ENGLAND

Abstract

NUCLEAR MAGNETIC RESONANCE IN LIQUIDS AND SOLIDS. The paper outlines the basic principles of nuclear magnetic resonance, trying wherever possible to compare and contrast the method with that of slow neutron scattering as a technique for studying the properties of condensed phases and especially of molecular and atomic motions. It is emphasized that this is not a review of nmr for an expert audience but has a pedagogical aim. It is hoped to give persons with a main interest in neutron scattering some appreciation of the scope and limitations of the nmr method. This is illustrated by recent results on one substance which covers many but by no means all of the important points.

1. INTRODUCTION

In the nuclear magnetic resonance technique the nucleus inside the material being studied is used as a probe which is sensitive in special ways to its surroundings. The nucleus, if it has a spin other than zero, may be regarded as a spinning bar magnet. By placing it in a static magnetic field it may be made sensitive, in first approximations, to static magnetic fields and to magnetic fields at the Larmor frequency (to be defined shortly) and of suitable polarization. The torque produced on the spinning bar magnet by the applied magnetic field causes it to reorient in a precessional motion about the direction of the applied field. The frequency of precession, the Larmor frequency, depends on the nucleus and on the circumstances, but is usually in the MHz range. The nucleus is then a sensitive radio receiver with a magnetic type antenna which is minute and is placed intimately within the material. It should be understood that even in a diamagnetic material there are substantial internal magnetic fields which may be in the range of milligauss to hundreds of gauss according to the material and that the nucleus may be sensitive to quite small magnetic fields. In ferromagnetic materials, and even in most paramagnetic materials, the internal magnetic fields are often too strong and the simple nuclear magnetic resonance behaviour is upset. The method is most powerful and useful therefore in diamagnetic materials. Metals may be studied, although there are technical difficulties.

It often happens that in a diamagnetic material the most important internal magnetic fields are due to the nuclei themselves either of the same or of a different type. If the nuclei, and therefore the atoms, are stationary, then this results in static local fields (except as discussed below). If the atoms or molecules containing the nuclei move, then the local fields vary with time. The static fields just mentioned are then usually reduced by averaging and at the same time one has the possibility of alternating magnetic fields associated with motion at or near the Larmor frequency to which the nucleus is sensitive. The behaviour of the nuclei is therefore an indirect indication of the motion of the atoms in which they are contained.

Nuclei with spin greater than one half have an electric quadrupole moment which may be regarded classically as due to a non-spherically symmetric distribution of the electric charge density. Such a charge distribution interacts with an electric field gradient. This can cause a reorientation of the nucleus and therefore of its magnetic dipole moment and so this electric interaction can be observed in nuclear magnetic resonance. If the interaction of the electric quadrupole moment with an electric field gradient is stronger than that of the magnetic dipole moment with the external magnetic field, or if the latter is absent, we may get electric quadrupole magnetic resonance. We shall usually be concerned here with the opposite situation where the magnetic interaction dominates. However, if the nucleus has $I > \frac{1}{2}$ then the electric interaction is almost always more important than the internal magnetic ones. We see therefore that nuclei may well be sensitive to electric fields within the material. This is of great interest since electric fields are more commonly encountered than magnetic ones inside materials. It often happens that the most important electric field gradient acting on a nucleus is that due to the electrons and nuclei in the molecule of which it forms a part. Apart from this, ions tend to produce important field gradients. If the molecules reorient or if other molecules or ions move, the field gradient experienced by a nucleus varies with time. Here also the nuclear orientation, and therefore the nuclear magnetic resonance effect, depends on the extent to which this time variation corresponds to the Larmor frequency of the nucleus.

It is clear then that the nucleus inside the material is subject to a variety of interactions which depend in various ways on itself and on its surroundings. One of the problems in magnetic resonance is to separate these interactions and to interpret the interactions in terms of the properties of the material in which the nucleus resides. Various techniques are available. One important technique for resolving the interactions for proton-containing materials is to change some or all of the protons to deuterons and in this respect it is in many ways similar to that used in neutron scattering.

The effective static magnetic field acting at a nucleus in a crystal in which no substantial motion takes place apart from thermal vibrations is sensitive, in suitable cases, to the structure of the crystal. The study of the magnetic resonance line shape is then to some extent analogous to the study of structure by neutron diffraction, in that distances between nuclei in crystals can often be determined or refined and in some cases information about structure can be obtained indirectly. The method is of particular interest for protons which are not readily accessible to neutron – or more so X-ray – analysis. The principal difference from conventional neutron or X-ray structural analysis is that magnetic resonance depends on essentially short-range interactions. It does not therefore give crystal structure information directly. In other words, it does not yield a structure factor S(Q).

The greater interest, however, lies in the determination of molecular and atomic motions and in some respects nmr gives similar information to that obtained from slow neutron scattering. It should be emphasized again, however, that the nuclear magnetic resonance method is not a scattering process and so the analysis of the results and the experiment itself is quite different. In particular the results do not yield the Van Hove space-time correlation function, $G(\vec{r}, \tau)$, or its Fourier transform $S(\vec{Q}, \omega)$ but rather a more complex correlation function, indeed various correlation functions depending on the different interactions, which cannot be expressed so simply and universally as $G(\vec{r}, \tau)$. One important difference as between slow neutron scattering and magnetic resonance is that in magnetic resonance the motion of the nuclei relative to the laboratory system is not in itself detectable. It is therefore not profitable to think in terms of the ability of the nucleus, or the system to which it is connected, to absorb or emit momentum and energy which leads directly to $S(\vec{Q}, \omega)$ in the slow neutron scattering experiment. A nuclear moment in a magnetic field is sensitive to direction and magnitude of an interaction and not to position as such. If the interaction with the given nucleus, 1, is the magnetic field due to another nucleus, 2, then the effect on the nucleus 1 due to 2 depends on the relative separation $\vec{r}_{12} = \vec{r}_1 - \vec{r}_2$ of the two nuclei and not on $\vec{r}_1$ or $\vec{r}_2$ and their variation with time as such. The observations depend on the correlation function of various functions of $\vec{r}_{12}$ which we shall call $f(\tau)$ and its Fourier transform $J(\omega)$. This is a more complex matter than the correlation function of $\vec{r}_1$ which arises in $G_s(\vec{r}, \tau)$. The distinct correlation function $G_d(\vec{r}, \tau)$ is more closely related but is 'less relative' than the magnetic resonance correlation functions. Thus the magnetic interaction of two nuclei depends on the probability $P(\vec{r}, \tau | \vec{r}_0)$ that their separation $\vec{r}_{12}$, has an initial value $\vec{r}_0$ and a value $\vec{r}$ at time τ later where $\vec{r}$ is always for the <u>same</u> pair of nuclei. This is in contrast with $G(\vec{r}, \tau)$ which is the probability that if there was an atom at $\vec{r}\,'$ at time 0, then there will be <u>any</u> atom at $\vec{r}\,' + \vec{r}$ at time τ later and which is given more formally by the expression

$$G(\vec{r}, \tau) = \frac{1}{N} \Big\langle \sum_{i,j} \delta[\vec{r} + \vec{r}_i(0) - \vec{r}_j(\tau)] \Big\rangle$$

Our correlation function is related to $G_s(\vec{r}, \tau)$ in the sense that we must consider motion of the same two nuclei but is related to $G_d(\vec{r}, \tau)$ in the sense that only the distance between two different nuclei is important. We may write the nmr correlation function in the form

$$P(\vec{r}, \tau | \vec{r}_0) = \frac{1}{N^2} \Big\langle \sum_{i \neq j} \delta[r_0 + r_i(0) - r_j(0)]\, \delta[\vec{r} + \vec{r}_i(\tau) - r_j(\tau)] \Big\rangle$$

It is clear that $P(\vec{r}, \tau | \vec{r}_0)$ cannot be expressed simply in terms of $G(\vec{r}, \tau)$. The more complex nature of P can be seen by considering the $\tau \to \infty$ limit when we find that

$$P \to V^{-2}\, g(r)\, g(r_0) \text{ whereas } G \to N/V$$

It is actually necessary to find the power spectrum typically of the quantity $r^{-3} Y_2^m(\theta, \phi)$ using $P(\vec{r}, \tau | \vec{r}_0)$. For a liquid a diffusion model is often used as an approximation for $G_s(\vec{r}, \tau)$ and could be used to estimate $G_d(\vec{r}, \tau)$ as for instance in Vineyard's approximation. A first approximation for $P(\vec{r}_1, \tau | \vec{r}_0)$ can be obtained by assuming that both the nuclei move independently according to the diffusion equation so that the diffusional motion of $\vec{r}_{12}$ can be found. We then have

$$P(r,\tau\,|\,r_0) = (8\,\pi D\tau)^{-3/2}\exp - |\vec{r} - \vec{r}_0|^2/8D\tau$$

with some ad hoc corrections to allow for $g(r)$ and $g(r_0)$. However, the actual interaction is relatively short range, e.g. it goes as r^{-3}, and so is important where the diffusion equation is least well obeyed. Nevertheless, the nmr interactions in liquids modulated by relative translational motion are quite well interpreted in terms of the self-diffusion constant, for example, we often find $T_1 \propto D$. Much more sophisticated analysis, including various types of 'jumps', has been applied for translation in crystals [1].

On the other hand, the magnetic resonance parameters may depend on orientation of the molecule in which the nucleus resides in a very direct manner. The magnetic interaction inside a molecule is sensitive only to reorientation and not to translation at all so that the reorientational correlation function is in principle directly accessible, and its variation with time. It would seem that in this respect magnetic resonance has some advantage over neutron scattering since in the latter case one cannot distinguish at all readily between the motion of a nucleus which is due either to a translational or to a reorientational motion if both occur together. Moreover, for reorientational motion alone the neutron scattering is, in principle, sensitive to the correlation functions of all orders Y_n^m(e.g. Sears 1966) whereas nmr is sensitive only to $Y_2^m(\theta,\varphi)$.

There is one interaction, the spin-rotation interaction, in magnetic resonance which depends on the molecular angular velocity. No analogous effect exists in slow neutron scattering, or indeed elsewhere, as far as I am aware.

It should be particularly noted that the magnetic resonance effect is sensitive in general to short-range interactions and to rather slow and large motions. It is virtually insensitive for instance to lattice vibrations since most of these are at frequencies very much above the MHz range and in any case only give rise to very small changes in the interactions. In other words, magnetic resonance tends to be insensitive to what are usually referred to as high-frequency co-operative modes of motion. The essentially short-range nature of the interactions is evident, for instance, from the fact that nothing drastic happens to the nmr parameters near the liquid-vapour critical point. The slower larger-scale motions to which magnetic resonance is sensitive tend to direct our attention to basically diffusive motions as already discussed, and to seek analogies to $G_s(\vec{r},\tau)$ in neutron scattering in spite of the fact that distinct interactions and therefore the distinct correlation function $G_d(r,\tau)$ would appear to be more relevant.

It is interesting to notice that, just as in neutron scattering, one is not able to obtain $G(\vec{r},\tau)$ because $S(\vec{Q},\omega)$ is known for only a small range of $\vec{Q}$ and ω, similarly in magnetic resonance we cannot really find $f(\tau)$ because we only know $J(\omega)$ for a very limited range of ω. However, perhaps this is just one more example of the almost universal experience of Statistical Physics that the information desired is the Fourier transform of the experimental result.

A great advantage of the magnetic resonance method is that the nuclear spin system is only very loosely coupled to the other degrees of freedom of the complex system in which it resides and its thermal capacity is extremely small. It is therefore possible to cause the nuclear spin system itself to depart severely from thermal equilibrium while leaving the rest of the material essentially in thermal equilibrium. In this way, therefore, the nuclear spin system is sensitive to the thermal fluctuations of the rest of the material in equilibrium. It seems fair to claim that the orientation of the nucleus is the most innocuous probe that can possibly be used. The energy of a nuclear moment is of order 10^{-3} meV and the local 'hotspot' due to a nucleus being wrongly oriented is extremely innocuous – certainly it has less effect than the energy change, of order meV produced by scattering of a thermal neutron. Consequently, the correlation functions in magnetic resonance have always been taken to be real quantities and the power spectra symmetrical in frequency and the disturbance of the system other than the nuclear spin has been ignored.

2. THE EXPERIMENT AND ITS ANALYSIS

Nuclei of magnetic moment $\vec{\mu}$ and spin $\hbar\vec{I}$ are placed in a steady magnetic field $\vec{B}$ and experience a torque $\vec{\mu} \times \vec{B}$ which causes them to precess at an angular frequency ω_L about the direction of $\vec{B}$ given by

$$\omega_L = \gamma H_0 \qquad (1)$$

where it is conventional that $\vec{B}$ is in the z-direction and has a magnitude H_0 and $\gamma = \mu/\hbar I$.

Quantum mechanically the nucleus can only have (2I + 1) discrete values of angular momentum in the field direction. Transitions between any two adjacent levels of the resulting equally spaced energy level system correspond to an energy change of $\hbar\omega_L$ where ω_L is given by Eq. (1).

If the nuclei are in thermodynamic equilibrium with the material at temperature T in a field H_0, a nuclear paramagnetic moment M_0 is produced in the direction of H_0 given by the Curie formula

$$M_0/H_0 = n\mu^2/3kT \qquad (2)$$

which corresponds to a Boltzmann distribution over the levels and where n is the number of nuclei per unit volume. If the equilibrium distribution is disturbed and the populations changed, the magnetization in the z-direction, M_z, is different from M_0, say M_{zi}. If then left alone, M_z reverts to M_0 and usually does so exponentially with time, i.e. (Fig. 1)

$$M_z(t) = M_0 - (M_0 - M_{zi}) \exp - t/T_1 \qquad (3)$$

This serves to define the spin-lattice relaxation time, T_1, and is so called because the process involves exchange of magnetic orientation energy with thermal energy of other degrees of freedom (known conventionally as a lattice even for a liquid or gas). The process may be represented as in Fig. 2(a).

If the probability of this happening is p, then it is easy to see that

$$1/T_1 \approx 2p \qquad (4)$$

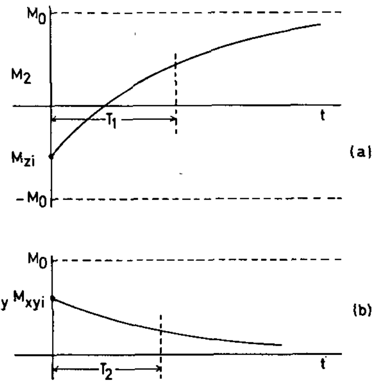

FIG.1. The relaxation of (a) the longitudinal and (b) the transverse nuclear magnetization.

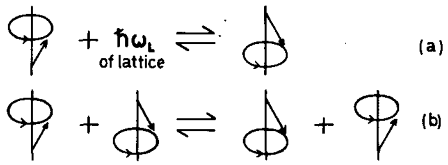

FIG.2. (a) Diagrammatic illustration of the interrelation between a spin and the 'lattice' which corresponds to the longitudinal relaxation and T_1. (b) The spin exchange process which gives one of the contributions to T_2.

All the interactions with the nucleus may contribute to p and so we must always add all contributions to $1/T_1$, e.g. we shall find it convenient to write

$$1/T_1 = 1/T_{1\,\text{inter d}} + 1/T_{1\,\text{intra d}} + 1/T_{1Q} + 1/T_{1\text{sr}} + \dots \tag{5}$$

where the various contributions to relaxation due to various interactions are defined below. In principle, the measurement of T_1 need not involve a magnetic resonance experiment at all but it is very convenient to do it this way. We can evidently disturb the system from equilibrium by applying radiation from outside with quanta of size $\hbar\omega_L$ and with suitable polarization. If we supply a strong pulse of such radiation, we might well expect to be able to reduce M_0 to zero. We can, in fact, produce a transverse magnetization M_{xy} which is proportional to M_z at the moment before the pulse and so measure $M_z(t)$ as it recovers from M_{zi} (which is usually zero) to M_0 and so determine the curve of Fig. 1(a) and hence T_1.

The outline of the experimental arrangement is shown in Fig. 3 but it should be clear that very considerable sophistication is required in practice. The disturbance from equilibrium is provoked by pulses from the gated transmitter at ω_L applied to the same or another orthogonal coil. The received signal is due to the precession of the transverse magnetization M_{xy} which induces an emf in the coil.

In equilibrium the transverse magnetization M_{xy} is zero, corresponding classically to incoherence in the phases of the precessing nuclei, or in quantum mechanics to the equilibrium density matrix being diagonal. The

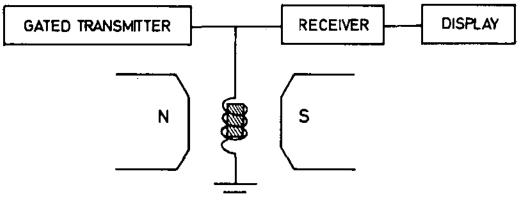

FIG.3. Idealized experimental arrangement showing the sample in a magnetic field and enclosed by a radio-frequency coil. R.F. energy at or near ω_L is applied to the specimen and the response is observed on a receiver.

transverse magnetization is destroyed both by processes as in Fig. 2(a) which involve the lattice, and by ones which do not, as indicated in Fig. 2(b), since both interrupt the phase of precession of the nucleus or limit the life-time of an orientational state.

We can see from Eq. (1) that if there are local fields, H_0 is replaced by $(H_0 + H_{loc})$ and H_{loc} varies for different nuclei and so therefore does ω_L. For the ensemble of nuclei any total transverse magnetization is lost by dephasing, or by a distribution of energy level spacings, and so this process also contributes to T_2 in addition to those in Fig. 2.

In first approximation the transverse magnetization decays exponentially to zero if left to itself (Fig. 1(b)) and so we describe the decay by a time T_2. T_2 is clearly quite different from T_1 but it so happens that $T_2 \leq T_1$. It may be more convenient to measure the line shape in steady state resonance rather than the decay of M_{xy}. In that case the line width is given by

$$\delta H = \gamma^{-1}\delta\omega \approx \gamma^{-1}T_2^{-1} \tag{6}$$

More precisely the absorption line is the Fourier transform of the decay curve of M_{xy}.

Now consider an explicit interaction of two nuclei, direct dipolar interaction. The classical form of the interaction is

$$\mathscr{H}_d = \frac{\vec{\mu}_1 \cdot \vec{\mu}_2}{r_{12}^3} - \frac{3(\vec{\mu}_1 \cdot \vec{r}_{12})(\vec{\mu}_2 \cdot \vec{r}_{12})}{r_{12}^5} \tag{7}$$

where $\vec{r}_{12}$ is in general time dependent. Only the local magnetic field at 1 due to 2 in the z-direction is important in view of the much larger applied field H_0 and this is given in Eq. (8) (see also Fig. 4):

$$H_{local} = \pm \frac{\mu}{r_{12}^3}(3\cos^2\theta_{12} - 1) \tag{8}$$

(note the appearance of the function $r^{-3}Y_2^0$ mentioned in section 1).
The spread in frequencies from Eq. (1) is $\Delta\omega_L = \gamma H_{loc}$ and clearly $T_2 \sim 1/\Delta\omega_L$. The additional dephasing due to the process of Fig. 2(b) increases the effective H_{loc} by the factor 3/2 and so decreases T_2 by the factor 2/3. This is the simplest example of possible structure determination by nmr.[1] The distance between the resonance lines is $2H_{loc}$ and so $\vec{r}_{12}$ may be determined. Clearly if $\vec{r}_{12}$ and θ_{12} are time dependent, the average of H_{loc}

---

[1] e.g. hydrated crystals [2].

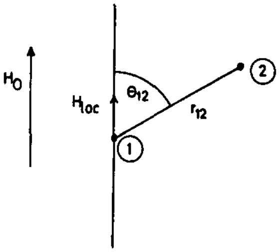

FIG.4. The effective local magnetic field at a nucleus (1) due to another nucleus (2).

tends to fall. However, it is a more subtle matter as to what time one should average over – it is actually the time T_2 itself.

If we regard the interaction, and now we speak quite generally, as a stochastic time dependent process, $\mathscr{H}_{\text{int}}(t)$, then we can evaluate the correlation function

$$\Phi(\tau) = \langle \mathscr{H}_{\text{int}}(t) \mathscr{H}_{\text{int}}(t+\tau) \rangle \tag{9}$$

where $\langle \ldots \rangle$ means a statistical average (and a quantum mechanical average if necessary). It will be convenient to write

$$\Phi(\tau) = \langle |\mathscr{H}_{\text{int}}(t)|^2 \rangle \phi(\tau) \tag{10}$$

The power spectrum $J(\omega)$ corresponding to $\phi(\tau)$ is given by the Wiener-Khintchine relation

$$J(\omega) = \int_{-\infty}^{\infty} \phi(\tau) \exp i\omega\tau \, d\tau \tag{11}$$

It is then clear that the effective static field contribution (Fig. 4 and Eq. (8)) and the uncertainty contribution (Fig. 2(b)) to T_2 depend on $J(0)$. The spin lattice contribution (Fig. 2(a)) depends on $J(\omega_L)$ – more generally on $J(2\omega_L)$ as well (see Eq. (14)). The contribution to T_1 also depends on $J(\omega_L)$ and possibly $J(2\omega_L)$, but in a different way. This time it is the probability of finding photons at a suitable frequency to cause the spin orientation transities of Fig. 2(a) and how these transitions affect M_z rather than M_{xy}.

It may be assumed for the sake of illustration that

$$\phi(\tau) = \exp - |\tau| / \tau_c \tag{12}$$

and then

$$J(\omega) = 2\tau_c / (1 + \omega^2 \tau_c^2) \tag{13}$$

Generally speaking, thermal motions get faster with increasing temperature and so τ_c falls with increasing temperature. It is clear that as τ_c falls $J(\omega_L)$ passes through a maximum at $\omega_L \tau_c = 1$ and that $J(0) = 2\tau_c$ falls steadily. Hence, T_1 which, apart from the slowly varying factor $\langle |\mathscr{H}_{\text{int}}(t)|^2 \rangle$, depends on $J(\omega_L)$, passes through a minimum whereas T_2 rises steadily with increasing temperature. T_1 depends on ω_L but, as a more refined analysis shows, T_2 does not (see Fig. 5).

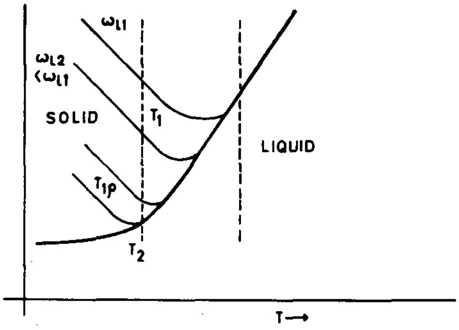

FIG. 5. The behaviour of the relaxation times T_1, T_2 and $T_{1\rho}$ as a function of the temperature of the material.

More explicitly, we can show that for the dipolar interaction between like spins (Eq. (7)) we get

$$1/T_1 = \frac{3}{2}\gamma^4\hbar^2 I(I+1)\sum_k{}' \left\{ J_{ik}{}^{(1)} \quad (\omega_I) + J_{ik}{}^{(2)} \quad (2\omega_I) \right\}$$

and (14)

$$1/T_2 = \gamma^4\hbar^2 I(I+1)\sum_k{}' \left\{ \frac{3}{8} J_{ik}{}^{(0)} \ (0) + \frac{15}{4} J_{ik}{}^{(1)} \ (\omega_I) + \frac{3}{8} J_{ik}{}^{(2)} \ (2\omega I) \right\}$$

where $J^{(0)}(\omega)$, $J^{(1)}(\omega)$ and $J^{(2)}(\omega)$ are the power spectra for the functions

$$F^{(0)} = r^{-3}(3\cos^2\theta - 1)$$

$$F^{(1)} = r^{-3}(\sin\theta\cos\theta e^{-i\phi})$$

and

$$F^{(2)} = r^{-3}\sin^2\theta e^{-2i\phi}$$

respectively, i.e. $r^{-3}Y_2^m(\Lambda)$. Equation (14) embodies a number of assumptions which we do not discuss here. The general behaviour corresponding to Eqs (14) is shown in Fig. 5.

Generally speaking, in liquids $\tau_c \sim 10^{-11}$ to 10^{-12} sec and since $\omega_L \sim 10^8$ sec^{-1} we have $\omega_L\tau_c \sim 10^{-3}$. In that case $J(\omega_L) \approx J(0)$ and $T_1 \approx T_2 \propto \tau_c^{-1}$. It may be noted that $J(0) = \int \phi(\tau)d\tau$ so that for a liquid we only get the integral of a correlation function and so T_1 is almost a macroscopic quantity (cf. $D = \frac{1}{3}\bar{v}^2 \int \phi_v(\tau)d\tau$).

Generally speaking, in solids $\tau_c > 10^{-4}$sec so that $\omega_L\tau_c > 10^4$ and so $T_1 >> T_2$, $T_1 \propto \tau_c$ and T_2 is independent of τ_c.

However, it may happen that minima are observed in solids and it may even happen in a solid that $\omega_L\tau_c \ll 1$ for some interactions (e.g. Fig. 6).

We must also mention another interesting experiment which effectively extends the Larmor frequency ω_L from the MHz region to the kHz region and even lower, without loss of sensitivity. It is of particular interest for solids since the most profitable region to be in is clearly near a minimum of T_1. If we produce a transverse magnetization, M_{xy}, say by a pulse, we can preserve it by placing parallel to it and rotating with it, at ω_L, a magnetic field which we call $\vec{H}_1$. If $H_1 >> H_{loc}$, the nuclei need an energy of order γH_1 to reorient and the dephasing due to H_{loc} is dominated by H_1 and so contributions to T_2 are almost suppressed. The decay of M_{xy} then becomes a 'T_1 process' but the energy involved is $\hbar\gamma H_1$ or $\hbar\omega_1$ instead of $\hbar\omega_L$. Hence M_{xy} now behaves like M_z except for replacement of ω_L by ω_1, so that

$$1/T_{1\rho} \sim J^{(\rho)}(\omega_1) \tag{15}$$

where $T_{1\rho}$ is the decay time of M_{xy} in precence of H_1 and $J^{(\rho)}(\omega)$ is a power spectrum similar to $J^{(1)}(\omega)$ and $J^{(2)}(\omega)$. Since $H_1 \ll H_0$, $\omega_1 \ll \omega_L$ and so we have effectively a low resonance frequency experiment. Thus may we get a $T_{1\rho}$ minimum in the solid even for relatively slow processes. By a further elaboration of the experiment, it is in some circumstances possible to measure a relaxation time T which is effectively equal to τ_c and so is a very direct measure of molecular motion [3].

3. AN ILLUSTRATIVE EXAMPLE

We can illustrate most of the points already made by reference to one substance which has recently been studied in great detail, namely hydrogen bromide and the mixture HBr/DBr.[2] Diagrammatic experimental results are given in Fig. 6 for the liquid up to the critical point under its own vapour pressure and for the three solid phases I, II and III for (i) the deuteron spin-lattice relaxation time, T_{1D}; (ii) the proton spin-lattice relaxation time, T_{1p}, in pure HBr at 21.5 and 9.0 MHz and also in 50% HBr/DBr at 21.5 MHz; (iii) the rotating frame spin-lattice relaxation time, $T_{1\rho}$, in HBr for H_1 = 14.5 and 5.3 G; (iv) T_2 for protons in HBr and in 50% HBr/DBr. It should be noted that Fig. 6 is a simplified and diagrammatic representation of the results and should not be used as data.

The deuteron spin-lattice relaxation time, T_{1D}, (N. B. the deuteron spin is $I_D = 1$) is controlled by the strongest relaxing mechanism, the quadrupole interaction inside the DBr molecule.

It is believed that the molecule reorients very rapidly both in the liquid and in the upper solid phase (I) so that $\omega_L\tau_c \ll 1$ and

$$1/T_{1D} = \frac{3}{8}\left(\frac{e^2qQ}{\hbar}\right)^2\tau_D \tag{16}$$

It is expected that $e^2qQh^{-1} \sim 250$ kHz and so τ_D is obtainable from T_{1D} and the values are in the order 10^{-13} sec as shown in Fig. 7. Figure 7 is diagrammatic and should not be used as data. In the lower temperature solid phases the reorientation is slower and asymmetrical and T_{1D} will not be discussed. The bromine spin-lattice times $T_{1Br^{79}}$ or $T_{1Br^{81}}$ are very short, since e^2qQh^{-1} is much bigger, and are estimated to be a few μsec.

---

[2] A detailed account of the results quoted will be found in Refs [4, 5].

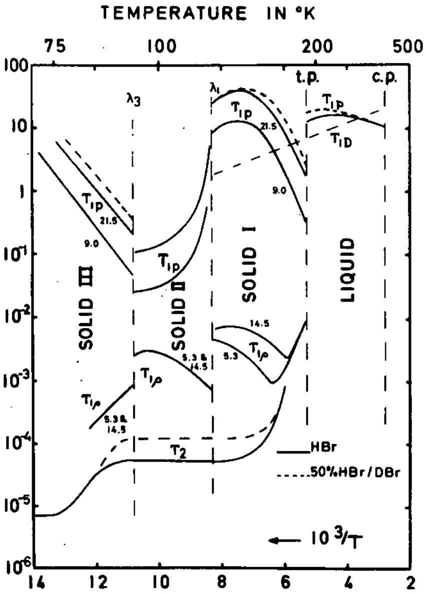

FIG. 6. Diagrammatic representation of nmr results on liquid and solid hydrogen bromide and deuterium bromide.

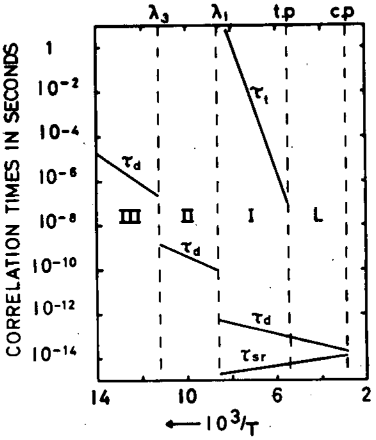

FIG. 7. Diagrammatic representation of the various correlation times as deduced from nmr for liquid and solid hydrogen bromide.

The proton spin-lattice relaxation time for the liquid behaves quite differently. This is because the mechanism controlling T_{1p} at lower temperatures is the proton intermolecular dipolar interaction – the quadrupole interaction is not present because $I = \frac{1}{2}$ for protons. This is shown by the increase in T_{1p} with deuteration since the deuteron dipole moment is much smaller than that of the proton and so $\langle |\mathscr{H}_{int}(t)|^2 \rangle$ gets smaller but τ_c remains much the same. However, at higher temperatures T_{1p} falls with increasing temperature and is independent of deuteration.

It is in fact then controlled by the spin-rotation interaction and yields a correlation time τ_{sr} for the molecular angular velocity. τ_{sr} turns out to be of the order of 10^{-14} sec or less and increases with increasing temperature while being less than τ_D. The situation in the liquid is complex. It should, in principle, be possible to separate the translational and reorientational molecular motion. It is expected that it will be found that for the translational contribution $T_{1\,\text{inter d}} \propto D$ where D is the self-diffusion constant. It is expected that the translational and reorientational molecular motions are very rapid and similar.

On solidification the T_{1p} value changes abruptly in contrast with T_{1D}. This is thought to be because the reorientational molecular motion is now much faster than the translational. For the interactions modulated by reorientational motion $\omega_L \tau_c \ll 1$ and the contribution to $1/T_1$ is small. But for the interaction modulated by the translational motions $\omega_L \tau_c > 1$ and the contribution to $1/T_1$ is reasonably short and we expect from Eq. (14) and Fig. 5 that

$$T_1 \propto \omega_L^2 \tau_t \qquad (17)$$

where we write τ_t instead of τ_c to emphasize that this is a translational motion. Also the main intermolecular interaction is between protons in different molecules and this is changed by deuteration. All these effects are observed, as seen in Fig. 6. The deduced values of τ_t are shown in Fig. 7.

If the interpretation of T_1 and these values of τ_t in phase I are correct, then the rotating frame relaxation time, $T_{1\rho}$ should show a minimum. This is indeed so, as shown in Fig. 6 and the deduced values of τ_t from $T_{1\rho}$ agree very well with those from T_1. Incidently, so do the values from the variation in T_2. As the temperature is lowered, τ_t increases and so does T_1 for this interaction so that eventually other contributions to T_1 take over (see Eq. (5)). We shall not discuss here the rather complex behaviour of T_1 (and of $T_{1\rho}$) in the lower temperature region of phase I.

We see that in phase II the behaviour of T_1 and $T_{1\rho}$ is not straightforward in that they do not obviously fit to any part of Fig. 5. The reason for this is that the proton relaxation is due to interaction with bromine nuclei whose relaxation is in turn controlled by quadrupole interaction and so the protons are connected indirectly to the lattice. In fact, $T_{1p} \propto \omega_L{}^2 T_{1Br}$ and $T_{1\rho} \propto 1/T_{1Br}$. T_{1Br} has a minimum at λ_3 so that T_{1p} have minima depending on ω_L whereas $T_{1\rho}$ has a maximum independent of ω_1. This rather involved argument, however, leads in the end to a correlation time for molecular reorientation which is in good agreement with that from dielectric absorption, which also reflects molecular reorientation. Furthermore, the reorientation is clearly not spherically symmetric, as may be expected because of the non-cubic structure in this phase. Translational motion must be very slow in this phase.

In the lowest temperature phase (III) the behaviour again becomes relatively simple and is surely asymmetric reorientation with no translation. The frequency dependence of T_{1p} suggests that $\omega_L \tau_c \gg 1$ and we are once more in the top-left region in Fig. 5, except that this time the interaction is modulated by reorientational rather than translational motion and it is this time not between protons but between protons and bromine nuclei. There is the additional complication that in this phase the bromine nucleus orientation is controlled by its strong molecular electric quadrupolar interaction. For $T_{1\rho}$, $\omega_1\tau_c \ll 1$ (since $\omega_1 \ll \omega_L$) and so we are on the right in Fig. 5 and $T_{1\rho}$ rises with temperature and its independent of ω_1. The deuteration independence of T_2 in phase III confirms that the protons' principle interaction is with bromine nuclei. The corresponding correlation times are shown in Fig. 7.

The line width (or T_2) is in good agreement with these conclusions but is not discussed here in detail.

4. CONCLUSION

It is hoped that this brief exposé of the nmr method and the illustrative example will give some feeling for the way in which it provides information about materials. We do not have time or space for a more thorough review of the application of the method to a wide variety of materials and the interested reader is directed to the Bibliography. It is clear nevertheless that the nmr method is supplementary and complementary to slow neutron scattering.

REFERENCES

[1] TORREY, H. C., Phys. Rev. 92 (1953) 962.

[2] PEDERSEN, B. F., HOLCOMB, D. F., J. chem. Phys. 38 (1963) 61.

[3] AILION, D., SLICHTER, C. P., Phys. Rev. Lett. 12 (1964) 168.

[4] NORRIS, M. O., STRANGE, J. H., POWLES, J. G., RHODES, M., MARSDEN, K., KRYNICKI, K., J. Phys. C. 1 (1968) 422.

[5] POWLES, J. G., KRYNICKI, K., to be published.

BIBLIOGRAPHY

Possibly the best introduction to nmr is: PAKE, G. E., in Solid State Physics 2, Academic Press (1956) 1-84.
A widely used introductory text is: ANDREW, E. R., Nuclear Magnetic Resonance, Cambridge University Press (1955).

Both of these are rather out of date but are still valuable.

The bible in the field is: ABRAGAM, A., Principles of Nuclear Magnetism, Oxford (1961).
The next most authoritative text is: SLICHTER, C. P., Principles of Magnetic Resonance, Harper and Row (1963).
For applications to metals see: KNIGHT, W. D., in Solid State Physics 2, Academic Press (1956) 93-137.
For a review of liquids see: POWLES, J. G., Ber. d. Bunsengesel, 67 (1963) 328; or Report of the XIV^e Colloque Ampère (1968).
For a review of solids see: ANDREW, E. R., ALLEN, P. S., J. Chim. phys. 1 (1966) 85.
For a review of polymers see: POWLES, J. G., Polymer 1 (1960) 219.

DISCUSSION

K.-E. LARSSON: In the interpretation of nuclear magnetic resonance experiments it is generally assumed that the angular self-correlation function decays exponentially with time, thus leading to a frequency distribution of simple Lorentzian type $\approx \tau_c/(1+\omega^2\tau_c^2)$. In general the frequency used in the investigation is of the order of megacycles, which makes $\omega\tau_c \ll 1$, unless the samples are investigated in a state of very high viscosity or low temperature.

I have two questions for Mr. Powles:
(1) If you lower the temperature of a sample to such an extent that you get into a region of slow molecular motions (resulting in $\omega\tau_c \approx 1$), you may be faced with an entirely different microscopic time and space structure from that obtaining at higher temperatures. Do you make any attempt in nmr experiments to draw inferences regarding the molecular motions at higher temperatures (where $\omega\tau_c \ll 1$) from the situation at lower temperatures (where $\omega\tau_c \approx 1$)? If so, what can you say about the reliability of the conclusions?

(2) If you measure at high temperatures, so that $\omega\tau_c \ll 1$, your relaxation time is simply inversely proportional to τ_c. Could there be any other possible shape of $f(\omega)$ which would also give $1/\tau_1 \sim \tau_c$? It should be noted that all neutron experiments without exception have shown that the assumption of an exponentially decaying self-correlation function (both for centre-of-gravity velocity and for angular velocity) is incorrect or, at best, only tells part of the story.

J.G. POWLES: It is true that for viscous liquids one may have $\omega\tau_c \sim 1$ and that then the nmr results are more directly sensitive to the form of the correlation function. This was found to be the case for instance, with glycerol (Hunt and Powles, Proc. phys. Soc. 88 (1966) 513). Moreover, it is also clear that as the temperature changes both the time scale and the form of the correlation function change, and the latter usually becomes more closely exponential, except of course for very short times. For low viscosity liquids we certainly have $\omega\tau_c \ll 1$ and $T_1 \propto \tau_c^{-1}$, where the factor of proportionality is a slowly varying function of temperature. Since τ_c is usually defined as $\int_0^\infty \phi(\tau)d\tau$, then we have $T_1 \propto \tau_c^{-1}$ for any $J(\omega)$ by definition! It is more sensible to say that $T_1^{-1} \propto J(0)$ and of course $J(0)$ depends on the form of $\phi(\tau)$. In general, therefore, nmr in low viscosity liquids is not very sensitive to the form of $\phi(\tau)$ for short times but rather to the overall behaviour, whereas neutron inelastic scattering appears to be very sensitive to the short-time behaviour. Attention to these two facts removes most of the apparent inconsistencies in the information given by the two methods of investigation.

E.E. SÁNDOR: There are two comments I should like to make on Mr. Powles' paper:

(1) Since in nmr the motion of the nuclei relative to the laboratory system is not in itself detectable, nor is the effect sensitive to lattice vibrations, nmr data can hardly be expected to be directly comparable with elastic or inelastic neutron scattering data in the majority of cases. On the other hand, nmr seems potentially a very powerful technique in studying relatively slow large-angle reorientations of molecules, such as accompany phase transitions in a number of molecular solids. However, nmr data should be used with great caution even in this field for the following reasons:

(a) The effect one observes in nmr is connected with the relative separation of the nuclei and with the reduction of this separation in time. Furthermore the nuclei studied in nmr are more often than not protons, whose motion is not always characteristic of the motion of the whole molecule to which the parent H-atom of the proton belongs. I am thinking of the possibility of proton tunnelling, proton hopping, proton conduction, etc. It is known, for example, that when H_2O and D_2O are mixed, HDO molecules soon appear in the mixture, which suggests that similar H-interchanges occur in pure H_2O as well.

(b) Since the nuclear spin system is very loosely coupled to the other degrees of freedom of the system under study, it is not a priori obvious that changes occurring in the nuclear spin system – such as observed in nmr – can be directly interpreted in terms of molecular motion.

(2) A possible check on the correct interpretation of nmr data may be furnished by dielectric relaxation studies – at least in cases where the molecules have appreciable dipole moment – provided that these studies can be extended to high enough frequencies, including the reorientational frequency of the molecules.

J.G. POWLES: I agree with your general remarks – in fact I was hoping that I had made all these points quite clear in my paper.

As regards your comment (1a), this possibility has been fully recognized in nmr studies for many years; in particular, proton exchange in water systems has been studied in great detail by Meiboom et al. Protons of course represent a rather special case in this respect. Incidentally, exception being made of course for the analytical applications, proton resonance is not as predominant as a superficial glance at the literature might lead one to think.

As regards your comment (1b), I agree that the nmr results cannot be directly interpreted in terms of molecular motion and a large part of my paper and of my oral presentation was devoted to trying to explain what in fact one has to do.

With reference to your comment (2), it is well known that dielectric relaxation studies are very valuable for the study of molecular reorientation. However, I was asked at this Symposium to explain the nmr technique, and so did not dwell on the subject of dielectric relaxation.

E.E. SÁNDOR: In the specific example of HBr discussed in the paper, what physical interpretation can be given to the nmr data recorded in the narrow temperature range separating the two highest solid-state transitions? I mean 'physical interpretation' as distinct from a purely phenomenological description of the nmr observations.

J.G. POWLES: Since I was using the example of solid HBr in a very general way, I did not discuss the considerable complexity of the pair of upper phase transitions. You will find this treated at length in the References of the paper.

H.Y. CARR: I very much approve of Mr. Powles' emphasis on a most important limitation of almost all nmr measurements; these measurements are sensitive to the relative separation of two nuclei and not to the nuclear positions and the variation of these positions with time as such.

However, as a very small footnote which may be of interest to some of us here, I wonder whether it should not be added that in one very special type of nmr measurement we are indeed rather directly sensitive to the positions of the nuclei and their variation with time. This is the spin-echo type of experiment with a fluid sample in an externally applied magnetic field gradient. In this kind of experiment the molecular translational self-diffusion coefficient is easily determined from the nuclear spin transverse relaxation time. Measurements are commonly made over times of 10^{-2}- 10^{-3} sec; with the advent of short high-intensity field gradient pulses we may soon use times of 10^{-5} – 10^{-6} sec. Unfortunately, there is little hope of achieving times shorter than this.

J.G. POWLES: It is true that the macroscopic self-diffusion constant, D, can be measured by the spin-echo method, and this method is probably the best one. I think it should be made clear, however, that this is not really an nmr experiment. In much the same way one would not say that a measurement of D by tracer methods is an investigation of a material by radioactivity.

J.W. WHITE: I understand that the relaxation rates which you measure may be dominated by one or more different physical interactions, so that the observable power spectrum may be the Fourier transform of functions involving dipole-dipole correlations, electric field gradient-nuclear quadrupole moment correlations, etc. Since some of these are sensitive only to particular molecular processes such as reorientation, are there cases where the 'same' correlation time has been measured independently through different interactions - presumably by placing different nuclei at strategic points in the molecule?

J.G. POWLES: Generally speaking the agreement is good when the proper conditions are complied with. An example is liquid benzene. We have measured, on the one hand, the proton relaxation times for a dilute solution of C_6H_6 in C_6D_6, and in this case the interaction is dipole-dipole and almost entirely intramolecular; also, the proton-proton distance is fixed. We therefore find the correlation time for the function $Y_2^m(\theta, \varphi)$ which varies with time because of molecular reorientation. On the other hand we have measured the deuteron relaxation time in C_6D_6 where the interaction is due almost entirely to the internal molecular electric field gradient. This again gives Y_2^m (but not for the same axis) and again the modulation is by molecular reorientation. The correlation times found are the same within experimental error.

J.W. WHITE: Have measurements been made in any cases at high enough fields to permit analysis of the non-exponential short-time parts of the correlation function?

J.G. POWLES: This is not a great problem in viscous liquids and in solids. You are probably thinking of low-viscosity liquids where the power spectrum, $J(\omega)$, is appreciable out to, say, 10^{11}Hz, whereas we can only measure its value at, say, 10^7 Hz. In this case we effectively see $J(0)$ which $\int_0^{\alpha} \varphi(\tau)\,d\tau$. We <u>do</u> therefore see a contribution due to $\varphi(\tau)$ at short times since these contribute to the integral and we do not have to assume that $\varphi(\tau)$ is exponential - although this is often a good first approximation for low-viscosity liquids unless short times are involved. To explore $J(\omega)$ (or $\varphi(\tau)$) in detail one would of course need large fields, of the order 10^7G, for low-viscosity liquids.

A. RAHMAN: In your paper you mention a simple form for $P(\vec{r}, \tau/\vec{r}_0)$. Do you do this because the experiment is not sensitive to a refined expression for the function P at short times?

J.G. POWLES: In general the experiments are quite sensitive to $P(\vec{r}, \tau \mid \vec{r}_0)$. However, in the case of low-viscosity liquids the relaxation time, T_1, is not very sensitive to P in that, for instance, one finds that $T_1 = CD$, where C is a constant and D is the macroscopic diffusion constant. Experiment and the simple theory give values for the constant C which differ by a factor of about two. An improvement in the expression for P should remove this discrepancy. It would be interesting to know the form of P, if only for purposes of 'computer argon'.

DYNAMICS OF SOLIDS

Chairmen: P.K.IYENGAR
J.L.YARNELL

Rapporteurs for this Session were:

P.D.RANDOLPH for SM—104/27, 56, 94, 97 and 115
U.DAHLBORG for SM—104/38, 58, 89, 59 and 80

All other papers were presented in the usual way.

LIQUID DYNAMICS FROM NEUTRON SCATTERING

K.-E. LARSSON
ROYAL INSTITUTE OF TECHNOLOGY,
STOCKHOLM, SWEDEN

Abstract

LIQUID DYNAMICS FROM NEUTRON SCATTERING. During the last three years (1965-67) the investigation of the dynamical behaviour of liquids by slow neutron scattering has developed along several different lines. Few new results have been reported on simple liquids, the most extensive being those on liquid lead and liquid argon. Several models for liquid dynamics were already developed and these, together with some new developments, have been tested against the neutron data obtained. Approximate dispersion relations and frequency distributions have been derived. The possible existence of a second Brillouin zone (approximate) in a liquid has been pointed out Attempts have been made to calculate the mean square displacement $<r^2(t)>$ for an atom in a liquid (sodium) on the basis of a given pair potential and to compare this to neutron results. The existence of a transient order in a simple liquid in space and time seems to be more firmly established.

For complex liquids a considerable advance in our understanding of the neutron results has occurred. Almost simultaneously models have been created and theories formulated which take the translational and rotational molecular motions into account. In particular, the motion of one of the simplest molecular liquids, methane, has been investigated and the scattered spectrum is relatively well understood as a hindered rotation combined with a vibrational and diffusive motion of the molecular centre of gravity. Similar results were obtained independently on more complex liquids leading to a similar conclusion: the molecular motion seems to be composed of (1) a rotational diffusion component consisting of two distinct parts created by motion in large and small steps respectively, and (2) a translational component for the centre of gravity which may be vibratory or diffusive. The nature of the quasi-elastic neutron scattering seems to be better understood. The connection with results obtained with other experimental techniques also seems to be more firmly established. This is particularly the case for the connection between infrared and Raman spectroscopy and neutron spectroscopy. A possible connection with dielectric, ultrasonic and nmr data is also indicated.

1. INTRODUCTION

During the last few years a series of neutron scattering experiments were made on liquids which further elucidate the basic properties of this state of matter. Experiments on simple liquids have given further insight into the nature of the diffusive and the vibratory nature of atomic motions of liquids. The existence and nature of collective effects of the atomic motions are shown in increasingly greater detail. The experience from the neutron experiments tends to be that the vibrational motions in liquids are short-time transients which die out into exponential decays after a few times 10^{-12} seconds. The local disturbances seem to range to about 10 Å round each atom.

Similarly the recent developments possible from the scattering experiments on molecular liquids have shown the importance of hindered rotations or reorientations of molecules round their centres of gravity. The indications from recent neutron scattering experiments are that reorientations are also of the nature of a transient oscillatory behaviour going over into an exponential damping for longer times. The possible collective nature of such torsional motions of molecules in liquids has not yet been demonstrated. The torsional behaviour deduced from neutron scattering experiments seems to be in agreement with deductions based on observations of infrared and Raman spectra.

2. GENERAL EXPERIMENTAL FACTS ABOUT SIMPLE LIQUIDS

From the first neutron scattering studies of single phonon excitations in solids at temperatures near the melting point it was concluded that phonons still exist a few degrees from the melting points [1, 2]. It was also found that their mean life-times are of the order of 10^{-12} seconds and their mean free paths a few Ångström units or of the order of one wavelength. It was also concluded that the interaction between a neutron and the phonon field results in a multiphonon spectrum which could be understood and quantitatively described on the basis of the incoherent approximation [1, 3]. The neutron spectrum scattered from a single crystal resulted in a few narrow lines determined by the energy and momentum conditions and the dispersion relations for the phonons. The spectrum scattered from a polycrystal is determined by an angular averaging process of the lattice orientation with respect to the neutron beam and consequently the spectrum was a wide one observed within certain broad limits which were also determined by the momentum condition and the dispersion relation. This spectrum could be understood and calculated on the basis of the theory of scattering from a harmonic lattice [4].

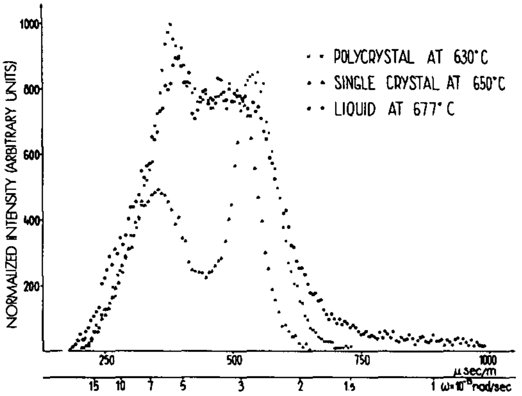

FIG.1. Observed neutron spectra scattered from liquid, polycrystalline and single crystal aluminium. Ingoing neutron energy at 1000 µsec/m. Angle of observation 60°. No quasi-elastic peak is observed. The similarity between liquid and polycrystalline spectra is demonstrated.

In a series of neutron scattering studies of various simple liquids, notably liquid metals [5, 6] near their melting points but also liquid argon [7, 8], it was concluded that the liquid scattering picture was remarkably similar to the corresponding polycrystalline scattering picture (Figs. 1, 2, 3). This similarity is particularly pronounced and temperature independent in the inelastic region which in the solid phase corresponds to the phonon excitation or de-excitation spectrum. In the near-elastic region pronounced broadenings occurred in the liquid spectrum of the corresponding sharp lines in the form of Bragg peaks for certain crystal orientations

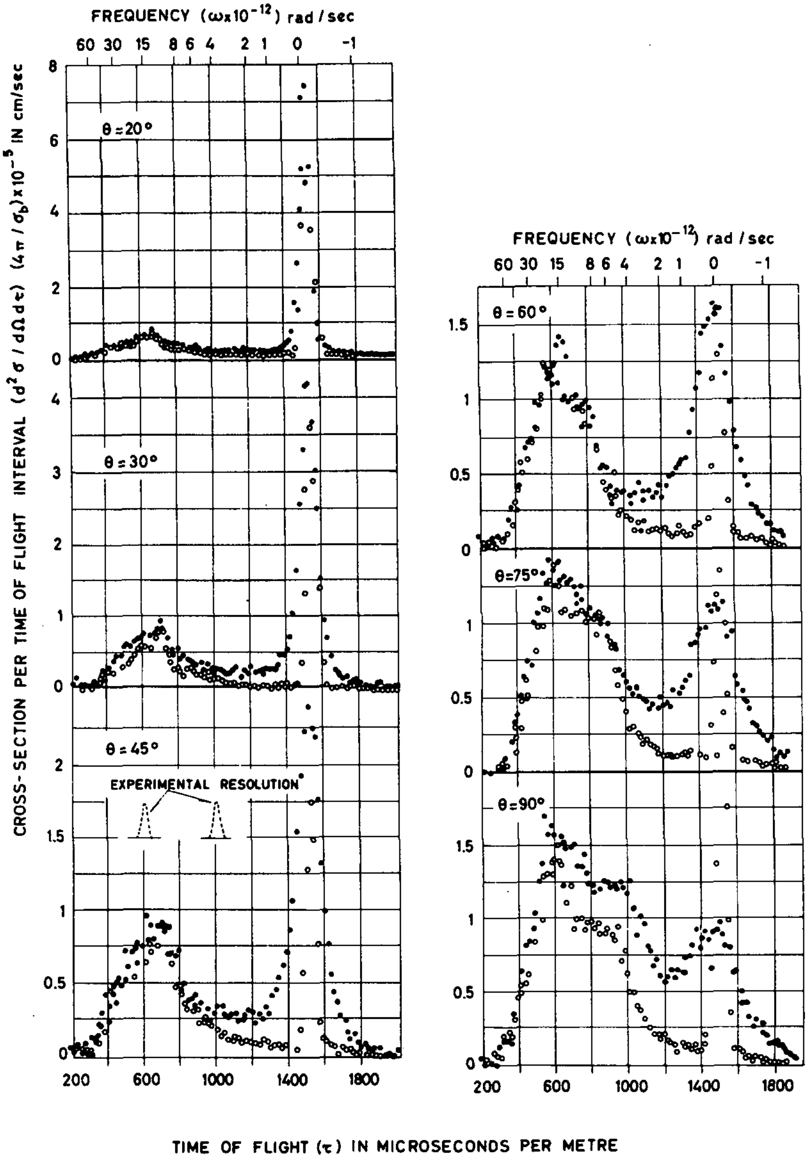

FIG. 2. Observed neutron spectra from solid and liquid sodium at various angles of observation. Ingoing neutron energy at 1520 μsec/m. A broadened quasi-elastic peak is observed in the liquid phase.

in the case of coherent solid scatterers and in the form of sharp elastically scattered lines for all orientations in the case of incoherent solid scatterers.

The features thus outlined are universal and have stimulated a number of attempts to understand the nature of atomic motions in simple liquids, mostly by creating models. A basic question, which has been dealt with

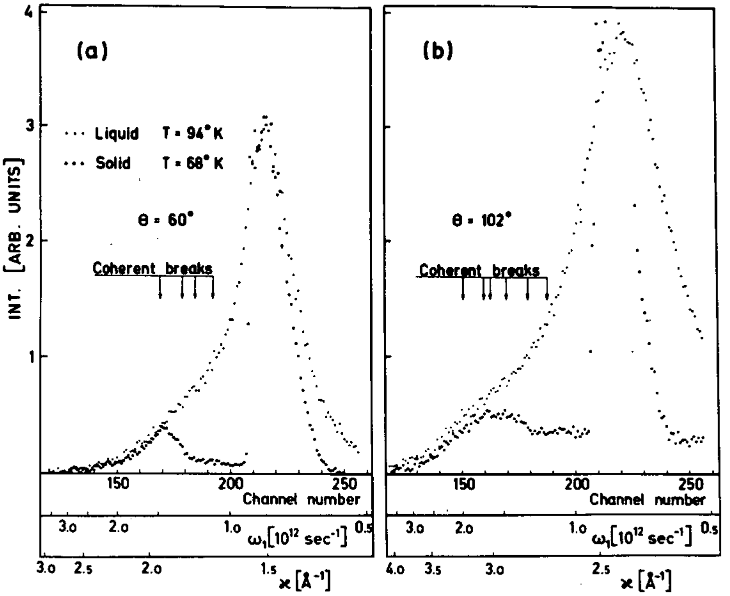

FIG.3. Observed neutron spectra from solid and liquid argon at 68 and 94°K respectively and at 60° and 102° angle of observation. A very broad quasi-elastic peak is observed in the liquid phase.

in great detail, is the shape of the velocity auto-correlation function $<\vec{v}(0)\cdot\vec{v}(t)>$ and its Fourier transform, which gives the frequency distribution $f(\omega)$ of the velocity correlation:

$$f(\omega) = \frac{4}{3\pi}\,\frac{M}{kT}\int_0^\infty <\vec{v}(0)\cdot\vec{v}(t)> \cos\omega t\,dt$$

In most models created so far one has separated the short-time behaviour of $<\vec{v}(0)\cdot\vec{v}(t)>$, which probably is of damped oscillatory character, and the long-time behaviour, which eventually becomes an exponential decay. Equivalently, the vibratory solid-like, short-time behaviour for times $t < 10^{-12}$ seconds and frequencies $\omega \gtrsim 2\times10^{12}$ sec^{-1} is often separated from the diffusive, long-time behaviour for $t > 10^{-12}$ seconds and frequencies $\omega \lesssim 2\times10^{12}$ sec^{-1}. Model work of this and a similar kind is mainly connected to observations on incoherent scatterers and the self motion of atoms [9-15].

The pronounced similarity between the polycrystalline and liquid spectra for coherent scatterers, which reveal collective motions, has suggested the idea of the existence of high-frequency collective excitations in liquids of a phonon-like nature. In such a case the frequency distribution $f(\omega)$ of $<\vec{v}(0)\cdot\vec{v}(t)>$, is given an interpretation quite similar to the frequency distribution of normal modes in a solid. In the low-frequency limit (in the hydrodynamic domain), corresponding to times of $t > 10^{-10}$ sec and distances of the order of 100 Å or more, it is known that sound waves can be propagated through the liquid. The question arises of to what degree longitudinal and transversal phonons of higher frequency may be transmitted through a liquid. These questions have been elucidated in a number of neutron scattering experiments from which dispersion relations in liquids like argon [7, 16], lead [6, 17], tin [6] have been derived. By applying various models to the neutron data, it has also been possible to derive – at least approximately or partially – the shape of the frequency distributions f(ω) for liquid sodium [6], lead [6] and argon [7]. In Brillouin scattering experiments [18] on liquid lead dispersion relations for both longitudinal and transversal phonons were observed.

The nature of the diffusive process and the transition region between the vibrational and the diffusive time regions has been studied in considerable detail [6, 19, 20]. The quasi-elastically scattered intensity, which reveals the details of the diffusive motions, has turned out to be dependent upon the liquid structure factor in an apparently simple way [21, 22].

3. THEORIES AND MODELS FOR DYNAMICS OF MONATOMIC LIQUIDS

The interpretation work on the neutron experiments always consists in calculating the cross-section or scattering function

$$S(\kappa, \omega) = \frac{1}{2\pi} \iint G(r, t)\, e^{i(\vec{\kappa}\vec{r} - \omega t)}\, d\vec{r}\, dt \qquad (1)$$

where the usual notation is used. For the self-motion

$$S_s(\kappa, \omega) = \frac{1}{2\pi} \iint G_s(r, t)\, e^{i(\vec{\kappa}\vec{r} - \omega t)}\, d\vec{r}\, dt \qquad (2)$$

is calculated. The aim of all theories is to calculate the time-displaced correlation functions $G(r, t)$ or $G_s(r, t)$. The calculation of $G_s(r, t)$ is the simpler task and is normally made in the Gaussian approximation, i.e. it is assumed that

$$G_s(r, t) = \frac{1}{(4\pi \rho(t))^{3/2}}\, e^{-r^2/4\rho(t)} \qquad (3)$$

Machine computations [23], which have taken higher-order terms of non-Gaussian type into account, have shown for some cases that the correction is not too large except in certain limited regions of κ in $S_s(\kappa, \omega)$, where it may amount to as much as 10-20%. The Gaussian approximation is a first-order approximation whose exactness is generally unknown.

3.1. Experience from incoherent scattering experiments

In spite of the basic simplicity of $G_s(r, t)$ in the Gaussian approximation, few attempts have been made to calculate the full dynamical picture. Very often the idea is used that $\rho(t)$ may be divided into a bound part, $\rho_B(t)$, more or less of a crystalline nature and a diffusive part, $\rho_D(t)$, for which simplified models are developed. Because the observed neutron spectra for incoherent scatterers are so much like those obtained from solids, simple models such as the Langevin model are ruled out. Modifications of it have, however, been created. One such model is the stochastic model of Rahman, Singwi and Sjölander [24]. In this model damped high frequency modes as in a solid are supposed to exist in a frequency range $\omega' < \omega < \omega_D$, where ω_D is determined by the equivalent Debye-temperature $\omega_D = k_B\Theta_D/\hbar$. Below ω' all modes are supposed to go into diffusion. Each atom is moving independently in the cave of neighbours. This is physically equivalent to saying that the onset of diffusion is delayed for a time $t_d = (MD/kt)(\omega_D/\omega')^3$ which may be $\gg t_\beta = MD/k_BT$, the Langevin delay time for diffusion. The velocity auto-correlation function predicted from the stochastic model consists of a sum of two terms, one simple exponential term corresponding to a modified Langevin diffusion case and an oscillatory term with exponential damping corresponding to a solid-like vibrational behaviour. The collective nature of the modes and the polarization of the high frequency modes is not considered since only the self-motion and $S_s(\kappa, \omega)$ is described.

A similar physical approach to the problem was made by Egelstaff and Schofield [25], who for simplicity assumed that $\rho_D(t) = D(\sqrt{t^2 + c^2} - c)$, where D is the self-diffusion coefficient and c is the delay time for the onset of diffusion such that $c = M^*D/k_BT$, where M^* is the apparent mass for diffusion, in general larger than the atomic mass M such that $c = (M^*/M)t_\beta$. Their approach only results in an expression for the quasi-elastic peak. Both models show the correct short and long-time behaviour of $\rho(t)$ and are very much of a quasi-crystalline character.

Similarly, the jump-diffusion models of Chudley and Elliot [26] and of Singwi and Sjölander [27] were of an extreme solid-like character and were developed only for the diffusive part of atomic motion, i.e. the quasi-elastic peak in the neutron spectrum. A modification by Oskotskii [28], which allows for a slow diffusion of the surrounding to the jumping atom, does not remove the basic solid-like nature of the pure jump model. It should, however, be noted that in general the Singwi-Sjölander model also allows for diffusion, a fact which is not often exploited.

A model which differs from those discussed above was presented by Sears [29] who assumed that an atom diffuses continuously at the same time as it performs vibrations round an ever-moving centre of oscillation. This itinerant oscillator model predicts an $f(\omega)$ which includes all atomic motions, whether diffusive or vibrational. The difficulty is, however, that the predicted $f(\omega)$ contains parameters which are not in general available at present.

The various models mentioned were tested against experiments. The stochastic model of Rahman, Singwi and Sjölander was tested against water data, which is unfortunate as water is a molecular liquid in which the vibrational and rotational motion of molecules or groups of molecules may radically add to the molecular centre of gravity motion as will be discussed below. Their model was also compared to low-resolution liquid lead data. Therefore it is fair to say that their model has not yet been tested against modern high-resolution data for a monatomic incoherently scattering liquid.

The idea that the diffusion process is delayed for a certain time t_d or c to give room for a vibrational motion to develop was tested in a monatomic liquid for liquid argon [30] and liquid sodium [6]. Both liquids are mixed incoherent and coherent scatterers. For the case of argon the self- and pair-correlation functions were derived for different times and the self correlation was isolated (Fig. 4). If the half-width of $G_s(r,t)$ as a function of time is derived from these curves, it is found that it can be fitted with an expression of the type $Dt + c = D(t - t_d)$. From the observed value of c it was deduced that a delay time of about 1×10^{-12} seconds exists in liquid argon at 84.5°K.

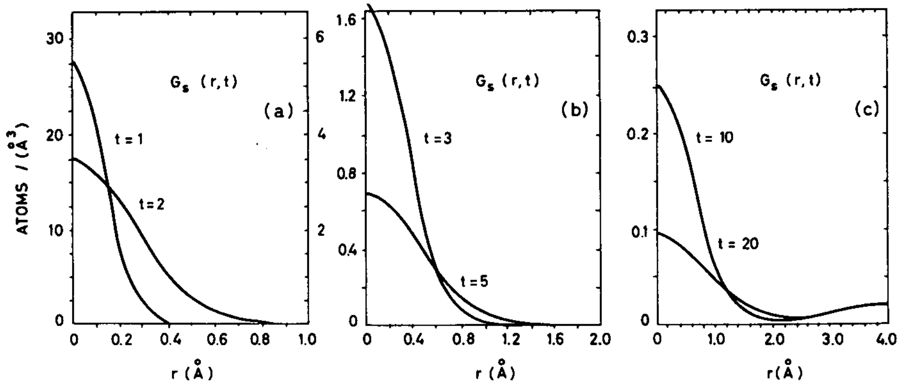

FIG. 4. Self-correlation function for different times in units of 10^{-13} sec derived from neutron spectra scattered from liquid argon at 84.5°K. The ordinate on the right-hand axis of (a) applies to $t = 2 \times 10^{-13}$ sec.

Liquid sodium was studied over a wide range of temperatures in such a low range of κ values ($\kappa < 1\,\text{Å}^{-1}$) that the structure dependent coherent scattering is practically absent. Under such circumstances $S_s(\kappa, \omega)$ is revealed in the observed neutron picture. Examples of observed neutron spectra were shown in Fig. 2. From the quasi-elastic scattering the natural width of the peak was derived and compared to the extreme jump-diffusion model version of the Singwi-Sjölander model, the modified jump-diffusion model of Oskotskii and Ivanov, which takes into account the effect of the jump in somewhat more detail, and the delayed diffusion model of Egelstaff and Schofield. As seen in Fig. 5, the extreme jump diffusion, in which the jump time is put = 0, is ruled out, whereas a mixed process (jump and continuous diffusion) may be claimed to fit the data. Typical values for the derived atomic displacements, derived from the relation $\overline{\ell^2} = 6D\tau_0$, are 2-2.5 Å and corresponding values of τ_0 are about 2×10^{-12} seconds. In reality, part of this length, $(\overline{\ell^2})^{1/2}$, is a jump distance and part of it is a continuous displacement. As pointed out elsewhere [31], the Singwi-Sjölander model in its full extent, when both jump and continuous diffusion is included, would probably also have fitted the data. As displayed in Fig. 6 the delayed diffusion model seems to fit the data for all temperatures and gives c values in a range of $1.1\text{-}1.5 \times 10^{-12}$ seconds. From these c values a value of M^*/M is found to be about 30, independent of temperature. This would in other words mean that if an atom moves, it makes its motion felt out to a distance of about 7 Å. This figure may be compared to the mean free path for phonons in solids near their melting points and of derived ranges of coherence in liquids discussed later on, which are of a similar order of magnitude.

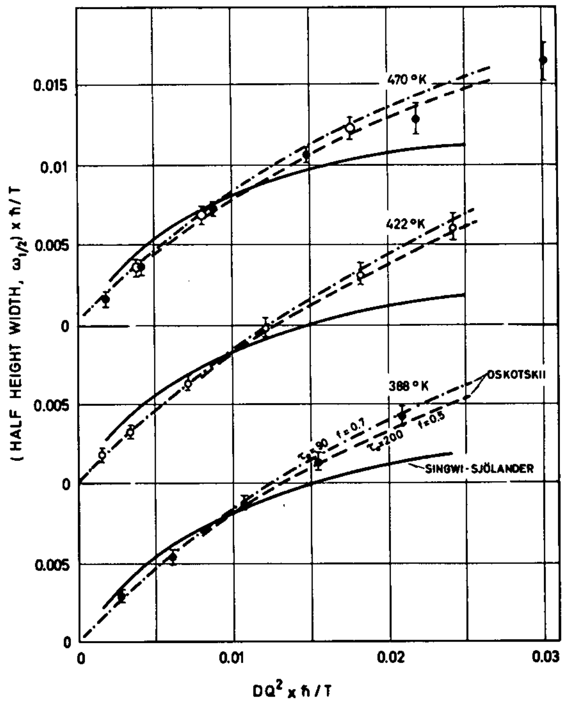

FIG. 5. Observed widths of the quasi-elastic peaks corrected for resolution from liquid sodium at various temperatures and compared to the predictions of: (1) the model of Singwi-Sjölander in its extreme jump version with e^{-2W} determined from peak intensities and with $\tau_0 = 2 \times 10^{-12}$ sec (full lines); (2) the model of Oskotskii with e^{-2W} determined from peak intensities using $\tau_0 = 5.4 \times 10^{-12}$ sec (dashed) and $\tau_0 = 2.4 \times 10^{-12}$ sec (dashed-dotted lines).

As in the Gaussian approximation, there is a simple connection between the scattering function and the width:

$$S_s(\kappa, \omega) = \frac{1}{2\pi} \int dt\, e^{-i\omega t - \kappa^2 \rho(t)} \tag{4}$$

It is in principle possible to calculate $S_s(\kappa, \omega)$ with $\rho(t)$ known. For liquid sodium an attempt was made to make use of the division of $\rho(t)$ into $\rho_B(t) + \rho_D(t)$ with $\rho_D(t) = D(\sqrt{t^2 + c^2} - c)$ and to use for $\rho_B(t)$ the expression developed for a solid

$$\rho_B(t) = \frac{kT}{M} \int_0^\infty d\omega \frac{f(\omega)}{\omega^2} (1 - \cos \omega t) \tag{5}$$

With such a model it would be possible to estimate what type of frequency distribution would be necessary to fit the experimentally observed $S_s(\kappa, \omega)$. Remembering the general similarities between polycrystalline and liquid spectra, it is natural to start as a first approximation with the phonon

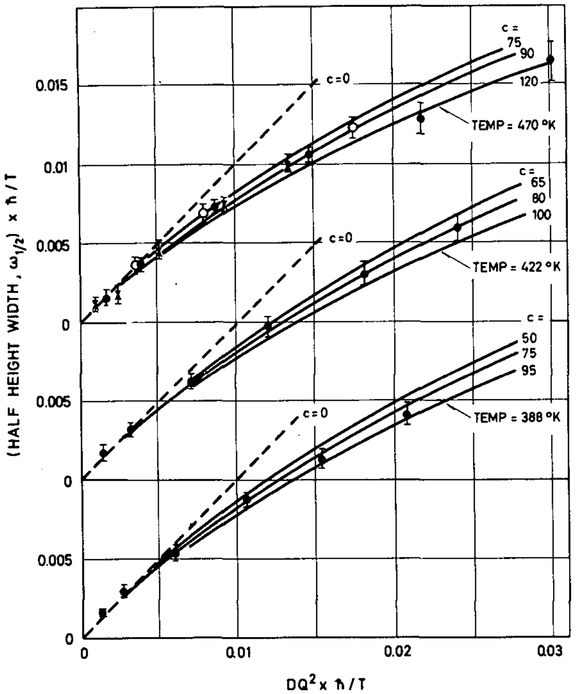

FIG. 6. Observed widths of the quasi-elastic peaks from sodium compared with the predictions of Ficks law (dashed line) and the delayed diffusion model of Egelstaff-Schofield (full line) for various values of t_d = c in units of ħ/T.

distribution in the solid. Then in the second approximation minor changes are made to make the calculated $S_s(\kappa, \omega)$ approach the measured one. In this way f(ω) for liquid sodium at 388°K was derived as shown in Fig. 7. It is seen that the main difference between the solid and liquid distributions is a displacement of the region of f(ω) corresponding to transversal modes of motion in the solid to lower frequencies and the appearance of the diffusive portion as $\omega \to 0$. It is clear that the velocity auto-correlation function $<\vec{v}(0)\cdot\vec{v}(t)$ corresponding to such a shape of f(ω) would have a similar damped oscillatory character as was, for instance, found by Rahman [32] in the machine computations on liquid argon.

Summing up the experience gained from neutron scattering experiments on simple, incoherently scattering liquids, it seems that:

(1) In a time of the order of $\sim(1\text{-}3)\times10^{-13}$ seconds an atom undergoes a relatively large displacement with $\rho(t) \simeq v^2t^2$ corresponding to the first part of $<\vec{v}(0)\cdot\vec{v}(t)> \simeq 1-\Omega^2t^2$, where Ω is some correlation frequency. This part of the motion may be likened to a jump. The relaxation time for the jump is τ_1 and $v\tau_1$ is the jump length ℓ.

(2) In a time of the order of $(1\text{-}3) \times 10^{-12}$ seconds the oscillations following the initial bigger jump are damped out. The relaxation time, τ_0, for the vibratory part of $<\vec{v}(0)\cdot\vec{v}(t)>$ is of the order of $(1\text{-}3)\times10^{-12}$ seconds.

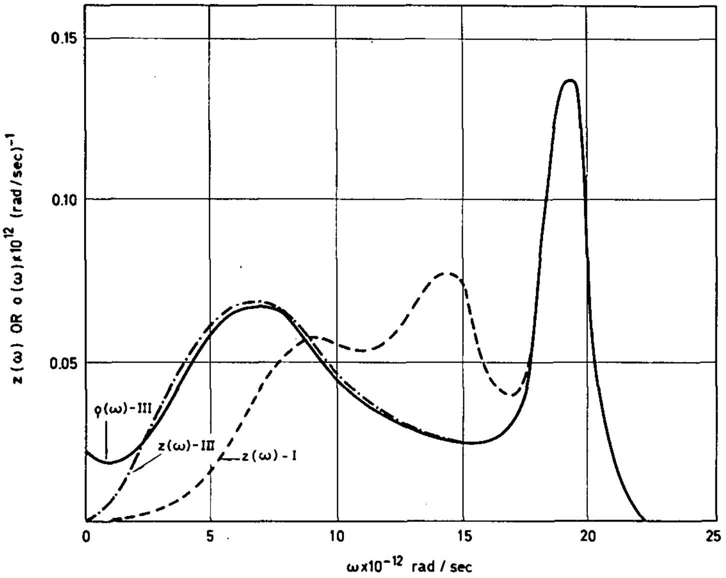

FIG.7. The frequency distribution f(ω) for liquid sodium necessary to fit the observed neutron spectrum (solid line, marked ρ(ω)-III) compared to the frequency distribution of normal modes in solid sodium (dashed line marked z(ω)-I).

(3) For times longer than τ_0 more than one period of the transient behaviour is considered. The damping is fairly complete and the atom is now said to diffuse away from its origin. The form of $\langle \vec{v}(0)\cdot\vec{v}(t)\rangle$ is dominated by an exponential decay.

(4) The two first phases mentioned above form the minimum cycle occurring in the diffusive process. The corresponding displacements may be described naively as $\overline{x^2} = \overline{\ell_x^2} + 2D_0\tau_0 = 2D(\tau_1 + \tau_0)$. It is therefore approximately correct to describe the diffusion process as a mixed process. The relative importance of the two components is reflected in the shape of f(ω).

3.2. Experience from coherent scattering experiments

As pointed out in section 2, the neutron scattering picture obtained from coherently scattering liquids very much resembles the results obtained on the polycrystalline solid phase (compare Fig.1). Attempts have been made to understand or predict these results. To obtain $S(\kappa, \omega)$, it is necessary to formulate a model for the time-displaced pair correlation function $G_d(r,t)$:

$$S(\kappa,\omega) = \frac{1}{2\pi}\iint G_s(r,t)\, e^{i(\vec{\kappa}\vec{r} - \omega t)}\, d\vec{r}dt + \frac{1}{2\pi}\iint G_d(r,t)\, e^{i(\vec{\kappa}\vec{r} - \omega t)}\, d\vec{r}dt \qquad (6)$$

The first attempt to calculate G(r, t) was the Vineyard convolution approximation [33]. In this approximation it was assumed that the probability of finding an atom at $\vec{r}$ and t was given by a folding of the static pair distribution function g(r') and the self-correlation function $G_s(\vec{r} - \vec{r}', t)$ such that

$$G_d(r, t) = \int g(\vec{r}')\, G_s(\vec{r} - \vec{r}', t) d\vec{r}' \tag{7}$$

The well-known physical limitation of this idea is that nothing prevents the atom moving from r' to r to get back to the origin during the time t. But as there is already an atom at the origin from the start, this means that the pair of atoms considered may penetrate each other. $S(\kappa, \omega)$ may in this approximation be written

$$S(\kappa, \omega) = S_s(\kappa, \omega)\ Z \tag{8}$$

where $Z = 1 + \gamma(\kappa)$ is the well-known liquid structure factor.

An apparently extreme model was formulated by Egelstaff [34], who used the cross-section formulated for a polycrystal [4] and made a generalization of it. The coherent one-phonon cross-section for a polycrystal is in the harmonic approximation shown to be a product of the incoherent cross-section and a structure factor:

$$S(\kappa, \omega) = S_s(\kappa, \omega) Z \tag{9}$$

with $Z = \sum_{\tau} \frac{\pi F_\tau}{2B\tau\kappa q}$

where B is the volume per nucleus in the crystal, $\vec{\tau}$ is a reciprocal lattice vector, $\vec{q}$ is the phonon wavevector, F_τ is the structure factor for the plane series specified by τ. Assuming that F_τ transforms into $1 + \gamma(\kappa)$, and the summation transforms into an integral over a sphere,

$$Z_{\text{solid}} = \sum_{\tau} \frac{\pi F_\tau}{2B\tau\kappa q} \rightarrow \frac{\pi}{2} \int \frac{4\pi\tau^2 d\tau (1 + \gamma(\tau))}{\tau\kappa q} \tag{10}$$

Furthermore, it is assumed that two polarizations are possible, also in a simplified analogy with the solid, for which a factor $(\vec{e}_q \cdot \vec{e}_\kappa)^2$ enters into the cross-section. Here $\vec{e}_q$ is a unit vector along the direction of polarization of the phonon and $\vec{e}_\kappa$ is a unit vector in the direction of $\vec{\kappa}$. It is easy to see that for a simplified description of the phonons as pure longitudinal and pure transversal it follows that $(\vec{e}_q \cdot \vec{e}_\kappa)^2 = \cos^2\Theta$ for longitudinal phonons and $= \sin^2 \Theta$ for transversal phonons. The final liquid structure factor is

$$(Z_{\text{liquid}})_{\substack{\text{longitudinal}\\ \text{transversal}}} = \frac{2\pi^2}{q^{\kappa}} \int_{\tau_{\min} = \kappa - q}^{\tau_{\max} = \kappa + q} \tau(1 + \gamma(\tau)) \begin{Bmatrix} \cos^2 \Theta \\ \sin^2 \Theta \end{Bmatrix} d\tau \tag{11}$$

In calculating $S(\kappa, \omega)$ in this approximation, the one-phonon form of $S_s(\kappa, \omega)$ derived for a solid is used with $f(\omega)$ divided into a longitudinal and a transversal part, for which the corresponding structure factors are calculated. The sum of the longitudinal and the two transversal parts forms $S(\kappa, \omega)$

$$S(\kappa, \omega) = S_s(\kappa, \omega)_{\text{long}} Z_{\text{long}} + S_s(\kappa, \omega)_{\text{trans}} \, Z_{\text{trans}} \tag{12}$$

A similar model formulated without the assumption of lattice vectors, τ, was formulated by Singwi [35-37]. To correct the obvious error of the convolution approximation, the atoms within a sphere of radius R, the so-called correlation range, round each atom are supposed to feel the motion of the central atom and are supposed to perform vibrational motions as in a solid for a limited time of order τ_0 as discussed above. The polarization of the phonon modes within the neighbourhood of each atom were, however, averaged out in the original work assuming an isotropic case. Outside the correlation range, R, it is assumed that the assumptions of the convolution approximation are valid. Consequently the scattering function is of the form

$$S(\kappa, \omega) = S_s(\kappa, \omega) Z \tag{13}$$

with

$$Z = 1 + \gamma(\kappa) + \frac{1}{6} q^2 L(R, \kappa, q) \tag{14}$$

where the term $\frac{1}{6} q^2 L(R, q, \kappa)$ is to be considered as correction term to the convolution approximation (for the most complete formulation of $L(R, q, \kappa)$ see Ref. [37]). Singwi showed that his formulas for $S(\kappa, \omega)$ and those of Egelstaff are identical for $\hbar\omega \ll 2k_BT$, $|q| \ll |\kappa|$ and $R \to \infty$. It was pointed out by Cocking [6] that the correspondence between the two models is more general and he showed that the condition $|q| < |\kappa|$ may be relaxed. Thus for <u>all</u> q of interest the results of the Egelstaff polycrystal model <u>without polarization included</u> is the limit for $R \to \infty$ of the Singwi model, provided $\hbar\omega < 2k_BT$, such that

$$1 + \gamma(\kappa) + \frac{1}{6} q^2 L(R = \infty, \kappa, q) = \frac{1}{2q\kappa} \int_{\kappa - q}^{\kappa + q} dx \, x[1 + \gamma(\kappa)] \tag{15}$$

When comparing the predictions of the three models above, the one-phonon cross-section for a solid has been used

$$S_s(\kappa, \omega) = \frac{\hbar}{2M} \kappa^2 e^{-2W} \frac{f(\omega)}{\omega \sinh \frac{\hbar\omega}{2k_BT}} \tag{16}$$

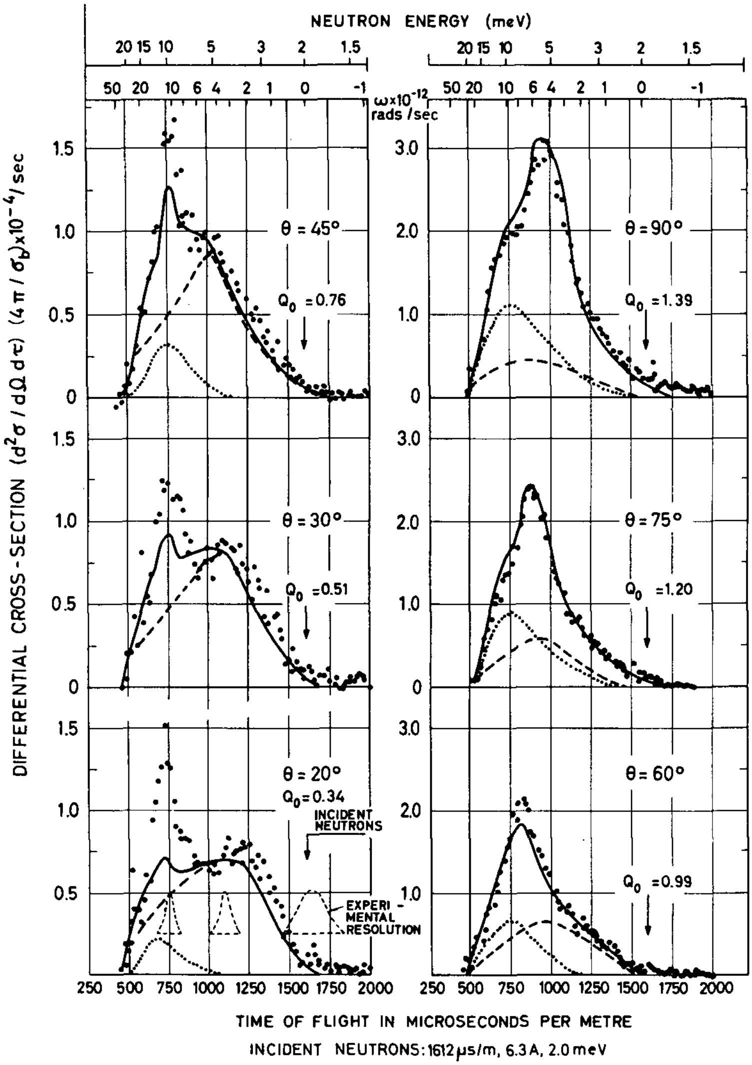

FIG. 8. Observed neutron spectra for liquid lead at 350 °C (melting point 327 °C) compared with calculated spectra using the generalized phonon model of Egelstaff. The multiphonon (dotted) and the multiple scattering (dashed) contributions have been added to the calculated one-phonon term to give the full curve (experimental data from Cocking).

in which f(ω) is divided into two parts of longitudinal and transversal nature respectively [5, 6]. If the scatterer is a mixed incoherent and coherent scatterer like liquid argon or sodium, then

$$a^2_{\text{total}}\, S(\kappa, \omega)_{\text{total}} = a^2_{\text{inc}}\, S_s(\kappa, \omega) + a^2_{\text{coh}}\, S(\kappa, \omega) \tag{17}$$

Also when comparing the theory and the experiment, the multiphonon contribution to the observed $S(\kappa,\omega)$ has to be subtracted, which may be done on the basis of the incoherent approximation as discussed in Section 2.

It also follows that only for given pairs of values of q and ω is a fit possible according to the nature of the models given. Therefore a dispersion relation can be derived. A basic quantity necessary for the computations is $f(\omega)$ but, as described above, one may start the fitting procedure by assuming the same $f(\omega)$ as for the corresponding high-temperature solid.

Following these lines, several experiments were performed in which the effects of collective motion in a simple liquid were tested [5-7, 16, 17]. In this paper the experiments on liquid lead and liquid argon will be discussed in some detail.

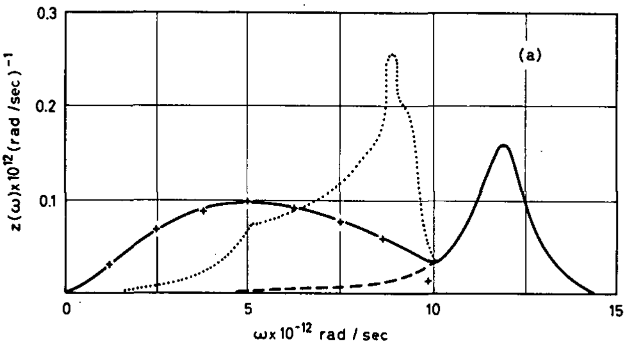

FIG. 9. Frequency distribution of liquid lead at 350 °C necessary to produce the best fit to the neutron data (solid line). Only the 'bound' part corresponding to $\rho_B(t)$ is given in the figure. The dotted curve gives the transversal part of $f(\omega)$ for solid lead. The longitudinal part of $f(\omega)$ (dashed curve and the upper peak) are taken the same for the solid and liquid phases.

Using very low-energy ingoing neutrons (6.3 Å, 2.0 meV) Cocking studied liquid lead (melting point 327°C) at 350°C for small κ values (most κ values studied fall between 1 and 2 Å^{-1}). As seen in Fig. 8, the calculated neutron distributions may be relatively well fitted to the observed ones for a considerable range of momentum transfers in the low range. To obtain the fit shown it was, however, necessary to use a frequency distribution differing from the one derived for the solid case, as seen in Fig. 9. The main difference occurs for the contribution of transversal waves.

Another set of experiments on liquid lead at 352°C was performed by Randolph and Singwi [17], who used higher ingoing neutron energies (15, 17 and 20 MeV) and therefore concentrated their studies on values of κ ranging from 1 to 5 Å^{-1}, thus covering the region where the structure factor $1+\gamma(\kappa)$ oscillates. In Fig. 10 their experimental data are compared to prediction of the convolution approximation of Vineyard, the modification of the convolution approximation by Singwi and the Egelstaff model including polarization of the quasi-phonons. The conclusion is that the extreme solid-like model of Egelstaff gives the best fit. The same fit would probably be obtained with the Singwi model if polarization effects were included.

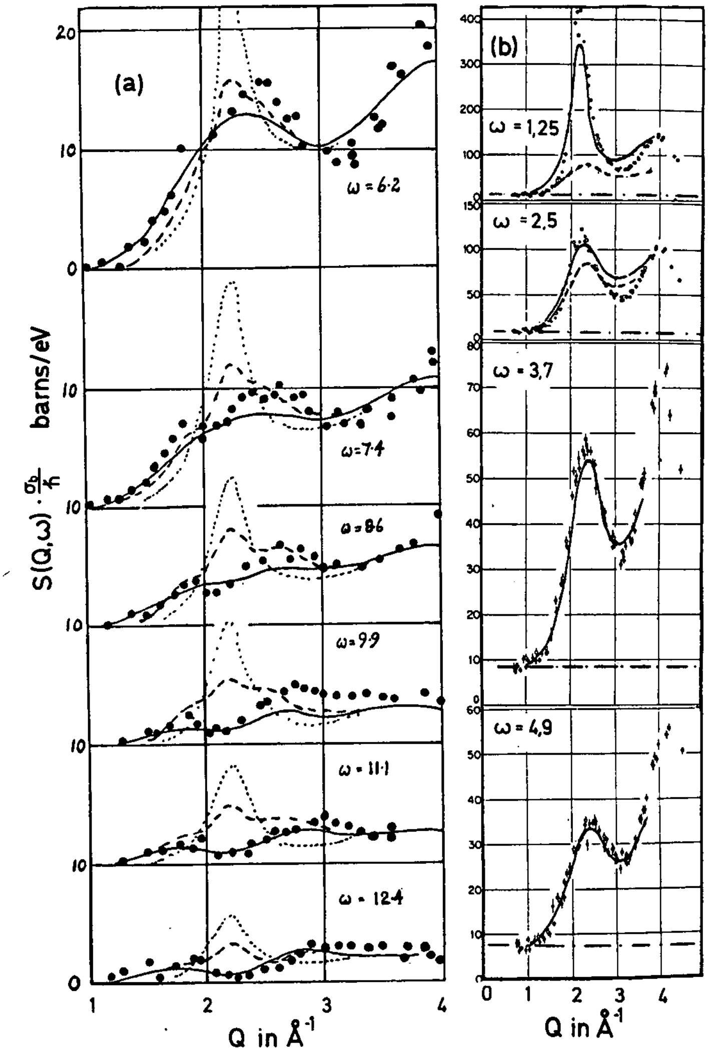

FIG. 10. Observed neutron spectra for liquid lead compared with the predictions of various models: (a) Dotted curve, convolution approximation (= Singwi model with R = 0); dashed curve, Singwi model with R = 20 Å and no polarization; full lines, Egelstaff model with polarization; (b) lower ω-data; comparison to Egelstaff model only. Multiple scattering level given by dash-dotted curve. At ω = 1.25 and 2.5 the one- and multi-phonon terms contribute as shown by dashed curve and the zero-phonon term is added to give full calculated curve.

In the experiments on liquid argon [7] at 94°K by Sköld and Larsson (5-MeV neutrons) a similar region of κ was covered, $1.5 < \kappa < 3.5\,Å^{-1}$, which is the region round the first diffraction peak at 2 $Å^{-1}$. Again the one-phonon term was isolated from the experimental data and compared to the models discussed above. As seen in Fig. 11, the observed $S(\kappa, \omega)$ develops a dip at the peak of the structure factor at 2 $Å^{-1}$ exactly as was observed

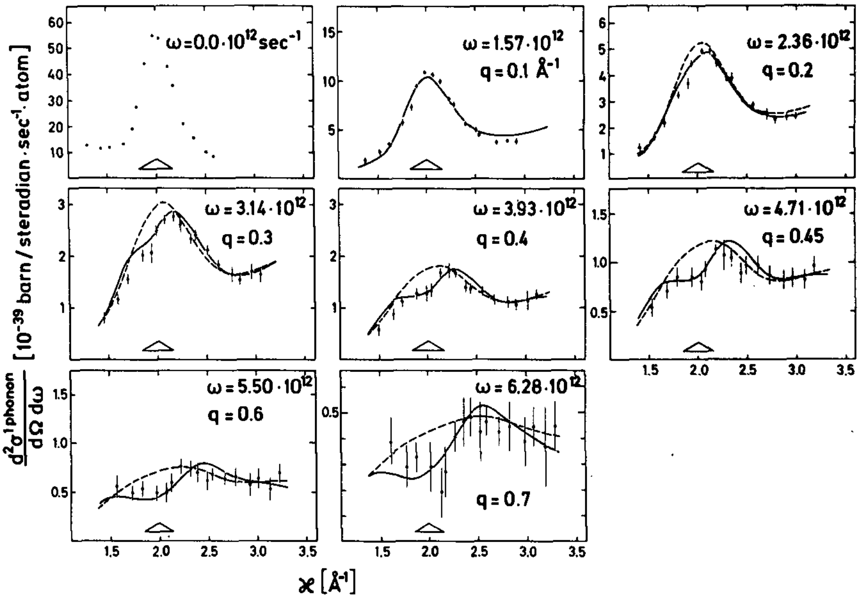

FIG. 11. Observed one-phonon cross-section for liquid argon at 94°K compared to the calculated cross-section for the Egelstaff model with the assumption of only longitudinal phonons existing in the liquid (full curve) and with the assumption of both longitudinal and transversal phonons (dashed curve). The values of q and ω result in a dispersion relation.

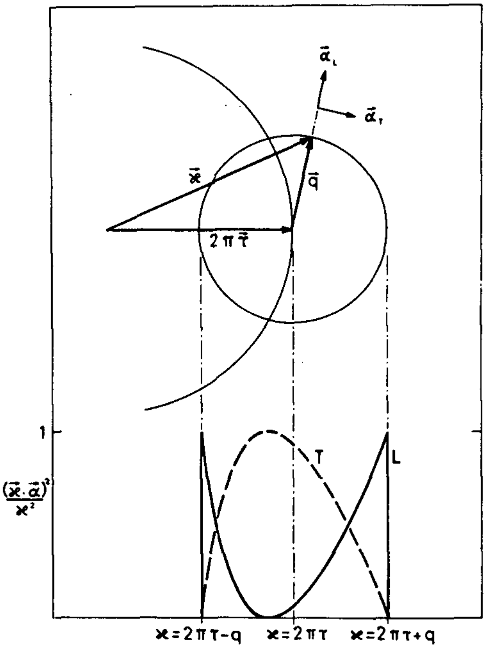

FIG. 12. Vector diagram for a coherent one-phonon process in a polycrystal and the resulting polarization factors. This will affect the structure factors $Z_{\text{longitudinal}}$ and $Z_{\text{transversal}}$ in formula (12).

for liquid lead (Fig. 10). The appearance of two peaks in S(κ, ω) for larger ω values indicates that the effect of polarization is very pronounced. As illustrated by Fig. 12, the polarization factor creates a double-peaked structure of Z_{long}. It thus seems that longitudinal collective modes exist at these high frequencies. As also seen in Fig. 12, the transversal modes on the other hand have a maximum near $\kappa = \tau$ which corresponds to $q = 0$. Therefore only longitudinal modes are observed as peaks (as in Fig. 11) because the contribution of the transversal modes is peaked where $1 + \gamma(\kappa)$ is peaked.

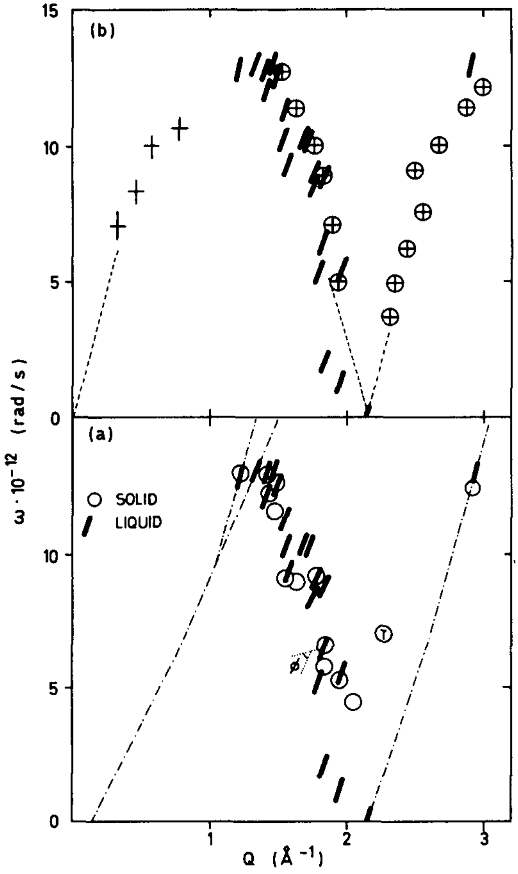

FIG. 13. Dispersion curves for liquid lead from various observed spectra: (a) Comparison between solid at 310°C and liquid at 350°C. The outer limits of the region of observation in κ-ω space are shown as dash-dotted lines. (b) ⊕ data of Randolph and Singwi from liquid lead at 352°C; / data of Cocking from liquid lead at 350°C; + data of Dorner et al. from liquid lead at 345°C.

For all simple liquids on which the Singwi model has been tested it is furthermore found that the range of the coherence parameter R has to be given a value of at least 10-20 Å. Larger values are possible but not smaller values.

For both liquids a dispersion relation was derived from the best fit corresponding to pairs of ω and q. The procedure used to obtain the dispersion relation is obvious from the presentation of $S(\kappa,\omega)$ versus κ for constant ω in which a fit is obtained for only one value of q for each ω value. This method to derive a dispersion relation is easily used when a wide range of κ values round the main diffraction peak of $1+\gamma(\kappa)$ is studied. The method was used by Randolph and Singwi on liquid lead and by Sköld and Larsson on liquid argon. Another method has been used by Kroó et al. Still another method proposes itself when very low ingoing neutron energies are used. The position of the inelastic peak itself gives a possibility of determining a pair of values of ω and κ, knowing that the inelastic intensity starts to rise just when $\kappa + q = \tau$ means that the corresponding q value is obtained when κ and τ are known. The τ value is taken as the value at the peak of the structure factor. This method was used by Cocking and Egelstaff [38] and Cocking [6] on liquid lead. As shown by Fig. 13, there is remarkable agreement between the average dispersion relation obtained in solid and liquid lead. Also the data of Cocking and those of Randoph and Singwi give a convincing agreement. The dispersion relations start out from the κ value of 2.2 $Å^{-1}$ corresponding to the main peak of the liquid structure factor for lead. It is seen that the dispersion relation measured directly by use of Brillouin scattering in liquid lead [18], which in the crystal language falls in the first Brillouin zone, for which $0 < \kappa < 1.1\ Å^{-1}$, seems to be symmetric to the one measured for $1.1 < \kappa < 2.2\ Å^{-1}$. This fact justifies the transfer of all the dispersion data to the 'first Brillouin zone'. This was in fact done for liquid argon for which the dispersion relation is shown in Fig. 14. As will be seen, the agreement between the various ways of analysis is satisfactory, showing the similarity of the basic physics of the two models. It should also be noted that no distinct differences are observed between liquid lead and liquid argon.

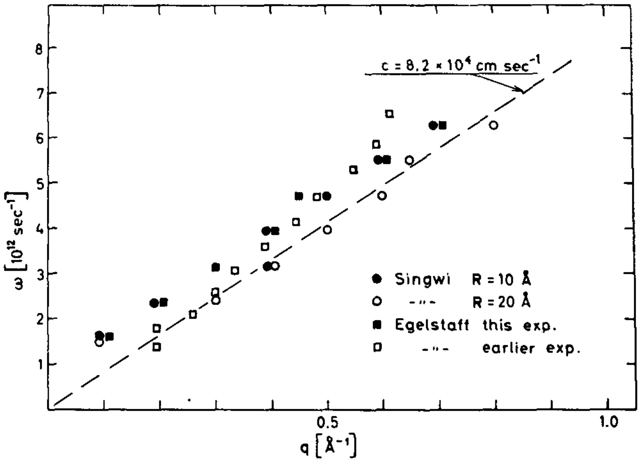

FIG. 14. Dispersion relation for liquid argon at 94°K. The measured q values belong to regions in ω-κ space round the main peak of the structure factor at $\kappa = 2\ Å^{-1}$.

It is of interest to point out that the tendency of the frequency distribution f(ω) derived from the liquid argon data shows some resemblance to the frequency distribution derived by Rahman [32] from his computer experiment (Fig. 15).

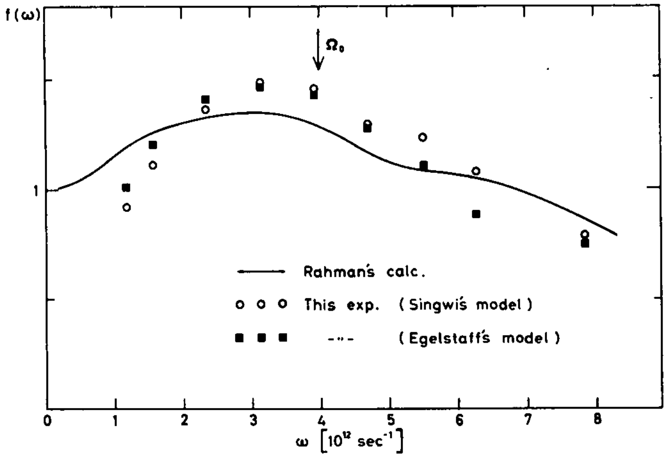

FIG. 15. Experimentally obtained frequency distribution f(ω) for liquid argon at 94°K compared to the calculated curve obtained by Rahman. Ω_0 is the characteristic frequency appearing in Sears itinerant oscillator model.

In the case of a coherent scatterer no quasi-elastic intensity is observed unless the κ value at the ingoing energy, $\hbar\omega_0$, corresponds to a value where $1 + \gamma(\kappa)$ has an appreciable value. Thus in Fig. 8 there is no quasi-elastic peak because of the small κ values used. In the liquid argon experiment there is always a quasi-elastic peak due to the incoherent component in $S(\kappa, \omega)_{\text{total}}$. If, however, the width of the peak is plotted against κ, one finds an oscillatory behaviour predicted [39] and observed earlier [30, 40]. The main variation of the width (compare Fig. 16) is in agreement with the simple diffusive behaviour corresponding to the assumption that $\rho(t) = Dt$ in the Gaussian approximation. The observed oscillations are connected to the coherent cross-section. It is well known that the convolution approximation with the simple diffusion approximation used to describe $S(\kappa, \omega)$ does not fulfil the elementary second-moment relation

$$\overline{\omega^2_{\text{coh}}} = \frac{k_B T \kappa^2}{M[1 + \gamma(\kappa)]} \tag{18}$$

It has been pointed out [21, 22] that if the calculating $S(\kappa, \omega)$ in the convolution approximation, the width function entering in the Gaussian approximation for $G_s(r, t)$ is taken as

$$\rho(t) = \frac{Dt}{1 + \gamma(\kappa)} \tag{19}$$

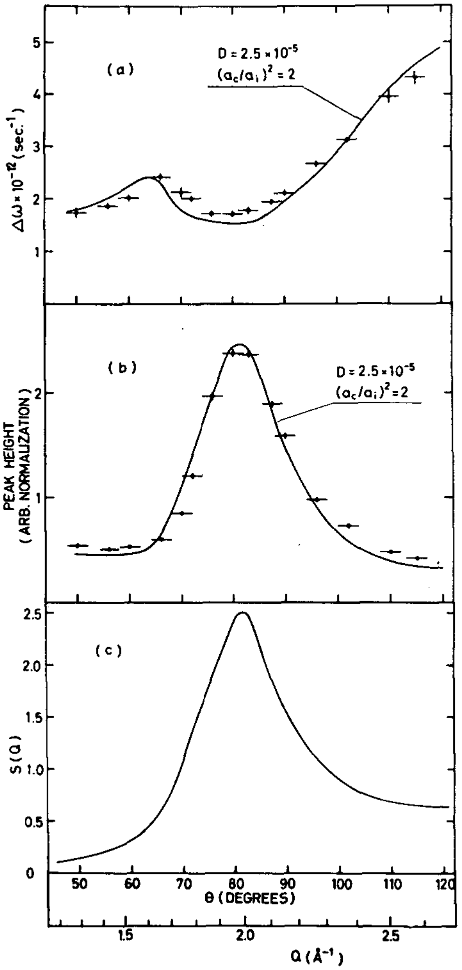

FIG.16. (a) Full width at half height of the quasi-elastic peak in the neutron spectrum from liquid argon at 94°K versus κ. The solid line calculated from formula (20). (b) Observed and calculated intensity at peak height. (c) Structure factor for liquid argon.

this failure is removed. Thus the quasi-elastic scattering for a mixed incoherent and coherent scattering like argon is calculated from

$$a^2_{\text{total}}\, S(\kappa,\omega)_{\text{total}} = a^2_{\text{inc}} \frac{D\kappa^2}{(D\kappa^2)^2 + \omega^2} + a_{\text{coh}} \frac{D\kappa^2}{\left[\dfrac{D\kappa^2}{1+\gamma(\kappa)}\right]^2 + \omega^2} \qquad (20)$$

If such an expression is used to calculate the width of the quasi-elastic peak, it is found that the oscillatory behaviour is accounted for relatively well (Fig.16). Also it is found that the peak intensity of the quasi-elastic peak is described correctly. Although the physical meaning of this construction is not clear, it seems tempting to speculate that the diffusion coefficient is structure dependent $D' = D/[1+\gamma(\kappa)]$, such that atoms at certain distances from a central atom, i.e. those in the quasi-stable shells round the atom at the origin corresponding to the maxima in g(r), show a lower mobility and lower diffusion constants than those atoms which move in between these shells.

To sum up the experiences on collective motions in liquids gained from coherent scattering of neutrons in monatomic liquids, the following conclusions may be drawn:

(1) The motion of an atom brings about an ordered reaction of the neighbouring atoms out to a distance of at least 10-20 Å.

(2) Within a short-time range of the order of 10^{-12} seconds the configuration round an atom is so rigid that the collective motions bear a strong resemblance to the phonons in the solid. The polarization of the travelling waves may be of the same importance as in a solid such that both longitudinal and transversal travelling waves exist.

(3) On the short-time scale it seems probable that the atoms in the shells of neighbours to any atom form a fairly rigid configuration and are less able to diffuse than those in between these shells.

It is seen that these conclusions are in satisfactory agreement with the conclusions drawn from the incoherent scatterers. The total picture obtained in one in which a stability of motion exists for a period of the order of a few times 10^{-12} seconds during which a transient behaviour occurs. This stability in time corresponds to a stability in space ranging to a distance of 10-20 Å from a selected atom. This may mean that a wave is damped out in about one or two wavelengths. The diffusive process seems to have an elementary cycle determined by a step and a damped vibration, a process which may be described as a mixture of one larger step and several smaller ones.

4. EXPERIMENTAL EVIDENCE FROM SCATTERING EXPERIMENTS ON MOLECULAR LIQUIDS

A great number of neutron scattering experiments were performed on molecular liquids of various degrees of complexity from methane [22, 41] and alcohols [42-45] to complex molecular liquids like cyclopentane [46], methylcyclohexane [46], water [47-49], glycerol [43, 44] and others. All these molecules contain hydrogen, which is an incoherent neutron scatterer and therefore all the motions of the protons are displayed in the observed neutron spectra. The broad inelastic spectra observed are associated with energy transfers in the translational, rotational and vibrational spectra of the molecule or its constituents. In one category of analysis of neutron scattering data on molecular liquids the interest is focussed upon this large energy transfer (ΔE) region with (say) 4 MeV $< \Delta E <$ 100 MeV. This region gives information mostly of the same nature as is obtained in Raman and infrared spectra, namely about the rotational-vibrational spectra. The main difference is that there are no selection rules effective in forming the scattered intensity in the neutron case, which in the case of electromagnetic radiation is a dominant feature. In another category of analysis the interest is focussed on near-elastic scattering, which gives information on the diffusive motions and on the transition region between diffusive, long-time motions and short-time motions [43, 44, 50]. In the ideal case of analysis both regions should be covered in one treatment. The difficulty of this problem has limited the number of theoretical attempts to simple cases [30, 41, 51-53].

In most of the interpretation work performed up to about 1965 upon the near-elastic neutron scattering from the molecular hydrogenous liquids it was assumed that the centre-of-gravity motion plays a leading role. No consideration was given to rotational effects [9-14]. In recent work it has been shown that the effect of molecular reorientations and librational motions play an important role in the time domain of neutron observations and have to be included in every theory or model that aims at an understanding of the scattering picture in the near-elastic region. This is particularly important for molecules containing heavier atoms (not methane) like carbon, oxygen etc. which may take part in a rotational reorientation (for instance pentane). The reorientational motions may be described by considering the angular auto-correlation function $\langle\vec{u}(0)\cdot\vec{u}(t)\rangle$ for the molecules, where $\vec{u}$ is a unit vector fixed to the molecule. From recent neutron experiments [22, 44, 46, 53] it seems probable that $\langle\vec{u}(0)\cdot\vec{u}(t)\rangle$ has a behaviour similar to $\langle\vec{v}(0)\cdot\vec{v}(t)\rangle$ for the centre-of-gravity motion.

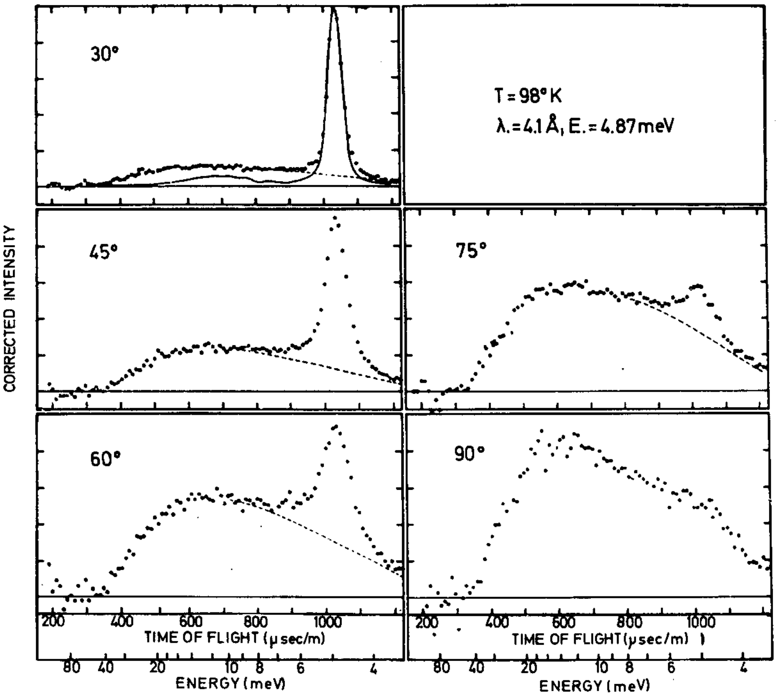

FIG. 17. Observed neutron spectra scattered from liquid methane at 98°K and various angles of observation showing the broad inelastic spectrum of rotational-translational nature and the quasi-elastic peak with a strong angular dependence of intensity and width. Ingoing neutron energy 5 meV corresponding to a wavelength of 4 Å.

The short-time behaviour of $<\vec{u}(0)\cdot\vec{u}(t)>$ is probably a damped oscillatory motion whose Fourier transform leads to a frequency distribution with contributions in both the long-time diffusive region at small ω values and in the short-time region of torsional oscillations at larger ω values. The scattered energy distribution of neutrons due to torsional oscillations and angular reorientations of a molecule is thus expected to look much like the spectrum obtained for the centre-of-gravity motion for an incoherent scatterer (compare Fig. 2 for liquid sodium). It is obvious that if the librational mass is large, the rotational part of the measured neutron spectrum may be concentrated near the ingoing energy because classically the rotational frequency is $\Omega = (kT/I)^{\frac{1}{2}}$, i.e. Ω is small for a large moment of inertia, I, of the molecule and the energy transfer, $\hbar\omega$, ought to be about $\approx \hbar\Omega$. On the other hand, for a molecule like methane where the protons are performing the rotational motions, or when a part of a molecule like a CH_3 group performs the free or hindered rotation, I is small and the rotational contribution to the observed neutron spectrum is expected to range out to large energy transfers, which is also observed. Examples of the spectra observed for liquid methane are shown in Fig. 17. Due to the different nature of the scattering from hydrogen (incoherent and large cross-section) and deuterium (mainly coherent and small cross-section), a method of identifying the motion is offered by a substitution technique [45]. Examples of the scattering from CD_3OH and CH_3OD are shown in Fig. 18, where one may also see that the rotational spectrum of the CH_3 group ranges out to large energy transfers, $\hbar\omega$, as for methane.

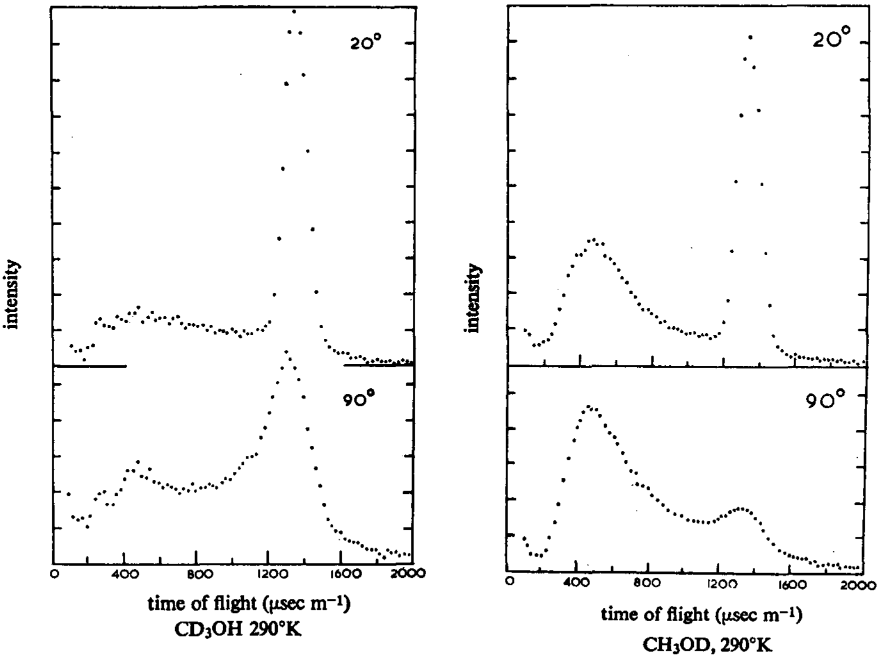

FIG. 18. Scattered neutron spectra obtained from CD_3OH and CH_3OD at 290°K and at scattering angles of 20° and 90°. Ingoing neutron wavelength 5.3 Å or 1340 μsec/m.

In contrast to these observations, Fig. 19 shows a high resolution study of the near-elastic scattering region for pentane from which it is seen that the hindered rotational motions of such a large and heavy molecule gives a scattered neutron spectrum close to the ingoing energy. It is also seen that in all cases a quasi-elastic peak is observed, the intensity of which decays rapidly with increasing κ (increasing angle of observation).

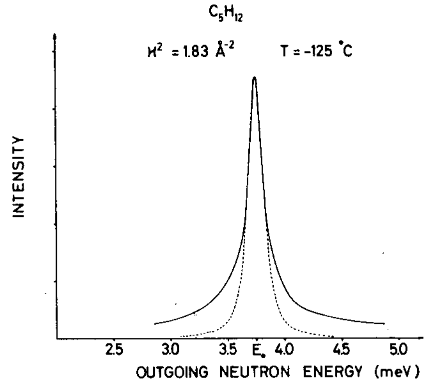

FIG. 19. Experimentally observed quasi-elastic region for pentane at 148°K for 3.74 meV ingoing neutron energy (full line). For comparison a Lorentzian curve of the same width as the central part of the peak is shown (dashed line). The observed shape suggests that the peak should be divided into two components: a narrow truly quasi-elastic and a broader, which may be inelastic in nature.

Considering only incoherent scattering of neutrons, the formulation of the complete self-correlation function $G_s(r,t)$ for a proton performing free or hindered rotational motion as well as vibrational motion relative to the centre of gravity of the molecule, which in turn may perform motions of the type discussed above for simple liquids, can in principle be formulated. The position, $\vec{r}$, of the scattering proton is expressed as the sum of a centre-of-mass position, $\vec{r}'$, and the position of the proton relative to the centre-of-mass $\vec{b} = \vec{r} - \vec{r}'$. For the centre-of-gravity motion, $g_e(r', t)$, as well as for the relative motion, $g_i(\vec{b}, t)$, a Gaussian distribution in space is assumed: the position of the proton at a certain time is given by

$$G_s(r,t) = \int g_e(\vec{r}', t)\, g_i(\vec{r} - \vec{r}', t)\, d\vec{r}' \qquad (21)$$

It is assumed that there is no coupling between the rotational and the translational motions such that $\vec{r}'$ and $\vec{b}$ are dynamically independent. It is easy to extend the formulation in the same approximation to include vibratory motions of the proton, which is, however, of little interest as the vibrations are exited only at higher temperatures and the zero-point amplitude of true vibrational motion is small.

The intermediate scattering function $\int G_s(r,t)\, e^{i\vec{\kappa}\vec{r}}\, d\vec{r} = F_s(\kappa, t)$ is simply

$$F_s(\kappa, t) = F_s(\kappa, t)_e \cdot F_s(\kappa, t)_i = e^{-\kappa^2 \rho(t)} \qquad (22)$$

where

$$\rho(t) = \rho_e(t) + \rho_i(t) = \langle [r'_\kappa(t) - r'(0)_\kappa]^2 \rangle + \langle [b_\kappa(t) - b_\kappa(0)]^2 \rangle \qquad (23)$$

where subscript κ denotes the vector component along κ. It is seen that the scattering function $S_s(\kappa, \omega)$ will be:

$$S_s(\kappa, \omega) = \int_{-\infty}^{+\infty} S_e(\kappa, \omega - \omega')S_i(\kappa, \omega')\, d\omega' \qquad (24)$$

All the physics of the rotational motion is hidden in the term $\langle (b_\kappa(t) - b_\kappa(0))^2 \rangle$, which might be written

$$\langle (b_\kappa(t) - b_\kappa(0))^2 \rangle = 2b_\kappa(0)^2 \left[1 - \frac{b_\kappa(t)\, b_\kappa(0)}{b_\kappa(0)^2}\right] = \frac{2}{3} b^2 \left(1 - \frac{b_\kappa(t)\, b_\kappa(0)}{b_\kappa(0)^2}\right) \qquad (25)$$

where $b_\kappa(t)b_\kappa(0)/\langle b_\kappa(0)^2 \rangle$ simply describes the correlation of a molecular axis at $t = 0$ with itself at a time t later. It is called the rotational correlation function. These functions are unknown for strongly hindered rotations, approximations have been proposed for the weakly hindered rotations [52], and exact expressions are available for the free rotations [51, 55]. In general it is to be expected that in the condensed state of matter the molecular rotations are more or less strongly hindered.
The limiting behaviours of the rotational correlation function for small times and for long times may be guessed as for the centre of gravity motion discussed in connection with simple liquids in section 3. At short times the correlation function ought classically to start as $1 - (kT/I)t^2$ giving $\rho_i(t) = (2b^2/3)(k_B T/I)t^2$. This is in strict analogy with the centre-of-gravity motion and simply means that the reorientation of a molecule occurs without interaction of forces from neighbours at the start. On the other hand, the long-time behaviour of the correlation function is expected to be an exponential decay. Such an assumption would lead to a simple diffusive behaviour for the molecular orientation at longer times. It would be reasonable to give $g_i(\vec{b}, t)$ in the long-time limit a form which could be found from a diffusion equation

$$D_r \Delta g_i(\vec{b}, t) = \frac{\partial g_i(\vec{b}, t)}{\partial t} \qquad (26)$$

where D_r is a rotational diffusion coefficient. Under certain assumptions [44] the solution of the equation gives a Gaussian form for $g_i(\vec{b}, t)$ with a width $\rho(t) = D_r t$. In such a case we have complete analogy between the rotational and the translational behaviours as evidenced in the behaviours of the correlation functions $\langle \vec{b}(t) \cdot \vec{b}(0) \rangle$ and $\langle v(t) \cdot v(0) \rangle$ and of $\rho_i(t)$ and $\rho_e(t)$ at short and long times. The important intermediate time range, which might accommodate an oscillatory behaviour of the rotational correlation function is, however, unknown.

An attempt was recently made to use information from optical experiments, infrared and Raman spectra, to calculate the scattering function for the case of weak hindering and an isotropic liquid. It was shown by Sears [52] that if $g_i(\vec{b},t)$ is assumed to be a function that only depends upon the angle between the two directions characterized by the angles Θ_0 and Θ of $\vec{b}$ at $t = 0$ and $t = t$, then $g_i(\vec{b},t)$ may be separated into an angular and a time-dependent part:

$$g_i(\vec{b},t) = g_i(\Theta_0,\Theta,\ t) = \frac{1}{4\pi} \sum_{\ell,m} F_\ell(t)\, Y_\ell^m(\Theta_0)\, Y_\ell^m(\Theta) \tag{27}$$

For all t one has $F_0(t) = 1$.
With this assumption it was shown that if $\kappa b < 1$, the intermediate scattering function may be written

$$F_i(\kappa,t) = 2 \sum_{\ell=0}^{\infty} (2\ell+1) j_\ell(\kappa b)^2 F_\ell(t) \tag{28}$$

where $j_\ell(\kappa b)$ is a spherical Bessel function. Therefore, the rotational scattering function $S_i(\kappa,\omega)$ is given by

$$S_i(\kappa\,\omega) = \sum_{\ell=0}^{\infty} (2\ell+1)\, j_\ell(\kappa b)^2\, S_\ell(\omega) \tag{29}$$

where

$$S_\ell(\omega) = \frac{1}{\pi} \int_0^\infty F_\ell(t) \cos\omega t\, dt \tag{30}$$

As the complete scattering function $S_s(\kappa,\omega)$ is a folding of $S_i(\kappa,\omega)$ and $S_e(\kappa,\omega)$, it is possible to obtain $S_s(\kappa,\omega)$ if some reasonable model is used to get $S_e(\kappa,\omega)$ and if the functions $F_\ell(t)$ are known. The functions $F_1(t)$ and $F_2(t)$ were obtained from a Fourier transform of bands in infrared and Raman spectra [56]. It is argued by Sears that the contribution from higher terms is small which is, however, disputed by Venkataraman et al. [22].

From the form of $S_s(\kappa,\omega)$ and as $F_0(t) = 1$ it is obvious that the three first terms in the expansion of $S_s(\kappa,\omega)$ are:

$\ell = 0$ $\quad S_0(\omega) = \delta(\omega) \qquad S_s(\kappa,\omega)_{\ell=0} = 2j_0(\kappa b)^2 S_e(\kappa,\omega)$

$\ell = 1$ $\quad S_1(\omega) = \frac{1}{\pi}\int_0^\infty F_1(t)\cos\omega t\, dt$

$$S_s(\kappa,\omega)_{\ell=1} = 6j_1(\kappa b)^2 \int_{-\infty}^{+\infty} S_e(\kappa,\omega-\omega')S_1(\omega')d\omega'$$

$$\ell = 2 \quad S_2(\omega) = \frac{1}{\pi}\int_0^{\infty} F_2(t)\cos\omega t\,dt$$

$$S_s(\kappa,\omega)_{\ell=2} = 10j_2(\kappa b)^2 \int_{-\infty}^{+\infty} S_e(\kappa,\omega-\omega')S_2(\omega')d\omega' \tag{31}$$

It is seen that the spherical Bessel function $j_0(\kappa b)^2$ acts like a Debye-Waller factor on the quasi-elastic peak which is caused by the centre-of-gravity motion.

Using these arguments and the itinerant oscillator model [15] for the centre-of-gravity motion, Sears calculated [53] the scattered spectrum for liquid methane and compared the result with measurements of Dasannacharya et al. [30] (Fig. 20). The main lines are reproduced by the theory but the detailed fit is moderately good.

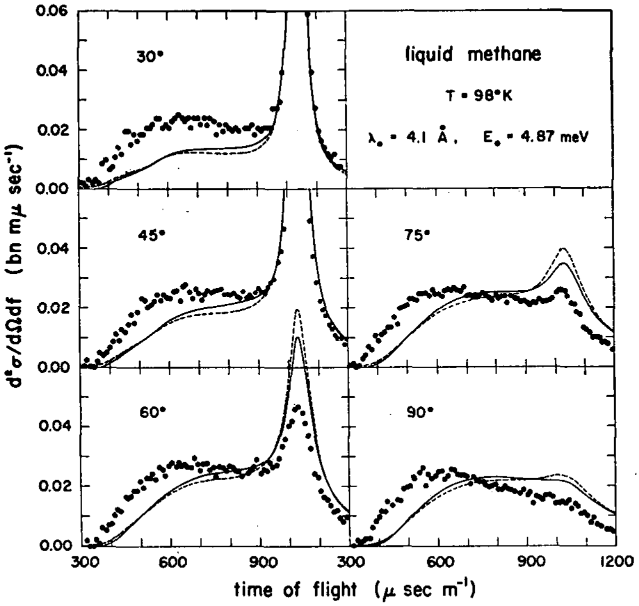

FIG. 20. Calculated time-of-flight distributions for liquid methane at 98°K on the basis of Sears theory compared to the observed distribution. Only three terms in the partial wave expansion of $S(\kappa,\omega)$ are included, namely for $\ell = 0$, 1 and 2.

The idea of identifying the rotational correlation function $<b_\kappa(t)\cdot b_\kappa(0)>$ with the Fourier transform of an infrared vibration band, $I(\omega)$, has been explored by Agrawal and Yip [57]. The method consists in writing

$$\frac{2}{3}b^2\left(1-\frac{b_\kappa(t)\,b_\kappa(0)}{b_\kappa(0)^2}\right)=\frac{2}{3}b^2\left[1-\int_{-\infty}^{+\infty}d\omega\,e^{i\omega t}\,I(\omega)\right] \qquad (32)$$

For liquid methane these authors described the centre-of-gravity motion by the Langevin equation. It was, however, found that to obtain a fit to the experimental data on methane, a value of the friction constant $\eta = 4\times10^{12}$ sec^{-1} had to be used instead of $\eta = 17\times10^{12}$ sec^{-1} derived from the measured diffusion coefficient and the Einstein relation $\eta = k_BT/MD$. This indicates that an effective mass M^* approximately four times the molecular mass has to be used to fit the liquid methane data by Harker and Brugger [58]. Figure 21 shows the various shapes of $\rho(t) = \rho_e(t) + \rho_i(t)$ which were tried.

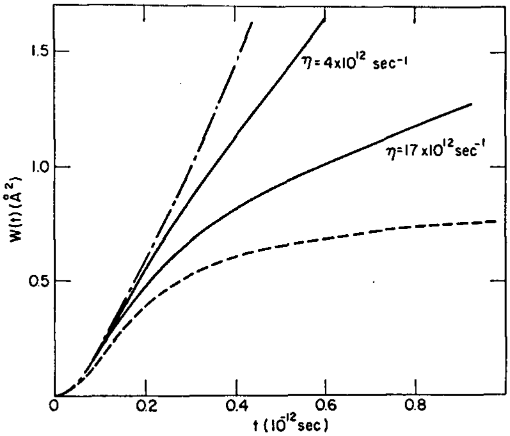

FIG. 21. Mean-square displacement $\rho(t) = \omega(t)$ of a proton in liquid methane as a function of time. The rotational contribution is calculated from Eq.(31) using optical data (dashed curve). The width produced by free translational motions (gas) is given by the broken line. The total $\rho(t) = \rho(t)_{\text{translational}} + \rho(t)_{\text{rotational}}$ is given by the solid lines for two values of the friction constant η in Langevins diffusion equation.

Following the ideas outlined above regarding the short and long-time behaviour of $<\vec{u}(0)\cdot\vec{u}(t)>$, a model for the combined rotational and translational motion was formulated by Larsson [44]. Essentially, the strongly hindered rotational motion is devided into two phases: during the average time, τ_1, the direction of $\vec{b}$ undergoes a larger change, a jump, followed by a diffusive random motion of $\vec{b}$ in small steps on which is superimposed an oscillatory motion which is of torsional character. The second phase of the motion is supposed to continue for a time τ_0. The period of the rotational diffusion cycle is thus $\tau_1 + \tau_0$, accomodating a jump and an oscillatory-diffusive motion. This motion is superimposed on the centre-of-gravity motion, which is in general supposed to be a mixture of large and small step diffusive motion. The cross-section is formulated in an extension of the Singwi-Sjölander formalism in which each step of motion is considered. Because of the considerable complexity of the expressions, only certain limiting cases have so far been considered. If the formulas are limited to cover only the quasi-elastic peak, and mainly its width, it is found that they may be fitted to the observations based on cold neutron scattering from propanol and glycerol and several other liquids [46], using a broad ingoing neutron spectrum. The conclusions of this analysis are:

(a) During a short time, say $(1\text{-}5) \times 10^{-13}$ sec, the direction of $\vec{b}$ changes over a distance of about 1-4 Å. This is a rotational jump.

(b) During a time of the order of $(1\text{-}5) \times 10^{-12}$ sec the direction of $\vec{b}$ oscillates and diffuses over a root-mean-square distance of order 0.5-1 Å.

(c) The correlation function $\langle \vec{b}_\kappa(t) \cdot \vec{b}(0)_\kappa \rangle$ must behave much like $\langle \vec{v}(0) \cdot \vec{v}(t) \rangle$ for the centre of gravity motion, showing a large and rapid decay in about 10^{-13}sec whereafter it oscillates up to about 10^{-12} sec and finally goes over to an exponential decay.

Finally from recent high-resolution studies on pentane and pentanol (compare Ref.[54]) in which a neutron spectrum of a width of 0.1 meV of an energy of 3.7 meV is used, it seems that the quasi-elastic peak in reality has a structure and is divided into a narrow central component and a broader one which may consist of two separate inelastic distributions on each side of the ingoing energy, E_0, and separated from E_0 by 0.5-1 meV. From the κ and temperature-dependence of the broad contribution it seems to follow the laws typical for a one-phonon spectrum. This indicates that the near-elastic scattering really has two components: one due to diffusive motions of the centre of gravity and due to small step proton motion relative to the centre of gravity; the other due to energy transfers in a torson spectrum. The origin of these components requires, however, a closer experimental and theoretical investigation.

CONCLUSIONS

The present neutron scattering of both monatomic and molecular liquids have revealed considerable detail of the nature of the diffusive process. The elementary cycles of the translational and the rotational motions seem to both consist of transient oscillatory phenomena of short duration. The stability of an atomic or molecular configuration in space over a time of the order of 10^{-12} seconds allows the existence of collective motions of phonon and probably also of torson character. Further high resolution work is necessary to solve the problems connected to the detailed understanding of these phenomena.

REFERENCES

[1] LARSSON, K.-E., DAHLBORG, U., HOLMRYD, S., Ark. Fys. 17 (1960) 369.

[2] BROCKHOUSE, B.N., ARASE, T., CAGLIOTI, G., SAKAMOTO, M., SINCLAIR, R.N., WOODS, A.D.B., Inelastic Scattering of Neutrons in Solids and Liquids (Proc. Symp. Vienna, 1960), IAEA, Vienna (1961) 531.

[3] SJÖLANDER, A., Ark. Fys. 14 (1958) 315.

[4] WEINSTOCK, R., Phys. Rev. 65 (1944) 1.

[5] DAHLBORG, U., LARSSON, K.-E., Ark. Fys. 33 (1965) 271.

[6] COCKING, S.J., Studies of the liquid state using the inelastic scattering of slow neutrons, Dissertation University of London (1967).

[7] SKÖLD, K., LARSSON, K.-E., Phys. Rev. 161 (1967) 102.

[8] CHEN, S.H., EDER, O.J., EGELSTAFF, P.A., HAYWOOD, B.C.G., WEBB, F.J., Phys. Lett. 19 (1965) 269.

[9] SINGWI, K.S., SJÖLANDER, A., Phys. Rev. 119 (1960) 863.

[10] OSKOTSKII, V.S., Soviet Phys.-Sol.State 5 (1963) 789.

[11] CHUDLEY, C.T., ELLIOTT, R.J., Proc. phys. Soc. 77 (1961) 353.

[12] EGELSTAFF, P.A., SCHOFIELD, P., Nucl. Sci. Engng 12 (1962) 260.

[13] RAHMAN, A., SINGWI, K.S., SJÖLANDER, A., Phys. Rev. 126 (1962) 997.

[14] ARDENTE, V., NARDELLI, G.F., REATTO, L., Phys. Rev. 148 (1966) 124.

[15] SEARS, V.F., Proc. phys. Soc. 86 (1965) 953.

[16] KROÓ, N., BORGONOVI, G., SKÖLD, K., LARSSON, K.-E., Phys. Rev. Lett. 12 (1964) 721.

[17] RANDOLPH, P.D., SINGWI, K.S., Phys. Rev. 152 (1966) 99.

[18] DORNER, B., PLESSER, T., STILLER, H., The Structure and Properties of Liquids, Disc. Faraday Soc. 43 (1967) 160.

[19] BROCKHOUSE, B.N., POPE, N.K., Phys. Rev. Lett. 3 (1959) 259.

[20] RANDOLPH, P.D., Phys. Rev. 134 (1964) A1238.

[21] SKÖLD, K., Phys. Rev. Lett. 19 (1967) 1023.

[22] VENKATARAMAN, G., DASANNACHARYA, B.A., RAO, K.R., Phys. Rev. 161 (1967) 133.

[23] NIJBOER, B.R.A., RAHMAN, A., Physica 32 (1966) 415.

[24] RAHMAN, A., SINGWI, K.S., SJÖLANDER, A., Phys. Rev. 126 (1962) 997.

[25] EGELSTAFF, P.A., SCHOFIELD, P., Nucl. Sci. Engng 12 (1962) 260.

[26] CHUDLEY, C.T., ELLIOTT, R.J., Proc. phys. Soc. 77 (1960) 353.

[27] SINGWI, K.S., SJÖLANDER, A., Phys. Rev. 119 (1960) 863.

[28] OSKOTSKII, V.S., Soviet Phys.-Sol.State 5 (1963) 789.

[29] SEARS, V.F., Proc. phys. Soc. 86 (1965) 953.

[30] DASANNACHARYA, B.A., RAO, K.R., Phys. Rev. 137 (1965) A417.

[31] LARSSON, K.-E., Inelastic Scattering of Neutrons (Proc. Symp. Bombay, 1964) 2, IAEA, Vienna (1965) 3; see particularly discussion pp 26, 27.

[32] RAHMAN, A., Phys. Rev. 136 (1964) A405.

[33] VINEYARD, G.H., Phys. Rev. 110 (1958) 999.

[34] EGELSTAFF, P.A., Rep. AERE-R4101 (1962).

[35] SINGWI, K.S., Phys. Rev. 136 (1964) A969.

[36] SINGWI, K.S., Physica 31 (1965).

[37] SINGWI, K.S., FELDMAN, G., Inelastic Scattering of Neutrons (Proc. Symp. Bombay, 1964) 2, IAEA, Vienna (1965) 85.

[38] COCKING, S.J., EGELSTAFF, P.A., Phys. Lett. 16 (1965) 130.

[39] de GENNES, P.G., Physica 25 (1959) 825.

[40] BROCKHOUSE, B.N., BERGSMA, J., DASANNACHARYA, B.A., POPE, N.K., Inelastic Scattering of Neutrons in Solids and Liquids (Proc. Symp. Chalk River, 1962) 1, IAEA, Vienna (1963) 189.

[41] DASANNACHARYA, B.A., VENKATARAMAN, G., Phys. Rev. 156 (1967) 196.

[42] SAUNDERSON, D.H., RAINEY, V.S., Inelastic Scattering of Neutrons in Solids and Liquids (Proc. Symp. Chalk River, 1962) 1, IAEA, Vienna (1963) 413.

[43] LARSSON, K.-E., OUEROZ DO AMARAL, L., IVANTCHEV, N., RIPEANU, S., BERGSTEDT, L., DAHLBORG, U., Phys. Rev. 151 (1966) 126.

[44] LARSSON, K.-E., Phys. Rev. 167 (1968) 171.

[45] ALDRED, B.K., EDEN. R.C., WHITE, J.W., The Structure and Properties of Liquids, Disc. Faraday Soc. 43 (1967) 169.

[46] de GRAAF, L.A., Dissertation Technical Highschool Delft (1968).

[47] SAKAMOTO, M., BROCKHOUSE, B.N., JOHNSON, R.H., POPE, N.K., J. Phys. Soc. Japan 17 Suppl. B-11 (1962) 370.

[48] HAYWOOD, B.C., J. nucl. Energy 21 (1967) 249.

[49] SZKATULA, A., FULINSKI, A., Physica 36 (1967) 35.

[50] LARSSON, K.-E., BERGSTEDT, L., Phys. Rev. 151 (1966) 117.

[51] SEARS, V.F., Can. J. Phys. 44 (1966) 1279.

[52] SEARS, V.F., Can. J. Phys. 44 (1966) 1299.

[53] SEARS, V.F., Can. J. Phys. 45 (1967) 237.
[54] DAHLBORG, U., FRIBERG, B., LARSSON, K.-E., PIRKMAJER, E., "New results on quasi-elastic scattering from some hydrogenous liquids", these Proceedings, SM-104/36.
[55] AGRAWAL, A.K., YIP, S., private communication (1968).
[56] GORDON, R.G., J. chem. Phys. 43 (1965) 1307.
[57] AGRAWAL, A.K., YIP, S., J. chem. Phys. 46 (1967) 1999.
[58] HARKER, Y.D., BRUGGER, R.M., J. chem. Phys. 42 (1965) 275.

DISCUSSION

G. JANNINK: The available energy resolution permits observation of departure from Lorentzian behaviour in these narrow quasi-elastic peaks. There are many predictions of non-Lorentzian shapes, reflecting several diffusive motions; however, none seems to be actually observable.

O.J. EDER: What is the physical meaning of the diffusion constant in the coherent scattering part?

K.-E. LARSSON: This meaning is naturally independent of the neutron scattering process: it is a property of the liquid investigated. But what I proposed in my paper was that the diffusion constant has a time structure as shown in the incoherent scattering case, and that it also has a spatial structure as indicated by the coherent scattering results. Of course, since it is an integral magnitude, the diffusion constant as normally studied is a number without any time or space dependence.

A. RAHMAN: The interpretation of scattering from liquid argon is apparently made in two quite contradictory ways. On the one hand, the method of scaling κ employs a purely diffusive Lorentzian, and on the other hand the extreme crystalline model likewise gives a good fit. Is this significant?

K.-E. LARSSON: We are still awaiting a theory which will be able to account simultaneously for the low-frequency diffusive motion and the high-frequency vibratory – you might say 'solid-like' - motion of an atom in a liquid. Until such a theory has been put forward we have to resort to approximations. When we say that a single Lorentzian with a width determined by simple diffusion behaviour fits the quasi-elastic line, this has to mean that the deviation from Langevin diffusive behaviour characterized by $t_\beta = MD/k_B T$ is small in the case of liquid argon. In the language I have used in the paper this means that the delay time for diffusion, which on the basis of your stochastic model may for instance be defined by $(\omega_D/\omega')^3$ $(MD/k_B T)$, does not deviate much from t_β. Subject to the limits of accuracy imposed by the experimental errors in respect of D and of the neutron scattering experiment, we do not observe this small difference. I believe that the frequency distribution for 'liquid argon' which Mr. Rahman has derived in his machine computations indicates a relatively small deviation from a Langevin behaviour. These facts taken together explain why an apparent contradiction occurs.

B. MOZER: My colleagues and myself have recently measured the inelastic spectrum of a completely incoherent metal alloy ($Cu_{52.5}$ $Ni^{62}_{47.5}$), in the solid and in the liquid states. The structure observed in the solid is completely smeared out in the liquid, especially the structure associated with transverse modes in the solid. Furthermore, high-energy excitations appear in the liquid which are not observed in the solid just below the melt. Out liquid frequency distributions do not resemble those assumed for similar fcc metals and indicate that some modifications are necessary for interpreting existing data. In addition anharmonic effects are noted which produce additional smearing of the solid spectra at high temperature; these effects should not be neglected in the theory of the liquid.

K.-E. LARSSON: On the whole I agree with what you say about the smearing out of the frequency distribution in a liquid. But I do not feel certain that an artificially created incoherent scatterer, like the copper-nickel system which you mention, will behave in the same way as pure melts of the types discussed in my paper. It is possible, is it not, that in the case of an alloy the properties undergo more profound changes after the melting point is passed. Until this question has been definitely cleared up, I consider that the data from the example you have chosen should not be assumed to be universally valid for a monatomic incoherent scattering system.

B.N. BROCKHOUSE: Can anyone explain why the correction to the simple diffusion model made by dividing D by S(Q) is effective, as it seems to be? At all events we should not think of it in terms of the convolution approximation: this approximation has been shown to be a bad one since the moment it was put forward, and it should have been discarded a decade ago! Perhaps a theoretical approach to the correction would indicate why it works.

K.-E. LARSSON: This is certainly an interesting point.

A. RAHMAN: The correction is in fact an artifice which scales κ for coherent scattering to match a κ in incoherent scattering, so as to satisfy the second-moment relation. It is in fact possible to carry the trick further and satisfy the fourth moment as well, by suitably scaling the frequency (or time). I do not think it is possible to produce interpretation of these scaling methods. The fact that scaling improves the fit with the experimental data only emphasizes how important it is that the second and fourth moments should be correctly given by a model.

B.N. BROCKHOUSE: But there is no reason to believe that the second moment theorem applies exclusively to the quasi-elastic part of the spectrum.

A. RAHMAN: This 'trick' - and I repeat the word "trick" advisedly, because it is not on any higher level - is in fact applicable to more than the quasi-elastic part. Yip and Desai have, I think, shown that it covers the inelastic part, and as I mentioned just now I have myself extended it to the fourth moment. It thus works well for the entire omega region.

K.-E. LARSSON: It seems to me that all the models for liquid dynamics put forward so far, including the machine computations, could be of equal value. There is at present no reason to favour one or the other approach to the problem. The model fitting made in connection with the neutron experiments has, however, given a rather clear indication that we are here dealing with a rapid transient phenomenon, which is strongly damped in time and space. Whether this transient is termed a 'phonon' or not seems largely immaterial.

B. DORNER: You explained the first maximum in the liquid structure factor in terms of an arrangement of several reciprocal lattice vectors.

Singwi, on the other hand, tries to explain the inelastic scattering from a liquid without introducing any reciprocal lattice vector. May I ask, therefore, whether you prefer a 'solid-like' interpretation?

K.-E. LARSSON: In a recent paper, Cocking showed that the Singwi and Egelstaff models are identical if the range of coherence R goes to infinity and if the polarization is not included. This means that in neither model is it necessary to postulate the existence of a reciprocal lattice vector. I am not particularly fond of a 'solid-like' interpretation of data: I prefer just to say that the neutron experiments indicate certain similarities in the high-frequency region.

PHONONS IN LIQUID BISMUTH STUDIED BY NEUTRON INELASTIC SCATTERING

E. TUNKELO, R. KUOPPAMÄKI AND A. PALMGREN
REACTOR LABORATORY,
TECHNICAL UNIVERSITY OF HELSINKI,
FINLAND

Abstract

PHONONS IN LIQUID BISMUTH STUDIED BY NEUTRON INELASTIC SCATTERING. Inelastic scattering of cold neutrons in liquid and solid polycrystalline bismuth was studied using the cold neutron facility at FiR 1 reactor in Helsinki. 5-MeV neutrons were incident on the sample and scattering angles ranging from 7.5° to 30° were used. The liquid sample used was at 280°C and the solid sample at 262°C. Similar peaks in the scattered intensity were observed both for liquid and solid samples. These were attributed to the coherent one-phonon scattering, thus leading to construction of a (ω, Q) relation similar to a dispersion curve, averaged over all possible directions of wavevectors. Both transverse and longitudinal branches of the acoustic modes were observed in the liquid as well as in the polycrystalline solid. Dispersion curves obtained for the liquid are similar to those of the solid, but the frequencies of the longitudinal branch are about 65% of those of the solid. This value is equal to the ratio of the sound velocities in liquid and solid bismuth. The intensity distribution of the scattered neutrons is analysed and it is shown that the peaks can be attributed to single phonon-like excitations, while contributions from higher Brillouin zones do not produce disturbing peaks. From this calculation it was further possible to conclude that the angle between the polarization vectors of the so-called transverse modes and the direction of propagation varies in the region of 70° to 110°.

1. INTRODUCTION

In liquids the kinetic energy of the particles is comparable with the interaction energy. Therefore the liquid phase cannot be extrapolated to an ideal state, for which the N-particle problem may be reduced to a number of one-particle problems. As a consequence the liquid state can be described rigorously for two limiting regions of space and time only: for very small times and distances, where all systems behave like a gas, and for very large times and distances, where the equations of hydrodynamics are valid. For the intermediate region the description is in most cases based on models which require experimental testing.

Inelastic scattering of neutrons offers, at least in principle, a method which allows the direct study of the collective exitations of the N-body problem. The double-differential cross-section of a coherent scatterer gives directly the energy-wavevector dependence or dispersion law of these exitations, as shown by Van Hove. Though experimental conditions limit the accessible time and space region where this is possible to 10^{-13} to 10^{-11} sec and 0.5 to 20Å which is only a part of the intermediate region mentioned, it is useful to try to find out what can be obtained by using this method.

As the experimental results of neutron inelastic scattering in liquids very much resemble those in solid materials [1, 2], it is tempting to use the same name, phonon, for the collective excitations in liquids as for those found in solids. This must be done, however, with a certain precaution, namely, remembering that this model applies only in the region of time and interatomic distances which are effective in the inelastic scattering experiment.

To study this effect in more detail, a series of measurements were performed using liquid bismuth as a scatterer at temperatures slightly above and below the melting point which is 271°C. Bismuth was selected as sample material for this study because it has several advantageous features as judged from the practical side of the work, and has not been studied before. Those advantageous features are: it is a heavy liquid so that a classical description of its atomic motion is good enough for the present purposes; it has a low melting point; and its scattering cross-section is completely coherent. A negative feature is that the crystal structure of bismuth is trigonal. This low symmetry would make a detailed study of individual phonons rather complicated, but it was thought that in a liquid in which there is an almost completely isotropic mixture of crystallites with different orientations, similar to that in a fine powder of solid material, this would not be a serious drawback.

2. EXPERIMENTAL METHOD

Measurements were performed using the cold neutron facility [3] at FiR 1. Beryllium-filtered neutrons were incident on the sample and the scattered neutrons were analysed using the time-of-flight technique. Two detectors with flight paths of about 3 metres were used simultaneously. Scattering angles at which measurements were performed were 7.5°, 10°, 12.5°, 16°, 20°, and 30° in order to get as small Q values as possible. The sample was in an electrically heated sample holder surrounded by a large thin-walled aluminium container which was filled with argon to prevent the bismuth from oxidization and to reduce air scattering.

The sample holder was in the form of a rectangular slab with windows made of 0.5 mm anodized aluminium. The sample thickness was 6.0 mm and its transmission was 0.85 and 0.91 when filled with liquid bismuth and solid bismuth powder, respectively. The bismuth used had a purity of 99.999% and the temperature of the sample was kept constant with an accuracy better than ± 2°C. The largest temperature variation over the surface of the sample was ± 3°C. Measurements were performed at sample temperatures of 262°C (solid) and 280°C (liquid).

Data runs and background runs were made consecutively and normalized to the time of measurement. Figures 1 and 2 show examples of data after subtraction of background correction for detector efficiency and air scattering. The calibration of the intensity is based on evaluation of detector efficiencies and solid angle and is therefore rather inaccurate.

3. RESULTS AND DISCUSSION

In the data one observes in both solid and liquid bismuth similar peaks, which may be attributed to phonons or phonon-like collective excitations. If these peaks are plotted in the (ω, Q) plane, a dispersion relation is obtained. This is shown in Figs 3 and 4 for liquid and solid, respectively. Peaks were accepted only if they were found to be statistically significant. In a few cases the identification of a peak was not evident and these were

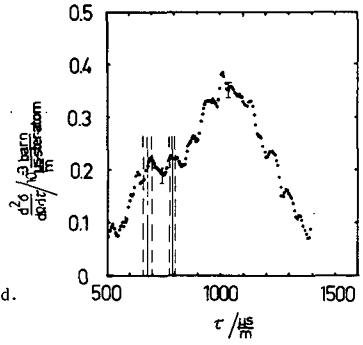

FIG. 1. Raw data at 16° for liquid bismuth, background subtracted.

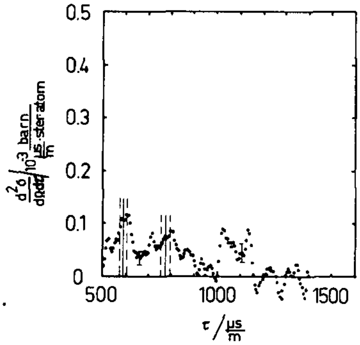

FIG. 2. Raw data at 16° for solid bismuth, background subtracted.

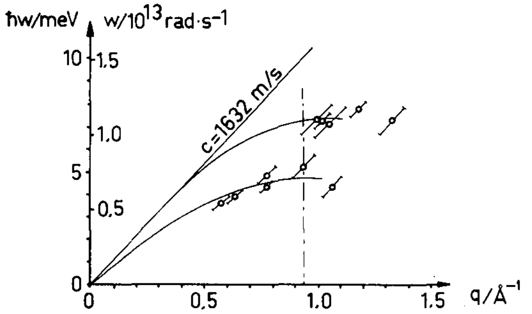

FIG. 3. Average dispersion curve for liquid bismuth as a function of the proper value of the wavevector.

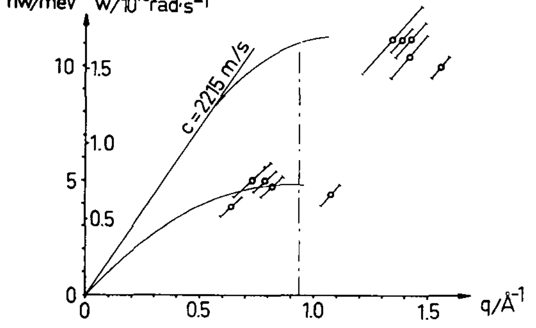

FIG. 4. Average dispersion curve for solid bismuth as a function of the proper value of the wavevector.

not included. The dispersion relations obtained are, of course, not directly comparable with the proper dispersion curves of phonons as they are not taken in any specific orientation of the crystal but are averages over all directions of the Q vector.

The dispersion relations are in agreement with those obtained through measurements with single crystals [4]. Both longitudinal and transverse branches seem to be observable. It is somewhat suprising that transverse phonons are observed in the first Brillouin zone. This may be understood as follows. The so-called transverse branch represents modes which are really transverse only in the symmetry directions. In the off-symmetry directions the polarization vector may have a small longitudinal component which will give enough intensity for these phonons to be observed. As this seems to be the case for both solid and liquid, one may conclude that the liquid has also in the atomic scale a rigidity which is strong enough to let transverse vibrations propagate and that their mean lifetime is at least of the order of the interaction time of the cold neutrons with the matter.

The frequencies of the longitudinal phonons in liquid bismuth is about 65% of those of similar phonons in the solid. This value is almost the same as the ratio of sound velocities in liquid and solid bismuth. The frequencies of the transverse modes are not appreciably changed when going from solid to liquid.

To understand the scattering completely, one should be able to interpret the scattered intensity completely, not only the position of the peaks observed. If the change of the wavevector (Q) in the scattering process were smaller than one half of the value corresponding to the distance of the closest lattice point of the reciprocal lattice, i.e. if the Q were in the first Brillouin zone, there would be no difficulty in interpreting the observed peaks. Now, however, because of experimental limitations it was impossible to go to smaller scattering angles than 7.5°. This means that quite a considerable part of the observed points is in the second Brillouin zone. Accordingly, there is a danger that intensity maxima could be produced through processes in which the lattice takes part of the change of momentum. This would lead to uncertainty in to what Q value the observed peak is to be attributed. To clarify the situation, calculations of all other processes ($\tau \neq 0$) were performed. These are reported in more detail later in this paper. This study shows that the observed peaks can be attributed to processes in which the momentum is transferred to the phonon only. All processes in which momentum is given to the lattice lead, at least under the present experimental conditions, to a rather broad distribution of scattered intensity. Thus the final conclusion is that the dispersion curves obtained really represent the properties of the collective excitations in liquid bismuth. Additionally one may show that the observed intensity of the transverse peaks implies that the polarization vector must have a longitudinal component which is on an average at least 25% of the transverse component, i.e. the angle between the polarization vector and direction of propagation varies in the region from 70° to 110°.

In the case of liquid bismuth a quasi-elastic peak is observed. In the solid there is nothing to be observed because the range of Q values of the experiment is smaller than the Q value for the first Bragg reflection. As bismuth is a completely coherent scatterer the 'quasi-elastic peak' should be attributed to elastic scattering corresponding to different values of the wavevector. The observed intensity corresponds approximately to the S(Q) values.

4. SCATTERING FROM HIGHER BRILLOUIN ZONES

The scattering cross-section is calculated, assuming the liquid to be composed of randomly oriented microcrystallites. The differential cross-section for scattering by phonon with frequency ω_f, wavevector q_f and polarization vector $\vec{\alpha}_f$ is, [5]

$$I_{\omega f} = \frac{\sigma_{coh}}{4\pi} \frac{k'}{k} e^{-2W}(e^{-\hbar\omega_f/k_B T} - 1)^{-1} \frac{2\pi^3\hbar(\vec{Q}\cdot\vec{\alpha}_f)^2}{BMN\omega_f}\delta(\vec{Q}-\vec{q}_f+2\pi\vec{\tau})$$

Here M is the mass of the scattering nucleus and B the volume of the unit cell, other symbols have their conventional meanings.

For the following calculations we want to separate the terms with $\tau = 0$ and $\tau \neq 0$, the former being the ones responsible for the single-phonon peaks. The latter is due to processes in which the lattice takes part of the momentum. To obtain the double-differential cross-section $d^2\sigma/d\Omega d\omega$ one has

(a) To integrate over all directions of q_f and α_f

(b) For terms $\tau = 0$, to integrate over all directions of τ

(c) To take a weighted average over ω_f and q_f.

For the last step detailed information of the phonon distribution is needed. This is approximated by assuming that the dispersion curve obtained from the experiment[1] is applicable in the first Brillouin zone. The calculations proceeded as follows [6].

Phonons were reduced to the first Brillouin zone. Their distribution in ω and q is shown in Fig. 5. In this calculation the local symmetry in the liquid bismuth was assumed to be the same as in the solid. Only phonons up to the third Brillouin zone were included in the detailed calculation. The error produced by this can be estimated as follows. If the Brillouin zones are approximated by concentric spheres, the proper value of the wavevector q_n of the phonon belonging to the nth Brillouin zone is defined by the inequation

$$n^{\frac{1}{3}} q_1 \geq q_n \geq (n-1)^{\frac{1}{3}} q_1$$

In actual fact we have to include additionally the fact that the phonons do not have an infinite lifetime. The dominant mechanism of disintegration of phonons is the three-phonon reaction where phonon with wavevector q_1 disintegrates to two phonons (q_2, q_3) in the presence of an anharmonic interaction. The probability of this process is proportional to the square of the matrix element of the interaction operator

$$(H_{if})^2 \sim (q_1 q_2 q_3)^2 \approx q^6$$

---

[1] The actual experimental data was represented with a smooth curve which resembles the dispersion in solid bismuth.

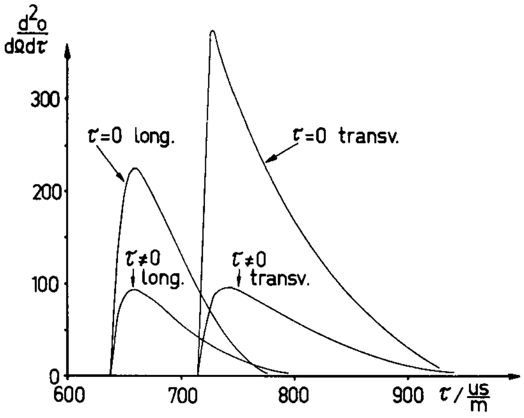

FIG. 5. Calculated inelastic cross-section for $\tau = 0$ and $\tau \neq 0$.

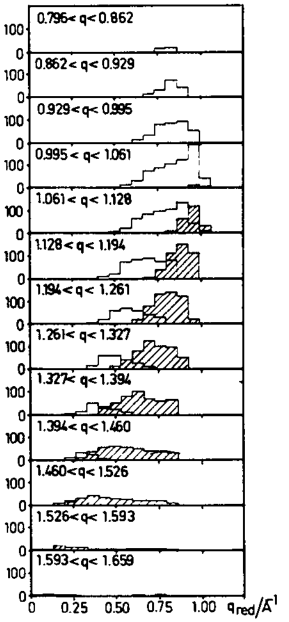

FIG. 6. Distribution in the proper value of reduced wavevector of the phonons. Open areas = second Brillouin zone, shaded areas = third Brillouin zone.

If we assume that the disintegration of phonons leads to two phonons which have approximately the same energy, the density of states is inversely proportional to the propagation velocity, we get for the transition probability $p \sim q^6 v^{-1}$. If the scattering length of the anharmonicities is constant, the collision density of phonons propagating with velocity v is pv. Thus the mean life of the phonons

$$\tau_p(q) = \frac{1}{pv} \sim q^{-6}$$

This factor actually limits the contribution from the higher Brillouin zones.

Accordingly, the number (N_n) of phonons with wavevector q_n satisfies the inequation

$$b(n^{\frac{1}{3}})^{-6} < N_n < b((n-1)^{\frac{1}{3}})^{-6}$$

where b is a constant. Thus approximately

$$N_n \approx \frac{1}{2}[(n-1)^{-2}+n^{-2}]b$$

If we assume that this formula applies even for n = 2, we get after integration

$$\frac{\text{Number of phonons in the zones 2-3}}{\text{Number of phonons in the zones 4-}\infty} = \frac{4}{5}$$

Accordingly, we may assume that the contribution from the fourth and higher zones is equal to what we calculate for the second and third zones.

The integrations of $I_{\omega f}$ were performed numerically and the result for a 16°scattering angle is shown in Fig. 6. The distribution lattice vectors were assumed to be given by the Fourier transformation S(Q) of the pair distribution function, which was taken from Ref. [7]. The averaging over the directions of the propagation vectors was done by assuming them to be isotropic. The fact that the transverse phonons in the first Brillouin zone would not give any intensity was corrected by assuming that they have a longitudinal component. If the average $\langle \vec{\alpha}_f \cdot \vec{q}/q \rangle^2$ is assigned a value of 0.06, the relative intensity of the longitudinal and transverse peaks can be made to fit with the experimental value. Thus one may conclude that the polarization vectors of the 'transverse modes' have a longitudinal component which is about 25% of the transverse component.

As the final conclusion of the calculation one can say that the $\tau = 0$ contribution can be separated from the $\tau \neq 0$ contributions and thus the peaks observed in the experimental data can be attributed to one-phonon scattering which finally means that the dispersion curves really represent the excitations in liquid bismuth.

ACKNOWLEDGEMENT

The authors are indebted to Prof. P. Jauho for fruitful discussions and encouragement.

REFERENCES

[1] COCKING, S.J., EGELSTAFF, P.E., Phys.Lett. 16 (1965) 130.
[2] RANDOLPH, P.D., SINGWI, K.E., Phys.Rev. 152 (1966) 99.
[3] TUNKELO, E., PALMGREN, A., Nucl. Instrum. Meth. 46 (1967) 266.
[4] YARNELL, J.L. et al., IBM J. Res. Develop. 8 (1964) 234.
[5] WEINSTOCK, R., Phys.Rev. 65 (1944) 1.
[6] EGELSTAFF, P.E., UKAEA Rep. AERE-R 4101 (1962).
[7] SHARRAH, P.C., PETZ, J.I., KRUH, R.F., J. chem. Phys. 32 (1960) 241.

MOLECULAR DYNAMICS IN LIQUID NITROGEN AND LIQUID BISMUTH INVESTIGATED BY COLD NEUTRON SCATTERING

N. MATEESCU, H. TEUTSCH, A. DIACONESCU
AND V. NAHORNIAK
INSTITUTE FOR ATOMIC PHYSICS,
BUCHAREST, ROMANIA

Abstract

MOLECULAR DYNAMICS IN LIQUID NITROGEN AND LIQUID BISMUTH INVESTIGATED BY COLD NEUTRON SCATTERING. The neutron scattering law $S(\vec{K},\omega)$ for liquid nitrogen at 77.4°K and liquid bismuth at 560°K was determined using a beryllium filter and time-of-flight technique. The scattered neutron spectra at scattering angles between 15° and 90° for liquid nitrogen and between 60° and 90° for liquid bismuth were measured. After making the necessary corrections for multiple scattering, the experimental results were compared with several theoretical models suggested for the scattering law. In the quasi-elastic range, the best agreement was obtained with the effective mass model. For liquid nitrogen it was found necessary to introduce the contribution of rotational diffusion. In the inelastic range, the dispersion law of quasi-phonons for both liquids was determined according to Egelstaff's quasi-crystalline model.

1. INTRODUCTION

Cold neutron scattering offers a sensitive method for the investigation of the dynamic behaviour of liquids. Information about the space-time correlation of molecular motion is provided by the scattering law $S(\vec{K},\omega)$. In the case of coherent scattering liquids, besides the diffusion motion the existence of a collective motion can also be noticed. Several authors [1-5] have studied such co-operative motions, comparing experimental results of neutrons scattered by monatomic liquids with the existing theoretical models.

Unfortunately, the mathematical formalism deduced on the basis of various models is only valid for restricted ranges in (K,ω) space. On the other hand, owing to the multiple parameters used in these theories, agreement with the experimental results in a given range does not necessarily express a final confirmation of the model in question. The study of new substances and finding new forms of comparison is therefore useful.

This paper contains the results obtained by cold neutron scattering by liquid bismuth - a perfect coherent monatomic scatterer - and by liquid nitrogen, for which collective motion can be studied in the case of a biatomic liquid.

A brief description of the main experimental results and their comparison with various theoretical models are given.

2. EXPERIMENTAL PROCEDURE

The measurements were carried out at the VVR-S reactor in Bucharest with the cold neutron time-of-flight spectrometer whose characteristic data are given in Ref. [6].

The measurements were made with a 4-mm thick sample at 11 scattering angles between 15° and 90° for liquid nitrogen and with a 10-mm thick sample at 6 scattering angles between 60° and 90° for liquid bismuth. The temperature of the liquid bismuth sample was 560 ± 2°K and that of the liquid nitrogen 77.4°K.

Besides the usual corrections, when subtracting the background the spectra measured with the empty container were corrected for the influence of the sample [7].

Because of the width of the incident neutron spectrum, neutrons of different energy and momentum transfers will contribute to the intensity I_f inside a time-of-flight channel. Instead of superposing various theoretical forms on the incident spectrum and thus comparing them with the experimental results, we used a special method [7] allowing to pass from $I_f(\varphi, \lambda)$ to $I_f(K, \hbar\omega)$ for each time-of-flight channel. It should be noted, however, that the $(K, \hbar\omega)$ values obtained for a given channel and for a certain scattering angle:

(a) Are specific for each experimental spectrum;
(b) Do not comprise $\hbar\omega \longrightarrow 0$; and
(c) Two pairs of values, $(K_1, \hbar\omega_1)$ and $(K_2, -\hbar\omega_2)$ are obtained for the quasi-elastic range.

3. EXPERIMENTAL RESULTS AND DISCUSSION

The spectra obtained for either liquid nitrogen or bismuth show a superposition of both quasi-elastic and inelastic ranges so that any real separation of the ranges is impossible. For this reason, we passed from the measured intensities to the symmetrical function $\tilde{S}(K, \hbar\omega)$, in accordance with the computed scale for $(K, \hbar\omega)$, by means of the following relation:

$$I(\varphi, \lambda) = \text{const}\ \frac{d^2\sigma}{d\Omega d\lambda} = \text{const}\ \frac{E_f^2}{\sqrt{E_i}}\, e^{-\frac{\hbar\omega}{2k_BT}}\, \tilde{S}(K, \hbar\omega) \tag{1}$$

where all the notation has the usual meaning.

The curves $\tilde{S}(K, \hbar\omega)_{\hbar\omega=\text{const}}$ were plotted and then the curves $\tilde{S}(K, \hbar\omega)_{K=\text{const}}$ were determined by interpolation. From the latter set of curves the momenta $\overline{\omega^0}$, $\overline{\omega^1}$, $\overline{\omega^2}$ and $\overline{\omega^4}$ were computed. The results of the ratios $\overline{\omega^1}/K^2$ and $\overline{\omega^2}/K^2$ are shown in Fig. 1. The deviations from a constant value of $\overline{\omega^2}/K^2$ and $\overline{\omega^2}/K^2$ for $K < 1.5$ Å^{-1} in the case of liquid nitrogen are due to multiple scattering. Correcting the results for multiple scattering [7], these points will be placed in the vicinity of the straight line determined by the points corresponding to $K > 1.5$ Å^{-1}.

The ratio $\overline{\omega^2}/\overline{\omega^1} = 2k_BT$ represents a test of the values obtained experimentally. Thus, $(2k_BT)^{N_2}_{\text{momentum}} = 13.84$ meV whereas $(2k_BT)^{N_2}_{\text{sample}} = 13.35$ meV, and $(2k_BT)^{Bi}_{\text{momentum}} = 96.10$ meV whereas $(2k_BT)^{Bi}_{\text{sample}} = 96.44$ meV. Taking into account the expression of the first momentum versus the recoil energy, $\overline{\omega^1} = E_rK^2$, the absolute normalization factor for the momenta and for $\tilde{S}(K, \hbar\omega)$ were determined. Thus, $\tilde{S}(K, \hbar\omega)$ is expressed in meV^{-1} and can be directly compared with the theoretical expressions.

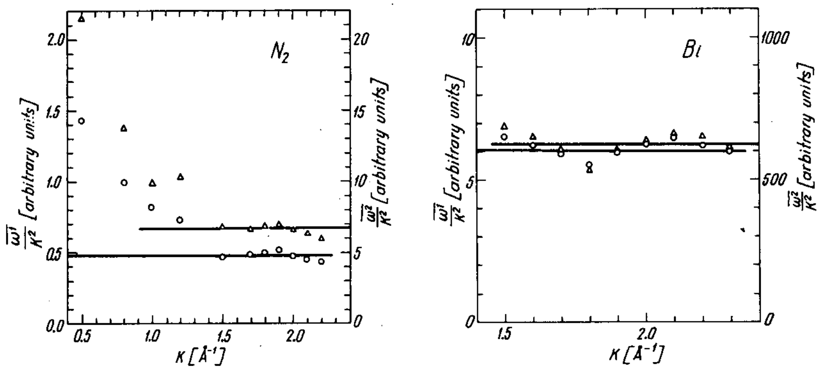

FIG.1. Ratios of the first and second moment to K^2: o - $\overline{\omega^1}/K^2$, Δ - $\overline{\omega^2}/K^2$.

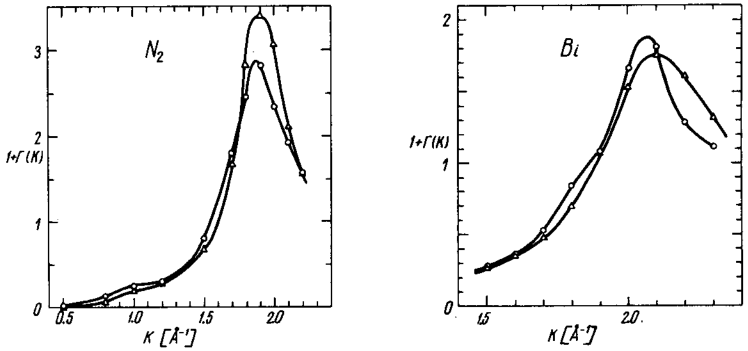

FIG.2. Functions 1 + Γ (K). Liquid nitrogen: o-this experiment, Δ-data of Henshaw et al. [8]; liquid bismuth: o-this experiment, Δ-data of Sharrah et al. [9].

By this normalization, $\overline{\omega^0}$ gives the 1+Γ(K) function directly. In Fig. 2 a difference may be noticed between our results and those obtained for nitrogen by Henshaw et al. [8] and for bismuth at 573°K by Sharrah et al. [9]. This difference would probably have been smaller if, in the integral of momentum, we had considered the geometry of the sample and the absorption of scattered neutrons in the sample [7].

By using de Gennes' approximation [10], a frequency Ω(K) and a diffusion coefficient D(K) was inferred from $\overline{\omega^4}$. The Lorentz form half-widths obtained in Vineyard's convolution approximation [11] with these values of D(K) are shown in Fig. 5, curve 6.

Quasi-elastic range

Two forms of presentation were selected for comparison of experimental results with various theoretical models:

(1) Half-widths at half-height ΔE
(2) Peak values $\tilde{S}(K, 0)$ of the scattering law.

Curve 1' of Fig. 3 represents the experimental half-width values of the $\tilde{S}(K, \hbar\omega)_{K=\text{const}}$ functions for liquid nitrogen. The half-widths of only the Lorentzian component of the experimental functions (curve 1) were determined from the peak values $\tilde{S}(K, 0)$ and $\overline{\omega^0}$, taking the resolution into account. The oscillation of curve 1' with respect to 1 in the neighbourhood of the diffraction peak is determined by an inelastic component extending, in this range, up to the half-width of the functions.

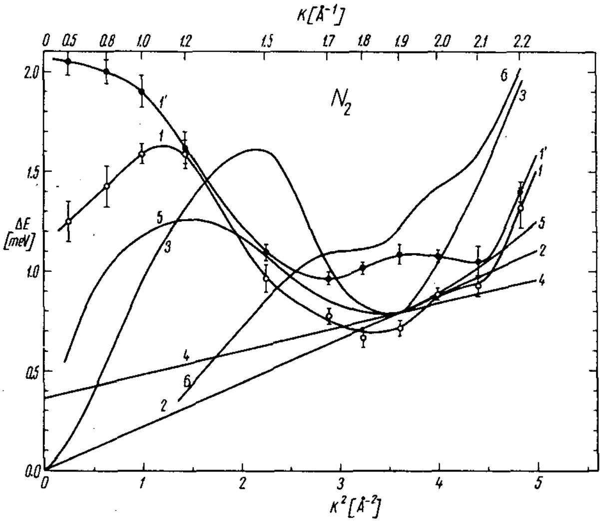

FIG. 3. Half-widths at half-height of function $\tilde{S}(K, \hbar\omega)_{K=\text{const}}$ for liquid nitrogen: 1'- experimental half-widths, 1- Lorentz component of experimental curves, 2- convolution approximation, 3- effective mass model, 4- convolution approximation with rotational diffusion, 5- effective mass model with rotational diffusion, 6- convolution approximation with D(K) from ω^4.

Curve 1 of Fig. 4 shows the experimental peak values $\tilde{S}(K, 0)$.

Curve 1 of Figs 3 and 4 was compared to various Lorentzian forms in accordance with various models. The parameters of the curves were so selected that at $K = 1.9$ Å^{-1} the $\tilde{S}(K, 0)$ values should correspond to the experimental ones.

Thus, curve 2 of Figs 3 and 4 represents the convolution approximation (relation (2) with $D_r = 0$) with the values $a^2_{\text{incoh}}/a^2_{\text{coh}} = 0.09$ [12] and $D = 3.4 \times 10^{-5}$ cm²/sec. As expected, there results from both representations that this model does not correspond to the experimental results for small K values. Singwi's correction function L(R, K) [13] is also not satisfactory, as can be seen from the corresponding correction term $\Delta\tilde{S}(K, 0)_L$ in Fig. 4.

Curve 4 in both figures represents the convolution approximation, in which a term for rotational diffusion was introduced in the intermediate function, and hence

$$\tilde{S}(K, \hbar\omega) = \left[1 + \Gamma(K) + \frac{a^2_{\text{incoh}}}{a^2_{\text{coh}}}\right] \frac{1}{\pi} \frac{1}{\hbar D K^2 + \hbar D_r} \frac{1}{1 + \left(\frac{\hbar\omega}{\hbar D K^2 + \hbar D_r}\right)^2} \qquad (2)$$

where $D_r = 0.50 \times 10^{12}\ s^{-1}$ is the rotational diffusion coefficient and $D = 2.0 \times 10^{-5}\ cm^2/sec$, the two constants being connected by relation (53) of Ref. [14]. This last case shows better agreement with the experimental results.

From the effective mass model [15] (relation (3) with $D_r = 0$) we obtain curve 3, with $D = 9.4 \times 10^{-5}\ cm^2/sec$.

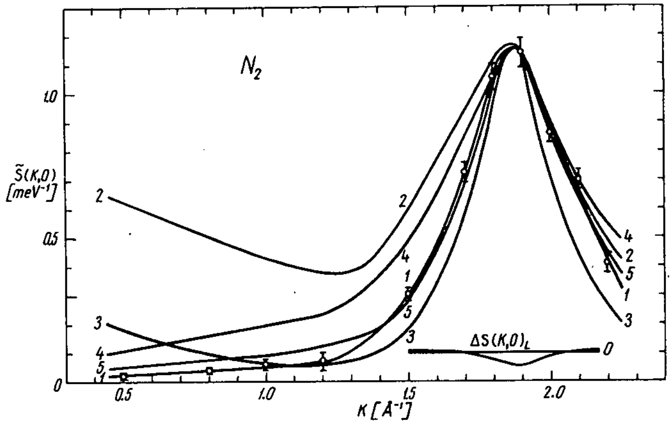

FIG.4. Peak values $\tilde{S}(K, 0)$ for liquid nitrogen: 1- experimental data, 2- convolution approximation, 3- effective mass model, 4- convolution approximation with rotational diffusion, 5- effective mass model with rotational diffusion.

By considering the rotational diffusion contribution according to relation

$$\tilde{S}(K,\hbar\omega) = [1+\Gamma(K)]\,\frac{1}{\pi}\,\frac{1}{\dfrac{\hbar DK^2}{1+\Gamma(k)}+\hbar D_r}\;\frac{1}{1+\left(\dfrac{\hbar\omega}{\dfrac{\hbar DK^2}{1+\Gamma(K)}+\hbar D_r}\right)^2}$$
$$+\frac{a^2_{incoh}}{a^2_{coh}}\,\frac{1}{\pi}\,\frac{1}{\hbar DK^2+\hbar D_r}\;\frac{1}{1+\left(\dfrac{\hbar\omega}{\hbar DK^2+\hbar D_r}\right)^2} \qquad (3)$$

curve 5 with constants $D = 3.2 \times 10^{-5}\ cm^2/sec$ and $D_r = 0.80 \times 10^{12}\ s^{-1}$ is obtained. It can be seen from Figs 3 and 4 that this form gives the best agreement with the experimental results and the values determined for the two diffusion constants are also in good agreement with those quoted by Sears [14] ($D = 3.7 \times 10^{-5}\ cm^2/sec$ and $D_r = 0.93 \times 10^{12}\ s^{-1}$). For still better agreement a value a^2_{incoh}/a^2_{coh} smaller than the one quoted would result.

In Figs 5 and 6 the results of measurements on liquid bismuth (curve 1) are compared with the convolution approximation (curve 2 with $D = 2.0 \times 10^{-5}\ cm^2/sec$) and with the effective mass model (curve 3 with $D = 3.6 \times 10^{-5}\ cm^2/sec$). The correction term computed on the

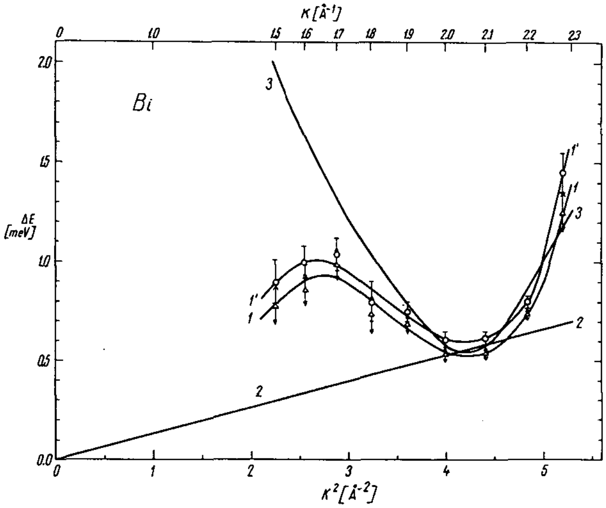

FIG.5. Half-widths at half-height of function $\tilde{S}(K, \hbar\omega)_{K=\text{const}}$ for liquid bismuth: 1- experimental half-widths, 2- convolution approximation, 3- effective mass model.

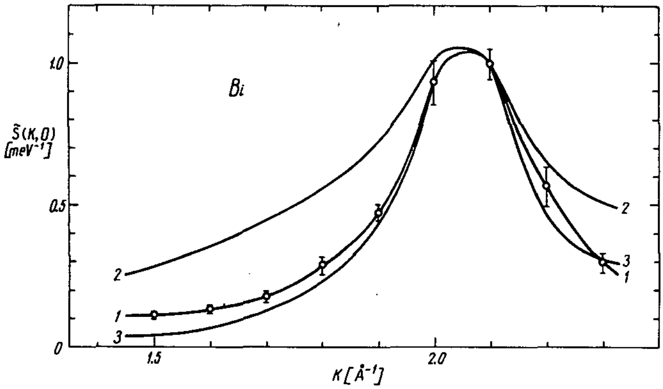

FIG.6. Peak values $\tilde{S}(K, 0)$ for liquid bismuth: 1- experimental data, 2- convolution approximation, 3- effective mass model.

basis of Singwi's theory is very small in the quasi-elastic range and cannot determine any improvement of the convolution approximation. In this case too the effective mass model gives the best agreement with the experimental results, especially in the vicinity of the diffraction peak.

Inelastic range

The following function was computed from the experimental results considering Singwi's theoretical model [13]:

$$Z(K, \hbar\omega) = \frac{S_{exp} - S_{multiphonon}}{S_{1\ phonon}\quad f(\omega)} = 1 + \Gamma(K) + \frac{a^2_{incoh}}{a^2_{coh}} + \operatorname{sech}\left(\frac{\hbar\omega}{2K_BT}\right)\frac{1}{6}\,\frac{\omega^2}{c^2}\,L\,(R, K, q) \tag{4}$$

where, for liquid nitrogen, we considered

$$f(\omega) = f(0)\, e^{-\left(\frac{\omega}{\omega_0}\right)^2} + A\omega^2 e^{-\frac{\omega}{\omega_D}} + B\,\frac{1}{2}\,\frac{I^2\omega^3}{(K_BT)^2}\, e^{-\frac{I\omega^2}{2K_BT}} \tag{5}$$

The parameters A, B and ω_0 were determined from the normalization condition of f(ω), considering three degrees of freedom for the first two terms and two degrees of freedom for the rotational term. The Debye temperature was taken for liquid state according to Mott's formula [16]. The following formula was obtained:

$$f(\omega)\left[\mathrm{meV}^{-1}\right] = 0.400\, e^{-\left(\frac{\hbar\omega}{0.253}\right)^2} + 0.0386\,(h\omega)^2 e^{-2\frac{\hbar\omega}{3.80}} + 0.0180\,(\hbar\omega)^3 e^{-0.150\,(\hbar\omega)^2} \tag{6}$$

For liquid bismuth we only considered for f(ω) the second term of Eq. (5) with $\hbar\omega_D$ = 2.5 meV.

The curves $Z(K, \hbar\omega)_{\hbar\omega = const}$ are shown in Fig. 7 and the function L(R, K, q) in Fig. 8 for liquid nitrogen in the range 5 meV< ħω < 2.5 meV. Their general aspect shows the existence of a dispersion law. The dispersion law of quasi-phonons was directly obtained from $Z(K, \hbar\omega)_{\hbar\omega = const}$ curves by noting the K values of the maxima.

Besides these results, the ones obtained for liquid nitrogen [17] using the methods of Egelstaff and of Kroó et al. [2] are shown in Fig. 9.

It can be observed that the values obtained from $Z(K, \hbar\omega)_{\hbar\omega = const}$ are in agreement with a linear dispersion law (corresponding to the velocity of sound) for high (ħω, q), while the other method is adequate for low values of (ħω, q). This result was determined by the fact that the first method was based on a considerable change of function $Z(K, \hbar\omega)_{\hbar\omega = const}$ with respect to 1 + Γ(K), which occurs for high values of ħω, while Kroó's method was based on a Gaussian approximation of the form of function $Z(K, \hbar\omega)_{\hbar\omega = const}$ which is valid for low values of ħω.

In the case of liquid bismuth, a third peak appears in function $Z(K, \hbar\omega)_{\hbar\omega = const}$ for ħω > 3 meV values, not shown in Fig. 9. This could account for the fact that for liquid bismuth L(R, K, q) does not agree with Singwi's theory.

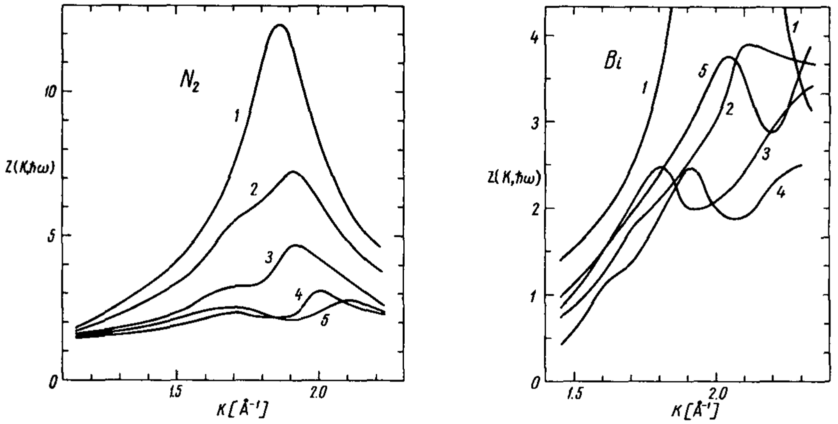

FIG. 7. Examples for function $Z(K,\hbar\omega)_{\hbar\omega=\text{const}}$. Liquid nitrogen: 1- $\hbar\omega$ = 0.5 meV, 2- $\hbar\omega$ = 1.5 meV, 3- $\hbar\omega$ = 2 meV, 4- $\hbar\omega$ = 2.5 meV, 5- $\hbar\omega$ = 3 meV. Liquid bismuth: 1- $\hbar\omega$ = 0.5 meV, 2- $\hbar\omega$ = 1.5 meV, 3- $\hbar\omega$ = 2 meV, 4- $\hbar\omega$ = 3 meV; 5- $\hbar\omega$ = 5 meV.

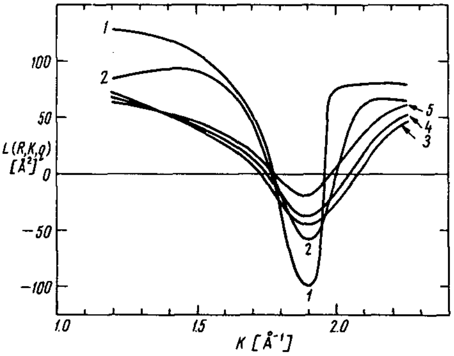

FIG. 8. Experimental values of L(R, K, q) for liquid nitrogen at various values of $\hbar\omega$: 1- $\hbar\omega$ = 2.5 meV, 2- $\hbar\omega$ = 3 meV, 3- $\hbar\omega$ = 4 meV, 4- $\hbar\omega$ = 5 meV.

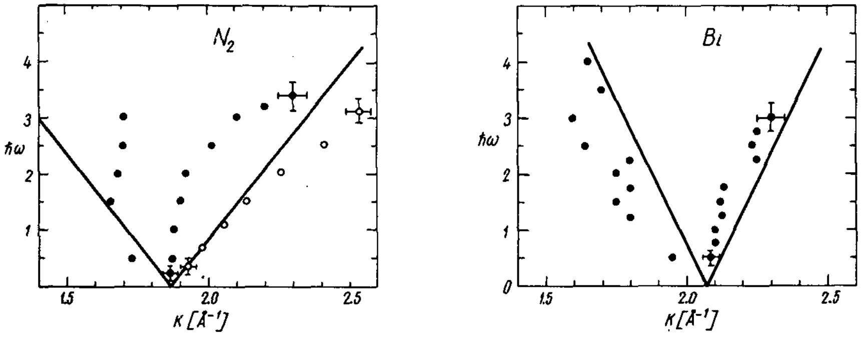

FIG. 9. Dispersion law for liquid nitrogen and liquid bismuth: ● - this experiment, ○ - our values published in Ref. [17]. The lines drawn represent the linear dispersion law corresponding to the velocity of sound.

REFERENCES

[1] EGELSTAFF, P.A., UKAEA Rep. AERE-R 4641 (1965).

[2] KROÓ, N., BORGONOVICI, G., SKÖLD, K., LARSSON, K.-E., Inelastic Scattering of Neutrons (Proc. Symp. Bombay, 1964) 2, IAEA, Vienna (1965) 101.

[3] DAHLBORG, U., LARSSON, K.E., Ark. Fys. 33 16 (1966) 271.

[4] RANDOLF, P.D., SINGWI, K.S., Phys. Rev. 152 (1966) 99.

[5] SKÖLD, K., LARSSON, K.E., Phys. Rev. 161 (1967) 102.

[6] BRUGGER, R.M., HARKER, Y.D., AEC Rep. IDO-17134 (1966) 38.

[7] MATEESCU, N., TEUTSCH, H., DIACONESCU, A., NAHORNIAK, V., to be published.

[8] HENSHAW, D.G., HURST, D.G., POPE, N.K., Phys. Rev. 92 (1953) 1229.

[9] SHARRAH, P.C., PETZ, J.J., KRUH, R.T., J. chem. Phys. 32 (1960) 241.

[10] DE GENNES, P.G., Physica 25 (1959) 825.

[11] VINEYARD, G.H., Phys. Rev. 110 (1958) 999.

[12] DONALDSON, R.E., PASSEL, L., BARTOLINI, W., Phys. Rev. 138 5B (1965) 1116.

[13] SINGWI, K.S., Physica 31 (1965) 1257.

[14] SEARS, V.F., Can. J. Phys. 44 (1966) 1279, 1299.

[15] ASCARELLI, P., CAGLIOTI, G., Nuovo Cim. 10 43B (1966) 375.

[16] MOTT, N.F., Proc. R. Soc. 146 (1934) 465.

[17] TEUTSCH, H., MATEESCU, N., NAHORNIAK, V., DIACONESCU, A., Phys. Lett. 22 (1966) 558.

INELASTIC SCATTERING IN LIQUID SODIUM AT SMALL MOMENTUM TRANSFER*

P.D. RANDOLPH
IDAHO NUCLEAR CORPORATION,
IDAHO FALLS, IDAHO,
UNITED STATES OF AMERICA

Abstract

INELASTIC SCATTERING IN LIQUID SODIUM AT SMALL MOMENTUM TRANSFER. The small momentum transfer region in simple liquids is of particular interest from the standpoint of examining the approach to the hydrodynamic limit and for studying diffusive and collective excitations. Measurements are reported on the inelastic scattering of slow neutrons from a sample of liquid sodium at 102°C in the κ region below the first diffraction maximum. The experiment was performed with the MTR phased chopper velocity selector at incident energies of 30 and 61 meV. To remove air scattering, an evacuated flight path subtending an 18.3° range of scattering angles was used. The measured spectra span the momentum transfer range $h\kappa$ of $0.3 \leq \kappa \leq 1.4$ Å^{-1} and an energy transfer range of $0 \leq \hbar\omega \leq 30$ meV. The quasi-elastic scattering was analysed after correction for coherent scattering and multiple elastic scattering. The behaviour is solid-like with a Debye-Waller coefficient of 0.22 Å^2. The widths of the quasi-elastic peaks are narrower than predicted by the simple diffusion model, but are in agreement with the jump-diffusion model with a residence time τ_0 of 1.5×10^{-12} sec. A broad peak or shoulder in the inelastic scattering appearing in all scattering angles at an energy transfer of 14 meV is primarily due to incoherent inelastic scattering. Its shape is in agreement with a Debye frequency spectrum but beyond the cut-off shows evidence of multiple inelastic scattering.

1. INTRODUCTION

We report here on a neutron inelastic scattering study of the single particle motion in liquid sodium just above its melting temperature. Sodium is partially an incoherent and partially a coherent scatterer, but it is one of the few simple metals which can be easily liquified with a relatively large fraction incoherent scattering. Its coherent cross section is 1.55 barns while the incoherent cross section is 1.85 barns [1].

There have been two earlier neutron scattering experiments on liquid sodium [2,3]. In a cold neutron experiment, Cocking [2] fit the shapes of the quasi-elastic peaks at 153°C to a model of Egelstaff and Schofield [4] in the range momentum exchange range $\hbar\kappa$ of $0.5 \lesssim \kappa \lesssim 1.5$ Å^{-1} assuming that in this low κ region no coherent effects were present. In another experiment using thermal neutrons, Randolph [3] measured the scattering law over a wide range of energy and momentum transfer. This experiment demonstrated clearly the appearance of coherent effects in the inelastic scattering for κ values $\gtrsim 1.5$ Å^{-1}.

In order that the single particle motion be the dominant contributions to the scattering, the experiment was performed in the region $\kappa \lesssim 1/2\ \kappa_o$ where κ_o is the position of the main diffraction maximum. In this region coherent effects are minimized though still present. The approach taken here to remove the remaining coherent scattering from observed quasi-elastic scattering is to subtract the coherent contribution using the

---

* Work performed under the auspices of the US Atomic Energy Commission.

measured structure factor, rather than calculate the contribution using a model such as the convolution approximation. In this experiment the main effort was directed toward obtaining the Debye-Waller factor, and studying the quasi-elastic widths. These give information about the nature and extent of solid like behavior in the liquid. In addition, qualitative information is obtained about the frequency spectrum of the velocity auto-correlation function.

2. DESCRIPTION OF THE EXPERIMENT

The experiment was performed using the MTR phased-chopper velocity selector [5]. In order to obtain small values of κ with thermal neutrons, small scattering angles are necessary. A cadmium lined, small angle evacuated flight path and scattering chamber was installed to remove air scattering. Scattering angles ranged from 3.3 to 18.3°, with a sample-to-detector flight path of 2.26 meters. The detectors were in 12 sets of two one-inch diameter, 10 atmosphere helium-3 proportional counters. Each bank of two counters subtended 1.4 degrees at the sample, giving a spread in κ of $\Delta\kappa \simeq \pm 0.06$ Å^{-1} for elastic scattering.

The sample was in the form of a rectangular slab with windows of 0.0025 cm vanadium, having a sample thickness of 0.635 cm and a measured transmission of 0.94. It was maintained at 102.6° ± 2°C by means of cartridge heaters in the sample frame.

Data runs were made at incident energies of 30.5 and 51.0 meV and the 12 angles spanned a κ range from 0.22 to 1.4 Å^{-1} for elastic scattering. Background runs were obtained by alternately cycling the filled sample holder and an empty holder into the beam at 10 minute intervals. The time-of-flight analyzer was used with 256 five μsec channels for each scattering angle. Fig. 1 shows an example of raw data for the 30 meV run at 11.53° and the resulting cross section. The intensity was calibrated using a vanadium standard. The measured energy resolution for elastic scattering as obtained from the shape of the forward beam bursts was 1.25 meV for the 30 meV data and 2.4 meV for the 51 meV data.

3. RESULTS

In Fig. 2 are shown representative plots of the inelastic partial differential cross section for the 30.5 meV data. As can be seen from Fig. 1, the quasi-elastic cross section is ≈ 50 times larger than the inelastic cross section. The inelastic data has some features of interest, which can be most easily observed on the short wavelength side of the elastic peaks. The main feature which appears for all scattering angles is a broad peak at $\lambda \sim 1.35$ to 1.4 Å which at the larger angles becomes a shoulder. Two other features appear in some of the angles. Thus there appears to be a small bump at $\lambda \sim 1.42$ Å and at 1.54 Å in some of the angles. If these are real, the fact that they appear only in some angles indicates they could be due to coherent inelastic scattering, i.e. excitation of quasi-phonons in the liquid. The statistical fluctuations of the data in this region however are sufficiently large that these little peaks or shoulders may not be real.

Quasi-Elastic Peaks. In liquid sodium the static structure factor $S(\kappa)$ has its main maximum at $\kappa_o = 2.02$ Å^{-1}. The quasi-elastic data of this experiment lies between 0.2 and 1.5 Å^{-1} and therefore arises predominantly from incoherent scattering. However the structure factor though small in this region is not zero, so that the observed quasi-elastic peaks have some coherent scattering. In addition, some multiple and inelastic scattering contributions are expected in the peak.

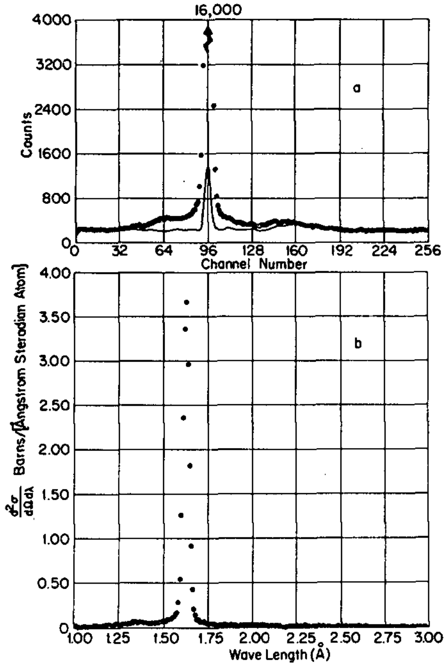

FIG.1. (a) Raw data at 11.5°. The elastic peak in the background is due to the vanadium windows of the sample. (b) Scattering cross-sections obtained from this data.

The quasi-elastic peaks have been analyzed to obtain the Debye-Waller factor for the liquid, and quasi-elastic widths have also been obtained. The Debye-Waller factor was obtained after correcting the data for estimated contributions for inelastic and multiple scattering, and further correcting for the known coherent contribution. In Fig. 2 are shown (dotted lines) the estimated combined contributions of multiple scattering and inelastic single scattering. These were estimated by eye, but approximate calculations of elastic double scattering show that these are reasonable values. The quasi-elastic peak was assumed to be the region between the vertical lines in Fig. 2. The correction for coherent contributions was calculated from the experiment structure factor $S(\kappa)$ given by Gingrich and Heaton [6]. The results are shown in Fig. 3a. This shows the uncorrected values for the integrated quasi-elastic peaks. Also shown are the contributions from coherent scattering and the estimated values of the inelastic and multiple scattering cross sections. Note that the combined multiple and inelastic contribution is of the same order and has about the same shape as the coherent contributions. At small κ, the total correction amounts to about 4 per cent and gradually rising to about 30 per cent at $\kappa = 1.4$ Å; in the latter range they cannot be considered negligible. Fig. 3b shows the

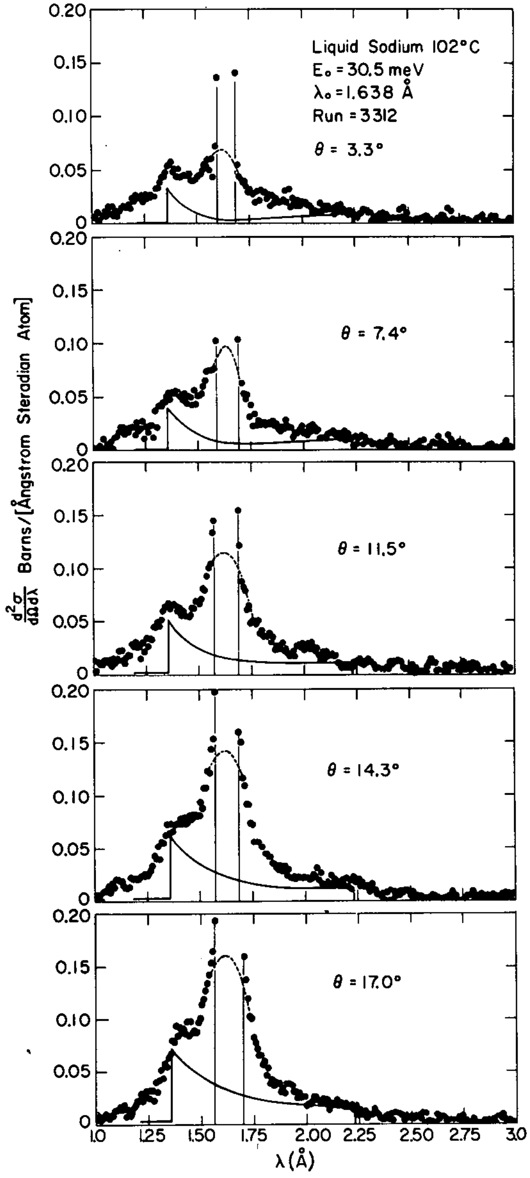

FIG. 2. Inelastic scattering cross-sections for liquid sodium. ----- Estimated multiple and inelastic scattering. ——— Cross-section for a Debye frequency spectrum including one and two phonon contributions. The vertical lines show the assumed boundary of the quasi-elastic peak.

corrected incoherent elastic cross sections combining data from both the 30 and 51 meV runs. The data have been least squares fit to

$$\frac{d\sigma}{d\Omega}\Big)_{\text{inc}} = \frac{\sigma_{\text{inc}}}{4\pi}\, e^{-a\kappa^2}$$

This is the form of the cross section for quasi-elastic scattering from a solid incoherent scatterer. The solid line in Fig. 3b shows the fit. The value of σ_{inc} given by this fit is 1.98 barns compared to the published value of 1.85 barns [1]. The Debye-Waller coefficient obtained is a = 0.221 Å^2. The value of σ_{inc} from this fit is 7 per cent higher than the published one. That this discrepancy is small gives confidence to the estimates of multiple scattering. If multiple elastic scattering were a relatively large effect in liquid sodium at these κ's, the measured elastic cross sections would be much higher than observed, due to contributions from elastic double scattering around the main maximum of S(κ).

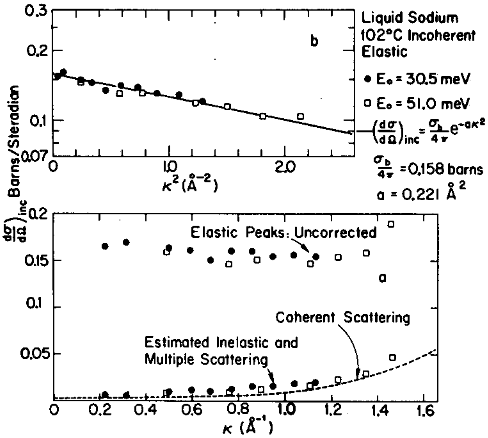

FIG.3. Angular distribution of the quasi-elastic peaks: (a) uncorrected data; (b) corrected distribution.

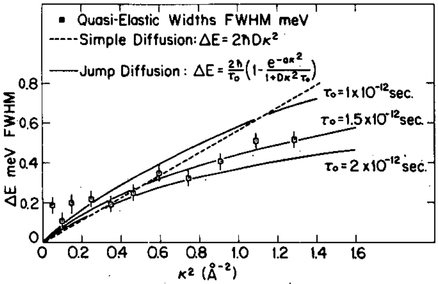

FIG.4. Widths of the quasi-elastic peaks for liquid sodium.

From the relation $a\kappa^2 = \kappa^2 R^2/6$, a value of 1.15 Å is obtained for the RMS displacement. The Debye temperature was evaluated using the relation [7]:

$$a = \frac{3\hbar^2}{M\kappa_B\Theta_D}\left[\frac{1}{x}\,\phi(x) + \frac{1}{4}\right]$$

where the symbols are defined in the reference. The resulting value is $\Theta_D = 103^\circ K$. This, as might be expected for a liquid, is somewhat smaller than the value of 114°K [8] obtained for room temperature solid sodium by x-ray diffraction methods.

Widths of the quasi-elastic peaks have been obtained from the 30.5 meV data which has the better energy resolution. These widths were corrected for energy resolution by assuming the time-of-flight distribution of the incident beam is Gaussian in shape, and that the natural line width is a Lorentzian in energy. The ratio of the Lorentzian width to the observed width ranges between 0.15 to 0.33, showing that most of the observed line width is due to the finite resolution of the incident beam. Fig. 4 shows the quasi-elastic widths plotted vs. κ^2. Also shown is the simple diffusion model, and several curves for the jump diffusion model [9] given by

$$\Delta E = \frac{2\hbar}{\tau_o}\left(1 - \frac{e^{-a\kappa^2}}{1 + D\kappa^2 \tau_o}\right)$$

The width given by this expression is the limiting case for jump diffusion when the jump time for an atom τ_1 is very much smaller than the characteristic time τ_o during which an atom is assumed to oscillate about a fixed position. In evaluating this expression the value of $D = 4.3 \times 10^{-5}$ cm²/sec has been taken for the macroscopic coefficient of self diffusion [10], and the Debye-Waller coefficient of $a = 0.22$ Å² as obtained in this experiment. At larger κ^2 the widths are narrower than the simple diffusion model predicts. This is characteristic of liquids. Above $\kappa^2 \approx 0.3$ Å^{-2} the jump diffusion model with a value of $\tau_o = 1.5 \times 10^{-12}$ sec gives the better fit. In the region below $\kappa^2 = 0.3$ Å^{-2}, the data lies above all the curves. In this region the energy resolution is too great a fraction of the observed total width to allow a good determination of the natural line width. In the cold neutron experiment of Cocking [2] a value of 3.6×10^{-12} sec was obtained on the assumption of jump diffusion for data analyzed at four angles in the range $0.5 < \kappa \leq 1.5$ Å^{-1}. We have not been able to explain this discrepancy.

Inelastic Scattering. The inelastic shoulder at $\lambda \approx 1.35$ Å appears in all the spectra (Fig. 3), and increases in amplitude with scattering angle. Since the single-scattering inelastic events in this κ region arise almost completely from incoherent scattering, the hump presumably is primarily due to the frequency spectrum of the velocity auto correlation function. It is expected however that there is a large contamination of multiple scattering. The amount of multiple scattering is of the same order as that present in the elastic case. However in the inelastic region the relative amount present is larger since the inelastic cross section is very small compared to the elastic peak (~1/50). Since we do not have an adequate way of calculating the multiple inelastic scattering contributions for both coherent and incoherent events, no quantitative analysis of the inelastic scattering was attempted. However some qualitative information can be obtained. The fact that a Debye-Waller factor can be obtained over a reasonable κ range together with the fit of the widths to a solid like model shows that the assumption of solid like behavior just above the melting point is a reasonable one. In this spirit the inelastic data has been analyzed in the one-phonon incoherent cubic approximation, i.e.

$$\frac{d^2\sigma}{d\Omega d\varepsilon} = \frac{\sigma_{inc}}{4\pi}\frac{k}{k_o} e^{-a\kappa^2}\frac{\hbar^2\kappa^2}{4M}\frac{e^{-\frac{\varepsilon}{2\kappa T}} G(\varepsilon)}{\varepsilon[\sinh \frac{\varepsilon}{2k_B T}]}$$

where $\varepsilon = E - E_0$ and $G(\varepsilon)$ is the "one-phonon" spectrum. The Debye-Waller coefficient used is the value obtained from the elastic peak analysis. Fig. 5 shows a typical $G(\varepsilon)$ for $\Theta = 14.30°$, together with error flags due to counting statistics. Positive values of the "phonon energy" indicate neutron energy loss, and the ordinate is in units of eV^{-1}. The spectrum has a single maximum for phonon energies in region of $\pm$(13 to 15) meV, and for energy transfer less than this has a shape similar to a Debye spectrum but rises faster. A value of 14 meV is taken as a reasonable cutoff value for the frequency spectrum ($\Theta_D = 162°K$). The longitudinal phonon branch in solid sodium in the 111 direction has a maximum at about 14 meV indicating a singularity in the frequency spectrum at this value. Above 14 meV, the observed liquid spectrum falls off rather slowly. Calculations of the two phonon scattering with a Debye spectrum shows that multiphonon contributions are very small in this κ range (see Fig. 2). Thus the extra contributions to the one phonon spectrum of Fig. 5 above 14 meV are presumably due to multiple inelastic scattering or possibly to new modes. Fig. 5 also shows the Debye spectrum with an assumed cutoff at 14 meV for both energy gain and loss events. The shapes below 14 meV are in reasonable agreement.

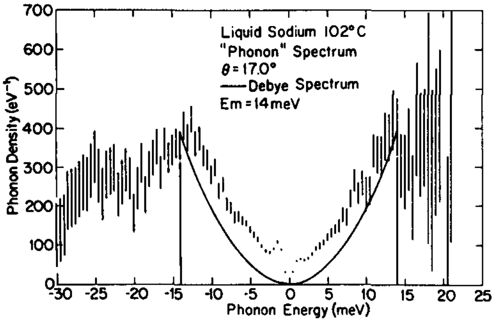

FIG.5. Typical frequency spectrum of the velocity auto-correlation function analysed in the one-phonon incoherent solid assumption. The error flags are due to counting statistics.

4. CONCLUSIONS

A slow neutron inelastic scattering experiment on liquid sodium in the momentum transfer range where the scattering is predominantly incoherent has been performed. Multiple scattering effects are relatively small in the quasi-elastic peaks, and large in the inelastic spectrum. From the quasi-elastic peaks a value of the Debye-Waller coefficient has been obtained and the quasi-elastic widths analyzed. A qualitative analysis of the inelastic spectrum shows a shape characteristic of a simple Debye type frequency spectrum for the velocity auto correlation function. The results are consistent with a solid like model of jump diffusion, having a Debye temperature of 103°K, and a mean vibrational time of residence $\tau_0 = 1.5 \times 10^{-12}$ sec.

5. ACKNOWLEDGEMENTS

The author is much in debt to Dr. W. R. Myers for many fruitful discussions and to Dr. R. M. Brugger for advice and encouragement.

REFERENCES

[1] United States Atomic Energy Commission Report BNL-325.
[2] COCKING, S. J., Inelastic Scattering of Neutrons in Solids and Liquids, I, IAEA, Vienna (1963) 227.
[3] RANDOLPH, P. D., Phys. Rev., 134 (1964) A1238.
[4] EGELSTAFF, P. A., SCHOFIELD, P. S., Nucl. Sci. Engng. 12 (1962) 260.
[5] BRUGGER, R. M., Thermal Neutron Scattering, EGELSTAFF, P. A., editor, Academic Press, London (1965) Chapter 2.
[6] GINGRICH, N. S., HEATON, L., J. Chem. Phys. 34 (1961) 873.
[7] BACON, G. E., Neutron Diffraction, Second edition, Oxford University Press (1962) 46.
[8] GSCHNEIDER, K. A., Solid State Physics 16 (1964) 270.
[9] SINGWI, K. S., SJOLANDER, A., Phys. Rev. 119 (1960) 863.
[10] NACHTRIEB, N. H., The Properties of Liquid Metals, Taylor and Francis Ltd., London (1967).

TEMPERATURE DEPENDENCE OF QUASI-ELASTIC SCATTERING OF COLD NEUTRONS FROM LIQUID ARGON*

W.S. ANDRUS AND H.R. MUETHER
BROOKHAVEN NATIONAL LABORATORY, AND
STATE UNIVERSITY OF NEW YORK AT STONY BROOK,
AND
H. PALEVSKY
BROOKHAVEN NATIONAL LABORATORY,
UPTON, LONG ISLAND, N.Y.,
UNITED STATES OF AMERICA

Abstract

TEMPERATURE DEPENDENCE OF QUASI-ELASTIC SCATTERING OF COLD NEUTRONS FROM LIQUID ARGON. The inelastic scattering of cold neutrons from liquid argon has been studied at a variety of scattering angles and sample temperatures on the slow chopper facility at the Brookhaven National Laboratory Graphite Research Reactor. The full beryllium-filtered incident spectrum was used to obtain time-of-flight spectra, and the quasi-elastic width was extracted by comparing the data to numerically generated spectra. The temperature dependence of the quasi-elastic peak at each angle was inconsistent with the free diffusion hypothesis. The data have been compared to the predictions of Singwi's model of coherent scattering from liquids.

INTRODUCTION

Experiments on the quasi-electric scattering of cold neutrons from simple liquids can provide considerable information about the atomic motions within the sample. An early calculation by Vineyard [1] showed that if diffusion takes place in a continuous, classical fashion, the incoherent scattering will be described by the expression

$$\frac{d^2\sigma}{d\Omega d\omega} \sim \frac{D\kappa^2}{(D\kappa^2)^2 + \omega^2} \qquad (1)$$

where κ and ω are the momentum transfer and energy transfer and D is the coefficient of self-diffusion. An indication of the departure from simple diffusive behaviour results from plotting the logarithm of the quasi-elastic width versus the reciprocal of the temperature. If diffusion is continuous, as opposed to the situation in solids where it proceeds by jumps, the plot will be linear and its slope will equal the activation energy for diffusion divided by Boltzmann's constant.

Singwi [2, 3] has proposed a model for coherent scattering from liquids which takes solid-like motions into account. He imagines a sphere of radius R drawn about an atom taken as the origin. All other atoms within the sphere are assumed to act in a rather solid-like way, and are treated

---

* This work was supported by the US Atomic Energy Commission.

in a quasi-harmonic approximation. Atoms outside the sphere are assumed to diffuse continuously, with a motion which is not conditioned by the presence of an atom at the origin. The resulting cross-section for quasi-elastic scattering with momentum transfer κ and energy transfer ω is

$$\frac{d^2\sigma}{d\Omega d\omega} = \frac{1}{4\pi}\,\frac{k}{k_0}\,a_{coh}{}^2\left\{\left[\frac{a_{inc}{}^2}{a_{coh}{}^2} + 1 + \Gamma(\kappa)\right]\frac{1}{\pi}\left[\frac{D\kappa^2}{(D\kappa^2)^2 + \omega^2}\right] + e^{-2M(0)}\,\frac{\kappa^2 K_B T}{12\,Mc^2}\,L(R,\kappa) f(\omega)\right\} \tag{2}$$

where k and k_0 are the momenta of the incident and scattered neutrons, a_{coh} and a_{inc} are the coherent and incoherent scattering lengths, and $\exp(-2M(0))$ is the Debye-Waller factor. The function $f(\omega)$ is the excitation spectrum, c is an appropriately averaged sound velocity, and $1 + \Gamma(\kappa)$ is the normalized diffraction pattern. The quantity $L(R, \kappa)$ is given by the expression

$$L(R,\kappa) = \frac{R^3}{4\sqrt{\pi}} \int_0^\infty k'\,\Gamma(k')\,e^{-\frac{R^2}{4}(\kappa - k')^2}\left[\frac{R^2}{2}(\kappa - k')^2 - 1\right] dk' \tag{3}$$

One primary goal of this work was the comparison of Singwi's prediction with experimental data over a broad temperature range.

EXPERIMENTAL PROCEDURE AND DATA ANALYSIS

The slow chopper and Graphite Research Reactor at Brookhaven National Laboratory have been used to collect data on the scattering of beryllium-filtered neutrons from liquid argon at three scattering angles and four temperatures covering half the range over which argon is a liquid. The samples were contained under 22 atmospheres pressure in a cylindrical aluminium holder whose wall thickness, in order to reduce background scattering, was 0.035 inches. The sample transmission against scattering was about 7%, and multiple scattering was reduced by sectioning the holder with cadmium discs. Data were collected at temperatures of 87, 97, 111 and 124°K; argon's triple point occurs at 84°K and its critical point at 151°K. The scattering angles, 45°, 65° and 80°, represented momentum transfers of 1.2, 1.7 and 2.0 $Å^{-1}$, respectively, for the 4 Å neutrons at the beryllium break. The diffraction peak in argon is at 2.0 $Å^{-1}$.

The data were corrected for the energy dependence of the transmission of the chopper and flight path and the energy-dependent detector efficiency. Argon is a mixed coherent and incoherent scatterer, with comparable scattering lengths for the two processes. Because the diffraction peak is at 2 $Å^{-1}$, the scattering at 80° is mostly coherent. At 45° there is very little coherent intensity, and approximately incoherent spectra result. Both coherent and incoherent contributions are present at 65°.

Extraction of the quasi-elastic widths from our data required some analysis. Curves were generated representing the folding of Lorentzians of various widths with a function representing our incident spectrum and with a Gaussian resolution function and a correction for diffraction effects. An additional contribution was added to represent incoherent scattering, for comparison with the data at 45° and 65°. The shape of the incoherent spectrum was assumed to be given by Eq.(1), and its intensity was computed from the diffraction pattern and the coherent and incoherent scattering lengths. The width of the incoherent spectrum was determined by assuming the scattering at 45° was incoherent.

The incident spectrum function was checked by verifying that after folding with a Gaussian it accurately reproduced the spectrum of neutrons elastically scattered from vanadium. Figure 1 shows this comparison, which also yielded the experimental resolution. Comparison of the generated curves with our data allowed us to determine the width of the Lorentzian that gave the best fit. One such comparison is shown in Fig. 2. These computations were performed on the IBM 7040 and automatic plotter at the Computing Center of the State University of New York at Stony Brook. The fitting process was aided by the fact that accurate values of the quasi-elastic width near the triple point had already been obtained by other groups [4, 5] using narrower incident spectra, so that useful criteria of good fit could be obtained by comparison to the earlier results.

RESULTS

Figure 3 shows semi-logarithmic plots of the quasi-elastic width as a function of the reciprocal of the temperature. The results at each scattering angle are consistent with linear behaviour, but the slope in each case is less than the activation energy. The slopes are 482 cal/mole at 45°, 288 cal/mole at 65° and 290 cal/mole at 80°. The activation energy for diffusion in argon under 22 atm pressure [6] is 705 cal/mole, indicating that diffusion in argon does not proceed in a continuous fashion.

Figure 4 shows fits of Singwi's prediction, Eq.(2), to our data. The expression is a sensitive function of the diffraction pattern at the temperature at which the scattering experiment is performed. While X-ray diffraction data on argon at elevated temperatures are available, there has been no neutron diffraction study in the region under investigation. Clayton and Heaton [7] have made a careful study of neutron diffraction in liquid krypton over a wide temperature range, however, and krypton and argon should be closely related through the theorem of corresponding states [8, 9]. On this assumption the krypton data have been transformed and used in Eqs (2) and (3).

DISCUSSION

The temperature dependence of the quasi-elastic width shown in Fig. 3 indicates that free diffusion is not an appropriate picture even for so weakly-interacting a liquid as argon. These results differ from the conclusion of Dasannacharya and Rao [4], obtained from data over a much narrower temperature range, that the slope in argon is equal to the activation energy and that diffusion is therefore continuous.

Although D in Eq.(2) is supposed to be the diffusion constant, the expression $D\kappa^2/[(D\kappa^2)^2 + \omega^2]$ is really meant to represent the incoherent

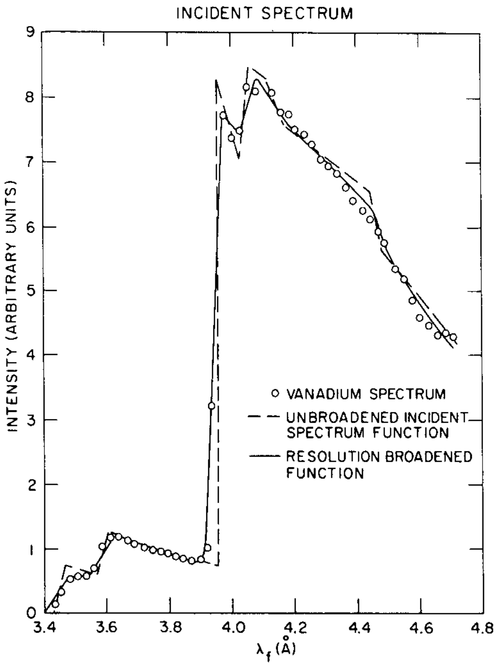

FIG.1. The function used to simulate the incident spectrum shown both before and after correction for experimental resolution. The open circles are the experimentally observed data on elastic scattering from vanadium.

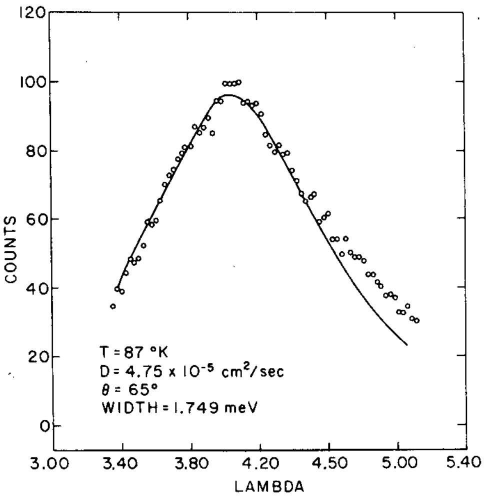

FIG.2. Comparison of the folding of a Lorentzian with the incident spectrum function and corrections for resolution resolution, incoherent scattering, and diffraction, to the data on scattering at 65 from argon at 87 K. The spectra are plotted as functions of the wavelength of the scattered neutron.

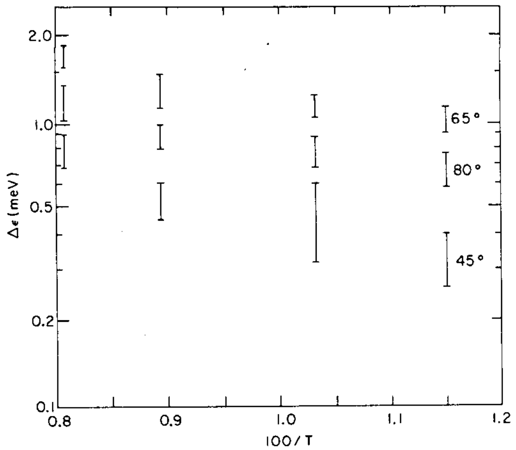

FIG.3. Logarithm of the quasi-elastic width versus the reciprocal of the temperature, at three values of the scattering angle. The data at each scattering angle are consistent with linear behaviour, but the slopes are not those predicted by the free diffusion picture.

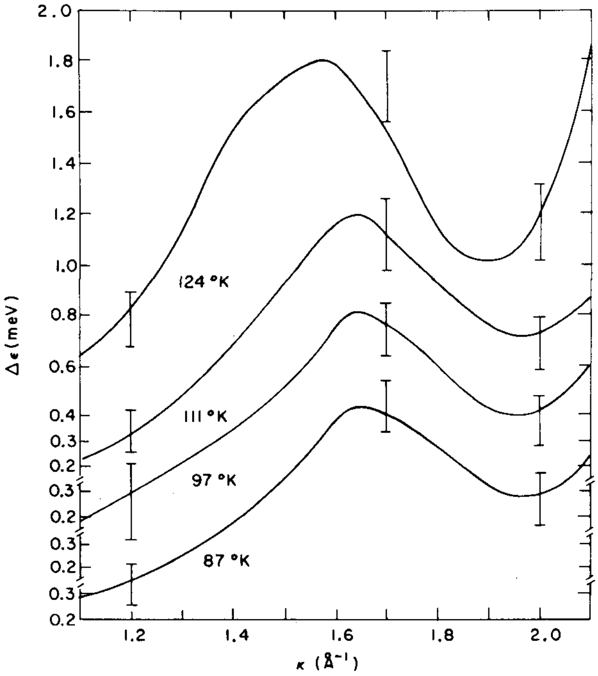

FIG.4. Comparison between Singwi's predictions and the experimental quasi-elastic widths at four temperatures. Note that the ordinates are referred to four different base lines.

spectrum. Since the incoherent width does not have the same temperature dependence as the diffusion constant, D was treated at each temperature as a free parameter. In each case, the result was consistent with the quasi-elastic width at 45°, where the scattering is mostly incoherent. The parameter R, representing the range over which solid-like motions are important, was chosen as 15 Å from the low temperature data, and was not allowed to vary. It would be interesting to acquire more data at higher temperature and investigate the temperature dependence of this parameter.

The parameter upon which Singwi's results depend most sensitively is c, which scales the oscillations in the quasi-elastic width with momentum transfer. The value of c was chosen from the low-temperature data, and was not allowed to vary, because the velocity of sound is not expected to change much. While a single value of c does produce agreement between theory and experiment over a broad temperature range, the value, 1.8×10^4 cm/sec, is about one-fifth the measured velocity of sound in liquid argon. Although sound velocity measurements are made at much lower frequencies than those of interest here, it is difficult to see how so much dispersion could be present. On the other hand, use of the measured sound velocity as c in Eq.(2) practically eliminates the coherent width oscillations, in disagreement with the data.

The use of a single value of the critical parameter c over this temperature range would nevertheless seem to be the most exacting test yet applied to the quasi-elastic predictions of Singwi's model.

REFERENCES

[1] VINEYARD, G.H., Phys. Rev. 110 (1958) 999.
[2] SINGWI, K.S., Phys. Rev. 136 (1964) A969.
[3] SINGWI, K.S., Physica 31 (1965) 1257.
[4] DASANNACHARYA, B.A., RAO, K.R., Phys. Rev. 137 (1965) A417.
[5] KROÓ, N., BORGANOVI, G., SKÖLD, K., LARSSON, K.-E., Inelastic Scattering of Neutrons (Proc. Symp. Bombay, 1964) 2, IAEA, Vienna (1965) 101.
[6] NAGHIZADEH, J., RICE, S.A., J. Chem. Phys. 36 (1962) 2710.
[7] CLAYTON, G.T., HEATON, L., Phys. Rev. 121 (1961) 649.
[8] VINEYARD, G.H., Phys. Rev. 119 (1960) 1150.
[9] SEARS, V.F., Can. J. Phys. 44 (1966) 867.

A QUASI-PHONON TREATMENT OF COHERENT NEUTRON SCATTERING BY LIQUID LEAD

S.J. COCKING
ATOMIC ENERGY RESEARCH ESTABLISHMENT,
HARWELL, DIDCOT, BERKS.,
ENGLAND

Abstract

A QUASI-PHONON TREATMENT OF COHERENT NEUTRON SCATTERING BY LIQUID LEAD. Two treatments which employ a phonon-like description of the relative motions of atoms in liquids have been compared. The method of Singwi introduces the concept of finite range of the excitation, while that due to Egelstaff takes some account of polarization of the modes. It is shown that the introduction of polarization is required to explain the observed results of coherent neutron scattering by liquid metals in agreement with the conclusions of Sköld and Larsson for liquid argon. Detailed comparison of the latter model with experimental results on liquid lead required the assumption of the spectral density of both longitudinal and transverse modes. The former was taken as the same as for the solid while the latter was derived from the best fits to the experimental data. The resulting calculation showed qualitative and semi-quantitative agreement with experimental data of Randolph and Singwi and of the author. Some limitations of the theoretical treatment are discussed.

1. INTRODUCTION

The similarity of frequency-wave number curves for excitations in the liquid and solid states for several monatomic systems has been shown [1]. These curves follow the broadly directionally independent longitudinal branch of the phonon dispersion curves observed with single crystals. These data thus provide evidence for the relevance of a quasi-phonon treatment of the relative motion of atoms in monatomic liquids. Extensions of phonon theory to the liquid state have been suggested [2, 3] and it is the purpose of the paper to compare these theories with one another and with experimental data on liquid lead.

2. THEORY

2.1. Egelstaff approach

The coherent scattering law $S(Q, \omega)$ for one-phonon scattering by a polycrystal of Bravais lattice has been obtained from expressions for a single crystal by averaging over all directions in the lattice [2]. Simplifying assumptions are introduced as

(i) The phonon dispersion curves are one, purely longitudinal and two, degenerate purely transverse branches; each branch being isotropic in the crystal lattice.

(ii) The phonon polarizations are resolved into purely longitudinal or transverse components.

Then

$$S(Q,\omega) = \sum_n Z_n(Q,\omega)\, S_{s,n}(Q,\omega) \tag{1}$$

where $S_s(Q,\omega)$ is the scattering law in the incoherent approximation and n refers to the 3 branches of the dispersion curves.

$$S_{s,n}(Q,\omega) = \frac{\hbar\, Q^2\, z(\omega)_n\, e^{-2w}}{2M\omega \sinh(\hbar\omega/2k_BT)} \qquad Z_n(Q,\omega) = \frac{\pi}{2BQq_n} \sum_{\tau=\frac{Q-q}{2\pi}}^{\tau=\frac{Q+q}{2\pi}} \frac{F\tau}{\tau}\, p_n \tag{2}$$

and p_n is the polarization factor $|\vec{Q}.\alpha_n|^2/Q^2$. (The notation is conventional; Eqs (1) and (2) are discussed in more detail in Refs [4] and [13] where expressions for the polarization factors are given.)

The factor p_n exhibits, for the longitudinal component, peaks at $Q = 2\pi\tau \pm q_L$ and falls to zero for $Q \approx 2\pi\tau$. For the degenerate transverse components, p_n has a broad maximum at $Q \approx 2\pi\tau$ and falls to zero at $Q = 2\pi\tau \pm q_T$.

Extension for the liquid was made by regarding the usual liquid structure factor S(Q) as a continuous distribution of reciprocal lattice spacings when, replacing the sum by an integral,

$$Z_n(Q,\omega) = \frac{1}{2Qq} \int_{Q-q}^{Q+q} dQ'\, Q'\, S(Q')\, p_n \tag{3}$$

If we ignore the term p_n in Eq. (3), then for $q \to 0$ $Z(Q,\omega) \to S(Q)$ giving Vineyard's convolution approximation (hereafter abbreviated VCA) while for the increasing q (i.e. increasing ω) the features of S(Q) become increasingly broadened. This broadening of the Q-dependent features of $S(Q,\omega)$ with increasing ω is indeed the general behaviour observed in liquid sodium [5], liquid lead [6] and liquid argon [7].

Examples of $Z(Q,\omega)$ including p_n are shown in Fig.1 to exhibit, for longitudinal components, peaks at $Q = Q_m \pm q_L$ (Q_m is the value of Q at the principal maximum of S(Q)) which at small q coalesce into a single peak at $Q = Q_m$. For transverse modes, the function, always peaked at $Q = Q_m$, is broadened as q increases. Thus in regions where longitudinal components dominate (that is, at high ω values) one may expect peaks in $S(Q,\omega)$ (plotted at constant ω) at Q values displaced from Q_m. This behaviour can indeed be seen in Fig. 2 for experimental data on liquid lead [6], and liquid argon [7].

2.2. Singwi approach

Singwi also used the idea of phonon-like modes to describe near-neighbour correlated motion but avoids the use of formulae involving the solid structure. Instead starting from the function I(Q,t) defined, as

$$2\pi \int d\omega e^{-i\omega t}\, S(Q,\omega) = I(Q,t) = \frac{1}{N} \sum_{i,j} \langle e^{i\vec{R}_i(0)\cdot\vec{Q}}\ e^{-i\vec{R}_j(t)\cdot\vec{Q}} \rangle$$

he writes $\vec{R}_j(t) = \vec{R}_j + \vec{u}_j(t)$ where $\vec{R}_j$ is the 'equilibrium' position of the atom and $\vec{u}_j(t)$ the displacement from this position, the 'equilibrium' position being assumed meaningful for a liquid for time $< 10^{-12}$ sec. Singwi described the displacement $\vec{u}_j(t)$ by a sum of travelled waves (phonons).

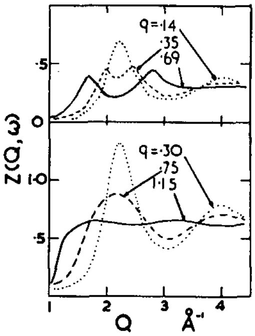

FIG.1. Examples of $Z(Q,\omega)$ at several values of q; upper and lower curves for longitudinal and transverse components respectively.

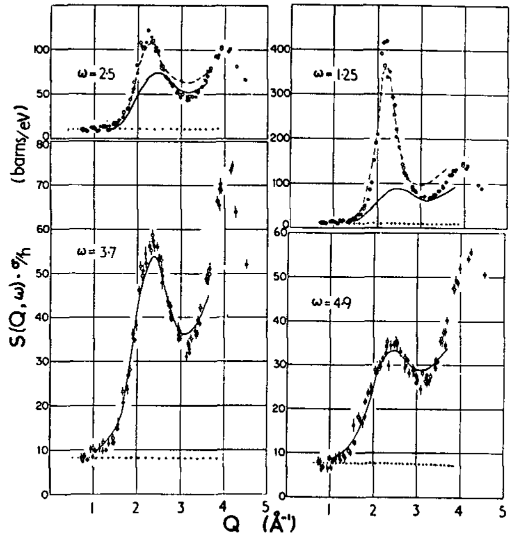

FIG.2. Experimental data [6] compared with the present calculations. Multiphonon and multiple (dotted) scattering are included to give the full curves. At $\omega = 1.25$ and 2.5, addition of the quasi-elastic component (negligible elsewhere) gives the broken curves.

No separation into longitudinal and transverse branches was attempted. (This is expressed in the Egelstaff treatment by dropping the specification n and setting $p_n = 1$, and is equivalent to assuming that all branches are degenerate.) Singwi expressed his result for single-phonon scattering as

$$S(Q,\omega) = [S(Q) + H(Q,\omega)]S_s(Q,\omega) \tag{4}$$

The liquid structure factor S(Q) being introduced as

$$S(Q) = \frac{1}{N} \int e^{iQ\cdot r} \sum_{i \neq j} \langle e^{i\vec{Q}\cdot\vec{R}_i} e^{-i\vec{Q}\cdot\vec{R}_j} \rangle \tag{5}$$

H(Q, ω) represents a correction to the VCA. In an extension, Singwi introduced a 'correlation range' R outside which the motion of atoms were uncorrelated, thus for $(R_i - R_j) > R$ the Vineyard convolution was assumed to apply. The transition between this region and the correlated region where phonon-like relative motion occurs was made using a cut-off function, $e^{-|R_i - R_j|^2/R^2}$. In this general form Singwi's result is (writing $\Delta = \sqrt{2}/R$)

$$H(Q, \omega) = \text{sech}\left(\frac{\hbar\omega}{2k_B T}\right) \frac{q^2}{6} L(\Delta, Q, q)$$

with

$$q^2 L(\Delta, Q, q) = \frac{3}{Qq} \int_0^\infty y[S(y) - 1] \left[\left\{ \int_{Q-q}^{Q+q} dx \frac{\left(e^{\frac{-(y-x)^2}{2\Delta^2}} - e^{\frac{(y+x)^2}{2\Delta^2}}\right)}{\sqrt{2\pi}\ \Delta} \right\} - 2q \left\{ \frac{e^{\frac{-(Q-y)^2}{2\Delta^2}} - e^{\frac{+(Q+y)^2}{2\Delta^2}}}{\sqrt{2\pi}\ \Delta} \right\}\right] \tag{6}$$

Singwi showed that for R → ∞ his result became identical to Eq. (3) with $p_n = 1$ in the limit $q \ll Q$. In fact the correspondence is more general since in the limit $R \to \infty (\Delta \to 0)$ the Gaussians may be replaced by Dirac δ-functions when integration over y gives

$$\frac{q^2}{6} L(\Delta, Q, q) = \frac{1}{2Qq} \int_{Q-q}^{Q+q} dQ' [S(Q') - 1] - [S(Q) - 1]$$

$$= \frac{1}{2Qq} \int_{Q-q}^{Q+q} dQ' S(Q')Q' - S(Q)$$

thus for $\hbar\omega/2k_B T \ll 1$, as is appropriate for all cases considered here,

$$S(Q) + H(Q, \omega) = \frac{1}{2Qq} \int_{Q-q}^{Q+q} dQ' S(Q')Q'$$

in exact agreement with Eq. (3) with $p_n = 1$.

Thus for all q the Egelstaff result (without the polarization factors) is identical with the Singwi result (in the limit R→∞). The assumptions made at Eqs(3) and (5) respectively thus are the same. This does not seem to have been generally appreciated. The results differ only in the separate introduction of polarization (Egelstaff approach) and of finite range ($R \neq \infty$) (Singwi approach).

A few remarks may indicate the origin of the features found in calculations using the Singwi formulation. For $R = \infty$, $H(Q, \omega)$ is $S(Q)$, broadened by the order q, minus $S(Q)$, and thus shows maxima at approximately $Q_m \pm q$; $[H(Q, \omega) + S(Q)]$ loses these maxima. However, when R is finite, $H(Q, \omega)$ is broadened by the order Δ ($= 0.07^{-1}$ for $R = 20$ Å) and $[H(Q,\omega) + S(Q)]$ retains minor inflexions near $Q_m \pm q$ while the peak at Q_m increases in amplitude with increasing R.

Singwi's formulation has been compared with data on liquid lead [6] and here the treatment introducing polarization effects is compared with these and other data on liquid lead.

To describe the total scattering we must add to the one-phonon term, multi-phonon and zero-phonon (elastic) contributions. The former will be calculated using the incoherent approximation. In a liquid the 'elastic' peak is broadened by diffusive motion and this is considered in the next section.

3. QUASI-ELASTIC SCATTERING IN LIQUID LEAD

The scattered spectra from liquid lead have been measured using 7.7, 6.3 and 4.1 Å incident neutrons [8]. For $Q_0 < 1.39$ Å^{-1} (Q_0 being Q at $\omega = 0$) the quasi-elastic peak was absent, though a strong peak was observed at $Q_0 \approx Q_m$. This was compared with the peak shape calculated for $S_s(Q, \omega)$ using the model of Egelstaff and Schofield [9], with experimental resolution included. The shape could be fitted using the parameters $D = 3.0 \times 10^{-5}$ cm^2/sec and $c = 3.5 \times 10^{-12}$ sec in this model. The absolute intensity also could be fitted using the VCA ($S(Q)$ taken from Ref. [10]) when an 'effective' Debye-Waller factor, $e^{-2W} = 0.653$, was included. Since the true peak width is several times narrower than the peak in $S(Q)$ at Q_m, the predicted shape is not markedly affected by using the VCA. Using $2W = Q^2(3T\hbar^2/MR_B\theta_D^2)$ we find a Debye temperature $\theta_D = 68$°K, a value somewhat lower than for the solid at the melting point [11]. Since we have no independent knowledge of the appropriate factors e^{-2W} or c, this comparison does not constitute a confirmation of the validity of the VCA to predict quasi-elastic scattering. However, we shall use it solely as an approximate description of quasi-elastic scattering near $Q = Q_m$ for comparison with the data of Ref. [6] employing e^{-2W} and c as determined here. In fact, the data for liquid lead and for liquid tin [12] and liquid gallium [13] all show that the total quasi-elastic peak intensity is very small for $Q < (Q_m - 0.3)$Å^{-1}, has a peak at Q_m narrower than that of $S(Q)$ and falls below $S(Q)$ for $Q > Q_m$. Thus the VCA is inaccurate in describing quasi-elastic scattering over a wide region of Q.

4. APPLICATION TO LIQUID LEAD AND COMPARISON WITH EXPERIMENT

Dr. R. Sharp (private communication) has obtained $z(\omega)$ from phonon dispersion curves for lead at room temperature. Taking the higher frequency branch to be near longitudinal he shows that the high frequency peak of $z(\omega)$ should be associated with predominantly longitudinal modes while the lower region is predominantly due to transverse modes. The observed similarity for solid and liquid in the longitudinal dispersion curves [8] suggests that the same $z_L(\omega)$ is appropriate for the liquid and the high frequency peak together with a low frequency tail with $z_L(\omega) = (B/2\pi^2 c^3)\omega^2$ ($c = 1.77 \times 10^5$ cm/sec) was used. Initially $z_T(\omega)$ for solid lead was also used and found to give an inadequate fit. The value of $z_T(\omega)$ at each value of ω was therefore determined as that value giving the best normalization to the experimental curves [6] at fixed values of ω. For $\omega > 10$ (here and elsewhere in units of 10^{12} rad/sec) the transverse component has been taken as zero.

Since we assume isotropy in each case, the dispersion relationships for the modes were thus made consistent with $z(\omega)$ using

$$z(\omega) = \frac{B}{2\pi^2} q^2 \left| \frac{dq}{d\omega} \right| \tag{7}$$

The resulting curve for longitudinal modes (which can be fitted by the expression $q_L = 0.056\omega(1 + 0.10(0.1\,\omega)^5)$ was consistent with the observed data [8]. The derivation of the final $z_T(\omega)$ and the resulting dispersion curve involved an iterative prodecure. It was found, however, that the resulting $S(Q, \omega)$ was not very sensitive to the chosen dispersion curve. For example, assuming a linear dispersion curve $\omega_T = c_T q_T$ with $c = 0.55 \times 10^5$ cm/sec gave results within 10% of those using the final curve; use of $c_T = 0.83 \times 10^5$ cm/sec gave $S(Q, \omega)$ which differed only by 15%.

Calculations using these functions are compared with the results of Ref. [6] in Fig. 3. For $\omega > 6.2$, Randolph and Singwi removed 'multi-

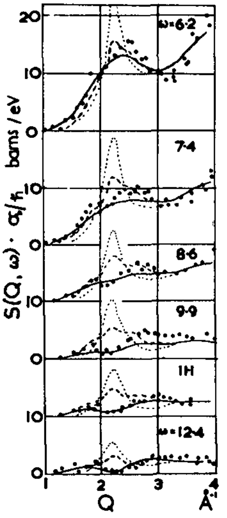

FIG. 3. Experimental data compared with the present calculations (full curves), the Singwi method (broken curves) and the VCA (dotted curves). The last two and the experimental data taken from [6].

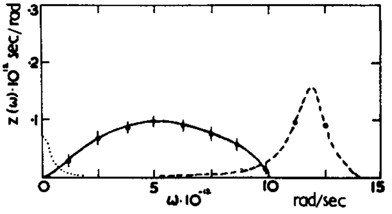

FIG.4. The spectral densities $Z_L(\omega)$ (broken curve) from independent data and $Z_T(\omega)$(full curve) from comparison with experimental data at the points shown. The spectral density for diffusing modes as implied by the present treatment is also shown (dotted).

phonon' and multiple scattering contributions so that the data shown can appropriately be compared with this 'one-phonon' calculation. For the two highest ω values only longitudinal modes contribute and the resulting peaks are displaced from Q_m (= 2.20 Å^{-1}) in experiment and theory. The absolute level calculated is generally satisfactory but the calculated maxima are less pronounced than in the observed data. Since the data were not corrected for experimental resolution the true maxima are probably more pronounced than is shown. At lower ω's the transverse contribution is increasingly dominant, and being peaked near $Q = Q_m$ tends to eliminate the minima. The absolute value of $S(Q, \omega)$ is fixed by the chosen values of $z_T(\omega)$ at each ω, the best fit values being shown in Fig.4.

The calculated results [6] using the Singwi theory show in Fig. 3 minor inflexions resulting from the use of a finite range, R = 20 Å, for the excitation. These correspond roughly to the observed maxima (for $\omega > 8.6$) but always retain a maximum at $Q = Q_m$ in contrast to the observations. The predictions of the convolution approximation, also from Ref. [6], are shown to be quite inadequate.

For $\omega < 6.2$, Ref. [6] give no calculations and make no correction to their data for multi-phonon effects. To extend the comparison with the present simple description into this region, a multi-phonon contribution has been calculated using the incoherent approximation and, together with the multiple scattering contribution, added to the 'one-phonon' calculation. Both corrections become relatively smaller as ω is reduced and since the multi-phonon term increases with Q^2, calculation was extended only to $Q = 3.7$ Å^{-1}. The comparison with the data in Fig. 2 shows acceptable agreement for $\omega = 4.9$ and 3.7.

At lower ω's the 'broadened zero-phonon' term makes a contribution. This was calculated as explained in section 3. The sum of all contributions gives only moderate fits to the data, the derived value of $z(\omega)_T$ especially for $\omega = 1.23$ is thus subject to a larger uncertainty, see Fig. 4. Integrating under the curves of Fig. 4 gives $\int_0^\infty z(\omega)d\omega = 0.33$ for longitudinal modes and 0.61 for transverse modes.

These calculations were also made for the experimental conditions [7] using 6.3-Å neutrons, using throughout the input data derived from the foregoing analyses.

The resulting curves are shown in Fig. 5 where the important contributions from both multiple scattering [7] and multi-phonon effects are added and resolution broadening has been made numerically. The agreement with the experimental data is remarkably good for $\theta > 45°$ but at lower

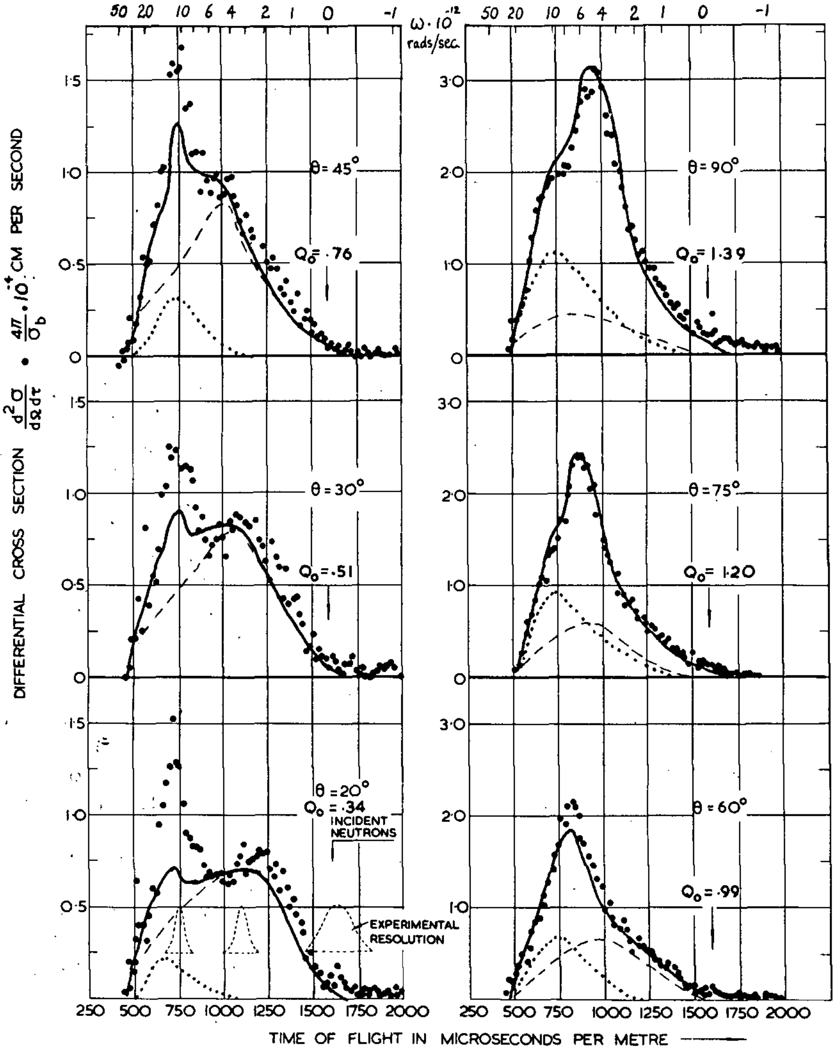

SCATTERED NEUTRON SPECTRA FROM LIQUID LEAD AT 350°C Plane Specimen (0·35cm)

INCIDENT NEUTRONS: 1612 μs/m, 6·3A, 2·0 meV

FIG.5. Experimental data [7] compared with present calculations. The multiphonon (dotted) and multiple scattering (broken curves) contributions are also shown.

angles the predicted 'longitudinal' peak is too small by a factor of order 2 at θ = 45° and 5 at θ = 20°.

5. BRIEF DISCUSSION

For ω > 10, where longitudinal modes dominate, the introduction of the longitudinal polarization factor is required to explain the observed features of the spectra. In the present calculations these features are found to be broader than is observed. At Eqs (3) and (5) the assumption is made that the initial structure $G(\vec{r}, 0)$, described by its transform $S(Q)$, persists for longer than the phonon lifetime . More accurately, the transform of $G(r, \tau)$ where τ is of the order of the phonon lifetime would be introduced. The expected trend with increasing τ is indicated by the following arguments.

Consider the total scattered intensity $S_\sigma(Q)$ viewed by a detector with Gaussian-shaped energy resolution of deviation, σ centred on elastic scattering. Then

$$S_\sigma(Q) = \int_{-\infty}^{\infty} d\omega\, e^{-\frac{\omega^2}{2\sigma^2}} S(Q, \omega) = \frac{\sigma}{\sqrt{2\pi}} \int d\vec{r}\, e^{-i\vec{Q}\cdot\vec{r}} \int dt\, e^{-\frac{t^2\sigma^2}{2}} G(\vec{r}, t)$$

Thus one views the transform of the time averaged structure over a period from zero to $1/\sigma$. The behaviour of $S_\sigma(Q)$ as σ decreases may be studied using the data of Refs [6] or [8]. The qualitative result that $S_\sigma(Q)$ always shows a peak at Q_m which narrows as σ decreases, while for $Q \gtrless Q_m$, $S_\sigma(Q)$ falls below $S(Q)$. This behaviour reflects the fact that the most persistent structural correlation is the mean interatomic distance.

It is therefore concluded that introduction of a time-dependent structure would yield more sharply defined features in $S(Q, \omega)$ as is required to fit the data. Observed phonon lifetimes increase with decreasing frequency [1]. Thus the required structure factor replacing $S(Q)$ is frequency dependent becoming more sharply peaked at lower frequencies.

For $\omega < 10$ where transverse components are postulated, the features associated with the longitudinal component are more evident in the experimental than in the calculated results. Sköld and Larsson [7] in a comparable analysis for liquid argon reach a similar conclusion. They therefore obtained $Z(\omega)$ assuming only longitudinal polarization, with consequent difficulties in normalization of the area of $Z(\omega)$. Improved fits can be achieved in the present analysis by a major modification of the assumed transverse dispersion curve and by introducing appreciable damping, while retaining $3/2 \int_0^\infty Z_T(\omega)d\omega \approx 3 \int_0^\infty Z_L(\omega)\, d\omega \approx 1$. This more arbitrary procedure is not detailed here.

REFERENCES

[1] COCKING, S.J., Adv. Phys. 16 62 (1967) 309; DORNER, B. et al., Disc. Faraday Soc. 43 (1968) 160.

[2] EGELSTAFF, P.A., AERE Reps N/R1164 (1958) and R.4101 (1962).

[3] SINGWI, K.S., Phys. Rev. 136 (1964) 969; Physica 31 (1965) 1257.

[4] COCKING, S.J., GUNER, Z., Inelastic Scattering of Neutrons in Solids and Liquids, (Proc. Symp. Chalk River, 1962) 1, IAEA, Vienna (1963) 237.

[5] RANDOLPH, P.D., Phys. Rev. 134 (1964) A1238.

[6] RANDOLPH, P.D., SINGWI, K.S., Phys. Rev. 152 (1966) 99.

[7] SKÖLD, K., LARSSON, K.-E., Phys. Rev. 161 (1967) 102.

[8] COCKING, S.J., EGELSTAFF, P.A., Phys. C. Ser. 2 1 (1968) 507.

[9] EGELSTAFF, P.A., SCHOFIELD, P., Nucl. Sci. Engng 12 (1962) 260.

[10] KAPLOW, R., STRONG, S., AVERBACH, B., Phys. Rev. 138 (1965) A1336.

[11] KAPLOW, R., AVERBACH, B., STRONG, S., J. Phys. Chem. Solids 24 (1964) 1195.
[12] NORTH, D., Thesis, University of Sheffield (1966).
[13] ASCARELLI, P., CAGLIOTTI, G., Nuovo Cim. 43B (1966) 375.

DISCUSSION

B. DORNER: I have a question and a comment on paper SM-104/27 by Tunkelo et al. First, in Fig. 6 of the paper why do you calculate contributions from transverse modes? When $\tau = 0$, κ, the momentum transfer, is parallel to q, the phonon wavevector, and under these conditions only longitudinal modes can be excited or de-excited. Secondly, not very long ago, Plesser, Stiller and myself contributed a paper on liquid lead to the Discussions of the Faraday Society (No. 43, 1967). In this paper we calculated the contribution of multiple scattering (in our case first elastic scattering and then inelastic), and it emerged that the transverse mode spectrum contributes very much more to the scattering inside the Brillouin zone around $\tau = 0$ than the longitudinal mode spectrum. I therefore believe that Mr. Tunkelo's lower peak is caused by multiple scattering, as in the case of our measurements on liquid and polycrystalline lead.

E. TUNKELO: As is stated in the paper it was assumed that, because of the anisotropy of the trigonal lattice, the modes which are transverse in the high-symmetry directions would generally have a polarization vector not exactly perpendicular to the direction of propagation. If the angle between the polarization vector and the direction of propagation differs from 90° on the average by 20°, the intensity shown in Fig. 6 is obtained. We made this assumption because the strength of the $\tau \neq 0$ contributions was insufficient to account for the peaks observed.

I quite agree with you that multiple processes are liable to produce the lower peak, and your criticism on this point is valid.

S.J. COCKING: May I offer a few explanatory remarks on my own paper (SM-104/115)? In the Egelstaff and the Singwi discussions of coherent scattering there is really only one model, namely, the imposition of a phonon-like description of the relative atomic motions. The different methods of introducing the liquid structure in the two approaches in fact give identical results. Thus, much discussion of the validity of a reciprocal lattice in a liquid is unnecessary and meaningless.

The finite range of the phonon and polarization of the phonon can in principle be introduced quite separately in either approach. The former was introduced only in Singwi's work and the latter only in Egelstaff's. The results presented in my paper demonstrate that the finite range extension alone does not adequately describe the data and so the derivation of a range parameter is not meaningful.

On the subject of the comparison of the value of τ_0 obtained from Singwi-Sjölander applied to sodium with that given in early work by myself, I should like to add that the values given in this previous work of mine were calculated and not derived from the measurements.

DIFFUSIVE MOTIONS IN BENZENE AND TOLUENE STUDIED WITH SLOW NEUTRONS

S. HOLMRYD AND G. NELIN
AB ATOMENERGI,
STUDSVIK, NYKÖPING,
SWEDEN

Abstract

DIFFUSIVE MOTIONS IN BENZENE AND TOLUENE STUDIED WITH SLOW NEUTRONS. The viscosity of benzene is described by the Arrhenius equation η = const. · $\exp(E/k_B T)$, where E is the activation energy for viscous flow. The viscosity of toluene, however, follows this law only in the higher temperature region of its liquid range, i.e. above the Arrhenius temperature T_A. In the whole normal liquid range the benzene molecule is supposed to be able to rotate many times about at least two symmetry axes between translational jumps. Davies and Matheson [1] suggest that the onset of non-Arrhenius viscosity behaviour in toluene occurs at that temperature at which rotation about two axes becomes restricted, while rotation about the third remains free.

Inelastic scattering experiments of slow neutrons have been performed on the two substances using a time-of-flight spectrometer for cold neutrons with an energy resolution of 12%. The quasi-elastic scattering has been studied for small momentum transfer as a function of temperature. Diffusion coefficients have been determined assuming a Lorentzian cross-section. The temperature dependence of the diffusion coefficient for benzene follows an exponential law, but the coefficient is a few times larger than the macroscopic coefficient, showing that a large amount of rotational diffusion exists. For toluene there is a change in the temperature dependence of the coefficient at about T_A. This is taken as an indication of a change in the number of degrees of rotational freedom of the toluene molecule around T_A. The methyl group in toluene has a low barrier to rotation ($\lesssim$500 cal/mole). Therefore the hindered rotation levels of the methyl group as well as molecular rotation will contribute significantly to the inelastic scattering spectrum which overlaps the quasi-elastic peak. The inelastic component is subtracted by extrapolation but the possible contribution of the CH_3 rotation to the quasi-elastic peak itself is neglected.

INTRODUCTION

Benzene and toluene have non-spherical molecules in which the intramolecular configuration is essentially fixed. The temperature dependence of the viscosity differs in these two substances. The viscosity of benzene follows in its entire normal liquid range (i.e. not in the supercooled region) the Arrhenius equation

$$\eta = \text{const.} \cdot \exp(E/k_B T) \tag{1}$$

where E is the activation energy for viscous flow, k_B the Boltzmann constant and T the absolute temperature. This equation fails, however, for liquid toluene below a temperature called the Arrhenius temperature.

Davies and Matheson [1] have for some hydrocarbons calculated and compared the free volume necessary for rotation of a molecule around three perpendicular symmetry axes through the center of gravity and the mean volume available to a molecule at the melting and boiling points and various other temperatures. They found that the molecules of a liquid following the Arrhenius law of viscosity are free to rotate about two or more axes. It is not important if one axis of rotation is restricted, since if rotation is occurring simultaneously and rapidly about the other two this is equivalent to rotation about the third axis. A rotation is called free, if a molecule is able to rotate 360° or more during the time between translational jumps. A liquid exhibiting both Arrhenius and non-Arrhenius viscosity behavior has free rotation about only one axis at lower temperatures while at higher rotation is possible about two or three axes. For that reason Davies and Matheson suggested that the onset of non-Arrhenius viscosity behavior occurs at that temperature at which rotation about two axes becomes restricted while rotation about the third remains free. In the Arrhenius region at least two rotational modes are free on the translational time scale and a molecule is able to reorient itself many times per translational jump. Here the viscosity is determined only by the probability that a molecule has sufficient energy to make a translational jump, and η is proportional to $\exp(E/k_BT)$. In the non-Arrhenius region a molecule may have sufficient energy to jump but it may not be in the correct position to do so, since this molecule and its neighbours are only free to rotate about one axis on the translational time scale. The viscosity is now determined by the probability that sufficient free volume is available. In that way there is a connection between the microscopic quantity molecular rotation and the macroscopic quantity viscosity. Finally, there ought to be some relation between viscosity and diffusion.

Information about diffusive motions in incoherently scattering liquids may be obtained from studies of quasi-elastic scattering of slow neutrons and especially from the broadening of the incident neutron spectrum as a function of temperature and momentum transfer. The dynamical aspects of the liquid which determine the width of the quasi-elastic peak are translational and vibrational motions of the center of gravity of the molecule and rotational and vibrational motions relative to the center of gravity by the whole molecule or a radical. A damped rotation gives a broadening of the incident neutron spectrum depending upon its relaxation time in relation to the time of other motions and to the neutron interaction time. Different degrees of rotational freedom would thus in principle be accessible by studies of the quasi-elastic scattering, but in practice the relations involved are complex. The purpose of this experiment was to investigate whether the change in the dynamics of toluene at the Arrhenius temperature (as shown in the viscosity behavior) depends upon a different number of degrees of freedom of rotation of the molecules above and below this temperature.

Benzene, C_6H_6, and toluene, $C_6H_5CH_3$, have their normal liquid range in the interval 279 - 353 °K and 178 - 383 °K respectively. The Arrhenius temperature of toluene is (288 ± 5) °K. The viscosity of both liquids is about the same, 0.5 - 0.6 cP at room temperature. Table I shows the calculations by Davies and Matheson [1] of molecular volumes, R_A, R_B, R_C respectively, required for rotation around symmetry axes and the available volumes, V_M V_A, V_B respectively, at the melting point, the Arrhenius temperature and the boiling point. The A axis is taken as the longest diameter through the center of gravity of the projection of the molecule, the B axis is taken perpendicular to the A axis in the plane of the projection and the C axis is perpendicular to the A and B axes. This definition of the A axis is not unique for benzene but the three possibilities are all equivalent.

Benzene and also toluene has in the past been carefully investigated by various methods, including inelastic scattering of neutrons. Quasi-elastic scattering of neutrons on benzene has been studied by Golikov et al. [2] but to our knowledge no such studies have been done on toluene.

TABLE I

Molecular volumes in $Å^3$

	R_A	R_B	R_C	V_M	V_A	V_B
Toluene	149	210	167	158	175	195
Benzene	143	137	127	145	-	160

EXPERIMENTAL RESULTS

The experiment was performed at the time-of-flight spectrometer at the Swedish reactor R2, which has been described elsewhere [3]. A beryllium filter and a semi-monochromatizing chopper are used in the incident beam. The incident wavelength is 4.1 Å and the spectrum width 0.6 meV giving an energy resolution of 12 %. The time resolution at the quasi-elastic peak is 1.2 %. Benzene and toluene of "pro analysi" quality were used. The sample was in the shape of a cylindric shell 0.2 mm thick, giving a transmission of 85 - 87 %. No corrections have been made for multiple scattering. De Graaf [4] has discussed this problem for hydrocarbons and gives some references to investigations of the subject, concluding that multiple scattering has a negligible effect on the quasi-elastic scattering. The background with empty container was measured both before and after a measurement with sample. The container also gives a peak at the incident energy, which at the maximum is at most 20 % of the quasi-elastic peak of the sample.

The inelastic background involved in the quasi-elastic peak was approximately determined from the time-of-flight spectrum, fig. 1, by tak-

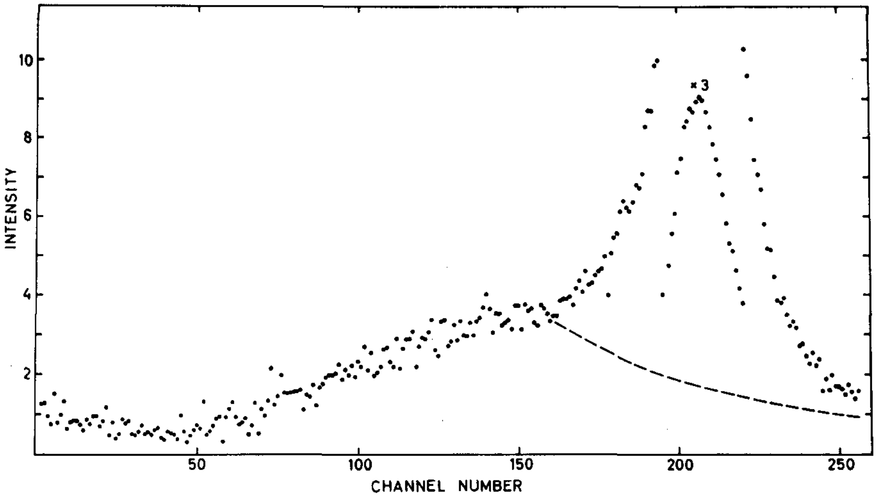

FIG.1. Time-of-flight spectrum of toluene at T = 333°K and θ = 30°. The broken curve shows the inelastic background which has been subtracted. (The wavelength λ = (0.02173 n - 0.418) Å, where n is the channel number.)

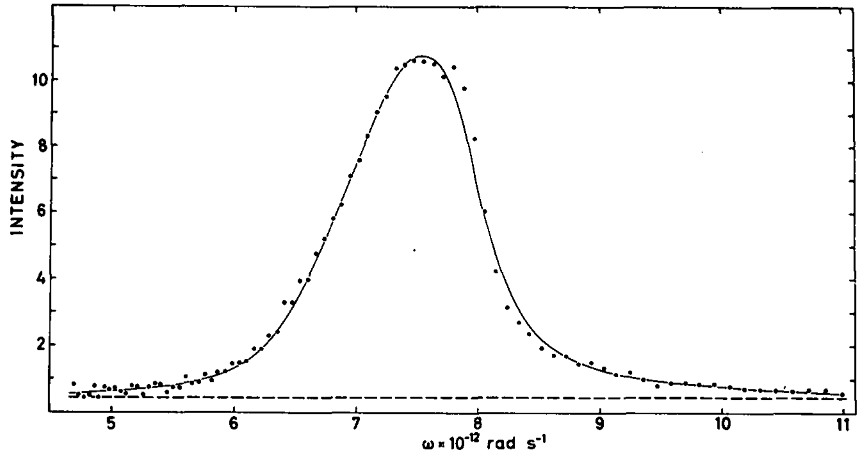

FIG. 2. Quasi-elastic peak of toluene at T = 243°K and θ = 30° in energy scale before subtraction of the inelastic background given by the broken line. The curve shows the best fit with a Lorentzian. The centre of gravity of the incident spectrum is 7.49×10^{12} rad/sec.

ing the intensity values at the wings of the quasi-elastic peak; when transformed to energy scale, these are very nearly constant. A constant background, fig. 2, of about this value was also subtracted from the peak in the energy scale in a way that gave the best fit to a Lorentzian folded with the incident spectrum. This value of the background always gave a reasonable fit to the wings in the time-to-flight spectrum. The broken curve in fig. 1 indicates this subtracted background in the time-of-flight scale. The spectrum shown represents the worst case in this sense. The intensity on the high-energy side is large and the quasi-elastic peak so broad that the available region on the low energy side is not sufficient to study the wing far out. The inelastic part, as indicated in fig. 1, has about the shape a free gas model would give. De Graaf [4] has used the free gas approximation of Krieger - Nelkin with an effective mass according to Sachs and Teller to calculate the inelastic background to be subtracted from the quasi-elastic scattering for some hexanes. At normalization he obtained a good fit to both wings, and the background determined agreed qualitatively with that estimated in this experiment. Even if the method of background calculation is open to objections, it is concluded that the error in the width of the quasi-elastic peak because of the uncertainty in the background will be rather small and of little importance, at least in a search for qualitative effects. The subtracted inelastic background amounted to 7 % of the quasi-elastic peak intensity.

The main interest is connected to the quasi-elastic peak after subtraction of the inelastic background. The cross section of the scattering is assumed to be of Lorentz form. A Lorentzian with various widths has been folded with the incident spectrum to give the best fit as described above. The fit was good except for toluene at the lowest temperatures. Fig. 2 shows the case with the largest disagreement between the calculated curve and the measurements. This deviation will be discussed later. The dip at the top of the peak is caused by aluminium in the path of the scattered beam.

The relation for simple diffusion,

$$\Delta E = 2\hbar \text{ "D" } \kappa^2 \tag{2}$$

was used to calculate the diffusion coefficients. The full width at half height ΔE, of the Lorentzian cross section corresponding to measurements at a scattering angle of 30° was used in this formula. $\hbar\varkappa$ is the momentum transfer. The value of $\varkappa^2$ at a scattering angle of 30° is 0.64 Å^{-2}. The diffusion coefficients thus obtained are ploted in fig. 3 for benzene and in fig. 4 for toluene as a function of reciprocal temperature. In the first of these figures the self diffusion coefficient of benzene is given for comparison. The values originate from Rathbun and Babb [5] as average values of measurements by them and others.

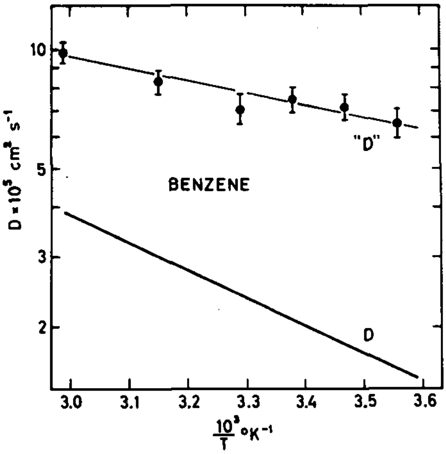

FIG.3. The apparent diffusion coefficient "D" of benzene. The self-diffusion coefficient D is given for comparison.

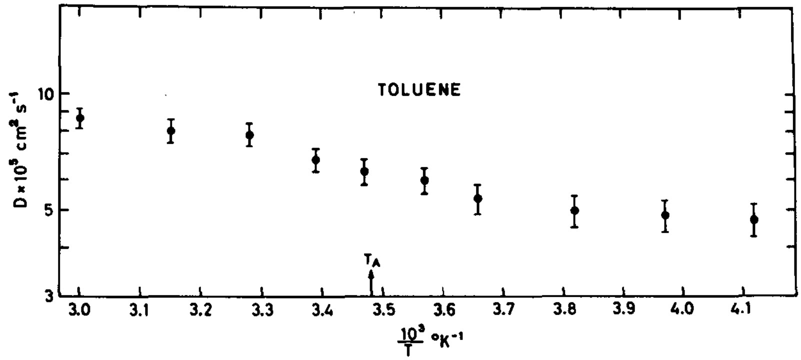

FIG.4. The apparent diffusion coefficient of toluene.

DISCUSSIONS

If the scattering does not follow the simple diffusion law, i.e. the width of the Lorentzian as a function of $\varkappa^2$ is not a straight line according to (2), the calculated "D"-values should be those given only by the slope at the origin. However, measurements for a smaller and a larger angle gave ΔE-values within the estimated error, together making a straight line through the origin as a function of $\varkappa^2$. The diffusion coefficients thus determined are the apparent diffusion coefficients depending upon the proton motions as seen by the neutron. To separate them from the self diffusion coefficient D they are indicated with inverted commas. The diffusion coefficient "D" of benzene plotted on a logarithmic scale as a function of inverse temperature follows a straight line, fig. 3.[x] The data for toluene show different slopes in different temperature regions, fig. 4, which is taken as an indication of an appreciable change in the rotational freedom of the toluene molecule at about $T_A = 288\ ^{\circ}K$.

Rush [6] suggests a value of less than 12 meV for the torsional oscillations in solid mesitylene in which the methyl group has no adjacent group and thus has a similar position to that in toluene. It is assumed that the inelastic contribution from the rotation of the CH_3 group could be subtracted as a part of the inelastic background. There could still be a contribution to the quasi-elastic peak, but it is believed that the influence on the widths is small, as the measured apparent diffusion coefficients for benzene and toluene have about the same values at higher temperatures (in the Arrhenius region) as would be probable. The temperature dependence of the motions of the CH_3 group ought to be smooth and any large change in the shape of the curve of the diffusion coefficients as a function of temperature would depend upon the motion of the whole molecule.

The great difference between the diffusion coefficient determined from the neutron scattering and the self diffusion coefficient shows the large number of rotational modes that exists [7, 8]. The translational vibratory spectrum is expected to be eliminated by the subtraction of the inelastic background. Benzene is able to rotate about one symmetry axis even in the solid phase near the melting point [9]. In the solid phase at 273 °K some broadening was obtained and the diffusion coefficient was about one third of the difference between "D" and D near the melting point. The solid phase of benzene will be investigated further to study the torsional motions.

Above 273 °K a folding with a Lorentzian cross section fits the experimental data quite well, but for lower temperatures toluene shows deviations on the high energy side. Dahlborg et al. [10] have studied neutron scattering from pentane and pentanol with a two-axis crystal spectrometer using the inverted filter method with BeO. The energy resolution is 0.1 meV and the energy transfers studied less than 1 meV. The inelastic background from the translational vibratory spectrum appears as small and flat. The experimental results show two peaks, one high and narrow the other low and broad. Dahlborg et al. found that it is possible to fit the quasi-elastic scattering with two Lorentzians which together give a width equal to the width obtained with this time-of-flight spectrometer when the inelastic background is subtracted according to the method described above. The temperature dependence of the sum of the intensity of the two Lorentzians was the same as that for the single Lorentzian obtained with the other spectrometer. The two peaks in the quasi-elastic peak may be explained as follows. The narrow Lorentzian corresponding to the higher central peak originates from translational and rotational diffusion of Brownian type. The broader one comes from strongly damped torsional oscillations of the molecule causing large jumps which contribute to the rotational part of the diffusion. The width of the broader peak is, however, almost independent of the momentum transfer, and for that

---

[x] One low point at 304 °K comes from a measurement showing unlikely intensity values, i.e. the deviation is likely to be caused by an occasional error.

reason it could be considered as inelastic scattering. In benzene and toluene there is a large contribution of hindered rotations of the whole molecule. The rotational part of the scattering will increase in relation to the translational one with decreasing temperature, as seen from the diffusion coefficients. For higher temperatures the Brownian diffusion peak is wide and a good fit is obtained for that peak superimposed on the rotational one. For toluene at lower temperatures the diffusive peak is narrower and the rotational peak still broad. Transitions between torsional levels of the molecule give energy transfers proportional to $\sqrt{kT/I}$, where I is the moment of inertia [10]. For heavy molecules as in the present case this means relatively small energy transfers giving a large contribution to the quasi-elastic peak in the whole liquid region. Therefore a single Lorentzian tends to be a bad approximation in the low temperature region. However, on the basis of other work [8, 10] it is believed that the single Lorentzian approximation in a qualitative sense gives the basic features of the diffusive processes hidden in the quasi-elastic peak in a correct way. If greater detail is required in the analysis it is necessary to have high-resolution data. The width of 0.6 meV of the incident spectrum used in this investigation does not permit a more penetrating analysis.

CONCLUSIONS

The diffusion coefficients "D" are determined from a quasi-elastic spectrum of considerable complexity. The interpretation of the results is for that reason difficult. The total rotational part is large and it will influence the "D" values to a great extent. The contribution from both the translational and the different rotational motions will change in the same direction for an altering hindrance of rotation of the molecule and tends to give qualitatively correct information. It is therefore believed that the change in the temperature dependence of the diffusion coefficients of toluene at about the Arrhenius temperature is likely to be caused by a change in the rotational freedom of the molecule.

If higher resolution measurements showed that the quasi-elastic spectrum separates into two components, the authors believe that the presently observed behavior of "D" for toluene would give similar effects: at higher temperatures the central narrower peak would be relatively wide, while at low temperatures it would be narrow and the single Lorentzian approximation would be worse. However, this would also correspond to an increased hindrance to rotational motion for decreasing liquid temperatures in agreement with the conclusions above.

The analysis and measurements will be continued mainly to obtain line width curves and Debye-Waller factors.

ACKNOWLEDGEMENT

The authors are indebted to Dr. K.E. Larsson for critical reading of the manuscript and to him and Mr U. Dahlborg for valuable discussions. Mr L. Karlén has given us skilful technical assistance.

REFERENCES

[1] DAVIES, D.B., MATHESON, A.J., J. Chem. Phys. 45 3 (1966) 1000. Trans. Far. Soc. 63 531 (1967) 596.

[2] GOLIKOV, V.V. et al., Inelastic Scattering of Neutrons II, IAEA, Vienna (1965) 201 (In Russian).

[3] HOLMRYD, S., SKÖLD, K., PILCHER, E., LARSSON, K.E., Nucl. Instr. Meth. 27 1 (1964) 61.

[4] de GRAAF, L.A., Thesis, Technische Hogeschool, Delft, The Netherlands (1967).

[5] RATHBUN, R.E., BABB, A.L., J. Phys. Chem. 65 6 (1961) 1072.

[6] RUSH, J.J., J. Chem. Phys. 47 10 (1967) 3936; 37 (1962) 234.

[7] LARSSON, K.E., BERGSTEDT, L., Phys. Rev. 151 1 (1966) 117.

[8] LARSSON, K.E., Phys. Rev. (1968) to be published.

[9] ANDREW, E.R., Physics Chem. Solids 18 1 (1961) 9.

[10] DAHLBORG, U., FRIBERG, B., LARSSON, K.E., PIRKMAJER, E., This conference Paper 36.

INELASTIC SCATTERING OF THERMAL NEUTRONS BY SOME BENZENE DERIVATIVES

V. TREPĂDUŞ AND D. BALLY
INSTITUTE FOR ATOMIC PHYSICS,
BUCHAREST, ROMANIA,
AND
V.A. PARFENOV AND V.G. LIFOROV
INSTITUTE FOR PHYSICS AND ENERGETICS,
OBNINSK, USSR

Abstract

INELASTIC SCATTERING OF THERMAL NEUTRONS BY SOME BENZENE DERIVATIVES. Thermal neutron scattering in phenol, hydroquinone and pyrogallol in the liquid state was investigated. The E_0 energy of incident neutrons was varied between 15 and 50 meV and the scattering angles between 5° and 108°. The quasi-elastic maximum width of scattered neutron spectra were determined for $(0.1\ \text{Å}^{-2} < \kappa^2 < 9\ \text{Å}^{-2})$. The obtained and computed values were compared by the Larsson-Bergstedt method. Very good agreement was obtained between the experimental and theoretical data for $\tau_0 = 10^{-12}$ sec; $\ell = 0.76$ Å. The result obtained can be explained by the contribution at the quasi-elastic maximum of neutron interactions with rotational oscillatory motion around an axis contained within a molecular plane. This interpretation can be justified by comparing our results with those obtained in the i.r. spectrum of benzene.

The transition corresponding to a wave number of approximately 60 cm^{-1} was observed in the quasi-elastic scattered neutron spectra of all substances studied and it was ascribed to molecular rotational oscillation around an axis contained within the molecule plane. The observed maxima in the three spectra corresponding to the wave numbers, 434 cm^{-1} (phenol), 412 cm^{-1} (hydroquinone) and 463 cm^{-1} (pyrogallol), are ascribed to superposing of the OH group vibration motions and benzenic ring deformation. A third maximum can be observed for hydroquinone and pyrogallol, corresponding to a wave number 150 cm^{-1}, characteristic for the hydrogen bond.

INTRODUCTION

Investigation of thermal neutron scattering has been the subject of several papers during the last few years. A compilation of these results can be found in Ref. [1]. In particular, diffusive motion in incoherent liquids where the hydrogen bond is present has been investigated. The comparison of results so obtained with cross-sections calculated for various models of the diffusive systems and with the data obtained by classical measurements suggested the complex character of the diffusive motion 'observed' by neutron scattering [2]. For these liquids it is expected that molecular rotational oscillations around one symmetrical axis of a molecule contribute to the diffusive motion observed by neutron physical methods, whose importance should depend on the neutron scattering temperature. For this investigations of organic compounds where the hydrogen bond is present are very important.

This paper reports the investigation of the diffusive motion and molecular dynamics of some benzene derivatives (phenol, hydroquinone, pirogallol). These substances were chosen because the benzene molecular structure and dynamics had been largely investigated by the methods of optical spectroscopy and by neutron physics methods. Therefore the interpretation of the motion modes modifications induced by hydrogen atoms substitution with OH groups is simplified by the possibility of referring the data obtained for these compounds to the data for benzene. The similarity existing between the hydrogen bond in phenols and alcohols allows further the correlation of data obtained during the investigation of these substances by neutron scattering. In this way the correctness of the model used for the description of diffusive motion in these last substances can be checked.

EXPERIMENTAL METHOD

The measurements were performed at the IBR-1 reactor of the Joint Institute for Nuclear Research (Dubna, USSR) using a time-of-flight spectrometer described elsewhere [3]. The energy E_0 of the incident neutrons has been varied over the range 15 to 50 meV. The scattered neutron spectra were taken at the following scattering angles: 5.5°; 8°; 21.5°; 38.9° using a 5.5-m flight path and at 67°; 92.2°; 105.3°; 108° using a 10.66-m flight path. The energy resolution of the spectrometer was better than 4%. The lack of precision of scattering angle, determined by geometry of the experimental arrangement, varied between 0.8° for the minimum scattering angle and 2.8° for scattering angles larger than 40°.

Measurements on phenol (60°C), hydroquinone (195°C) and pyrogallol (150°C) were carried out. The plane-shaped samples, having a thickness of 0.04 to 0.06 cm, were placed at 45° to the incident beam. Within the energy region covered in the experiment, the transmission of the samples was in all cases greater than 90%. The experimental data have been corrected for absorption in samples and container walls, detector efficiency and absorption in flight path. The multiple scattering, estimated according to Vineyard's method [4], was smaller than 5%. The central region (around the value $E = E_0$) of the scattered neutron measured spectrum is proportional with convolution between the device resolution function and the partial differential cross-section, the last being described by the sum of cross-sections for a diffusive system and for a monatomic gas. To extract the quasi-elastic component from the experimental data, the measured intensities were compared with the computed ones by introducing the actual width of quasi-elastic maximum and the monatomic gas mass as parameters [5].

RESULTS

The analysis of the quasi-elastic component of the scattered neutron spectra in the three substances investigated have permitted the determination of the values $\Delta E = f(k^2)$. The results obtained on phenol are shown in Fig. 1. Analogous results were obtained for the other two substances. In all cases the OH group presence suggests a dynamical behaviour of the molecules in liquid state analogous to the behaviour of aliphatic alcohol molecules. Therefore, it is expected that in the case of aromatic alcohols a treatment method of proton motions in hydrogenate complex liquids suggested by Larsson and Bergstedt [6] may be applied too. The viscosity

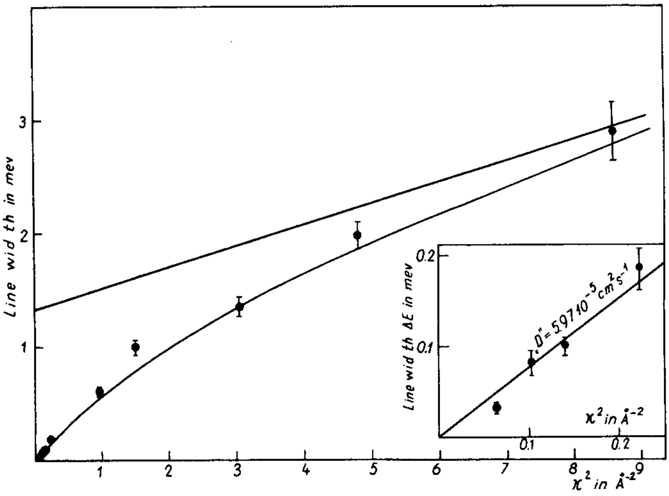

FIG.1. Observed widths of quasi-elastic lines for phenol. The solid line corresponds to the best fit of the theoretical width given in Ref. [6] and the straight line represents the asymptote of this curve intersecting the ΔE axis at $2\hbar/\tau_0$.

of phenol is 1.575 cP at 60°C [7], hence this liquid corresponds approximately to the third case dealt with in Ref. [6]: the time τ_1' during which the molecule is unbound is much larger than τ_0', the time during which the molecule is bound, and than τ_0, the internal mean life-time for a proton in an equilibrium position. The slope at the origin of the curve $\Delta E = f(\kappa^2)$ in 2 ℏ units equals in this case the diffusion apparent coefficient [6]: $''D'' = D + \tau_0^{-1} [1/2\, \ell^2 + < r_i^2/6 >]$ where D is the true macroscopic diffusion constant, ℓ is the proton jump length in the molecule, $<r_i^2/6>$ is the mean square value of the thermal cloud produced by proton motion. The "D" value 5.95×10^{-5} cm^2/sec was determined by approximating all experimental data obtained for $\kappa^2 < 0.2$ Å^{-2} with a straight line. The D value was determined from the relation: $D \sim T^{3/4} M^{-1/4} \eta^{-1/2}$ (T = liquid temperature in degrees K, M = molecular mass) by using the measured values for benzene at 25°C : D = 2.27 cm^2/sec [8], and $\eta = 0.599$ cP [9]. Thus $D = 1.45 \times 10^{-5}$ cm^2/sec was obtained for phenol at 60°C. It was found that the quantity $<r_i^2/6>$ determined by measuring the quasi-elastic maximum area was equal to 0.16 Å^{-2}. The values of ℓ and τ_0 have been obtained by successive approximations using relation (35 a) of Ref. [6]. The best fit of experimental data was obtained for $\ell = 0.76$ Å and $\tau_0 = 10^{-12}$ sec. This value of τ_0 corresponds to a torsional oscillation of the molecule around an axis contained in the plane of the molecule, with a 33.3 cm^{-1} wave number. The value of the quantity τ_0 is affected by both the proper measure errors and the errors resulting from the approximations carried out in computing of the line width ΔE. Therefore it can be expected that the value thus obtained, i.e. the frequency value, should correspond only approximately to the actual value of the molecular oscillation frequency.

The phenol molecule is plane; the OH group is located in the benzenic ring plane [10]. It was expected that within the model used for the description of the quasi-elastic component the molecule oscillatory motion should be carried out around an axis included in the molecular plane. The height of the potential barrier for internal rotation of OH group in phenol determined by Kojima [11] from the study of microwave spectra of phenol vapour was found to be 3.15 ± 0.3 kcal/mol at room temperature. Because it is normally expected that the activation energy for oscillatory motion is much lower than this value, it can be supposed that such motion will leave unchanged the position of hydroxyl groups. In this case this type of molecular motion must find its correspondent amongst the modes of benzene molecular motion.

The benzene investigation in solid state at 0°C, performed by Raman spectrometry by Frühling [12], led to the observation of four characteristic wave numbers $\nu_2 = 63$ cm^{-1}; $\nu_4 = 105$ cm^{-1}; $\nu_1 = 35$ cm^{-1}; $\nu_3 = 69$ cm^{-1}; the first two were ascribed to some rotational oscillation around an axis contained in the molecular plane and the last two to the rotational oscillation around the axis normal to the molecular plane. Later on Ichishima and Mizushima [13] by analysing again the Raman spectrum of solid benzene, concluded that the frequencies ν_1 and ν_4 correspond to the rotational oscillation around an axis contained within the molecular plane.

The investigation of the inelastic scattering of cold neutrons in liquid benzene led to a further observation of the frequency of 63 cm^{-1} associated with a rotational oscillation of the molecule (see for instance Ref. [14]). Therefore the results obtained during the experimental investigations of low frequencies characteristic of benzene molecules may be considered as representing a proof of data obtained in the study of the quasi-elastic component of the scattered neutron spectrum on phenol. In Fig. 2 our data on phenol and those for ethyl alcohol at 20°C ($\eta = 1.129$ cP) [15], propyl alcohol at 50°C ($\eta = 1.129$ cP) [16] and oleic acid at 60°C ($\eta = 1.40$ cP) [17] are shown. The diffusion coefficients of the last three substances have the following values (expressed in 10^5 cm^2/sec): 2, 5 and 5.2 respectively, while the true diffusion coefficients have the values (in the same units): 0.89, 1.1 and 5. Owing to sterical hindrance of the benzenic ring it is expected that the molecular associations in phenol will be weaker than in alcohols [8]. This would explain why $\tau_0' \ll \tau_1'$ in phenol while $\tau_0' \gg \tau_1'$ in propyl alcohol, although in these substances the viscosities are comparable and the molecular association mechanisms are analogous. As concerns the ethyl alcohol it is expected that the curve $\Delta E = f(\kappa^2)$ is analogous to that of propyl alcohol. A more detailed investigation of the quasi-elastic maximum width in the range of small κ^2 would contribute to a better explanation of the diffusion mechanism in this liquid. The curves $\Delta E = f(\kappa^2)$ for oleic acid and phenol are rather similar. Although the comparison is limited by the lack of experimental data on oleic acid, it can be appreciated that the curve $\Delta E = f(\kappa^2)$ for this liquid tends to its asymptotic value more rapidly than in phenol. The difference between the two curves could also be assigned to the fact that molecular associations for phenols are weaker than for aliphatic molecules containing OH or COOH groups.

The measured spectrum of scattered neutrons in phenol is shown in Fig. 3; the data obtained at two scattering angles were included in the plotting to illustrate the reproducibility of the observed characteristic points of the spectrum. A first spectrum inflection located around the value 57 cm^{-1} can, by analogy with the benzene spectrum, be ascribed to rotational oscillation around an axis contained within the molecular plane. This frequency is found practically in the same position of the scattered neutron spectrum in hydroquinone (Fig. 4) and pyrogallol (Fig. 5.)

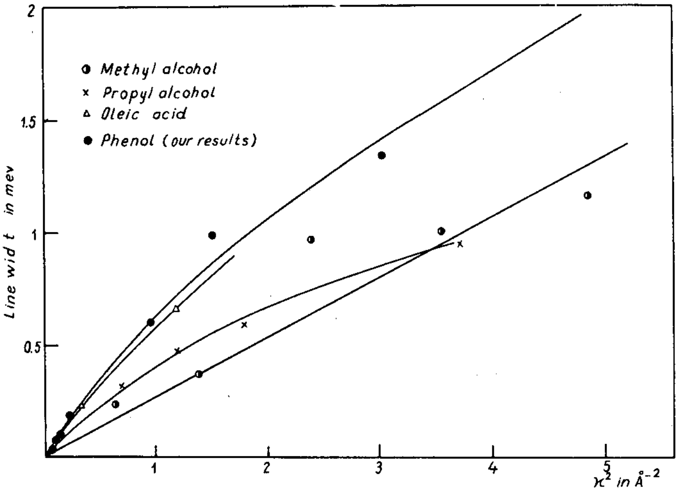

FIG.2. Experimental data $\Delta E(\kappa^2)$ for methyl alcohol [15], propyl alcohol [16] and oleic acid [17].

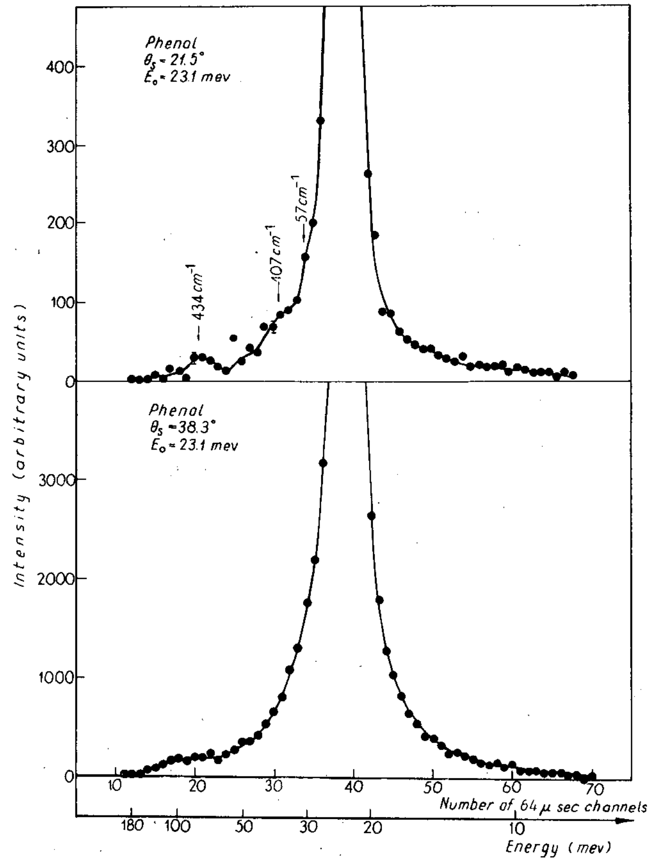

FIG.3. Observed spectrum of neutrons scattered by phenol.

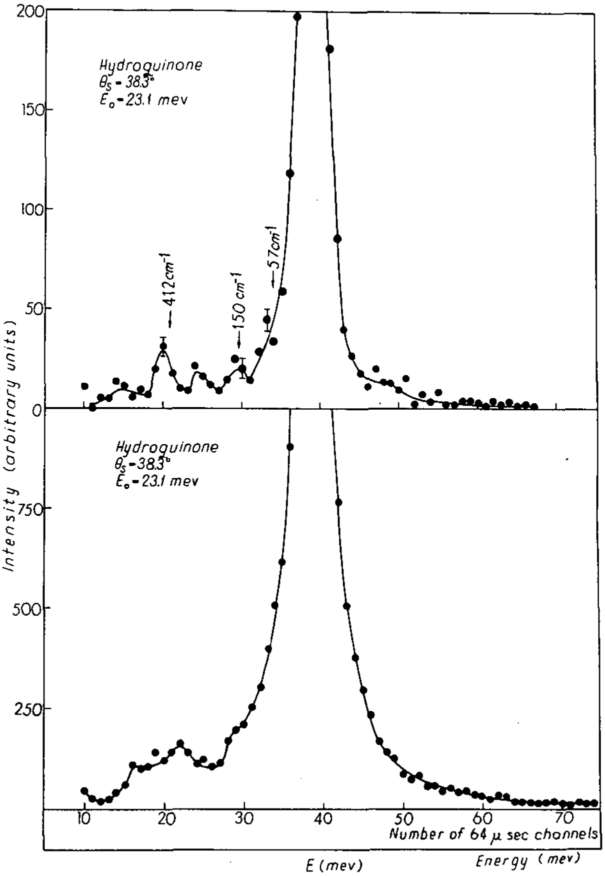

FIG. 4. Observed spectrum of neutrons scattered by hydroquinone.

The investigation of the i.r. absorption spectrum of liquid phenol, carried out by Hidalgó and Otero [19] led to the observation of two lines of approximately equal intensity, to which correspond the wave numbers 419 cm^{-1} and 452 cm^{-1}. The first line is associated with OH group vibration, the second is connected with deformation vibrations of the benzenic ring. The observed maximum within the spectrum of neutrons scattered in phenol (Fig. 3) corresponding to a wave number of 434 cm^{-1} can be interpreted as the superposition of maxima corresponding to the above-mentioned frequencies.

It should be mentioned that Evans [20], by investigating the infrared and Raman spectrum of liquid phenol, has observed in this region a wide maximum at 410 cm^{-1} in the i.r. and at 413 cm^{-1} in the Raman spectrum, which has been ascribed to benzenic ring deformation.

In the case of liquid hydroquinone the infrared spectrum contains the frequency 412 cm^{-1} associated with benzenic ring deformation and the frequency 410 cm^{-1} associated with OH group vibration [19]. The maximum of the inelastically scattered neutron spectrum in hydroquinone (Fig. 4) located at about 410 cm^{-1} can be thus ascribed to superposing of the

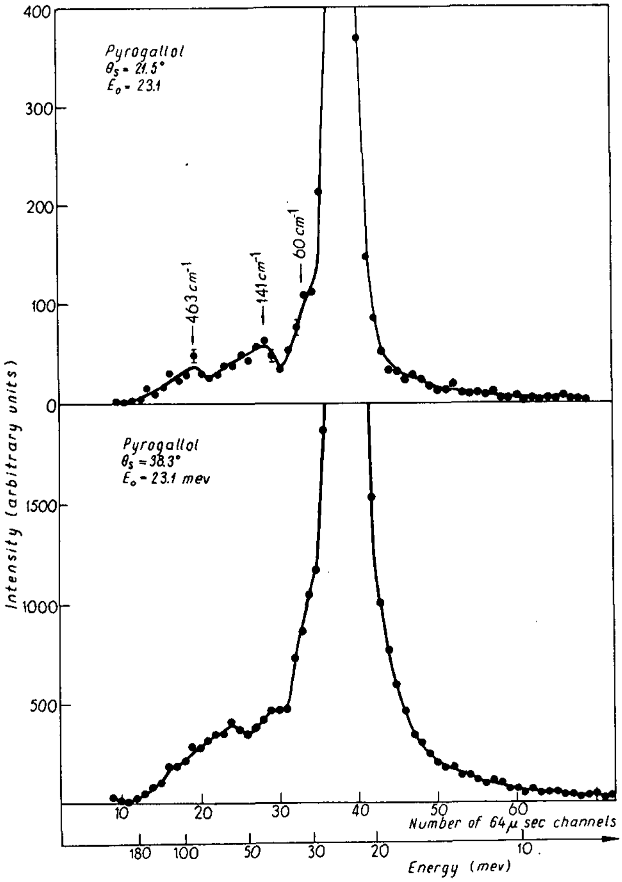

FIG. 5. Observed spectrum of neutrons scattered by pyrogallol.

contributions of two motion modes in neutron scattering. This spectrum presents also a maximum corresponding to a frequency of about 150 cm^{-1}, probably due to hydrogen bond oscillation. Indeed the absorption spectrum in the infrared domain for hydroquinone at 190° points to the presence of one wide absorption band extending between 140 - 220 cm^{-1}, centred approximately around the value 175 cm^{-1} [21] and ascribed to the above-mentioned motion modes.

The two maxima observed within the scattered neutron spectrum in pyrogallol (Fig. 5) and located around the frequencies 141 cm^{-1} and 463 cm^{-1} can be ascribed by analogy with data obtained for hydroquinone in the following way: the first maximum is due to the hydrogen bond oscillation and the second to superposing of the contributions of deformation oscillations of the benzenic ring and OH group vibrations.

REFERENCES

[1] Thermal Neutron Scattering, (EGELSTAFF, P.A., Ed.) Academic Press, London (1965) 347.

[2] LARSSON, K.-E., Inelastic Scattering of Neutrons (Proc.Symp.Bombay, 1964) 2, IAEA, Vienna (1965) 3; GOLIKOV, V.V., ZHUKOVSKAYA, I., SHAPIRO, F.L., SHKATULA, A., Inelastic Scattering of Neutrons (Proc.Symp.Bombay, 1964) 2, IAEA, Vienna (1965) 201.

[3] BONDARENKO, I.I., LIFOROV, V.G., NIKOLAEV, M.N., ORLOV, V.V., PARFENOV, V.A., SEMENOV, V.A., SMIRNOV, V.I., TURTCHIN, V.F., Inelastic Scattering of Neutrons in Solids and Liquids (Proc. Symp.Chalk River, 1962) 1, IAEA, Vienna (1963) 127.

[4] VINEYARD. G.H., Phys.Rev.110 (1958) 999.

[5] BALLY, D., TREPĂDUŞ, V., CARUTASU, I., to be published.

[6] LARSSON, K.-E., BERGSTEDT, L., Phys.Rev. 151 (1966) 117.

[7] SURYANARAYANA, C.V., SOMASNERDARAM, K.M., Acta Chim. Acad.Sci.Hung. 19 (1959) 337.

[8] FALCONE, D.R., J. phys.Chem. 71 (1967) 2754.

[9] GRUNBERG, L., Trans.Faraday Soc. 50 (1954) 1293.

[10] PAULING, L., The Nature of the Chemical Bond, Cornell University Press, Ithaca, 3rd ed. (1960) 490.

[11] KOJIMA, T., J. phys.Soc.Japan 15 (1960) 284.

[12] FRÜHLING, A., J. chem.Phys. 18 (1950) 1119.

[13] ICHISHIMA, I., MIZUSHIMA, S., J.chem.Phys. 18 (1950) 1687.

[14] ZEMLYANOV, M.G., TCHERNOPLEKOV, N.A., Inelastic Scattering of Neutrons in Solids and Liquids (Proc. Symp. Chalk River, 1962) 1, IAEA, Vienna (1963) 297.

[15] SAUNDERSON, D.H., RAINEY, V.S., Inelastic Scattering of Neutrons in Solids and Liquids (Proc. Symp.Chalk River, 1962) 1, IAEA, Vienna (1963) 413.

[16] LARSSON, K.-E., QUEROZ do AMARAL, L., IVANCHEV, N., RAPEANU, S., BERGSTEDT, L., DAHLBORG, U., Phys.Rev. 151 (1966) 126.

[17] LARSSON, K.-E., DAHLBORG, U., Physica 30 (1964) 1561.

[18] PIMENTEL, G.C., McCLELLAN, A.L., The Hydrogen Bond. W.H. Freeman and Co., London (1960) 20.

[19] HIDALGO, A., OTERO, C., Spectrochim\ Acta 16 (1960) 528.

[20] EVANS, J.C., Spectrochim.Acta 16 (1960) 1382.

[21] STANIEVICZI, A.E., Optika Spectrosk. 14 (1964) 781.

THERMAL NEUTRON INELASTIC SCATTERING BY METHYL ALCOHOL AND METHYL MERCAPTAN*

T.E. SAMPSON AND J.M. CARPENTER
DEPARTMENT OF NUCLEAR ENGINEERING,
THE UNIVERSITY OF MICHIGAN,
ANN ARBOR, MICH.,
UNITED STATES OF AMERICA

Abstract

THERMAL NEUTRON INELASTIC SCATTERING BY METHYL ALCOHOL AND METHYL MERCAPTAN. Thermal neutron inelastic scattering spectra of room temperature methyl alcohol (CH_3OH) and methyl mercaptan (CH_3SH) in the liquid state are reported. The principal feature of the spectra of both liquids is the narrow quasi-elastic peak prominent at low momentum transfers which merges into a broad band of energy transfers extending to energies greater than 100 meV at larger momentum transfers. For momentum transfers in the range 1-6 Å^{-1} the spectra for CH_3SH have a greater width than those for CH_3OH. This is attributed to the effect of the strong hydrogen bonding in CH_3OH which hinders both the rotation and translation of the methanol molecule, whereas hydrogen bonding in methyl mercaptan is believed to be quite weak. Measurements of the quasi-elastic line widths for small momentum transfers are also presented.

No prominent maxima are found in the inelastic spectra for either material. For CH_3OH a broad band of energy transfers in the range from 60-100 meV is attributed to the O-H out-of-plane deformation frequency. There is some evidence to support several weak events of under 20 meV. For CH_3SH there is also a broad high-energy band between 70 and 110 meV and the possibility of weak events in the low-energy region.

1. INTRODUCTION

Methyl alcohol (CH_3OH) and methyl mercaptan (CH_3SH) are both slightly asymetric top molecules which exhibit hindered internal rotation of the OH and SH groups about the symmetry axis of the methyl group. This is one of the dynamical features of methanol that has caused it to be extensively studied by optical techniques. Analysis of microwave spectra has yielded gas phase values of 374.8 cm^{-1} for the barrier height of CH_3OH [1] and 443.9 cm^{-1} for the barrier hindering internal rotation in CH_3SH [2].

The liquid phase values of these barriers are less well known. No data have been reported for CH_3SH while for CH_3OH a broad band centered about 670 cm^{-1} is attributed to the OH out of plane bending mode [3,4,5]. This frequency is greatly increased in the liquid because of the association of CH_3OH molecules by strong hydrogen bonding. Hydrogen bonding in CH_3SH is believed to be quite weak [6].

Total neutron scattering cross sections have been reported for the gaseous and liquid phases of both molecules [7]. These results display the effect of association in the liquid phase of methanol and indicate that it is possible that there is no perturbation of the hindered internal rotation in methyl mercaptan in the gas to liquid transition.

Cold neutron inelastic scattering measurements on liquid CH_3OH [8] and two deuterated species [9] have been analyzed in terms of the simple

---

* Work supported by The National Science Foundation.

diffusion model [10]. The neutron inferred diffusion constants are in good agreement with macroscopically measured diffusion coefficients. To our knowledge no inelastic neutron scattering data has been reported for CH_3SH.

The purpose of this paper is to present some preliminary results comparing the thermal neutron inelastic scattering cross sections of CH_3OH and CH_3SH in the liquid state at room temperature. It is hoped that these experiments will yield information on the effects of association and liquid state interactions on the hindered internal rotational frequencies of these molecules. Quasielastic line widths for several values of momentum transfer are also presented.

2. EXPERIMENTAL DETAILS

2.1 Time of flight spectrometer

These data were taken at The University of Michigan Phased Rotor Time of Flight Spectrometer [11] facility at the 2 MW Ford Nuclear Reactor. This facility is similar to the former Chalk River Scattering Law apparatus developed by Egelstaff and co-workers [12]. The scattered neutrons are detected at the end of a 2 m flight path by a bank of 7 five inch square Li^6F-ZnS scintillation detectors at a scattering angle of 90°. A second detector bank containing three detectors was used at scattering angles of 47.5° and 22°. Signal and background counts taken with a dummy target are stored in a 1024 channel time of flight analyzer. The sample and dummy targets were alternated on an eight minute counting cycle, six minutes for the sample and two minutes for the dummy. Data for two scattering angles were accumulated simultaneously. A range of incident energies from 18 meV to 46 meV was investigated with 6 us channel widths used below 30 meV. Above 30 meV both 4 us and 8 us channel widths were used.

The beam size is 1.0 in. by 1.25 in. at the target position with an intensity ranging from 1.7×10^5 n/min at 18 meV to 6×10^5 n/min at 46 meV. The energy resolution $\Delta E/E_0$ (FWHM) for elastic scattering is 7.4%. A typical set of scattering data was obtained in a 4-5 day run.

2.2 Samples

Reagent grade methanol (99.96% CH_3OH) was used after checking its density and boiling point. The methanol was contained in a 3.75 in. diam. sample holder [13] with .005 in. thick stretched aluminum foil windows. Nominal sample thicknesses of .015 in. and .010 in. were used although bulging of the foil windows increased this thickness somewhat. Target transmissions measured with the target at a 45° angle to the incident beam ranged from .77 to .92.

The methyl mercaptan samples (99.5% minimum purity) were obtained from the Matheson Company and were used without further purification. The sample was held as a liquified gas under its own vapor pressure of 15 psig in a welded aluminum container with a .040 in. wall thickness in the 1.5 in. by 3 in. target area. Sample thicknesses of .020 in. and .010 in. were used with target transmissions ranging from .8 to .9 at a 45° target angle.

2.3 Data reduction

After point for point background subtraction (corrected to equal counting times), the net counts are corrected for detector efficiency and averaged linearly over three points. An alternate data reduction program smooths both the signal and background over adjacent points with a 1:2:1 weighting before background subtraction and corrections for detector efficiency are made.

2.4 Multiple scattering

No corrections for multiple scattering have been made. Data taken with a target transmission of .8 do not appear to differ from those with a transmission of .9. As discussed by Slaggie [14], this does not necessarily mean that multiple scattering is not present; it most certainly is. It may mean, however, that multiple scattering is relatively insensitive to target transmission in this range. Existing beam intensity makes extensive experiments with samples of transmission greater than .9 impractical.

3. RESULTS AND DISCUSSION

3.1 Inelastic spectra

Inelastic scattering spectra from CH_3OH and CH_3SH are presented in Figures 1-4. The data are normalized to each other in such a way as to give equal average cross sections in a small range about zero energy transfer. The spectrometer resolution shown by the triangles has been calculated according to the formulation of Royston [15].

3.1.1 Methyl alcohol

Figure 1 displays the large energy transfer portion of the relative time of flight cross section of CH_3OH for several incident energies. The data for incident energies of 18 meV and 35 meV have been summed from two independent runs at each energy. The characteristic feature of these data is the appearance of a broad band of energy transfers in the region from 60-100 meV. This appears in the same region as a band in CD_3OH at 68 meV noted by Aldren et al. [9]. A very broad band centered around 80 meV in the i.r. spectrum of liquid CH_3OH has been assigned to the O-H out of plane bending mode [3,5]. The same assignment has been made for the Raman spectrum of the liquid [4]. Aldren et al. did not assign the band they noted at 68 meV but it appears that both it and the broad band observed in these experiments arise from the O-H out of plane bending mode. The data of Aldren et al. are especially useful in this assignment since scattering from the methyl protons is suppressed by deuteration.

This mode goes over to the hindered internal rotation or torsional oscillation in the gas phase with a 1-0 transition energy of approximately 30 meV [3,16,17]. The energy shift of this mode arises from the strong hindrance of the motion of the hydroxyl proton due to hydrogen bonding in the liquid state.

Relative time of flight cross sections for two different experimental conditions are shown in Figures 2a and 2b. These spectra seem to exhibit some structure at an energy transfer of 10-12 meV. From many other spectra observed there is also consistent, but weak evidence to indicate an event of 5-7 meV. Assignment of these events is difficult. Aldren et al. note

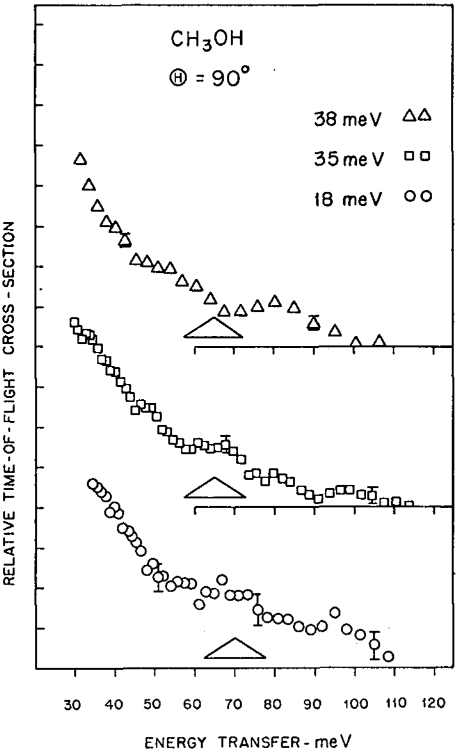

FIG. 1. CH$_3$OH relative TOF cross-sections for large energy transfers.

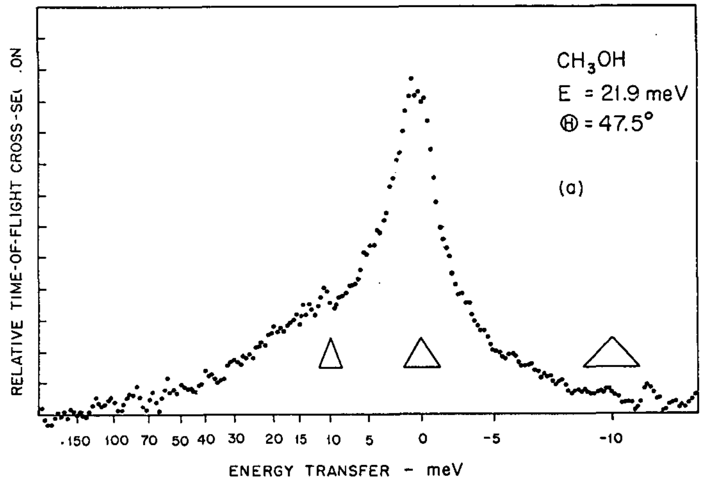

FIG. 2a. CH$_3$OH relative TOF cross-section.

a peak at 5 meV in CH$_3$OD. Raman lines at 8 and 16 meV have tenatively been described in terms of possible rotational oscillations of the CH$_3$OH units in dimers and trimers about the hydrogen bond [4]. The origin of the 10-12 meV event in our data is uncertain.

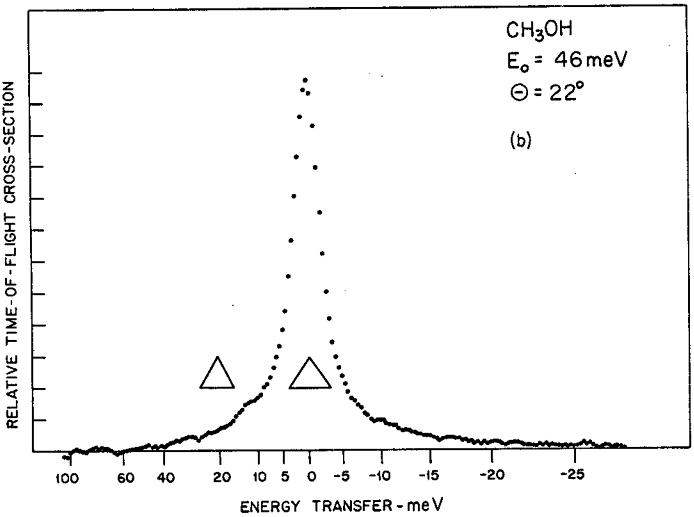

FIG. 2b. CH_3OH relative TOF cross-section.

3.1.2 Methyl mercaptan data

Large energy transfer data for CH_3SH at several incident energies are shown in Figure 3. These data also exhibit a high energy band, here in the 70-110 meV region. Spectroscopic data on CH_3SH are not as complete as those for methanol. However, Raman measurements in the liquid [18] and i.r. measurements in the gas phase [19] show two vibrations in this region, the C-S stretching mode at 702 cm^{-1} (87 meV) and the S-H in plane bending mode at 805 cm^{-1} (100 meV). Our data probably exhibit the effects of both motions.

In Figures 4a and 4b, complete spectra are presented for two different experimental conditions. Several other spectra in addition to that shown in Figure 4a exhibit structure in the 20-30 meV region. If the torsional oscillation frequency is unhindered in the liquid, this frequency would be expected to appear around 25 meV.

There is evidence to support the idea that molecular motions in liquid CH_3SH are not hindered strongly. Total neutron cross section measurements were noted in section 1. The limited optical data available show little shift in the vibrational frequencies in the gas-liquid transition. NMR measurements [6] also indicate that hydrogen bonding is quite weak. Our neutron measurements of quasielastic line widths (see section 3.2) indicate that proton motions are not hindered as strongly as in CH_3OH. This evidence indicates that it is possible that the torsional oscillation frequency is the same in the liquid and gas phases of CH_3SH. While our inelastic neutron scattering data do not firmly establish the torsional frequency in the liquid state, they are not inconsistent with the value of 25 meV expected if the motion is free.

Diffusive broadening of the quasielastic peak prevents identification of the 5 meV event shown in Figure 4b in any other spectra we have taken at larger momentum transfers. Higher resolution data at lower momentum transfers are needed to confirm this peak.

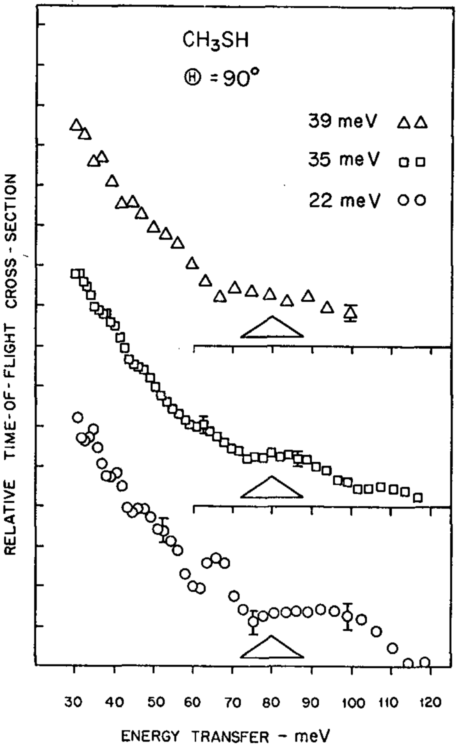

FIG.3. CH$_3$SH relative TOF cross-sections for large energy transfers.

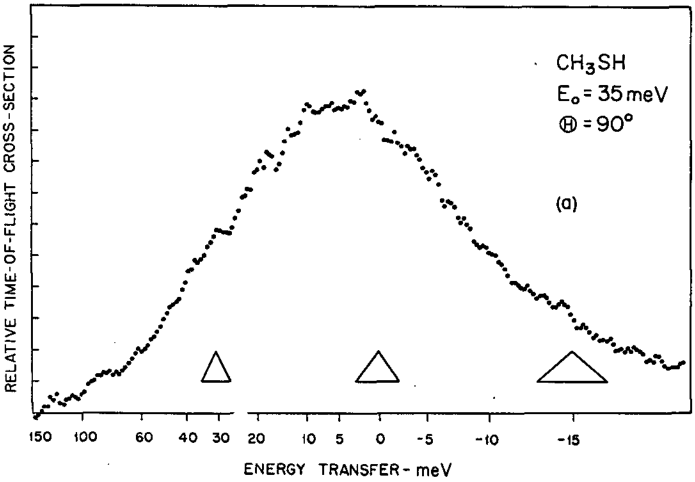

FIG.4a. CH SH relative TOF cross-section.

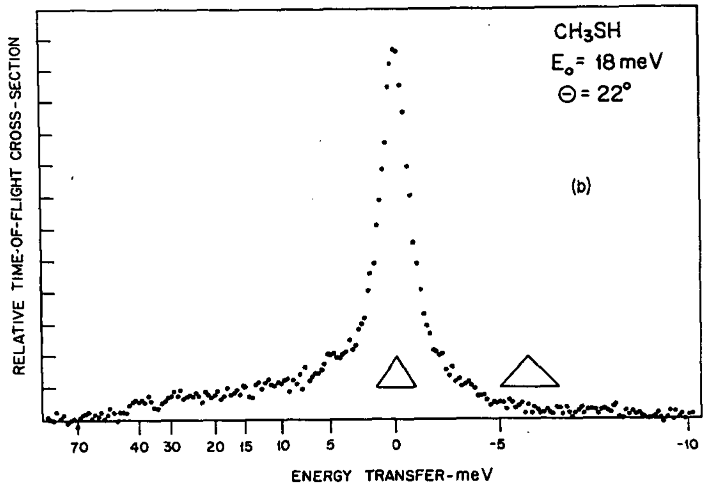

FIG.4b. CH_3SH relative TOF cross-section.

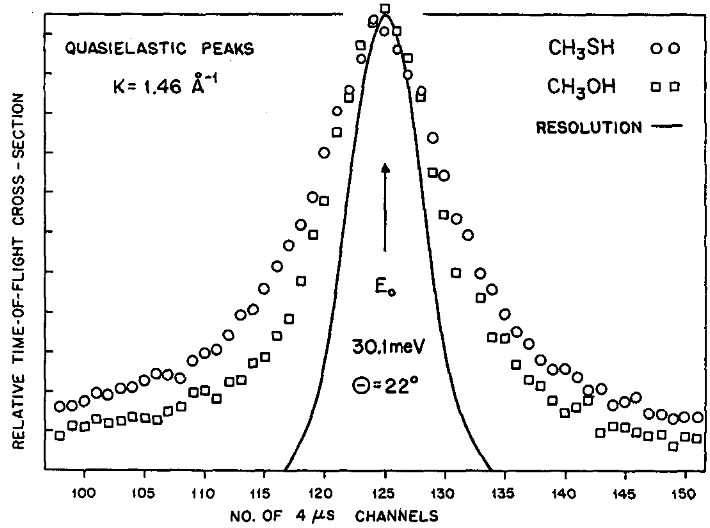

FIG.5. Comparison of quasi-elastic peaks for CH_3OH and CH_3SH.

3.2 Quasielastic line widths

Preliminary measurements of the quasielastic line widths for both molecules have been made. A comparison of typical spectra with the instrumental resolution function as measured by scattering from a .125 in. thick vanadium slab is shown in Figure 5. All three curves have been arbitrarily normalized at the peak. The line widths were extracted from the measured spectra with the usual assumption that the measured spectrum is the convolution of a lorentzian line shape and a gaussian resolution function.

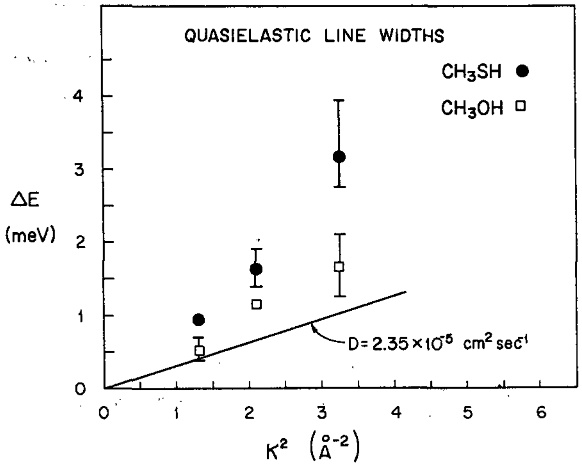

FIG. 6. Quasi-elastic line widths for CH_3OH and CH_3SH.

Figure 6 displays the results of these line width measurements. The line width predicted by simple diffusion theory [10] for CH_3OH using the macroscopically measured value of the diffusion constant at a temperature of 25°C ($D = 2.35x10^{-5}$ cm^2sec^{-1}) [20] is also shown.

The data for methanol fall consistently above the prediction of the simple diffusion model and above the cold neutron data of Saunderson and Rainey [8] and of Aldren et al. [9] whose data were consistent with a diffusion constant of $D = 2.1x10^{-5}cm^2sec^{-1}$. No comparison with simple diffusion theory can be made for CH_3SH since viscosity and diffusion data are not known.

The analysis of these data is considerably more difficult than that of the previously mentioned cold neutron data. The nearly symmetrical shape of the observed spectra in the wings of the peaks makes subtraction of the "inelastic background" difficult. The instrumental resolution of the cold neutron measurements is also superior to ours making such measurements easier to interpret.

Nevertheless, our data clearly show that the widths for CH_3SH are consistently larger than those for CH_3OH. This is observed not only for the data of Figure 6 but for all data observed thus far covering a momentum transfer range up to 6 $\mathring{A}^{-1}$. This is further evidence of the effect of the hindrance of molecular motions in methanol from hydrogen bonding compared to the free or less hindered motions in methyl mercaptan.

4. CONCLUSIONS

Thermal neutron inelastic scattering data have been reported for methyl alcohol and methyl mercaptan in the liquid phase at room temperature. For CH_3OH a high energy band in the 60-100 meV region has been assigned to the strongly hindered O-H out of plane bending motion. A similar band in the 70-110 meV region for CH_3SH probably arises from two vibrational modes in this region. Our data do not firmly establish the value of the torsional frequency for liquid CH_3SH but they are not inconsistent with the value of 25 meV expected if the motion is not hindered. Several energy transfers of under 15 meV have been noted in the two materials but can not be conclusively assigned from these data.

Quasielastic line widths measured for CH_3OH are larger than previous cold neutron results [8,9]. Line widths for CH_3SH are larger than those for CH_3OH for all momentum transfers observed up to 6 A^{-1}. This is further evidence for the idea that molecular motions in CH_3SH are much less hindered than in hydrogen bonded CH_3OH.

REFERENCES

[1] IVASH, E. V. and DENNISON, D. M., J. chem. Phys. 21 (1953) 1804.

[2] KOJIMA, T., J. phys. Soc. Japan 15 (1960) 1284.

[3] STUART, A. V. and SUTHERLAND, G. B. B. M., J. chem. Phys. 20 (1952) 1977.

[4] KRISHNAN, K., Proc. Indian Acad. Sci. 53A (1961) 151.

[5] FALK, M. and WHALLEY, E., J. chem. Phys. 34 (1961) 151.

[6] KRYNICKI, K. and POWLES, J. G., Proc. phys. Soc. Lond. 83 (1964) 151.

[7] BOROWSKI, F. and RŻANY, H., Nukleonika 10 (1965) 201.

[8] SAUNDERSON, D. H. and RAINEY, V. S., Inelastic Scattering of Neutrons in Solids and Liquids I IAEA, Vienna (1963) 413.

[9] ALDREN, B. K., EDEN, R. C. and WHITE, J. W., Disc. Faraday Soc. 43 (1967) 169.

[10] VINEYARD, G. H., Phys. Rev. 110 (1958) 999.

[11] ZWEIFEL, P. F., University of Michigan Report 03712-5-F (1964).

[12] EGELSTAFF, P. A., COCKING, S. J. and ALEXANDER, T. K., Inelastic Scattering of Neutrons in Solids and Liquids IAEA, Vienna (1961) 165.

[13] SAMPSON, T. E. and CARPENTER, J. M., Nuclear Instr. and Meth. 50 (1967) 179.

[14] SLAGGIE, E.L., Neutron Thermalization and Reactor Spectra (Proc. Symp. Ann Arbor, 1967) 1, IAEA, Vienna (1968) 311.

[15] ROYSTON, R. J., Nuclear Inst. and Meth. 30 (1964) 184.

[16] KOEHLER, J. S. and DENNISON, K. M., Phys. Rev. 57 (1940) 1006.

[17] BURKHARD, D. G. and DENNISON, K. M., J. mol. Spectroscopy 3 (1959) 304.

[18] VENKATESWARAN, S., Indian J. Phys. 5 (1930) 219.

[19] SKERRETT, N. P. and THOMPSON, H. W., Trans. Faraday Soc. 36 (1940) 812.

[20] RATHBUN, R. E. and BABB, A. L., J. phys. Chem. 65 (1961) 1072.

STUDY OF THE SOLID-LIQUID TRANSITION IN CYCLOHEXANE BY COLD NEUTRONS

V. TARINĂ
INSTITUTE FOR ATOMIC PHYSICS,
BUCHAREST, ROMANIA

Abstract

A STUDY OF THE SOLID-LIQUID TRANSITION IN CYCLOHEXANE BY COLD NEUTRONS. Measurements of total cross-section and double-differential cross-sections versus temperature for cyclohexane below and above the melting point were performed. The incident wavelength for total cross-section was 10.2 Å, while the double-differential cross-sections were measured using Be-filtered neutrons. The temperature was varied continuously between -20 and +20°C. A thermostat which kept the temperature constant to a precision better than ± 0.05°C was used. In this work the following problems are considered: (1) the comparison of the measured total cross-section of solid cyclohexane with that calculated by Kothari and Singwi for polycrystals; (2) determination of the Debye temperature for liquid cyclohexane; (3) the evaluation of a disorder entropy at the melting point transition; and (4) the existence of a 'homophase' premelting in the melting process of cyclohexane.

INTRODUCTION

Solid-liquid transition investigations on various substances are interesting not only to obtain detailed knowledge of the transition itself, but also because of the information they yield for the general study of the liquid state. Atomic or molecular vibrational motion is one of the physical parameters whose changes play an important part in this transition. It can be successfully investigated by means of low-energy neutrons. The temperature-dependence measurements of total cross-section for low-energy neutrons within the phase-transition range carried out till now have been directed towards the general aspect of the problem [1, 2]. In particular, cyclohexane total cross-section measurements in a large temperature range around the melting point allowed the determination of the total cross-section of protons bound in cyclohexane molecules [3].

In this paper the results of total cross-section and cold neutron inelastic scattering measurements carried out on solid and liquid cyclohexane near the melting point are reported. Cyclohexane was selected because its solid state crystallizes in a cubic system and for its properties as a 'globular' substance. Because of its properties, this molecular crystal can be likened to solidified noble gases and therefore it can be considered as a monatomic crystal whose atoms are changed in more complex units, i.e. molecules.

EXPERIMENTAL METHOD

Inelastic scattering measurements were carried out with beryllium-filtered neutrons in a set-up previously described [4]. The total cross-section measurements were performed by using 10.2-Å monochromatic neutrons from a mechanical monochromator [5] and a filter consisting of 35 cm monocrystalline bismuth and 15 cm monocrystalline lead. The resolution was $\Delta\lambda/\lambda \simeq 15\%$ at $\lambda = 10.2$ Å. The sample was a 0.043-cm layer of pure cyclohexane (99.99%) in an aluminium holder with a wall thickness of 0.15 cm. The holder was placed within an aluminium cylinder tightly sealed and containing dry air to prevent water deposits during measurements carried out at low temperatures. The sample cooling was performed by circulation of pressurized nitrogen vapour with a variable flow, passing through an aluminium pipe frame attached by a cadmium sleeve to the sample holder. The temperature was measured by means of a thermistor. To prevent errors in temperature read-off due to thermal inertia during the passage through the transition point, the thermistor was fitted within the sample. The thermistor sensitivity around the transition point was 0.2 Ω at 0.1°C. The thermistor was calibrated before the measurements were made and checked on their completion. By using the thermistor calibration, the sample temperature was continuously read off by a bridge method with an accuracy better than 0.05 degC. A thermostat using water as coolant was used for measurements at constant temperature. The temperature on the sample varied less than 0.01 degC due to thermal inertia at a variation of ±0.05 degC of thermostat water temperature.

RESULTS AND DISCUSSION

The total cross-section measurements were carried out by temperature continuous variation between -20 and + 20°C. The measured sample transmission at different temperatures ranged between 0.55 and 0.65. The intensities were registered for temperature increments of about 0.1 degC. The final cross-section values have been obtained by averaging over 1 degC several series of measurements. The results are shown in Figs 1 and 2. It should be observed that the total cross-section jump is not obtained at the same temperature if the measurements are carried out by sample cooling (Fig. 1) or heating (Fig. 2). During cooling the jump occurs just at the freezing point, while during heating this jump occurs at 8.5 degC before the melting point. Moreover, at the same temperature variation velocity the jump at the transition point occurs suddenly during sample

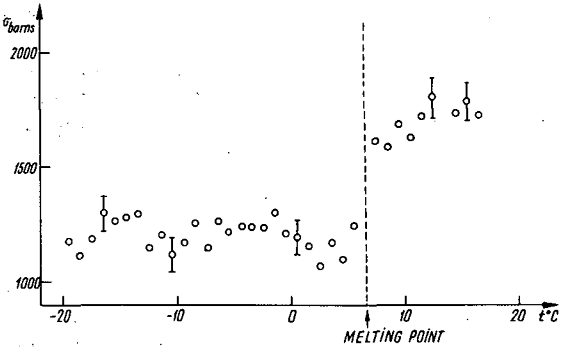

FIG.1. Total cross-section of cyclohexane versus temperature obtained by cooling the sample.

cooling, while during sample heating the jump spreads over 4 degC. When heating the sample, no other change occurs during the passage through the melting point and the total cross-section increases gradually with temperature. This behaviour can be associated with a 'homophase' premelting due to either vibrational anharmonicity of the formation of an anomalously high number of defects before reaching the melting point [6]. Data about adiabatic compressibility in this range [6] confirm this conclusion. Unfortunately, data about the variation of the specific heat at constant pressure (C_p) with temperature of this substance near its melting point are not available.

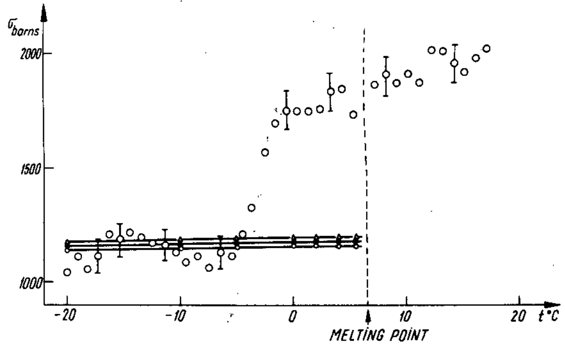

FIG. 2. Total cross-section of cyclohexane versus temperature obtained by heating the sample.

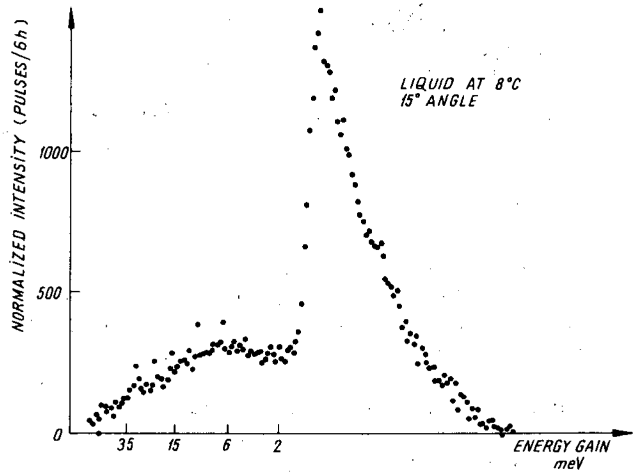

FIG. 3. Spectrum of scattered neutrons on liquid cyclohexane at 8°C and 15° angle.

The hypothesis concerning the influence of some impurities or pressure increase within the holder containing the sample can be omitted because the jump appears in the total cross-section just at the freezing point when cooling the sample. We intend to continue total cross-section measurements with other globular and non-globular substances to elucidate the contribution of the true premelting process.

The measurements of inelastic scattering were carried out at a 15° scattering angle and temperatures of 5 and 8°C, both at 1.5 degC from the melting point (6.5°C). The two curves with intensities normalized at the same measurement time (background subtracted) are shown in Figs 3 and 4. For solid cyclohexane, peaks corresponding to 28 meV (226 cm^{-1}), 5 meV (40.3 cm^{-1}) and 3.2 meV (25.8 cm^{-1}) energy transfer (of which the 28-meV peak is better resolved) can be observed in the inelastic part. These peaks can be associated with cyclohexane lattice acoustic branch frequencies. The two spectra obtained from the solid and the liquid phases are almost identical. It can be thus inferred that no essential change appears during the solid-liquid transition for the lattice vibrations acoustic branch, hence liquid cyclohexane just near the melting point can be considered as a quasi-crystalline melt.

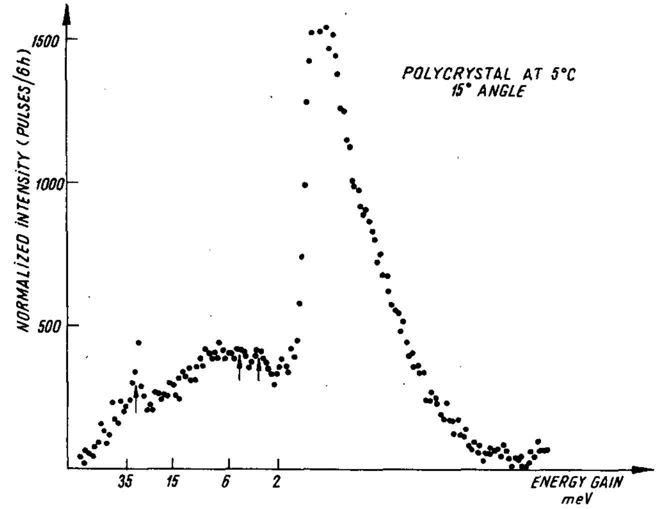

FIG.4. Spectrum of scattered neutrons on solid cyclohexane at 5°C and 15° angle.

Kitaigorodski [7] reported that the Debye approximation is also valid for molecular crystals when in computing thermodynamic functions only the lattice vibrations are considered. On the other hand, cyclohexane has a fcc lattice and, because it belongs to the 'globular' molecules class, it can be likened to a monatomic crystal [6]. The preceding discussion suggests the comparison of the measured total cross-section against temperature with the theoretical one, computed for cubic monatomic polycrystals with the Debye temperature as a parameter. The following version of the Kothari-Singwi formula [8] was used:

$$\sigma_s = -2\,(S+s)\,\frac{2m_0}{\hbar^2 M}\,\alpha E + \frac{3(S+s)m_0}{M\sqrt{E}}\,(k_0\,\theta_D)^{1/2}\Big[\Big(\frac{2}{5}\,\frac{T}{\theta_D} - \frac{1}{7} + \frac{1}{54}\,\frac{\theta_D}{T}\Big) + \frac{E}{k_0\theta_D}\,\Big(\frac{5}{3}\,\frac{T}{\theta_D} - \frac{1}{2}\,\frac{5}{84}\,\frac{\theta_D}{T}\Big) + \frac{E^2}{k_0^2\theta_D^2}\,\Big(\frac{7}{4}\,\frac{T}{\theta_D} - \frac{7}{24} + \frac{7}{240}\,\frac{\theta_D}{T}\Big) + \frac{E^3}{k_0^3\,\theta_D^3}\,\Big(\frac{3}{8}\,\frac{T}{\theta_D} + \frac{3}{16} - \frac{1}{96}\,\frac{\theta_D}{T}\Big)\Big] \qquad (1)$$

valid for $E \ll k_0\, \theta_D\ ,\ T \gg \theta_D\ ,\ M > 10\ a.m.u$

where $S = 4\pi\, \bar{a}^2, \quad s = 4\pi\, (\overline{a^2} - \bar{a}^2)$

a is the scattering length, m_0 is the neutron mass, ħ is Planck's constant, M is the molecular mass, E is the energy

$$\alpha = \frac{3\hbar^2}{k_0 \theta_D} F, \quad F = \frac{1}{4} + \frac{T}{\theta_D}\, \varphi\left(\frac{\theta_D}{T}\right), \quad \varphi(z) = \frac{1}{z} \int_0^z \frac{\beta\, d\beta}{e^{\beta} - 1}$$

k_0 is the Boltzmann constant, θ_D is the Debye temperature, and T is the absolute temperature. In our case: E = 0.00081 eV, $\theta_D \sim 60$°K, T = 253°K - 293°K, M = 84.16 a.m.u. and S + s = 978 barns (sum of incoherent scattering cross-sections of hydrogen atoms in the cyclohexane molecule). The total cross-section $\sigma_t = \sigma_s + \sigma_a$, where σ_s is given by Eq. (1), and σ_a is the absorption cross-section.

Function $\sigma_t(T)$ computed according to formula (1) is shown in Fig. 2. The $\theta_D(T)$ values used in the computations were obtained by linear extrapolation in the investigated temperature range of the straight line obtained between -80 and - 20°C by ultrasonic velocity measurements [9]. The difference of ~20% between the two sets of θ_D values given in Ref. [9] leads to a 1.8% difference in calculated $\sigma_t(T)$ values.

Also shown in Fig. 2 is the $\sigma_t(T)$ function computed for the two extreme energy values given by experimental arrangement resolution ΔE. This energy uncertainty lead to a ~1.7% variation in $\sigma_t(T)$. If $\sigma_t(T)$ is written as a function of θ only, the following equation is obtained:

$$\sigma_t = a_0 + \frac{a_1}{(\sqrt{\theta})^7} + \frac{a_2}{(\sqrt{\theta})^5} + \frac{a_3}{(\sqrt{\theta})^3} + \frac{a_4}{\sqrt{\theta}} + \frac{a_5}{\theta^2} + a_6 \sqrt{\theta} + a_7 (\sqrt{\theta})^3 \tag{2}$$

where the coefficients a_i are functions of T and E. For a given energy value, the coefficients a_i are very slowly varying functions of T in the range of interest. A typical plotting of $\sigma_t(\theta_D)$ function for T = 268°K is seen in Fig. 5. For a measured average value of σ_t = 1150 barns found for solid cyclohexane, two solutions for the Debye temperature θ_s are obtained: θ_s = 10°K and θ_s = 60°K. From Fig. 2 the value of σ_t = 1750 barns can be taken for the total cross-section of the liquid phase near the cross-section jump. This value leads to a Debye temperature for the liquid of θ_L = 7.5°K obtained from Fig. 5.

As suggested in Ref. [8], a disorder entropy at the melting point may be evaluated through the following relationship between θ_L, θ_s and $\Delta S = \alpha' k_0$:

$$\frac{L - \alpha' k_0 T_M}{3 k_0 T_M} = \ln \frac{1 - \exp(-\theta_S / T_M)}{1 - \exp(-\theta_L / T_M)}$$

Here L is the latent heat of melting, T_M is the temperature of melting, θ_s, θ_L are the Debye temperatures for solid and liquid respectively, and α' is a parameter to be determined. Using the values: $\theta_s = 60°K$ and $\theta_L = 7.5°K$, a negative value of $\alpha' = -4.5$ is obtained. The other set of values, $\theta_s = 10°K$ and $\theta_L = 7.5°K$, give an α' value of $\alpha' = 0.56$. In this case $\Delta S = 1.11$ cal/mole deg, a value lower than that of $\Delta S = 2$ cal/mole deg obtained from calorimetric measurements [6].

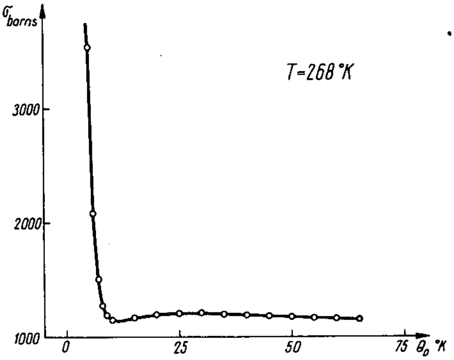

FIG. 5. Total cross-section versus θ_D for T = 268°K, computed by using relation (2).

A more detailed investigation of the disorder entropy at the melting point obtained from cross-section measurements at low-energy neutrons is planned.

ACKNOWLEDGEMENTS

The author is indebted to Dr. D. Bally for his interest in this work. He is also particularly grateful to E. Tarină for helping in carrying out the experiments, Mrs. H. Teutsch and N. Mateescu's group for supplying their apparatus for measurements of inelastic spectra. Many thanks are due to V. Ene for technical assistance.

REFERENCES

[1] EGELSTAFF, P.A., Thermal Neutron Scattering, Academic Press, London and New York (1965).
[2] HEINLOTH, K., Z. Phys. 163 (1961) 218.
[3] SCHMIDT, U., Atomkernenergie 11 (1966) 39.
[4] TEUTSCH, H., MATEESCU, N., NAHORNIAK, V., DIACONESCU, A., TIMIŞ, P., Rev. Roum. Phys. 9 (1964) 737.
[5] BALLY, D., TARINĂ, E., PÎRLOGEA, P., Rev. sci. Instrum. 32 (1961) 297.
[6] UBBELOHDE, A.R., Melting and Crystal Structure, Clarendon Press, Oxford (1965).
[7] KITAIGORODSKI, A.I., Kristallografia 7 (1962) 195.
[8] KOTHARI, L.S., SINGWI, K.S., Solid State Phys. 8 (1959) 109.
[9] GREEN, J.R., SCHEIE, C.E., J. Phys. Chem. Solids 28 (1967) 383.

THE DYNAMICS OF LIQUID H_2O AND D_2O AND SOLID H_2O FROM THE INELASTIC SCATTERING OF EPITHERMAL NEUTRONS*

O.K. HARLING
PACIFIC NORTHWEST LABORATORY,
RICHLAND, WASH., UNITED STATES OF AMERICA

Abstract

THE DYNAMICS OF LIQUID H_2O AND D_2O AND SOLID H_2O FROM THE INELASTIC SCATTERING OF EPITHERMAL NEUTRONS. An extensive series of neutron inelastic scattering measurements has been made on liquid H_2O and D_2O at 299°K and on solid H_2O at 268°K. Double differential cross-sections for H_2O were obtained for energy transfers to 0.6 eV and momentum wave vector transfers ($\Delta\bar{p}/\hbar$) to 32 $Å^{-1}$ while for D_2O the energy and momentum transfer range was 0.2 eV and 9.5 $Å^{-1}$, respectively. All measurements were obtained with the Battelle rotating crystal spectrometer using initial neutron energies of 0.101 to 0.616 eV. Scattering angles ranged from 15 to 155°. The measured differential cross-sections exhibit considerable structure in energy corresponding to the torsional motions and the intramolecular bending and stretching modes of the H_2O molecule. Instrumental resolution was adequate to obtain information about the widths of some of these transitions.

The angular dependence of scattering associated with the excitation of a definite mode, in a solid or liquid, can be expected to depend upon the shape of the potential well in which the dynamical unit moves. In the case of the present measurements on ice, it was possible to determine the angular dependence of the inelastic scattering from the torsional band. The experimental differential cross-section for excitation of these modes is found to be in good agreement with the angular dependence calculated for inelastic scattering from a symmetric harmonic oscillator potential.

Spectral density functions for the proton and deuteron have been obtained using an extrapolation technique. These density functions extend to higher energy transfers than previously published neutron results, and include the intramolecular bending modes of the water molecule. The mean squared amplitudes of the proton and deuteron clouds are derived from the spectral density functions. These amplitudes are found to be in agreement with neutron diffraction studies of D_2O but are smaller than values obtained by other investigators who measured the Debye-Waller factor for quasi-elastically scattered slow neutrons.

I. INTRODUCTION

There have been numerous neutron scattering studies of H_2O. An article by Springer(1) provides a comprehensive review of most of the work prior to 1961. More recent work includes the cold neutron studies of Larsson and Dahlborg,(2) and Golikov et al.(3) Down-scattering studies for energy transfers less than ∿0.15 eV have been reported by McMurry, Russell and Brugger,(4) Haywood,(5) and Mostovoi et al.(6) Low resolution measurements with energy transfers to 0.25 eV have been obtained by Kottwitz and Leonard(7) using a three axis crystal spectrometer. Measurements with energy transfers to 0.63 eV, have been published by Kirouac et al(8) for liquid H_2O. Harling(9,10) has reported neutron downscattering results on water and ice which included the observation of resolved intramolecular vibrations in H_2O.

---

* Work performed under US Atomic Energy Commission Contract AT (45-1)-1830.

Room temperature D_2O has also been studied previously by neutron inelastic scattering, although not as extensively as light water. Larsson and Dahlborg(11) have used beryllium filtered cold neutrons in upscattering to study heavy water dynamics, Haywood(12) used a four-rotor phased chopper for downscattering measurements with energy transfers to about 3 kT, and Whittemore(13) has used an electron linac and chopper for measurements with initial energies to 0.646 eV.

In the present paper an extensive series of slow neutron inelastic downscattering measurements on solid and liquid H_2O and D_2O are presented and discussed. A numerical compilation of cross section results has been published previously.(14) The measurements reported here were made on thin samples of liquid and solid. The energy transfer range ~0.0-0.6 eV with corresponding momentum wave vector transfers ($\vec{k} = \Delta\vec{P}/\hbar$) up to $32Å^{-1}$ has been investigated for H_2O while energy and momentum transfers to ~0.2 eV and 9.5 $Å^{-1}$ were used for D_2O. This range includes the highest energy bound proton motions in H_2O. The double differential cross sections, obtained from the scattered neutron spectra, exhibit some clearly resolved peaks corresponding to the hindered rotation and the high energy bending and stretching vibration of the H_2O molecule. The energies and neutron scattering widths of some of these modes have been obtained. Some preliminary results on inelastic scattering from heavy ice are also presented.

Spectral density functions have been derived using an extrapolation technique. These distributions give information about the modes of motion of H_2O and D_2O. The angular dependence of the inelastic scattering under the hindered rotation band in light ice, has been determined experimentally and compared with the dependence expected from a simple theoretical model.

Mean squared amplitudes of the proton and deuteron clouds have been obtained from the Debye-Waller factor for the entire range of inter and intra molecular motions of the water molecule. This result is compared with that obtained from other neutron scattering experiments and x-ray results.

II. EXPERIMENTAL PROCEDURES

The slow neutron downscattering technique was employed to excite translational, rotational and vibrational degrees of freedom up to and including the highest frequency intramolecular stretching modes of the H_2O molecule. The scattered neutron spectra were obtained with the Battelle Rotating Crystal Spectrometer (RXS).(15,16) A number of initial neutron energies were used ranging from 0.1 eV to 0.6 eV. The energy width of the incident neutrons ranged from approximately 1% at 0.1 eV to 3.5% at 0.6 eV. These small initial energy spreads, with time bursts of about 10 μs at the sample, gave a relatively high resolution which was narrower than the structure observed. Scattered neutron spectra were measured by time-of-flight at scattering angles from 15 to 155 degrees.

Liquid water samples were contained between 0.025 cm-thick aluminum sheets while the ice samples were built up in thin layers on a 0.158 cm-thick aluminum backing plate which was cooled by conduction from the edges. Transmission of the scattering samples was in the range of 90-93% for initial energies to 0.3 eV and ~80% for the measurements made with 0.6 eV neutrons. Additional experimental details are to be found in Reference 14.

III. DIFFERENTIAL CROSS SECTIONS

Examples of the measured double differential cross sections are shown in Figs. 1 to 5. Cross sections are given in barns per steradian per eV per H or D atom and are plotted versus the reduced energy transfer, $\beta = \Delta E/kT$, for each detector angle. Resolutions on energy transfer are shown as triangles which are given for selected values of β in some of the figures. These resolutions represent the total resolution except where they are shown in the quasi-elastic peaks, there they represent the energy spread only of the incident neutrons, i.e., ΔE_0.

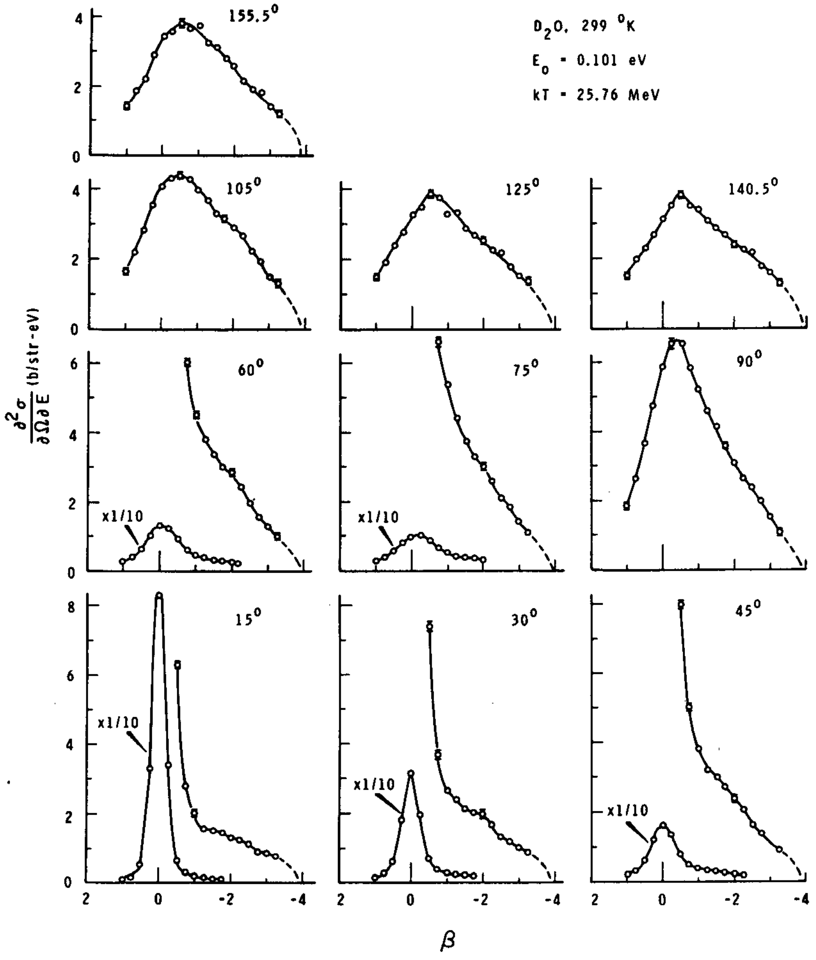

FIG.1. Double-differential cross-sections for D_2O at 299°K with E_0 = 0.101 eV.

The doubly differential cross section results for D_2O at 299°K and 272°K are presented in Figs. 1 and 2. A broad band near the energy corresponding to the hindered rotation is evident in the liquid cross section curves, particularly those at small scattering angles in Fig. 1. Preliminary results for solid D_2O are shown in Fig. 2. The hindered rotational band which has a maximum near 70 meV is much more pronounced than in the liquid. Measurements on liquid D_2O were also made with initial neutron energies of 0.213 eV, these showed the torsional modes but did not give clear indication of a well resolved peak due to the bending vibration, comparable to that which was found in H_2O.

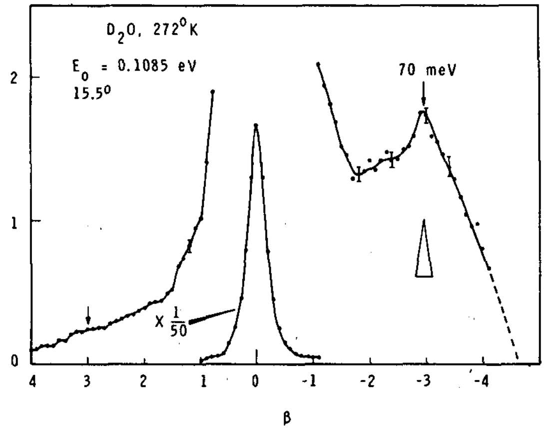

FIG. 2. Double-differential cross-section of D_2O at 272°K.

There is clear evidence for excitation of H_2O torsional modes in the double differential cross sections of Fig. 3, which were obtained with an E_0 = 151.5 meV. For the liquid this band is broad and not clearly separated from the elastic peak. Due to this broadness it is difficult to define an energy for the centroid of the band. However, it appears that a value somewhere between 60 and 70 meV is consistent with the experimental cross section curve. For solid H_2O the rotation band is clearly separated from the elastic peak and the centroid of the band appears near 93 meV while its width is ∿63 meV at the 15° scattering angle. As the scattering angle is increased the torsional band in ice continues to be distinct from the broadened elastic peak. For small energy changes, i.e., for those between the torsional band and elastic peak, the differential cross sections in ice are substantially smaller than those in room temperature water. This decrease in the lower frequency modes has also been observed in cold neutron measurements.(11) and in optical Raman work.(17)

Some cross sections for light water and ice at an initial energy of 304 meV are presented in Fig. 4. With this high an energy the intramolecular vibration, corresponding to the bending of the H-O-H angle, can be excited. The upper part of Fig. 4 shows a well resolved peak for the 15° detector, corresponding to the excitation of this molecular vibration in liquid H_2O. The broad continuum under the narrow peak is probably due to multiphonon scattering events. Spectrometer resolution is more than

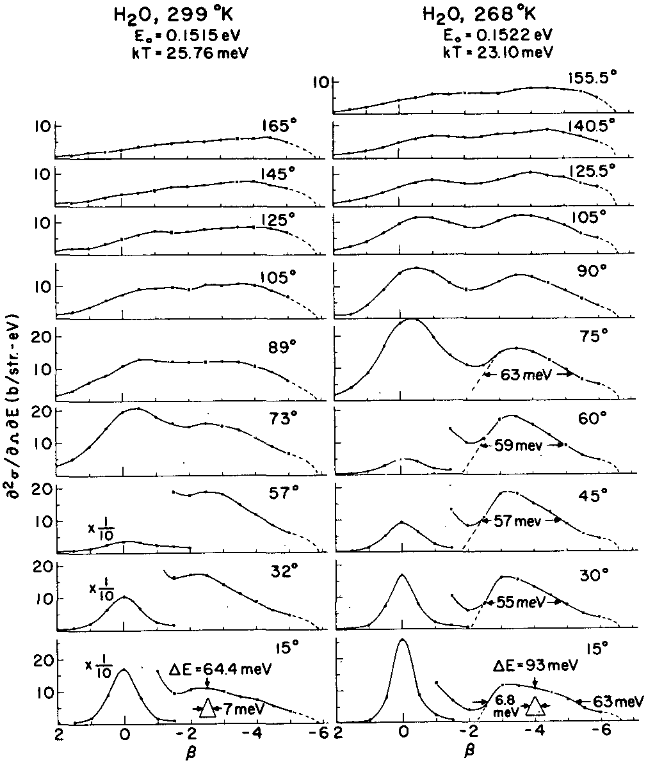

FIG.3. Double-differential cross-sections of H_2O at 299 and 268°K, $E_0 = 0.15$ eV.

adequate to permit unfolding of the level width. After correction for resolution a width of 23 meV centered at 206 meV is obtained. In the lower half of Fig. 4, the ice cross section curve, the rotational excitations are clearly resolved at an energy transfer of ∿90 meV. The resolution corrected width of the band is ∿57 meV in good agreement with the lower E_0 measurements. A peak centered near 206 meV undoubtedly corresponds to the bending mode of vibration. There is also some indication of multiple excitations involving the strong rotational levels. These multi-phonon peaks occur at β values of ∿8 and ∿12. The double excitation of the $\beta \approx 4$ rotational peak overlaps the vibrational peak and prevents an accurate determination of the width of the vibrational component.

Initial neutron energies of ∿0.6 eV were also used to measure the scattering cross sections of light water and ice. With these excitation energies the neutron scattering is sensitive to all the possible molecular motions and the highest frequency bound motions of the H atom. The cross section results for 268°K light ice are shown in Fig. 5. The results for the 15° scattering angle exhibit considerable structure in the form of multiple peaks corresponding to the symmetric and asymmetric stretching modes. Spectrometer resolution was ∿22 meV on energy transfer in the region of the high frequency intramolecular vibration peaks and since the

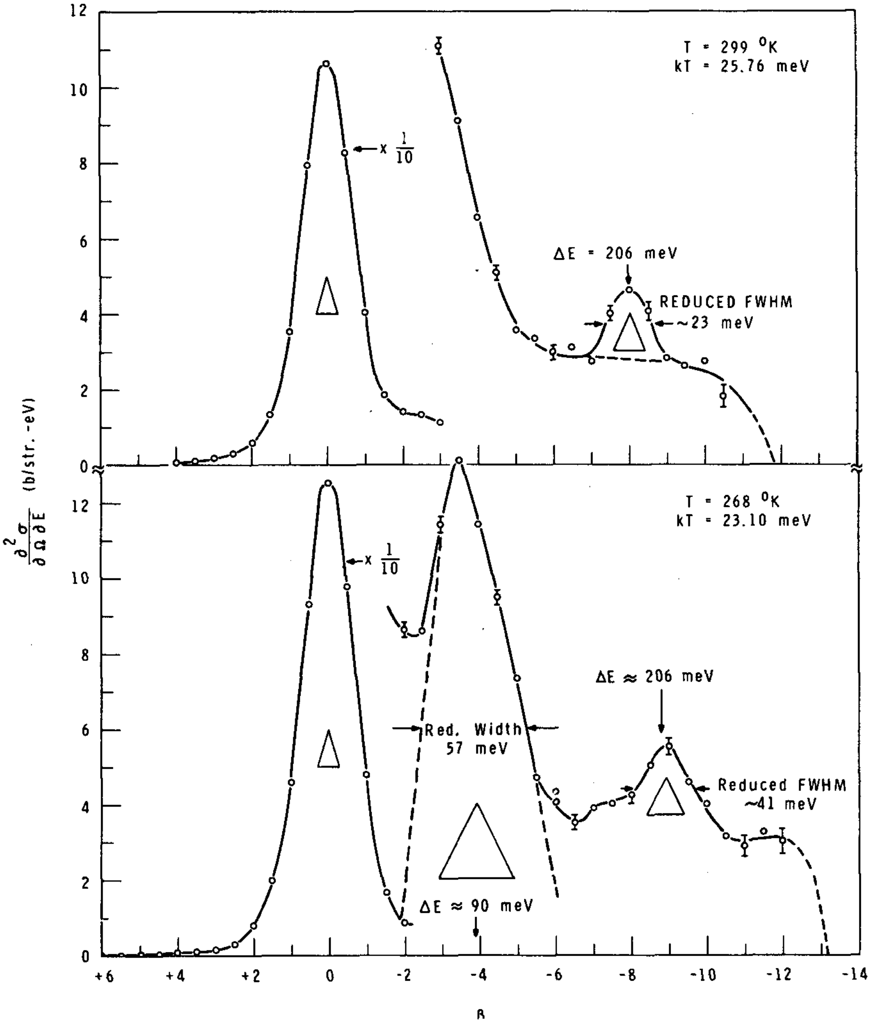

FIG. 4. Double-differential cross-sections of H_2O at 299 and 268°K, $E_0 = 0.304$ eV, $\theta = 15°$.

structure observed is considerably wider than this resolution, there should be no significant distortion due to instrumental effects. There is a well resolved peak at 427 meV and two smaller peaks centered near 485 and 531 meV. The scattering results for the 299°K liquid are similar to those for ice but the structure is not as pronounced.

In Table I are listed the energies and energy widths obtained from the neutron spectra. Representative results from cold neutron upscattering measurements, and from optical spectroscopy are included for comparison. The energy widths are the resolution corrected full widths at half maximum (FWHM). The width given for the rotational band in ice is obtained from an average of the

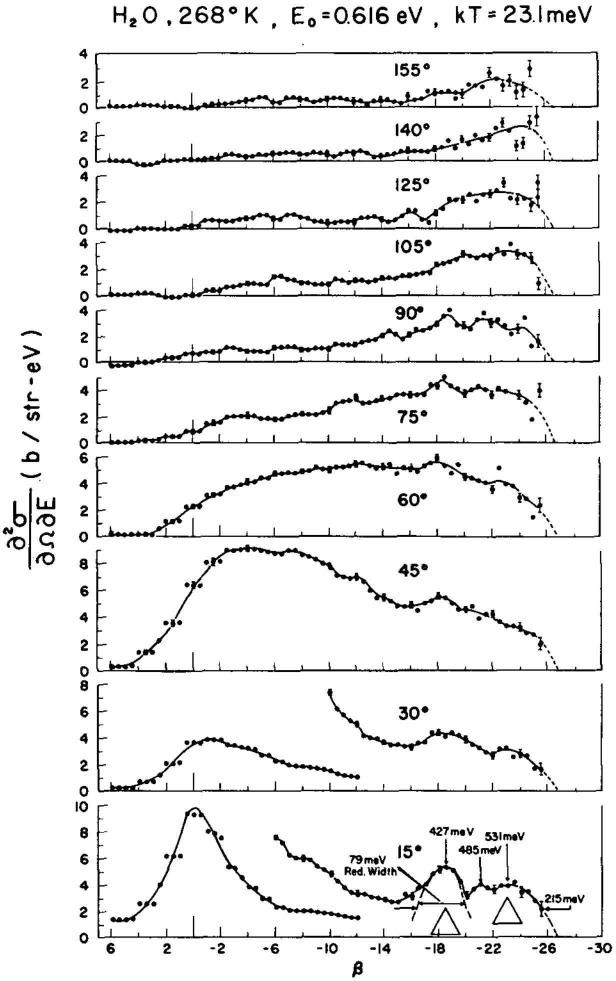

FIG.5. Double-differential cross-sections of light ice at 268°K, E_0 = 0.616 eV.

results for the three smallest scattering angles. The present downscattering results and the cold neutron scattering measurements of Larsson and Dahlborg(2) are in good agreement regarding the location and width of the rotational band while two broad components centered at somewhat higher energy than that obtained in the neutron results, are seen in Raman optical spectra. The energy of 206 meV obtained in the present neutron scattering work for the bending vibration is in excellent agreement with both the Raman(17) and infrared(18,20) results. The narrower widths observed for the bending mode in the optical results, compared to the present neutron result, indicate that there is probably a substantial excitation of low frequency modes along with the pure vibrational transition. The neutron results for the highest frequency vibrational band, indicate consistently higher average energies and widths than the optical results. The much greater

TABLE I. ENERGIES AND WIDTHS OF ROTATIONAL AND VIBRATIONAL LEVELS IN LIQUID AND SOLID H_2O. TEMPERATURE IN °K, ENERGIES IN meV.

	H_2O						
	T	E_r	ΔE_r	E_{V_1}	ΔE_{V_1}	E_{V_2}	ΔE_{V_2}
Present results from neutron downscattering	299	$\sim$64		206	23	$\sim$450 $\sim$530	
	268	88	$\sim$58	206	$\sim$41	$\sim$427 $\sim$485 $\sim$531	$\sim$79
Ref. [2] neutron upscattering	295	70	$\sim$80				
	270	80	$\sim$55				
Ref. [21] infrared	298	87		204	16	420	
Raman	298	$\sim$56,97		205		420	$\sim$52
Ref. [18] Raman	313			205	20		
	299					421	$\sim$62
	273					406	$\sim$57
Ref. [19] infrared	$\sim$100	106	30	205		400	30
Ref. [20] Raman	77					383	$\sim$40
	D_2O						
Preliminary neutron downscattering results	272	$\sim$70					
Ref. [2] Cold neutron upscattering	275	$\sim$63	$\sim$60				

probability of multiphonon interactions in the neutron case would produce a wider band shifted to higher β. Present down scattering results on D_2O ice are in agreement with the cold neutron upscattering results.(2)

IV. ANGULAR VARIATION OF THE INELASTIC SCATTERING FROM THE TORSIONAL MODES IN ICE

The single differential cross sections, $\partial\sigma/\partial\Omega$, for the inelastic scattering from the torsional modes in light ice are presented in Fig. 6. This figure also includes the results of a

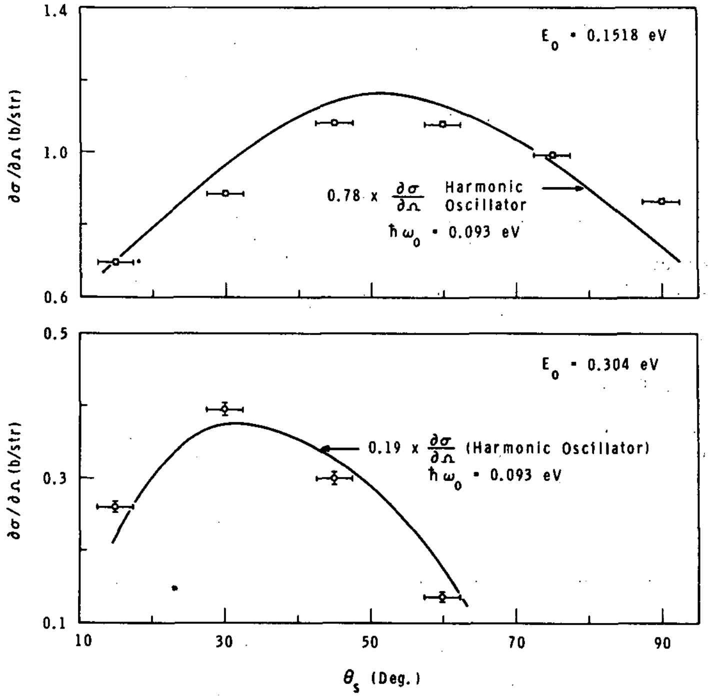

FIG. 6. Angular distribution of inelastic scattering from torsional modes in light ice.

calculation based on a simple model by Fermi$^{(21)}$ which assumes the proton to be bound in a symmetric harmonic potential. Equation 1 gives the theoretical

$$\frac{\partial\sigma}{\partial\Omega} = \frac{\sigma_b}{4\pi}\sqrt{\frac{E_1}{E_o}}\;\frac{(E_o+E_1-2\sqrt{E_oE_1}\cos\theta_s}{\hbar\omega_o} \times$$

$$\exp\left[-\frac{1}{\hbar\omega_o}(E_o+E_1-2\sqrt{E_oE_1}\cos\theta_s)\right] \qquad (1)$$

result for scattering of neutrons from initial energy E_o to final energy E_1 at a scattering angle θ_s, with the excitation of a single vibration quantum of energy $\hbar\omega_o$, and σ_b is the bound atom hydrogen cross section 81.4 barns. The theoretical cross sections are shown for an oscillator energy of 93 meV. The area under the theoretical curves has been normalized to the area under the experimental distribution. Normalization factors of 0.78 and 0.19 were used respectively with the E_o = 0.152 eV and 0.304 eV data. A normalization constant less than one is to be expected since the rotational mode is not the only degree of freedom excited during the neutron scattering. The root mean squared deviation of the experimental points from the theoretical curve is ~10% for both curves in Fig. 6. The angular dependence of the partial cross sections for inelastic scattering from the rotational levels in ice, are consistent with theoretical predictions based on the simple Fermi model with its spherical harmonic oscillator potential. This of course does not rule out that calculated scattering distributions using other potential shapes could not fit the data as well or better than the isotropic harmonic oscillator potential. There is clearly considerable averaging taking place in the neutron scattering experiment discussed here. The sample is polycrystalline so that there is no fixed orientation for the molecules with respect to the incident neutrons. Furthermore, the actual proton potential is basically harmonic though certainly not spherically symmetric.$^{(1,22)}$

V. SPECTRAL DENSITY

Spectral density functions, $\rho(\beta)$, for heavy water and for light water and ice are presented in Figs. 7 and 8. The method used to extract the density functions follows that of Egelstaff and Schofield.$^{(23)}$ In this procedure an initial estimate of $\rho(\beta)$ is obtained by extrapolation of the experimental scattering law $S(\alpha,\beta)$ or $S(\alpha,\beta)/\alpha$ to zero α. The initial $\rho(\beta)$ is used to regenerate the differential cross sections or the scattering law with the aid of program Leap.$^{(24)}$ The $\rho(\beta)$ is then adjusted and the process is reiterated until satisfactory agreement between calculated and experimental scattering cross sections is obtained.

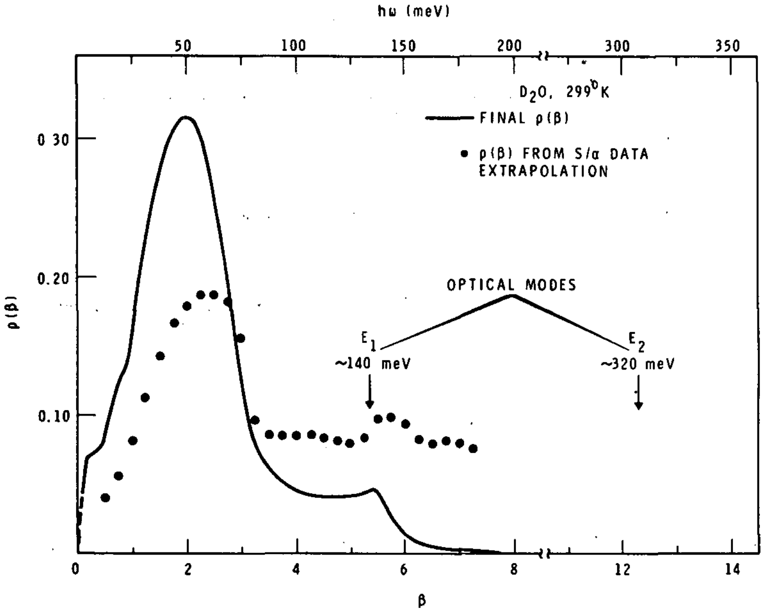

FIG. 7. Spectral density functions for D_2O at 299°K. Weight assigned to stretching modes near 320 meV is 0.25.

The spectral density function for heavy water is presented in Fig. 7. It is comprised of a continuous distribution of modes which extends to $\beta \approx 7.5$ and has peaks near $\beta = 2$ and $\beta = 5.5$ corresponding to the hindered rotational band and the bending mode of the D_2O molecule. A single delta function mode with a weight of 0.25 is used to represent the stretching vibrations near $\beta = 12.4$.

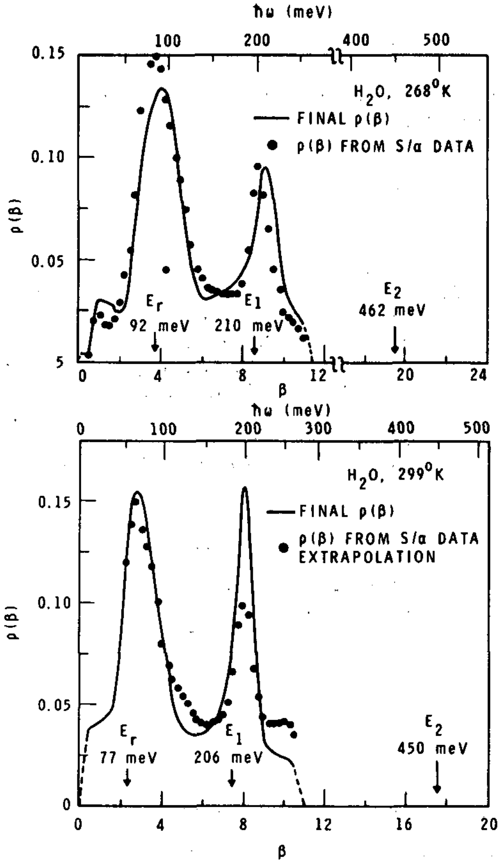

FIG. 8. Spectral density functions for H_2O at 268 and 299°K. The weight assigned to the high-frequency stretching modes is 0.30 and 0.40 respectively for the water and ice.

Spectral density functions for light water and ice are given in Fig. 8. The high frequency stretching modes of the H_2O molecules have been accounted for with a single delta function, while a continuous $\rho(\beta)$ has been obtained for modes up to $\beta \approx 11$. Pronounced peaks corresponding to the bending vibration and the torsional modes are seen in this part of $\rho(\beta)$. At the smallest energy changes corresponding to $\beta \leq 1$ or 2 the present experimental results do not have adequate resolution to provide significant new information. Furthermore, there is still some disagreement (11,25,26,27,28,29) regarding the shape of $\rho(\beta)$ in this region. In view of this a smooth distribution was used in the present work with an area which is comparable to that found in a recent determination by Haywood.(29) Figures 7 and 8 also include the initial estimates of $\rho(\beta)$ which are obtained from the extrapolation of the scattering law data to zero momentum transfer.

The mean squared amplitude of molecular vibration (u^2), is related to the Debye-Waller factor in the following manner

$$e^{-2W} = e^{-\bar{k}^2 u^2} = e^{-\alpha\lambda} \tag{2}$$

where the Debye-Waller coefficient λ is obtained from an integral over the spectral density function

$$\lambda = 2 \int_0^\infty \frac{1}{\beta} \coth \beta/2 \; \rho(\beta) d\beta. \tag{3}$$

The u obtained in this manner corresponds to the rms amplitude in a solid without diffusion. Values of u obtained from the present results are 0.26, 0.23, and 0.15 Å for 299°K D_2O, 299°K H_2O and 268°K light ice respectively. These results are comparable to the neutron diffraction results of Peterson and Levy(22) which give an average u of 0.200 Å for D_2O at 233°K. However, present results are considerably lower than the amplitudes of 0.38Å and 0.4 Å obtained respectively by Larsson et al(26) and by Brockhouse(30) for room temperature H_2O using the quasi-elastic scattering of cold neutrons.

ACKNOWLEDGMENTS

The author wishes to thank Drs. D. A. Kottwitz, W. D. McCormick and B. R. Leonard, Jr. for useful discussions concerning this work and Dr. L. C. Schmid for his continuing interest and support.

REFERENCES

[1] SPRINGER, TASSO, Nuckeonik 3, 110 (1961).

[2] LARSSON, K.E., DAHLBORG, U., Reactor Sci. and Technol., 16, 81 (1962).

[3] GOLIKOV, V.V., ZUBOVSKA, I., SHAPIkO, F.L., SZKATULA, A., JANIK, J., "Inelastic Scattering of Neutrons in Solids and Liquids," Vol. II, p. 201, IAEA, Vienna (1965).

[4] McMURRY, H.L., RUSSELL, G.J., BRUGGER, R.M., Nucl. Sci. and Eng., 25, 248 (1966).

[5] HAYWOOD, B.C., AERE Report R-4484 (1964).

[6] MOSTOVOI, V.I., DYBAREV, V.S., EREMEAV, I.P., ISHMAEV, S.P., SADIKOV, I.P., SALTYKOV, Y.S., TARABANKO, V.A., CHERENYSHOV, A.E., Proceed. of Third Int. Confer. on the Peaceful Uses of Atomic Energy, Geneva A/Conf. 28/P/367 (1964).

[7] KOTTWITZ, D.A., LEONARD, B.R., JR., "Inelastic Scattering of Neutrons by Solids and Liquids," Vol. I., p. 359, IAEA, Vienna, (1963).

[8] KIROUAC, G.J., MOORE, W.E., ESCH, L.J., SEEMAN, K.W., YEATER, M.L., Sm 96/64, IAEA Conference on Neutron Thermalization, Ann Arbor, Michigan, July 1967.

[9] HARLING, O.K., Physics Letters, 22, 15 (1966).

[10] HARLING, O.K., Proc. Am. Crystal. Assoc., Atlanta, Georgia, p.37, (Jan. 1967).

[11] LARSSON, K.E., DAHLBORG, U., Inelastic Scattering of Neutrons in Solids and Liquids, Vol. I., p. 317, IAEA, Vienna, (1963).

[12] HAYWOOD, B.C., "A Compilation of the Scattering Law for Heavy Water at 22°C and 150°C," AERE-R-4582 (1964). Harwell.

[13] WHITTEMORE, W.L., "Differential Neutron Thermalization," Annual Summary Report, Oct. 1, 1965 through Sept. 30, 1966, USAEC Report GA-7439, (Feb. 1967).

[14] HARLING, O.K., U.S. Atomic Energy Commission Report, BNWL-436, June 1967.

[15] HARLING, O.K., Rev. of Sci. Instr., 37, 697-709 (1966).

[16] See these Proceedings.

[17] CROSS, P.C., BURNHAM, J., LEIGHTON, P.A., J. Am. Chem. Soc., 59, 1134, (1937).

[18] BERTIE, J.E., WHALLEY, E., J. Chem. Phys. 40, 1637,(1964).

[19] TAYLOR, J.J., WHALLEY, E., J. Chem. Phys. 40, 1660,(1964).

[20] WALRAFEN, G.E., J. Chem. Phys., 40, 3249 (1964).

[21] FERMI, E., Ricerca Sci. VII-2, 13 (1936).

[22] PETERSON, W., LEVY, H.A., Acta Cryst., 10, 70 (1957).

[23] EGELSTAFF, P.A., Nucl. Sci. Eng., 12, 250 (1962) and EGELSTAFF, P.A., SCHOFIELD, P., Nucl. Sci. Eng., 12, 260, (1962).

[24] McLATCHIE, R.C.F., To be Published.

[25] HUGHES, D.J., PALEVSKY, H., KLEY, W., TUNKEL, E., Phys. Rev., 119, 872, (1960).

[26] LARSSON, K.E., HOLMRYD, S., OTNES, K., "Inelastic Scattering of Neutrons in Solids and Liquids," p. 329, IAEA, Vienna (1961).

[27] SAFFORD, A.J., NAUMANN, A.W., 1965 and 1966 Saline Water Conversion Reports, U. S. Dept. of the Interior.

[28] SAKAMOTO, M., BROCKHOUSE, B.N., JOHNSON, R.C., POPE, N.K., J. Phys. Soc., Japan, Suppl., BII, 17, 370 (1962).

[29] HAYWOOD, B.C., Journ. of Nucl. Energy, 21, 249 (1967).

[30] BROCKHOUSE, Nuovo Cimento, Vol. 9, Suppl. 1, 45 (1958).

DISCUSSION

J.W. WHITE: I should just like to comment on the paper by Holmryd and Nelin (SM-104/38) and especially on the temperature-dependent diffusional activation energy for toluene which they reported. In molecules where the protons are in different chemical environments it is most important to try and separate the different contributions to D. This can often be done by the atomic substitution method (Ref.[45] of Mr. Larsson's review paper (SM-104/200)). We have actually done this for $C_6H_5CH_3$, $C_6H_5CD_3$ and some similar compounds, and find that the diffusion coefficients are different. This suggests that the anomalous temperature dependence found may be due to a combination of effects.

S. HOLMRYD: Mr. White has indeed broached a very important problem in referring to the influence of the torsional motions of the CH_3 group in toluene on the measured diffusion coefficients and activation energy. The latter is not measured for the group in toluene and the value varies over a wide range for different substances. It is, however, believed by Nelin and myself that there ought not to be any abrupt change in the temperature dependence of the activation energy and that the measured discontinuity for toluene depends upon a change in the number of degrees of rotational freedom of the whole molecule; the curve of the diffusion coefficients should thus give qualitatively correct information.

J.G. POWLES: The inelastic neutron scattering results on liquid benzene reported in paper SM-104/38 show an effective diffusion constant larger than the macroscopic diffusion constant, and this is attributed to reorientational motion of the benzene molecules. It may be of interest to mention that these results are consistent with the nmr data in liquid benzene (Molec. Phys. 10 (1966) 155; 11 (1966) 515 and 13 (1967) 253), where it is shown that the molecule reorients faster than it translates and that the activation energy for reorientation is about 1.9 kcal $mole^{-1}$ and for translation is about 3.0 kcal $mole^{-1}$ over a wide temperature range. The apparent diffusion constant obtained by neutron inelastic scattering has an activation energy of about 1.7 kcal $mole^{-1}$, and so the fact that the neutrons see the reorientational rather than the translational motion appears to be confirmed.

I would also like to make the general observation that measurements over a small temperature range on liquids can be misleading. A liquid exists from the melting point (and can often be supercooled) to the critical point, and this whole range ought to be covered. In fact, in my opinion, one really needs coexistence values; pressure measurements are therefore highly desirable and even moderate pressures (say up to 2000 atm) can be quite helpful.

T. SPRINGER: The optical molecular vibrational peaks shown in the reduced spectra $p(\omega)$ in Harling's paper (SM-104/80) have a considerable width. Is this mainly due to resolution, or to the dispersion of the corresponding optical vibration branches?

O.K. HARLING: The instrumental resolution is given in the figures to my paper and is considerably better than the observed widths. The reduced widths, i.e. those corrected for the resolution function of the instrument, are therefore not significantly affected by the instrumental resolution. The widths observed are, however, influenced by multiple excitations involving optical modes and low-frequency modes, e.g. translational excitations. Using the present knowledge of the spectral density function, it is in fact easy to show that the width of the 206-meV peak in H_2O for the E_0 = 304-meV experiment is strongly influenced by the low-frequency translational modes.

L.A. de GRAAF: In connection with the papers of Holmryd and Nelin (SM-104/38) and of Tarina (SM-104/59), I should like to present some results on translational and rotational motions in cyclohexane and cyclopentane. These globular compounds were studied by scattering of 4-Å neutrons using a rotating-crystal spectrometer[1]. The broadening of the quasi-elastic peaks as a function of momentum transfer observed at different temperatures has been interpreted in terms of a model proposed by Larsson and Bergstedt[2] for complex hydrogenous liquids. To include hindered reorientational motions of the rigid molecules, this model was modified by considering the rotational jumps as being not instantaneous, and calculating the average jump velocity. Also the mean square radius of the thermal cloud for the librational motions was not assumed to be much larger than that for the centre-of-mass motions, contrary to the assumption of Larsson and co-workers. From the fit of the derived line-width formulae to the experimental data, relaxation times for diffusional and rotational motions (τ_0' and τ_0 respectively), and average distances covered by a proton during a rotational jump, l_1, have been obtained. The intensity of the quasi-elastic peaks is found to be mainly governed by the centre-of-mass motions. Figure A shows the mean square radii of the thermal clouds. For cyclohexane these are in good agreement with values calculated from Debye temperatures obtained from sound velocity measurements[3], indicated as solid lines in Fig.A. In Fig.B the parameters obtained for cyclopentane are shown. In the solid phases I and II the behaviour of the relaxation time for rotational motions, τ_0, the mean jump time, τ_1, and the mean jump distance, l_1, seems to be continuous, which is consistent with the small entropy change at the I → II transition. In the

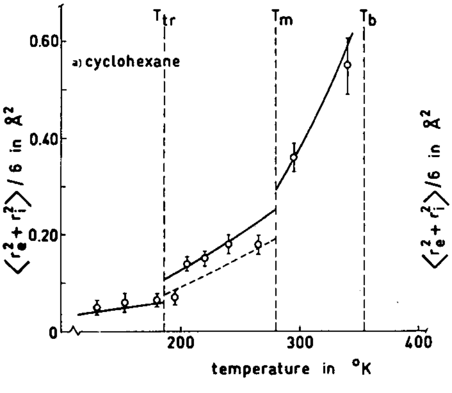

FIG.A. Values of $\langle r_e^2 + r_i^2 \rangle /6$ derived from the intensities of the quasi-elastic peaks measured in cyclohexane.

---

[1] De GRAAF, L.A., Thesis, Technische Hogeschool Delft (1968); De GRAAF, L.A., Physica (to be published).

[2] LARSSON, K-E., BERGSTEDT, L., Phys. Rev. 151 (1966) 117.

[3] GREEN, J.R., SCHEIE, C.E., J. Phys. Chem. Solids 28 (1967) 383.

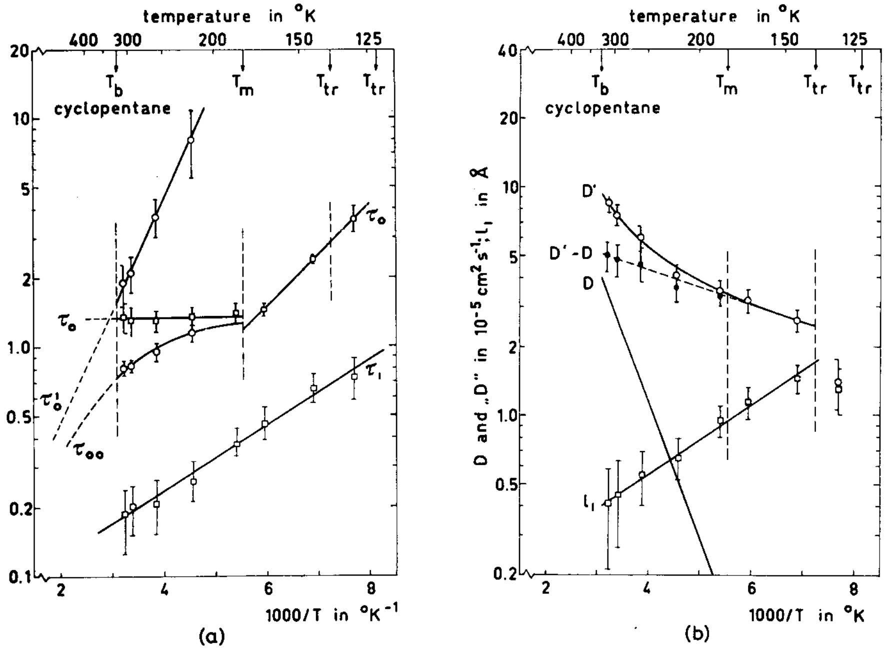

FIG.B. (a) Relaxation times for the motions in cyclopentane derived from the line width data.
(b) Apparent diffusion coefficient and jump distance for cyclopentane derived from the line width data. The macroscopic diffusion coefficient is given for comparison.

liquid, τ_0 was found to be essentially constant. This indicates that the barrier hindering the reorientations is strengthened when the mobility of the neighbouring molecules is enhanced by an increase in temperature. The larger collision frequency is also reflected in the decrease of the jump distance and jump time obtained.

For a transition in the solid state the entropy change at the transition approximates R ln Q, where Q is the ratio of the number of equilibrium orientations statistically occupied in the two phases. In this way jump distances of about 0.8 Å were calculated for both cyclohexane and cyclopentane, and are in fairly good agreement with the neutron results.

As in the results of Holmryd and Nelin a substantial difference between macroscopic and apparent diffusion coefficients is observed.

КОЭФФИЦИЕНТ САМОДИФФУЗИИ ЭТАНА ВБЛИЗИ КРИТИЧЕСКОЙ ТОЧКИ ЖИДКОСТЬ-ПАР

Л.А.БУЛАВИН, А.В.ВОРОНЕЛЬ,
Ю.М.ОСТАНЕВИЧ, А.П.СИМКИНА,
А.В.СТРЕЛКОВ
ОБЪЕДИНЕННЫЙ ИНСТИТУТ ЯДЕРНЫХ
ИССЛЕДОВАНИЙ, ДУБНА,
СССР

Abstract — Аннотация

SELF-DIFFUSION COEFFICIENT OF ETHANE NEAR THE LIQUID-GAS TRANSITION POINT. As has been shown in a series of papers by I.R. Krichevsky and his co-workers, the diffusion coefficient of small amounts of impurities in a pure substance is sharply reduced in the neighbourhood of the liquid-gas transition point. We attempted to observe similar alterations in the self-diffusion coefficient near the transition point of ethane by using cold neutron quasi-elastic scattering.

The IFR reactor and an arrangement consisting of a beryllium filter in front of a detector were used for the measurements. The energy resolution of the assembly was ~ 0.025 meV, and the observed smearing-out of the energy of the quasi-elastically scattered neutrons was $\Delta E \simeq 0.15$ meV at a scattering angle of $6 \pm 2.5°$.

With an alteration of the sample temperature (in $(T - T_C)/T_C$ units) from 3×10^{-5} to 6×10^{-2}, no changes greater than 0.03 meV were observed in the quasi-elastic line width.

Thus, we found no significant changes in the self-diffusion coefficient near the liquid-gas transition point in the pure substance. A final evaluation of the upper limit of changes in the self-diffusion coefficient requires corrections to be made for multiple scattering, final angular resolution, etc., and is given in the text of the paper.

КОЭФФИЦИЕНТ САМОДИФФУЗИИ ЭТАНА ВБЛИЗИ КРИТИЧЕСКОЙ ТОЧКИ ЖИДКОСТЬ-ПАР. Как было показано в серии работ И.Р.Кричевского и сотрудников, коэффициент диффузии малых примесей в чистом веществе резко уменьшается вблизи критической точки жидкость-пар чистого вещества. В связи с этим нами предпринята попытка обнаружить аналогичные изменения коэффициента самодиффузии вблизи критической точки в этане с помощью квазиупругого рассеяния медленных нейтронов.

Для измерений использовался реактор ИБР и геометрия с бериллиевым фильтром перед детектором. Энергетическое разрешение установки составляло ~0,025 миллиэлектронвольт, наблюдавшееся размытие энергии квазиупруго рассеянных нейтронов $\Delta E \approx 0{,}15$ миллиэлектронвольт при угле рассеяния $6 \pm 2{,}5°$.

При изменении температуры образца (в единицах $(T - T_c)/T_c$) от $3 \cdot 10^{-5}$ до $6 \cdot 10^{-2}$ не обнаружено каких-либо изменений ширины квазиупругой линии, превышающих 0,03 миллиэлектронвольт.

Таким образом, нами не обнаружено существенных изменений коэффициента самодиффузии вблизи критической точки жидкость-пар чистого вещества. Окончательная оценка верхней границы изменений коэффициента самодиффузии требует введения поправок на многократное рассеяние, конечное угловое разрешение и т.д. и будет приведена в тексте доклада.

ВВЕДЕНИЕ

В последнее время различными методами получены интересные данные о поведении коэффициента диффузии вблизи критической точки жидкость-пар. И.Р.Кричевский с сотрудниками в серии работ [1] показал, что в двухкомпонентной системе с малым содержанием второго компонента коэффициент диффузии малого компонента стремится к нулю при приближении системы к критической точке жидкость-пар. Экспериментально наблюдалось уменьшение коэффициента диффузии до 10^{-7} см^2/сек в системе CO_2 – J и до $2\cdot10^{-12}$ см^2/сек в системе Cl_2 – Cl. Качественно похожий результат для диффузии электронов в ^{4}He недавно был получен Риччи [2].. Результаты этих опытов находятся в согласии с теоретическими предсказаниями [3], которые, однако, не позволяют дать наглядную микроскопическую интерпретацию явления.

Число экспериментальных работ, посвященных исследованию коэффициента самодиффузии D_c в чистом веществе вблизи критической точки, значительно меньше, а результаты их порой носят противоречивый характер.

Так, Бата и др. [4], исследуя квазиупругое рассеяние нейтронов в эфире, обнаружили уменьшение уширения квазиупругого пика, что, возможно, соответствует уменьшению коэффициента самодиффузии вблизи критической температуры.

Набл и Блуме [5] с помощью метода спинового эха заметили немонотонность на температурной зависимости ρD_c для этана, однако, окончательных заключений о поведении коэффициента самодиффузии вблизи критической точки жидкость-пар сделано не было.

Траппеньер и др. [6], исследуя тем же методом метан, не обнаружили каких-либо аномалий D_c вблизи критической точки. И, наконец, недавно, исследуя капиллярным методом диффузию изотопа ^{36}Ar в естественной смеси, де Паз [7] также пришел к выводу об отсутствии изменений коэффициента самодиффузии вблизи критической точки.

В данной работе изложены результаты исследований коэффициента самодиффузии этана вблизи критической точки жидкость-пар методом квазиупругого рассеяния медленных нейтронов.

ЭКСПЕРИМЕНТ

1. Образец. Мы считаем необходимым подробно сообщить параметры исследуемых образцов, поскольку от них в значительной степени зависит проявление всех особенностей, связанных с критическим сотоянием.

Образец (рис.1) размерами 25 × 25 × 1 см состоял из 60 трубок из нержавеющей стали диаметром 5 мм и толщиной стенки 0,22 мм, расположенных так, что непостоянство толщины слоя этана было минимальным. Для уменьшения влияния гравитационного эффекта трубки располагаются горизонтально. Они наполнены этаном до критической плотности ($\rho_c = 0{,}2048 \pm 0{,}0007$ г/см^3). Хроматографический анализ используемого этана выявил присутствие следующих примесей: азот 0,02%, кислород 0,004% и пропилен 0,017% (% объемные). Объем образцов определялся при комнатной температуре и атмосферном давлении с точностью 0,01%. При наполнении образцов вводилась поправка на увеличение объема, связанное с нагреванием трубок до критической температуры и расширением их под действием давления. Показанная на рис.2 гистограмма распределения числа трубок по плотности позволяет утверждать, что заполнение их было критическим с точностью не меньше, чем 0,8%. Коэффициент пропускания нейтронов с энергией $5{,}2\cdot10^{-3}$ эв через пустые трубки составляет 0,88.

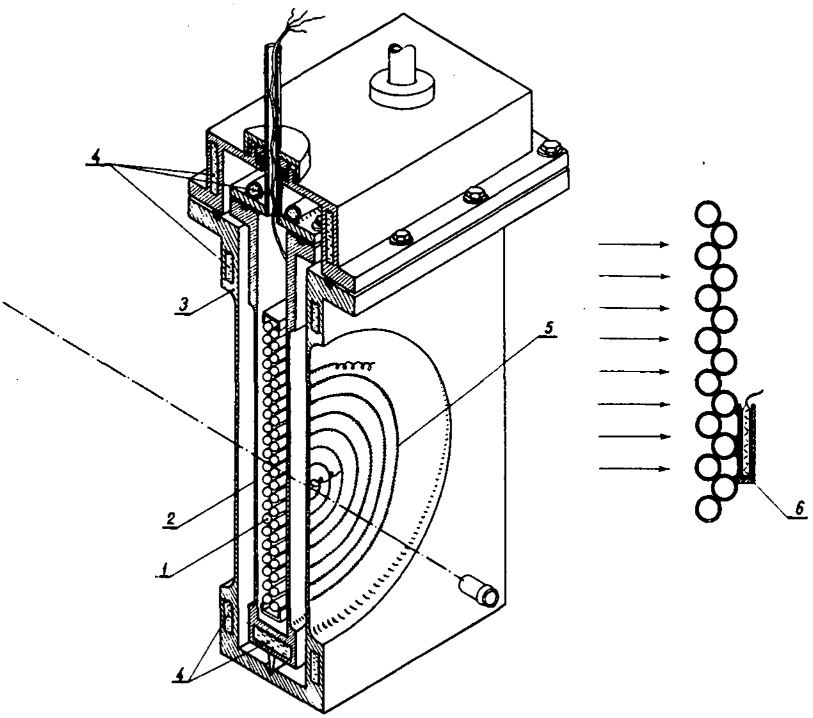

Рис.1. Общий вид контейнера с образцами. 1 – трубки с этаном; 2, 3 – внутренняя и наружная алюминиевые коробки; 4 – проточная термостатированная вода; 5 – дополнительный нагреватель на окнах; 6 – платиновый термометр сопротивления.

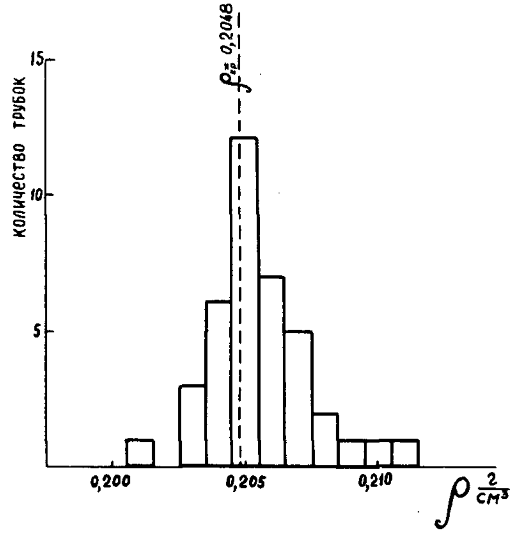

Рис.2. Распределение трубок по плотности, полученное при контрольном определении плотности после измерений рассеяния нейтронов.

2. Термостатирование. Для термостатирования образцы с этаном помещались в специальный контейнер, состоящий из двух вставленных друг в друга разборных алюминиевых коробок, каждая из которых омывалась термостатированной водой. На боковых стенках контейнера имелись окна для пропускания нейтронного пучка, которые были основным источником температурных градиентов на образце. Для устранения этих градиентов на окна были нанесены вспомогательные нагреватели. Откачка полости между коробками до 10^{-2} мм рт.ст. не привела к заметному улучшению температурной стабилизации и снижению температурных градиентов на образце. Коэффициент пропускания нейтронов с энергией $5{,}2\cdot10^{-3}$ эв через пустой контейнер составляет 0,94. Измерение температуры образца производилось платиновым термометром сопротивления с точностью абсолютной градуировки ±0,01 °С. Температурные градиенты на образце измерялись дифференциальными медь-константановыми термопарами. Нестабильности и неоднородность температуры образца во время измерений не превышали ±0,005 °С. В качестве критической температуры этана нами было принято значение $T_c = (32{,}33 \pm 0{,}01)$ °С*.

3. Рассеяние. Рассеяние нейтронов исследовалось методом бериллиевого фильтра перед детектором (рис.3) на импульсном реакторе ИБР Объединенного института ядерных исследований [8].

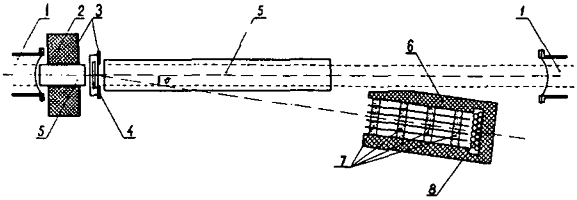

Рис.3. Геометрия опыта. 1 – вакуумный нейтроновод; 2 – коллиматор; 3 – коллиматоры из кадмия; 4 – образцы с этаном; 5 – тонкостенные алюминиевые трубы, наполненные гелием; 6 – защита детектора; 7 – бериллий; 8 – пропорциональные счетчики.

Образец располагался на пролетной базе 37,5 метров, что обеспечивало аппаратурное разрешение $2\cdot10^{-5}$ эв для энергии $5{,}2\cdot10^{-3}$ эв. Рассеяние от контейнера с пустыми трубками составляет 30% от рассеяния на контейнере с трубками, наполненными этаном. Показанный на рис.3 фильтр с разнесенным бериллием имеет в 15 раз меньшее пропускание для тепловых нейтронов, чем обычно используемый фильтр с плотной упаковкой. При толщине бериллия 16 см пропускание фильтра равнялось $1{,}5\cdot10^{-4}$ для $E_n > 5{,}2\cdot10^{-3}$ эв и 0,4 для $E_n < 5{,}2\cdot10^{-3}$ эв. Детектором нейтронов служила батарея из 17 пропорциональных счетчиков, наполненных BF_3 (80% ^{10}B) с площадью ≈ 700 см^2 и эффективностью 60% для нейтронов с энергией $5{,}2\cdot10^{-3}$ эв.

На описанной установке нами были выполнены две независимые серии измерений: с углом рассеяния $\theta = (8{,}5 \pm 2{,}5)^\circ$ и плотностью этана $\rho = (1{,}03 \pm 0{,}008)\rho_c$, а также с углом рассеяния $\theta = (6 \pm 2{,}5)^\circ$ и плотностью этана $\rho = (1{,}00 \pm 0{,}008)\rho_c$. Измерения в основном велись при $T > T_c$, так как при $T < T_c$ этан становится двухфазным и, при использованной нами

---

* Выражаем благодарность В.А.Смирнову и Ю.Р.Чашкину, определившим по нашей просьбе значения ρ_c и T_c.

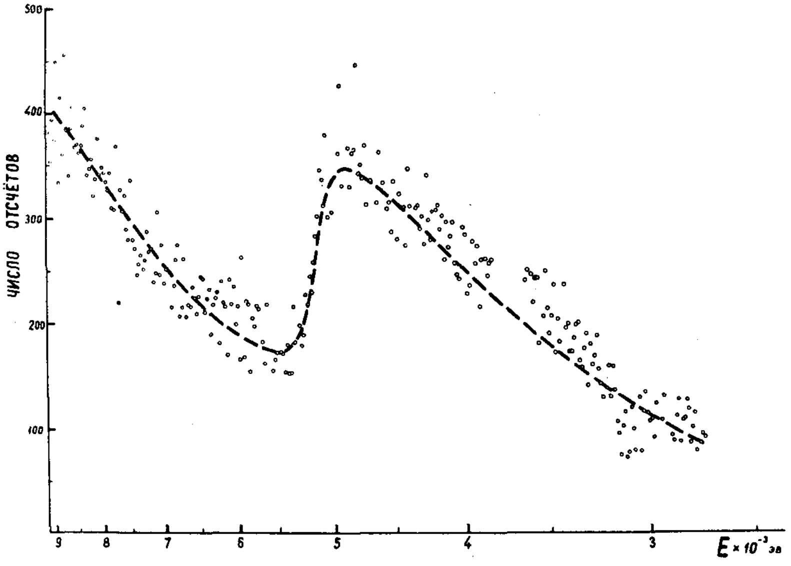

Рис.4. Аппаратурный спектр для рассеяния на угол 6°.

геометрии, интерпретация результатов невозможна. За 100 часов измерений при фиксированной температуре для коэффициента самодиффузии достигалась точность 25%. На рис.4 представлен типичный аппаратурный спектр после вычитания фона от рассеяния на контейнере с пустыми трубками.

РЕЗУЛЬТАТЫ ИЗМЕРЕНИЙ И ОБСУЖДЕНИЕ

Для определения уширения квазиупругого пика аппаратурный спектр после коррекции на посторонний фон и рассеяние от контейнера без этана аппроксимировался методом наименьших квадратов с помощью выражения:

$$F(x) = Ax^2 + Bx + C + \tfrac{1}{2}(\alpha x^2 + \beta x + \gamma)\left[1 + \frac{2}{\pi}\,\text{arctg}\,\frac{x - x_0}{\Gamma/2}\right] \qquad (1)$$

где x – номер канала временного анализатора,

x_0 – номер канала, в котором находится центр бериллиевой границы для упругого рассеяния.

Параметр $\Gamma/2$ соответствует полуширине лоренцовского члена в дважды дифференциальном сечении квазиупругого рассеяния при энергии бериллиевого края. Аппроксимирующее выражение (1) может быть получено из точного, если сделать следующие допущения:

1) интенсивность в спектре падающих нейтронов мало изменяется в пределах ширины квазиупругого пика;

2) относительное изменение κ^2 в тех же пределах также достаточно мало;

3) эффективность детектора в тех же пределах может быть представлена в виде единичной ступеньки, равной 0 при $E'_{\text{п}} > E_{\text{Be}}$ и 1 при

$E_n^! < E_{Be}$ ($E_n^!$ – энергия рассеянного нейтрона, E_{Be} – энергия бериллиевой границы);

4) медленно изменяющиеся компоненты наблюдаемого спектра (неупругое, квазиупругое при $E_{Be} - E_n^! \ll \Gamma$ и многократное рассеяние) в окрестностях E_{Be} могут быть аппроксимированы квадратичными многочленами.

Из-за незначительности наблюдаемого уширения погрешности в определении Г за счет перечисленных допущений оказываются малыми по сравнению с ошибкой, обусловленной недостаточной статистической точностью. Качество аппроксимации видно из рис.4, на котором пунктирная линия соответствует выражению (1).

Полученное из (1) значение Г исправлялось на аппаратурное разрешение Γ_0, на влияние второй пролетной базы и на конечное угловое разрешение детектора следующим образом:

$$\Gamma = \Gamma \frac{\bar{\nu}^2}{\nu_1 \nu_2} \frac{1}{1+\frac{L_2}{L_1}} - \Gamma_0 \qquad (2)$$

где $\bar{\nu}$ – средний угол рассеяния,
ν_1, ν_2 – предельные значения углов рассеяния,
L_1, L_2 – длины первой и второй пролетной базы соответственно.

Эта поправка (полученная в предположении лоренцовской формы аппаратурного разрешения и рассеянного спектра, а также незначительности самих поправок), в конечном счете не превышает 10% от Г. Несмотря на сравнительно большую толщину образца ($n\sigma \approx 0{,}7$), многократное рассеяние не влияет на ширину квазиупругого пика. Это связано с быстрым уменьшением квазиупругой части дважды дифференциального сечения при увеличении угла рассеяния. Весьма малое уширение квазиупругого пика, равное $\approx 3 \cdot 10^{-4}$ эв, позволяет ограничиться рассмотрением только двукратного квазиупругого рассеяния. Оценки показывают, что интенсивность двукратного квазиупругого рассеяния составляет не более 2% от интенсивности однократного квазиупругого рассеяния.

Если допустить, что уширение квазиупругого пика после перечисленных исправлений целиком обусловлено классической диффузией молекул этана, то коэффициент самодиффузии может быть легко получен:

$$D_c = \frac{\Gamma_{испр.} E_{Be}}{x_0 h \kappa^2} \qquad (3)$$

где E_{Be} – энергия бериллиевой границы.

Применимость приближения классической диффузии требует более детального обсуждения. Как было показано Подгорецким и Степановым [9], рассеяние нейтронов на плотном газе может отражать как максвелловское распределение скоростей, так и диффузионное движение молекул, в зависимости от условий эксперимента. Критерием применимости диффузионного приближения является выполнение неравенства:

$$z = \frac{2k_B T}{M \kappa^2 D^2} >> 1$$

где M – масса диффундирующей молекулы. В нашем эксперименте

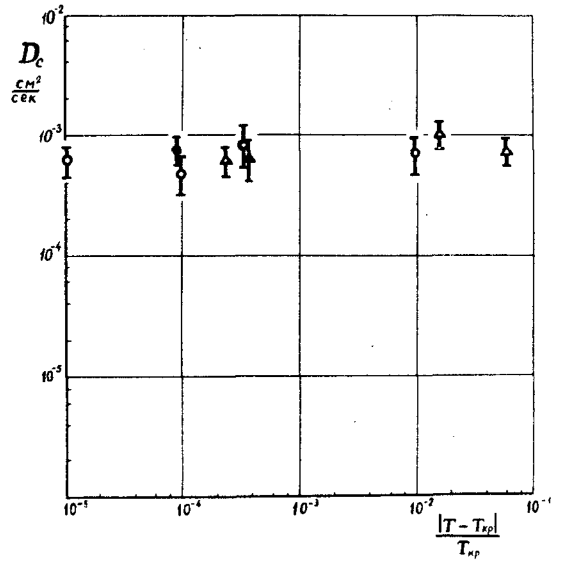

Рис.5. Зависимость коэффициента самодиффузии этана от температуры. Δ – угол рассеяния 6°, 0 – угол рассеяния 8,5°. Зачерненные точки относятся к двухфазной области ($T < T_c$).

$z = 12{,}5$ и 6,2 для углов рассеяния 6° и 8,5° соответственно, что и позволяет пользоваться диффузионным приближением. Другим доводом в пользу применимости диффузионного приближения является наблюдаемая пропорциональность между Γ и κ^2, что при двух углах рассеяния дает совпадающие значения D_c.

На рис.5 представлены наши результаты для разных температур и двух углов рассеяния. Из этого рисунка видно, что приближение к критической температуре вплоть до $\frac{T - T_c}{T_c} \approx 10^{-5}$ не влияет на коэффициент самодиффузии с точностью 30%. Наше среднее значение

$$D_c = (6{,}8 \pm 0{,}7)\cdot 10^{-4}\ см^2/сек$$

находится в хорошем согласии со значением

$$D_c = (6{,}3 \pm 0{,}1)\cdot 10^{-4}\ см^2/сек$$

найденным в [5], и со значением $6{,}10^{-4}$, полученным в приближении $D_c \approx \frac{1}{\rho}$ из значения D_c при нормальных условиях [10].

Отсутствие существенных особенностей в поведении D_c вблизи критической точки при временах наблюдения $\approx 5\cdot 10^{-12}$сек, характерных для нашего эксперимента, а также результаты Траппеньера и др. [6] для времен 10^{-4} сек, и де Паза [7] для времен диффузии 10^4 сек, по-видимому, подтверждают отсутствие аномалий D_c для всего доступного наблюдению интервала времен диффузии. Подробный результат получил Кавасаки [11], исследуя коэффициент самодиффузии в двухатомной решетке в приближении зависящей от времени модели Изинга.

В заключение авторы выражают искреннюю благодарность профессору Ф.Л.Шапиро, предложившему данный эксперимент; профессору И.Р.Кричевскому, любезно предоставившему чистый этан; профессору Я.И.Яшину за выполнение хроматографического анализа этана в его лаборатории и В.И.Лазину за большую помощь при выполнении эксперимента.

ЛИТЕРАТУРА

[1] КРИЧЕВСКИЙ, И.Р., ХАЗАНОВА, Н.Е., ЛИВШИЦ, Л.Р., ДАН СССР, 141 (1961) 397; ХАЗАНОВА, Н.Е., ЛЕСНЕВСКАЯ, Л.С., ЖФХ, 40 (1966) 464; ХАЗАНОВА, Н.Е., ЛЕСНЕВСКАЯ, Л.С., ЖФХ, 40 (1966) 76; КРИЧЕВСКИЙ, И.Р., ЦЕХАНСКАЯ, Ю.В., ПОЛЯКОВА, З.А., УФЖ, 12 (1967) 137; ХАЗАНОВА, Н.Е., УФЖ, 12 (1967) 244.

[2] MODENA, I., RICCI, F.P., Phys. Rev. Lett. 19 (1967) 347.

[3] КРИЧЕВСКИЙ, И.Р., РОТТ, Л.А., ДАН СССР, 136 (1961) 1938.

[4] BATA, L., KOSZO, E., KROO, N., PAL, L., Phys. Lett. 24A (1967) 57. BATA, L., KISZI-KOSZO, E., KROO, N., MUZSNAY, L., PAL, L., SZLAVIK, F., ZSIGMOND, C., Preprint KFKI 2457, Budapest, 1966.

[5] NOBLE, J.D., BLOOM, M., Phys. Rev. Lett. 14 (1965) 250.

[6] TRAPPENIERS, N.J., OOSTING, P.H., Phys. Lett. 23 (1966) 445.

[7] DE PAZ, M., Phys. Rev. Lett. 20 (1968) 183.

[8] БАЙОРЕК, А., ПАРЛИНЬСКИ, К., ШАПИРО, Ф.Л., Препринт ОИЯИ Р-1899, Дубна, 1964.

[9] ПОДГОРЕЦКИЙ, М.И., СТЕПАНОВ, А.В., ЖЭТФ, 40 (1961) 561; ПОДГОРЕЦКИЙ, М.И., СТЕПАНОВ, А.В., Препринт ОИЯИ Р-588, Дубна, 1960.

[10] БРЕТШНАЙДЕР, С., "Свойства газов и жидкостей". Химия, М. 1966, стр.455.

[11] KAWASAKI, K., Phys. Rev. 150 (1966) 285.

DISCUSSION

O.J. EDER: Did you observe gravitational effects? Close to the critical point you would, I imagine, obtain critical conditions only in a very thin layer of the sample. If therefore there was on the average a large beam covering the sample, I should expect the occurrence of differences if the relative position of the sample to the beam were changed. Was this the case?

V.V. GOLIKOV: As I said, the sample consisted of a set of metal tubes, about 5 mm in diameter, horizontally located in order to minimize the gravitational effect. When, on a previous occasion, measurements were made with a different disposition of the tubes, a gravitational effect was in fact observed.

O.J. EDER: How large was the beam?

V.V. GOLIKOV: About 20 × 20 cm.

O.J. EDER: Are not the beam sizes in neutron scattering experiments normally much smaller?

L.A. de GRAAF: The 20 cm width of the beam is necessary to get a reasonable intensity at 30 m distance from the reactor core.

H.Y. CARR: It might be assumed from the questions about beam size that the relevant height for estimating gravitational corrections is the 20-cm dimension of the beam. Surely this assumption is incorrect: if the horizontal tubes 5 mm in diameter were separately sealed – and I imagine they were – the relevant height would be only 5 mm, a very respectable height as fluid critical measurements go. Were the horizontal heights indeed separately sealed?

V.V. GOLIKOV: Yes, they were.

H.Y. CARR: Of more serious concern may be the temperature control (uniformity and stability). I understand that this temperature control was of the order of a hundredth of a per cent only. For ethane this is about 30 millidegrees, or perhaps more. On the basis of other fluid critical neighbourhood experiments (including our own recent nmr work with xenon at Rutgers) I should expect some important critical phenomena to start only at about 30 millidegrees, or less, from the critical point. This includes effects closely related to molecular diffusion. I should therefore be particularly interested to know how good the temperature control was.

V.V. GOLIKOV: The temperature instability and gradient during the measurements were less than ± 0.005°C.

COLLECTIVE MODES IN LIQUIDS AND NEUTRON SCATTERING*

M. NELKIN AND P.J. ORTOLEVA
CORNELL UNIVERSITY,
ITHACA, N.Y., UNITED STATES OF AMERICA

Abstract

COLLECTIVE MODES IN LIQUIDS AND NEUTRON SCATTERING. Using linear response theory and the fluctuation-dissipation theorem, G(r, t) for a classical fluid is expressed in terms of the solution of the Liouville equation with a precisely defined initial condition. The special form taken by the s-particle distribution functions at zero time is essential in identifying the non-equilibrium problem studied with the particular equilibrium fluctuation of direct interest in neutron scattering. Earlier calculations of G(r, t) from approximate kinetic theories can now be systematically derived within the usual framework of non-equilibrium statistical mechanics.

A simple approximation which exhibits many of the observed collective features of neutron scattering data is a linearized Vlasov equation with the interatomic potential replaced by -kT times the direct correlation function, c(r). Calculations in this approximation illustrate the importance, for interpreting neutron scattering data, of solving the relevant initial value problem rather than considering dispersion relations for the collective modes. In this approximation the direct solution of the initial value problem for S(Q, ω) is straightforward. Comparisons with molecular dynamics results are presented.

1. INTRODUCTION

A kinetic description of the Van Hove correlation functions has been extensively developed in recent years [1]. This description has been theoretically justified for dilute gases [2] and applied with considerable success to Brillouin scattering by gases [3, 4]. More recently, it has been extended to approximate calculations for dense gases using the Enskog theory [5]. In its original Boltzmann equation form, this approach is irrelevant to the liquid state. There are, however, many aspects of the kinetic approach which are more generally valid.

In particular the calculation of an equilibrium time dependent correlation function can always be restated in terms of a non-equilibrium problem involving the relaxation of a small well-defined initial disturbance. In section 2 we develop a detailed treatment of this equivalence for the case of the density-density correlation function G(r, t) of a classical monatomic fluid. By recasting the calculation of G(r, t) as the solution of a non-equilibrium initial value problem, we are able to consider neutron scattering as a specific problem in non-equilibrium statistical mechanics without requiring any separate physical consideration of the subtleties of fluctuation theory. The price we pay for this conceptual simplification is in the strong sensitivity of our results to the specific initial conditions of the problem. By working with the Laplace transform

---

* Work supported by the US Atomic Energy Commission under contract AT(30-1) 3326.

of the appropriate Liouville equation, this initial condition appears explicitly in the formal development, and enters naturally in the choice of approximate solutions. This will be demonstrated in section 3 of this paper.

A striking feature of many recent neutron scattering experiments is the observation of broad but definite inelastic peaks in monatomic liquids. Theoretical descriptions of these peaks [6] tend to emphasize the idea of elementary excitations in classical liquids [7]. In these theoretical treatments the restoring force giving rise to the collective motions is obtained from the short-time behaviour of various relevant correlation functions. The observed peaks are sufficiently broad, however, that the Maxwell distribution of initial velocities plays an important role. This role cannot be included correctly by merely looking for the dispersion relation for the collective modes.

This is reminiscent of the situation in dilute gases when wavelength and mean free path are comparable. To calculate correctly the sound-wave peaks which occur in the frequency distribution of scattered light under those conditions, it is necessary to properly solve an initial value problem using the appropriate kinetic equation (in that case the linearized Boltzmann equation). A calculation of the sound-wave dispersion relation under the same circumstances is both more difficult and irrelevant.

To exploit this analogy in the case of neutron scattering by liquids we need an approximate theory which still gives a soluble initial value problem. Our approximate kinetic equation containing a restoring force must properly reflect the short-time behaviour of $G(r, t)$. In a recent paper, such an approximate kinetic equation has been proposed and solved [8]. It showed many qualitatively sensible features even though it was based on a very crude short-time approximation. Only the second frequency moment of $S(K, \omega)$ was given correctly. The interesting dynamical information contained in the fourth moment (which is essential in the calculation of dispersion relations for collective modes [6]) was completely omitted. In the present paper we derive the approximate kinetic equation of Ref. [8] in a systematic way from the formal development described above. In this context, better approximations are naturally suggested. Calculations with these improved approximations are in progress.

2. FORMAL DEVELOPMENT

Consider a classical fluid in thermodynamic equilibrium in a weak gravitational potential $\phi(\vec{r})$. At $t = 0$ this fictitious potential is suddenly shut off, and the initially inhomogeneous equilibrium state relaxes to a final uniform equilibrium state. We wish to calculate the density of the fluid $n(\vec{r}, t)$ for $t > 0$ to first order in $\phi(\vec{r})$. Through the use of linear response theory and the fluctuation dissipation theorem, this is given by

$$n(\vec{r}, t) - n_0 = -n_0\beta \int d^3r' \, \phi(\vec{r}') \, [G(\vec{r} - \vec{r}', t) - n_0] \tag{1}$$

where $\beta = (kT)^{-1}$.

Since we will be concerned throughout only with terms of first order in $\phi(\vec{r})$, it is convenient to work with functional derivatives with respect to $\phi(\vec{r})$. For example, Eq. (1) can be written in the equivalent form

$$\hat{n}(\vec{r}, \vec{r}\,', t) \equiv -\left.\frac{\delta n(\vec{r}, t)}{\beta\delta\phi(\vec{r}\,')}\right|_{\phi=0} = n_0[G(\vec{r}-\vec{r}\,', t) - n_0] \tag{2}$$

Equation (2) reduces at $t = 0$ to a well-known result of equilibrium statistical mechanics [9]. Rather than derive Eq. (2) in the conventional way, it is more useful here to set up the Liouville equation for this problem and to demonstrate directly that the excess density does yield the correlation function of interest.

We represent our fluid as a classical N particle system with Hamiltonian

$$H = \sum_{j=1}^{N} \frac{p_j^2}{2m} + V(\vec{r}_1 \ldots \vec{r}_N) \tag{3}$$

The time evolution of the system can be described by a phase function $f_N(x, t)$ which obeys the Liouville equation

$$\frac{\partial f_N}{\partial t} = iLf_N \tag{4}$$

which has the formal solution

$$f_N(x, t) = \exp(iLt)\, f_N(x, 0) \tag{5}$$

In Eqs (4) and (5) x represents a point in 6N-dimensional phase space. A phase point describes the positions and momenta of all the atoms in the fluid. The Liouville operator is given by

$$iL = +\sum_{j=1}^{N} \left(-\frac{\vec{p}_j}{m} \cdot \frac{\partial}{\partial \vec{r}_j} + \frac{\partial V}{\partial \vec{r}_j} \cdot \frac{\partial}{\partial \vec{p}_j} \right) \tag{6}$$

At $t = 0$ the inhomogeneous equilibrium distribution is

$$f_N(x, 0) = \frac{\exp[-\beta(H+W)]}{\int dx \exp[-\beta(H+W)]} \tag{7}$$

where

$$W = \int \rho(\vec{r}\,')\, \phi(\vec{r}\,')\, d^3r' \tag{8}$$

and

$$\rho(\vec{r}) = \sum_{j=1}^{N} \delta(\vec{r} - \vec{r}_j) \tag{9}$$

is the density operator of the system.

To first order in $\phi(\vec{r})$ we have, by direct calculation from Eq. (7),

$$\hat{f}(\vec{r}, x, 0) \equiv -\frac{\delta f_N(x, 0)}{\beta\delta\phi(\vec{r})}\bigg|_{\phi=0} = [\rho(\vec{r}) - n_0] f_{eq} \tag{10}$$

where

$$f_{eq} = \frac{\exp(-\beta H)}{\int dx \exp(-\beta H)} \tag{11}$$

is the equilibrium distribution function when $\phi = 0$. Since the Liouville equation is linear, and $iLf_{eq} = 0$, the distribution function to first order in $\phi(\vec{r})$ evolves in time according to

$$\hat{f}(\vec{r}, x, t) \equiv -\frac{\delta f_N(x, t)}{\beta\delta\phi(\vec{r})}\bigg|_{\phi=0} = \exp(iLt)\hat{f}(\vec{r}, x, 0) \tag{12}$$

The excess density to first order in $\phi(\vec{r})$ is given by

$$\hat{n}(\vec{r}, \vec{r}', t) = \int dx\, \rho(\vec{r})\hat{f}(\vec{r}', x, t) \tag{13}$$

Using Eqs (10) and (12) we have

$$\hat{n}(\vec{r}, \vec{r}', t) = \int dx\, \rho(\vec{r}) \exp(iLt)[\rho(\vec{r}) - n_0] f_{eq} \tag{14}$$

thus verifying Eq. (2). For actual calculation, it is more convenient to work with Fourier transforms with respect to $\vec{r}$:

$$f(\vec{K}, x, t) = \int d^3r \exp(-i\vec{K}\cdot\vec{r})\hat{f}(r, x, t) \tag{15}$$

$$F(K, t) = \frac{1}{V}\iint d^3r\, d^3r' \exp[i\vec{K}\cdot(\vec{r}-\vec{r}')]\hat{n}(\vec{r}, \vec{r}', t) \tag{16}$$

(Note that in Eq. (15) the Fourier transform is only with respect to $\vec{r}$ and that $f(K, x, t)$ is still a phase function.)

Substituting Eqs (10), (12) and (14) into Eqs (15) and (16) gives

$$F(K, t) = \frac{1}{V}\int dx\, \rho_{-\vec{K}} f(\vec{K}, x, t) \tag{17}$$

and

$$f(\vec{K}, x, t) = \exp(iLt)\, \rho_{\vec{K}} f_{eq} \tag{18}$$

where

$$\rho_{\vec{K}} = \sum_{j=1}^{N} \exp(-i\vec{K}\cdot\vec{r}_j) \tag{19}$$

Combining Eqs (17) and (18) yields the familiar result

$$F(K, t) = \frac{1}{V}\int dx\, \rho_{-\vec{K}} \exp(iLt)\, \rho_{\vec{K}}\, f_{eq} \tag{20}$$

$$= \frac{1}{V} \langle \rho_{-\vec{K}} \exp(iLt)\, \rho_{\vec{K}} \rangle = \langle \rho_{-\vec{K}}(0)\, \rho_{\vec{K}}(t) \rangle \frac{1}{V}$$

Comparison of Eq. (17) with Eq. (20) shows clearly the changed point of view in calculating F(K, t) from the solution of an initial value problem. The two density operators appear symmetrically in Eq. (20), which is the conventional starting point for neutron scattering calculations. In Eq. (17) one of the density operators appears explicitly as the excess density that we are calculating by integrating over the distribution function at time t. The second density operator is implicit in the initial value of the function $f(\vec{K}, x, t)$. It remains to employ this artificially imposed asymmetry in determining useful approximate solutions for the Liouville equation obeyed by $f(\vec{K}, x, t)$.

3. KINETIC EQUATIONS

Since the initial value of $f(\vec{K}, x, t)$ plays a crucial role we work with the Laplace transform

$$g(\vec{K}, x, s) = \int_0^\infty \exp(-st)\, f(\vec{K}, x, t)\, dt \tag{21}$$

The Liouville equation for $g(\vec{K}, x, s)$ is

$$(s - iL)\, g(\vec{K}, x, s) = \rho_{\vec{K}} f_{eq} \tag{22}$$

In Eq. (22) the Liouville operator operates only on the phase variables. The dependence on $\vec{K}$ and s arises entirely from the explicit appearance of s and $\rho_{\vec{K}}$ in the equation. The excess density is given by

$$n(K, s) = \int dx\, \rho_{-\vec{K}}\, g(\vec{K}, x, s) \tag{23}$$

$$= \int dx\, \rho_{-\vec{K}}\, (s - iL)^{-1}\, \rho_{\vec{K}}\, f_{eq}$$

The neutron scattering cross-section is given by

$$S(K, \omega) = 2 \lim_{\epsilon \to 0^+} \operatorname{Re} n(K, i\omega + \epsilon) \tag{24}$$

The expansion of n(K, s) in powers of 1/s is readily obtained from Eq. (23). The coefficients, as expected, are the moments of S(K, ω)

$$n(K, s) = \frac{1}{V} \sum_{n=0} \frac{1}{s^{n+1}} \langle \rho_{-\vec{K}} (iL)\ \rho_{\vec{K}} \rangle \tag{25}$$

The terms in Eq. (25) can be calculated directly using the results of de Gennes [10]

$$\frac{n(K,s)}{n_0} = \frac{S(K)}{s} - \frac{K^2}{M\beta s^3} + \ldots \tag{26}$$

To develop approximate kinetic equations, we first separate the kinetic and potential parts of the Liouville operator

$$(s - iL_0)g = \rho_{\vec{K}} f_{eq} + iL_1 g \tag{27}$$

where

$$iL_0 = -\sum_{j=1}^{N} \frac{\vec{p}_j}{m} \cdot \frac{\partial}{\partial \vec{r}_j} \qquad iL_1 = +\sum_{j=1}^{N} \frac{\partial V}{\partial \vec{r}_j} \cdot \frac{\partial}{\partial \vec{p}_j} \tag{28}$$

We then introduce a one-particle distribution function

$$\mathscr{F}(\vec{K},\vec{p},s) = \frac{1}{V}\int dx \left(\sum_{j=1}^{N} \exp(i\vec{K}\cdot\vec{r}_j)\, \delta(\vec{p}-\vec{p}_j)\right) g(\vec{K},x,s) \tag{29}$$

whose integral over momenta is given by

$$n(K,s) = \int d^3p \; \mathscr{F}(\vec{K},\vec{p},s) \tag{30}$$

Carrying out the appropriate operations on Eq. (27) gives

$$\left(s - \frac{i\vec{K}\cdot\vec{p}}{m}\right) \mathscr{F}(\vec{K},\vec{p},s) = f_M(p)\, S(K) + A \tag{31}$$

where our massive ignorance is contained entirely in the function

$$A = \frac{1}{V}\int dx \left(\sum_{j=1}^{N} \exp(i\vec{K}\cdot\vec{r}_j)\, \delta(\vec{p}-\vec{p}_j)\right) iL_1 g(\vec{K},x,s) \tag{32}$$

In Eq. (31)

$$f_M(p) = (\beta/2\pi m)^{3/2} \exp(-\beta p^2/2m) \tag{33}$$

is a normalized Maxwellian distribution, and S(K) is the static structure factor

$$n_0 S(K) = \frac{1}{V}\int dx\, \rho_{-\vec{K}}\rho_{\vec{K}}\, f_{eq} = \langle \rho_{-\vec{K}}\rho_{\vec{K}} \rangle \frac{1}{V} \tag{34}$$

Equation (32) is just the first equation in the BBGKY hierarchy associated with the Liouville equation for our problem (i.e. Eq. (22) or Eq. (27)). As discussed in the introduction, we want to make approximations which preserve the initial condition and the kinetic behaviour, but treat the intermolecular forces in terms of their effects at short times. In other words we want to approximate the unknown function A in a way consistent with its known behaviour at large values of s. To do this in a non-trivial way, we must make an assumption concerning the approximate functional form for A. The assumption we have used so far is

$$A = R\, n(K, s) \tag{35}$$

We then expand

$$R = \frac{A}{n(K, s)} = R_0 + \frac{R_1}{s} + \ldots \tag{36}$$

in powers of $1/s$ and keep as many terms as our stamina allows. Using Eqs (22) and (32) we have

$$R = \frac{1}{n(K, s)} \frac{1}{V} \int dx \left(\sum_{j=1}^{N} \exp(i\vec{K} \cdot \vec{r}_j)\, \delta(\vec{p} - \vec{p}_j) \right) (iL - iL_0)(s - iL)^{-1} \rho_{\vec{K}} f_{eq} \tag{37}$$

In order that the resulting approximate kinetic equation give $n(K, s)$ correct to order $1/s^3$ it is necessary to keep the first two terms in the expansion of Eq. (36). After some calculation (which we carry out in appendix A) we find that R_1 is identically zero and that

$$R_0 = \frac{-i\vec{K} \cdot \vec{p}}{m} \left(1 - \frac{1}{S(K)}\right) f_M(p) \tag{38}$$

Our lowest order approximation is thus obtained by combining Eqs (31), (35), (36) and (38) to give

$$\left(s - i\frac{\vec{K} \cdot \vec{p}}{M}\right) \mathscr{F}(\vec{K}, \vec{p}, s) = f_M(p)\, S(K) - \frac{i\vec{K} \cdot \vec{p}}{M} f_M(p) \left(1 - \frac{1}{S(K)}\right) n(K, s) \tag{39}$$

Equation (39) is just the linearized Vlasov equation with the interparticle potential $v(K)$ replaced by

$$V_{eff}(K) = -\frac{1}{\beta} C(K) = -\frac{1}{\beta n_0} \left(1 - \frac{1}{S(K)}\right)$$

This is just the equation which was written down on more intuitive grounds in Ref. [8]. A closely related derivation of this equation has been given by Lebowitz and Percus [11]. As discussed there this equation can be integrated easily to give an analytic expression for $n(K, s)$ and thus for $S(K, \omega)$. This is clearly a very crude approximation, but it gives a simple expression in closed form for $S(K, \omega)$ with no adjustable parameters. Since the publication of Ref. [8], we have compared the predictions of this equation with Rahman's molecular dynamics calculations [12] for liquid argon.

This comparison is shown in Fig. 1 for the current-current correlation function $\omega^2 S(K,\omega)$. The Vlasov calculation is from Eq. (13) of Ref. [8]. The quantitative agreement is clearly not very good. The most straightforward approach to get improved results is to keep more terms in the expansion in Eq. (36) while retaining the assumed functional form of Eq. (35). We are also investigating improvements in the assumed functional form of Eq. (35) which retain the advantage of allowing a calculation of $S(K,\omega)$ in closed form. It appears promising that a tractable approximation to the Liouville equation will be found which is capable of reasonable quantitative description of neutron inelastic scattering data.

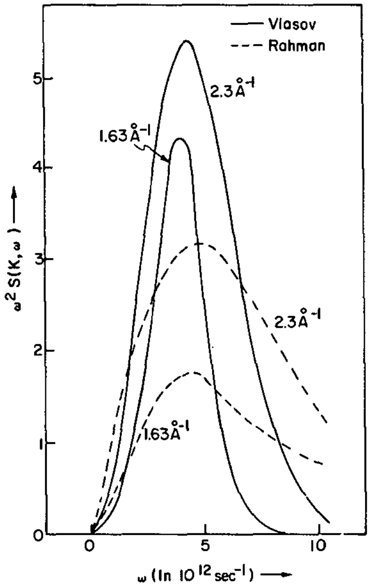

FIG. 1. The current-current correlation function $\omega^2 S(K,\omega)$ is plotted against ω for Rahman's molecular dynamics calculation of liquid argon and for the approximate theory of this paper and Ref. [8]. The density is 1.407 g/cm^3 and the temperature is 76°K.

APPENDIX

To carry out the expansion of Eq. (37) in powers of 1/s we use Eq. (26) and note that iL_0 can be replaced by

$$\alpha = i\vec{K}\cdot\vec{p}/m$$

We thus have

$$R_0 = (C_1 - \alpha C_0)/NS(K)$$

$$R_1 = (C_2 - \alpha C_1)/NS(K)$$

where

$$C_n = \int dx \left(\sum_{j=1}^{N} \exp(i\vec{K}\cdot\vec{r}_j)\, \delta(\vec{p} - \vec{p}_j) \right) (iL)^n \rho_{\vec{K}} f_{eq}$$

$$n = 0, 1, 2$$

Noting that $iL\rho_{\vec{K}} f_{eq} = (iL\rho_{\vec{K}}) f_{eq}$, and that

$$iL\rho_{\vec{K}} = \sum_{j=1}^{N} \frac{i\vec{K}\cdot\vec{p}_j}{m} \exp(-i\vec{K}\cdot\vec{r}_j)$$

we thus have

$$C_1 = N\alpha f_M(p), \qquad C_0 = NS(K)\, f_M(p)$$

To calculate C_2 we operate twice with iL to give

$$C_2 = dx \sum_{k=1}^{N} \exp(i\vec{K}\cdot\vec{r}_k)\, \delta(\vec{p} - \vec{p}_k) \sum_{j=1}^{N} \left[\left(\frac{i\vec{K}\cdot\vec{p}_j}{m} \right)^2 + \frac{i\vec{K}}{m} \cdot \frac{\partial V}{\partial \vec{r}_j} \right] \exp(-i\vec{K}\cdot\vec{r}_j) \;\; f_{eq}$$

In evaluating C_2 we use the well-known result [10]

$$\left\langle \frac{\partial V}{\partial \vec{r}_j} F \right\rangle = \frac{1}{\beta} \left\langle \frac{\partial F}{\partial \vec{r}_j} \right\rangle$$

so that the terms with $j \neq k$ cancel, and $C_2 = N\alpha^2 f_M(p)$ and $R_1 = 0$.

REFERENCES

[1] NELKIN, M., VAN LEEUWEN, J.M.J., YIP, S., Inelastic Scattering of Neutrons (Proc. Symp. Bombay, 1964) 2, IAEA, Vienna (1965) 35-57.
[2] VAN LEEUWEN, J.M.J., YIP, S., Phys. Rev. 139 (1965) A1138.
[3] NELKIN, M., YIP, S., Phys. Fluids 9 (1966) 380.
[4] GREYTAK, T.J., BENEDEK, G.B., Phys. Rev. Lett. 17 (1966) 179; GREYTAK, T.J., Ph.D. thesis, M.I.T. (1967) unpublished.
[5] RANGANATHAN, S., NELKIN, M., J. chem. Phys. 47 (1967) 4056.
[6] NOSSAL, R., ZWANZIG, R., Phys. Rev. 157 (1967) 120; NOSSAL, R., Phys. Rev. 166 (1968) 81.
[7] ZWANZIG, R., Phys. Rev. 156 (1967) 190.
[8] NELKIN, M., RANGANATHAN, S., Phys. Rev. 164 (1967) 222.
[9] PERCUS, J.K., in The Equilibrium Theory of Classical Fluids (FRISCH, H.L., LEBOWITZ, J.L., Eds), W.A. Benjamin, Inc. New York (1964); see in particular Eq.(5.1) of Percus' lectures.
[10] De GENNES, P., Physica 25 (1959) 825.
[11] LEBOWITZ, J., PERCUS, J.K., private communication (1967).
[12] RAHMAN, A., Phys. Rev. Lett. 19 (1967) 420.

DISCUSSION

J.A. YOUNG: I believe your results are similar to those obtained using the random phase approximation. What would you say is the connection here?

M.S. NELKIN: The calculation we have done so far can be described as a modified random phase approximation (RPA), as discussed by Ranganathan and myself in Ref.[8] of the paper. The present derivation shows, however, that an RPA description is not physically relevant to our basic approximation scheme.

ANALYSIS OF NEUTRON SCATTERING EXPERIMENTS ON LIQUIDS

A.K.AGRAWAL, R.C. DESAI AND S. YIP
MASSACHUSETTS INSTITUTE OF TECHNOLOGY,
CAMBRIDGE, MASS., UNITED STATES OF AMERICA

Abstract

ANALYSIS OF NEUTRON SCATTERING EXPERIMENTS ON LIQUIDS. The influence of atomic and of molecular motions on the spectrum of inelastically scattered neutrons is analysed in terms of classical correlation functions. In the case of incoherent scattering the approach is based on the use of a Gaussian intermediate scattering function and a mean square displacement, which for a molecular system consists of separate translation and rotation components. An interpolation model which gives the correct behaviour at short and long times is used to describe the centre-of-mass motions. This model has no adjustable parameters if the mean square force and the diffusion coefficient are known. The rotational effects are treated through an angular correlation function which can be calculated for a gas of spherical, linear, and symmetric molecules. For liquids the function is obtained from the Fourier transform of an infrared vibration band.

For coherent scattering the interpolation model is used in conjunction with the effective-mass approximation, which is an improvement over the Vineyard convolution approximation in that the second moment sum rule is now satisfied.

The analysis is applied to recent experiments on liquid argon, sodium, lead, methane and hydrogen in liquid argon. Comparison is made in terms of the differential cross-section (on an absolute scale) and of the variation of quasi-elastic peak width with momentum transfer. The general conclusion is that the interpolation model, the effective-mass approximation, and the angular correlation functions obtained from infrared data (in the case of methane) allow us to obtain all the qualitative features observed in the neutron experiments.

1. INTRODUCTION

Because there is no general microscopic theory of liquids, analysis of neutron scattering measurements invariably has to rely on model calculations. The most extensive theoretical development has been concerned with the description of individual particle motions in a liquid [1]. A number of phenomenological models [2] have been proposed for the purpose of interpreting incoherent scattering experiments. To treat coherent effects, the problem of collective motions must be taken into account. Here the status of the theory is less satisfactory since an effective general procedure for computing the time-dependent density correlation function is still lacking. Further theoretical attention is also needed in the case of molecular liquids. The effects of intermolecular torque on the processes of molecular reorientation have been largely ignored in explicit calculations of neutron spectra; consequently most of the current information on potential barrier has to be inferred from total cross-section data [3].

In this paper we present analyses of several liquid experiments using a systematic method of calculation. Even though the method itself is not new, the specific model used and its range of applicability have not been fully explored previously. For incoherent scattering we employ a description of translational motions which has the correct general behaviour and which is mathematically quite tractable. For coherent scattering the same model is used in conjunction with a convolution-type approximation which has given encouraging results in recent studies. In both cases the calculations require as parameters only those quantities which can be either directly measured or computed from well-defined expressions. For scattering by molecular systems effects due to the rotational motions of the molecules are known to be important. Instead of proposing a model to describe the dynamics, we consider a method whereby infrared spectroscopy data can be directly utilized in computing the neutron spectra. Moreover, this procedure is formulated as an integral part of the overall calculation.

Specific calculations have been carried out for liquid argon, sodium, lead, methane, and hydrogen in liquid argon, and the computed scattered intensities have been compared with experimental data. In all cases qualitative agreement is obtained, and in several comparisons the agreement may be regarded as quantitative. These results should be of value in clarifying the information content of existing neutron measurements on liquids and in delineating the problems for future studies.

2. SIMPLE LIQUIDS

The description of translational motions which will be used for all our liquid calculations is an interpolation model which has been discussed recently [4]. It is called an interpolation model because it is constrained to give the correct behaviour at both short and long times. The physical assumption of the model is that the effects of the liquid environment can be represented by those of an external potential which itself is changing with time. Initially the atom undergoes vibrations in the potential 'cage', but eventually the restoring forces decay into a frictional background and the atom is then able to diffuse. In contrast to other models which also attempt to combine solid-like motions with diffusion, it should be noticed that here the oscillatory and diffusive behaviour are consequences of the same potential, and in this way both are governed by the shape of the potential well and the manner in which it decays.

If we take the external potential to be a parabolic well with a simple exponential relaxation, then the parameters characteristic frequency ω_0 (the spring constant) and the relaxation time τ_0 completely specify our description. In this case analytical expressions can be found for the velocity autocorrelation function and related quantities. One has

$$\psi(t) = \langle v(t)\ v(0)\rangle / \langle v^2 \rangle$$

$$= e^{-\frac{t}{2\tau_0}} \left[\cos \Omega t + \frac{1}{2\tau_0 \Omega} \sin \Omega t \right] \tag{1}$$

The spectral density of $\psi(t)$ is

$$f(\omega) = \frac{2}{\pi} \int_0^\infty dt \cos \omega t\ \psi(t)$$

$$= \frac{2}{\pi} \frac{\omega_0^2 / \tau_0}{(\omega^2 - \omega_0^2)^2 + (\omega/\tau_0)^2} \tag{2}$$

and the mean square displacement function W(t) becomes

$$\begin{aligned} W(t) &= \frac{1}{3}\left\langle [\vec{r}(t) - \vec{r}(0)]^2 \right\rangle \\ &= 2\int_0^t dt'\,(t-t')\left\langle v(t')\,v(0)\right\rangle \\ &= 2\left\{ \frac{\omega_0^2 - \frac{1}{\tau_0^2}}{\omega_0^4} + \frac{t}{\omega_0^2\tau_0} + \frac{e^{-t/2\tau_0}}{\omega_0^4} \right. \\ &\quad \left. \times \left[\left(\frac{1}{8\tau_0^3\Omega} - \frac{3\Omega}{2\tau_0} \right) \sin\Omega t - \left(\omega_0^2 - \frac{1}{\tau_0^2} \right) \cos\Omega t \right] \right\} \end{aligned} \tag{3}$$

where $\Omega^2 = \omega_0^2 - (1/4\tau_0^2)$. Inspection of these results shows clearly that $\psi(t)$ has a damped oscillatory behaviour. The spectral density also resembles a damped oscillator except that it has a finite value at zero frequency, the latter being related to a finite self-diffusion constant. From Eq. (3) one can show that W(t) starts like t^2 and attains a linear growth at long times. Its behaviour at intermediate times can be rather complex and depends on the values of ω_0 and τ_0. These two parameters can be specified self-consistently. The physical quantities needed for their determination are the mean-square force on an atom and the self-diffusion constant D. By simply requiring Eq. (2) to give the correct second frequency moment as well as the zero-frequency limit we find

$$\begin{aligned} \omega_0^2 &= \int_0^\infty d\omega\,\omega^2 f(\omega) \\ &= \frac{1}{3M}\left\langle \nabla^2 U \right\rangle \end{aligned} \tag{4}$$

and

$$\tau_0 = \frac{T}{M\omega_0^2 D} \tag{5}$$

The energy and angular differential cross-section can be written as [1][1]

$$\frac{d^2\sigma}{d\Omega\,d\omega} = \frac{k_f}{k_i}\, e^{-\frac{\omega}{2T}}\, e^{-\frac{\kappa^2}{8mT}} \left[a_{coh}^2\, S(\kappa,\omega) + a_{inc}^2\, S_s(\kappa,\omega) \right] \tag{6}$$

where $\omega = E_f - E_i$, $\vec{\kappa} = \vec{k}_f - \vec{k}_i$; and the two exponential factors account for detailed balance and recoil effects. Functions $S(\kappa, \omega)$ and $S_s(\kappa, \omega)$ are given by

$$S(\kappa,\omega) = \frac{1}{\pi}\int_0^\infty dt\,\cos\omega t\; F(\kappa, t) \tag{7}$$

$$S_s(\kappa,\omega) = \frac{1}{\pi}\int_0^\infty dt\,\cos\omega t\; F_s(\kappa, t) \tag{8}$$

---

[1] In units of $\hbar = k_B = 1$.

It will be understood that the intermediate scattering functions F_s and F will be calculated classically. Our model calculations actually begin with the intermediate scattering functions. For the former we write

$$F_s(\kappa, t) = e^{-\frac{\kappa^2}{2} W(t)} + \text{non-Gaussian terms} \tag{9}$$

In a classical treatment the scattering functions are even in t. One sees, therefore, the interpolation model will give a short-time expansion of F_s that is correct to t^4, or equivalently the second and fourth frequency moments of S_s are treated properly.

A direct calculation of $F(\kappa, t)$ is a difficult problem, and thus far for liquids most of the attempts have utilized convolution-type approximations [5, 6]. Recently the so-called effective mass approximation [6] has been proposed and this appeared to provide a simple and reasonably accurate procedure for estimating the coherent effects. One assumes that

$$F(\kappa, t) = [1 + \Gamma(\kappa)]\, e^{-\frac{\kappa^2}{2} \frac{W(t)}{[1+\Gamma(\kappa)]}} \tag{10}$$

where $\Gamma(\kappa)$ is the Fourier transform of $n[g(r)-1]$, n being the density and g(r) the equilibrium pair distribution function. The essential advantage of Eq. (10) over the original convolution approximation is that without introducing any parameter the second frequency moment of $S(\kappa, \omega)$ is now preserved. As is well known, the De Gennes narrowing effect [7] cannot be obtained if the second moment is violated. Unlike the interpolation model, the effective-mass approximation is known to fail in the limit of small momentum and energy transfers.

Equations (3) and (6) to (10) enable one to analyse inelastic scattering experiments on simple liquids completely. We have applied this approach to liquid argon, sodium, lead and to hydrogen in liquid argon. The parameters used in these computations are summarized in Table I. For argon the derived full widths at half maximum of the quasi-elastic peak are compared with the experimental values obtained by Sköld and Larsson [8]

TABLE I. PHYSICAL PARAMETERS OF VARIOUS LIQUIDS AND THEIR BOUND-ATOM CROSS-SECTIONS

	Ar	H_2 in Ar	Na	Pb
Temp (°K)	94.4	100	373	625
ω_0 (sec^{-1} × 10^{12})	6.7	15	12.9	9
τ_0 (sec × 10^{-12})	0.178	0.153	0.139	0.124
D (10^{-5} cm^2/sec)	2.43	12	5.8	2.46
$4\pi a^2_{coh}$ (10^{-24}cm^2)	0.47	1.19[a]	1.55	11.4
$4\pi a^2_{inc}$ (10^{-24}cm^2)	0.23	79.7[a]	1.85	0

[a] Values for bound hydrogen atoms; the coherent contribution was neglected in actual computations.

in Fig. 1. This shows that the above-mentioned narrowing phenomenon in the region of first diffraction maximum is reasonably well treated by the combination of interpolation model and effective-mass approximation. Comparison of absolute intensities at constant momentum and energy transfers also show quite satisfactory agreement. The values of ω_0 and τ_0 used in this calculation are determined from computer experiments [9]. In this case one can also compute ω_0 directly from Eq. (4) since g(r) is known and a Lennard-Jones (6-12) potential may be used for U.

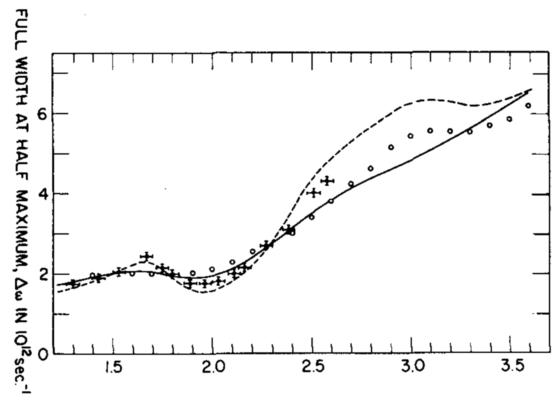

FIG.1. Full width at half maximum of the scattered neutron energy distribution as a function of κ for liquid argon at 94.4°K. Crosses - experiment of Sköld and Larsson; solid line - interpolation model DCA [10] (τ_0 = 10^{-12} sec); dashed line - interpolation model + EMA; open circles - interpolation model + DCA (τ_0 = 10^{-12} sec).

The parameters ω_0 and τ_0 for sodium are also obtained from computer studies [10] using a long-range-order potential. The computed scattering function is shown in Fig. 2 at three fixed values of energy transfer. The experimental points are taken from the smooth curves reported by Randolph [11]. A similar comparison [12] is given for lead in Fig. 3. Here we have used the measured value of D and a value of ω_0 estimated from a Debye temperature of 88°K. For the range of energy transfers shown the agreement between absolute calculation and data is reasonable. The discrepancy at small κ, is believed to be mostly due to the effective-mass approximation. An indication of this defect may be seen by a study [13] of the fourth frequency moment of S.

The incoherent spectra of hydrogen in liquid argon, as measured by Eder, Chen and Egelstaff [14], are shown in Fig. 4. The theoretical curves correspond to values of ω_0 and τ_0 which are more or less those suggested by Eder et al. The results given include the effects of ortho-para transition as well as rotational elastic scattering. It can be observed that the interpolation model and the itinerant oscillator description of Sears give qualitatively similar spectra, the quantitative difference being that the former shows more intensity in the inelastic region and less intensity in the quasi-elastic peak. This distinction will not be so pronounced if a large value of D were used in the itinerant oscillator calculation.

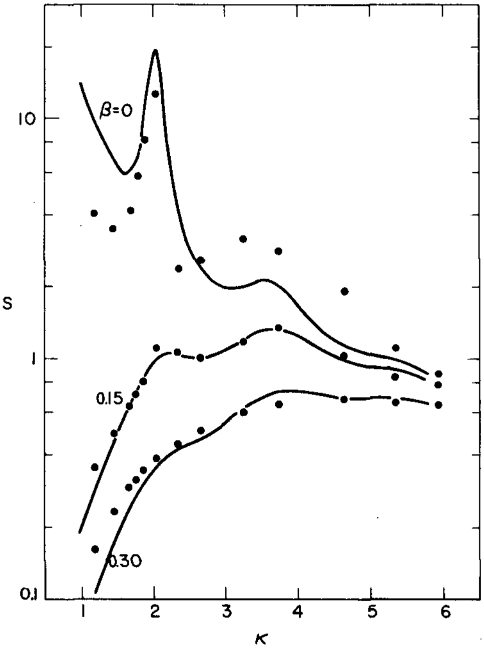

FIG. 2. S(α, β), as defined by Randolph [12], as a function of κ for various values of β(= ω/T), for liquid sodium at 373°K ($\alpha = \kappa^2/2Mt$). Solid curve is obtained with the interpolation model and effective-mass approximation. Open circles are the experimental values from Randolph.

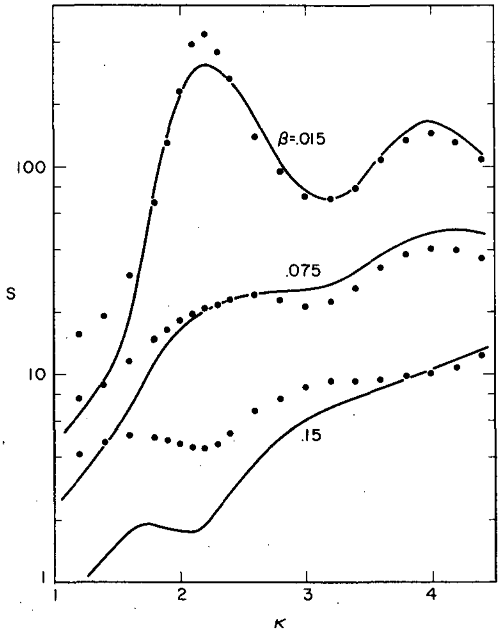

FIG. 3. $S_R(\kappa, \omega)$, as defined by Randolph and Singwi [13], as a function of κ for various values of β, for liquid lead at 625°K. Solid curve is obtained through the interpolation model and effective mass approximation. Open circles are the experimental values from Randolph and Singwi.

3. MOLECULAR SYSTEMS

The method of analysis described in the preceding section can be readily generalized to molecular liquids. The inclusion of intramolecular vibrations is straightforward, but this is usually not necessary because the incident neutron energies are insufficient to excite any level. On the other hand, rotational effects are known to have an appreciable influence especially in the inelastic region [3]. To make the calculations tractable it has been necessary to assume that translation-rotation couplings can be neglected. This is an approximation made in all existing computations although very little is known about the extent to which it is justified.

The simplest treatment of the rotational problem is to assume that molecules in a liquid rotate freely. With this approximation one can compute rigorously the rotational contributions to the cross-section [15]. However, such an approach undermines at the outset the purpose of studying rotational dynamics in condensed systems. If one is to distinguish molecular reorientation processes in gases from those in liquids and solids, clearly it is essential that explicit considerations be given to the effects of intermolecular torque. An alternative is to utilize experimental information provided by a different technique. This is the approach followed in our calculations.

Calculations based on the Gaussian approximation can also be formulated for molecular systems [16]. Assuming no translation-rotation interactions, we decompose the mean square displacement function of an atom in a molecule into separate contributions due to centre-of-mass motions and angular displacements. By writing

$$W(t) = W_t(t) + W_r(t) \tag{11}$$

we have

$$\begin{aligned} W_t(t) &= \frac{1}{3}\langle[\vec{R}(t) - \vec{R}(0)]^2\rangle \\ W_r(t) &= \frac{1}{3}\langle[\vec{b}(t) - \vec{b}(0)]^2\rangle \end{aligned} \tag{12}$$

$$= \frac{2}{3} b^2 \, [1 - F_1(t)] \tag{13}$$

$$F_1(t) = \frac{1}{b^2}\langle\vec{b}(t) \cdot \vec{b}(0)\rangle \tag{14}$$

where $\vec{r} = \vec{R} + \vec{b}$, $\vec{R}$ being centre-of-mass position of the molecule and $\vec{b}$ the bond distance measured from $\vec{R}$. Because we ignore intramolecular vibrations, $\vec{b}(t)$ varies in orientation but not in magnitude. The function $F_1(t)$ is seen to describe the correlation of a molecular axis at $t = 0$ with itself at a time t later. Its time dependence is, of course, determined by the molecular reorientation processes characteristic of the system.

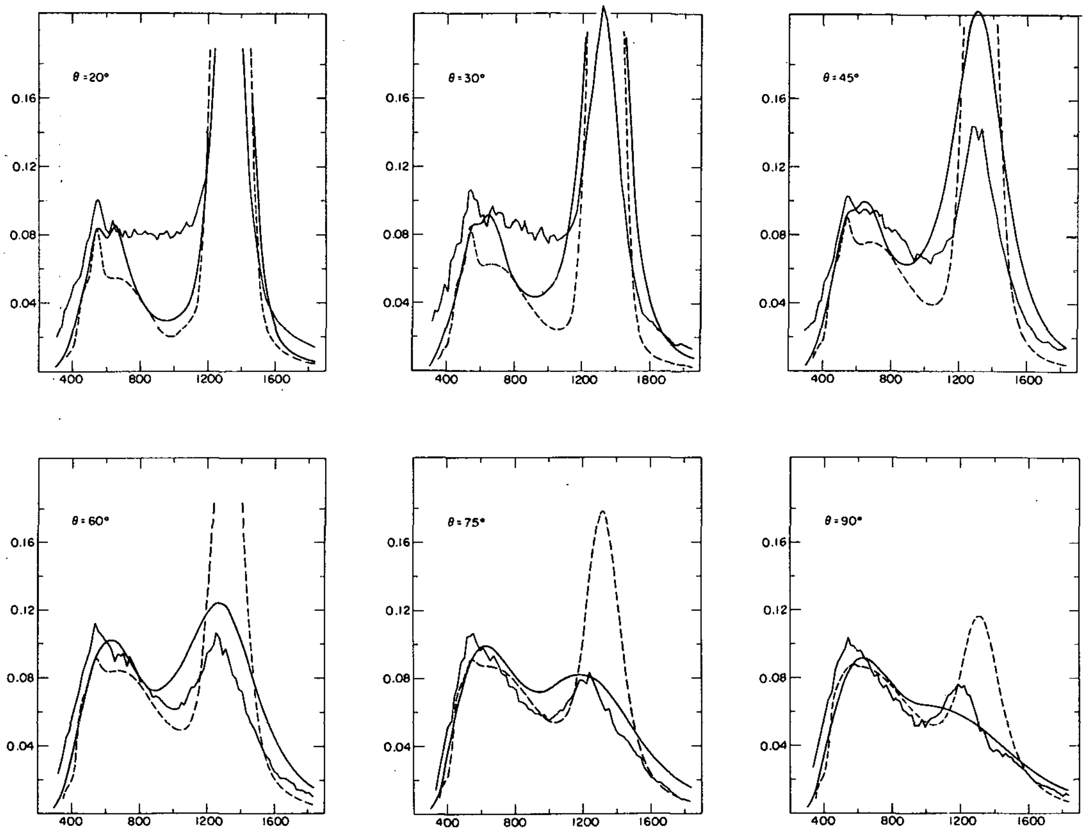

FIG.4. Energy distribution of neutrons scattered by hydrogen in liquid argon at 100°K and 26.5 atm., as a function of time of flight for various scattering angles, θ. Solid curve – interpolation model; dashed curve – Sears itinerant oscillator model; jagged curve – experiment. Abscissa is time-of-flight in μsec/m and ordinate is cross-section in mb Sr^{-1} μsec^{-1}.

The addition of W_r in Eq. (11) enables us to extend our previous calculations to molecular systems. The differential cross-section for incoherent scattering becomes [17]

$$\frac{d^2\sigma}{d\Omega d\omega} = \frac{k_f}{k_i}\, a_{inc}^2\, e^{-\frac{\omega}{2T}}\, e^{-\frac{\kappa^2}{8Mt}G(T)}\, \widetilde{S}_s(\kappa, \omega) \tag{15}$$

where

$$\widetilde{S}_s(\kappa, \omega) = \frac{1}{\pi}\int_0^\infty dt \cos \omega t\, e^{-\frac{\kappa^2}{2}W(t)} \tag{16}$$

The temperature-dependent quantity G(T) is defined by

$$G(T) = 8MT \int_0^\infty d\omega \frac{f(\omega)}{\omega^2}\left(\cosh \frac{\omega}{2T} - 1\right) \tag{17}$$

where $f(\omega)$ is a generalized spectral density, related to the mean square displacement by

$$W(t) = 2\int_0^\infty d\omega \frac{f(\omega)}{\omega^2}(1 - \cos \omega t) \tag{18}$$

G(T) is close to unity for monatomic systems - in agreement with Eq. (6). It can be very different from unity for polyatomic systems. Thus far our results are still general. The dynamical properties of the medium are given by Eq. (12) and the function $F_1(t)$.

In the case of gases, $W_t(t) = (T/M)t^2$ so the only problem is to determine $F_1(t)$ for a rigid rotator of the correct symmetry. Approximate results for spherical, linear and symmetric molecules have been derived [16]; these are respectively

$$F_1(t) = \frac{1}{3} + \frac{2}{3}(1 - t^{*2})\, e^{-t^{*2}/2} \tag{19}$$

$$F_1(t) = M\left(-\frac{1}{2}, \frac{1}{2}, \frac{t^{*2}}{2}\right) e^{-t^{*2}/2} \tag{20}$$

$$F_1(t) = g(t^*) \cos^2\emptyset + \frac{1}{2}\,[1 + g(t^*)]\, e^{-\frac{I_z - I}{2I_z}t^{*2}} \sin^2\emptyset \tag{21}$$

where $t^* = (T/I)^{\frac{1}{2}}\, t$, $\emptyset$ is the angle between $\vec{b}$ and the symmetry axis (along z), and M(a, b, x) is Kummer's confluent hypergeometric function [18]. $g(t^*)$ is $F_1(t)$ as defined by Eq. (20). For spherical molecules $F_1(t)$ shows a minimum region but remains positive at all times whereas the linear molecule result becomes negative. The symmetric molecule can have different behaviour, depending on the value of $\emptyset$. Notice that if $\emptyset = 0$ then Eq. (21) reduces to Eq. (20).

Equations (19) and (21) have been used to compute the cold-neutron spectra of gaseous methane and ammonia measured by Webb [19]. Comparison between calculation and experiment at a scattering angle of 20° is

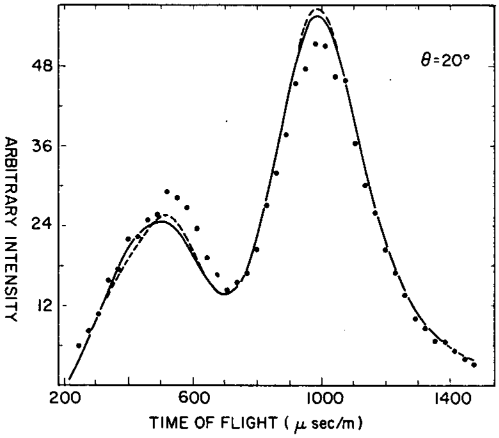

FIG. 5. Time-of-flight spectra of neutrons scattered by methane gas at T = 295°K. Experimental points are given as closed circles and theoretical results are shown as solid (Gaussian approximation) and dashed (exact quantum mechanical) lines respectively. Calculated spectra have been averaged over an incident spectrum (mean energy 4.87 meV) and are area normalized.

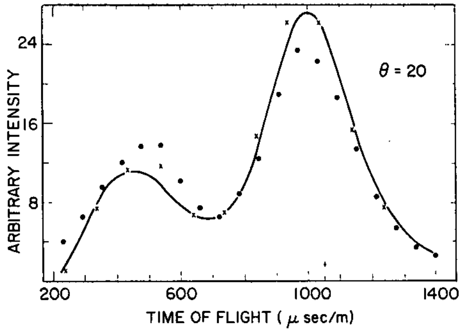

FIG. 6. Time-of-flight spectra of neutrons scattered by ammonia gas at T = 295°K. Experimental points are given as closed circles and the Gaussian approximation is shown by the solid line. Exact results are indicated by crosses. Calculated spectra have been averaged over an incident spectrum (mean energy 4.87 meV) and are area normalized.

shown in Figs 5 and 6. Also given are exact quantum mechanical results [15]. For methane we have estimated the rotational non-Gaussian corrections, and when the leading non-Gaussian correction term is included, the final result is found to agree with the quantum calculation to within about 1%. Similar comparisons at larger scattering angles show equally satisfactory agreement. In the case of ammonia, the present approach reduces the amount of computation time by a factor of about 200-300 relative to an exact treatment.

The method just described is applicable also to liquids. Unfortunately it has not been feasible to compute $F_1(t)$ in terms of an appropriate model. For a spherical rotator undergoing small-step angular displacements one has [20]

$$F_1(t) = \exp\left[- \frac{2}{\xi^{*2}} \left(\xi^* t^* - 1 + e^{-\xi^* t^*} \right) \right] \qquad (22)$$

where $\xi^* = (1/IT)^{\frac{1}{2}}\xi$, ξ being the rotational friction constant. Equation (22) is a one-parameter description in which ξ can be related to the mean square torque. This expression has not been used in neutron scattering calculations to any appreciable extent. In the absence of a proper theoretical description, we may turn to other experimental techniques for information about $F_1(t)$ for liquids. It has been shown by Gordon [21] that for isotropic rotations $F_1(t)$ is just the Fourier transform of a properly normalized infrared vibration band, $\hat{I}(\omega)$. This means

$$F_1(t) = \int_{-\infty}^{\infty} d\omega\ \hat{I}(\omega)\ e^{-i\omega t} \tag{23}$$

which is a connection between an optical absorption band shape and the energy distribution of inelastically scattered neutrons. We have applied Eq.(23) to recent cold-neutron measurements on liquid methane as reported by Venkataraman, Dasannacharya and Rao [6]. For W_t we use the interpolation model of section 2 with the measured value of diffusion coefficient and $\omega_0 = 11 \times 10^{12}$ sec^{-1} as obtained by law of corresponding states. The comparison at 98°K is shown in Fig. 7. Figure 8 shows the full width at half maximum of the quasi-elastic peak. The generalized spectral density, as defined in Eq. (18), can be computed in this form

$$f(\omega) = f_t(\omega) + \frac{2}{3} b^2 \omega^2\ \hat{I}(\omega) \tag{24}$$

where $f_t(\omega)$ is given by Eq.(2). This result is shown in Fig. 9 along with a frequency function extracted from thermal neutron data on solid methane by Harker and Brugger [22]. The resemblance between the liquid and solid spectra is striking. A free spherical rotator, on the same scale, would show a peak at a much lower frequency and the width would be different from that derived from infrared data.

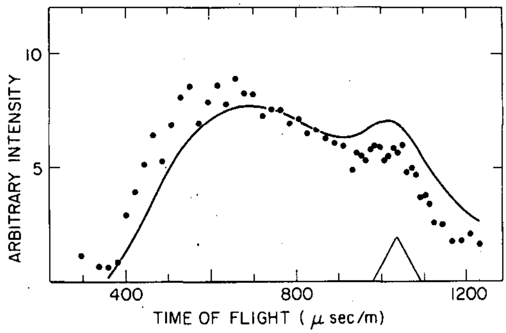

FIG.7. Time-of-flight spectra of neutrons scattered by liquid methane at T = 98°K. Experimental points are given as closed circles and theoretical results are shown by solid line. Calculated spectrum has been averaged over the indicated incident neutron spectrum (mean energy 4.87 meV) and is area normalized.

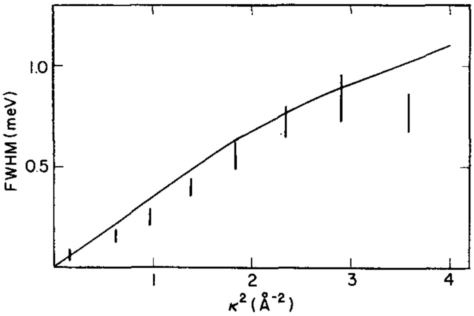

FIG.8. Full width at half maximum of the quasi-elastically scattered neutron energy distribution as a function of κ^2 for liquid methane at 98°K. Vertical bars are experimental data while solid curve is the theoretical one.

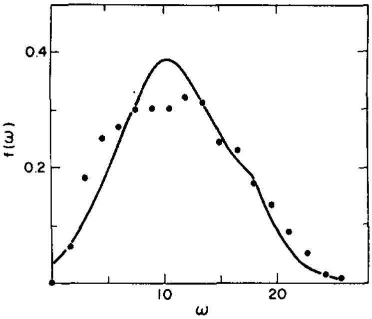

FIG.9. The generalized frequency distribution function f(ω) in 10^{-12} sec, versus the frequency ω, in 10^{12} sec^{-1} for liquid methane at 98°K. Solid circles are results extracted by Harker and Brugger for solid methane at 22.1°K. Harker and Brugger's results have been area normalized to the theoretical one.

4. DISCUSSION

One of the most useful calculational procedures in the theory of neutron scattering by simple liquids is the Gaussian approximation. It provides a relation between the scattered neutron intensity and the velocity autocorrelation function, a quantity which also can be studied by means of computer molecular dynamics experiments [9]. The correlation function and its spectral density are quantities of fundamental interest [23] in current theories of non-equilibrium phenomena in liquids, therefore the Gaussian approximation enables us to bring the neutron experiments into closer contact with recent theoretical developments as well as with other experimental techniques. Since procedures now exist for treating non-Gaussian corrections, this approach can be made as accurate as the mean square displacement function permits [9, 24]. In this spirit the interpolation model plays a useful role as a means of correlating neutron data with computer results and with physical quantities such as the diffusion constant, the mean square force, and the relaxation time. The simplicity of the model and the fact that analytical expressions for $\psi(t)$, f(ω) and W(t) are available should greatly facilitate its application. In so doing one is assured of a description which satisfies the requirements of proper behaviour at short and long times [4].

The extension of Gaussian approximation to molecular systems is both physically reasonable and mathematically convenient. Although it is well known that the scattering function of free rotators is not Gaussian [25], we have shown that a Gaussian approach yields quite accurate results in the case of methane and ammonia [16]. Again, one can take into account the non-Gaussian corrections, which in liquids can be expected to be even less significant. The use of rotational correlation functions has the same advantages as the case of velocity autocorrelation in translations. The fact that $F_1(t)$ can be measured by infrared spectroscopy further enhances the utility of this method [26].

The numerical results presented in this work include liquid metals as well as an inert gas liquid. Although additional computations and comparisons with experiment are needed before definite conclusions can be reached, certain qualitative trends can now be observed. In general, all the qualitative features of the experiment are reproduced whether they pertain to coherent or incoherent effects. This implies that with the type of approximations we have discussed one should begin to look for a more quantitative agreement. Specifically, the effective-mass approximation appears to work well at small energy transfers but significant discrepancy sets in at higher energy transfers in the case of liquid metals. On the other hand, this approximation gave surprisingly good results over the entire experimental range in argon. For incoherent scattering there is a consistent tendency to underestimate the intensity of inelastic scattering and overestimate the elastic scattering. In the case of hydrogen in liquid argon this is at least partly due to the interpolation model and the choice of ω_0 and τ_0 values. It is possible that the discrepancy, which is most pronounced at small scattering angles, signifies the inadequacy of a single relaxation process. Also for both methane and hydrogen in argon there are uncertainties associated with the treatment of rotations. In methane other attempts of using infrared data in neutron scattering calculations showed the same behaviour [27], consequently the lack of quantitative agreement still remains to be clarified.

ACKNOWLEDGEMENTS

We would like to thank Dr. P.D. Randolph and Dr. K.R. Rao for sending us their experimental results. The computations were done, in part, at the MIT computation centre. This work was supported by the Army Research Office-Durham, The National Science Foundation and Project SQUID of the US Office of Naval Research.

REFERENCES

[1] SJÖLANDER, A., in Thermal Neutron Scattering (EGELSTAFF, P.A., Ed.), Academic Press Inc., New York (1965); also EGELSTAFF, P.A., An Introduction to the Liquid State, Academic Press Inc., New York (1967).

[2] RAHMAN, A., SINGWI, K.S., SJÖLANDER, A., Phys. Rev. 126 (1962) 997; ARDENTE, V., NARDELLI, G.F., REATTO, L., Phys. Rev. 148 (1966) 124; SEARS, V.F., Proc. phys. Soc. 86 (1965) 953; NAKAHARA, Y., TAKAHASHI, H., Proc. phys. Soc. 89 (1966) 747; DAMLE, P.S., SJÖLANDER, A., SINGWI, K.S., Phys. Rev. 165 (1968) 277.

[3] JANIK, J.A., KOWALSKA, A., in Thermal Neutron Scattering (EGELSTAFF, P.A., Ed.), Academic Press Inc., New York (1965).

[4] DESAI, R.C., YIP, S., Phys. Rev. 166 (1968) 129.

[5] VINEYARD, G.H., Phys. Rev. 110 (1958) 999; SINGWI, K.S., Phys. Rev. 136 (1964) 969; Physica 31 (1965) 1257.

[6] SKÖLD, K., Phys. Rev. Lett. 19 (1967) 1023; VENKATARAMAN, G., DASANNACHARYA, B.A., RAO, K.R., Phys. Lett. 23 (1966) 226; Phys. Rev. 161 (1967) 133.

[7] de GENNES, P.G., Physica 25 (1959) 825.

[8] SKÖLD, K., LARSSON, K.-E., Phys. Rev. 161 (1967) 102; see also Ref. [4].

[9] RAHMAN, A., Phys. Rev. 136 (1964) A 405; NIJBOER, B.R.A., RAHMAN, A., Physica 32 (1966) 415.

[10] PASKIN, A., RAHMAN, A., Phys. Rev. Lett. 16 (1966) 300.

[11] RANDOLPH, P.D., Phys. Rev. 134 (1964) A1238.

[12] RANDOLPH, P.D., SINGWI, K.S., Phys. Rev. 152 (1966) 99.

[13] DESAI, R.C., YIP, S., Phys. Lett. 25A (1967) 211.

[14] EDER, O.J., CHEN, S.H., EGELSTAFF, P.A., Proc. phys. Soc. 89 (1966) 833.

[15] RAHMAN, A., Nucl. Energy, Part A: Reactor Sciences 13 (1961) 128; YIP, S., Thesis, University of Michigan (1962); GRIFFING, G.W., Phys. Rev. 124 (1961) 1489; 127 (1962) 1179; LURIE, N.A., J. chem. Phys. 46 (1967) 352; VENKATARAMAN, G., RAO, K.R., DASANNACHARYA, B.A., DAYANIDHI, P.K., Proc. phys. Soc. 89 (1966) 379; YOUNG, R.C., Bull. Am. phys. Soc. 8 (1963) 512.

[16] AGRAWAL, A.K., YIP, S., Phys. Rev. (July 1968).

[17] AGRAWAL, A.K., YIP, S., in Proc. Symp. Molecular Dynamics and Structure of Solids, National Bureau of Standards, 1967, to be published.

[18] ABRAMOWITZ, M., STEGUN, I.A., Eds, Handbook of Mathematical Functions, Dover, New York (1965).

[19] WEBB, F.J., Inelastic Scattering of Neutrons in Solids and Liquids (Proc. Symp. Chalk River, 1962) 1, IAEA, Vienna (1963) 457; Proc. phys. Soc. 92 (1967) 912.

[20] STEELE, W.A., J. chem. Phys. 38 (1963) 2411.

[21] GORDON, R.G., J. chem. Phys. 43 (1965) 1307.

[22] HARKER, Y.D., BRUGGER, R.M., J. chem. Phys. 46 (1967) 2201.

[23] RICE, S.A., GRAY, P., The Statistical Mechanics of Simple Liquids, Interscience Publishers, New York (1965).

[24] DESAI, R.C., NELKIN, M.S., Nucl. Sci. Engng 24 (1966) 142; DESAI, R.C., J. chem. Phys. 44 (1966) 77.

[25] SCHOFIELD, P., in Proc. Brookhaven Conf. Neutron Thermalization 1 (1962), RB1 USAEC Rep. BNL-719.

[26] AGRAWAL, A.K., YIP, S., J. chem. Phys. 46 (1967) 1999.

[27] SEARS, V.F., Can. J. Phys. 45 (1967) 237; RAO, K.R., Venkataraman, G., DASANNACHARYA, B.A., Can. J. Phys. 45 (1967) 3185.

DISCUSSION

B. MOZER: Does your self-correlation function satisfy the sum rule of integrating overall energy transfer, i.e. $\int \langle e^{i\vec{K}\cdot\vec{x}_i(t)} e^{-i\vec{K}\cdot\vec{x}_i(0)} \rangle e^{i\omega t} d\omega = 1$? Your model is similar to the Bohm-Pines method with individual and collective components including their interaction terms.

S. YIP: The interpolation model gives correctly the zeroth moment of $S_s(K, \omega)$, and likewise the second and fourth moments. The basic idea of the model is very old, and we can trace it all the way back to Maxwell in viscoelastic theory and Drude in electrodynamics.

O.J. EDER: Have you taken into account the quantum effects in the rotational part of the intermediate scattering function by going from the real time to Schofield's time?

S. YIP: The angular correlation function we get from optical data is a classical correlation function, i.e. we take a cosine transform of $I(\omega)$, which is taken to be symmetric. In using this correlation function to compute neutron scattering, we have indeed used a displaced time variable. Among other things this procedure gives rise to a Debye-Waller factor which depends on the rotational contribution to the spectral density f(ω).

J.W. WHITE: The correlation function which you derive from infrared data (Eq.(23)) is of course a dipole moment correlation function. It therefore has the nature of a pair correlation function and I should be glad if you would comment on its use for calculating incoherent neutron scattering spectra.

S. YIP: You are quite right about the cross terms which normally would be present in the dipole-dipole correlation function. On the other hand, it is a good approximation to consider the intramolecular vibrations in different molecules to be uncorrelated. This means that if you look at the shape of a near infrared vibration band (I(ω) in our notation), you get mainly information about autocorrelation in the orientation of a molecule. If you look at far infrared data, then indeed we should worry about correlation effects between different molecules which appear through translation-rotation interactions as well as intermolecular torques.

J.G. POWLES: Mr. Yip reported that the inelastic neutron scattering spectrum for methane does not differ much as between the solid and the liquid states. This is what I would expect, because it is known from nmr data that the reorientational motion is hardly changed on solidification and is probably faster than translation in the liquid. Since inelastic scattering of neutrons is sensitive to the fastest motion it is just seeing reorientation and hence the results are consistent with those obtained by nmr.

CURRENT FLUCTUATIONS IN CLASSICAL LIQUIDS*

A. RAHMAN
ARGONNE NATIONAL LABORATORY,
ARGONNE, ILL., UNITED STATES OF AMERICA

Abstract

CURRENT FLUCTUATIONS IN CLASSICAL LIQUIDS. Molecular dynamics data on an argon-like liquid are used to determine the spectrum of current density fluctuations in the system. It is found that for given wave-number κ the frequency spectra of the longitudinal and the transverse current fluctuations have a well-defined peak. The position of this peak depends on κ and for the longitudinal currents the dependence is closely related to the structure factor $S(\kappa)$ of the system; for transverse currents the dependence is less marked.

Estimates of the life-times of the fluctuations have been obtained from the shape of the spectra. The unique role of molecular dynamics for the study of transverse current correlations is discussed.

DEFINITIONS

In this paper we shall report the calculation of space-time fluctuations of current density in an argon-like dense classical fluid. For this calculation the trajectories of the particles were obtained by the method of molecular dynamics; it has been shown in recent years that this is a useful method for the study of such fluids for their equilibrium[1] and non-equilibrium properties.[2]

The current $\underset{\sim}{J}$ and number density Q at position $\underset{\sim}{r}$ and time t, in a system of N particles having positions $\underset{\sim}{r}_i(t)$ and velocities $\underset{\sim}{v}_i(t)$, $i = 1, \ldots, N$, are defined as

$$\underset{\sim}{J}(\underset{\sim}{r},t) = N^{-\frac{1}{2}} \sum_{j=1}^{N} \underset{\sim}{v}_j(t)\ \delta(\underset{\sim}{r} - \underset{\sim}{r}_j(t)) \qquad (1)$$

$$Q(\underset{\sim}{r},t) = N^{-\frac{1}{2}} \sum_{j=1}^{N} \delta(\underset{\sim}{r} - \underset{\sim}{r}_j(t)) \qquad (1'$$

respectively. Their Fourier components for wave vector $\underset{\sim}{\kappa}$ are, respectively,

$$\underset{\sim}{J}(\underset{\sim}{\kappa},t) = N^{-\frac{1}{2}} \sum_{j=1}^{N} \underset{\sim}{v}_j(t)\ \exp(i\underset{\sim}{\kappa}\cdot\underset{\sim}{r}_j(t)) \qquad (2)$$

$$Q(\underset{\sim}{\kappa},t) = N^{-\frac{1}{2}} \sum_{j=1}^{N} \exp(i\underset{\sim}{\kappa}\cdot\underset{\sim}{r}_j(t)) \qquad (2'$$

---

* Based on work performed under the auspices of the US Atomic Energy Commission.

The scalar product $\underset{\sim}{\kappa}\cdot\underset{\sim}{J}(\underset{\sim}{\kappa},t)$ will be denoted by $J_{\parallel}(\underset{\sim}{\kappa},t)$, and referred to as the longitudinal component of $\underset{\sim}{J}(\kappa,t)$. Similarly the component in a fixed direction in space normal to $\underset{\sim}{\kappa}$ will be devoted by $J_{\perp}(\underset{\sim}{\kappa},t)$ and referred to as the transverse component; for uniformity with the definition of $J_{\parallel}$ we shall include in $J_{\perp}$ a factor κ, equal to the magnitude of $\underset{\sim}{\kappa}$.

The auto-correlations in time of $J_{\parallel}$, $J_{\perp}$ and Q are defined as

$$C_{\parallel}(\underset{\sim}{\kappa},t) = \langle J_{\parallel}(\underset{\sim}{\kappa},o)\, J_{\parallel}^{*}(\underset{\sim}{\kappa},t)\rangle \tag{3}$$

$$C_{\perp}(\underset{\sim}{\kappa},t) = \langle J_{\perp}(\underset{\sim}{\kappa},o)\, J_{\perp}^{*}(\underset{\sim}{\kappa},t)\rangle \tag{3'}$$

$$F(\underset{\sim}{\kappa},t) = \langle Q(\underset{\sim}{\kappa},o)\, Q^{*}(\underset{\sim}{\kappa},t)\rangle \tag{3''}$$

respectively. In the above definitions $\langle\ldots\rangle$ denotes thermal averaging. The frequency spectra of the time correlations defined above will be denoted by $C_{\parallel}(\underset{\sim}{\kappa},\omega)$, $C_{\perp}(\underset{\sim}{\kappa},\omega)$ and $S(\underset{\sim}{\kappa},\omega)$, respectively and will be given by equations of the type $C_{\parallel}(\underset{\sim}{\kappa},\omega) = \int_{o}^{\infty} C_{\parallel}(\underset{\sim}{\kappa},t)\cos\omega t\, dt$.

The functions $C_{\parallel}$, $C_{\perp}$ and F have been defined with vector $\underset{\sim}{\kappa}$ as argument; for fluids these functions will depend on the magnitude $\kappa = |\underset{\sim}{\kappa}|$. In the rest of the paper, when any of the functions $C_{\parallel}$, $C_{\perp}$ or F is shown with magnitude κ as argument, it will imply that the function of vector $\underset{\sim}{\kappa}$ has been averaged over all orientations of $\underset{\sim}{\kappa}$ with respect to the system.

SOME PROPERTIES OF $C_{\parallel}$, $C_{\perp}$ AND F

At any time t, for a classical system, the positions and velocities of the particles are statistically independent and hence, using Eqs. (2) and (3), we get

$$C_{\parallel}(\underset{\sim}{\kappa},t = o) = C_{\perp}(\underset{\sim}{\kappa},t = o) = \kappa^{2}k_{B}T/M \tag{4}$$

where k_B is the Boltzmann constant, T the absolute temperature and M the mass of the particles which are all assumed to be identical.

The correlation $F(\underset{\sim}{\kappa}, t = o)$ is the Fourier transform of the pair correlation function $g(\underset{\sim}{r})$; it will be denoted by $S(\underset{\sim}{\kappa})$ and will be referred to as the structure factor. The relation between $g(\underset{\sim}{r})$ and $S(\underset{\sim}{\kappa})$ is of course

$$S(\underset{\sim}{\kappa}) - 1 = 8\pi^3 n\, \delta(\underset{\sim}{\kappa}) + n \int d\underset{\sim}{r}(g(\underset{\sim}{r}) - 1) \exp(i\underset{\sim}{\kappa}\cdot\underset{\sim}{r}) \tag{5}$$

where n is the average number density. As $\underset{\sim}{\kappa} \to o$, apart from the $\delta(\underset{\sim}{\kappa})$ part, the structure factor is determined by macroscopic fluctuations of density and is given by

$$S(o) = nk_BT\, \chi_T \tag{6}$$

where χ_T is the isothermal compressibility of the system.

Using the continuity equation, $Q(\underset{\sim}{\kappa}, t) = iJ_{\parallel}(\underset{\sim}{\kappa}, t)$, we get the relation[3]

$$C_{\parallel}(\underset{\sim}{\kappa}, t) = -\frac{d^2}{dt^2} F(\underset{\sim}{\kappa}, t) \tag{7}$$

and hence

$$C_{\parallel}(\underset{\sim}{\kappa}, \omega) = \omega^2 S(\underset{\sim}{\kappa}, \omega) \tag{8}$$

From Eq. (7) it follows that

$$F(\underset{\sim}{\kappa}, t) = S(\underset{\sim}{\kappa}) - \int_o^t (t - u)\, C_{\parallel}(\underset{\sim}{\kappa}, u)\, du \tag{9}$$

Thus, in general, for long times,

$$F(\underset{\sim}{\kappa}, t = \infty) = S(\underset{\sim}{\kappa}) + \int_o^{\infty} u\, C_{\parallel}(\underset{\sim}{\kappa}, u)\, du \tag{10}$$

and

$$o = \int_0^\infty C_\parallel(\underset{\sim}{\kappa},u)\ du \tag{11}$$

In particular, for fluids, since $F(\underset{\sim}{\kappa},t = \infty) = 0$,

$$S(\underset{\sim}{\kappa}) + \int_0^\infty uC_\parallel(\underset{\sim}{\kappa},u)\ du = 0 \tag{12}$$

For a detailed discussion of the small time behavior of $C_\parallel$, $C_\perp$ and F the reader is referred to a recent paper by Forster Martin and Yip.[4]

METHOD OF CALCULATION

In molecular dynamics the trajectories of the N particles are calculated with periodic boundary conditions;[2] thus, a cubic box, of side L, volume L^3, containing N particles, is repeated an infinite number of times along each side of the cube. It then follows that for this infinite system only those Fourier components are not zero for which $\underset{\sim}{\kappa} = (2\pi/L)(\nu_1, \nu_2, \nu_3)$, the ν's being positive or negative integers. Moreover, for these special values of $\underset{\sim}{\kappa}$, it is enough to calculate the functions defined above using the positions and velocities of the N particles situated inside one of the infinite number of identical boxes.

For a chosen $\underset{\sim}{\kappa}$, knowing the positions and velocities of the N particles as a function of time, we can calculate $J_\parallel$, $J_\perp$ and Q and hence their auto-correlation; then, for a suitably chosen $\Delta\kappa$, by adding the results for all $\underset{\sim}{\kappa}$ in a shell defined by the magnitudes κ, $\kappa + \Delta\kappa$, and dividing by the number of vectors $\underset{\sim}{\kappa}$ in the shell, we get the auto-correlations as a function of κ. It is obvious that for small values of κ this averaging over angles of $\underset{\sim}{\kappa}$ will be statistically less satisfactory than at large values; this effect will be mentioned again when the results are presented.

The calculations reported here were made on an argon-like system of 500 particles at T = 76°K and ρ = Mn = 1.407 g/cc. A Lennard-Jones (6,12) potential was used with a depth of 120°K the minimum in the potential being at 3.817 Å (i.e. the usual parameter σ is equal to 3.4 Å).

RESULTS FOR LONGITUDINAL CURRENTS

The structure factor, $S(\kappa)$, is shown in Fig. 1. As explained in the previous section this is really a histogram with

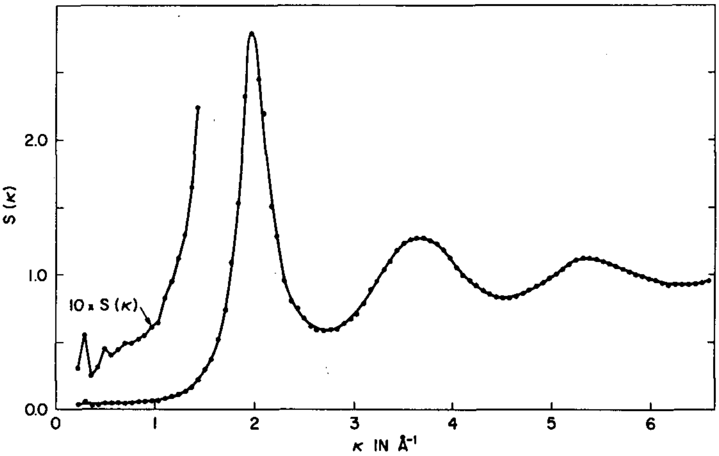

FIG.1. The structure factor $S(\kappa) \equiv F(\kappa, t = 0)$ for the argon-like fluid calculated from molecular dynamics data. The small κ region is shown on an expanded vertical scale.

$\Delta\kappa = 1/15\ A^{-1}$ even though it has been drawn as a smooth curve. On the same figure, with a scale expanded by a factor of 10, we have shown the small κ region of the data; this is to show the scatter of the data in the statistically least favorable region. The asymptotic value $S(o)$ is unattainable in a system of a few hundred particles but the data indicates a value of approximately 0.04; it is quite remarkable that even an assembly of only 500 particles gives a qualitatively good indication of the value of a macroscopic elastic constant, namely, the isothermal compressibility; using $S(o) = 0.04$ and Eq. (6) we get $\chi_T = 1.6 \times 10^{-10}$ cm^2 dynes^{-1}, the experimental value[5] at 84°K being 2.0×10^{-10} cm^2 dynes^{-1}.

We have shown above that, as a consequence of the continuity equation, the second derivative of $-F(\kappa,t)$ is $C_{\parallel}(\kappa,t)$; its value at $t = o$ is equal to $\kappa^2 k_B T/M$ and is unrelated to $F(\kappa,o) \equiv S(\kappa)$, the spatial structure of the system. Figure 2 shows the calculated value of $C_{\parallel}(\kappa,t = o)$ as a function of κ; it also shows $\kappa^2 k_B T/M$ for $T = 76°K$. The agreement is quite satisfactory.

In Fig. 3 we have plotted for various κ the normalized, dimensionless quantities, $C_{\parallel}(\kappa,t)/C_{\parallel}(\kappa,t = o)$, as a function of time. Notice that around $\kappa = 2\text{Å}^{-1}$, where $S(\kappa)$ is a maximum (Fig. 1), the variation of $C_{\parallel}(\kappa,t)$ is slower than at all other values of κ, and around $\kappa = 1\text{Å}^{-1}$ it is faster. This is obviously related to the fact that there is considerable short range order in the system so that for a certain wavelength, namely $\lambda \sim 2\pi/2$ Å, neighboring particles get displaced by about the same amount thus producing small restoring forces. The faster changes occurring at twice this wavelength have a similar qualitative explanation in terms of out of phase displacement of immediate neighbors.

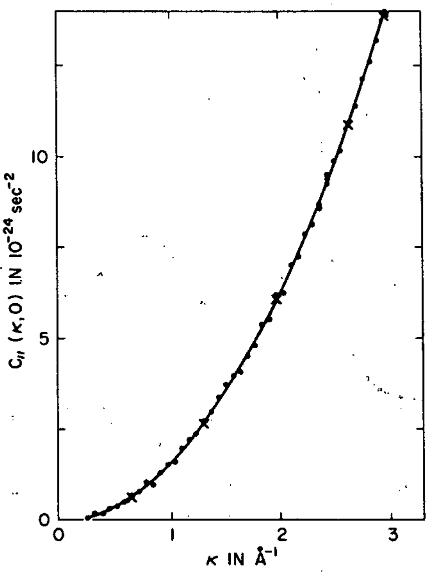

FIG. 2. .... $C_{||}(\kappa, t = 0)$ or $\langle J_{||}(\kappa, 0)\, J_{||}^{*}(\kappa, 0)\rangle$ from molecular dynamics data; $\kappa^2 k_B T/M$ for T = 76°K is shown as xxx.

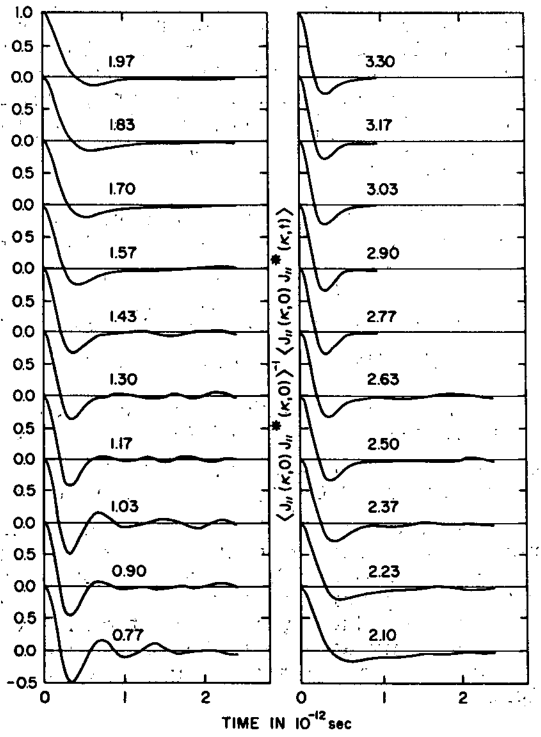

FIG. 3. Time dependence of $C_{||}(\kappa, t)/C_{||}(\kappa, t = 0)$ for various κ.

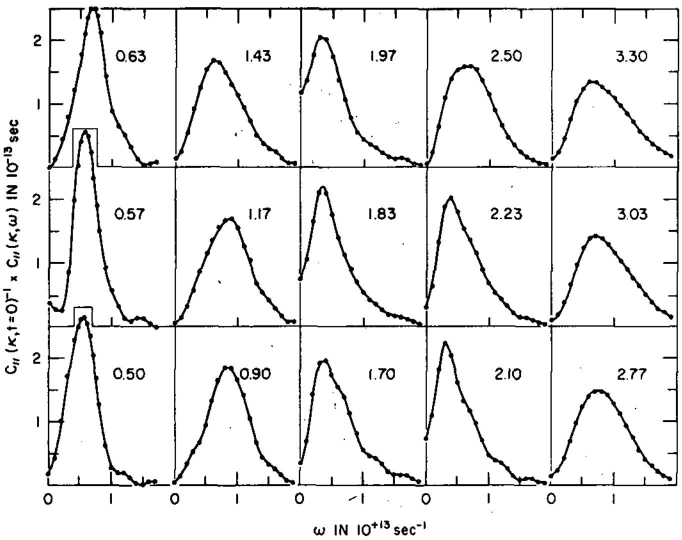

FIG.4. Fourier transform of functions shown in Fig.3. Area under each curve is $\pi/2$.

Figure 4 shows the harmonic analysis of the functions of time shown in Fig. 3. The curves in Fig. 4 are therefore equal to $C_{\parallel}(\kappa,\omega)/C_{\parallel}(\kappa,t = o)$; the area under each curve shown in Fig. 4 is $\pi/2$.

The value of the calculated $C_{\parallel}(\kappa,\omega = o)$ for κ in the region $2Å^{-1}$ is considerably different from zero; this violates Eq. (11). This is because, for these κ, the decay of $C_{\parallel}(\kappa,t)$ with time is slow (see Fig. 3) and Eq. (11) is fulfilled only when $C_{\parallel}(\kappa,t)$ is known for much longer times than were calculated. However, already at $\omega = 0.5 \times 10^{13}$ sec^{-1} the effect of this incompleteness in $C(\kappa,t)$ is quite negligible.

The curves $C_{\parallel}(\kappa,\omega)$ shown in Fig. 4 give a dispersion curve without ambiguity. Figure 5 shows the values $\omega_{max}(\kappa)$ at which $C_{\parallel}(\kappa,\omega)$ attains its maximum for specified κ. As seen from this figure the dependence of $\omega_{max}(\kappa)$ on κ is closely related to the structure $S(\kappa)$ which has been redrawn in Fig. 5 for reference.

A second maximum in $\omega_{max}(\kappa)$ is also seen in Fig. 5; it occurs at $\kappa \sim 2.8Å^{-1}$ where $S(\kappa)$ shows a minimum. This is the first time that such an effect has been demonstrated unambiguously in the dispersion of current fluctuations in fluids.

Each curve shown in Fig. 4 has an area equal to $\pi/2$. This means that the spread of a curve around $\omega = \omega_{max}(\kappa)$ will be large if the height at that ω is small. Since the life-time of a fluctuation is inversely related to the width of the frequency response we can consider the height at $\omega = \omega_{max}(\kappa)$ of each curve shown in Fig. 4 to be the life-time of the respective fluctuation.

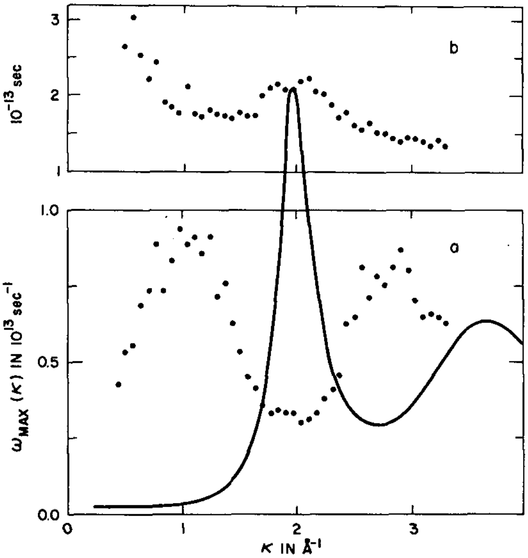

FIG.5. (a) Dispersion $\omega_{max}(\kappa)$ of longitudinal current fluctuations. (b) Height of the transforms shown in Fig.4. This can be considered to be a life-time as explained in the text. The structure factor $S(\kappa)$ is redrawn from Fig.1 to show its relation with the dispersion of longitudinal currents.

This is shown in the upper part of Fig. 5. As expected, for small κ, i.e. for long wave lengths the longitudinal current fluctuations have appreciably longer life-time than for large κ.

THE HYDRODYNAMIC REGION

In the hydrodynamic region, i.e. for long wave lengths, $S(\kappa,\omega)$, the frequency response to density fluctuations, consists of three distinct lines, one having a maximum at $\omega = o$ (the Rayleigh line of light scattering) and two (the Brillouin components) having maxima at $\omega = \pm c\kappa$, c being the velocity of sound. If we assume that each Brillouin component has a Lorentzian shape[6] in the immediate neighborhood of its maximum and that the Lorentzian has a width $\delta\kappa^2$, follows that $\omega^2 S(\kappa,\omega)$, i.e. $C_{\|}(\kappa,\omega)$ has a dispersion given by

$$\omega_{max}(\kappa) = \kappa(c + \delta^2 c^{-1}\kappa^2) \qquad (13)$$

With decreasing κ, since the width $(\delta\kappa^2)$ of the density fluctuations goes to zero faster than the peak position $(c\kappa)$, these fluctuations become increasingly well defined harmonic oscillations; in that case, current fluctuations, being the second time derivatives of density fluctuations, will also oscillate with about the same frequency. Hence for small κ the dispersion of current and density fluctuations will coincide.

At small κ, $\omega_{max}(\kappa)$ has an upward curvature (Eq. 13); however, around $\kappa = 1Å^{-1}$ it has negative curvature (Fig. 5). We may thus consider the region of κ where $\omega_{max}(\kappa)$ has a point of inflection as the region separating the hydrodynamic and the microscopic or kinetic region in the fluid. Beyond this region density fluctuations will get damped and cease to propagate. However, current fluctuations will continue to propagate with a frequency and life-time strongly dependent on the structure $S(\kappa)$; eventually, for large κ, they will depend only on single particle modes and will not be collective coordinates anymore.

RESULTS FOR TRANSVERSE CURRENTS

With molecular dynamics data we can calculate $C_\perp(\underset{\sim}{\kappa},t)$ as simply as the longitudinal correlation $C_\parallel(\underset{\sim}{\kappa},t)$. Hence the method of calculation need not be mentioned; we shall present just the results of the calculation of $C_\perp(\kappa,t)$ and $C_\perp(\kappa,\omega)$. Firstly, let us note that $C_\perp(\underset{\sim}{\kappa},t)$ does not satisfy a condition like Eq. (11) for $C_\parallel(\kappa,t)$; hence $C_\perp(\underset{\sim}{\kappa},\omega = o) \neq 0$. Also, transverse current fluctuations change interparticle distances only by small amounts and hence the restoring force is also small irrespective of the value of κ.

Figure 6 shows the frequency, $\omega_{max}(\kappa)$, at which $C_\perp(\kappa,\omega)$ attains a maximum. For small κ the value of the transform at

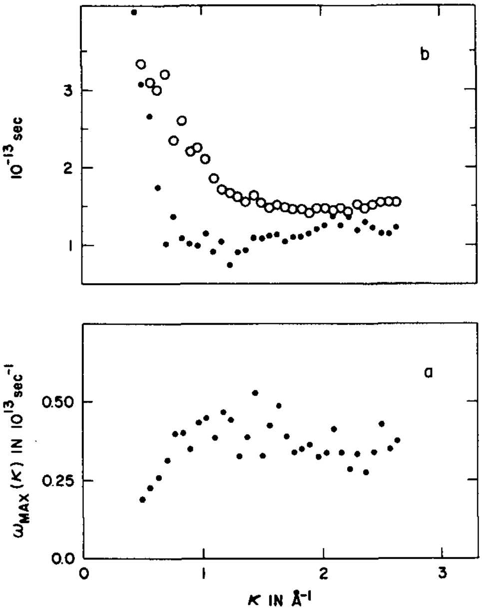

FIG.6. (a) Dispersion $\omega_{max}(\kappa)$ of transverse current fluctuations. (b) .... value of $C_\perp(\kappa,\omega)/C_\perp(\kappa,t=0)$ at $\omega = 0$. oooo value of $C_\perp(\kappa,\omega)/C_\perp(\kappa,t=0)$ at $\omega = \omega_{max}(\kappa)$.

$\omega = 0$ rises so rapidly that eventually the curve $C_{\perp}(\kappa,\omega)$ shows no maximum at a non-zero frequency. This is seen in the upper part of Fig. 6 from the plotted values of $C_{\perp}(\kappa,\omega)$ at $\omega = 0$ and at $\omega = \omega_{\max}(\kappa)$.

There is much to be desired in the precision with which the quantities shown in Fig. 6 were determined. In calculating $J_{\perp}(\underset{\sim}{\kappa},t)$ we have taken only one direction in space normal to $\underset{\sim}{\kappa}$. The statistics will improve on considering the transverse current correlations in both the directions normal to $\underset{\sim}{\kappa}$. These calcutions are in progress.

However, we have a quantitative indication of how transverse current fluctuations behave in space and time. Theoretical attempts to understand this aspect of fluids have thus become possible.

ROLE OF MOLECULAR DYNAMICS IN THE THEORY OF FLUIDS

Apart from their intrinsic interest, the results shown in Fig. 6 give an indication of the possibilities of the method of molecular dynamics for the study of dense classical fluids. There is no other method available at present for investigating transverse currents in fluids. In molecular dynamics we have complete information about a completely defined classical system and hence it is capable of giving numerical data for any function of the positions of the particles (and any higher derivatives of the positions). $\underset{\sim}{J}$ and Q, defined in the first section, are examples of such functions. However, as shown elsewhere,[7] the method makes it possible to investigate other useful correlations as well, which, up to now, have not found a place in the formal structure of the statistical mechanics of dense fluids.

A knowledge of the wave length region where density fluctuations, or phonons, cease to propagate in dense fluids will be very useful, and in the future, with larger computer memories and speeds, it will become possible to have precise numerical data on this question. This aspect of the dynamics can of course be investigated with inelastic neutron scattering as well.

ACKNOWLEDGEMENT

The method of spatial Fourier analysis used here was suggested to the author by M. Kalos and J. Lebowitz. I thank Lester Guttman for a critical reading of the manuscript which helped to improve the presentation.

REFERENCES

[1] L. Verlet, Phys. Rev. **159**, 98 (1967); **165**, 201 (1968).

[2] A. Rahman, Phys. Rev. **136**, A405 (1964).

[3] A. Rahman, Phys. Rev. Letters, **19**, 420 (1967).

[4] D. Forster, P. C. Martin, S. Yip, Phys. Rev. (under publication).

[5] *Argon, Helium and the Rare Gases*, G. A. Cook, Ed. (Interscience Publishers, Inc., New York, 1961), Vol. 1, p. 366.

[6] L. D. Landau, E. M. Lifshits, *Electrodynamics of Continuous Media* (Pergamon Press, New York, 1960), p. 391.

[7] A. Rahman, J. Chem. Phys. **45**, 2585 (1966).

DISCUSSION

K.-E. LARSSON: What physical meaning should be attached to the minimum in the current-current correlation function at the maximum of the structure factor?

A. RAHMAN: A wave for which $\kappa \sim 1$ Å^{-1} displaces neighbouring particles against each other, and the hard core collision produces a large energy change. At $\kappa \sim 2$ Å^{-1} the displacement of first neighbours is about the same, but lack of complete order nevertheless produces some energy even for this wavelength.

K.-E. LARSSON: On the basis of your interpretation of this correlation function, what do you consider to be the physical difference between your formulation of the κ dependence of the current and the picture of a κ-dependent coefficient of diffusion being smaller where $S(\kappa)$ is larger?

A. RAHMAN: I am unable to see any relation between the two. What I have calculated is a property of the current density in the system which, conceptually, is nothing new. The concept of a κ-dependent diffusion constant is on the other hand not very clear to me.

M.S. NELKIN: Can you comment on the experimental observation in liquid metals that the frequency and lifetime at $\kappa = 1$ Å^{-1} are approximately independent of temperature?

A. RAHMAN: I think that the quantity will depend more on volume than on temperature. The analysis of molecular dynamics data has not yet been extended to cover any appreciable variation of temperature and density.

B. MOZER: Do your data allow you to predict the shortest wavelength for high-energy phonons in your model of a liquid? It would be helpful to know this number for purposes of interpreting the high-energy excitations as observed in some of the measurements. Crude arguments would lead one to believe that the shortest wavelength is about the average nearest neighbour distance, as it is in the solid.

A. RAHMAN: I am not certain that I fully understand your question. At all events I would say that there is no distinct wave number beyond which, suddenly, the single particle motion alone is of significance. At large κ, of course, this motion is of significance, but the transition is, I think, a gradual one.

S. YIP: I have two questions. First, have you looked at the stress-stress correlation function? Secondly, how meaningful is it to extrapolate your spectral densities to lower κ?

A. RAHMAN: A preliminary analysis of the time correlations whose integrated value gives the viscosity has yielded a value of viscosity two or three times larger than the observed level.

In reply to your second question, use of the 500-particle system – as explained in the paper – means that at low κ there is a lack of statistics, which makes it difficult to obtain conclusive results. This is particularly true at the lowest κ, namely $2\pi/L$, where L is the size of the box used in the calculation.

THE THEORY OF HIGH-FREQUENCY DENSITY FLUCTUATIONS IN LIQUIDS

P. SCHOFIELD
THEORETICAL PHYSICS DIVISION,
ATOMIC ENERGY RESEARCH ESTABLISHMENT,
HARWELL, DIDCOT, BERKS., ENGLAND

Abstract

THE THEORY OF HIGH-FREQUENCY DENSITY FLUCTUATIONS IN LIQUIDS. The aim of this work is to obtain a theoretical understanding of the close similarity which is observed, particularly in metals, between the neutron scattering in a polycrystal just below the melting point and in the liquid just above the melting point, for frequencies greater than that characterizing the basic diffusive mechanism ($\sim 10^{12}$ sec^{-1}).

The starting point is an approximation to the equivalent of the 'one-phonon' cross-section in the solid. Successive approximations are discussed leading finally to a 'quasi-harmonic' approximation. This reduces the problem to the solution of a pair of coupled integral equations involving the two and three particle equilibrium distribution functions. For a crystalline solid at low temperature these equations give correctly the phonon dispersion laws. The form of the equations indicate a qualitative agreement with the experimental results. In particular, the strong angular correlation of two particles relative to a third at small separations is shown to give an effect similar to that of the 'orientational averaging' in the one-phonon cross-section for a polycrystal,, and to lead to the appearance of transverse excitations in the scattered neutron spectrum.

1. INTRODUCTION

The aim of this paper is to present a theory of the van Hove correlation function, $G(\vec{R}, t)$, appropriate to the 'solid-like' regime of dense liquids near the melting point. This regime is characterized by distances of the order of the interatomic spacing, and times shorter than the characteristic time for the diffusive motion of the atoms. The latter, inferred from the study of quasi-elastic incoherent neutron scattering, is of the order of 10^{-12}sec [1].

The solid-like regime is, of course, that studied by inelastic neutron scattering. The characteristic observation, in particular so far as metals are concerned, is that the scattering from the liquid is very similar to that observed from the polycrystalline solid just below the melting point (e.g. Ref. [2]). The interpretation of the result in the solid is straightforward: a neutron scattered in a particular crystallite of the polycrystal with change of momentum $\vec{Q}$ and energy $\hbar\omega$ can create or destroy a phonon of wavevector $\vec{f} = \vec{Q} + \vec{\tau}$ and energy $\omega(\vec{f}) = \omega$, where $\vec{\tau}$ is a vector of the reciprocal lattice. The spectrum of scattered neutrons from a polycrystal for a fixed $\vec{Q}$ then contains the aggregate of all frequencies ω for which these conditions are satisfied for different orientations of the crystallites.

This interpretation depends on the translational symmetry of the crystal lattice in a twofold manner: first, in that the excitations of the system of a given frequency (the phonons) are basically plane waves, so that the displacement of an atom about an 'equilibrium' site $\vec{R}$ is proportional to $\exp\{i(\vec{f}\cdot\vec{R} - \omega(\vec{f})t)\}$ and second in that the equilibrium sites themselves lie on a lattice, so that $\vec{R}$ is of the form $(n_1\vec{a} + n_2\vec{b} + n_3\vec{c})$ where $n_1 n_2$ and n_3

are integers[1]. In a disordered system, such as a liquid, neither of these conditions is necessarily satisfied. It is clear therefore that the explanation of the similarity in scattering from solid and liquid must be sought in rather different terms.

Previous theories of the coherent scattering in liquids by Egelstaff [3] and by Singwi [4] have restricted attention to the second of the two points mentioned above – by taking account of the disordered structure of the liquid, but retaining the assumption of plane wave excitations. Egelstaff [3] uses an ad hoc generalization of the one-phonon cross-section for a polycrystal by replacing the sums over reciprocal lattice vectors by an integral over an appropriate range of the 'structure-factor' S(Q). Singwi [4], on the other hand, gives a straightforward generalization of the theory for a solid in terms of displacement correlation functions for the correlations of atoms within a range R, but assumes the motion of atoms outside this range to be statistically independent. His result for the 'one-phonon' cross-section involves an integral over the spherically symmetric pair distribution function, g(R).

One obvious weakness of these theories is that averages over g(R) are not equivalent to the sum over lattice sites. g(R) represents an average over all configurations of particles except those at O and $\vec{R}$, while the lattice specifies one particular equilibrium configuration. The same remark applies to the relation between $S(\vec{Q})$ and the reciprocal lattice. A second consideration, which is discussed in greater detail below, is that averages of this sort take no account of angular correlation in the system: in the lattice structure such correlations are present – and important in the neutron scattering interpretation.

In the theory presented here, we start by obtaining an approximate expression for the equivalent of the 'one-phonon' cross-section for high frequencies, in terms of velocity-averaged velocity correlation functions. These satisfy a set of differential equations depending on the second derivative of the interatomic potential. Two further major approximations are made – the 'quasi-harmonic' approximation and the 'average field' approximation. Even with these approximations, the equations are still extremely complicated, but their form demonstrates the qualitative features of the solutions and illustrates the important role played by the angular correlations present in the three-particle distribution function.

In section 4, the problem is considered more generally. It is shown that the 'one-phonon' part considered so far can be regarded, with a slight modification, as the first term in a cumulant expansion for the intermediate scattering function.

2. THE ONE-PHONON CROSS-SECTION

The scattering law, S(Q, ω) for coherent scattering in an isotropic system, can be written as the Fourier transform of the 'intermediate' function I(Q, t) which is the correlation function for density fluctuations in the system. We shall consider throughout a monatomic system

$$I\ (Q,t) = \left< \sum_j e^{-i\vec{Q}.\vec{r}_j(o)} \sum_i e^{i\vec{Q}.\vec{r}_i(t)} \right> \qquad (1)$$

---

[1] More precisely, the requirement is that $\vec{R}$ should have this form for distances large compared to the mean free path of the phonons. This is true for the polycrystal but not for the liquid.

If I tends to zero as t tends to infinity, we may write alternatively, for $Q \neq 0$

$$S(Q,\omega) = \frac{Q^2}{\omega^2} C_L(Q,\omega) = \frac{Q^2}{\omega^2} \cdot \frac{1}{2\pi} \int_{-\infty}^{\infty} V_L(Q,t)\, e^{i\omega t}\, dt \tag{2}$$

where $C_L(Q,\omega)$ is the Fourier transform of the longitudinal current correlation function [5]

$$\begin{aligned} V_L(Q,t) &= -\frac{1}{Q^2} \ddot{I}(Q,t) \\ &= \left< \sum_j v_j^L(o)\, e^{-i\vec{Q}\cdot\vec{r}_j(o)} \sum_i v_i^L(t)\, e^{i\vec{Q}\cdot\vec{r}_i(t)} \right> \end{aligned} \tag{3}$$

where $v_i^L(t)$ is the component of velocity parallel to $\vec{Q}$. The 'one-phonon' part of $V_L(\underline{Q},t)$ will be defined by

$$V_L^{(1)}(Q,t) = \left< \sum_j v_j^L(o)\, e^{-i\vec{Q}\cdot\vec{r}_j(o)} \sum_i v_i^L(t)\, e^{i\vec{Q}\cdot\vec{r}_i(o)} \right> \tag{4}$$

i.e. by replacing $r_i(t)$ by $r_i(o)$. The correction to this will be small, provided $\vec{Q}(\vec{r}_i(t) - \vec{r}_i(o))$ is small compared to unity — that is, for sufficiently small Q, provided that t is small enough so that the atom has not moved far from its initial position. The nature of this approximation will be seen more precisely in section 4.

Alternatively let us define velocity-averaged velocity correlation functions

$$f_{ij}^{\alpha\beta}(t) = \frac{M}{kT} \overline{v_j^{\beta}(o)\, v_i^{\alpha}(t)} \tag{5}$$

where the bar denotes an average over the initial velocity distribution (so that f_{ij} is a function of the initial configuration of all the particles) and functions $f^{\alpha\beta}(\vec{R},t)$ obtained by averaging $f_{ij}(t)$ over all configurations with the constraint that atoms i and j have an initial separation $\vec{R}$ and $f_s(t)$ the configurational average of $f_{ii}(t)$. For an isotropic system, symmetry demands that

$$f^{\alpha\beta}(\vec{R},t) = f_{11}(R,t)\, \ell^{\alpha}\ell^{\beta} + f_{\perp}(R,t)\, (\delta^{\alpha\beta} - \ell^{\alpha}\ell^{\beta}) \tag{6}$$

where ℓ^{α} is the direction cosine of $\vec{R}$. Now we can re-write Eq. (4):

$$\frac{M}{NkT} V_i^{(1)}(Q,t) = f_s(t) + 2\pi n_o \int_0^{\infty} R^2 dR \int_{-1}^{1} d\mu\, g(R)\, e^{iQR\mu} \Big[f_{11}(R,t)\mu^2 + f_{\perp}(R,t)\,(1-\mu^2) \Big] \tag{7}$$

where N is the total number of atoms, n_0 the mean number density and $g(R)$ the pair distribution function. Note that $f_s(t)$ is the velocity autocorrelation function which plays an important role in the 'self' part of $S(Q, \omega)$.

3. THE QUASI-HARMONIC APPROXIMATION

It is easy to show that if $\Phi_N(\vec{r}_i(t))$ is the interatomic potential then

$$\frac{d^2}{dt^2}\overline{v_j^\beta(o)\,v_i^\alpha(t)} = -\frac{1}{M}\sum_k \overline{\left(\frac{\partial^2\Phi_N}{\partial r_i^\alpha\,\partial r_k^\gamma}\right)_t v_j^\beta(o)\,v_k^\gamma(t)} \tag{8}$$

Further, if Φ_N can be expressed as a sum of pair potentials, then Eq. (8) may be written

$$\frac{d^2}{dt^2}\overline{v_j^\beta(o)\,v_i^\alpha(t)} = -\sum_{k\neq i}\overline{\phi_{ik}^{\alpha\gamma}(t)\,v_j^\beta(o)\left[v_i^\gamma(t) - v_k^\gamma(t)\right]} \tag{9}$$

where the 'dynamical matrix' $\phi_{ik}^{\alpha\gamma}$ is given by

$$\frac{1}{M}\frac{\partial^2\Phi_N}{\partial r_i^\alpha\,\partial r_j^\beta} = \sum_{k\neq i}\phi_{ik}^{\alpha\beta}(\delta_{ij} - \delta_{ik}) \tag{10}$$

At this stage we make the crucial approximation of the theory. Under the assumption that during the times in which we are interested the environment of an atom does not change much, we assume that we can take $\phi_{ik}(t)$ to be time independent. This we call the 'quasi-harmonic' approximation, since it is equivalent to the assumption of harmonic forces. With this approximation, we can now write Eq. (9) in terms of the f_{ij}, obtaining separate equations for i equal and not equal to j,

$$\ddot{f}_{jj}^{\alpha\beta} = \sum_{k\neq j}\phi_{jk}^{\alpha\gamma} f_{jj}^{\gamma\beta}(t) - \sum_{k\neq j}\phi_{jk}^{\alpha\gamma} f_{kj}^{\gamma\beta}(t) \tag{11}$$

$$\ddot{f}_{ij}^{\alpha\beta}(t) = -\phi_{ij}^{\alpha\gamma} f_{jj}^{\gamma\beta}(t) + \Big(\phi_{ij}^{\alpha\gamma} + \sum_{k\neq ij}\phi_{ik}^{\alpha\gamma}\Big) f_{ij}^{\gamma\beta}(t) - \sum_{k\neq ij}\phi_{ik}^{\alpha\gamma} f_{kj}^{\gamma\beta} \tag{12}$$

The initial conditions are

$$f_{ij}^{\alpha\beta}(o) = \delta_{ij}\,\delta^{\alpha\beta}; \quad f_{ij}(o) = 0 \tag{13}$$

This is the set of equations which must be solved for each initial configuration to give the quasi-harmonic one-phonon cross-section. Direct solution for each configuration is clearly not feasible, so we adopt the procedure of averaging the equations over all but one, two ... n particles. This given a hierarchy of equations for functions $f^{\alpha\beta}(\vec{R}_1; \vec{R}_2 \ldots \vec{R}_n, t)$, the velocity correlation functions for atoms originally at the origin and $\vec{R}_1$, given atoms initially at $\vec{R}_2 \ldots \vec{R}_n$. The equations are, in principle to be solved by a truncation procedure. Here we shall consider just the lowest order truncation corresponding to the assumption that the velocity correlation function depends only on the initial separation of the atoms involved and not on the detailed environment, i.e. we replace f_{ij} (t) in Eqs (11) and (12) by $f(\vec{R}, t)$, and f_{jj} (t) by f_s (t). This we call the 'average field' approximation. The principal weakness of this approximation is concerned with the strong repulsive part of the potential at short distances. A particle initially very close to the one or two atoms under consideration will have a strong effect on the initial time development of the correlation functions. We shall indicate later in the paper how this may be overcome.

Making this assumption, one obtains a pair of coupled integral equations for $f_{\parallel}$ (R, t) and $f_{\perp}$ (R, t) involving both the pair distribution function g(R) and the three-particle distribution function $g(\vec{R}, \vec{S})$. These equations will not be given here, but are discussed elsewhere [6]. It is more revealing to discuss more generally the Fourier transform of the equation for $f^{\alpha\beta}(\vec{R}, t)$. Writing

$$G^{\alpha\beta}(\vec{Q},\omega) = \int_{-\infty}^{\infty} dt\; e^{i\omega t} \left[f_s(t)\, \delta^{\alpha\beta} + n_0 \int d\vec{R}\; g(R)\; e^{i\vec{Q}\cdot\vec{R}} f^{\alpha\beta}(\vec{R},t) \right] \tag{14}$$

one obtains in the average field approximation

$$\begin{aligned} \omega^2\, G^{\alpha\beta}(\vec{Q},t) = {} & - i\omega\, \delta^{\alpha\beta} + G^{\alpha\gamma}(\vec{Q},\omega) \left[\tilde{\phi}^{\gamma\beta}(\vec{Q}) - \tilde{\phi}^{\gamma\beta}(o) \right] \\ & - n_0^2 \int\!\!\int d\vec{R}\; d\vec{S} \left[g(\vec{R},\vec{S}) - g(R)\, (g(S) - n_0^{-1}\, \delta(\vec{R} - \vec{S})) \right] \\ & \times \phi^{\alpha\gamma}(\vec{R})\; f^{\gamma\beta}(\vec{S}) \left[e^{i\vec{Q}\cdot(\vec{R} - \vec{S})} - e^{i\vec{Q}\cdot\vec{R}} \right] \end{aligned} \tag{15}$$

with

$$\tilde{\phi}^{\alpha\beta}(\vec{Q}) = n_0 \int d\vec{r}\; g(R)\; e^{i\vec{Q}\cdot\vec{R}}\; \phi^{\alpha\beta}(\vec{R}) \tag{16}$$

The form of Eq. (15) shows the important effect of the angular correlations in a disordered system and demonstrates qualitatively the analogue of the orientational averaging in the polycrystal. The first term in brackets in the integral on the right-hand side of Eq. (15) is a measure of the angular correlation between particles at $\vec{R}$ and $\vec{S}$ relative to an atom at the origin. If it is neglected, then for an isotropic system Eq. (15) may be solved to give, via Eqs (14) and (2), $C_L(Q, \omega)$ and the corresponding correlation function for transverse fluctuations $C_T(Q, \omega)$

$$C_{L,T}(Q,\omega) \propto \delta(\omega^2 - \omega^2_{L,T}(Q)) \tag{17}$$

with

$$\omega_L^2(Q) = 2\pi\, n_o \int_0^{\infty} g(R)\, R^2\, dR \int_{-1}^{1} d\mu \left[\phi_{\parallel}(R)\, \mu^2 + \phi_{\perp}(R)(1-\mu^2)\right](1-\cos QR\mu) \tag{18}$$

$$\omega_L^2(Q) = \pi\, n_o \int_0^{\infty} g(R)\, R^2\, dR \int_{-1}^{1} d\mu \left[\phi_{\parallel}(R)\, (1-\mu^2) + \phi_{\perp}(R)(1+\mu^2)\right](1-\cos QR\mu) \tag{19}$$

The effect of the last term on the right-hand side of Eq.(15) can be considered as giving a coupling between the longitudinal and transverse modes given by Eqs (18), (19). That is, the angular correlations in the system give rise to a 'structural broadening' of the one-phonon scattering analogous to the orientational averaging in the polycrystal.

It is worth noting that Eq. (15) also gives the correct result for a single crystal at low temperatures. Here the pair distribution function $g(\vec{R})$ depends on the vector $\vec{R}$ and can be approximated by a sum of delta functions at the lattice sites, as can the higher distribution functions. In this case, the last term in Eq. (15) does vanish and the resulting equations are then the usual ones determining the phonon dispersion laws [6].

4. THE GENERALIZED GAUSSIAN APPROXIMATION

The relation between $S(Q, \omega)$ and $V_L(Q, t)$ given in Eq. (2) suggests a form of cumulant expansion for the former, analogous to that used for the 'self' term, i.e. to write

$$I(Q,t) = \left\langle \sum_i \sum_j \exp i\, \vec{Q}\cdot(\vec{r}_i - \vec{r}_j)\, \exp(-F_{ij}(\vec{Q},t)) \right\rangle \tag{20}$$

and to consider the expansion of $F_{ij}(\vec{Q}, t)$, in powers of Q. From Eq.(3) it is seen that the leading term in $F_{ij}(\vec{Q}, t)$ is second order in Q and is given by

$$F_{ij}(\vec{Q},t) = Q^{\alpha} Q^{\beta} \frac{kT}{M} \int_0^t (t-t')\, f_{ij}^{\alpha\beta}(t')\, dt' + O(Q^3) \tag{21}$$

Further it may be shown [6] that under the conditions, (a) the displacement of an atom is a linear function of its initial velocity and the initial force on it; and (b) the initial forces, as well as the initial velocities have a

Gaussian distribution, then all the higher terms vanish. These conditions are only rigorously satisfied for harmonic forces, but neglect of higher terms could be a useful approximation as proved in the theory of the self term.

Alternatively Eq. (20) may be written

$$\frac{1}{N} I(Q,t) = < \exp \{ - Q^{\alpha} Q^{\beta} \ F_{ii}^{\alpha\beta} (t) \} >$$

$$+ n_o \int g(R) \ e^{i\vec{Q}\cdot\vec{R}} < \exp \{-Q^{\alpha} \ Q^{\beta} \ F_{ij}^{\alpha\,\beta} (t) \} >_{\vec{R}} d\vec{R} \qquad (22)$$

where $<\ldots.>_R$ denotes a configurational average given that atoms i and j have an initial separation $\vec{R}$. Equation (22), which gives correctly the expansion of $I(Q, t)$ up to t^4, shows how the convolution approximation breaks down. The convolution approximation corresponds to an approximation in which $F_{ij}(t)$ is replaced by $F_{ii}(t)$.

The evaluation of the scattering law in the Gaussian approximation may now be performed as in the incoherent case by separating the asymptotic time dependence of $F_{ij}(t)$:

$$F_{ij}(t) = |t| \int_0^{\infty} f_{ij} \ (t') \ dt' \ - \int_0^{\infty} t' \ f_{ij}(t') \ dt' + F'_{ij}(t) \qquad (23)$$

In the phonon expansion the first two terms should be retained in the exponent. This modifies the 'one-phonon' cross-section calculated in section 2 by (a) a diffusive broadening, from the first term in Eq. (23) and (b) a configuration dependent Debye-Waller factor coming from the second term.

5. DISCUSSION

In this paper, we have discussed a theory which we believe contains the essential features of the high frequency density fluctuations in a liquid, and is capable of explaining the structure of the spectrum of inelastically scattered neutrons. Unfortunately the equations determining the one-phonon spectrum, even in the average field approximation, are extremely complex, requiring a knowledge not only of $g(R)$ but also the three-particle distribution function $g(\vec{R}, \vec{S})$.

However, to obtain quantitative results, a further complication arises from the hard-core repulsion of the interatomic potential. When a pair of atoms are initially very close together, they will tend to fly apart very rapidly, violating the condition of the quasi-harmonic approximation. This implies that the dynamical matrix $\phi(R)$ must be cut off at some appropriate distance R_0. Such a cut-off is implicit in the full set of Eqs (11) and (12). If we take time Fourier transforms and solve Eq. (11) for $f_{jj}(\omega)$ and substitute in Eq. (12), the principal effect is to modify the second term on the right-hand side of Eq. (12) to cancel $\phi_{ij}^{\alpha\gamma}(\vec{R})$ for values of R for which it is much greater than ω^2. However, this procedure has not been carried through in detail.

Finally, it should be remarked that the generalized Gaussian approximation fails in the limit Q tends to zero, where $S(Q, \omega)$ is determined by hydrodynamic considerations [5]. For example, the longitudinal viscosity which is given by $\lim_{\omega \to 0} \omega^4 \lim_{Q \to 0} \frac{1}{Q^4} S(Q, \omega)$ [7] requires terms up to Q^4 in the expansion of $F(\vec{Q}, t)$ (Eq. (21)).

REFERENCES

[1] EGELSTAFF, P.A., Advances in Physics 11 (1962) 203
[2] LARSSON, K.E., "Experimental Results in Liquids", Ch.8, Thermal Neutron Scattering (EGELSTAFF, P.A., Ed), Academic Press, London and New York (1965).
[3] EGELSTAFF, P.A., UKAEA Rep. AERE - R4101 (1962).
[4] SINGWI, K.S., Phys. Rev. 136, (1964) A969.
[5] SCHOFIELD, P., "Experimental Knowledge of Correlation Functions in Simple Liquids", Ch.13, The Physics of Simple Liquids (TEMPERLEY, H.N.V., Ed.), North Holland, Amsterdam (1968).
[6] SCHOFIELD, P., to be published.
[7] EGELSTAFF, P.A., An Introduction to the Liquid State, Academic Press, London and New York (1967), 184.

DISCUSSION

B. MOZER: I am going to repeat to you the question I asked Mr. Rahman: what is the shortest phonon wavelength that can be observed in your model of a liquid?

P. SCHOFIELD: One of the points which I am trying to stress in the paper is that it does not make sense to talk of short wavelength 'phonons' in disordered systems. If you are asking, in effect, what is the highest frequency in the velocity autocorrelation, the answer is that the theory I have described does not really throw any new light on this problem.

NEW RESULTS ON 'QUASI-ELASTIC' SCATTERING FROM SOME HYDROGENOUS LIQUIDS

U. DAHLBORG, B. FRIBERG, K.-E. LARSSON AND E. PIRKMAJER*
ROYAL INSTITUTE OF TECHNOLOGY,
STOCKHOLM, SWEDEN

Abstract

NEW RESULTS ON 'QUASI-ELASTIC' SCATTERING FROM SOME HYDROGENOUS LIQUIDS. A study of the 'quasi-elastic' scattering of cold neutrons from pentane and pentanol by use of the inverted filter technique is reported. The total energy resolution of the spectrometer in this investigation was varied from 0.10 to 0.13 meV at the beryllium oxide cut-off. It is found that in no case hitherto studied has the total 'quasi-elastic' cross-section the shape of a single Lorentzian but is made up of two components, a narrow central peak and a broader underlying part. From their intensity variation it is concluded that the narrow peak is of an elastic nature while the broader underlying distribution has an inelastic origin. The width of the central peak for liquid pentane and for pentanol in the low viscosity region is understood from measured or extrapolated translational diffusion constants, while for lower temperatures another diffusion mechanism, probably rotational diffusion, is responsible for the width.

A comparison is made with results obtained from two time-of-flight spectrometers, using the whole or only a part of the cold spectrum to define the energies of the neutrons hitting the sample. It is found that both of the two components observed in the inverted filter investigation are included in the quasi-elastic peak in the time-of-flight cases. It is shown that both the width dependence and the intensity dependence of κ of the time-of-flight results can be fully reproduced by an appropriate sum of the new results. The quasi-elastic peak is thus probably of a true almost elastic origin as well as of an inelastic origin. It is concluded that very high resolution both on the monochromator and on the analyser side is required to reveal the true nature of the near elastic neutron scattering spectra.

INTRODUCTION

Knowledge of the nature of the molecular motions in complex liquids has increased considerably during the last decade. The neutron scattering technique has in this respect proved its usefulness. Many different experimental methods [1-6] have been used and many models for interpretation of the data obtained in terms of characteristic constants for the atomic and the molecular motions have been developed [7-13]. In general, the quasi-elastic differential scattering cross-section was in the first approximation found to be Lorentzian in shape and this fact has been used when extracting appropriate parameter values out of the data. However, this has to be considered only as a first approximation. In no case has the experimental resolution been good enough to draw a definite conclusion about the validity of the approximation. It has not been clear how much of the quasi-elastic intensity may really be described by a single Lorentzian.

To study this problem an experimental apparatus with a very good resolution is needed. Since the Stockholm reactor is relatively weak as a neutron source, the inverted filter technique was chosen. The technique was introduced by Stedman and independently by Stiller and Danner [14] in the late fifties but has not been exploited to its full capacity before. The advantage with this method of measuring shapes and widths of quasi-elastic cross-sections lies in the fact that it is possible to achieve good resolution simultaneously with reasonable intensity at a low cost. It is, however, an experimentally difficult method requiring the greatest care in production and treatment of data.

In this report measurements on pentane and pentanol, performed both at the inverted filter spectrometer and at two time-of-flight spectrometers having different degrees of monochromation, will be discussed. Earlier only a few investigations of these liquids had been published [1,2, 15-17]. The idea behind this particular choice was to compare two similar liquids one of which is hydrogen bonded and the other is not.

One of the main results in the high-resolution measurements at the inverted filter spectrometer is that the 'quasi-elastic' peak is made up of two components, one having an elastic origin and the other an inelastic origin. It is found that the quasi-elastic peak obtained at time-of-flight spectrometers can be fully reproduced as a sum of the two components obtained at the inverted filter spectrometer. The width as well as the intensity variation of the peak can be accounted for in this way. The conclusion is drawn that, in cases where the instrumental energy resolution is no better than ~ 0.2 meV, both components contribute in observed widths and Debye-Waller factors.

Because of the different mechanisms active in forming the observed spectrum, it is concluded that the direct filter method is inferior to the inverted filter method, particularly with regard to the analysis of quasi-elastic scattering.

EXPERIMENTAL METHODS

Since 1966 a crystal spectrometer using the inverted filter technique for defining the energies of the neutrons registered in the detector has been in operation at the Stockholm reactor. The instrument was constructed in such a way that a good resolution in studies of elastic and near-elastic scattering could be achieved and it was meant to be complementary to the time-of-flight spectrometer using the full cold spectrum. The first measurements made at spectrometers using this method were reported in 1960 [14]. Since then, however, only little effort has been made to exploit the technique to its full capacity.

Figure 1 shows a horizontal section of the instrument. One of the most intricate problems connected with the use of a crystal spectrometer is the higher order neutrons reflected from the monochromator crystal. The solution adopted here is to eliminate them by a suitable choice of filters. A 30-cm polycrystalline beryllium block is placed in the beam before the monochromator crystal. This filter allows neutrons with energies less than 5.2 meV to reach the Pb(III) monochromator crystal. In this way a beam of monoenergetic neutrons hitting the sample is brought about. To be registered in the detector the scattered neutrons have to pass through a 20-cm polycrystalline piece of beryllium oxide. The cross-section of beryllium oxide is such that only neutrons with energies less than 3.74 meV are transmitted. Both filters are cooled to liquid nitrogen temperature to increase their transmission. The choice of a beryllium filter to eliminate high-order neutrons and a Pb(III) monochromator crystal restricts the energy interval that can be studied to 2.9 meV < E < 5 meV. In some

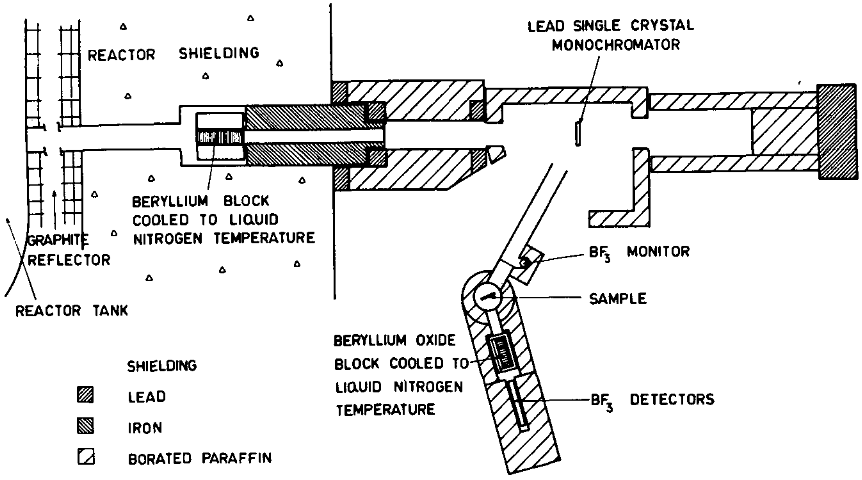

FIG.1. Horizontal section of the inverted beryllium oxide filter spectrometer.

particular cases we found it too narrow but for most of the results to be reported here it is wide enough.

The count rate in the detector is given by

$$J(E_0) = A\ N(E_0) \int_0^{E_c} T(E)dE \int_0^{\infty} R(E'-E_0)\ \frac{d^2\sigma(E' \rightarrow E)}{d\Omega\, dE'}\, dE' \qquad (1)$$

where $J(E_0)$ is the count rate in the detector for a particular choice of the glancing angle Θ which specifies E_0 through the Bragg condition; A is a factor, independent of energy, which is determined by the geometry; $N(E_0)$ is the total number of neutrons impinging on the sample per time interval; E_c is cut-off energy of the beryllium oxide filter; T(E) is the transmission function of the beryllium oxide filter experimentally found to be independent of energy; $R(E'-E_0)$ is the energy distribution of the neutrons hitting the sample.

To measure $N(E_0)$ accurately enough is quite a complicated task as the monochromator crystal has been chosen as large as possible in order to get good intensity. The size of the crystal is $7.5 \times 15\ cm^2$. Accordingly, the size of the neutron beam hitting the sample varies considerably over the whole angular interval. Moreover, the monochromator is not expected to be an ideal single crystal but most probably the reflection power varies over its surface. $N(E_0)$ is determined by placing a detector with known efficiency curve at the sample position and measuring its count rate as a function of crystal setting. This count rate is then used to calibrate the monitor counter in the beam between the monochromator crystal and the sample. The values obtained were tested on a vanadium run and were found to have an accuracy better than 1% over the whole energy region.

The resolution function $R(E'-E_0)$ has been found experimentally to be very close to a Gaussian, the width of which varies with energy. In the set of measurements to be discussed below the half width of the Gaussian was 0.13 and 0.10 meV at 3.74 meV.

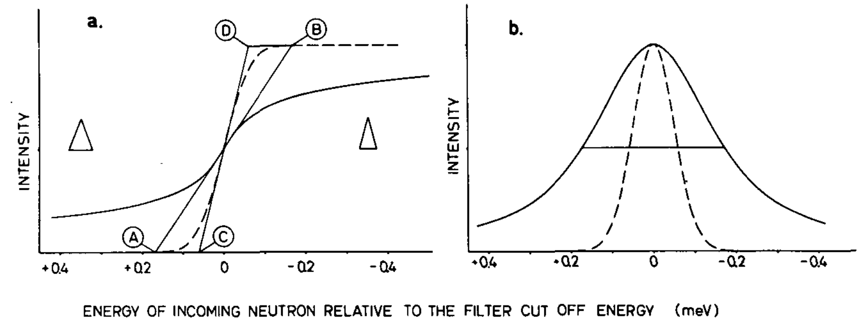

FIG. 2. Comparison of possible data treatments: (a) full curve: idealized one-component intensity distribution; broken curve: measured resolution distribution; (b) differentiated curves obtained from the distributions in (a). The resolution is indicated by the triangles.

In principle, a measured intensity distribution $J(E_0)$ can be treated in two ways. First, if the shape of the quasi-elastic cross-section is known and if only the width remains to be obtained, a direct comparison between experimental spectra and spectra calculated with Eq. (1) might be feasible. A well-known difficulty is, however, that the quasi-elastic peak has to be separated from the inelastic component which is of a hindered translational nature. As a matter of fact the same type of complication arises in this case as in an experiment using the full cold spectrum (see below). The principle of analysis is shown in Fig. 2a. The full curve shows an idealized one-component intensity distribution corrected to constant ingoing neutron intensity. The broken curve gives the vanadium pattern. From the full curve, actually representing the maximum broadening possible to determine with this instrument, it is obvious that the determinations of points A and B can be very difficult. In the case of a Lorentzian cross-section a direct comparison between the two projections L(AB) and L(CD) gives its width ΔE through

$$\frac{L(AB)}{L(CD)} = \frac{e^{-\lambda}}{1-\mathrm{erf}\,(\sqrt{\lambda})} \qquad (2)$$

where

$$\lambda = \ell n\, 2 \left[\frac{\Delta E}{(\delta E)_{res}}\right]^2$$

It was found that in no case reported here was this treatment satisfactory as the uncertainty in determining L(AB) was to large. This was mainly due to the arbitrariness in the separation between the quasi-elastic and the inelastic contributions. However, this procedure will be accurate enough for jump diffusion in solids and related problems.

Another method is to differentiate the measured intensity distribution and compare with calculated spectra. Equation (1) gives

$$I(E_0) = \frac{d\,\frac{J(E_0)}{N(E_0)}}{dE_0} = \int_0^\infty R(E'-E_0)\,\frac{d^2\sigma(E'\rightarrow E_c)}{d\Omega\, dE'}\,dE' \qquad (3)$$

Figure 2b shows the patterns in Fig. 2a differentiated. In this case one gets more direct information about the shape of the cross-section and also the separation between quasi-elastic and inelastic scattering is usually easier to perform. The differentiation eliminates the effect of the wide-energy window for the detected neutrons and the total resolution of the instrument is given by the energy width of the spectrum of the impinging neutrons. However, the uncertainty in an experimental intensity distribution is not displayed in a differentiated curve, because in performing the differentiation a mean value of a number of experimental points is taken. To keep the error of the differentiated curve as small as possible, it is very important that every detail of the experimental technique is known to great accuracy and also to have very good counting statistics. The width of the resolution function is indicated by the triangles. The variation with energy is rather small but of sufficient magnitude to account for a slight assymmetry which has been seen in the experimental curves. In deriving half-value widths no account has been taken of the resolution variation.

It is instructive to compare the intensity distribution of scattered neutrons given by Eq. (1) with the corresponding distribution obtained from a normal beryllium-filter time-of-flight spectrometer. The count rate in the detector in the latter case is given by

$$B(E) = A\ T_{ch}(E) \int_0^{\infty} R(E'-E)\ dE' \int_0^{(E_0)_{max}} I(E_0)\ \frac{d^2\sigma(E_0 \to E')}{d\Omega dE_0}\ dE_0 \qquad (4)$$

where A is a factor independent of energy; $T_{ch}(E)$ is the chopper transmission function if the chopper is placed after the sample, in other cases $T_{ch}(E) = 1$; $R(E'-E)$ is the resolution function on the analysing side; and $I(E_0)$ is the energy spectrum of the neutrons hitting the sample.

From Eq. (4) it is seen that in no way can the width of the ingoing spectrum $I(E_0)$ be extracted or eliminated from the measured spectrum shape. The only proper method of analysis consists in assuming a cross-section, calculating a theoretical B(E) and comparing it with the measured spectrum. The method is then quite insensitive in distinguishing between a Lorentzian cross-section and, for example, a cross-section which is a sum of two Lorentzian components. Only if $I(E_0)$ is a very narrow energy distribution, is there any hope of seeing fine details in B(E).

MEASUREMENTS

The liquids studied were pentane and amylalcohol (pentanol) in a temperature region covering almost the whole liquid range interval. The idea behind this particular choice was to compare two liquids with similar molecules, one being hydrogen bonded the other not hydrogen bonded.

The sample thickness used corresponds to a transmission of about 85%. No correction for multiple scattering was made as it was thought to be small. The temperatures were electronically controlled to be constant within 0.2°C and the temperature gradient over the sample area at the lowest temperatures was about one degree.

All measured patterns are corrected as described above and two examples are showed in Fig. 3.

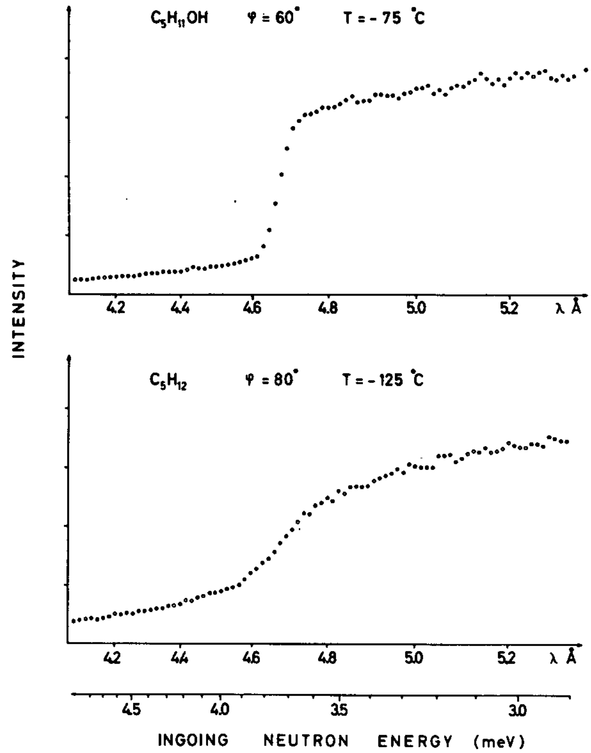

FIG.3. Examples of corrected measured intensity distributions.

EXPERIMENTAL RESULTS

Typical differentiated spectra obtained at the inverted beryllium oxide filter spectrometer on pentane at different scattering angles and temperatures are displayed in Fig. 4. At low temperatures and at small momentum transfers the patterns naturally divide into two parts, one central narrow peak and one broad underlying distribution. The separation between the two components becomes more and more complex the higher the temperature and the momentum transfer. In all other hydrogenous liquids studied hitherto, such as pentanol, glycerol and propanol, the same tendency has appeared. The measurements on pentane at -140°C need some extra explanation. Though the melting point of pentane is -130°C, we believe that the measurements were performed on liquid pentane or at least in a solid phase which is much like a liquid. The reason for this is that different results were obtained when reaching -140°C from the cold or the hot side. When cooling the sample to ~ -150°C and then increasing the temperature to -140°C an inelastic spectrum rich in detail and characteristic of a solid was obtained at the beryllium filter time-of-flight spectrometer, while when cooling directly to -140°C a more liquid-like inelastic spectrum resulted.

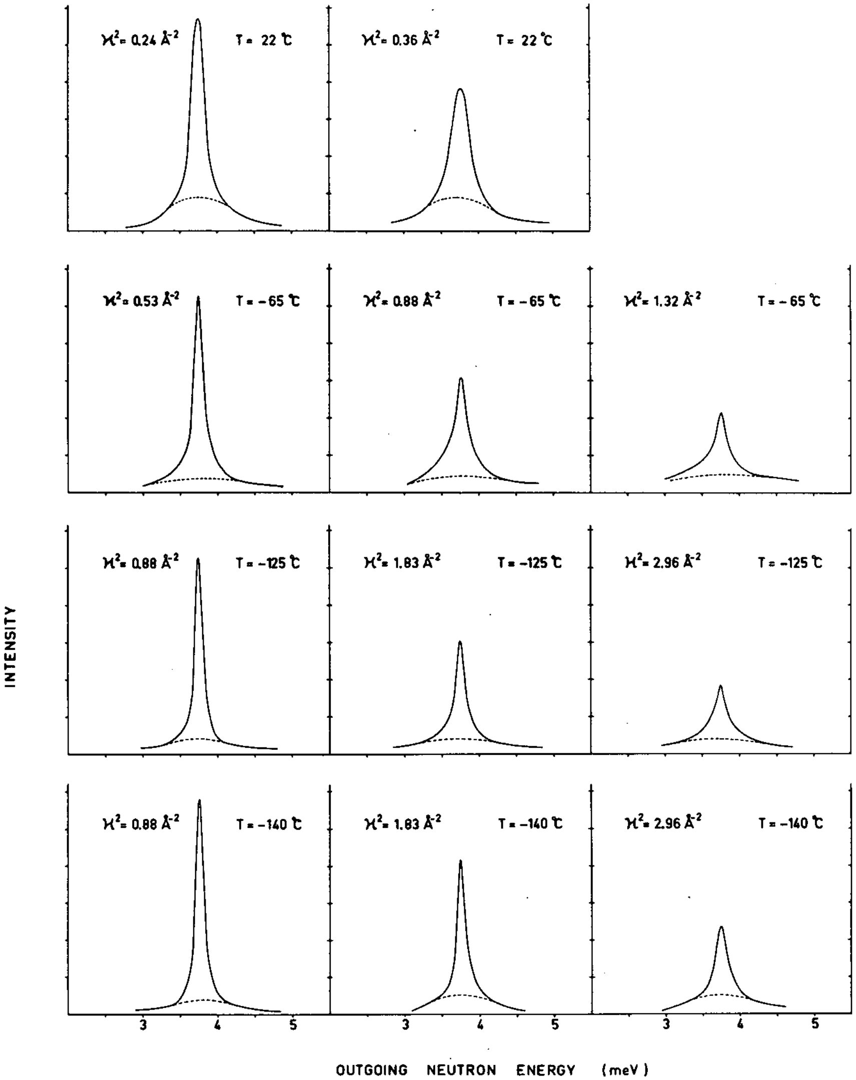

FIG.4. Differentiated spectra obtained from measurements on pentane at different temperatures and scattering angles.

To determine the nature of the two parts, their total intensities as functions of κ are shown in Fig. 5 for two particular cases, pentane at -140°C and pentanol at -45°C. Two interesting features are obvious, namely: (1) the intensity of the central peak is governed by a single exponential, which we call a Debye-Waller factor. Thus

$$I(\kappa)_{\text{central}} = e^{-a^2\kappa^2} \tag{5a}$$

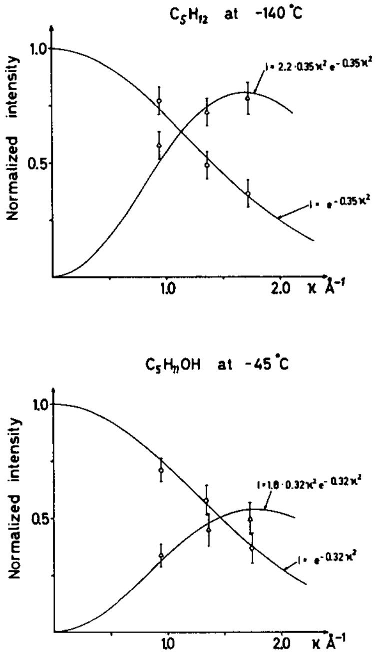

FIG.5. Intensity variation of the two observed components of the near-elastic cross-section for pentane at -140 °C and pentanol at -45 °C.

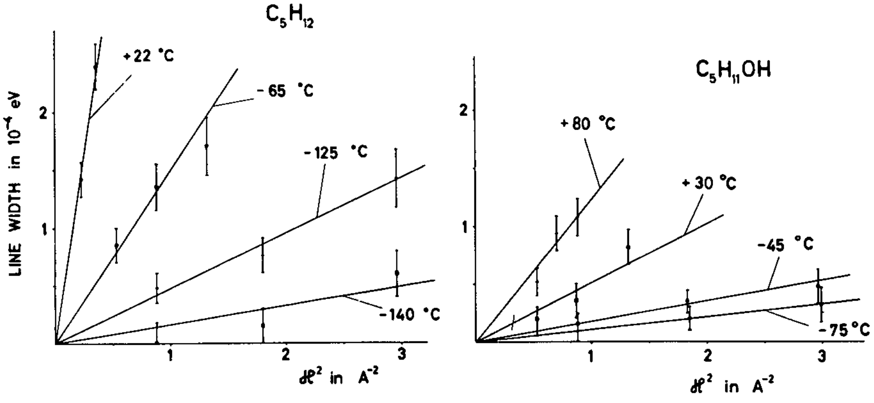

FIG.6. Line width of the central peak for pentane and pentanol.

(2) the intensity of the broad underlying distribution is increasing with κ^2. The integrated intensity is found to obey a law

$$I(\kappa)_{\text{broad}} = A\,\kappa^2\,e^{-a^2\kappa^2} \tag{5b}$$

The conclusion which can be drawn is that the central peak is of quasi-elastic origin while the broad distribution is of inelastic origin. We start the analysis with the central peak.

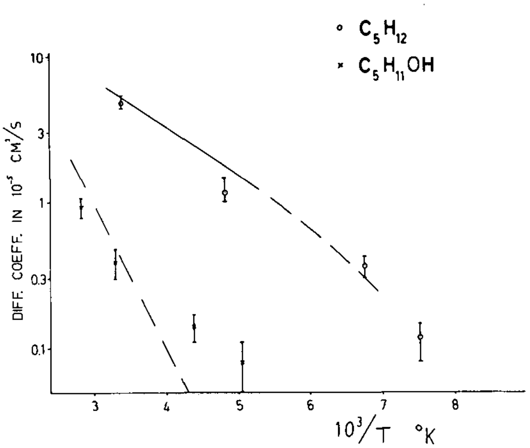

FIG.7. Derived diffusion coefficients for pentane and pentanol. Full curve represents measured values with spin echo methods while broken curves indicate extrapolations (see text).

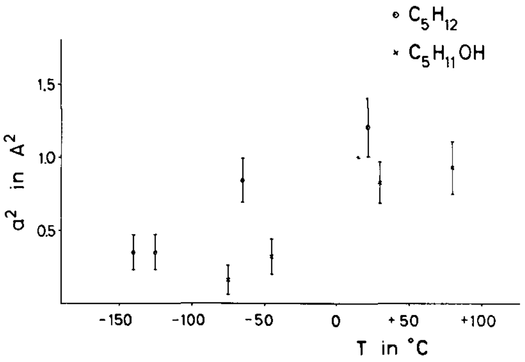

FIG.8. The temperature variation of a^2 determining the intensity of the central peak through $I \sim e^{-a^2\kappa^2}$.

Assuming a Lorentzian cross-section and a separation between the central and the underlying components as given by the broken curves in Fig. 4, a natural width of the central peak for pentane is obtained and is shown in Fig. 6 together with corresponding results for pentanol. In both liquids the points are fitted very well by straight lines through the origin indicating a diffusion mechanism as responsible for the intensity. As a matter of fact, if the relation $\Delta E = 2\hbar D\kappa^2$ is assumed, values are obtained for the diffusion constant D for pentane which are in good agreement with the ones measured by spin echo methods (Fig. 7). The macroscopic D values are, however, measured only in the temperature region +30°C > T > -80°C [18]. For lower temperatures an extrapolation is made with the use of measured viscosity values [19] (broken curve). For pentanol the diffusion constant has not been experimentally determined but measurements are in preparation at this laboratory. The broken curve is obtained through an extrapolation from lower alcohols. The activation energy for diffusion is almost constant for ethyl- propyl- and butyl-alcohol [20] and an average value is assumed for pentanol. Thus the slope of the curve is rather sure but the absolute values are uncertain within

± 25%. The uncertainty in the extrapolation can probably not account for the difference between the macroscopically and the neutron measured values at low temperatures. In this temperature range the viscosity is of the order of 1 poise or larger and a mechanism other than translational diffusion must be responsible for the width of the central peak, for example rotational diffusion. For the same reason the D value for pentane at -140°C, where pentane is expected to be in the solid phase, might be of rotational origin. At higher temperatures when the translational diffusion constant is about 10^{-5} cm^2/sec or larger, the relatively small rotational component should be impossible to see.

As mentioned above, the intensity variation of the central peak is governed by a factor $e^{-a^2\kappa^2}$. The temperature dependence of a^2 is shown in Fig. 8. The values for the two liquids are fitted very well by parallel curves. The absolute values are large and if one identifies $a^2 = \langle r_i^2 \rangle /6$, r_i is equal to 2.7 Å for pentane at room temperature. The only motion which can give such large r_i values is a rotational motion and thus it results in an indication that both translational and rotational motions contribute in the central peak. Then for large D values the intensity of the central peak is determined by the rotational motion and the width is determined by the translational diffusion. No variation of the width of the broad distribution with κ^2 has been found but it grows somewhat broader when the temperature increases. The constant A in Eq. (5b) was further found to have the same temperature variation as a^2. Accordingly the total intensity in the elastic region can be written as

$$I = e^{-a^2\kappa^2} + B \cdot a^2 \kappa^2 e^{-a^2\kappa^2} \tag{5c}$$

where for pentane $B = 2.2 \pm 0.1$ and for pentanol $B = 1.8 \pm 0.1$.

COMPARISON WITH THEORIES AND DISCUSSION

Recently Sears in a series of papers [10-12] has derived scattering cross-sections for molecules where both translational and rotational motions of the molecules are taken into account. A limiting assumption in Sears' treatment is that no interaction between the two types of motion occur. The general expression for the scattering cross-section is a partial wave expansion in terms of the angular momentum transfer.

Thus if all nuclei in the molecule but the protons are disregarded in treating the scattering process we have

$$\frac{d^2\sigma}{d\Omega dE} = \sum_{\ell=0}^{\infty} \frac{d^2\sigma_\ell}{d\Omega dE} \tag{6}$$

where

$$\frac{d^2\sigma_0}{d\Omega\, dE} = N \frac{k}{k_0} \frac{b^2}{\hbar} \sum_{\nu=1}^{n} j_0(\kappa r_\nu)^2 \, S'_{inc}(\vec{\kappa}, E) \tag{6a}$$

$$\frac{d^2\sigma_\ell}{d\Omega\, dE} = N \frac{k}{k_0} \frac{b^2}{\hbar} e^{\beta E} (2\ell + 1) \sum_{\nu=1}^{n} j_\ell(\kappa r_\nu)^2 \int_{-\infty}^{+\infty} S'_{inc}(\vec{\kappa}, E - E')\, S_\ell(E')\, dE' \tag{6b}$$

and

$$S'_{inc}(\vec{\kappa}, E) = e^{-\beta E}\, S_{inc}(\vec{\kappa}, E)$$

$$S_\ell(E) = \frac{1}{\pi}\int_0^\infty F_\ell(t+i\beta)\cos\frac{Et}{\hbar}\,dt$$

$$\beta = \frac{1}{2K_BT}$$

$F_\ell(t)$ is a rotational relaxation function essentially the same as the dipole correlation functions empirically obtained by Gordon from infrared and Raman data [8], r_ν denotes the position of a nucleus relative to the centre of mass of the molecule. $S_{inc}(\vec{\kappa}, E)$ is the incoherent cross-section in this case assumed to be given by

$$S_{inc}(\vec{\kappa}, E) = \frac{\hbar}{2\pi}\;\frac{\hbar D\kappa^2}{(\hbar D\kappa^2)^2 + E^2} \tag{6c}$$

Expansion (6) is rapidly convergent for $\kappa_r \lesssim 1$ and it is in most cases enough to include only the first two terms.

The difficulty in comparing Sears theory with our experimental data lies in the summation over all hydrogens in the molecule (coherence effects are neglected). The structure of the pentane and pentanol molecules is complicated and also many isomeric forms exist.

One way to overcome the problem is to try to introduce a representative average R_ℓ value through

$$j_\ell(\kappa\, R_\ell)^2 = \frac{1}{n}\sum_{\nu=1}^{n} j_\ell(\kappa\, r_\nu)^2 \tag{7}$$

A fit to pentane at -140°C yields R_0=1.0Å and R_1 = 1.4Å. That R_0 is smaller than R_1 can be understood from the functional forms of the spherical Bessel functions. Assuming that S_{inc} is described by the simple diffusion formula, it seems, however, difficult to account for the variation of a^2 with temperature. Other features from the theory do fit the experiment, such as the fact that the total elastic cross-section is made up by at least two components and also that the width of the broader underlying intensity distribution shows, if any, only a small dependence on κ. In the comparison with Sears' theory it has to be remembered that the weak hindering approximation was adopted. It may very well be that the hindering of the molecular rotations is fairly strong, at least in the lower temperature ranges of the liquid state.

The intensity variation of the broad underlying distribution suggests another approach. It has been customary to take formulas valid for the solid state over to the liquid, for example, to obtain frequency distributions. The justification has been the solid-like behaviour of a liquid. Including a rotational part in his treatment, Hahn [21] has shown that in energy gain processes the one-phonon and one-torson cross-sections for a molecular cubic crystal can, if all interactions between rotational and translational motions are neglected, be written as

$$\frac{d^2\sigma}{d\Omega\, dE} = N\, b^2\, \frac{k}{k_0}\, 2\pi\, \frac{\hbar^2\kappa^2}{2E}\, \frac{1}{e^{2\beta E}-1}\, e^{-a^2\kappa^2} \left[\frac{Z_r\, g_t}{3M}\, f_t(E) + \frac{g_r}{2m}\, f_{rot}(E) \right] \tag{8}$$

where Z_r is the number of atoms participating in the rotation; M is the molecular mass; m is the mass of one of the atoms participating in the rotation; g_t, g_r are parameters which are functions of κ and of a^2; and $f_t(E)$, $f_{rot}(E)$ are frequency distributions for hindered translations and hindered rotations of the molecule, respectively. The main contribution from $f_t(E)$ to the scattering falls outside the energy region covered in this experiment and will be neglected.

Rewriting Eq. (8) and using the same formalism as in the phonon case [22], we get

$$\frac{d^2\sigma}{d\Omega\, dE} \sim \frac{1}{M_r}\, (2\, W)_{rot}\, e^{-(2W)_{rot}}\, f_{rot}(E)\, \frac{1}{E^2} \tag{8a}$$

Here g_r has been put equal to one, which is valid only for small $(2W)_{rot} = a^2\kappa^2$. From a comparison with the empirical Eq. (5c) it is seen that both the κ dependence and the temperature dependence of the broad underlying distribution is properly predicted from Eq. (8a). This gives strong support to the idea that torsional vibrations with the molecule as unit occur in the liquid phase as well. Also a possible interpretation of the constant B in terms of an effective rotating mass can be made. The fact that the numerical value of B is smaller for pentanol than for pentane should then reflect the larger hindrance for rotation in a hydrogen-bonded liquid.

Thus a phenomenological description of the measured intensity in the 'quasi-elastic' region may be created. The scattering function can, according to the results presented above, be written as

$$S(\vec{\kappa}, E) = \int_{-\infty}^{+\infty} S_{diff}\, (\vec{\kappa}, E - E')\, S_{rot}(\vec{\kappa}, E')\, dE' \tag{9}$$

where

$$S_{diff}\, (\vec{\kappa}, E) = \frac{\hbar\, D\kappa^2}{(\hbar\, D\kappa^2)^2 + E^2}$$

$$S_{rot}\, (\vec{\kappa}, E) = e^{-(2W)}\, \mathrm{rot} \left[\frac{\hbar\, D_{rot}\, \kappa^2}{(\hbar\, D_{rot}\, \kappa^2\,)^2 + E^2} + C\, \frac{(2W)_{rot}}{M_r}\, f_{rot}(E) \right] \frac{1}{E^2}$$

The constant C should be possible to calculate from molecular data. Concerning the shape of the torson spectrum $f_{rot}(E)$ nothing definite can be said from this experiment. Qualitatively the following remarks can be made. By assuming a molecular rotational correlation function of the same shape as those derived by Gordon from infrared and Raman work [8], that is, putting

$$<\vec{u}(0)\cdot\vec{u}(t)> = \cos \Omega t\ e^{-t/\tau} \tag{10}$$

where $\vec{u}$ is a unit vector connected to the molecule, one arrives at

$$f_{rot}(E) = \frac{\hbar}{2\tau}\left[\frac{1}{\frac{\hbar^2}{\tau^2} + (E - \hbar\Omega)^2} + \frac{1}{\frac{\hbar^2}{\tau^2} + (E + \hbar\Omega)^2}\right] \tag{11}$$

Thus a satellite line with a width $2\hbar/\tau$ will appear on each side of the ingoing energy which is broadened by rotational diffusion. Assuming that the molecules are in their straight zig-zag form, the moment of inertia is of the order of 5×10^{-38} g cm^2. From the equipartition law

$$\Omega = \left(\frac{k_B T}{I}\right)^{\frac{1}{2}} \tag{12}$$

we get $\hbar\Omega \sim 0.4$ meV at -140°C. To resolve the two satellite lines from the central line is an almost impossible task. Experimentally a broad distribution having a width $\sim 2\hbar[(1/\tau) + \Omega + D\kappa^2]$ should be expected. This agrees very well with our results. Also the small temperature and small κ dependence of the width can be qualitatively understood in this way.

COMPARISON BETWEEN DIFFERENT TECHNIQUES USED FOR QUASI-ELASTIC SCATTERING EXPERIMENTS

Many methods have been used for measurements of line-width curves on complex liquids. We compare here as typical examples three spectrometers in Sweden:

(1) The time-of-flight spectrometer in Stockholm [23] using the full cold spectrum where the width of the impinging neutron distribution is ~ 2 meV

(2) The time-of-flight spectrometer in Studsvik [24] where a chopper is used to cut away the low-energy tail of the cold spectrum and when working in conjunction with a Be filter results in a width ΔE_0 of the impinging neutron distribution of 0.6 meV

(3) The inverted beryllium oxide filter spectrometer in Stockholm described above.

The main difficulty in obtaining line-width data in the time-of-flight cases is to separate the quasi-elastic component out of the total scattering pattern. The procedure has been discussed earlier in detail [1]. Once the separation is made, one has, however, also to relate the width in time Δt_{obs} of the quasi-elastic peak to the width in energy ΔE_{nat}. To establish this relation, one usually has assumed a cross-section consisting of a single Lorentzian component. As shown above, the quasi-elastic cross-section is, however, made up of two components. The question is now whether the previous assumption of a single Lorentzian will invalidate all earlier analyses of quasi-elastic scattering. It is important to investigate whether the broad underlying component is contained within the part of the cross-section earlier called the quasi-elastic or not and, if it is, how large an error is introduced in using the relation between Δt_{obs} and ΔE_{nat} derived from the assumption of a single Lorentzian cross-section. It is certainly of interest to compare in detail results obtained with different techniques. For this purpose we chose pentane measurements at -125°C and +22°C.

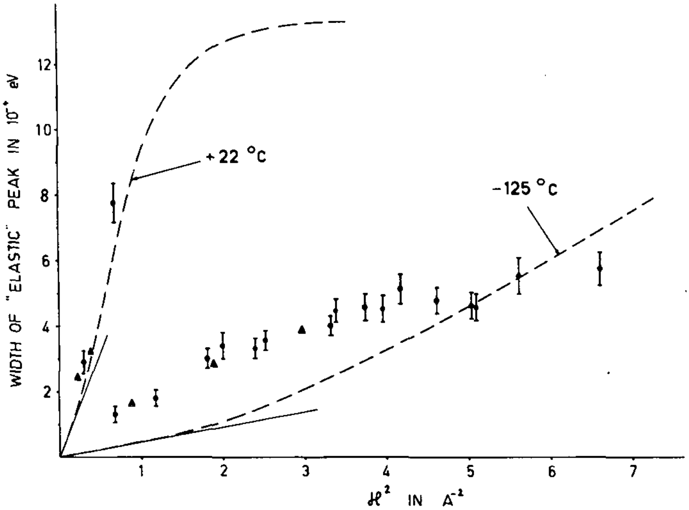

FIG.9. Line-width results obtained with different methods for pentane at two temperatures. Open circles are measured at the time-of-flight spectrometer in Stockholm and filled circles in Studsvik. The curves represent results obtained with the inverted filter technique (see text).

Figure 9 shows line-width results obtained from the three spectrometers. Open circles are from the time-of-flight spectrometer in Stockholm and filled circles from Studsvik. The straight lines through the origin are best fits to measured points from the inverted filter spectrometer. An important test of the reliability of the data is to see if the time-of-flight results can be understood in terms of the inverted filter technique results. Thus the resolution was unfolded from the scattering picture shown in Fig.4 and the corresponding time-of-flight scattering pattern was calculated from Eq. (4). Line width values shown by triangles in Fig.9 were obtained from the calculated distributions. The conclusion is that the different scattering patterns do not stand in contradiction to each other but rather describe the same thing. It also means that in the time-of-flight values both components seen in the inverted filter measurements are included in what has been called the quasi-elastic peak. The numerical values for the line widths derived from the time-of-flight spectrometers probably do not allow a detailed physical interpretation. Thus in both cases the resolution $\Delta E_0/E_0$ is too poor to resolve the two components. The broken curve in Fig. 9 represents the half width of the total cross-section as measured for $\kappa^2 < 3$ and calculated for larger κ^2 values from

$$I(\kappa, E) = e^{-a^2\kappa^2} \frac{\hbar D\kappa^2}{(\hbar D\kappa^2)^2 + E^2} + 2.2\, a^2 \kappa^2\, e^{-a^2\kappa^2} \frac{c}{c^2 + E^2} \qquad (13)$$

This formula has no theoretical background but it describes the inverted filter results rather accurately. That one experimental point from the time-of-flight measurements falls below the extrapolated curve is probably not significant but has its origin in the uncertainty of the determination of the parameters in Eq. (13). On the contrary one would expect all time-of-flight results to fall above the calculated curve and that the difference should

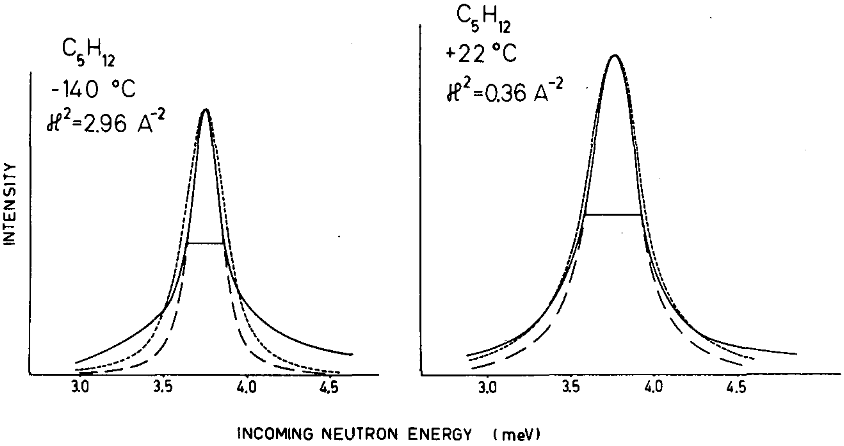

FIG.10. Cross-sections derived from measurements at different types of spectrometers. Full curve: inverted filter spectrometer result; broken curve: Lorentzian cross-section folded with the inverted filter spectrometer resolution function; dotted curve: Lorentzian cross-section from the time-of-flight analysis folded with the inverted filter spectrometer resolution function.

be smaller when the central peak grows broader. One could also expect that when the total cross-section approaches the shape of a single Lorentzian the different methods should yield the same results. This tendency is actually seen for the +22°C measurements. To elucidate the situation further the different cross-section shapes are compared in Fig. 10. The full curve describes the inverted filter spectrometer result. The broken curve is a Lorentzian, folded with the resolution function. The half width of the compounded function is the same as the total half width of the full curve. The dotted curve is the Lorentzian cross-section resulting from the time-of-flight analysis folded with the resolution function of the inverted filter spectrometer. The deviation from a Lorentzian shape of the cross-section lies mainly in the wings and is smaller at +22°C than at -125°C.

Thus it must be concluded that the rapid rise of the line-width curves for small values of κ^2 yielding apparent diffusion coefficients considerably larger than macroscopically measured ones is probably caused by the relatively poor resolution $\Delta E_0 / E_0$ such that both the true quasi-elastic and the rather narrow inelastic distributions have contributed to the width values from the smallest κ^2 values and up. The single Lorentzian description of the quasi-elastic peak used until now because of lack of good resolution data may be said to give a zero-order approximation to the true picture. It is obvious from Fig. 10 that the average between the two distributions observed with high resolution and described by Eq. (13) is in fact obtained by the single Lorentzian description. Therefore, although the numerical values of constants derived from the low resolution data are uncertain, the main trend and the basic physics probably was correctly brought out by the earlier low resolution data and the corresponding analysis [2, 9, 13].

The intensity variation of the total quasi-elastic intensity as seen in the time-of-flight experiments has been fully reproduced from the inverted filter results. This means that also in this respect earlier derived values contain contributions from both quasi-elastic and inelastic scattering. In some cases deviations from a single $e^{-a^2\kappa^2}$ dependence have been reported [1, 25]. According to the results presented above this is an indication that inelastic scattering is contributing.

CONCLUSIONS

The intensity distribution formerly called the 'quasi-elastic' scattering is made up of two components, one which is really quasi-elastic and one which has an inelastic origin. To separate the two components a high resolution is needed.

The motion of a molecule in a complex liquid is described by a translational motion upon which a rotational motion is superimposed. The rotational motion is probably more or less hindered.

The rotational motion probably has two components corresponding to small steps (quasi-elastic peak) and large steps (inelastic contribution). The small step motion would correspond to rotational diffusion and the large step motion to rotational jumps in which the molecule changes its torsional energy.

ACKNOWLEDGEMENT

The authors are indebted to Mr. S. Holmryd for valuable help and discussions in connection to the measurements in Studsvik and to Mr. N. M. Butt for his participation in the data treatment.

REFERENCES

[1] LARSSON, K.-E., DAHLBORG, U., Physica 30 (1964) 1561.
[2] LARSSON, K.-E., QUEROZ do AMARAL, L., IVANTCHEV, N., RAPEANU, S., BERGSTEDT, L., DAHLBORG, U., Phys. Rev. 151 (1966) 126.
[3] DASANNACHARYA, B.A., VENKATARAMAN, G., Phys. Rev. 156 (1967) 196.
[4] ALDRED, B.K., EDEN, R.C., WHITE, J.W., Disc. Faraday Soc. 43 (1967) 169.
[5] RUSH, J.J., J. chem. Phys. 47 (1967) 3936.
[6] de GRAAF, L.A., Thesis, Delft (1968).
[7] STILLER, H., Inelastic Scattering of Neutrons (Proc. Symp. Bombay, 1964) 2, IAEA, Vienna (1965) 179.
[8] GORDON, R.G., J. chem. Phys. 44 (1966) 1830.
[9] LARSSON, K.-E., BERGSTEDT, L., Phys. Rev. 151 (1966) 117.
[10] SEARS, V.F., Can. J. Phys. 44 (1966) 1279.
[11] SEARS, V.F., Can. J. Phys. 44 (1966) 1299.
[12] SEARS, V.F., Can. J. Phys. 45 (1967) 237.
[13] LARSSON, K.-E., Phys. Rev. 167 (1968) 171.
[14] STILLER, H.H., DANNER, H.R., Inelastic Scattering of Neutrons in Solids and Liquids (Proc. Symp. Vienna, 1960), IAEA, Vienna (1961) 363.
[15] RAPEANU, S., Rev. Rom. Phys. 11 (1966) 265.
[16] SAUNDERSON, D.H., RAINEY, V.S., Inelastic Scattering of Neutrons in Solids and Liquids (Proc. Symp. Chalk River, 1962) 1, IAEA, Vienna (1963) 413.
[17] RAPEANU, S., ILIESCU, N., Phys. Lett. 26A (1967) 72.
[18] DOUGLASS, D.C., McCALL, D.W., J. phys. Chem. 62 (1958) 1102.
[19] GILLER, E.B., DRICKAMER, H.G., Ind. Eng. Chem. 41 (1949) 2067.
[20] PARTINGTON, J.R., HUDSON, R.F., BAGNALL, K.W., J. chem. Phys. 55 (1958) 77.
[21] HAHN, H., Inelastic Scattering of Neutrons (Proc. Symp. Bombay, 1964) 2, IAEA, Vienna (1965) 279.
[22] SJÖLANDER, A., Ark. Fys. 14 (1958) 315.

[23] LARSSON, K.-E., DAHLBORG, U., HOLMRYD, S., OTNES, K., STEDMAN, R., Ark. Fys. 16 (1959) 199.

[24] HOLMRYD, S., SKÖLD, K., PILCHER, E., LARSSON, K.-E., Nucl. Instrum. Meth. 27 (1964) 61.

[25] LARSSON, K.-E., Inelastic Scattering of Neutrons (Proc. Symp. Bombay, 1964) 2, IAEA, Vienna (1965) 3.

DISCUSSION

J.J. RUSH: I believe you said in your oral presentation that your results indicated a displacement of about 2.7 Å which you associated primarily with the reorientation of the methyl groups. This would seem unusual, since such a reorientation would involve a motion of the hydrogens around the molecular chain through a 120° angle and a distance only about half that which you mentioned. Would you please comment on this?

B. FRIBERG: I said that a CH_3 rotation can make some contribution to this substantial displacement; I would stress, however, that the largest contribution most probably comes from a hindered oscillation of the molecule as a whole.

J.W. WHITE: Could you tell me whether the activation energies which you measured for diffusion in these two materials are the same as the activation energies for viscosity?

B. FRIBERG: We have not performed the calculation in question; especially in the case of propanol, no activation energy could be found, because measurements are not made in that material. We therefore merely extrapolated the lower hydrocarbons, and used the activation energy arrived at by that method.

J.W. WHITE: May I suggest that it would be quite interesting to plot the activation energy for the ratio of the diffusion coefficient which you measure divided by the viscosity, at the temperature concerned?

B. FRIBERG: Thank you for that useful suggestion.

H.H. STILLER: Regarding the temperature dependences of the diffusion constants, you observe good agreement with macroscopic values for pentane and poor agreement, at low temperatures, for pentanol. Could this not just be due to the motions of the hydrogens at the hydrogen bonds? Therein lies, after all, the main difference between the two substances.

B. FRIBERG: Let me emphasize that it is more or less a guess on our part that the poor agreement between the measured 'diffusion' coefficient and the extrapolated values, shown by the broken curve in Fig. 7, is due to rotational diffusion. However, in the solid phase of pentane a broadening of the quasi-elastic peak was seen. The reason for this broadening must be a reorientation process, and we believe the same explanation to be valid for pentanol at low temperatures.

BRILLOUIN SCATTERING OF NEUTRONS FROM LIQUID CO

K. MIKA, B. DORNER AND H.H. STILLER
INSTITUT FÜR FESTKÖRPER- UND NEUTRONENPHYSIK,
KERNFORSCHUNGSANLAGE JÜLICH,
FEDERAL REPUBLIC OF GERMANY

Abstract

BRILLOUIN SCATTERING OF NEUTRONS FROM LIQUID CO. The energy distributions of neutrons scattered from liquid and from solid β-CO are measured with a triple-axis spectrometer in the constant κ mode of operation for very small values of $\kappa(|\vec{\kappa}| \leq 0.65$ Å^{-1}), such that for the excitation of collective motions of wavevector $\vec{q}$ one has $\vec{\kappa} = -\vec{q}$ (Brillouin scattering). Multiple scattering, which may invalidate this condition, is largely suppressed by inserting a Cd honeycomb into the sample. Brillouin scattering is the only method by which in polycrystals and liquids peaks in the distribution of scattered neutrons represent single excited states of collective motions.

In solid β-CO longitudinal phonons are observed in this way. Their dispersion, averaged over all lattice directions, is determined; the longitudinal sound velocity is found to be 1500 m/sec. In liquid CO a large amount of small energy transfers is observed. This must result from a large difference between the isothermal and the adiabatic compressibility. Its energy width is discussed in terms of diffusion, free rotations and hydrodynamics. It is shown, that diffusion makes a small contribution only. The scattering due to free or quasi-free rotations is calculated in the Krieger-Nelkin approximation. After subtracting this contribution from the experimental inelastic data, Brillouin peaks are again well separated. From their position a dispersion law for longitudinal phonons in liquid CO can be derived, with a sound velocity of 1200 m/sec.

If the ω dependence of the scattered intensity at different κ values is described by hydrodynamics, the quasi-elastic peak comes out to be broadened by heat conductivity and a contribution of Brillouin peaks can be seen as a shoulder. A best fit to the experimental data is obtained with values for the heat conductivity and for the viscosity, which are smaller than the macroscopic ones.

1. INTRODUCTION

The coherent inelastic scattering of neutrons is governed by the conservation of energy

$$\pm \hbar\omega = \frac{\hbar^2}{2m}\,(k_0^2 - k_1^2) \tag{1}$$

and by interference conditions, which also may be interpreted as conservation of momentum. With single crystals the interference condition is

$$\vec{\kappa} \equiv \vec{k}_0 - \vec{k}_1 = 2\pi\vec{\tau} - \vec{q}$$

where $\vec{k}_0$ is the wavevector of the incident, $\vec{k}_1$ the wavevector of the scattered neutrons, $\vec{q}$ the wavevector of an excited or de-excited collective particle motion and $2\pi\vec{\tau}$ a reciprocal lattice vector, m the neutron mass. $h\vec{\tau}$ is the momentum taken up by the crystal without energy change.

With polycrystals and, even more so, with liquids the question of what part of the momentum transfer $\hbar\vec{\kappa}$ is taken up by the system without energy change is extremely complicated [1, 2]. Uncertainties with respect to this question render the interpretation of experimental observations quite difficult. As has been shown already [3], these difficulties are avoided only if the experiment is conducted such that with certainty $\tau = 0$. We call this scattering Brillouin scattering. The interference condition is then

$$\vec{\kappa} = -\vec{q} \tag{2}$$

As with single crystals, such an experiment yields peaks in the distribution $S_{coh}(\vec{\kappa},\omega)$ of scattered neutrons, which each represent one excited state of collective motions, because the peaks will appear at those values of the experimental variables, which satisfy Eqs (1) and (2) together with the dispersion relation

$$\omega = \omega_s(\vec{q}) \tag{3}$$

Under condition (2) the only averaging which enters the experiment results from a possible directional dependence of $\omega_s(\vec{q})$. It has been shown [4] that usually this averaging is not serious from an experimental point of view.

Brillouin scattering has two disadvantages: (i) as the inelastic coherent scattering cross-section is proportional to $(\vec{\kappa}\cdot\vec{e}_{s\vec{q}})^2$, where $\vec{e}_{s\vec{q}}$ is a unit vector in the direction of polarization of the excited wave, condition (2) means that only certain modes can be excited, for instance, for sound waves longitudinal modes only; (ii) as illustrated in Fig. 1, rather large incident energies $E_0 = \hbar^2k_0^2/2m$ and small scattering angles Φ are necessary to fulfil condition (2); both these requirements restrict the accessible solid angles.

In the following we report the results of scattering experiments carried out under condition (2) on liquid CO at 77.3°K. For comparison measurements were also performed on solid polycrystalline β-CO at 63.1°K, under the same experimental conditions. CO is liquid between 81.6°K and 68.1°K. The β-phase of the solid is stable between 68.1°K and 61.6°K. In this phase the molecular centres of masses are arranged in nearly close-packed hexagonal structure ($a = 4.11$ Å, $c = 6.79$ Å), while the molecular orientations appear to be unordered [5]. It has been assumed that the molecules either rotate freely or perform precessions around the c-axis [6].

2. EXPERIMENTAL RESULTS

The measurements were carried out with a triple-axis spectrometer at the FRJ-2 reactor in Jülich, using the constant-κ method. Neutrons of energy $E_0 = 30.9$ meV were selected from the reactor spectrum by Bragg reflection from the 220 planes of a Pb single crystal. The energies of the scattered neutrons were analysed by Bragg reflection from the same

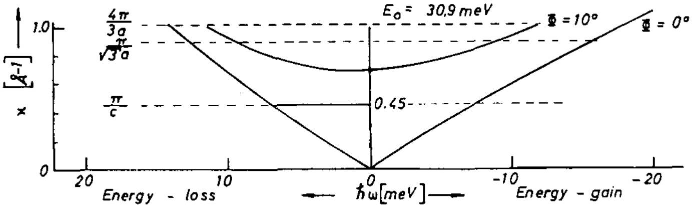

FIG.1. The region in the κ - ω plane covered by the present experiment under condition $\vec{\kappa} = -\vec{q}$. The curves represent Eqs.(1) and (2) after elimination of k_1. With β-CO the boundaries of the Brillouin zone for the symmetry directions are: π/c for (0001), $\frac{4}{3}\pi/a$ for $(01\bar{1}0)$ and $\frac{1}{\sqrt{3}}$ π/a for $(10\bar{1}0)$.

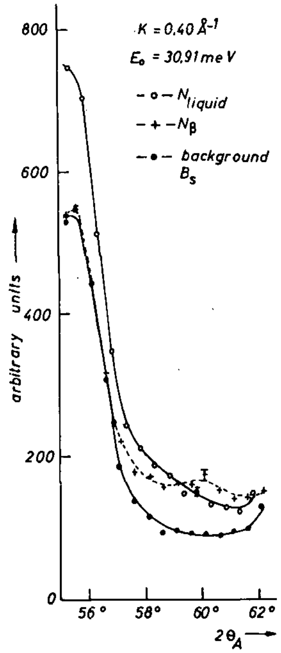

FIG.2. Typical experimental results, without any corrections. The elastic line is at $2\theta_A = 55°30'$.

planes of a second Pb crystal. The scattering angle Φ was varied simultaneously with the Bragg angle θ_A between 10° and 1°50'.

CO, 99.995% pure obtained from Air Liquide, was condensed into a layer of 12 mm thickness, giving a transmission of 83%. To reduce multiple scattering a honeycomb of cadmium, 10 mm wide, was inserted into the sample container. The temperature of 63.1°K, the triple point of N_2, was reached by pumping on N_2. A possible texture of the solid sample was reduced by repeatedly cooling below 61.6°K, the phase transition point of CO. The reduction of texture was observed from intensities of Bragg reflections.

Figure 2 shows, without any corrections, some typical experimental results. Figure 3 shows all results obtained, after subtraction of background and conversion from an analysing Bragg angle to an energy scale. The back-

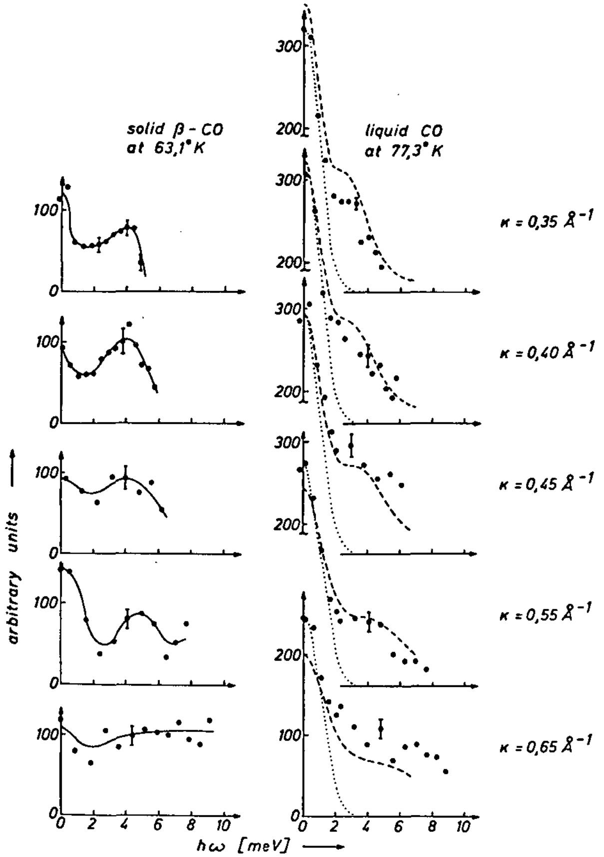

FIG. 3. Experimental results after background correction. The broken lines are calculated from hydrodynamics with Eq. (5) with parameters given in the next. The dotted lines give the contribution of free rotations calculated with Eq. (4).

ground was determined by measuring (a) the scattering from the empty, but cooled sample container, B_s (Fig. 2), and (b) by covering the sample with cadmium, B_0. $B = B_0 + \vartheta(B_s - B_0)$ was subtracted from the data, where ϑ is the sample transmission.

In addition, a measurement was carried out to determine the intensity at $\omega = 0$ as a function of κ. The results are shown in Fig. 4.

3. DISCUSSION

The peaks in $S(\kappa, \omega)$ observed with polycrystalline β-CO (Fig. 3) can only represent longitudinal acoustical phonons, because no peaks appear at smaller ω. Figure 5 shows the dispersion, $\omega_\ell(q)$, of these phonons. Apparently in β-CO the frequencies of optical phonons and of possible torsons are so high that they could not be observed with the present conditions for Brillouin scattering (see Fig. 1). Actually, with $\kappa = 0,55$ Å^{-1} condition $\tau = 0$ is no longer fulfilled in the c-direction. It can be shown,

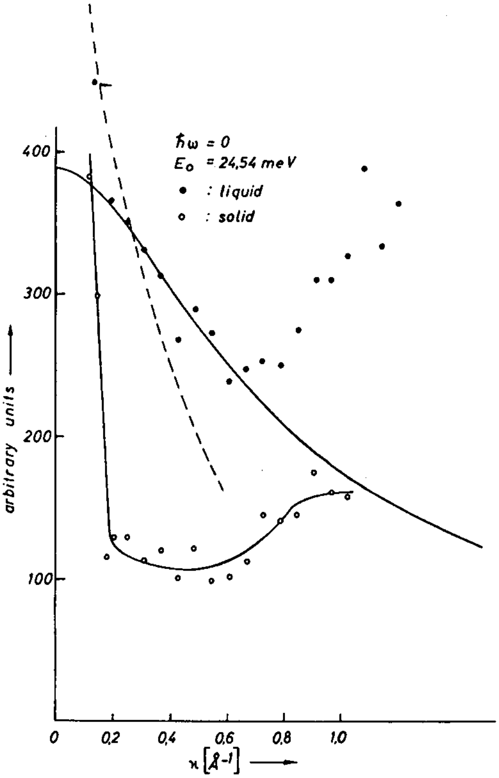

FIG.4. Results of measurements for $\omega = 0$: ○ solid, ● liquid. The curves fitted to the liquid points are: ——— calculated for free rotations, - - - - calculated from the hydrodynamical theory of Mountain. For $\kappa > 0.7$ Å^{-1} the liquid points show the increase to the first diffraction maximum at 1.83 Å^{-1}, the height of which is about 9000 counts. The curve joining the solid points has no theoretical meaning. The steep descent below $\kappa = 0.2$ Å^{-1} is predominantly due to multiple intragrain scattering in solid CO.

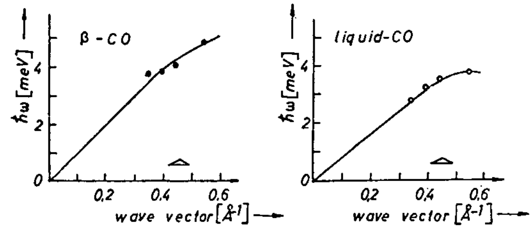

FIG.5. Phonon dispersion in solid β-CO and in liquid CO. The sound velocities are: $c_{\text{solid}} \approx 1500$ m/sec, $c_{\text{liquid}} \approx 1200$ m/sec.

however, that the a-directions contribute considerably more scattered intensity, because $\omega_\ell(\kappa, \vartheta, \varphi)$ has, for constant κ and as a function of the directions, only a maximum or minimum in the c-direction, whereas in one of the symmetry directions of the hexagonal plane a saddlepoint can be expected. Therefore in the frequency distribution for constant κ no peak will appear for frequencies around the c-direction [4].

The experimental results for liquid CO (Fig. 3) are quite different. In comparison to the results with β-CO, the most striking difference lies in the appearance of a strong peak at $\omega = 0$. As has been shown earlier [3], such a peak may result from multiple scattering, but since the transmissions of the solid and the liquid sample were equal and since owing to the Cd honeycomb the scattering volume elements were cubic with both samples, multiple scattering also should have been equal. Hence it can be safely assumed that the appearance of the elastic peak is physically significant for the liquid state of CO. In liquid CO the difference between the isothermal and the adiabatic compressibility, proportional to $(c_p/c_v - 1)$, which for neutron scattering determines the intensity for small κ, must be large. The isothermal compressibility gives the intensity for $\kappa \to 0$, while the adiabatic compressibility described the contribution of sound waves. c_p/c_v is unknown for liquid CO; for liquid N_2 which has very similar properties as CO, as well as for liquid O_2 a value of $c_p/c_v = 1.91$ is tabulated in Ref. [7]. There seem to be three possible explanations for the broadening ω: (i) diffusion, (ii) rotations of small frequencies, for instance free rotations, (iii) a large heat conductivity [8, 9].

Diffusion can make only a small contribution. In the convolution approximation [10] it would give

$$S_{\mathrm{coh}}^{\mathrm{diff}}(\kappa, \omega) = (1 + \gamma(\kappa)) \frac{D\kappa^2}{\omega^2 + (D\kappa^2)^2}$$

where $1 + \gamma(\kappa)$ is the structure factor of the liquid and D the self-diffusion constant. With $D = 2.9 \times 10^{-5}$ cm^2 sec^{-1} [11], for $\kappa = 0.5$ Å^{-1} the width of the peak should be about 30 times smaller than the observed one. A contribution from rotational diffusion, as recently discussed by Larsson [12], also must be expected to be small, since the viscosity of liquid CO has the small value of 1.92×10^{-3} poise at 77°K [13]. In the following we discuss the other two possibilities.

We assume that also in the liquid equilibrium positions for the molecular centres of masses, $\vec{R}_i^0$, are sufficiently well defined, and hence write for the position of atom ν of molecule i

$$\vec{R}_i^\nu(t) = \vec{R}_i^0 + \vec{u}_i(t) + \vec{r}_i^\nu(t)$$

$\vec{u}_i$ is the displacement of the centre of mass and $\vec{r}_i^\nu$ the rotational displacement. Then, if these two displacements are independent of each other, as with free rotations,

$$S(\vec{\kappa},\omega) = \sum_i \sum_{\nu,\mu} a_i^\nu a_i^\mu \int dt\, e^{-i\omega t} \langle e^{i\vec{\kappa}[\vec{u}_i(t) - \vec{u}_i(0)]} \rangle$$

$$\times \left\{ \langle e^{i\vec{\kappa}[\vec{r}_i^\nu(t) - \vec{r}_i^\mu(0)]} \rangle - \langle e^{i\vec{\kappa}\vec{r}_i^\nu(t)} \rangle \langle e^{-i\vec{\kappa}\vec{r}_i^\mu(0)} \rangle \right\}$$

$$+\sum_{i,j}\sum_{\nu,\mu} a_i^{\nu} a_j^{\mu} e^{i\vec{\kappa}(\vec{R}_i^0-\vec{R}_j^0)}\int dt\, e^{-i\omega t}$$

$$\times\langle e^{i\vec{\kappa}[\vec{u}_i(t)-\vec{u}_j(0)]}\rangle\langle e^{i\vec{\kappa}\vec{r}_i^{\nu}(t)}\rangle\langle e^{-i\vec{\kappa}\vec{r}_j^{\mu}(0)}\rangle$$

The a^{ν} are the scattering amplitudes for the O and C atoms, respectively. The first term represents scattering, which is incoherent with respect to the molecules, the last term is coherent scattering. By carrying out a phonon expansion for the $\vec{u}_i$ to zero order only, one obtains, following Krieger and Nelkin [14],

$$S(\kappa,\omega) = \frac{1}{\kappa}\left(\frac{2\pi\overline{M}}{k_B T}\right)^{\frac{1}{2}} \exp\left[-\frac{\overline{M}\,\omega^2}{2k_B T\kappa^2}\right] e^{-2W}$$

$$\times\left\{N\left[(a_c^2+a_0^2)+2a_c a_0\frac{\sin 2\kappa r}{2\kappa r}-(a_c+a_0)^2\left(\frac{\sin\kappa r}{\kappa r}\right)^2\right]\right.$$

$$\left.+(a_c+a_0)^2\left(\frac{\sin\kappa r}{\kappa r}\right)^2 F(\kappa)\right\} \qquad (4)$$

where $F(\kappa)$ is some structure factor, $\overline{M}$ is the effective mass from the Sachs-Teller mass tensor and $2r = 1.12$ Å is the O-C distance. In Eq. (4) the mass difference of O and C atoms has been neglected.

It is seen that for $\kappa\to 0$ the term $[\ldots]$, the incoherent scattering, disappears. The coherent term, however, remains finite as the structure factor $F(\kappa)$ will approach the same value as the well-known liquid structure factor $1+\gamma(\kappa)$. For small κ, $F(\kappa)$ may be assumed to be constant and given by the difference of the isothermal and adiabatic compressibility. Under this assumption the solid curve in Fig. 4 represents Eq. (4) for $\omega = 0$ after folding with a resolution function $\exp[-(\hbar\omega)^2/\Delta^2]$ with $\Delta = 0.77$ meV) and with $F(\kappa)$ and $\overline{M}$ as fitting parameters. $\overline{M}$ turned out to be 0.84 M, where M is the molecular mass. For entirely free molecules one expects $\overline{M} = 0.60$ M, for fixed centres of masses with free rotations $\overline{M} = 1.50$ M. Figure 5 represents a phonon dispersion $\omega(q)$ for liquid CO, obtained by subtracting from the experimental data the calculated inelastic scattering due to free rotations.

The broken curve in Fig. 4 represents the scattering for $\omega = 0$ as a function of κ, calculated with the hydrodynamic theory of Mountain [9], that is, assuming the elastic peak to be broadened by heat conductivity,

$$S_{coh}(\kappa,\omega) = \frac{1}{\pi}\,\rho\, k_B T\, \chi_s\left\{\left(\frac{c_p}{c_v}-1\right)\frac{D_T\kappa^2}{\omega^2+(D_T\kappa^2)^2}\right.$$

$$\left.+\frac{1}{2}\Gamma\kappa^2\left[\frac{1}{(\omega+c\kappa)^2+(\Gamma\kappa^2)^2}+\frac{1}{(\omega-c\kappa)^2+(\Gamma\kappa^2)^2}\right]\right\}$$

(5)

where ρ is the mass density, χ_s the adiabatic compressibility,

$$D_T = \frac{\lambda}{\rho\, c_p}$$

$$\Gamma = \frac{1}{2}\left[\frac{1}{\rho}\left(\frac{4}{3}\,\eta + \zeta\right) + D_T\left(\frac{c_p}{c_v} - 1\right)\right]$$

λ is the heat conductivity, η and ζ are the first and second viscosity, respectively. A best fit to the experimental data was obtained with the following values : $c_p/c_v = 1.91$, $c_p = 14.41$ cal/degree mole, $\lambda = 1.87 \times 10^{-4}$ cal/cm sec degree, $(4/3\,\eta + \zeta) = 1.41 \times 10^{-3}$ poise, $c = 1200$ m/sec, $\rho = 0.80$ g cm^{-3}. With these values a rather good fit, better than the one for $\omega = 0$, could be obtained for the inelastic scattering data (see Fig. 3). Not all these values, however, agree with the ones determined macroscopically. c_p/c_v, c and ζ are unknown for liquid CO. For the heat conductivity and for the first viscosity, macroscopic measurements have given $\lambda = 3.55 \times 10^{-4}$ cal/cm sec degree, $\eta = 1.92 \times 10^{-3}$ poise [13]. Two different values of the sound velocity in liquid N_2 are given; $c = 866$ m/sec [7] and $c = 1044$ m/sec [15, 16].

This discrepancy with respect to the transport coefficients may indicate that for the wavelengths and frequencies relevant to the neutron experiment, hydrodynamics with frequency independent coefficients are no longer valid, although the hydrodynamic criterion for the existence of phonons [8] is fulfilled:

$$(D_T \kappa^2)^2 \ll c^2 \kappa^2$$

The hydrodynamic theory of Kadanoff and Martin [8] gives less good agreement. Their theory could be fitted to the experimental data only by assuming $c \gtrsim 1500$ m/sec.

The experimental results can be described approximately with free rotations as well as with hydrodynamics. It seems likely that both dynamical processes contribute. A determination of the relative amount of the contributions should be possible by Brillouin scattering experiments on a monatomic liquid of similar c_p/c_v, for instance Ne. Such experiments are planned.

ACKNOWLEDGEMENTS

The authors wish to thank Professor Dr. T. Springer for his continuous support, Dr. Th. Plesser for many helpful discussions and Mr. F. Fredel for his assistance with the experiments.

REFERENCES

[1] EGELSTAFF, P.A., AERE Rep. N/R 1164 (1953).

[2] KROÓ, N., BORGONOVI, G., SKÖLD, K., LARSSON, K.-E., Inelastic Scattering of Neutrons in Solids and Liquids (Proc. Symp. Bombay, 1964) 2, IAEA, Vienna (1965) 101.

[3] DORNER, B., PLESSER, Th. and STILLER, H.H., The Structure and Properties of Liquids, Disc. Faraday Soc. 43 (1967) 160.

[4] MIKA, K., Phys. Stat. Sol. 21 (1967) 279.

[5] VEGARD, L., Z. Phys. 88 (1934) 235.

[6] JORDAN, T.H., SMITH, H.W., STREIB, W.E., LIPSCOMB, W.N., J. chem. Phys. 41 (1964) 756.

[7] ROWLINSON, J.S., Liquids and Liquid Mixtures, Butterworths Scientific Publications, London (1959).

[8] KADANOFF, L.P., MARTIN, P.C., Ann. Phys. 24 (1963) 419.

[9] MOUNTAIN, R.D., Rev. mod. Phys. 38 (1966) 205.

[10] VINEYARD, G.H., Phys. Rev. 110 (1958) 999.

[11] CINI CASTAGNOLI, G., Physica 30 (1964) 953.

[12] LARSSON, K.-E., Roy. Inst. of Techn. Stockholm, to be published in Phys. Rev.

[13] JOHNSON, V.J., Properties of Materials at Low Temperatures (Phase 1), Pergamon Press, Oxford (1961).

[14] KRIEGER, T.J., NELKIN, M.S., Phys. Rev. 106 (1957) 290.

[15] KAYE, G.W., LABY, T.H., Tables of Physical and Chemical Constants, Longmans, Green and Co., London, New York, Toronto (1959) 62.

[16] TEUTSCH, H., MATEESCU, N., NAHORNIAK, V., DIACONESCU, A., Phys. Lett. 22 (1966) 558.

HIGH-ENERGY EXCITATIONS IN LIQUID HELIUM

A.D.B. WOODS AND R.A. COWLEY
ATOMIC ENERGY OF CANADA LTD.,
CHALK RIVER, ONT., CANADA

Abstract

HIGH-ENERGY EXCITATIONS IN LIQUID HELIUM. The scattering of neutrons from liquid helium at 1.1°K has been studied by use of a rotating crystal spectrometer and a triple-axis crystal spectrometer. Measurements were made at both larger energy and momentum transfers than in earlier experiments where the existence of phonons and rotons was demonstrated. An additional ill-defined excitation branch was found at momentum transfers, Q, of less than $2\mathrm{Å}^{-1}$. Its intensity was comparable with that of the phonon branch, its mean energy was almost constant at about 24°K and its full-width at half height was approximately equal to its energy. At larger momentum transfers the mean energy of this excitation increased and, above $3\mathrm{Å}^{-1}$, was almost the free particle energy, $\hbar^2Q^2/2M$. The width of this scattering increased, on average, linearly with Q, up to the limit to the measurements, $9\mathrm{Å}^{-1}$, and in magnitude was consistent with an independent particle model and McMillan's ground state wave function of liquid helium. Additional structure was also observed in the width, however, and this possibly arises from the creation of vortex rings.

The experiments described in this paper are part of a continuing program to study the excitations in liquid helium. A review of the work up to 1965 and references to earlier work have been given previously [1]. At that time measurements of the one-phonon excitation had been carried out to a momentum of $3.8\ (\mathrm{Å})^{-1}$. However, at that momentum, most ($\gtrsim$ 98% beyond $3.36\ (\mathrm{Å})^{-1}$) of the scattering occured at higher energies than the one-phonon excitation. It was the object of the experiments reported here to determine the nature of that scattering.

The scattering at large momentum has also been the subject of some theoretical interest by Miller, Pines and Nozieres [2] and more recently by Hohenberg and Platzman [3]. The scattering at large momentum and energy transfers yields information about the response of the liquid at small distances and short times. An independent particle model is then likely to be a good approximation. A free helium atom with momentum $\hbar\vec{p}$ has an energy of $\hbar^2p^2/2M$, where M is the mass of the helium atom. If a neutron is scattered by this atom with momentum transfer $\hbar\vec{Q}$, the momentum of the helium atom is $\hbar(\vec{p} + \vec{Q})$ and its energy is $\hbar^2|\vec{p} + \vec{Q}|^2/2M$. The energy transfer to the helium atom is then

$$\frac{\hbar^2}{2M}\ (Q^2 + 2\vec{p}.\vec{Q})\,.$$

The scattering cross-section $S(\vec{Q},\omega)$ is then proportional to

$$\sum_{\vec{p}} n(\vec{p})\ \delta\left(\hbar\omega - \frac{\hbar^2}{2M}\ (Q^2 + 2\vec{p}.\vec{Q})\right), \qquad (1)$$

where $\hbar\omega$ is the energy transfer and where $n(\vec{p})$ is the initial momentum distribution of the helium atoms.

On this model a measurement of an energy distribution at fixed momentum transfer yields a direct measurement of the momentum distribution, $n(\vec{p})$. Of particular interest is that in the superfluid state there is expected to be a macroscopic occupation of the zero momentum state. This leads to a sharp peak in the energy distribution at an energy of $\hbar^2Q^2/2M$, superimposed on a broad distribution resulting from the non-zero momentum components. A measure of the relative intensity of these two components provides a direct measure of $n(0)$. As pointed out by Hohenberg and Platzman [3] however this theory is no doubt too simple, because it neglects the scattering of the excited particle. This scattering will tend to broaden both the whole distribution and the sharp peak which might arise from the zero momentum component.

Most of the experiments were conducted with the rotating crystal spectrometer at Chalk River [4]. The monochromator planes (220), (331) and (511), enabled measurements to be made out to a momentum transfer of 6 $(\text{Å})^{-1}$. Two typical distributions are shown in Fig. 1. The improvement in these results over those obtained earlier [1] is largely due to the modifications described in ref. [4].

The distributions shown in Fig. 1 were obtained by subtracting a flat background (arising from fast neutrons) from the time of flight spectrum of a particular detector and then converting them to an energy distribution. As the energy varies so the momentum transfer varies but the change in the momentum transfer across the distributions is quite small; for example for the distribution shown in the lower part of Fig. 1, energy transfers of 125°K and 225°K correspond to 5.52 $(\text{Å})^{-1}$ and $5.15(\text{Å})^{-1}$. Hence it is reasonable to treat these distributions as having approximately a constant momentum transfer.

Measurements at larger momentum transfers to 9 $(\text{Å})^{-1}$ were made with a triple axis crystal spectrometer in its constant $|\vec{Q}|$ mode of operation. The results are very similar, when corrected for the experimental resolution, as shown in the region of overlap of the measurements in Fig. 2. In all, extensive measurements have been made at 1.1°K and 4.2°K and measurements at a few momentum transfers at intermediate temperatures.

The distributions shown in Fig. 1 are broad but peaked distributions with a width much greater than the experimental resolution. They are also almost symmetric in energy about their maxima. The centres of the peaks for momenta beyond 2.8 $(\text{Å})^{-1}$, where the one-phonon part of the scattering is negligible, are very close to the free particle energy, $\hbar^2Q^2/2M$. The widths of the peaks at 1.1°K are shown in Fig. 2.

It is of interest to compare these results with the predictions of the independent particle model. The centres of the peaks are in excellent agreement with the model. The model also predicts that the width of the distributions should be

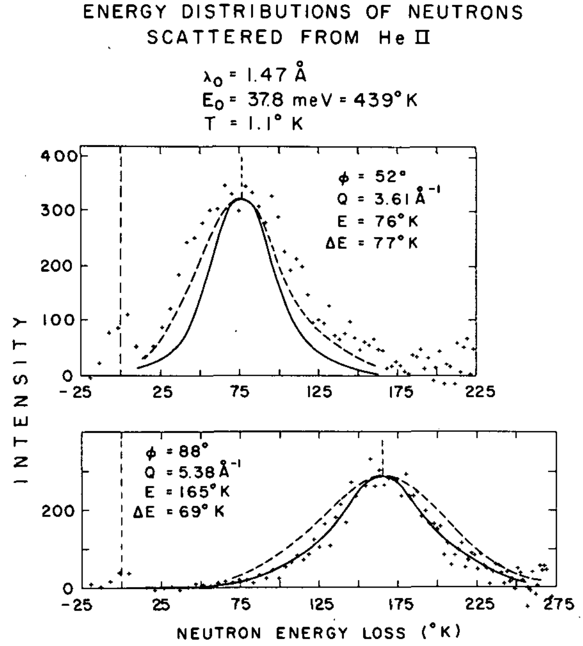

FIG.1. Two scattered neutron distributions obtained with the rotating crystal spectrometer. The solid and dotted curves are the distributions calculated with n(0) = 0.11 and n(0) = 0 respectively, and with the wave function of Ref. [5] for the other particles.

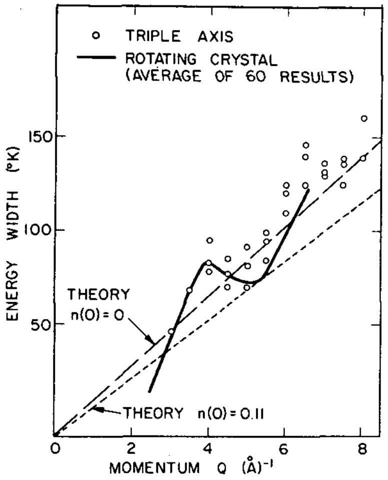

FIG.2. The full width at half height of the distributions obtained with the rotating crystal spectrometer, solid line, and triple-axis crystal spectrometer, open circles. The theoretical curves are for the same calculations as Fig.1.

proportional to the momentum transfer, $\vec{Q}$. This is in qualitative agreement with the experimental results, but not in detailed agreement.

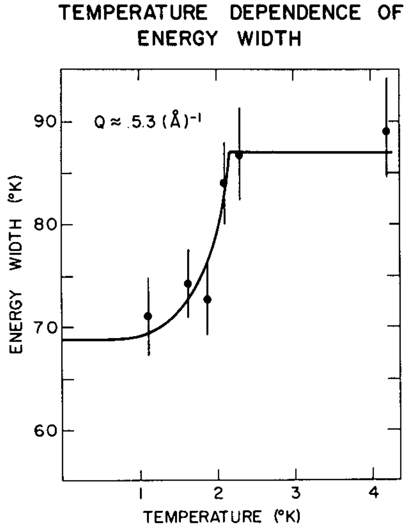

FIG. 3. The full width at half height of the distributions with momentum transfer of 5.38 $\mathrm{\AA}^{-1}$. The solid curve is calculated assuming n(0) is temperature dependent in the same way as the superfluid density.

More quantitative calculations of the model can be made by substituting McMillan's calculations [5] of $n(\vec{p})$ into Eq. 1. Although Realto and Chester [6] have shown his wavefunction to be inadequate at small momenta the difference is insignificant for our purposes.

The results of two calculations are shown in Figs. 1 and 2. In one calculation we assume $n(0) = 0$, and in the other $n(0) = 0.11$ [5] and the n(0) peak is broadened to about one third of the width of the main peak. At a momentum transfer of 5.38 $(\mathrm{\AA})^{-1}$ the former calculation gives a width which is significantly larger than the experimental results, while the latter calculation gives excellent agreement with experiment. At a momentum transfer of 3.61 $(\mathrm{\AA})^{-1}$ both calculations are significantly narrower than the experimental results.

These calculations suggest that most of the width at a momentum transfer of 5.38 $(\mathrm{\AA})^{-1}$ arises from the initial momentum distribution of the helium atoms, and that the peak from the zero momentum state is smeared out by the collisions of the excited atom. The smearing is of the same order of magnitude as that estimated by Hohenberg and Platzman [3], although possibly somewhat larger in detail.

In order to test further the above description of the scattering with a momentum transfer of 5.38 $(\mathrm{\AA})^{-1}$, the temperature dependence of the width was measured shows a marked increase near the λ-point as shown in Fig. 3. The theoretical calculation is based on the temperature dependence expected for the n(0) contribution assuming that the distribution of the remainder of the atoms remains unchanged with temperature. The agreement is clearly very satisfactory and strongly supports both the above description of the scattering and McMillan's wave function for the ground state [5].

There is one further feature which is as yet unexplained. This is the increase in the width of the distributions for momentum transfers near 3.5 $(\text{Å})^{-1}$ and 6.5 $(\text{Å})^{-1}$. One possible explanation of these increases is that the excited helium atoms at these energies have just the energy required to create small vortex rings of one and then two quanta of circulation. The energy of the excited helium atoms at the start of the increases in width are about 50°K and 200°K respectively which are in reasonable agreement with the energy of small vortex rings about 3 Å in radius [7].

These experiments have shown the existence of single particle like excitations in liquid helium and that they behave in a manner predicted by an independent particle model. The width of the distributions at some momentum transfers near 5.5 $(\text{Å})^{-1}$ is in agreement with that expected from calculations of the ground state wavefunction [5]. Unfortunately the scattering of the excited atoms is sufficiently large that no peak from the condensate was observed at 1.1°K. However measurements of the temperature dependence of the width suggest that n(0) is about 10% of the particles at 1.1°K. The experiments also suggest that the scattering of the excited particles shows some resonances at certain energies, possibly these arise from the spontaneous creation of small vortex rings by the excited atoms.

ACKNOWLEDGEMENTS

The authors are very grateful for the invaluable technical assistance of E.A. Glaser, R. Dutkiewicz, R. Campbell, and A. Betts. One of us (R.A.C.) is grateful for helpful discussions and comments from colleagues, especially G. Chester, at the Laboratory of Atomic and Solid State Physics where it was his pleasure to be a visitor.

REFERENCES

[1] WOODS, A.D.B., "Quantum Fluids", Ed. BREWER, D.F., North Holland, Amsterdam (1966).

[2] MILLER, A., PINES, D., NOZIERES, P., Phys. Rev. 127 (1962) 474.

[3] HOHENBERG, P.C., PLATZMAN, P.M., Phys. Rev. 152 (1966) 198.

[4] GLASER, E.A., WOODS, A.D.B., COWLEY, R.A. (this conference) and BROCKHOUSE, B.N., "Inelastic Scattering of Liquids from Solids and Liquids", IAEA, Vienna (1961) 113.

[5] McMILLAN, W.L., Phys. Rev. 138 (1965) A442.

[6] REALTO, L., CHESTER, G.V., Phys. Rev. 155 (1967) 88.

[7] CHESTER, G.V. (private communication).

DISCUSSION

O.K. HARLING: I should like first to congratulate Messrs Wood and Cowley on this work, which may represent the first experimental evidence for the existence of a Bose condensate. One could wish that there were many more equally fundamental experiments which could be undertaken with present neutron scattering techniques.

I have two or three questions for Mr. Cowley. First, should not the areas under both theoretical curves in Fig. 1 be equal, since the total particle density is a constant?

R.A. COWLEY: What you say is quite correct, but the point is that the curves in Fig. 1 were normalized to peak height, not to the areas.

O.K. HARLING: Thank you. What were the running times and the sample transmission percentages?

R.A. COWLEY: Sample transmission was about 92%. The sample was made up as a cylinder, of length much greater than the diameter, and with cadmium sheets inside, located at 3/8-in. intervals, intended to reduce the multiple scattering in the vertical direction. The typical running times on the rotating crystal spectrometer were about one week for each angle.

O.K. HARLING: As shown in Fig. 2, there is still some evidence for collective modes of excitation. Would not this indicate that the momentum transfers which you used may still be too low to permit the study of the momentum distribution of single helium particles?

R.A. COWLEY: Measurements at larger momentum transfers would be very useful but difficult. We believe, however, that we have reached the region in which the independent-particle model is valid.

W. GISSLER: For your expression for the scattering correction you have neglected the coherence effect; helium is a coherent scatterer. Could this neglect influence the width of your peak?

R.A. COWLEY: We do not think so, as we are dealing with high energy and momentum transfers for which a single-particle model is appropriate. S(q) is very close to unity at the momentum transfers of the experiment.

B. MOZER: Is your resolution time-of-flight resolution, or energy resolution of the incoming beam, or both?

R.A. COWLEY: The instrumental resolution is about 10% of the width studied, and arises both from the uncertainties in time of flight and from the mosaic spread of the monochromator.

INVESTIGATION OF THE DYNAMICAL PROPERTIES OF LIQUID-GAS SYSTEMS BY COHERENT COLD NEUTRON SCATTERING NEAR THE CRITICAL POINT

L. BATA AND N. KROÓ
CENTRAL RESEARCH INSTITUTE FOR PHYSICS,
HUNGARIAN ACADEMY OF SCIENCES,
BUDAPEST, HUNGARY

Abstract

INVESTIGATION OF THE DYNAMIC PROPERTIES OF LIQUID-GAS SYSTEMS BY COHERENT NEUTRON SCATTERING NEAR THE CRITICAL POINT. Inelastic coherent neutron scattering was chosen because of the relatively higher momentum transfers involved for the investigation of the dynamic behaviour of liquids in the critical region where $Q >> 1$. The critical state of the CO_2 and CS_2 samples was first confirmed by elastic cold neutron scattering measurements, carried out at small angles (1.5°, 2°, 2.5°). The scattered intensities at fixed angles as a function of temperature exhibited maxima at the critical point due to density fluctuations. To study the dynamics of these fluctuations inelastic neutron scattering measurements were performed in a wide angular region, keeping the values of Q_{el} smaller than that of the first diffraction peak and varying the temperature from room temperature to critical and higher. The results are explained in terms of the hydrodynamic approximation at small momentum transfer, as due to scattering by isobaric and adiabatic density fluctuations, characteristic of the dynamics of the critical state.

1. INTRODUCTION

In recent years considerable attention has been paid to critical phenomena. Inelastic neutron scattering has become a successful tool in these studies. In fact, our knowledge of the critical fluctuations in magnetic systems is based mainly on neutron scattering results [1]. It seems therefore reasonable to extend neutron scattering investigations to critical phenomena in liquid-gas systems. The critical region can be characterized by $Q\xi >> 1$. Here Q stands for the momentum transfer and ξ for the characteristic correlation length of the critical fluctuations [2].

For the time being no model is available which could be used for describing the neutron scattering in the critical region. However, it is expected that in the case of $Q\xi \ll 1$ the scattering function of the isobaric and adiabatic density fluctuations can be expressed in terms of the hydrodynamic model as

$$S^{coh}(Q,\omega) = \frac{1}{R^2(\kappa^2+Q^2)}\left\{\frac{C_p-C_v}{\pi C_p}\,\frac{D_T Q^2}{\omega + (D_T Q^2)^2} + \frac{C_v}{\pi C_p}\left[\frac{\Gamma Q^2}{(\Gamma Q^2)^2+(\omega+cQ)^2}+\frac{\Gamma Q^2}{(\Gamma Q^2)^2+(\omega-cQ)^2}\right]\right\} \tag{1}$$

where R is a length slowly varying with temperature and density [3], κ^{-1} is the two-body correlation length, C_p and C_v are the values of the specific heat at constant pressure and volume, respectively. D_T is the heat diffusion coefficient, c is the velocity of sound, Γ is a coefficient inversely proportional to the lifetime of the sound modes, depending on the shear and bulk viscosities of the system [4].

Even if this model does not hold near the critical temperature T_c and for large values of Q, i.e. if $Q\xi \gg 1$, it may serve as a qualitative guide for the following reasons. Sound modes are expected to exist in the critical region, the dispersion relation $\omega_Q = cQ$ is thought to be still valid, the lifetime Γ^{-1} of the sound modes must be finite and there should exist also isobaric density fluctuations. Moreover, the temperature dependence of the total scattered intensity could be also described by Eq. (1) on introducing at large values of Q instead of the term $\{R^2(\kappa^2 + Q^2)\}$ some function s(Q, T), representing the dependence of the total scattered intensity on scattering angle and temperature.

2. EXPERIMENTAL

The experiments were performed on critically loaded CO_2 and CS_2 samples. The transmission for CO_2 was 94%, that for CS_2 85%. CO_2 was chosen because its thermodynamic constants near the critical point have been already determined [5] and CS_2 because it is liquid at room temperature and can be thus conveniently investigated over a wide range of temperatures. Each sample is a pure coherent neutron scatterer.

The critical points were determined in CO_2 from small-angle (1.5°, 2°, 2.5°) scattering experiments using Be-filtered cold neutrons and a small-angle scattering spectrometer. For CS_2 neutrons of $\lambda = 1.15$ Å wavelength and a neutron diffractometer were used.

The inelastic scattering data observed at different temperatures and angles were measured with the time-of-flight spectrometer described in Ref. [6].

For the interpretation of data, $\epsilon = T - T_c/T_c$ was considered instead of the absolute temperature near the critical point. The critical behaviour of the system was observed in the $10^{-2} \leq \epsilon \leq 10^{-1}$ region.

3. RESULTS AND DISCUSSION

Figure 1a shows the critical behaviour exhibited by the cold neutron scattering in CO_2 at small angles with Q = 0.034, 0.046 and 0.058 Å^{-1}. A similar type of temperature dependence was observed in CS_2, (Fig. 1b) for $Q_0 = 0.28$ Å^{-1}. The same effect appears over a wide range of momentum transfer for values of Q smaller than that corresponding to the first diffraction peak. This region is shown in Fig. 2 for CS_2. The inelastic neutron spectra were studied in the momentum transfer region marked by the arrow. The changes in intensity are thought to be due to density fluctuations.

At room temperature, for scattering angles $\vartheta < 40°$ the width of the quasi-elastic spectra increases with increasing angles, while for angles $\vartheta > 40°$ the width of the quasi-elastic spectra decreases owing to the de Gennes [7] narrowing effect. The measured width of the spectra is much smaller than the value predicted from the hydrodynamic approximation

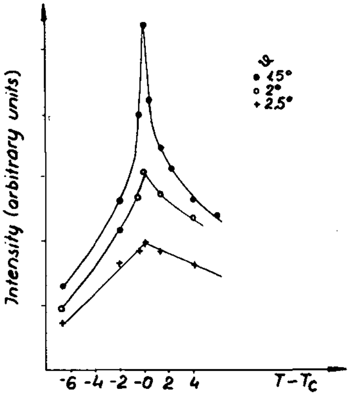

FIG.1a. Critical scattering of Be-filtered cold neutrons by CO_2. Temperature dependence of intensity at different scattering angles.

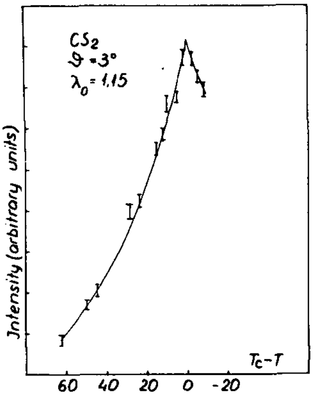

FIG.1b. Temperature dependence of scattered neutrons with λ_0 = 1.15 Å by CS_2 at $\vartheta = 3°$ scattering angle.

taking into account only the heat diffusion process and the classical value [8] of the heat diffusion coefficient, i.e. $D_T = 1.26 \times 10^{-3}$ cm²/sec. The fit of the model yields $D_T = (1.4 \pm 0.3) \times 10^{-4}$ cm²/sec.

The scattering spectra exhibit, in addition to the quasi-elastic, an adjacent, apparently inelastic contribution which can be explained by the presence of sound modes with dispersion relation $\omega_Q = cQ$, called Brillouin-Mandelstamm modes in the hydrodynamic model. The velocity of ultrasound measured in CS_2 at room temperature as 1.5×10^{-5} cm/sec [9] is in good agreement with the inelastic maxima in the spectra observed at different angles.

At higher temperatures, near the critical point the velocity of sound decreases to the order of $C \approx 1 \times 10^4$ cm/sec and the Brillouin peak appears very close to the central (quasi-elastic) line even at great angles, as seen in Fig. 3 in the spectrum taken at $\vartheta = 50°$. At $\epsilon = 0.04$ the width of the spectra increases rapidly (as Q^2) with increasing angle up to $\vartheta = 26°$, for $\vartheta > 26°$ the width continues to change more slowly (Fig. 4). The values of the half height are marked on the curves by arrows. The solid lines show simple Lorentzians [1] folded with the ingoing spectrum using the

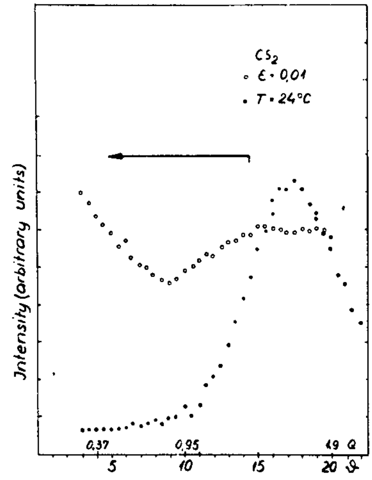

FIG.2. Angular distribution of elastically scattered neutrons from CS_2 sample at room temperature and when $\epsilon = 0.01$. Neutron wavelength $\lambda_0 = 1.15$ Å.

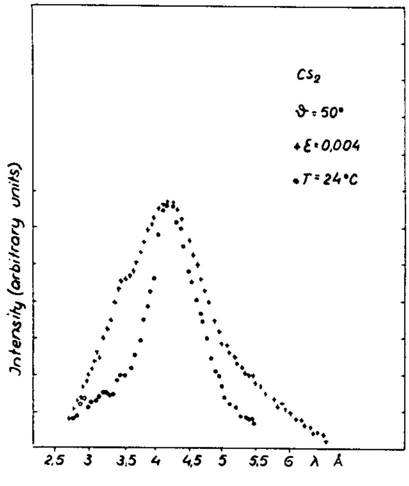

FIG.3. The scattered neutron spectra on CS_2 at room temperature and near to critical point.

largest reasonable values of D_T. This curve gives for the heat diffusion coefficient at $\vartheta = 20°$, $D_T(\epsilon = 0.04) = 3 \times 10^{-4}$ cm^4/sec. It is clearly apparent from the figures that a Lorentzian scattering function cannot describe the measured spectra because it cannot account for the inelastic contributions appearing in the spectra at positions varying with the scattering angle. This inelastic contribution can be interpreted from both scattering on sound modes described by the hydrodynamic model and the relation $\omega_Q = CQ$.

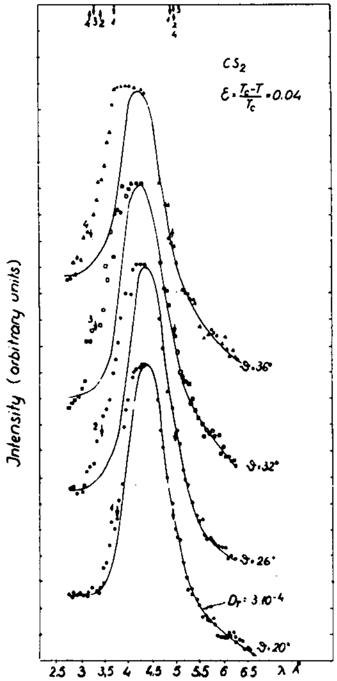

FIG.4. Inelastically scattered neutron spectra on CS_2 at $\epsilon = 0.04$ and various angles. The solid lines in the figure indicate the folding of in-going spectra with Lorentzian scattering function when $D_T = 3 \times 10^{-4}$ cm²/sec at $\vartheta = 20°$ and $D_T = 4 \times 10^{-4}$ cm²/sec in other cases. The arrows show the positions of the measured half-width values at various angles.

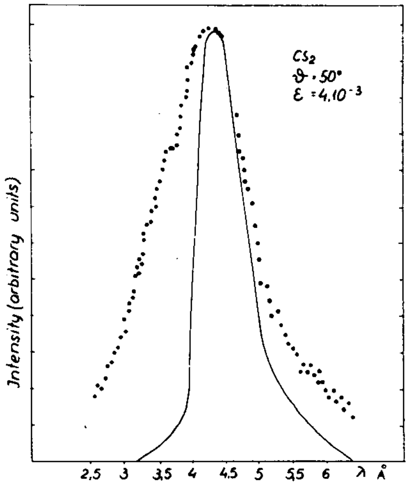

FIG.5. The measured scattered neutron spectra near to critical point with $\epsilon = 4 \times 10^{-3}$ and the calculated one with $D_T = 10^{-5}$ cm²/sec.

If the classical Van der Waals equation were valid near the critical point, the heat diffusion constant would have the form

$$D_T = \frac{\lambda_0}{\rho_c TR} \left\{ |T - T_c| + \frac{3}{4} T_c \left(\frac{V - V_c}{V_c} \right)^2 \right\} \tag{2}$$

where λ_0 is the coefficient of heat conduction, ρ_c is the critical density, R is the universal gas constant and V is the specific volume. Using the value of $D_T = 10^{-5}$ cm^2/sec at $\epsilon = 0.004$ calculated from Eq. (2), the heat diffusion contribution to Eq. (1) is shown along with the measured spectrum in Fig. 5. The clearly apparent great discrepancy in the region of large Q can be explained, at least partially, by the scattering sound modes. Unfortunately the values of c, C_v, C_p and Γ near T_c are not known and the contribution from the sound modes in Eq. (1) cannot be evaluated.

The value of c around T_c in CO_2 is known [10]. As an example of the CO_2 runs, the measurements at 60° are to be seen in Fig. 6. Qualitatively the same effects were observed as in the case of CS_2. The positions of the sound peaks shift towards smaller energies if $\epsilon \to 0$, in agreement with the reported data [10]. The horizontal bars in the figure indicate

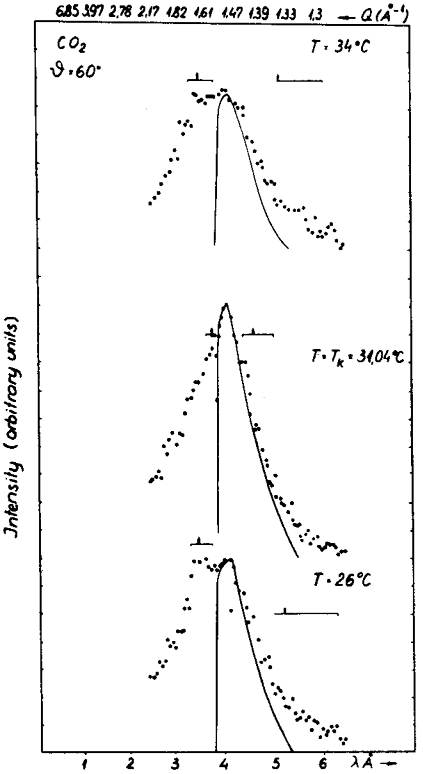

FIG. 6. The inelastically scattered neutron spectra at $\vartheta = 60°$ at various temperatures and $\epsilon = 1 \times 10^{-3}$, $\epsilon = 1.3 \times 10^{-4}$ and $\epsilon = 1.6 \times 10^{-3}$. The solid lines in the figure indicate the ingoing spectrum, the arrows the positions of the Brillouin scatterings.

the full width at half height for infinite lifetime of sound modes. The measured distribution is seen to be definitely broader. The narrowing of the central line near T_c should be also observed. This indicates a decrease in D_T near the critical temperature.

CONCLUSIONS

It is seen that the scattering spectra measured at different angles cannot be described by a simple Lorentzian function. The large inelastic contributions observed near the quasi-elastic spectra can be explained by the presence of sound modes considered in terms of the proposed hydrodynamic approximation as Brillouin modes. The inelastic contribution varies with the scattering angle as defined by the relation $\omega_Q = cQ$ and exhibits the same temperature dependence as that of the sound velocity, c.

The comparison of the observed inelastic contribution with the adiabatic term in Eq. (1) could not be performed since the separation of the isobaric and adiabatic spectra seems to be extremely difficult without any satisfactory theory and sufficiently reliable thermodynamic data (specific heat, viscosity, thermal conductivity, velocity of sound etc.).

ACKNOWLEDGEMENTS

Authors are indebted to Professor L. Pál for his continued interest in the measurements and to Dr. Cs. Hargitai for useful discussions and to Dr. É. Kisdi-Koszó, for writing the programmes.

REFERENCES

[1] JACROT, B., KONSTANTINOVIC, I., PARETTE, G., CRIBIER, D., Inelastic Scattering of Neutrons in Solids and Liquids (Proc. Symp. Chalk River, 1962) 2, IAEA, Vienna (1963) 317.

[2] HALPERIN, B.I., HOHENBERG, P.C., Phys. Rev. Lett. 19 (1967) 700.

[3] Van HOVE, L., Phys. Rev. 95 (1954) 249; 1374.

[4] LANDAU, L.D., LIFSITZ, E.M., Fluid Mechanics, Pergamon Press (1959).

[5] MICHELS, A., Physica 28 (1962) 1216.

[6] BATA, L., KISDI, É., KROÓ, N. PÁL, L., Internal KFKI Rep. 2/1966.

[7] De GENNES, P.G., Physica 25 (1959) 825.

[8] VINEYARD, G.H., Phys. Rev. 110 (1958) 999.

[9] FABELINSKII, I.L., Molekularnoje Rassejanie Sveta "Nauka", Moscow (1965).

[10] Handbuch der Physik, 11 1, Springer-Verlag, Berlin (1961) 190.

DISCUSSION

O.J. EDER: Did you evaluate the thermal diffusion coefficient as a function of temperature, and does the result agree with Cummins' LASER scattering data?

N. KROÓ: Yes, we did study the temperature dependence of D_T but our results do not agree with those obtained from classical measurements.

We have not compared our data with those from Cummins' LASER experiments.

B. DORNER: One normally speaks of Brillouin scattering only if κ lies inside the Brillouin zone around $\tau = 0$. At scattering angles of 50° or 60° and with an incoming wavelength of 4 Å I believe that you are outside the Brillouin zone around $\tau = 0$. Inside that zone Brillouin scattering occurs only if the velocity of the incoming neutrons is higher than the sound velocity in the sample, at least when the experiments are performed involving neutron energy loss. Outside the zone this restriction no longer applies.

N. KROÓ: I agree. We have seen the Brillouin scattering in the zone around $\tau = 0$, and I may perhaps mention in addition that $\tau \neq 0$ scattering could also be observed. It is of course correct that the Brillouin scattering could be seen only under conditions of energy gain due to the restriction in question. It is precisely for this reason that we performed all these measurements in neutron energy gain, and not in loss.

T. SPRINGER: You performed measurements at temperatures very close to T_c, where the correlation length is large (100Å or so). Interpreting your peak as you have done, may one infer the existence of collective modes with a wavelength much smaller than the correlation length of the critical fluctuations?

N. KROÓ: Yes, one may.

P. SCHOFIELD: Is it certain, in your diffusion measurements, that the scattering is still incoherent, and that the increase in S (κ) does not give a coherent contribution?

N. KROÓ: Yes, I think it is. The angular distribution of the quasi-elastically scattered neutron intensity does not exhibit the behaviour characteristic of coherent critical scattering.

RELAXATION SPECTROSCOPY IN LIQUIDS

C.J. MONTROSE AND T.A. LITOVITZ
THE CATHOLIC UNIVERSITY OF AMERICA,
WASHINGTON, D.C., UNITED STATES OF AMERICA

Abstract

RELAXATION SPECTROSCOPY IN LIQUIDS. Ultrasonic measurements are sensitive to those molecular motions which contribute to the relaxation of stress. These are related to rearrangement of the liquid structure and generally involve displacement of the molecules' centres of mass. Dielectric relaxation and depolarixed light scattering experiments, on the other hand, permit observation of rotational motions about the molecules' centres of mass. The aim of this review is to explore the interrelationships among these various relaxation processes.

The observed distributions of dielectric relaxation times can be accounted for by assuming that the ultrasonically determined structural relaxation time characterizes the 'environmental memory' of a molecule in the liquid and is therefore a rate-determining step in the dielectric relaxation process. The ratio of dielectric to structural relaxation times τ_D/τ_p is the critical parameter in determining the width of the dielectric distribution. This same idea is also used to relate the magnitudes of τ_D and the relaxation time associated with depolarized Rayleigh scattering, τ_{OR}, to the nature of the molecular reorientation mechanism in a liquid. Molecular reorientation is assumed to proceed by a series of angular steps, the size of the steps being determined by the environmental life-time τ_p. When $\tau_D \gg \tau_p$ the steps are small and the reorientation is described by simple rotational diffusion; when τ_D and τ_p become comparable, the angular steps increase and the mechanism approaches jump reorientation. It appears that in a liquid the structural relaxation time plays a role analogous to the time between collisions in a gas, insofar as it gives the basic environmental correlation time, fundamental to all the diffusional motions of a molecule.

1. STRUCTURAL RELAXATION IN LIQUIDS

The structure of liquids, in contrast to that of crystalline solids, lacks long-range order and, in addition, the short-range order that does exist is imperfect. Because the degree of order changes under an applied stress, the liquid exhibits a compressibility which contains a structural contribution β_r. Further because this structural change is not instantaneous, the compressibility is found to decrease with increasing frequency from a low-frequency value β_0 to a high-frequency limit β_∞. These values differ by the relaxational or structural compressibility β_r, that is, $\beta_0 = \beta_r + \beta_\infty$.

In an ultrasonic or Brillouin scattering experiment the quantity measured is a complex frequency dependent modulus $K_c(\omega)$. Depending upon the details of the experiment, this may be either the bulk or shear modulus or some combination of these. These moduli are related to the Fourier-Laplace transform of the appropriate stress correlation function [1, 2]. For example, the complex bulk modulus is given by

$$K_c(\omega) = K(\omega) + i\omega\eta_v(\omega) = K_0 + \frac{i\omega}{VkT}\int_0^\infty dt\, e^{-i\omega t}\langle J(0)\,J(t)\rangle \qquad (1.1)$$

where $K(\omega)$ and $\eta_v(\omega)$ are the frequency-dependent bulk modulus and viscosity; $K_0 = \beta_0^{-1}$ is the static bulk modulus, V is the volume of the system, k is Boltzmann's constant, T is the temperature and J is the mean normal stress. The brackets $\langle \cdots \rangle$ denote an ensemble average over the initial states of the system.

If the stress correlation function decays exponentially in time then we obtain $K_c(\omega)$ in the form [3]

$$K_c(\omega) = K(\omega) + i\omega\eta_v(\omega) = K_0 + K_r \frac{\omega^2\tau_v^2}{1+\omega^2\tau_v^2} + i\,K_r \frac{\omega\tau_v}{1+\omega^2\tau_v^2} \qquad (1.2)$$

where τ_v is the structural relaxation time at constant volume and $K_r = \beta_r/\beta_0\beta_\infty$ is the relaxational contribution to the modulus. The behaviour of $K(\omega)$ is illustrated in Fig. 1(a). In some circumstances it is useful to discuss a complex compressibility $\beta_c(\omega) = K_c(\omega)^{-1}$, in which case the appropriate relaxation time is $\tau_p = (\beta_0/\beta_\infty)\tau_v$, the relaxation time at constant pressure. Observe from Eq. (1.2) that the volume or bulk viscosity η_v is given by

$$\eta_v = \lim_{\omega \to 0} \eta_v(\omega) = K_r\tau_v = \beta_r\tau_p/\beta_0^2 \qquad (1.3)$$

An equation similar to Eq. (1.2) can also be written for the complex shear modulus. At low frequencies, we find, in analogy with Eq. (1. 3), that $\eta_s = G_\infty \tau_s$ where η_s is the shear viscosity, G_∞ is the high frequency shear rigidity and τ_s is the shear relaxation time.

In practice it often turns out that an exponential stress correlation function, and therefore Eq. (1.2) does not adequately represent the data [4]. This can be seen by comparing the two curves in Fig. 1(a). In such cases the results can be described in terms of a distribution of relaxation times $g(\tau)$. Equation (1.3) and the analogous equation for η_s are still valid except that τ_v, τ_p and τ_s must now be interpreted as average relaxation times.

Experimentally it is found that shear and bulk processes are closely related. In such diverse liquids as metals, oxides, molten salts and organic compounds one finds that [3]

$$\tau_v \approx \tau_s; \qquad \eta_v \approx \eta_s; \qquad K_r \approx G_\infty \qquad (1.4)$$

This is interpreted as indicating that similar molecular motions and similar structural rearrangements are involved in relieving either a shear or bulk strain.

We must next inquire as to the microscopic significance of the relaxation times τ_v, τ_p and τ_s. Since even in the Brillouin scattering experiment one is observing liquid behaviour on a scale greater than 1000 Å, it is not obvious that these relaxation times reflect molecular time scales. That they do, in fact, characterize motions on a microscopic scale is indicated by the comparison of τ_p values with residence times τ_r (determined by quasi-elastic neutron scattering) shown in Table I. The similarity of the values indicates that τ_p is indeed characteristic of elementary diffusive motions in liquids.

It has been remarked that, in general, the stress correlation function is non-exponential; a single relaxation time is not sufficient to describe

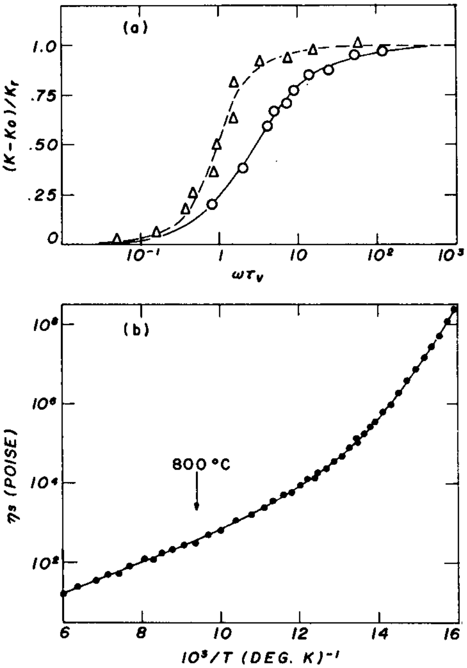

FIG.1. (a) the reduced bulk modulus for B_2O_3 at 650°C (O) and above 800°C (Δ); the dashed curve is from Eq.(1-2). (b) The variation of η_s with T in B_2O_3(data from Refs [7] and [14]).

TABLE I. COMPARISON OF STRUCTURAL RELAXATION TIMES WITH DIFFUSIVE RESIDENCE TIMES IN LIQUIDS

Liquid	T(°C)	$\tau_p(10^{-12}$ sec)	$\tau_r(10^{-12}$ sec)
Water	1	4.3[a]	3.1[b]
	25	2.0[a]	2.0[b]
1-Propanol	- 10	18 [13]	11.2[c]
	-100	15000 [13]	580[c]
Sodium	100	3[d]	1.0[e]

[a] SLIE, W.M., DONFOR, A.R., LITOVITZ, T.A., J. chem. Phys. 44 (1966) 3712.

[b] SAFFORD, G.J., NAUMANN, A.W., SCHAFFER, P.C., A Neutron Scattering Study of Water and Ionic Solutions, Tech. Rep. Union Carbide Corporation, Tuxedo, N.Y. (1967).

[c] LARSSON, K.-E., QUEROZ do AMARAL, L., IVANCHEV, N., RIPEAUNU, S., BERGSTEDT, L., DAHLBORG, U., Phys. Rev. 151 (1966) 126. These authors quote two relaxation times, one they call the hydrogen bond life-time, the other the mean time between intramolecular rotational jumps. We have quoted the former time here.

[d] Estimated from the data of JARZYNSKI, J., LITOVITZ, T.A., J. chem. Phys. 41 (1964) 1290 by assuming β_r is given by the difference between liquid and solid compressibilities at the melting temperature.

[e] Data of Cocking and Randolph as quoted by EGELSTAFF, P.A., Rep.Progr.Phys. 29 (1966) 33.

experimental results. We must, therefore, ask what are the factors that govern the distribution of relaxation times. Litovitz and co-workers [5, 6] observed that in liquids where single relaxation behaviour was found, the viscosity exhibited an Arrhenius temperature dependence $\eta_s \sim \exp(H^*/RT)$. In liquids where distributions of relaxation times were found, the viscosity was non-Arrhenius. To test the hypothesis that this correlation was not accidental, Litovitz and Macedo [7] studied molten B_2O_3, a liquid where the viscosity shows non-Arrhenius behaviour only below 800°C as shown in Fig. 1(b). From Fig. 1(a) it is apparent that the correlation is real. Above 800°C single relaxation behaviour was measured, while at lower temperatures a distribution of relaxation times was found.

While this indicates that distributed correlation functions and non-Arrhenius viscosity behaviour probably have a common explanation, of itself it does not provide that explanation. However, the latter effect has been accounted for by various authors [8, 9] who point out that for a molecule to move, a certain local free volume must be present. If the liquid structure is relatively close-packed, co-operative molecular motions are needed to attain this free volume. Since the required degree of co-operation is temperature dependent, a non-Arrhenius viscosity results. These same co-operative effects imply that the probability of a diffusive step, which depends upon the instantaneous environment of a molecule, can vary in time. This leads to a non-exponential structural break-up and thus to a distribution of relaxation times.

2. DIELECTRIC RELAXATION IN LIQUIDS

The application of an electric field tends to orient the permanent dipole moments of molecules in a liquid producing a net polarization; when the field is removed the polarization decreases to zero. This process is termed dielectric relaxation and is characterized by a relaxation time τ_D. Debye [10] has pointed out that a close relationship exists between viscosity and τ_D as is evidenced by their similar temperature dependences. In view of this, we shall consider together the reorientational motion performed by the dipole and the process by which a structural rearrangement occurs.

Similar to the structural relaxation situation, it is found that certain liquids exhibit a distribution of dielectric relaxation times and others a single relaxation time [11-13]. To account for this, McDuffie and Litovitz [6] suggest that regions of short-range order exist in the liquid and that these are continually breaking up and reforming. This structural break-up is co-operative and does not generally follow a simple rate process. Molecular rotation cannot take place except during those times when the structure is randomized. Thus the structural relaxation time becomes a rate-determining parameter in the dielectric relaxation process.

Table II lists structural and dielectric relaxation parameters for several liquids. Notice that in every liquid $\tau_D/\tau_p > 1$ in accordance with the McDuffie-Litovitz proposal that τ_p is rate-determining. Observe also that in all cases a distribution of structural relaxation times was found but that in two liquids a single dielectric time was observed. The structural distributions are, in fact, always broader than the dielectric ones. This and the fact that the dielectric distribution is narrowest for larger values of τ_D/τ_p are explained as follows: When $\tau_D \approx \tau_p$, the co-operative aspects of the structural break-up

TABLE II. STRUCTURAL AND DIELECTRIC RELAXATION PARAMETERS FOR SEVERAL LIQUIDS
Unless otherwise noted, the data are from Ref. [3].

Liquid	τ_D/τ_p	Dielectric distribution width[a]	Structural distribution width[a]
Glycerol	1.5	4.0	100
2-Methyl Pentanediol 2, 4	2.5	2.4	4.2
Butanediol 1, 3	4.2	2.4	9.0
1-Octanol	55[b]	1.0[c]	4[b]
1-Propanol	88 [13]	1.0 [13]	10 [13]

[a] The width is defined here as the ratio of the frequencies where the dielectric constant or compressibility has fallen by 90% to the frequency where it has fallen by 10%. The case of single relaxation is normalized to unity.

[b] MONTROSE, C.J., unpublished data.

[c] MacGREGOR, D., M.S. Dissertation, Catholic University of America (1966).

are reflected in the dielectric behaviour in that a distribution of dielectric times is observed; however, when τ_D is significantly larger than τ_p the co-operative details of the structural process are averaged out and a narrow dielectric distribution results.

Experimental support of this idea was obtained by Kono, McDuffie and Litovitz [13] who studied the dielectric distribution in mixtures of glycerol and 1-propanol. In this system the ratio τ_D/τ_p could be varied from near one to almost 100 by changing the propanol content. The results of their measurements are plotted in Fig. 2. The dielectric distribution does indeed narrow as τ_D/τ_p is increased.

To explain why $\tau_D \gg \tau_p$ in 1-propanol, Kono et al. [13] assumed that both relaxation times were given by an expression exp $(H^*/RT + V^*/V_f)$, as suggested by Macedo and Litovitz [14]. In this expression H^* is the activation energy associated with local structure and is assumed the same for both structural and dielectric processes. V_f is the local free volume and V^* is the critical local volume needed for flow or reorientation. By assuming that dielectric and structural processes involve rotations about different molecular axes, one can easily reason that in essentially ellipsoidal molecules the critical free volume needed for dipolar reorientation V_D^* is greater than that for structural rearrangements V_S^*.

3. DISCUSSION OF MOLECULAR REORIENTATION

3.1. General theory

Because of this interpretation in terms of different molecular motions or rotations, it is appropriate to consider the reorientational motion of molecules in a liquid. We assume that the liquid is composed of rigid mole-

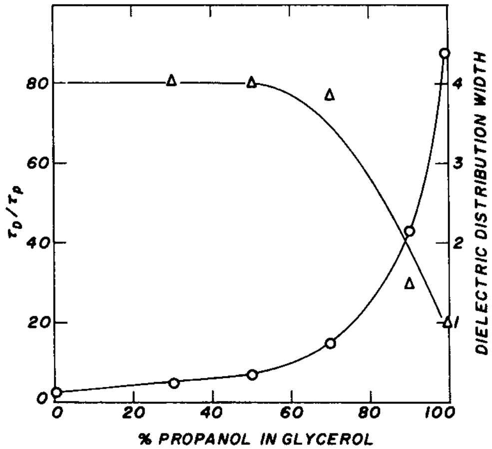

FIG. 2. The ratio τ_D/τ_p (O) plotted against mole% 1-propanol in glycerol at -60°C. The points (Δ) show the variation in the dielectric distribution width with propanol content (data from Ref.[13]).

cules. Let the vector $\vec{R}$ locate the centre of mass of a molecule and let $\vec{R}+\vec{r}$ locate a second point within the molecule, $\vec{r}$ being fixed with respect to the molecule. We define a quantity $f(\vec{\Omega}_0, \vec{\Omega}, t)\, d\vec{\Omega}_0\, d\vec{\Omega}$ as the probability that the direction of $\vec{r}$ lies within $d\vec{\Omega}_0$ about $\vec{\Omega}_0$ at time t=0 and within $d\vec{\Omega}$ about $\vec{\Omega}$ at time t. For an isotropic liquid $f(\vec{\Omega}_0, \vec{\Omega}, t)$ depends only upon the angle between $\vec{\Omega}_0$ and $\vec{\Omega}$ and can therefore be expanded as

$$f(\vec{\Omega}_0, \vec{\Omega}, t) = (1/4\pi) \sum_{\ell=0}^{\infty} \sum_{m=-\ell}^{\ell} Y_{\ell m}(\theta_0, \varphi_0)^* \, Y_{\ell m}(\theta, \varphi) f_\ell(t) \tag{3.1}$$

where the $f_\ell(t)$ are time correlation functions independent of m and where the angles (θ_0, φ_0) and (θ, φ) characterize the directions of $\vec{\Omega}_0$ and $\vec{\Omega}$ respectively. The only conditions imposed on $f(\vec{\Omega}_0, \vec{\Omega}, t)$ are that it be bounded and single valued. We require the normalization $1 = \int d\vec{\Omega}_0 \int d\vec{\Omega}\, f(\vec{\Omega}_0, \vec{\Omega}, t)$ and the initial value $f(\vec{\Omega}_0, \vec{\Omega}, 0) = (1/4\pi)\,\delta(\vec{\Omega}_0 - \vec{\Omega})$. The orientational behaviour of a molecule is then completely specified by the functions $f_\ell(t)$.

To understand the general nature of these functions, it is useful to consider a specific of molecular reorientation. Perhaps the simplest such model is to assume simple rotational diffusion. In this case $f(\vec{\Omega}_0, \vec{\Omega}, t)$ satisfies the differential equation

$$D_r \left\{ \frac{1}{\sin\theta} \frac{\partial}{\partial\theta} \left(\sin\theta \frac{\partial}{\partial\theta} \right) + \frac{1}{\sin^2\theta} \frac{\partial^2}{\partial\varphi^2} \right\} f = \frac{\partial f}{\partial t} \tag{3.2}$$

where D_r is the coefficient of rotational diffusion. The solution to Eq.(3.2) is easily obtained and the $f_\ell(t)$ are then evaluated. We find

$$f_\ell(t) = \exp\{-\ell(\ell+1) D_r t\} + \exp\{-t/\tau_\ell\} \tag{3.3}$$

The spectral distribution of these functions $\sigma_\ell(\omega)$ are given by the Fourier cosine transform

$$\sigma_\ell(\omega) = (1/\pi)\frac{\ell(\ell+1)D_r}{\ell^2(\ell+1)^2 D_r^2 + \omega^2} = (1/\pi)\frac{\tau_\ell}{1+\omega^2\tau_\ell^2} \qquad (3.4)$$

for $\ell \geqq 1$. The spectra are Lorentzian lines centred at $\omega = 0$ of half widths $\Gamma_\ell = 1/\tau_\ell = \ell(\ell+1)D_r$. Thus for simple diffusion a plot of Γ_ℓ versus $\ell(\ell+1)$ yields a straight line of slope D_r. This is analogous to the situation in translational diffusion where simple diffusion leads to spectra of half width $D\kappa^2$ [15]. For rotational diffusion the angular momentum $\ell(\ell+1)$ appears in place of the linear momentum κ^2.

3.2. Dielectric relaxation

In the dielectric relaxation experiment one observes the reorientation of permanent molecular dipoles $\vec{p}$ whose motion we shall assume to be the same as that of the entire molecule. The interaction of the dipoles with the imposed electric field $\vec{E}$ is given by $-pE\cos\theta$ so that in the dielectric relaxation experiment one observes the time correlation function, $F_D(t) = \langle\cos\theta(t)\cos\theta(0)\rangle$, given by

$$F_D(t) = \int d\vec{\Omega}_0 \int d\vec{\Omega}\, f(\vec{\Omega}_0, \vec{\Omega}, t)\cos\theta\cos\theta_0 \qquad (3.5)$$

Using Eq.(3.1) in this and recognizing that $\cos\theta = P_1(\cos\theta)$ gives (to within a multiplicative constant) $F_D(t) = f_1(t)$. Thus dielectric relaxation measurements allow one to pick out and observe the time dependence of the $\ell = 1$ term in $f(\vec{\Omega}_0, \vec{\Omega}, t)$.

3.3. Depolarized light scattering

In the depolarized light scattering experiment again the effects of molecular rotation are significant. Light of a given linear polarization illuminates the sample and the scattered light is observed to have components of polarization both parallel and perpendicular to the polarization of the incident beam. Because the scattering can be thought of as radiation from the dipoles induced by the incident beam, it follows that if the molecular polarizability tensor is isotropic (i.e. a scalar), then only scattered light with the polarization characteristic of the incident beam is observed. On the other hand, if the polarizability is anisotropic, a depolarized component will be observed. Moreover, the frequency spectrum of this depolarized light will be related to the molecular rotation.

In the case where the molecule exhibits one symmetry axis, its polarizability tensor α depends only upon two independent parameters which we shall take to be its eigenvalues α_1 and α_2. In this case the scattered field, which is governed by the induced dipole moment $\alpha \cdot \vec{E}$, where $\vec{E}$ is the incident field, exhibits separately the behaviour of the isotropic polarizability $(\frac{1}{3}\,\mathrm{Tr}\,\alpha)$ and of the anisotropic part $(\alpha_1 - \alpha_2)$. This latter part gives contributions to the induced dipole moment parallel and perpendicular to the incident field which are proportional to $(\alpha_1-\alpha_2)(\cos^2\theta - \frac{1}{3})$ and $(\alpha_1 - \alpha_2)\,e^{\pm i\varphi}\sin\theta\cos\theta$

respectively. We recognize these as second-order spherical harmonics so that the frequency spectrum of the scattered light is governed by time correlation functions

$$F_{OR}(t) = \langle Y_{2m}\{\theta(t)\varphi(t)\}^* Y_{2m}\{\theta(0)\varphi(0)\}\rangle \qquad (3.6)$$

These are calculated as

$$F_{OR}(t) = \int d\vec{\Omega}_0 \int d\vec{\Omega} f(\vec{\Omega}_0, \vec{\Omega}, t)\, Y_{2m}(\theta, \varphi)^* Y_{2m}(\theta_0, \varphi_0) \qquad (3.7)$$

With the help of Eq. (3.1) we obtain $F_{OR}(t) = f_2(t)$. Therefore depolarized light scattering allows observation of the $\ell = 2$ terms in $f(\vec{\Omega}_0, \vec{\Omega}, t)$.

3.4. Inelastic neutron scattering

Incoherent neutron scattering is, of course, also sensitive to the effects of molecular rotation. In this case the appropriate time correlation function is that part of the intermediate scattering function related to the rotational motion of a molecule about its centre of mass. Sears [16] has shown this to be

$$\mathscr{Y}(\vec{\kappa}, t) = \sum_{\ell=0}^{\infty} (2\ell+1)\,[j_\ell(\kappa r)]^2 f_\ell(t) \qquad (3.8)$$

where the j_ℓ are the spherical Bessel functions. Equation (3.8) means that incoherent neutron scattering measures all of the Legendre components in $f(\vec{\Omega}_0, \vec{\Omega}, t)$. It is therefore difficult to extract the functions $f_\ell(t)$ from the neutron data especially as the scattered spectrum includes contributions from motion of the molecules' centres of mass as well as coherent scattering.

4. ORIENTATIONAL RELAXATION IN LIQUIDS

Very little information is available on orientational relaxation as determined by the method of Rayleigh scattering [17]. Pinnow, Candau and Litovitz started a systematic investigation of orientational relaxation in liquids [18]. This included the alkyl-bromides having linear chains from 2 to 16 carbon atoms in order to explore effects of increasing molecular volume. In addition, measurements were made in the polyethylene glycols as well as 1-octanol, butanediol 1,3 and glycerol.

Typical depolarized spectra are shown in Fig. 3. The scattered light consists at each temperature of a single line centred about the incident laser frequency. The width of this line was interpreted as a reciprocal orientational relaxation time $1/\tau_{OR}$ and τ_{OR} was found to increase with increasing chain lengths. Also for each liquid the relaxation time increased as the temperature was lowered. Over the limited temperature range measured the data fit the Arrhenius form $\tau_{OR} = A \exp(H^*/RT)$.

A feature of the data as shown in Fig. 4 is the nearly linear behaviour of the logarithm of the orientational relaxation times versus the number of

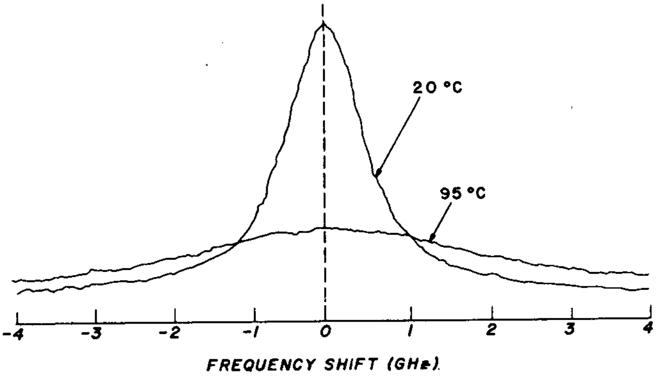

FIG. 3. Typical depolarized spectra taken in bromododecane at two temperatures.

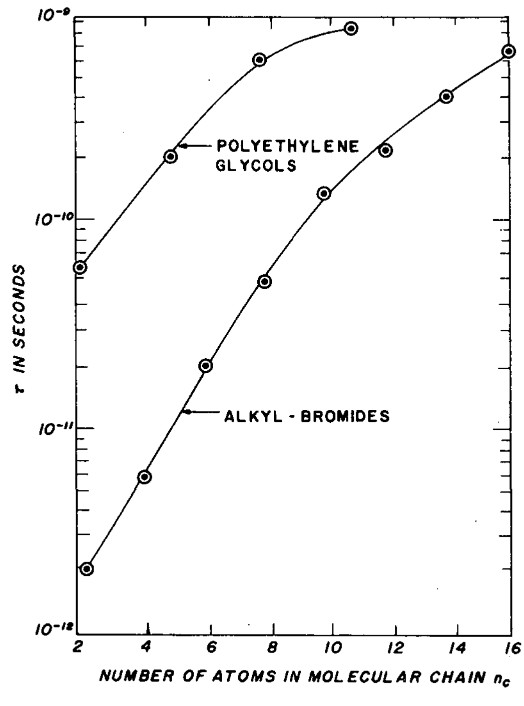

FIG. 4. The variation of τ_{OR} with the number of atoms in the molecular chain at 25°C for two homologous families of liquids.

atoms, n_c which is assumed to be roughly proportional to the molecular length L. The initial slopes for the two families are nearly the same, even though the type of bonding in the liquids varies greatly. This linear behaviour persists up to $n_c \approx 8$ where an apparent saturation begins. This saturation effect is due to the inexactness of the assumption that the number of atoms in a molecular chain is proportional to its length. Recent X-ray measurements of alkyl-bromide end-to-end distances L [19], indicate that

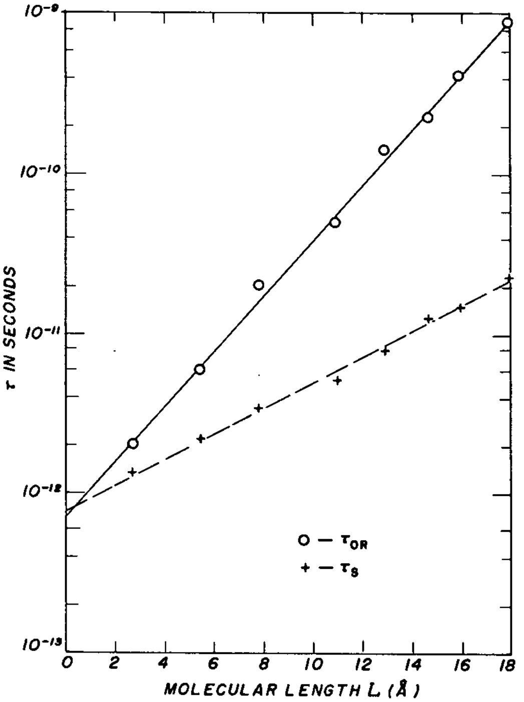

FIG. 5. Chain-length dependence of orientation and shear relaxation times of the alkyl-bromides at 25°C.

while for small molecules L is directly proportional to n_c; for larger molecules folding of the chain limits L. When the logarithm of the relaxation times are plotted against the actual chain lengths, the linear plot of Fig. 5 results. This linear variation can be accounted for by the free volume model proposed by Doolittle [20] and extended by Macedo and Litovitz [14]. In this model the relaxation time is determined by the combined probability of (1) breaking directed bonds such as the hydrogen or bromine bond, and (2) having sufficient local free volume to accomplish the desired molecular motion. Thus one writes, as in section 2,

$$\tau_{OR} = \tau_0 \exp\{H^*/RT + (V^*/V_f)\} \qquad (4.1)$$

where τ_0 is a constant equal to h/kT according to classical rate theory [21]. The free volume $V_f = V_m - V_0$, where V_m and V_0 are the average molecular volume at temperature T and 0°K respectively. The variation of τ_{OR} with chain length is associated with changes in (V^*/V_f) since V^* clearly increases with n_c. Doolittle [20] using PVT data has evaluated $\delta V_0/\delta n_c$ and has shown that as a function of n_c, V_0 changes much more rapidly than V_f. Pinnow et al. [18] have shown that $\delta V^*/\delta n_c$ for the alkyl bromides is nearly the same as $\delta V_0/\delta n_c$ for the normal alkanes. This indicates that for orientational motion the minimum local excess free volume V^* approximately equals the molecular volume V_0. The intercept values of τ_{OR} (i.e. $V^* = 0$) are determined only by τ_0 and H^*. Thus, for example, the intercept of τ_{OR} for the glycols is 30 times greater than that for the alkyl-bromides reflecting the stronger H-O...H bond relative to the Br...H bond.

It is instructive to compare the shear and orientational relaxation times. The values of τ_s are plotted in Fig. 5. It is evident that the slope of the τ versus L curves is greater for the orientational time. This result is consistent with the hypothesis (section 2) accounting for the fact that $\tau_D \gg \tau_p$ in 1-propanol.

This discussion suggests that orientational relaxation involves rotation of the total molecule about a minor axis. Assuming, as in propanol, that the shear flow involves a motion about a major axis, then V^*_{OR} should be greater than V^*_s which would predict that $\tau_{OR}/\tau_s > 1$, as actually observed in Fig. 5. The fact that τ_{OR} and τ_s have the same intercept in this figure (within the uncertainties in estimating τ_s) is consistent with the idea that both shear and orientational motion require the same H^* to break the end bonds, but that different volumes are swept out in the course of the motion.

5. MECHANISM OF REORIENTATION

In this section we use a comparison of the $\ell = 1$ (dielectric) and $\ell = 2$ (orientational) terms in $f(\vec{\Omega}_0, \vec{\Omega}, t)$ to obtain further insight into the nature of the molecular reorientation process. We do this by considering another model for reorientation, and examining its predictions concerning the various $f_\ell(t)$. We have seen that the simple diffusion model predicts that

$$\tau_1/\tau_2 = \tau_D/\tau_{OR} = 3 \tag{5.1}$$

Experimental deviations of this ratio from the value 3 mean that this simple idea is inadequate. Simple diffusion can occur only when the angular displacements are large enough to include several diffusive steps. Since the dielectric relaxation experiment involves the loss of correlation of the first-order Lengendre polynomial, a rotation of approximately 68° is required for $\langle P_1\{\cos\theta(t)\}\, P_1\{\cos\theta(0)\}\rangle$ to fall to e^{-1} its initial value. Similarly since orientational relaxation involves the $\ell = 2$ terms, a rotation of 39° is required for $\langle Y_{2m}\{\theta(t)\varphi(t)\}^*\, Y_{2m}\{\theta(0),\varphi(0)\}\rangle$ to fall by e^{-1}. This means that for simple diffusion to be an accurate description of the motion (at least for $\ell = 1$ or 2), the average angular step must be much less than 39°. For larger diffusive steps (or higher values of ℓ) we must use some more sophisticated model of rotational diffusion which takes into account the nature of the angular steps. We shall consider what is essentially a jump rotational diffusion model. The basic considerations are: (1) a molecule in a liquid oscillates about an equilibrium orientation which remains unchanged for a residence time τ_r; (2) the molecule is then suddenly displaced through an angle ϵ to a new equilibrium orientation; (3) molecular reorientation occurs by a repetition of these steps. The rotational motion of a molecule is therefore to be treated as an angular random walk problem. Ivanov [22] has considered just such a random walk problem and has found that $f_\ell(t) = \exp(-t/\tau_\ell)$ where τ_ℓ is given by

$$\frac{1}{\tau_\ell} = \frac{1}{\tau}\left\{1 - \frac{1}{2\ell+1}\int_0^{\pi} d\epsilon\, w(\epsilon)\, \frac{\sin(\ell+1/2)\epsilon}{\sin(\epsilon/2)}\right\} \tag{5.2}$$

$w(\epsilon)\,d\epsilon$ is the probability that an angular jump will be in the range ϵ to $\epsilon + d\epsilon$ and τ is the average time between jumps. We have evaluated this assuming a random distribution of jump angles

$$w(\epsilon) = w_0 \exp(-\epsilon/\theta_0) \tag{5.3}$$

where w_0 is a constant ensuring normalization and θ_0 is a parameter. For $\ell = 1$ we obtain

$$\frac{1}{\tau_1} = \frac{2}{3\tau}\left\{\theta_0^2 - 2\left(e^{\pi/\theta_0} - 1\right)^{-1}\right\}\Big/\left\{1+\theta_0^2\right\} \xrightarrow[\theta_0 \to 0]{} \frac{2\theta_0^2}{3\tau} \tag{5.4}$$

and the ratio τ_1/τ_2 as a function of θ_0 is given by

$$\frac{\tau_1}{\tau_2} = 3\,\frac{\dfrac{1+8\theta_0^2}{5} - e^{-\pi/\theta_0}\left(\dfrac{8\theta_0^2}{5} + \dfrac{13}{5} + \dfrac{2}{5\theta_0^2}\right)}{(1+4\theta_0^2) - e^{-\pi\theta_0}\left(4\theta_0^2 + 3 + \dfrac{2}{\theta_0^2}\right)} \approx \frac{3}{5}\,\frac{5+8\theta_0^2}{1+4\theta_0^2} \tag{5.5}$$

the expression on the far right holding to better than 3% for $\theta_0 \leq \pi$. These expressions can also be given in terms of the average jump angle $\bar{\epsilon}$ which is related to θ_0 by

$$\bar{\epsilon} = \theta_0 - \pi/(e^{-\pi/\theta_0} - 1) \xrightarrow[\theta_0 \to 0]{} \theta_0 \tag{5.6}$$

The ratio τ_1/τ_2 in Eq. (5.5) falls from the value 3 in the $\theta_0 = 0$ limit to a value 1.2 in the limit $\theta_0 \to \infty$ (in terms of $\bar{\epsilon}$ these limits correspond to $\bar{\epsilon} = 0$ and $\bar{\epsilon} = \pi/2$ respectively). This behaviour is illustrated in Fig. 6. It is therefore possible to use the combined dielectric and depolarized light scattering results to evaluate the average jump angle in the molecular reorientation process.

As they stand these results cannot be used to predict values of τ_1/τ_2 since $\bar{\epsilon}$ is not known a priori. To proceed further we must ask for more information concerning those factors which determine the size of the reorientational steps. In this context we again consider the McDuffie-Litovitz hypothesis advanced earlier in connection with the origin of the distributed dielectric correlation function. The breaking up and reforming of the local liquid structure is now pictured as a fluctuation in the local free volume. Molecular reorientation is assumed to occur only when the local structure has been sufficiently randomized, that is, when the fluctuation has supplied sufficient local free volume. When this occurs the molecule reorients more or less freely until the liquid structure re-forms (the critical local volume needed for reorientation disappears) at which time the motion is stopped. It must then wait for the next fluctuation to occur. The size of the angular step is therefore determined by the relative magnitudes of the 'free' rotation rate, while the structure is randomized and the rate at which this randomization occurs. If the randomized state persists for a comparatively long time, $\bar{\epsilon}$ will be large and so-called 'jump' reorientation takes place. If the randomized state is relatively short-lived, then small angular steps result and the simple diffusion limit is approached. The parameter

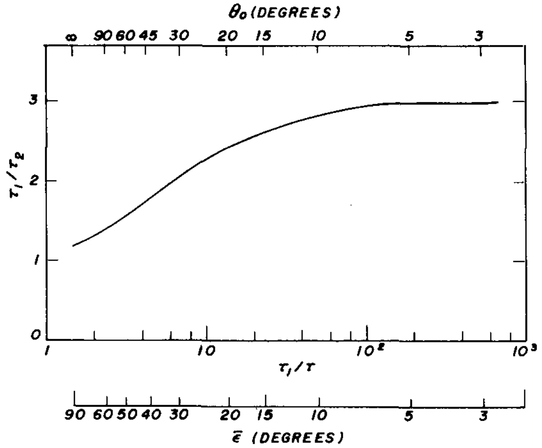

FIG. 6. The variation of the ratio τ_1/τ_2 with θ_0, $\bar{\epsilon}$ and τ_1/τ_2.

TABLE III. COMPARISON OF EXPERIMENTAL AND CALCULATED VALUES OF τ_1/τ_2

Liquid	$(\tau_D/\tau_p)^a$	(τ_D/τ_{OR}) exp [18]	(τ_1/τ_2) calc.
1-Octanol	55	3.0	2.92
Butanediol 1, 3	4.2	1.8	1.74
Glycerol	1.5	1.0	1.2

[a] See Table II.

which then governs the size of the average jump angle $\bar{\epsilon}$ is now τ_{rot}/τ where τ_{rot}^{-1} is the rotational speed of the molecule in transit and τ, the average time between jumps, is now interpreted as characterizing the rate of structural randomization in the liquid. To characterize the rotational speed we shall use τ_1 instead of τ_{rot} simply because this latter parameter is experimentally inaccessible. We propose, further, that the quantity τ is simply the average relaxation time for volume fluctuations at constant pressure (see section 1), that is, we assume that $\tau = \tau_p$. The ratio τ_1/τ_2 is now given in terms of τ_1/τ or equivalently τ_D/τ_p by combining Eqs (5.4) and (5.5). For τ_1/τ values of greater than about 3 we have to better than a few per cent

$$\frac{\tau_1}{\tau_2} \approx 3\,\frac{(\tau_1/\tau) + 9/10}{(\tau_1/\tau) + 9/2} \qquad (5.7)$$

The exact result of τ_1/τ_2 versus τ_1/τ is plotted in Fig. 6.

From Table III, in which we have shown three liquids in which adequate orientational, dielectric and structural relaxation data are available, the agreement is seen to be quite reasonable. This is especially the case when we realize that the quantities τ_p, τ_D and τ_{OR} are all subject to experimental uncertainties of the order of 10%. There is one inconsistency in this view: Independent of the ratio τ_1/τ we have obtained exponential correlation functions $f_\ell(t)$, while earlier we related this ratio to the existence of distributed correlation functions. This is a result of directly applying Ivanov's [22] formula, Eq. (5.2), which tacitly assumes a single structural relaxation time.

In conclusion the following picture emerges. It appears that in a liquid the structural relaxation time plays a role analogous to that of the time between collisions in a gas. Physically the analogy holds in that these times characterize the time scale over which the environment of a molecule remains essentially unchanged. Alterations in this environment (structural break-up in a liquid, collisions in a gas) effect a loss of memory of the molecule of its previous dynamic state. In this picture all those diffusional modes of motion involving the molecule as a unit are closely connected with this environmental memory time.

REFERENCES

[1] ZWANZIG, R., A.Rev.phys.Chem. 16 (1965) 67.

[2] MONTROSE, C.J., SOLOVYEV, V.A., LITOVITZ, T.A., J.acoust.Soc.Am. 43 (1968) 117.

[3] LITOVITZ, T.A., DAVIS, C.M., "Structural and shear relaxation in liquids", Physical Acoustics 2A (MASON, W.P., Ed.), Academic Press, New York (1965) 282.

[4] HERZFELD, K.F., LITOVITZ, T.A., Absorption and Dispersion of Ultrasonic Waves, Academic Press, New York (1959).

[5] GRUBER, G., LITOVITZ, T.A., J.chem. Phys. 40 (1964) 13.

[6] McDUFFIE, G.E., LITOVITZ, T.A., J. chem. Phys. 37 (1962) 1699.

[7] MACEDO, P., LITOVITZ, T.A., Phys. Chem. Glasses 6 (1965) 69.

[8] WILLIAMS, M., LANDEL, R., FERRY, J., J.Am. chem. Soc. 77 (1955) 3701.

[9] BUECHE, F., J. chem. Phys. 30 (1959) 748.

[10] DEBYE, P., Polar Molecules Dover, New York (1945).

[11] LITOVITZ, T.A., McDUFFIE, G.E., J. chem. Phys. 39 (1963) 729.

[12] DENNEY, D.J., COLE, R.H., J. chem. Phys. 23 (1955) 1767.

[13] KONO, R., LITOVITZ, T.A., McDUFFIE, G.E., J. chem. Phys. 45 (1966) 1790.

[14] MACEDO, P.B., LITOVITZ, T.A., J.chem. Phys. 42 (1965) 245.

[15] SJÖLANDER, A., "Theory of neutron scattering by liquids", Thermal Neutron Scattering (EGELSTAFF, P.A., Ed.), Academic Press, New York (1965).

[16] SEARS, V.F., Can.J. Phys. 44 (1966) 1299.

[17] The only published data is that of STARUNOV, V.S., Optics Spectrosc. 18 (1965) 165 and ZAITSEV, G.I., STARUNOV, V.S., Optics Spectrosc. 19 (1965) 497.

[18] PINNOW, D.A., CANDAU, S.J., LITOVITZ, T.A., J. chem. Phys. (to be published).

[19] BRADY, G.W., WASSERMAN, E., WELLENDORF, J., J. chem. Phys. 47 (1967) 855.

[20] DOOLTTTLE, A.K., J. appl. Phys. 22 (1951) 1471.

[21] EYRING, H., EYRING, E.M., Modern Chemical Kinetics,Reinhold, New York (1963).

[22] IVANOV, E.N., Sov. Physics JETP 18 (1964) 1041.

DISCUSSION

K.-E. LARSSON: During your oral presentation you stated that one is justified in assuming that the reorientational and centre-of-gravity motions are not coupled. Is there any experimental or other evidence for this statement?

T.A. LITOWITZ: This is not too easy to answer, but certainly I can say that if there is any coupling, it is not a serious factor from the experimental point of view.

S. YIP: Regarding the question whether one can assume that translations and rotations are approximately separable in liquids, I think that we can learn a good deal from computer molecular dynamics experiments. Such calculations are at present being carried out at Columbia University for diatomic liquids such as CO, and we can expect to hear the results in the near future.

J.G. POWLES: I believe that the large ratio of the dielectric relaxation time to the structural relaxation time may be due at least partially to the fact that the molecules are flexible, and so it is possible that the heavy or strongly-interacting dipolar end of the molecule reorients slowly, while the rest of the chain can move more rapidly by some approximation to link motion. This possibility could of course be readily checked by nmr, and a start on this was made some years ago for n-octyl bromide and n-octyl alcohol (Proc. phys. Soc. 75 (1960) 617).

SYMPOSIUM ON NEUTRON INELASTIC SCATTERING

HELD AT COPENHAGEN, 20-25 MAY 1968

CHAIRMEN OF SESSIONS

Session A	W. HÄLG	Switzerland
	J. ALS-NIELSEN	Denmark
	Yu.M. KAGAN	Union of Soviet Socialist Republics
SessionsB	P.K. IYENGAR	India
	J.L. YARNELL	United States of America
Session C	A.G. SJÖLANDER	Sweden
	R.D. LOWDE	United Kingdom
Session D	D. JOVIĆ	Yugoslavia
	T. RISTE	Norway
Special Session	H. MAIER-LEIBNITZ	Federal Republic of Germany

SECRETARIAT OF THE SYMPOSIUM

Scientific Secretary	J. DILNICAR	Division of Research and Laboratories, IAEA
Administrative Secretary	H.H. STORHAUG	Division of Scientific and Technical Information IAEA
Editor	C.N. WELSH	Division of Publications, IAEA
Records Officer	N.W.A. JONES	Division of Languages, IAEA

AUTHOR INDEX

Arabic numerals underlined refer to the first page of a paper.
Other Arabic numerals refer to a contribution to the discussions.
This index refers only to Volume I, a complete index
for both volumes will be found at the back of Volume II.

TRANSLITERATION INDEX

Бровман Е.Г.	Brovman, E.G.
Булавин Л.А.	Bulavin, L.A.
Воронель А.В.	Voronel, A.V.
Землянов М.Г.	Zemlyanov, M.G.
Каган Ю.	Kagan, Yu.
Миронов С.П.	Mironov, S.P.
Останевич Ю.М.	Ostanevich, Yu.M.
Симкина А.П.	Simkina, A.P.
Стрелков А.В.	Strelkov, A.V.
Сырых Г.Ф.	Syrykh, G.F.
Холас А.	Holas, A.

IAEA SALES AGENTS

Orders for Agency publications can be placed with your bookseller or any of our sales agents listed below:

ARGENTINA
Comisión Nacional de
Energía Atómica
Avenida del Libertador
General San Martin 8250
Buenos Aires - Suc. 29

AUSTRALIA
Hunter Publications,
23 McKillop Street
Melbourne, C.1

AUSTRIA
Georg Fromme & Co.
Spengergasse 39
A-1050, Vienna V

BELGIUM
Office international de librairie
30, avenue Marnix
Brussels 5

BRAZIL
Livraria Kosmos Editora
Rua do Rosario, 135-137
Rio de Janeiro

Agencia Expoente Oscar M. Silva
Rua Xavier de Toledo, 140-1° Andar
(Caixa Postal No. 5.614)
São Paulo

BYELORUSSIAN SOVIET SOCIALIST REPUBLIC
See under USSR

CANADA
The Queen's Printer
Ottawa, Ontario

CHINA (Taiwan)
Books and Scientific Supplies
Service, Ltd.,
P.O. Box 83
Taipei

CZECHOSLOVAK SOCIALIST REPUBLIC
S.N.T.L.
Spolena 51
Nové Město
Prague 1

DENMARK
Ejnar Munksgaard Ltd.
6 Nörregade
Copenhagen K

FINLAND
Akateeminen Kirjakauppa
Keskuskatu 2
Helsinki

FRANCE
Office international de
documentation et librairie
48, rue Gay-Lussac
F-75, Paris 5^{e}

GERMANY, Federal Republic of
R. Oldenbourg
Rosenheimer Strasse 145
8 Munich 8

HUNGARY
Kultura
Hungarian Trading Co. for Books
and Newspapers
P.O.B. 149
Budapest 62

ISRAEL
Heiliger and Co.
3 Nathan Strauss Street
Jerusalem

ITALY
Agenzia Editoriale Internazionale
Organizzazioni Universali (A.E.I.O.U.)
Via Meravigli 16
Milan

JAPAN
Maruzen Company Ltd.
6, Tori Nichome
Nihonbashi
(P.O. Box 605)
Tokyo Central

MEXICO
Librería Internacional
Av. Sonora 206
Mexico 11, D.F.

NETHERLANDS
N.V. Martinus Nijhoff
Lange Voorhout 9
The Hague

NEW ZEALAND
Whitcombe & Tombs, Ltd.
G.P.O. Box 1894
Wellington, C.1

NORWAY
Johan Grundt Tanum
Karl Johans gate 43
Oslo

PAKISTAN
Karachi Education Society
Haroon Chambers
South Napier Road
(P.O. Box No. 4866)
Karachi 2

POLAND
Ośrodek Rozpowszechniana
Wydawnictw Naukowych
Polska Akademia Nauk
Pałac Kultury i Nauki
Warsaw

ROMANIA
Cartimex
Rue A. Briand 14-18
Bucarest

SOUTH AFRICA
Van Schaik's Bookstore (Pty) Ltd.
Libri Building
Church Street
(P.O. Box 724)
Pretoria

SPAIN
Librería Bosch
Ronda de la Universidad 11
Barcelona

SWEDEN
C.E. Fritzes Kungl. Hovbokhandel
Fredsgatan 2
Stockholm 16

SWITZERLAND
Librairie Payot
Rue Grenus 6
1211 Geneva 11

TURKEY
Librairie Hachette
469, Istiklâl Caddesi
Beyoğlu, Istanbul

UKRAINIAN SOVIET SOCIALIST REPUBLIC
See under USSR

UNION OF SOVIET SOCIALIST REPUBLICS
Mezhdunarodnaya Kniga
Smolenskaya-Sennaya 32-34
Moscow G-200

UNITED KINGDOM OF GREAT BRITAIN AND NORTHERN IRELAND
Her Majesty's Stationery Office
P.O. Box 569
London, S.E.1

UNITED STATES OF AMERICA
National Agency for
International Publications, Inc.
317 East 34th Street
New York, N.Y. 10016

VENEZUELA
Sr. Braulio Gabriel Chacares
Gobernador a Candilito 37
Santa Rosalía
(Apartado Postal 8092)
Caracas D.F.

YUGOSLAVIA
Jugoslovenska Knjiga
Terazije 27
Belgrade

IAEA publications can also be purchased retail at the United Nations Bookshop at United Nations Headquarters, New York, at the news-stand at the Agency's Headquarters, Vienna, and at most conferences, symposia and seminars organized by the Agency.

In order to facilitate the distribution of its publications, the Agency is prepared to accept payment in UNESCO coupons or in local currencies.

Orders and inquiries from countries where sales agents have not yet been appointed may be sent to:

Distribution and Sales Group, International Atomic Energy Agency,
Kärntner Ring 11, A-1010, Vienna I, Austria

INTERNATIONAL
ATOMIC ENERGY AGENCY
VIENNA, 1968

PRICE: US $15.-
Austrian Schillings 388.-
(£6.5.0; F.Fr. 73,50; DM 60,-)